THE EFFECTS OF VARIOUS PORPHYRIN

SPECIES ON THE DECOMPOSITION AND

HYDROGENATION OF HYDROCARBONS

by

IAN D. CARNELL

A thesis submitted for the degree of Ph.D.

School of Chemical Engineering,

The University of Birmingham.

July 1989

UNIVERSITY OF BIRMINGHAM

University of Birmingham Research Archive

e-theses repository

TO ROGER

gone forever

forgotten never

ACKNOWLEDGEMENTS

SYNOPSIS

A tubular reactor was designed and constructed in order that the decomposition of hydrocarbon gases and vapours could be studied. Product distributions and kinetic data obtained from the cracking of n-butane agreed with the values available in the literature. From these results a reaction mechanism for the thermal decomposition of n-butane was proposed.

The cracking of 2,2-dimethylbutane was investigated and a reaction mechanism postulated following the acquisition of product spectra and the calculation of kinetic data. This mechanism differed from others found in the literature.

Base etioporphyrin was synthesised by two unrelated routes.

A concentrate containing approximately two per cent petroporphyrins was isolated from Tia Juana Pesado topped crude.

After demonstrating that porphyrins are thermally stable up to a temperature of $540^{\circ}C$ the effects of nine different porphyrin species towards the cracking of 2,2-dimethylbutane were examined. All nine were shown to act as cracking catalysts. Following consideration of the product distributions and kinetic data obtained from the study of porphyrin catalysis a reaction mechanism has been proposed. This is based on increasing the rate of homolytic bond cleavage.

Porphyrins were shown to catalyse the decomposition of 1-hexene over the temperature range 325 to $450^{\circ}C$. At a temperature of $150^{\circ}C$ three porphyrins catalysed the hydrogenation of 1-hexene.

ABBREVIATIONS

A.C.S.	AMERICAN CHEMICAL SOCIETY.
β	restraining coefficient.
d	density.
CP	CHEMICALLY PURE
2,2-DMB	2,2-dimethylbutane.
DMF	dimethylformamide.
DMG	dimethylglyoxime.
DPEP	deoxophylloerythroetioporphyrin.
Ea	activation energy.
FID	flame ionization detector.
FSD	FULL SCALE DEFLECTION
ID	internal diameter.
k_1	first order rate constant.
mb/d	million barrels per day.
m/e	relative molecular mass divided by electronic charge.
M.I.	molecular ion.
MW	molecular weight.
nmr	nuclear magnetic resonance.
OECD	Organisation for Economic Co-operation and Development.
OD	outside diameter.
ppm	parts per million.
R	gas constant.
RMM	relative molecular mass.
SLR	standard laboratory reagent.
T	absolute temperature. (K)
TJP	Tia Juana Pesado.
TLC	thin layer chromatography.
TMS	trimethylsilane.
TPD	temperature programmed decomposition.

TPP	tetraphenylporphyrin.
TPR	temperature programmed reduction.
UV	ultra violet.
v	volume.
vol	volume.
W	WEIGHT
wt	weight.

1.   <u>INTRODUCTION</u>

1.1   <u>Crude Oil Refining Economic Situation</u>

Outside of the United States of America much of the post war growth

in the consumption of residual fuel oil arose from it displacing coal

from its traditional markets. This displacement depended upon fuel oil

price competitiveness. The trend came to an abrupt halt as a result of

the 1973-74 crude oil price rises and was put into reverse with the

further increases of 1979-80. Between 1979 and 1982 fuel oil consumption

in the OECD declined by 31% whereas total oil consumption only fell

by 13%.

The crude oil price rises of 1973-74 halted the substitution of fuel

oil for coal in most major markets, but did not significantly reverse the

trend of the last twenty years, except in power generation. Once the

initial economic impact of crude oil price rises on fuel oil consumption

was absorbed, the use of fuel oil stagnated while growth, more modest

than previously, returned to most of the rest of the crude oil barrel.

The 1979-80 crude oil price increases produced a more fundamental

shift in the demand for oil. Residual fuel oil ceased to be competitive

with coal in most bulk steam raising and direct heat process applications.

Allied with more intense conservation and the general economic recession,

both of which were the by-product of crude oil price escalation, fuel

oil consumption fell sharply, accounting for 73% of the decline in crude

oil consumption between 1979 and 1982 (1).

Due to the sharp change in the energy supply and demand structure,

the energy consuming nations launched policies for the development and

introduction of such alternative energy sources as natural gas, coal,

oil shale, oil sand, nuclear power and renewable energy supplies.

The introduction of natural gas, coal and other alternative energy sources was particularly active in the energy intensive industries, such as steel and cement production and the efforts of energy savings were promoted at the same time (2). A summit meeting of the oil consuming countries in Venice in June 1980 saw the approval by its members of a comprehensive energy development strategy that was founded on the following :-

1) Alternative energy supplied to increase by 15-20 mb/d (million barrels per day) of crude oil equivalent by 1990.

2) Doubling coal production and use by 1990.

3) Expanding the application of nuclear power (3).

High boiling point fractions are becoming increasingly important contributors to future crude oil supplies because of rapidly depleting resources that can be easily processed (4) and projections indicate that crude oils will tend to have a higher sulphur content and yield more residuum over the next ten years (5). Thus, there is an increased dependence on heavy crude oils. Therefore, diversion of residuum from its traditional role in heavy fuel oil to separation and conversion units which produce lighter products will continue (6). However, there is a natural limit to the extent that modification of existing facilities can cope with this situation and the application of new residual oil upgrading processes and the addition of residuum conversion capacity will become necessary (7).

1.2   The Fractionation of Crude Oil

Crude oil may be fractionated in several ways according to the chemical or physical methods employed.

By analytical methods, it may be separated into the various classes

of, or individual compounds contained in an oil. Alternatively a crude oil can be split into arbitrary fractions depending upon solubility in various solvents or it may be fractionated according to boiling point range.

1.2.1 Fractionation by Compound Type

Crude Oil is a complex mixture of three basic hydrocarbon types, alkanes, cycloalkanes and aromatics, together with small amounts of compounds of sulphur, nitrogen, oxygen and metallic compounds.

1.2.1.1 Alkanes (32% of crude oil)

All of the normal alkanes from C1 to C_{33} have been isolated. The most abundant branched chain alkanes are those with a methyl group on number two carbon followed by 3-methyl and 4-methyl monosubstituted compounds. There are very few disubstituted alkanes. The ethyl group is also rarely found, the tendency being for a dimethyl rather than a monoethyl compound. The methyl group is by far the most common alkyl substituent in crude oil regardless of the hydrocarbon type.

1.2.1.2 Cycloalkanes (21% of crude oil)

The monocycloalkanes are the most abundant. Due to ring strain in other monocycloalkanes only cyclopentanes and cyclohexanes are present in appreciable amounts in the lower boiling fractions of crude oil. In contrast to the alkanes, the most abundant cycloalkanes are those with the largest number of substituents. However, the most common substituent is once again the methyl group. Bicycloalkanes come in assorted ring sizes but all of those isolated have five or six carbon atoms in each ring.

1.2.1.3 <u>Aromatics</u> (47% of crude oil)

All of the mononuclear aromatics boiling up to 190°C have been isolated in addition to miscellaneous species boiling above 190°C. The more thermodynamically stable 1,3-dialkyl or 1,2,4-trialkyl benzenes are more abundant than the 1,2-dialkyl benzenes. Methyl groups are the prevalent substituent although ethyl and higher carbon number alkyl groups also occur.

The higher molecular weight mononuclear aromatics generally belong to the aromatic-cycloalkane sub-class. These compounds have the benzene ring joined to a cycloalkane ring through two common adjacent carbon atoms. The cycloalkane ring is commonly cyclopentane, cyclohexane or a multi-ring combination of these.

All of the dinuclear aromatics contain two benzene rings with two common carbon atoms. The most abundant are 2-methyl and 1-methylnaphthalene, in that order. Tri and tetranuclear aromatics have also been isolated. The higher boiling fractions of crude oil are rich in polynuclear aromatics and aromatic-cycloalkane types of hydrocarbon.

1.2.1.4 <u>Non-hydrocarbon constituents</u>

There are many different types of non-hydrocarbon compounds in crude oil including hydrogen sulphide, inorganic salts, water and organic compounds containing sulphur, nitrogen and oxygen. Only the sulphur, nitrogen and oxygen compounds are present in sufficient quantities to be of economic interest and this interest is mostly negative.

The sulphur compounds in crude oil are complex, relatively unstable and break down during refining processes to give simpler compounds. A large portion of the sulphur compounds in high temperature crude oil

fractions consist of benzthiophenes (8). The removal of these compounds is important because of the adverse effect that they have on catalyst life in subsequent processing. Nitrogen compounds, such as porphyrins, also act as catalyst poisons.

Oxygen compounds occur both in crude oil and its distillates from which, due to their acidic nature, they may be quite easily separated. Oxygen containing compounds are generally not a serious problem in the various catalytic refinery processes.

1.2.2   <u>Fractionation by Boiling Point Range</u>

The composition of hydrocarbons can be identified by boiling point range. As this range increases, the proportion of alkanes and alkenes decreases and the concentration of alicyclics and aromatics increases, therefore structures become more complex. Compounds with the highest boiling point consist mainly of condensed polycyclics. The carbon number of an alicyclic is approximately 20, when the boiling point is 350°C, increasing to around 30 and 40 as the boiling point rises to about 450°C and 550°C respectively (8).

Table 1 shows the approximate boiling ranges of the major fuel products obtained from crude oil. There are three broad classes; naphthas, middle distillates and residue. The latter is used as fuel oil after cutting or diluting with suitable middle distillate in order to adjust the vicosity (9).

1.2.3   <u>Fractionation by Solubility</u>

The fractionation of crude oil can be made on the basis of solubility in various solvents. In the United Kingdom the standard separation

procedure is detailed in BS 2000: Part 143: 1983 (10).

1.2.3.1 __Carboids__

Carboids are components of very high carbon content. They are carbon disulphide insoluble and account for a maximum of 2% of the crude oil make up.

1.2.3.2 __Carbenes__

Carbenes are insoluble in tetrachloromethane and toluene but soluble in solvents such as pyridine and carbon disulphide.

1.2.3.3 __Asphaltenes__

Asphaltenes are n-heptane soluble but toluene insoluble. The name asphaltene was originally proposed in 1837 to describe the fractionation of charcoal using several solvents. It was first stated in 1928 that asphaltenes were precipitated by solvents having a surface tension below 250×10^6 Nm^{-1}. Asphaltenes tend to have an almost constant carbon to hydrogen ratio of about 10 to 1, despite their source.

1.2.3.4 __Maltenes or Petrolenes__

These can be described as being the non-asphaltene compounds of asphalt. Maltenes are n-heptane soluble and can be further separated into oils and resins by chromatography (11,12).

Following exhaustive extraction with the low molecular weight solvents propane and pentane, only 17.3% of a sample of Santa Maria Valley crude oil remained. Subsequent extraction with n-hexane,

n-heptane and iso-octane reduced this figure by 2.1%. The remaining

15.2% of the crude oil had resisted the solvent or dispersive action

of the aliphatic hydrocarbons up to nine carbon atoms, including a

branched chain member. These experiments confirmed that asphaltic bodies

were precipitated by hydrocarbons having a surface tension below 250 x

10^6 Nm^{-1}, as all of the above solvents were below this figure. When

the 15.2% fraction of the crude remaining after the aliphatic extractions

was treated with cyclohexane, having a surface tension of 250 x 10^6 Nm^{-1},

only 8.35% of the original crude oil remained. This was, in effect, the

peeling off of the naphthenic layer protecting the high molecular weight

aromatic nuclei of the asphaltic crude system. Subsequent extraction

with benzene, having a surface tension of 285.6 x 10^6 Nm^{-1} dissolved

or dispersed all but about one per cent of the original crude oil (13).

1.2.3.5   The Chemical and Physical Properties of Asphaltenes

Asphaltenes are very dark brown or black friable solids that have

no definite melting point (12). They melt with swelling and decompose

over the temperature range 180 to 280°C. They are almost insoluble in

alcohols and low molecular weight n-alkanes, are slightly soluble in

ether and acetone and are soluble in benzene, chloroform and carbon

disulphide (14).

An x-ray powder photograph of a precipitated asphaltene is typical

of that of an amorphous solid. Asphaltenes can be separated from oils

by precipitation, centrifugation at very high speed or by the action

of an electric field (15).

In general, asphaltenes are highly resistant to chemical oxidation

e.g. with alkaline permanganate. The slow rate of oxidation has led to

the conclusion that most of the heteroatoms contained in the asphaltic fraction, particularly nitrogen and sulphur, are protected in chains or rings (15).

The concentration of sulphur, oxygen and nitrogen in asphaltenes is quite high. During the genesis of asphaltene, the graphatisation process is interrupted due to the divalent nature of the sulphur and oxygen atoms and the trivalent nature of nitrogen. In this case, the incomplete formation of the tessellations of hexagons will prevent the complete aromatisation of the fused benzenoid network. Thus holes or gaps will be formed and these centres will be the sites of donor atoms. Metals will be able to complex into these sites which cannot be removed by acid washings (16).

Asphaltenes are a solubility classification comprising condensed aromatic nuclei which carry alkyl and alicyclic systems with heteroatoms scattered throughout in various locations. They contain carbon (80-90%), hydrogen (7-8%), nitrogen (0.7-1.8%), sulphur (3-12%) and oxygen (0.2-4%). The precise elemental composition depends on the source of the crude oil and its subsequent treatment but the carbon to hydrogen atomic ratio is almost constant, the greatest variation occurring in the figures quoted for heteroatom content.

The asphaltenes and resins exist in the crude oil in a colloidal form and the oil system may be regarded as a transition from the high molecular weight, fused ring, aromatic, polar micelle of the asphaltene through the less polar and less aromatic resins to the low molecular weight, non-polar hydrocarbons of the bulk crude oil (13,17). In such a system the maltenes act as the disperse phase and the resins are important in maintaining colloidal stability. No distinct interface

around the nucleus or at the micelle boundry exists (8,12,13).

The environment of the asphaltene species is important in determining both its size and shape.

Microstructure :- Individual asphaltene particles appear to consist of a core of five stacked sheets held together by $\overline{\Lambda}$ - $\overline{\Lambda}$ interactions and/or hydrogen bonding. The distance between the planes in the stacks is 3.55 to 3.70 Å, the average height of a stack being 16.0 to 20.0 Å with an overall sheet diameter of 8.5 to 15.0 Å. Arbitrary short range bonding distances of 0.5 to 20.0 Å make the asphaltene particle approximately circular with a diameter of 20 to 100 Å.

Macrostructure :- There are molecular interactions, or orders, at distances of 20 to 2000 Å. The quoted figures for the molecular mass of an asphaltene particle range from a few hundred to about half a million and the value obtained seems to be dependent upon the method of estimation (12).

A value of 50 kJmol^{-1} has been calculated for the energy of association between vanadium and an asphaltene species (12). Crude oil components such as asphaltenes do not appear to influence the rate of thermal degradation of metalloporphyrins and there is evidence that the thermal treatment of crude oils will not form additional metalloporphyrins via the depolymerisation of complexes contained in the asphaltene fraction (18).

1.3   The Problem

There is a trend in petroleum refining to process increasing proportions of high boiling products by cracking and there is an economic

incentive to extract more light distillate from the crude oil during

the primary distillation. As a consequence of the latter point,

atmospheric distillation is being replaced by deeper cutting vacuum

distillation. However, the maximum yield of valuable light distillate

is limited by the highest permissible flash zone temperature. Beyond

this, the least stable components of the crude oil begin to crack, leading

to a loss of vacuum and/or lower pipe still capacity. This results in the

degradation of both the distillate and residue product qualities. It has

been indicated that this cracking can be attributed to the asphaltene

content and more specifically the metal porphyrin components of the

crude oil.

1.4.   The Occurrence of Trace Metals in Crude Oils

1.4.1   Nickel and Vanadium in Crude Oils

The most abundant trace metals in crude oils are nickel and vanadium.

The concentration of vanadium can vary from as little as 0.1 ppm to

as much as 1200ppm. Vanadium has been found in all of the crude oils

originating from Iran and while the vanadium content of the Iranian

paraffinic base crude was low it has also been noted that some crude

oils with a high vanadium content were available. These also contained

comparatively large amounts of nickel and sulphur (19).

Vanadium is generally more abundant than nickel but this is not

always the case. For example, certain African and Indonesian crude oils

have higher nickel contents than vanadium (20). The view upon the nature

of the bonding of vanadium in crude oil and some crude oil products,

has undergone changes in the past. The original hypothesis that vanadium

occurred in crude oil asphaltenes in the form of inorganic salt crystals was later disproved by the detection of vanadyl porphyrins in various crude oils, asphalts and oil shales from different deposits. From an analysis of the electron spin resonance spectra of many crude oil and crude oil fraction samples it was concluded that the nature of the bonding of vanadium in crude oil occurs exclusively in the form of organometallic complexes of VO^{2+} ions of porphyrinic or non-porphyrinic nature (21).

Boscan crude oil residue has one of the highest metal concentrations known, but upon distillation little metal appears in the distillate boiling below 500°C. Above 500°C, however, the metal content of the distillate increases dramatically and is probably all porphyrinic. Iranian light crude residue was distilled in a similar manner and metals were again found in the fractions boiling in excess of 500°C. Vanadium concentration reached a maximum in the fraction that boiled between 550 and 600°C and the nickel content rose steadily with increasing temperature. Iranian light crude oil has a metal content an order of magnitude less than Boscan crude oil but it still showed the same behaviour on distillation. For comparison, Forties crude oil, which contains relatively little metal, was distilled. Again the same behaviour on distillation was observed with metal appearing in distillates boiling above 500°C. However, most of the metal remained in the residue which had a boiling point in excess of 650°C. The metalloporphyrin complexes present in crude oil are sufficiently volatile to appear in crude oil distillate fractions boiling below 500°C whereas the non-porphyrinic metal complexes are not volatile and remain in the high boiling residue (20). Both nickel and vanadium cause problems for the oil industry as they both form compounds which are surface active agents, are corrosive and act as catalyst poisons (20). However, the presence

of vanadium is essential in keeping the homogeneity of crude oil. Many physical properties such as flow, viscosity, etc., depend upon the geometrical arrangement of vanadium sites (16,22). The configuration of the nitrogen, sulphur and oxygen heterogeneous donor atoms about these sites is probably analagous to that in compounds such as β-diketones, β-ketoimides, salicylaldimides, mono- and di-thio-β-diketones and dithiocarbamates (23).

1.4.2   Vanadium in Natural Environments

The occurrence of vanadium is extremely widespread in nature. All types of igneous rocks and solids contain an average of 100 ppm of vanadium, although its concentration in sea water is much lower at about 0.002 ppm (16). All living organisms contain vanadium from 0.15 to 2 ppm. Certain land plants such as Amanita muscaria and marine animals such as Pleurobranchas plumula contain vanadium in concentrations as high as 0.65%, on a dry weight basis (24). Biochemically, vanadium is involved in processes ranging from nitrogen fixation to the inhibition of cholesterol synthesis (16).

1.4.3   Trace Metals (other than Ni or V) in Crude Oils

Although metals other than vanadium and nickel are sometimes to be found in crude oils, their concentrations will be at least an order of magnitude lower than the total vanadium plus nickel content (25).

Examination of 15 different Hungarian crude oils revealed that they contained exclusively stable nickel and vanadyl porphyrins. Complexes formed with other metals or free porphyrins could not be detected (26).

A Californian tertiary crude oil was found to contain iron, mercury, zinc and cobalt in sufficiently large quantities such that porphyrin complexes of these metals could be easily detected. None were found (17). It is believed that trace metals in crude oils, other than vanadium and nickel, are incorporated into the crude oil and behave in a very similar manner to non-porphyrinic nickel and vanadium. It has been concluded that, except for nickel and vanadium, the trace element content of crude oils could be reduced to a negligible level by centrifuging or other procedures designed to remove suspended particulate matter or a dispersed aqueous phase (17).

1.4.4   Non-Porphyrinic Nickel and Vanadium

It is indicated by experiment that the trace metal content of a crude oil, especially the vanadium and nickel content, is related to the porphyrin concentration. However, on a molar basis the amount of porphyrin present is always inadequate to account for the total level of vanadium and nickel (Table 2) (27). Although porphyrins occurring in crude oil have been widely studied very little is known about the nature of the non-porphyrinic metal present (20).

The non-porphyrinic metal compounds are found almost exclusively in the very heavy, unextractable portion of the asphaltenes. They are subjected to strong association effects which minimise the possibilty of their removal and recovery by either physical or chemical methods (25).

It has been found that the non-porphyrinic metals that are acid extractable have relative thermal stabilities similar to those of the metalloporphyrins (18). The non-porphyrinic nickel and vanadium in crude oil either occupies "holes" in the asphaltene sheets that are

bounded by heteroatoms or are present in the form of metalloporphyrin type complexes that are strongly associated to the asphaltene by $\bar{\Lambda}$ - $\bar{\Lambda}$ bonding (17). Asphaltenes are undersaturated with metal ions and sites in the sheet-like structure are available for metal ion complexing (17).

The origin of the non-porphyrinic nickel and vanadium is not known. It may have been incorporated into the asphaltene structure from the original organic source material, replaced other metal cations in the asphaltene or been incorporated by complexation from aqueous or solid phases during the migration or maturation of the crude oil. It has been demonstrated that vanadium and to a lesser extent nickel, are taken up by asphaltenes from aqueous solutions. It has been postulated that the co-ordinating sites were formed slowly during the asphaltene diagenesis and that while the oil was dispersed in the source rock these sites were rapidly filled by nickel or vanadium cations. It has also been suggested that the non-porphyrinic vanadium in the asphaltenes was the source of vanadium introduced into the petroporphyrin structures during the conversion of the source material to the metalloporphyrins found in crude oil (17). However, they undoubtedly arose because nickel and vanadyl porphyrins are the most thermodynamically stable metalloporphyrins and transmetallation between an ion such as magnesium and either nickel or vanadyl would occur during the early stages of diagenesis.

1.4.5   ## The Variation of Trace Metal Concentration
with Depth of Burial

Out of all of the possible metalloporphyrins it is likely that only the vanadyl and nickel porphyrins would survive the geological conditions due to their high thermodynamic stability (17). In addition to this there

appears to be a direct relationship between the vanadium to nickel ratio and the age or depth of the crude oil deposit.

Vanadyl porphyrin complexes were detected in crude oils from the Volgograd region of the USSR by spectroscopic methods. The concentration of the complexes in the oil decreased with depth, the relationship being especially obvious below a production depth of 1800 m (28).

In contrast to the Volgograd crude oil, samples from the Kura River region of the USSR were found to contain nickel, but no vanadyl porphyrins. In this case the concentration of nickel porphyrins increased with deposit depth (29). An exactly analagous position to this was shown by samples of crude oil taken from the Sangachaly Sea and Duvannyi Sea fields (30).

It was reported that in Boscan distillate the nickel porphyrins were confined to the aromatic fraction and the vanadyl porphyrins were contained in the resins. (31). Further, it was estimated that the molar ratio of vanadyl to nickel porphyrins was in the order of 13.

Within the range of values of the V/Ni ratios reported two distinct trends are indicated. The lighter the oil the lower the ratio and the younger the oil the higher the ratio. It has been indicated that the greater the depth of burial the greater the degradation of the hydro-carbon material. From the trend indicated by the metals ratio of Lower Cretaceous oils it may be concluded that the vanadium-hydrocarbon complex in oils is less stable than the corresponding nickel complex (32).

1.4.6   The Effect of Trace Metals in Crude Oils

Crude oils contain complex organometallic compounds which are very stable and relatively non-volatile. Consequently these compounds do not decompose in normal refinery operations and are therefore concentrated

in residual fuel oils and high boiling distillate feedstocks (19).
Among these vanadium, particularly in the presence of sodium and oxygen,
causes external corrosion. Although the vanadium content of fuel oil
may be less than 100ppm, it can become concentrated to greater than
50% in the resulting ash upon combustion (Table 3). Accumulation of
vanadium occurs on heat receiving surfaces at the time and place of high
temperature combustion and ash particles are generally carried in the
gas stream to be deposited upon impinged metal surfaces. Instances of
oxide dripping from ships boilers and their supports have been observed.
The oxide of vanadium which is stable in air at elevated temperatures
is the pentoxide, V_2O_5, which melts at $670^\circ C$. Mixtures with certain
other metals can reduce this already low melting point even further.
Since the corrosion resistance of high temperature alloys arises from
the development of an adherent diffusion-resistant barrier which separates
the metal from its corrosive environment, the formation of a corrosion
product which will flow off and leave the metal essentially unprotected
would be deleterious (33).

The presence of metals in distillate charge stocks greatly increases
gas and coke yields while reducing the production of gasoline (34,35).
Investigations show that small amounts of metal complexes often remain
in partially refined crude oil products such as thermally cracked
distillates and deasphalted stocks. It has been shown that nitrogenous
materials cause copious sludge formation in furnace oils and
metalloporphyrin complexes adversely affect the stability of fuels (36).

Vanadium acts as a catalyst poison, particularly in refining processes
such as hydrocracking. It is deposited onto the surface of the solid
catalyst and reduces its catalytic activity. Accumulation of vanadium

on the process catalyst may also promote undesirable side reactions (19).

Metalloporphyrins are powerful interfacially active agents which promote the formation of a stable emulsion of crude oil with water and also play an important role in the displacement of crude oil from reservoir surfaces (4).

Vanadium contributes to harmful physiological effects such as lung disease arising from the industrial combustion of fuels and the resultant ejection of vanadium oxides into the atmosphere. In addition, heterocyclic atoms present in crude oil are major sources of pollutants such as SO_2 and NO_x (22).

1.4.7   <u>The Removal of Trace Metals from Crude Oils</u>

The removal of metals from crude oil has proved difficult, as reagents powerful enough to effect demetallation tend to alter the other organic materials that are present (37). Traditionally, strong acids such as sulphuric or methane sulphonic acid have been used. Reduction procedures in a basic medium also bring about deep seated changes to a crude oil sample.

The removal of metals presents a complex problem as they are chelated or complexed with ligands that are completely compatible with crude oil, their concentration is low and they can exhibit catalytic effects during conversion. However, certain reagents have been used successfully to demetallate samples of crude oil under mild conditions, such as chlorine, sulphuryl chloride and dinitrogen tetroxide, which do not alter the crude oil matrix (16).

1.5 Porphyrins and Metalloporphyrins

1.5.1 The Structure of Porphyrins

The nucleus of all porphyrin molecules is a large cyclic structure composed of four pyrrole rings linked at their alpha positions by -CH- groups, referred to as methine bridges. These four bridge positions are known as meso positions and are designated alpha, beta, gamma and delta positions. The eight other peripheral positions that are available for substitution are called beta positions and are designated by the numbers one to eight (Fig 1). Replacement of the hydrogen atoms in the beta positions gives rise to a wide variety of porphyrins (38).

The simplest porphyrin structure is porphine whereby all of the meso and beta positions are occupied by hydrogen atoms (Fig 1). The methine bridges establish conjugated linkages between the component pyrrole nuclei forming a more extended resonance system. Although the resulting structure retains much of the inherent character of the pyrrole components, the larger conjugated system gives increased aromatic character to the porphine molecule. The extended resonance lends remarkable stability to all porphyrin molecules and it has been reported that porphine is stabilized by resonance to the extent of 1046 kJmol^{-1} (39) (c.f. benzene; 151 kJmol^{-1}) (40).

Pyrrole, like other heterocyclic molecules, differs from homocyclic aromatic compounds in that it is quite reactive at the position alpha to the nitrogen atom and tends to form dimers, trimers and higher condensation products in which the fundamental pyrrole structure is preserved to a marked degree. The reactivity of the pyrrole nuclei in porphine is greatly reduced, partially because of the increased aromatic character but primarily due to the reactive alpha positions now being blocked (39).

The classical structure for porphine (Fig1), and its derivatives, indicates eleven conjugated carbon-carbon double bonds as well as nitrogen atoms bearing lone pairs of electrons. The molecular orbital interpretation of the porphine molecule indicates a conjugated set of $26\bar{\pi}$ electrons, 20 being donated to the system by carbon atoms, two each by the -NH- groups and one each by the tertiary nitrogen atoms. The electron energies suggest a strongly aromatic molecule. The $\bar{\pi}$ bond order shows that the inner ring contains the greater part of the aromatic character as the outer bonds have a higher bond order and are largely insulated from the inner ring by bonds of a low order. By this theory the molecule approximates to the structure shown in Fig. 2. (41).

X-ray analysis of the porphine molecule has shown it to be approximately planar, consisting of rapidly interconverting tautomers, as four "half-hydrogen" atoms were calculated for the two inner hydrogen atoms (42). Porphine has a four-fold axis of symmetry with respect to the bond distances and angles and it has been definitely established by x-ray diffraction studies on the free base that the inner hydrogen atoms are situated opposite each other rather than adjacent (43). The two inner pyrrole protons can be replaced, thus allowing the nitrogen atoms to chelate with various metals to form metalloporphyrins (38,43). The bonding of the metal ions to the porphyrin molecule is largely covalent in character (39).

An evaluation of the ligand field stabilization energies has been made indicating preferential configurations of electrons in the orbitals of the complexing metals. The two metals that are predominant are those with three and eight d electrons, i.e. vanadium and nickel respectively. In the vanadium atom the three electrons occupy the three low energy d.xy,

d.xz and d.yz orbitals. The corresponding nickel electrons occupy the three low energy levels in spin paired orbitals (six electrons) and in each of the high energy $d.z^2$ and $d.x^2-y^2$ orbitals in single assignments (two electrons). The other possibilities for metals in the series are less stable.

The foregoing has assumed an octahedral orientation for the complexes, but nickel porphyrins are generally considered to have a square planar co-ordination arrangement. Thus nickel complexes should be relatively stable because the eight d electrons can be accomodated in the four low energy d.xy, d.yz, d.xz and $d.z^2$ orbitals.

The vanadium complex probably cannot assume any form other than an octahedral configuration due to the fact that it is not a complex of V^{2+} but rather VO^{2+} and should be referred to as the vanadyl and not vanadium complex. There is no space within the plane of the porphyrin molecule for accommodation of the oxygen atom. Therefore it must occupy a position outside the plane, either above or below, at one of the points of the octahedron (39) (Fig 3).

There is considerable evidence that the two additional ligand points lying above and below the plane of the porphyrin molecule in the octahedral arrangement are generally occupied by solvent molecules (39). It is commonly agreed that porphyrin molecules are substantially planar and x-ray diffraction data has shown that insertion of the vanadyl group into free base octaethylporphyrin had a minimal effect on the geometry of the porphyrin core (44). It has been reported (45) that nickel etioporphyrin I is slightly non-planar, two of the pyrrole rings being bent up and two bent down, relative to the plane formed by the meso carbon atoms, with the metal atom lying in the plane of the porphyrin ring (46). However,

deviations from planarity are small and bond lengths indicate a high degree of symmetry (Fig 4).

1.5.2 The Chemical Properties of Porphyrins

Porphyrins generally are high melting point solids that are stable to the actions of mineral acids (41). The conjugated porphine ring system is heat stable and can be halogenated, nitrated or sublimed without destroying the macrocyclic structure (47). Porphyrins are diacidic bases that exhibit amphoteric properties. They react readily with sodium hydroxide to form sodium salts through the replacemnt of the two imine hydrogen atoms and form salts with hydrochloric acid through the addition of two extra protons to the centre of the porphyrin ring (39). pK values indicate that the acidic groups are very weak in aqueous solution.

It has been reported that gamma radiation is effective in destroying porphyrins (39).

Free porphyrins are only moderately stable; however reaction to form metalloporphyrins increases their stability considerably (39).

A vanadium petroporphyrin separated from Santa Maria Valley crude oil was stable to heat treatment at $125^{\circ}C$ in the presence of water, at $110^{\circ}C$ in the presence of 35% orthophosphoric acid and was not affected by electrical fields. However, it appeared to start to decompose at about $450^{\circ}C$ (13).

Apparently the thermal decomposition of both nickel and vanadyl petroporphyrins is a first order process, since the first order rate constants do not change significantly over a three fold increase in metalloporphyrin concentration. The Arrhenius activation energies

calculated from the rate constants are 180 kJmol^{-1} for the vanadyl porphyrin and 192 kJmol^{-1} for the nickel porphyrin. The rate constant for the vanadyl complex is approximately 1.7 times larger than the corresponding value for the nickel porphyrin (18) (Figs 5 and 6).

The stability of metal complexes of etioporphyrin I in relation to the direct attack of acid was studied and resistance to sulphuric acid was found to increase in the order Cu (II), Ni (II), Fe (III) and VO (II) (39). It has been suggested that a shorter metal to nitrogen bond length indicates a more stable metalloporphyrin with respect to demetallation (43). The removal of the metal from vanadyl porphyrins requires vigorous conditions. Vanadyl octaethylporphyrin was not demetallated by treatment with refluxing trifluoracetic acid for 18 hours nor by contact with phosphoric acid at 180° for one hour. Partial demetallation occured with an hydrobromic/acetic acid mixture when held at 100°C for four hours. Concentrated sulphuric acid at room temperature for 15 minutes or 75% sulphuric acid at 100°C for one hour both caused effective demetallation but 50% sulphuric acid at 100°C for 15 minutes failed to generate a detectable quantity of the free base (48).

The most distinct differences in the polarities of porphyrins are caused by the presence or absence of carboxylic acid side chains (36). Similar conclusions were also drawn from the chromatographic behaviour of petroporphyrins which indicated that structural changes around the periphery of the porphyrin nucleus significantly affected their polarity (49).

Correlations of interfacial activity and porphyrin content showed that the petroporphyrin complexes identified were among the major contributors to the interfacial activity and film forming tendencies

exhibited by a sample of Californian crude oil (50).

1.5.3   The Spectra of Porphyrins

Complexes of transition metals with chlorins and porphyrins do not exhibit fluorescence (39) but they do give characteristic visible spectra. Porphyrins dissolved in organic solvents and in dilute alkali have a typical absorption spectrum, exhibiting four bands in the visible region and a very strong Soret band in the near ultra violet. In strong acids the bands in the visible range are reduced to two (37).

Chemical substitution on the porphyrin nucleus does not substantially alter the visible spectrum since there is no direct interference with the general resonance configuration of the molecule (39). The relative intensities of some of the bands may change but the Soret band is least affected by structural variation (51).

Absorptions in the visible region occur at about 620, 565, 530 and 500 nm and are labelled bands I, II, III, and IV respectively. The relative intensities of these four main bands forms the basis for the classification of porphyrins into three main spectral types, namely etio, phyllo and rhodo. The type of spectrum tends to be indicative of the molecular structure of the porphyrin. In the etio type spectrum the relative intensities of the bands decreases progressively from IV to I. In the phyllo type spectra the decreasing order of band intensity is IV, II, III, I. Rhodo type spectra show band III as the most intense, followed by bands IV, II, and I (52). In addition there is a fourth type of spectrum, known as the chlorin type in which band I is the most intense and is shifted to about 650 nm or even longer wavelengths. Band IV is the next most intense and the intermediate bands are quite weak.

This type of spectrum is characteristic of many chlorophyll derivatives and of some porphyrins that contain a large number of unsubstituted beta positions (38).

In contrast to the four band visible spectrum of the porphyrins, the metalloporphyrins of major interest to geochemists exhibit a two band spectrum. The two bands for nickel etioporphyrin in neutral solution are found at 550 and 514 nm whilst those for vanadyl etioporphyrin are found at 570 and 531 nm. The shift to longer wavelenghths, as compared to the square planar nickel chelate, can be considered to be the consequence of additional coordination with an oxygen atom to yield a pentacoordinate complex.

The position and intensity of the metalloporphyrin visible absorption bands are, in general, even less sensitive to alterations by substituents than are the spectra of the free base porphyrins (53).

The absolute limit of detection of metal porphyrin complexes on the basis of the Soret band at approximately 400 nm is 1.6×10^{-8} moles for vanadyl complexes and 3.0×10^{-8} moles for nickel complexes, based on a solution concentration of about 5g dm^{-3} and the use of 1 cm cells (26).

1.5.4   The Occurrence of Porphyrins in Crude Oils

Of the many porphyrins, chlorins and tetrahydroporphyrins arising in biological systems only a few persist in crude oil and related substances. However, these few are very widespread in their occurrence.

Porphyrins have been found in crude oil, oil shales, coal and other bituminous materials in concentrations of less than one ppm in some light crude oils and up to 0.4% in certain oil shales. They are usually

found as a metal complex but free porphyrin bases have been reported, very little being known about them. This is because methods for detection and analysis of free porphyrin bases in crude oils are not well developed and also the concentration of these compounds is very low, only accounting for about one per cent of the total porphyrin content at best (39).

At present, only average properties and typical structures can be given on the basis of combined degradation and mass spectrometic studies. Oxidation of porphyrins to maleimides, using strong acids to effect bond cleavage at the methine bridges, has traditionally been used as a tool for structural analysis. While much important structural data concerning a porphyrin mixture is made available by this method, a great deal is also lost. Total reconstruction of the structures of the components of a porphyrin mixture cannot be accomplished because oxidation destroys bridges and a mixture containing four times as many components is obtained (53).

One of the two most commonly reported porphyrins occurring in crude oils is deoxophylloerythroetioporphyrin (Fig 7) having a molecular weight of 476 and a systematic name of 1,3,5,8-tetramethyl-2,4,7-triethyl-6, gammaethane porphine $(C_{32}N_{36}N_4)$. The name of this petroporphyrin is commonly abbreviated to DPEP. The second metalloporphyrin commonly found in crude oil is etioporphyrin, the structure and nomenclature of which is given in Fig. 8. The systematic name for etioporphyrin III, which has a molecular weight of 478, is 1,3,5,8-tetramethyl-2,4,6,7-tetraethylporphine (39).

An examination of Boscan distillate, which has a high concentration of petroporphyrins, by mass spectroscopy revealed, in addition to the

usual DPEP and etioporphyrins, three other, more minor, series. These were di-DPEP, rhodo-etio and rhodo-DPEP, the latter two more commonly being combined under the single heading of rhodoporphyrins. The structures of the three minor series of petroporphyrins are given in Figs 9,10, and 11 respectively (20).

In addition to the presence of DPEP and etioporphyrins in Romashkino asphalt, visible spectroscopy also revealed a small quantity of rhodoporphyrins. These were said to exhibit either an alkylbenzoporphyrin or monocycloalkano-alkylbenzoporphyrin structure (21).

It has been reported (20) that the extra ring in rhodoporphyrins confers extra stability to the molecule. Rhodoporphyrins seem less volatile than other petroporphyrins, as shown by the distillation of Iranian light residue. The $600-650^\circ C$ fraction contained 39% of the total rhodoporphyrins present whereas the $500-550^\circ C$ distillate only held 9%.

Rhodoporphyrins have been reported to occur in a number of geological materials but always in coexistance with the more abundant DPEP and etioporphyrins (49).

Porphyrins are virtually universal constituents of crude oils, irrespective of the origin of the oil. Porphyrins were found in 85 out of 99 samples of Polish crude oils examined from various deposits and various formations (54). Samples of 20 Romanian crude oils were all found to contain porphyrins and their concentration was described as a linear function of the total nitrogen content (55). Thus, with porphyrins occurring in nearly every crude oil it would perhaps be reasonable to expect similar chlorin and tetrahydroporphyrin compounds to occur as well, especially since crude oil is normally associated with highly reducing environments. However, tetrahydroporphyrins have not been

reported and only a few isolated occurrences of chlorin compounds have been noted (39).

The DPEP to etio petroporphyrin ratio has been calculated for a number of crude oil samples and there appears to be a direct relationship between this ratio and the depth of the crude oil deposit. The ratio varies from about 0.2 up to a value of around 6, with a decrease in the value of the ratio as the depth of the deposit increases (16).

The relative intensities of the bands in the visible spectrum of La Paz crude oil indicated a mixture of DPEP and etio porphyrins with the latter type predominate. This was confirmed by mass spectroscopy and a DPEP to etio ratio of 0.56 was calculated for the oil (49). It has been reported (56) that crude oil asphaltenes contain higher concentrations of porphyrins than the crude oil from which they have been isolated. The relative concentration of the DPEP series was significantly higher in the La Paz asphaltenes than in the oil. The increase in the DPEP content was reflected by a DPEP to etio ratio increase to 0.96. This indicates that the asphaltenes tend to preferentially concentrate the DPEP species (49).

Carboxylated porphyrin complexes in crude oil are common but not abundant. North American and Venezuelian oils showed that carboxylated porphyrins made up less than 5% of the porphyrin material present in young oils with an even smaller proportion in older oils (39). It has also been reported that the concentration of carboxylated porphyrins in all crude oils is much lower than that of the corresponding decarboxylated compound, usually being at least an order of magnitude lower (27). A study of Bachaquero residuum precluded the presence of porphyrins containing carboxylic ester side chains due to the resistance

of the extracted porphyrins to undergo hydrolysis in the presence of
alcoholic sodium hydroxide (34). However, the presence of porphyrins
with carboxylated side chains may be more common, and their concentration
greater, than previously reported. The methods of concentration and
separation discriminates against carboxylated porphyrins as they are
probably too strongly absorbed in the asphaltene fraction to be easily
removed by presently used methods (57). Additionally, any polar porphyrins
separated from the crude oil may be lost, or at best only traces recovered,
due to retention by chromatographic stationary phases during purification
stages (52). This has led to the commonly held belief that most of the
porphyrins occurring in crude oil and other bituminous substances are
totally decarboxylated or that decarboxylated porphyrins cannot be
distinguished (57).

1.5.5   Porphyrin Content vs Sulphur Concentration

Examination of a large number of crude oil samples showed that oils
containing less than 0.7% sulphur are either very low or totally devoid
of porphyrins, while the porphyrin content of high sulphur samples is
between 100 and 1000 times greater than the former case (58).

There is a definite relationship between the sulphur content of a
crude oil and the vanadyl porphyrin level. This is demonstrated by the
Utah and Madagascar oil sand deposits in which very heavy crude oils
are found with a very low sulphur content, this being less than 0.5%.
There is a correspondingly low vanadyl porphyrin content, which amounts
to only about 15ppm (27,39). This can be compared with the case of the
Athabasca tar sands which have a 5% sulphur content and a similarly
high vanadyl porphyrin content of about 500 ppm (27,39). However, the

converse also appears to be true and crude oils that have a low sulphur content seem to exhibit a relatively high concentration of nickel porphyrins (27,39).

Thus in a high sulphur crude oil petroporphyrins are predominately in the form of vanadyl complexes (up to 90%) while in samples with a low sulphur content porphyrins occur mainly as nickel complexes (58).

1.5.6   The Occurrence of Porphyrins in Nature

Amino acid analysis was carried out on a fraction of a crude oil from Lower Cretaceous strata that contained vanadyl porphyrins and a number of amino acids including glucine, alanine, serine, glutamic acid, aspartic acid, leucine and isoleucine were found in the hydrolysates of the isolated porphyrin fraction. These results were interpreted as being the residues of proteins originally bonded to biogenic pigments (59).

The main biochemical function of porphyrins and their derivatives in nature is to provide carriers for metals which it is necessary to confine to a small space for the purposes of chemical reaction (60). The first porphyrin to be found in nature as a crystallised mineral has recently been reported. The nickel porphyrin was found as tiny flakes in a drill core at a depth of 764 metres in the Green River formation of Uintah County, Utah. The soft and fragile crystals were purple in colour, with an adamantine lustre. Visible and mass spectra showed the crystals to be mainly a C_{31} nickel DPEP together with about 14% of the free base porphyrin (53).

1.5.6.1   Porphyrins in Coal

Coal has long been known to contain porphyrins, believed to be made
up of mainly etioporphyrins. Hodgson, et al (27) have studied two coals,
a subbituminous coal and a lignite, both containing porphyrins of the
etio type, some with free carboxylic acid side chains. Two features
were apparent from the porphyrins occurring in coal.

a)   The concentration was very low.

b)   The pigment was not of the chlorophyll type, a pigment class which
might have been expected if coal were believed to arise from plant material.
Both observations were explained in terms of oxidation effects. In the
first case oxidation causing total destruction of the pigment and in the
second significantly changing the structure of the original chlorophyll
type molecule, in which the fifth isocyclic ring was broken, giving rise
to etio type pigments. The porphyrins present were extracted by the
method of hydrobromic/acetic acid digestion which cleaves any metal to
porphyrin bonds. This method was found to be necessary as milder extraction
methods failed to extract any porphyrins, probably because of the strong
absorptive capacity of coals. Thus it was impossible to determine if the
porphyrins extracted by this method were associated with metal ions
or not.

1.5.6.2   Porphyrins in Peat

A sample of peat from the Edmonton area of Canada showed chlorin
pigments to be present at a concentration of 750 ppm, based on dry weight.
Chlorins are dihydroporphyrins which might therefore be regarded as
hydrogenation or reduction products of porphyrins. Chlorophyll is, for
example, a very well known chlorin pigment. Generally, chlorins are less

stable than the corresponding porphyrin, are green in colour and exhibit a visible spectrum differing from the type shown by porphyrins. The pigments found in peat were mainly carboxylated free chlorins and their esters. Carboxylated metal chlorin complexes were present at a concentration at least an order of magnitude lower than the concentration of the carboxylated free chlorins and their esters combined. Metal porphyrin complexes were present to the extent of approximately 0.5% of the total pigment concentration and were mainly of the carboxylated type (27).

1.5.7   Porphyrin Homologous Series

The complexity of the naturally occurring petroporphyrin mixtures is emphasised by very strong evidence which suggests the presence of structural isomers. In addition, complete structural characterisation of individual petroporphyrins is rendered difficult by a large number of homologues for different structural series which occur in geological materials (49).

The number of petroporphyrins present in any crude oil is large because in each of the etio, DPEP and rhodo series the homologues commonly span the range of C_{26} to C_{40} (6 to 20 methylene groups) giving a total of at least forty groups of isomers. It has been estimated that the total number of metalloporphyrin isomers in a given crude oil may exceed 10^5. However oxidative degradation and mass spectrometric data make it quite clear that not all of the possible isomers are present in detectable quantities. One group, the polymethine substituted phylloporphyrins are not present, the evidence for which is the absence of characteristic absorption bands in the electronic spectra.

A second and much larger group, the identically beta substituted (e.g. methyl/methyl; ethyl/ethyl) porphyrins are also absent from crude oil, as samples oxidised to maleimides showed no traces of dimethyl or diethylmaleimides. The reason for the absence of geoporphyrin structures with two identical beta substituents is not clear, but the absence of such structures eliminates a vast group of possible isomers. For example, in the case of etioporphyrins, if only one asymmetrical substitution is present, four isomers are possible. If, however, symmetrical as well as asymmetrical substitution is present, the number of isomers rises to thirteen. In a simple case, Lloydminser oil, only etio series porphyrins are present. All of the etioporhyrins present in the sample were composed of combinations of five asymmetrically beta substituted pyrroles. Methyl/hydrogen; ethyl/hydrogen; methyl/ethyl; methyl/propyl and ethyl/propyl. No other combinations were experimentally determined. Summing the C_{28} to C_{34} isomers in the etio series gives the possible number of structurally differing porphyrins as 1081. Porphyrins in the DPEP series present a complex problem in estimating isomer number and no detailed values have been produced (53).

Oxidative degradation of La Paz petroporphyrins produced the same pattern of alkyl-substitution in the etio series as detailed above. Other maleimides such as dimethyl, diethyl and methyl/isopropyl were absent and the most abundant component was the methyl/ethyl homologue. This indicates that the alkyl-substituents are limited to methyl, ethyl and n-propyl and that unsubstituted positions are present (49). Mass spectrometry is an obvious tool for studying the structural spread of petroporphyrins. However, the use of this technique was hampered for many years due to the non-volatility of porphyrins. The problem was

solved by the use of solid probe inlets and the first mass spectrum
of a porphyrin to be published was that of nickel etioporphyrin,
appearing in 1960 (53). Following initial investigations, the first
report of the use of mass spectrometry to characterise naturally
occurring porphyrins was in 1966 (47). Mass spectrometry has now become
a standard method of identifying and characterising porphyrin mixtures
from geological sources. Polar groups, such as carboxyl, decrease the
already limited volatility of the porphyrin so greatly that good quality
spectra of these species are difficult to obtain (53).

The parent molecular ions of a geoporphyrin mixture fell into two
major homologous series with peaks appearing in each series every 14
mass units. Alkylporphyrins of the etio series have a molecular weight
of 310 ± 14 n, where n is a positive integer. Those of the DPEP series
havē a molecular weight of 308 ± 14 m where, m is a positive integer of
two or greater. In addition to the two major series of porphyrins
present in crude oil minor series attributed to rhodoporphyrins have
also been found. In this case homologous series at molecular weights
of 458 ± 14 n and 456 ± 14 n are observed in the mass spectrum (53).

The petroporphyrins of a Cretaceous crude oil, La Paz, from Western
Venezuela, were shown to be a mixture of etio and DPEP homologues
maximising at C_{30} and C_{31} respectively. Minor amounts of rhodoporphyrins
were also shown to be present. TLC afforded fractions, which were shown
by mass spectroscopy to contain up to 80% of a single weight species.
Oxidative degradation of the petroporphyrins to maleimides followed
by mass spectrometric analysis of the TLC fractions indicated that some
of the porphyrins were to a large extent incompletely substituted.
The molecular ions of the predominant etioporphyrins, which represented

64% of the total ion current due to molecular ions, form an envelope with m/e values at 310 ± 14 n, where n varies from 7 to 19, with a maximum at mass 450. The molecular ions of the DPEP series consist of an homologous series with m/e values of 308 ± 14 n, where n varies from 7 to 19. This series has a maximum mass value at 462, which is one $-CH_2-$ equivalent higher than the maximum for the etio series. This bimodal distribution, with the relative maxima of both series differing by a mass of 14 units, is typical of the petroporphyrins detected in a wide range of geological materials (49).

The porphyrins of an oil shale and Wilmington crude oil from California were shown to be similar and contain at least two homologous series. The porphyrins were alkylsubstituted and contained from seven to thirteen methylene substituents per molecule (47).

From Baxterville crude oil, an homologous series of etioporphyrins was found of mass 310 ± 14 n, where n varied from 5 to 15, and from Rozel Point crude oil a series was similarly found by mass spectroscopy with a mass of 308 ± 14 n for the DPEP species (57).

The vanadyl petroporphyrins originating from a West Siberia crude oil were found to consist of homologues of alkyl, cycloalkyl and bicycloalkyl species with between 6 and 26 alkyl substituents (61).

Petroporphyrins from Boscan crude oil are reported to be in the range C_{28} to C_{39}. However, in the heavier Boscan distillate all five porphyrin types were observed with the following order of abundance, DPEP $>$ etio $>$ di-DPEP $>$ rhodo-etio = rhodo-DPEP. The mass spectrum of the concentrate containing the vanadyl porphyrins indicated a spread from C_{25} up to C_{60}, with a peak at C_{32} (20, 31). In an examination of Baxterville crude oil it was noted that porphyrins possessing the rhodo

type visible spectrum had nominal masses of an homologous series four
mass units lower than the DPEP series. On the basis of high resolution
mass spectroscopy it is quite certain that only the elements of carbon,
hydrogen and nitrogen are present in these petroporphyrins and that
oxygen is absent (57).

Rhodoporphyrins were also detected in samples of La Paz crude oil
and it was determined that they covered the range C_{30}-C_{39} (49).

An homologous series of vanadyl etioporphyrins of mass $375 + 14 n$
was found by mass spectrometric methods, to exist in Romashkino asphalt.
A corresponding series of vanadyl DPEP species was also found. This
series fell on the mass range of $373 + 14 m$ and the number of carbon
atoms in the saturated substituents on the basic porphine structural
unit was found to be between seven and sixteen. The mass spectrum of the
vanadyl porphyrin concentrate obtained from chromatographic separations
indicated that a series of rhodoporphyrins was also present obeying the
mass relationship $425 + 14 n$ (21).

Petroporphyrins extracted from asphaltenes with methylsulphonic
acid were reported to fall into two major, DPEP and etio, and one minor,
rhodo, series. The two major series were homologues of the structures
given in Figs 7 and 8 and the relative distribution of each series formed
a roughly Gaussian distribution peaking at the structures given above
(48).

The relative concentration of DPEP homologues was found to be
significantly higher in asphaltenes than in crude oil with the C_{31} DPEP
being the most abundant component. In contrast to the oil petroporphyrins,
the molecular mass distribution of porphyrins derived from asphaltenes
covers the narrower carbon number range of 27 to 35. These differences

could be attributed to the fact that the petroporphyrins are incorporated into the asphaltic host by forming $\bar{\Lambda}$ to $\bar{\Lambda}$ molecular complexes with the asphaltene fractions and that the incorporation of petroporphyrins in the asphaltic host will be affected by their polarity. This would result in the preferential inclusion of the DPEP species. Petroporphyrins that have been isolated from geological materials with a high asphaltene content, e.g. Gilsonite, which is a naturally occurring asphaltite, Athabasca tar sands and Green River Shale, have demonstrated that they have high DPEP to etio ratios (commonly 1.5-5.0) and narrow carbon number distributions (C29-C35). Due to the preferential concentration of the DPEP homologues in the asphaltic fractions, any process which produces a change in the asphaltene content, such as migration, natural deasphalting or expulsion from the source rock at different stages of maturation, could produce a significant change in the petroporphyrin content and the relative abundance of the DPEP and etio series (49). Thus different crude oils contain homologous series of petroporphyrins that have differing spreads of carbon numbers depending upon their geochemical histories (31).

1.5.8 Petroporphyrin Genesis

Even though porphyrins account for only a trace of the carbon present in crude oil the chemistry of these tetrapyrrole pigments has made a major impact on geology and the earth sciences. The significance of these compounds was recognised in 1934 by Alfred Treibs at the Technische Hochschule in Munich (62) when he discovered that a wide variety of crude oils and bitumens contained porphyrins. He stated; "The findings compel extensive geological conclusions. The demonstration

of porphyrin is just as sure and exact as the spectroscopic detection of an element. The proof that chlorophyll bearing plants played a decisive part in the formation of bitumens and crude oils of various origins and of all geologic ages is brought out with full certainty". From this beginning the science which is today called organic geochemistry developed (53). Treibs isolated and identified two of the major metalloporphyrins present in crude oils and shale, namely vanadyl DPEP and vanadyl etioporphyrin (31). A second type of metallochelate, present in much lower concentrations, was tentatively, but as it turned out incorrectly, identified by Treibs as iron porphyrin. A later re-examination in 1948 using a porphyrin mixture rich in the second chelate revealed that nickel rather than iron was the second porphyrin type present (53).

While porphyrins may be formed directly from pyrroles under extreme conditions it is now generally agreed that petroporphyrins are of biogenic origin. Thus petroporphyrin metal complexes may be regarded as the stable end products of the partial breakdown of the primary source material of crude oil and it is clear that many pigments in living organisms would degrade and stabilise to porphyrin structures (19,39). In 1936 Treibs published his famous reaction sequence in which DPEP and etioporphyrins could be derived from chlorophyll or heam (Fig 12) and the knowledge of the composition of metalloporphyrins in crude oil has been evolving over the last 50 years (31).

The presence of an isocyclic ring in a petroporphyrin structure is usually interpreted as an indication that these pigments were originally derived from chlorophyll. In photosynthetic organisms several types of chlorophyll have been identified chlorophylls (a, b, c, d and e), bacteriochlorophylls (a, b and c) and chlorobium chlorophylls (of which

there are several types). Chlorophyll a (Fig 13) is the most abundant,
being common to all autotropic organisms, except pigmented bacteria.
Chlorophyll b is found with chlorophyll a in some algae and higher
plants. Chlorophylls c, d and e are also found associated with chlorophyll
a in algae. Bacteriochlorophylls are found in a number of purple and
brown bacteria and chlorobium chlorophylls are associated with
chlorophyll a in green bacteria (39). Thus petroporphyrins are believed
to be the degradation products of plant chlorophylls (20), and while it
is easy to reach such a conclusion it may be an oversimplification (39),
so care must be exercised in choosing the specific starting pigment.
If it is assumed that chlorophyll a is the initial starting compound
and the abundance of this species in nature strengthens this suggestion,
then a sequence of simple reactions could be used to account for the
development of pigments in crude oil and would define to some
considerable degree the chemical environment of the genesis of crude
oil (27). The crude oil in the Santa Maria Valley is produced from the
diatomaceous Monterey shale of the Miocene period and the oil is now
present in the reservoirs where it was originally formed. Thus, no
migration of the crude has taken place and any present constituent is
the product of elements existing at the time the oil was formed. The
evolution of an oil is a process of degradation and the more complex
molecules in the structures of ancient flora and fauna have tended to
degrade to compounds containing only carbon and hydrogen. The residual
elements, such as the metals, either separate from the resulting crude
oil and become part of the matrix, or remain in certian stable molecular
configurations, such as the porphyrins, which are compatible with the
bulk hydrocarbons (13).

A typical sequence of discrete reactions which could convert chlorophyll a into a porphyrin type structure is:-

1.   Demetallation - removal of Mg from chlorophyll a.

2.   Saponification - breakdown of ester groups.

3.   Hydrogen transfer - vinyl saturation and aromatisation.

4.   Reduction - oxygen removal.

5.   Decarboxylation - removal of -COO- groups.

6.   Metal complexing - addition of VO or Ni (27,39).

If chlorophyll a was the major source of petroporphyrins then C_{32} DPEP with a methyl, ethyl substitution pattern would be the expected stable end product. In Boscan crude oil C_{32} DPEP is the major constituent and the methyl, ethyl maleimide is the major oxidation product (31).

It has been suggested that the etio series arose from the DPEP series of petroporphyrins rather than heam. The mechanism remains unclear but thermal conversion of DPEP to etioporphyrin was postulated on the basis of the release of isocyclic ring strain (53). Mass spectrometric analysis of the products arising from experiments using naturally occurring porphyrin mixtures showed partial to complete conversion of the DPEP to etio series, depending upon time and temperature of exposure. At the same time the centre of the etio series mass distribution shifted one methylene unit lower than that of the DPEP series (53).

In order to explain the generation of a large number of isomeric petroporphyrins from a relatively small number of biogenic precursors it has been suggested that porphyrins are subjected to transalkylation reactions in the geological environment. Thus, alkylporphyrins may undergo transalkylation on acidic minerals over geological time periods and this has been demonstrated by in vitro experiments designed to

simulate geological conditions (49). Octaethylporphyrin did not undergo

transalkylation when left to stand in concentrated sulphuric acid for 22

days at ambient temperature. However, when vanadyl octaethylporphyrin

was mixed with alumina and heated in vacuo at $245^{\circ}C$ for 19 days, and the

metalloporphyrins were recovered and recrystallised, mass spectroscopy

clearly demonstrated the presence of higher homologues. Upon impregnating

a range of supports, including the natural clay minerals illite and

montmorillonite, with vanadyl octaethylporphyrin from solution, the mass

spectra of the total extracts were recorded following thermal treatment.

There was clear evidence that up to 20% transethylation had occurred.

These results support the hypothesis that the various homologues series

of petroporphyrins have arisen via natural minerals, such as alumino-

silicates, catalysing intermolecular transalkylation processes (63).

The oxidative degradation of La Paz petroporphyrins shows that their

range of alkyl substituents is quite small with only methyl, ethyl and

n-propyl groups being detected and only certain combinations of

substituents occurring. Transalkylation would be expected to produce

a wider range of substituents and also a larger number of combinations

of substituent pairs on the pyrrole nuclei. Thus the relative simplicity

of the alkyl substitution pattern of the La Paz petroporphyrins suggests

that transalkylation reactions have not taken place to any significant

extent in this particular case and that dealkylation processes may have

played an important role in their geological history. It has been suggested

that an alternative origin for the higher molecular weight petroporphyrin

homologues could be a series of biogenic precursors with a basic carbon

skeleton containing more than 32 atoms. Chlorobium chlorophylls, with an

extended carbon skeleton range, have been isolated and characterised and

could have given rise to the substitution patterns observed among petroporphyrins (49).

Although the di-DPEP structure is rarely mentioned in the literature, it has been shown to be more abundant in crude oils than rhodoporphyrins and is said to arise from condensation of the vinyl group of chlorophyll a (31).

The diagenic route to rhodoporphyrins may start with multi carboxylic acid or ester porphyrins such as mesoporphyrin, coroporphyrin or uroporphyrin and proceed via cyclisation and aromatisation. An alternative mechanism involves the dehydrogenation of the isopropyl group of chlorobium chlorophyll followed by ring closure with neighbouring methyl groups (24).

Simple and predictable extensions plus the original Treibs reactions produce mixtures of porphyrins with carbon skeletons in the range C_{26} to C_{32}, all containing an isocyclic ring.

Treibs reaction	Name	Extension
2	Saponification	Elimination
3	Vinyl group reaction	Devinylation
4	Dehydrogenation	Demethanation
5	Decarboxylation	β-cleavage decarboxylation

Substantially greater reworking of the carbon skeleton is required to produce the C_{32} up to C_{40} structures than for the degradative case. A

partial and tentative list of reactions that might produce porphyrins
of C_{32} and greater includes; Diels-Alder, alkylation and dimerisation.
The reactions involved here may also lead to carbon numbers of less than
32. To distinguish C_{26} to C_{32} porphyrins produced by these rearrangements
from those resulting from simple degradation would require much more
structural information than is presently available.

1.5.8.1   Deesterification

It has been assumed historically, either implicitly or explicitly,
that the process of deesterification was hydrolysis. However, concurrent
hydrolysis and dehydration must occur in order to account for the
observed products. This has led to the suggestion that elimination
rather than hydrolysis is the common deesterification route.

1.5.8.2   Oxidation - Reduction

The environment in buried sediments is unique in NATURE IN several respects,
including the facts that water is present and molecular oxygen is
excluded. Thus, oxidation and reduction reactions must occur together
and for every donor there must be an acceptor. Just below the sediment -
water interface the reduction potential will be sufficiently large to
reduce isolated, and even conjugated double bonds. Treibs originally
proposed the direct intramolecular transfer of hydrogen atoms 7 and 8
in the chlorin structure to the vinyl group. However, it now seems more
likely that other components in the sediments are reactants in these
conversions and a free radical mechanism has been proposed to account
for the saturation of the vinyl group.

1.5.8.3 Aromatisation

The dehydrogenation of the chlorin system to the porphyrin structure at first appears to be a simple aromatisation. This is analagous to the conversion of cyclohexadiene to benzene and indeed, simple chlorins are readily dehydrogenated to porphyrins. However, this is not so for chlorophyll itself or its derivatives and these compounds can be aromatised only under severe conditions. The ease of dehydrogenation of the chlorins to porphyrins depends largely on the presence, or absence, of a gamma substituent or an isocyclic ring. Aromatisation is much more difficult with the presence of such groups and molecular hydrogen is probably not the product of this reaction, a free radical mechanism being proposed as the most likely.

1.5.8.4 Decarboxylation

Decarboxylation of the propionic acid group was perceived as thermally equivalent to CO_2 loss from aliphatic acids. However, the free radical decarboxylation mechanism shown in Fig 14 has been proposed. Homolytic cleavage of the hydrogen to oxygen bond gives a radical that loses CO_2. The new radical can either abstract a hydrogen atom or couple with an oxygen donor to yield an acid one carbon atom less than the original acid. The process could repeat, eventually leading to the loss of three carbon atoms.

A second mechanism involving breakage of the carbon to carbon bond beta to the porphyrin ring is also a possibility. The bond is doubly activated, being beta to both the aromatic system and the carbonyl group. The activation energy for the beta-cleavage route may be sufficiently low as to make the two carbon loss the preferred route.

1.5.8.5 Devinylation

In the laboratory, fusion of vinyl substituted porphyrins with resorcinol at 190°C for 15 minutes produces adducts which break down under mildly acidic conditions to yield devinylated porphyrins. Even though no such adducts have been separated from any crude oil, large quantities of hydroxy-substituted compounds are present and such adducts do form under mild conditions. The above was thus suggested as the most likely mechanism for the formation of beta unsubstituted petroporphyrins.

1.5.8.6 Demethanation

The ethyl, hydrogen beta substitution pattern is quite common to some petroporphyrins. However, none of the simple dealkylation reactions, e.g. oxidative decarboxylation or devinylation, yield this pattern. Thus, demethanation, in competition with dehydrogenation was proposed as a route to the observed ethyl, hydrogen beta substitution pattern.

1.5.8.7 Etio series generation

Geoporphyrins of the etio series (310 + 14 n) may constitute up to half of the total petroporphyrins. Strongly alkaline conditions will open the isocyclic ring in chlorophyll to yield a chlorin. However, conditions under which these reactions proceed are not conducive to pigment survival and apparently only a minor portion of the etioporphyrins arose by this route.

Based upon experimental evidence and oxidative degradation data, it would appear than an unsymmetrical cleavage of the 6,δ-ethano bridge is favoured. The diradical so generated can undergo a complex array of

reactions including hydrogen abstraction and/or oxidation. However, any reaction leading to a 6-methyl substituent seems to play a small part, as no dimethyl maleimide is observed upon the oxidative degradation of petroporphyrins. Hence the δ-ethano radical is somehow favoured and degradation of this radical would lead to the resonance stabilised porphoryl radical.

1.5.8.8   Alkylation

Since the first detailed mass spectrometric report of homologous series of petroporphyrins it has become increasingly unlikely, as investigations have progressed, that chlorobium chlorophylls could be petroporphyrin precursors and the originally suggested mechanism of transalkylation still stands.

Interpretation of the structural data shows that the carbon skeleton of chlorophyll has been altered in two ways; substitution on the aromatic system and on the beta alkyl substituents.

There is strong evidence for intermolecular porphyrin transalkylation under conditions that are geochemically accessible.

1.5.8.9   Diels-Alder Adducts

It is known that vinyl substituted porphyrins produce Diels-Alder adducts with a number of dienophiles. Thus, benzoporphyrins may be formed by Diels-Alder adduct formation with benzoquinone homologues followed by diagenic dealkylation and aromatisation (Fig 15).

Plastiquinone is present in substantial amounts in photosynthetic organisms and could thus act as a dienophile.

1.5.8.10   <u>Dimerisation</u>

Dimerisation of porphyrin molecules could possibly occur through either:-

a)   dimerisation of porphoryl radicals arising by either isocyclic
      ring opening or decarboxylation

      or

b)   Diels-Alder condensation through the acrylic acid side chain of
      chlorophyll c.

Whether nickel and vanadium were originally present in the porphyrins
in a biochemically useful form is open to speculation, but this seems
unlikely. It is more probable that porphyrin precursors and metals came
from separate sources. The introduction of metals into porphyrins in
the laboratory proceeds rapidly under acidic conditions, so if it is
assumed that the remains of metal concentrating organisms, or the like,
were present in the oil forming beds then sufficient time, temperature
and a favourable acidity could permit the formation of these complexes
(60). However, metal complexes of pigments indistinguishable from vanadyl
chlorins occur in all early environments, most significantly the
structure of living plants. This focuses attention on the possibility
that vanadyl porphyrins present in crude oil arose from compounds in
plants other than chlorophylls. The sequence of environmental reactions
for vanadyl porphyrin production from chlorin precursors is thus
simplified to; hydrogen transfer, reduction and decarboxylation. By this
route the most difficult step in accounting for the presence of vanadyl
pigments in crude oil is overcome. The complexing of the vanadyl ion
with the pigment is not necessarily a reaction in the genesis environment
but rather a prior reaction occurring in the plants..There is no evidence

for the presence of nickel complexes either in very early genesis environments or in plants. The entire sequence of reactions previously discussed appears to be required to explain the presence of nickel porphyrins in crude oil. However, the complexing of nickel with a free base porphyrin is accomplished much more easily than the corresponding complexation with the vanadyl ion (27).

1.5.9   Metalloporphyrins as catalysts

Upon the addition of magnesium complexes of porphyrins to boiling tetralin a certain amount of the dye was destroyed with intense red luminescence which persisted for a few minutes. The same effect was found with the zinc complex but the luminescence was less intense and more persistant (64). This is a description of the first found report of a metalloporphyrin catalysing a chemical reaction. Since this paper appeared in 1938 metalloporphyrins have been found to catalyse many types of reaction including oxidation, reduction, isomerisation, decarbonylation and others.

1.5.9.1   Oxidation Reactions

Mercaptans are oxidised to disulphides in the sweetening of light petroleum distillates by air oxidation with cobalt tetraphenylporphyrin-tetrasulphonate acting as catalyst (65).

Co (III) and Fe (III) porphyrins were found to catalyse the autoxidation of cyclohexene to allylic hydroperoxides, which decompose to yield 2-cyclohexenone as the main product (66). Cobalt (II) tetra-phenylporphyrin catalysed the autoxidation of acetaldehyde to give peracetic acid quantitatively. The para-substituents of the phenyl

groups on the porphyrin were found to influence the catalytic activity (67).

The catalytic oxidation of aldehydes by cobalt tetraphenylporphyrin was found to proceed by oxygen activation of the central metal atom and subsequent hydrogen abstraction from the aldehyde (68). Transition metal derivatives of tetrakis(p-methoxyphenyl)porphyrin were found to activate the anodic oxidation of sulphur dioxide (69). Ketoamides were the primary products of the cobalt and copper porphyrin catalysed oxidation of indoles (70).

It was discovered that the addition of unsaturated hydrocarbons to Co (II) porphyrins in non-aqueous solution caused immediate oxidation of the Co (II) to Co (III), followed by degradation. Oxidation occurs if the dielectric constant of the solvent is higher than that of the alkene. This suggests that the solvent has to be more polar than the alkene in order to aid electron transfer (71).

It was found that the oxidation of ascorbic acid was catalysed by copper hematoporphyrin (72). The manganese (II) chloride complex of tetraphenylporphyrin and the phase transfer reagent trioctylmethyl-ammonium chloride act synergically to promote the oxidation of both alcohols and hydrocarbons (73).

Cyclohexylbenzylhydroperoxide was prepared by the oxidation of cyclohexylbenzene with oxygen in the absence of light and in the presence of copper or nickel tetraphenylporphyrin (74).

Cobalt octaethylporphyrin catalysed the autoxidation of squalene to yield three isomeric epoxides and two alpha, beta unsaturated aldehydes as the main products (75).

1.5.9.2   Reduction Reactions

Copper and cobalt tetraphenylporphyrins were found to catalytically reduce nitric oxide in the presence of hydrogen at elevated temperatures (76,77). Degassed solutions of N-methylpyrrolidine and nitrophenol in benzene containing tin (IV) or germanium (IV) tetraphenylporphyrindichloride were irradiated with visible light, of wavelength greater than 500nm, to give aniline, azoxybenzene and azobenzene as the reduction products of nitrophenol and N-methylpyrrole as the dehydrogenation product of N-methylpyrrolidine (78).

1.5.9.3   Other Reactions

Aryl, alkyl and cycloalkylaldehydes were decarbonylated by the di, triphenylphosphineruthenium complex of tetraphenylporphyrin under ambient conditions (79). Cobalt tetraphenylporphyrin catalysed the electrochemical cleavage of butylbromide in non-aqueous media (80).

Aromatic nitro-compounds were converted to the respective isocyanate by treatment with carbon monoxide over palladium tetraphenylporphyrin (81,82). The copper (III) chloride complex of tetraphenylporphyrin was found to catalyse the isomerisation of quadricyclene to norbornadiene (83,84).

It was evident from the experimental results that both vanadyl and nickel tetraphenylporphyrin were inefficient catalysts for both the hydrodesulphurisation and hydrodenitrogenation of atmospheric gas oil, vacuum gas oil and a synthetic oil (85).

1.6.   The Cracking of Hydrocarbons

1.6.1   Catalytic vs Thermal Cracking

Catalytic cracking proceeds via a carbonium ion mechanism, unlike thermal cracking which involves free radicals. Due to the difference in reaction mechanism the product spectrum is also different. Catalytic cracking yields larger quantities of C_3 and C_4 compounds, branched alkanes and alkenes as well as aromatic compounds, which have a beneficial effect on the composition of motor fuels (86).

1.6.2   Catalytic Cracking

The main advantages of catalytic cracking over thermal cracking when processing crude oils lie in the maximisation of light hydrocarbon production at C_4 rather than C_2 (Fig 16) and a higher yield of light gasoline compounds. Catalytically cracked gasoline also has a higher proportion of branched alkanes, cycloalkanes and aromatics, all of which increase the quality of gasoline.

Unlike thermal cracking, catalytic cracking is an ionic process involving carbonium ions.

The formation of carbonium ions in catalytic cracking can occur in three ways (Fig 17).

1.   Addition of a proton from the acid catalyst to an alkene produces a carbonium ion in a reversible reaction. A proton may then leave the carbonium ion from a carbon atom other than the one to which the original proton became attached. The initial alkene may have been formed from a free radical produced by thermal cracking. This is one of the ways in which alpha alkenes are converted to internally unsaturated alkenes

during catalytic cracking.

2. Carbonium ions may also be formed by the abstraction of a hydride ion from a saturated hydrocarbon by the acid catalyst or

3. A carbonium ion.

The acid catalysts first used in catalytic cracking were amorphous solids composed of approximately 87% silica and 13% alumina for low alumina catalysts, and 75%-25% for high alumina catalysts. However, these have now been superseded by zeolites. The catalytic action of amorphous silica-alumina catalysts has been well established as a function of Lewis acid and Bronsted acid sites. The Lewis acid sites abstract a hydride ion from an alkane as shown in Fig 18. Bronsted acid sites form carbonium ions by protonation of a carbon to carbon double bond as given in Fig 19. Both acid sites appear to be operative, with the ratio being dependent on the degree of catalyst hydration, the amount of water in the feed having a marked influence on the catalyst activity.

Zeolite catalysts appear to be able to promote both acid catalysed carbonium ion reactions and reactions occurring by a free radical mechanism. The chemistry occurring at the catalytic sites in zeolites is not well understood and because the product distribution is different from that obtained when silica-alumina catalysts are used it is apparent that the situation is more complex in relation to zeolites.

Thus, as the process catalysts used produce the carbonium ions, the reactions of these ions produce the desired products.

Isomerization is effected by both hydride and methide (CH_3^-) shifts. The hydride shift (Fig 20) moves the positive charge to the next carbon atom. The stability trend is towards the centre of the molecule, which accounts for the isomerisation of alpha alkenes to internal alkenes under

carbonium ion conditions. The methide shift results in skeletal rearrangement as shown in Fig 21. The initial shift is followed by a hydride shift to give the more stable tertiary carbonium ion. This type of reaction accounts for the conversion of normal-alkanes to iso-alkanes.

Beta fission is the cracking reaction of catalytic cracking (Fig 22). The carbon to carbon fission takes place on either side of the carbonium ion, with the smallest fragment usually containing at least three carbon atoms. The new carbonium ion rearranges before it can undergo beta fission which is one reason for the low yield of C_2 compounds. Cyclisation takes place by carbonium ion addition to a carbon to carbon double bond in the same molecule (Fig 23).

Cyclic alkenes and aromatics can be accounted for by a two step hydrogen transfer sequence. The first is a proton transfer and the second a hydride ion transfer (Fig 24). A continuation of this sequence converts the cyclic carbonium ion to an aromatic hydrocarbon.

The hydride ion transfer reaction is an important ion molecule reaction between carbonium ions and hydrocarbons. For simple alkyl carbonium ions, the rate of hydride transfer is independent of the source of the reacting ion. This implies that the reactant carbonium ion must be capable of readily rearranging, by a hydride shift sequence, to the reacting structure regardless of the structure of the initially formed ion. The reaction rate is deteremined by the hydrocarbon molecule with which the carbonium ion is reacting (87).

1.6.3   Thermal Cracking

The first paper detailing the mechanism of thermal cracking, by the free radical pathway that is generally recognised today, appeared in

1931 (88). From what is today regarded as the definitive paper on the
subject, a series of thirteen articles (88-100) was released dealing
with subjects as diverse as bond strengths in organic molecules (92),
through the combination of methyl groups with metallic mercury (96),
to the decomposition of ethyl nitrite (100). However, even 25 years ago,
understanding of the mechanism of alkane pyrolysis was little better
than rudimentary. Not only was there dispute regarding the relative
roles of molecular and radical chain processes, but quantitative results
were limited and conflicting. The turning point came with the advent of
gas chromatography, which allowed a detailed analytical approach providing
large volumes of comprehensive data rapidly. The almost immediate
consequence was that a number of research groups, working along
independent lines, were able to unequivocally establish the radical chain
nature of thermal cracking reactions. Subsequent development was swift
and within a decade the general features of the early stages of the
pyrolysis of all alkanes in the C_2 to C_5 range were well established.
The intervention of vessel walls and both the homogeneous and hetero-
geneous effects of traces of oxygen have been studied in great detail,
and the eventual observation that isopentane pyrolysis can be almost
stopped by appropriate wall treatment constituted the final and most
convincing evidence for the totally radical chain nature of these
pyrolyses (101).

Hydrocarbon free radicals are formed by the first order homolytic
cleavage of a carbon to carbon bond. Relative bond energies determine
which bonds will break. For carbon to carbon bonds these energies are
about 331, 314, and 310 $kJmol^{-1}$ for primary, secondary and tertiary bonds
respectively. The carbon to hydrogen bonds are shorter (1.09 Å) than the

carbon to carbon bonds (1.54 Å) and stronger (87). Due to this it is
necessary to consider only the cleavage of the carbon to carbon bonds as
possible initiation reactions (88). This was confirmed by work with
isobutene where carbon to hydrogen bond rupture did not exceed five
per cent of the total initiation (101).

According to radical chain theory small alkyl radicals quickly
accumulate to a steady state concentration (102). Once formed, a radical
may react with one of the surrounding hydrocarbon molecules, decompose
into a compound and a smaller radical or diffuse to the wall of the
reaction vessel and be absorbed there.

A methyl radical can only undergo one reaction. It will abstract a
hydrogen atom from a molecule of the surrounding hydrocarbon to leave
a free radical containing the same number of carbon atoms as the original
hydrocarbon.

Radicals higher than methyl can undergo two types of reactions:
1. They may abstract a hydrogen atom from the surrounding hydrocarbon
molecules that contain the same number of carbon atoms.
2. They may decompose either by giving up a hydrogen atom to form a
compound with the same number of carbon atoms as the original compound
or they may break into a compound and a smaller free radical (88),
usually an ethyl or methyl radical or a hydrogen atom (103). The relative
rates of the decomposition of large radicals is determined by the resonance
stability of the new radicals, as shown in Table 4 (102).

When any free radical, except methyl, is formed it can decompose
either into a hydrogen atom and a compound containing a carbon to carbon
double bond or into a smaller free radical and a compound containing a

carbon to carbon double bond (88). Thus, when a straight chain alkane decomposes, the yield is a lower alkene and a lower alkane, the alkene always being the shorter of the two. From Table 5 it can be seen that the relative probability of bond rupture with respect to the location of a carbon to carbon bond in an alkane is greatest between the first and second carbon atoms in the chain (104). Therefore at low pressures alkanes thermally decompose to yield mainly methane and ethane (105).

A distinctive property of hydrocarbon free radicals is their inability to undergo isomerisation of the type involving migration of an alkyl group. As a result thermal cracking produces no branching that is not already present in the feed compound. Free radicals do not undergo a shift of the unpaired electron from one carbon atom to the next in the chain and the only migration of a hydrogen atom occurs when primary free radicals are sufficiently long that they can coil back on themselves and abstract a hydrogen atom to form an internal free radical (87).

Few studies have been made on the pyrolysis of alpha alkenes, yet they are the primary major products of alkane cracking and secondary reactions involving alkenes must be important in moderate to high severity cracking. The product distribution from the thermal cracking of alpha alkenes resembles that of the corresponding normal alkane except that small quantities of dialkenes and cycloalkenes are also present. A high yield of $C_n H_{2n}$ compounds was rationalised by a concerted molecular mechanism and the remaining products were accounted for by free radical mechanisms like that of Rice's (88) for alkane pyrolysis. Thus, in an analogy to alkane decomposition, small radicals abstract a hydrogen atom from the alkene reactant to form 'parent radicals'. The parent radicals decompose via beta scission or hydrogen atom elimination until a radical which will not readily decompose is formed. This radical

abstracts a hydrogen atom from the reactant alkene to form a new parent radical and the chain continues (106). Organic decompositions are therefore regarded as chain reactions in which certain radicals start a cycle of reactions at the end of which they are regenerated and start a new cycle. The atoms or groups regenerated are called chain carriers. In this way the composition of the products is practically independent of the primary decomposition of the hydrocarbon and is determined almost exclusively by the chain cycle (88).

2.   EXPERIMENTAL MATERIALS, EQUIPMENT AND METHODS

2.1   Materials Used

2.1.1   Chemicals used in the synthesis of
                      etioporphyrin (isomeric mixture)

2.1.1.1

Reagents	Purity
methanol	99+ %
trans-2-pentenoic acid	> 98%
sulphuric acid	95% $^w/_w$
sodium hydride	Dry. 97%
tosyl methyl isocyanide	-
lithium aluminium hydride	95+ %
formaldehyde	37% $^w/_v$ aqueous solution
hydrochloric acid	36.5-38.0% $^w/_w$

2.1.1.2

Solvents	Purity
methanol	99 + %
diethyl ether	-
dimethylsulphoxide	99 + %
tetrahydrofuran	99 + %
ethanol	anhydrous. denatured
1,2-dichloroethane	99%

2.1.1.3

Compounds used in purification etc.	Purity
sodium hydrogen carbonate	99 + %
sodium sulphate	anhydrous
calcium chloride	anhydrous
ethyl acetate	99.5%
sodium hydroxide	97 + %

Trans-2-pentenoic acid was supplied by Fluorochem Ltd.

All other chemicals were supplied by Aldrich Chemical Co. Ltd.

2.1.2   <u>Chemicals used in the synthesis</u>

                 <u>of etioporphyrin I</u>

2.1.2.1

<u>Reagents</u>	<u>Purity</u>
red phosphorus	99%
ethanol	anhydrous, denatured
iodine	A.C.S.
2,4-pentandione	99 + %
potassium carbonate	99 + %
acetic acid	glacial, 99.8%
t-butylacetoacetate	99%
sodium nitrite	97%
zinc dust	-325 mesh
bromine	-
formic acid	98-100% w/w SLR

2.1.2.2

<u>Solvents</u>	<u>Purity</u>
ethanol	anhydrous, denatured
acetone	99 + %
glacial acetic acid	99.8%
petroleum ether	A.C.S.
methanol	99 + %
tetrachloromethane	99%

2.1.2.3

Compounds used in purification,

etc.	Purity
copper wire	99.9%
4A molecular sieve	8-12 mesh
calcium chloride	anhydrous, $\sim$ 8 mesh
sodium chloride	99 + % A.C.S.

Formic acid was supplied by Fisons Ltd.

All other chemicals were supplied by Aldrich Chemical Co. Ltd.

2.1.3   Chemicals used in metalloporphyrin

synthesis

2.1.3.1

Reagents	Purity
sodium acetate	anhydrous. 99%
vanadyl sulphate	$\sim$ 96%
nickel (II) acetate tetrahydrate	-
tetraammineplatinum (II) dichloride	99.1% and 95.3% $^W/_{w}$
tetraamminepalladium (II) dichloride	88.40% $^W/_{w}$
base hematoporphyrin IX	-

2.1.3.2

Solvents	Purity
acetic acid	glacial, 99.8%
benzene	thiophene free
methanol	99 + %
dimethylformamide	99%
trichloromethane	stabilized with $\sim$ 0.75% ethanol

Vanadyl sulphate was supplied by Fluorochem Ltd.

The platinum (II) and palladium (II) complexes were supplied by the Johnson Matthey Technology Centre.

All other chemicals were supplied by Aldrich Chemical Co. Ltd.

2.1.4   Chemicals used in the quantitative
               gravimetric determination of palladium

Compounds	Purity
ethanol	anhydrous. denatured
dimethylglyoxime sodium salt	-
sulphuric acid	-
ammonium hydroxide	A.C.S.
nickel (II) sulphate	99%

Dimethylglyoxime sodium salt and sulphuric acid were supplied by B.D.H. Ltd.

All other chemicals were supplied by Aldrich Chemical Co. Ltd.

2.1.5   <u>Chemicals used in the preparation and</u>

                        <u>analysis of the petroporphyrin concentrate</u>

Material	Purity
Tia Juana Pesado topped crude oil	-
n-heptane	99%
toluene	99%
diphenylmethane	99%
acetonitrile	99%
2,2,4-trimethylpentane	99 + %
silica gel	for chromatographic analysis 60 - 120 mesh
benzene	thiophene free
aluminium oxide 90	Brockmann activity II to III "Merck" 1097
trichloromethane	stabilized with~0.75% ethanol

Silica gel and aluminium oxide 90 were supplied by B.D.H. Ltd.

Tia Juana Pesado topped crude oil was supplied by Shell U.K. Ltd.

All other chemicals were supplied by Aldrich Chemical Co. Ltd.

2.1.6   Materials used in supported

catalyst preparation

2.1.6.1

Support material	Supplier
60 - 120 mesh silica gel	B.D.H. Ltd.
alpha alumina	Strem Ltd.

2.1.6.2

Catalyst phase	Supplier
base etioporphyrin	own preparation
nickel etioporphyrin	own preparation
vanadyl etioporphyrin	own preparation
platinum etioporphyrin	own preparation
palladium etioporphyrin	own preparation
base hematoporphyrin IX	Aldrich Chemical Co. Ltd.
nickel hematoporphyrin IX	own preparation
vanadyl hematoporphyrin IX	own preparation
petroporphyrin concentrate	own preparation

2.1.6.3

Solvent	Purity
trichloromethane	stabilized with $\sim$ 0.75% ethanol
tetrachloromethane	99%

Solvents were supplied by Aldrich Chemical Co. Ltd.

2.1.7   <u>Materials used for temperature</u>

<u>programmed decomposition</u>

<u>Material</u>	<u>Purity</u>
helium	99.995%
5A molecular sieve	8 - 12 mesh

Helium gas was supplied by B.O.C. Ltd.

5A molecular sieve was supplied by Aldrich Chemical Co. Ltd.

2.1.8   <u>Chemicals used in cracking reactions</u>

<u>Feed Materials</u>	<u>Purity</u>
n-butane	CP grade 99%
2,2-dimethylbutane	98%

<u>Diluent gas</u>	<u>Purity</u>
helium	99.995%

n-butane was supplied by Air Products Ltd.

2,2-dimethylbutane was supplied by Aldrich Chemical Co. Ltd

helium was supplied by B.O.C. Ltd.

2.1.9 <u>Materials used in the gas chromatographic</u>

<u>separation of hydrocarbons</u>

<u>Gases</u>	<u>Grade</u>
nitrogen	commercial "white spot"
hydrogen	commercial high purity
air	-

Both nitrogen and hydrogen were passed through oxy traps prior to use.

<u>Column packing</u>

60 - 120 mesh silica gel

All gases were supplied by B.O.C. Ltd.

The silica gel was supplied by Hopkin and Williams Ltd.

2.1.10 <u>Materials used for temperature</u>

<u>programmed reduction</u>

<u>Material</u>	<u>Supplier</u>
5% hydrogen/95% argon	B.O.C. Special Gases
5A molecular sieve	Aldrich Chemical Co Ltd

2.1.11 <u>Materials used in the hydrogenation</u>

<u>of 1-hexene</u>

<u>Material</u>	<u>Supplier</u>
5% hydrogen/95% argon	B.O.C. Special Gases
1-hexene	Aldrich Chemical Co. Ltd

2.2   <u>Experimental equipment</u>

2.2.1   <u>Analytical Spectra</u>

Mass spectra were obtained using a Kratos MS 80 RF mass spectrometer.

Proton magnetic resonance spectra were obtained using a Varian XL

100 c.w. nmr spectrometer.

Infra red spectra were obtained using a Perkin Elmer Model 157

recording IR spectrometer.

Ultra violet spectra were obtained using a Pye Unicam SP8 - 400

UV/VIS spectrophotometer.

2.2.2   <u>Chromatographic separations</u>

Gas chromatographic separations were performed using the following

equipment.

chromatograph.-:-	Pye Unicam 304 series dual FID
integrator :-	Pye Unicam DP101
chart recorder :-	Phillips PM 8251

All analytical equipment employed for analysis was used according

to the manufacturers recommendations as set down in the relevant

instruction manual.

2.3.   Experimental methods

2.3.1.   Etioporphyrin synthesis

2.3.1.1   Synthesis of isomeric mixture of etioporphyrin

2.3.1.1.1   Preparation of methyl trans-2-pentenoate (107)

According to the equation given in Fig 25, 166 cm^3 of methanol was placed in a 1000 cm^3 round bottomed flask. To this was added 92 cm^3 of trans-2-pentenoic acid and 2.3 cm^3 of concentrated sulphuric acid was delivered from a burette, one drop every 30 seconds. Following all additions a reflux condenser was attached to the flask and the mixture was refluxed for approximately 12 hours. After being allowed to cool to ambient temperature the mixture was poured into 500 cm^3 of distilled water contained in a separating funnel. The upper layer of crude ester was removed and subsequently washed with 200 cm^3 of distilled water, 50 cm^3 of saturated sodium hydrogen carbonate solution and a further 100cm^3 of distilled water. The crude ester was dried by being allowed to stand over 11g of anhydrous sodium sulphate. Following filtration the ester was distilled and the fraction boiling between 142 and 143°C collected as pure product.

2.3.1.1.2   Preparation of methyl 4-ethylpyrrole-3-carboxylate (108)

8.568 g of sodium hydride was weighed out, using a glove box that contained an atmosphere of dry nitrogen and placed in a dry 5000 cm^3 four necked, round bottomed flask, that had been previously flushed with dry nitrogen. The round bottomed flask was continually flushed with dry nitrogen and fitted with a reflux condenser protected by a calcium chloride guard tube, a stirrer and a dropping funnel, which was also

protected by a calcium chloride guard tube. 555cm^3 of dry diethyl ether was added and the stirrer was switched on during the addition in order to form a suspension. A solution of 58.09 g of dry tosyl methyl isocyanide and 34.2 cm^3 of dry methyl trans-2-pentenoate in dry diethyl ether/dimethyl sulphoxide (2.1 = 992 cm^3 : 496 cm^3) was made up and added to the suspension in a dropwise manner. The reaction, according to the equation given in Fig 26, started to reflux due to the exotherm and was terminated 15 minutes after the addition of the above mixture was complete. The sodium hydride residues remaining at this stage were destroyed by the careful addition of ethyl acetate, after the liquid had been decanted off the solid.

The remaining solution was slowly added, until any reaction ceased, to 3000 cm^3 of distilled water contained in a 5000 cm^3 beaker. The ethereal layer was separated and the aqueous portion was split into 6 x 500 cm^3 aliquots, each being extracted three times with 125 cm^3 of diethyl ether. The ether layers were combined and upon removal of the ether a mid-brown liquid product resulted, which was used in the following synthetic step in the unpurified state.

2.3.1.1.3 <u>Preparation of 3-ethyl-4-methylpyrrole</u> (109)

54.264 g of lithium aluminium hydride was weighed out, using a glove box containing a nitrogen atmosphere, and placed in a 5000 cm^3 four necked, round bottomed flask. The flask was fitted with a stirrer, reflux condenser protected by a calcium chloride guard tube, a nitrogen supply and a dropping funnel. After the flask had been purged with nitrogen the stirrer was switched on and sufficient dry tetrahydrofuran added to form a slurry with the lithium aluminium hydride. The remainder

of the 2500 cm^3 of tetrahydrofuran was mixed with 49.6 cm^3 of dry methyl 4-ethylpyrrole-3-carboxylate and added to the flask at such a rate that the mixture gently refluxed. Following the addition of the pyrrole/solvent mixture, the whole was allowed to reflux for a further 15 minutes, as the reaction according to Fig 27 proceeded. Decomposition of the excess hydride was effected by the dropwise addition in succession of, 55 cm^3 of water, 55 cm^3 of 15% sodium hydroxide solution and sufficient water to ensure that all reaction had ceased. Efficient stirring was ensured throughout the additions. Inorganic solids were removed by filtration under reduced pressure and the aqueous phase split into 500 cm^3 aliquots, each being extracted four times with diethyl ether. The ethereal layers were combined and the ether removed by simple distillation. Any remaining residues of ether were removed under reduced pressure to yield the crude product which was a dark brown oil. This was vacuum distilled, and the fraction boiling at 88°C under 11 mm Hg was collected as the pure product.

2.3.1.1.4 Preparation of etioporphyrin (110)

A solution of 122 cm^3 of 37% aqueous formaldehyde was placed in a three necked, 5000 cm^3 round bottomed flask fitted with a reflux condenser and stirrer. To this, 1112 cm^3 of ethanol and 56 cm^3 of one molar hydrochloric acid were added and the mixture heated to about 55°C. After heating to this temperature a mixture of 13.5 cm^3 of 3-ethyl-4-methyl pyrrole in 1112 cm^3 of ethanol was added from a dropping funnel. The whole mixture was stirred at 55°C for one hour and then allowed to cool and stand at ambient temperature for three days, while the reaction in Fig 28 proceeded.

Following this time period, the mixture was diluted with water

(about 1:2) and neutralised using a dilute solution of sodium hydroxide.

Approximately 2 dm^3 aliquots were extracted using a downward displace-

ment extractor, of dimensions shown in Fig 29, utilising 1,2-dichloro-

ethane as solvent. Following extraction and separation, the chlorinated

solvent was removed by simple distillation and the residue evaporated to

dryness. The dark brown/black residue was powdered and washed with cold

methanol. Following filtration the porphyrin remaining on the filter

paper was further washed with cold methanol until the washings ran clear.

The resulting purple microneedles of etioporphyrin were dried under

reduced pressure.

2.3.1.2 Synthesis of etioporphyrin I

The overall reaction sequence, up to and including the synthesis

of base etioporphyrin I is given in Fig 30.

2.3.1.2.1 Ethyl iodide synthesis

2.3.1.2.1.1 Preparation of ethyl iodide (107)

400 g of red phosphorus was added to a quantity of distilled water

such that a thin slurry was formed. This mixture was boiled for about

15 minutes and then allowed to cool. When the red phosphorus had settled,

the excess liquid was decanted and the remaining solid boiled again with

a fresh portion of distilled water. This process was repeated again.

Finally the red phosphorus was filtered and washed with boiling water

until the washings were neutral. The collected solid was dried in an

oven set just above 100°C for 24 hours.

313 g of dry red phosphorus was weighed out and placed in a three

necked, 5.0 dm^3 round bottomed flask that had been fitted with a stirrer,

reflux condenser and separating funnel. Sufficient ethanol was run into the flask from the separating funnel to form a smooth slurry with the red phosphorus.

1600 g of coarsely powdered iodine was weighed out and added in about 2 g portions to approximately 1500 cm^3 of ethanol. The addition was performed quite quickly, but the heat of the exothermic dissolution was allowed to dissipate before each portion was added.

The alcoholic solution of iodine was added to the red phosphorus slurry from the separating funnel. The mixture was stirred at all times. Following the addition, the mixture was heated and refluxed for about one hour, allowing the reaction to proceed according to Fig. 31.

Following this period of time the condenser was rearranged for simple downward distillation and the product formed was collected.

The product was stored in a sealed container containing a short coil of clean copper wire and some 4A molecular sieve.

2.3.1.2.1.2   Azeotropic mixture of ethyl
                     iodide and ethanol

Analysis by infra red spectroscopy of the liquid product obtained from the preparation described in 2.3.1.2.1.1 demonstrated that a mixture of compounds was present.

Ethanol and ethyl iodide are mutually soluble and form an azeotropic mixture. The presence of ethanol was confirmed and an estimation of the proportion of ethyl iodide in the mixture was made using gas chromatography.

2.3.1.2.1.3   <u>Chromatograph conditions used for the</u>

<u>separation of ethanol and ethyl iodide</u>

column   :-   6' x ¼" O.D. x 4 mm I.D. glass column.

packing :-   Chromosorb 102   80-100 mesh.

column temperature   :- $225^{o}C$ isothermal.

detector temperature :- $250^{o}C$

injector temperature :- $250^{o}C$

helium pressure   :-   23.5 psig at column head.

hydrogen pressure   :-   18.5 psig

air pressure   :-   7 psig

2.3.1.2.2   <u>Preparation of 3-ethyl-2,4-pentandione</u> (111,112)

A three necked, 5 dm^{3} round bottomed flask was fitted with a reflux condenser protected by a calcium chloride guard tube, a stirrer and a wide necked funnel. Into this was placed 984 cm^{3} of dry acetone and 1016 cm^{3} of 2,4-pentandione. The stirrer was switched on and 1122 g of anhydrous potassium carbonate was added to the flask, followed by 795 cm^{3} of ethyl iodide. The whole mixture was refluxed for a total period of 24 hours, allowing the reaction given in Fig. 32. to proceed. Following this, the mixture was cooled to ambient temperature and then filtered. The resulting filtrate was distilled and the fraction boiling over the range 178 - $182^{o}C$ was collected.

2.3.1.2.3   <u>Preparation of t-butyl 4-ethyl-3,5-</u>

                       <u>dimethylpyrrole carboxylate</u> (111,112)

A 5 dm^3 round bottomed flask was fitted with a stirrer, separating

funnel, reflux condenser and thermometer. 944 cm^3 of glacial acetic

acid was placed in the flask and to this was added 836 cm^3 of

t-butylacetoacetate. This solution was then cooled in an ice bath such

that the temperature was below $10^{\circ}C$.

424 g of sodium nitrite was dissolved in 943 cm^3 of distilled water

and this was added to the stirred t-butylacetoacetate solution at such

a rate (dropwise) that the temperature of the contents of the flask was

maintained between 10 and $12^{\circ}C$.

Following the addition of the sodium nitrite solution the mixture

was cooled to between -4 and $-5^{\circ}C$ for a period of one hour by the use

of an ice/salt bath. The mixture was subsequently stirred for 12 hours

at room temperature.

680 cm^3 of 3-ethyl-2,4-pentandione was dissolved in 184 cm^3 of

glacial acetic acid and added to the above mixture, causing the formation

of a bright orange colouration. 659 g of zinc dust was then added slowly,

whilst stirring, until a temperature of $80-85^{\circ}C$ was reached. This

temperature was maintained by further additions of zinc dust. Following

the addition of all of the zinc dust, the mixture was refluxed for a

period of two hours to allow the reaction outlined in Fig. 33. and

detailed in Fig. 34. to proceed. The hot mixture was subsequently poured

into 15 dm^3 of cold water. The resulting solid was filtered under reduced

pressure.

1712 cm^3 of ethanol was heated over a water bath and all alcohol

soluble constituents of the solid were dissolved. This solution was

filtered hot, under reduced pressure in order to remove the zinc residues. Upon cooling, the filtrate yielded white, needle-like crystals of the required pyrrolic product. The filtrate was allowed to stand overnight to encourage crystal formation. The pyrrolic product was filtered from the alcoholic solution under reduced pressure and the white, needle-like crystals washed with a small volume of cold ethanol.

The crude product was recrystallised from the minimum quantity of ethanol and finally dried in an air oven set at 40°C.

2.3.1.2.4   <u>Preparation of etioporphyrin I</u> (112)

A round bottomed flask of 3 dm^3 capacity was fitted with a reflux condenser, a stirrer and a separating funnel. 133g of t-butyl 4-ethyl-3,5-dimethylpyrrole carboxylate was dissolved in 560 cm^3 of glacial acetic acid and this acidic solution was placed in the flask.

93 cm^3 of bromine was dissolved in 420 cm^3 of glacial acetic acid and this solution was placed in the separating funnel. The acidic bromine solution was added to the contents of the flask in a dropwise manner ensuring efficient stirring throughout. The mixture was maintained at approximately ambient temperature by placing the flask in a cold water bath. After the mixture had been stirred continuously for about 18 hours the pyrromethene product was filtered, washed with petroleum ether and dried under reduced pressure.

The pyrromethene product was placed in a 1 dm^3 single necked, round bottomed flask and refluxed with 376 cm^3 of formic acid for three hours allowing the reaction outlined in Fig 35 and detailed in Fig 36 to proceed. Following this time period excess formic acid was distilled off and the resulting residue was dissolved in 665 cm^3 of tetrachloromethane.

This solution was evaporated to dryness and the solid crushed to a fine powder in a pestle and mortar.

Initial product purification was carried out using solid/liquid extraction. The above powder was placed in an extraction thimble and a Soxhlet extraction apparatus was employed using methanol as the solvent. When extraction was complete the thimble and its contents were dried in an air oven.

Following this, repeated recrystallisations (a total of five times) were performed in order to complete the purification process. The crude porphyrin was dissolved in the minimum quantity of hot tetrachloromethane which was then left to cool slightly. Cold methanol was added to the porphyrin solution to effect crystallisation such that the final tetra-chloromethane : methanol volume ratio was approximately 1:3.

2.3.2   Metalloporphyrin synthesis

2.3.2.1   Vanadyl ion insertion into etioporphyrin (113)

51 cm^3 of glacial acetic acid was placed into a 100 cm^3 round bottomed flask fitted with a reflux condenser and stirrer. To this was added 1.58 g of sodium acetate, 0.80 g of vanadyl sulphate and 0.500 g of etioporphyrin. The mixture was refluxed for four hours and then allowed to cool to ambient temperature, the reaction proceeding as shown in Fig. 37.

The mixture was subsequently transferred to a beaker, diluted with 40 cm^3 of distilled water, covered with a watch glass and allowed to stand for two days to induce crystal growth. The crystals formed were filtered and washed with distilled water until the filtrate was colourless

(i.e. until the blue colour of the vanadyl salt had disappeared). The product was dried at about 35°C under reduced pressure to yield a dark purple crystalline powder. The crude vanadyl etioporphyrin was dissolved in the minimum quantity of hot benzene, followed by the slow addition of hot methanol (so that the final methanol:benzene ratio = 3:1). After cooling to ambient temperature the purple platelets so produced were washed with cold methanol and dried at about 35°C under reduced pressure.

This preparation was performed a second time using a scale up factor of ten for all reagents.

2.3.2.2 <u>Nickel ion insertion into etioporphyrin</u> (114)

50 cm^3 of dimethylformamide were placed in a 100 cm^3 round bottomed flask and heated to reflux. When the solvent was boiling, 0.500 g of etioporphyrin was added and one minute was allowed to elapse allowing complete dissolution of the porphyrin. Following this 2.6 g of nickel (II) acetate tetrahydrate was added to the mixture which was refluxed for three hours, following the reaction given in Fig. 38.

After this time period the mixture was allowed to cool to ambient temperature when it was diluted with 40 cm^3 of distilled water. The metalloporphyrin formed was filtered, washed with cold methanol and dried at about 35°C under reduced pressure. The crude product was dissolved in the minimum quantity of hot trichloromethane and treated slowly with hot methanol, such that the final methanol:trichloromethane ratio was 3:1. The crystals obtained upon cooling were filtered, washed with cold methanol and dried at approximately 35°C under reduced pressure.

This preparation was performed a second time using a scale up factor of ten for all reagents.

2.3.2.3   <u>Preparation of platinum etioporphyrin I</u>

2.20 g (0.00653moles at 99.1% pure) of tetraammineplatinum (II) dichloride was dissolved in about 10 cm^3 of distilled water. This was added to a mixture of 300 cm^3 of DMF and 50 cm^3 of distilled water contained in a 1000 cm^3 round bottomed flask. This mixture was heated to reflux and 2.60 g of etioporphyrin I was added. The whole was then refluxed for a period of three hours.

After this time period the mixture was allowed to cool to ambient temperature when it was diluted with 350 cm^3 of distilled water. The crude metalloporphyrin was filtered, washed with cold methanol and dried.

The crude platinum etioporphyrin I was purified by recrystallization. This was performed by dissolving the crude product in the minimum quantity of hot trichloromethane allowing this solution to cool and then adding an excess of cold methanol to facilitate crystallization.

This synthesis was performed a second time using 1.90 g (0.00542 moles at 95.3% pure) of tetraammineplatinum (II) dichloride and 2.60 g of etioporphyrin. In all other respects the two syntheses were identical.

2.3.2.4   <u>Palladium etioporphyrin I synthesis</u>

2.3.2.4.1   <u>Preparation of palladium etioporphyrin I</u>

1.81 g (0.00652 moles at 88.40% pure) of tetraamminepalladium (II) dichloride was dissolved in about 10 cm^3 of distilled water. This was added to 350 cm^3 of DMF contained in a 1000 cm^3 round bottomed flask. This mixture was heated to reflux and 3.346 g of etioporphyrin I was added. The whole was then refluxed for a period of three hours.

After this time period the mixture was allowed to cool to ambient

temperature when it was diluted with 350 cm^3 of distilled water. The crude metalloporphyrin was filtered, washed with cold methanol and dried.

The crude palladium etioporphyrin I was purified by recrystallization. This was performed by dissolving the crude product in the minimum quantity of hot trichloromethane, allowing this solution to cool and then adding an excess of cold methanol to facilitate crystallization.

2.3.2.4.2 Incomplete substitution of palladium

Following the initial filtration of the product it was noticed that the filtrate was yellow in colour. This suggested that a quantity of the palladium salt was still present in the solution and had not reacted with the etioporphyrin I.

2.3.2.4.3 Quantitative gravimetric determination of palladium (115)

A quantity of solvent consisting of 50% ethanol 50% water (v/v) was made up. An excess of the sodium salt of dimethylglyoxime was placed in this solvent and the undissolved salt remaining was filtered off.

The palladium solution was acidified using sulphuric acid and the pH of the solution was adjusted to about three.

The DMG solution was added to the palladium solution and the whole was warmed to encourage formation and coagulation of the Pd DMG salt.

After being allowed to cool, the precipitate was filtered using an ashless filter paper to obtain the solid.

It was verified that all palladium ions present in the solution had been precipitated by ensuring than an excess of DMG was present in the filtrate thus :- A small sample of the filtrate was taken and neutralised using a dilute ammonium hydroxide solution. To this a small quantity of nickel sulphate solution was added and an excess of DMG was indicated by the presence of a gelatinous brick red precipitate of nickel dimethylglyoxime.

When filtration was complete the filter paper was washed with distilled water and the washings periodically tested as above until it was indicated that no DMG anions were present. The filter paper and retained solid were subsequently dried in an air oven set at 110°C.

After drying, the filter paper and precipitate were placed in a pre-weighed fused silica crucible. The crucible and contents were gently heated in a muffle furnace ensuring no losses from the crucible. When the crucible reached red heat the door of the furnace was closed and left overnight.

Following ignition, volatilization of the organic components and reduction of the palladium dimethylglyoxime salt to palladium metal, the crucible was cooled, left to equilibrate with the surrounding atmosphere and weighed to constant weight.

2.3.2.5   <u>Preparation of vanadyl hematoporphyrin IX</u>

250 cm^3 of glacial acetic acid was placed in a three necked, 500 cm^3 round bottomed flask fitted with a stirrer and reflux condenser. To this was added 7.60 g of sodium acetate, 3.90 g of vanadyl sulphate and 3.0 g of base hematoporphyrin IX. This mixture was heated to boiling and then refluxed for a period of four hours, after which it was allowed

to cool to ambient temperature.

The contents of the flask was transferred to a 1000 cm^3 beaker, diluted with 200 cm^3 of cold distilled water, covered with a watch glass and allowed to stand for eighteen hours to facilitate crystal growth.

The crystals thus formed were washed with water until the blue colour of the vanadyl salt was no longer in evidence (i.e. colourless), washed with cold methanol and then dried in an air oven.

The crude vanadyl hematoporphyrin IX was purified by dissolving the solid in the minimum quantity of hot DMF, allowing the whole to cool to ambient temperature and then adding a slight excess of cold water to ensure complete crystallization. The vanadyl hematoporphyrin IX was finally filtered under reduced pressure and dried in an air oven set at 110°C.

2.3.2.6.   Preparation of nickel hematoporphyrin IX

240 cm^3 of dimethylformamide was placed in a 500 cm^3 round bottomed flask and heated until reflux conditions were established. 3.0 g of base hematoporphyrin IX was added to the flask and a few minutes were allowed for complete dissolution. 12.5 g of nickel (II) acetate tetrahydrate was added to the porphyrinic solution and the whole was refluxed for a period of three hours.

Following this, the flask and contents were allowed to cool and then diluted with cold distilled water. The nickel hematoporphyrin IX thus formed was filtered under reduced pressure, washed with cold methanol and dried in an air oven.

The crude nickel hematoporphyrin IX was purified by dissolving the solid in the minimum quantity of hot DMF, allowing the whole to cool to ambient temperature and then adding a slight excess of cold water to ensure complete crystallization. The nickel hematoporphyrin IX was finally filtered under reduced pressure and dried in an air oven set at 110°C.

2.3.3	<u>Preparation and analysis of a petroporphyrin</u> <u>concentrate from Tia Juana Pesado</u> (topped crude)
2.3.3.1	<u>Determination of asphaltene content</u> <u>of Tia Juana Pesado (topped crude)</u>(10)

n-Heptane and TJP were added to a 500 cm^3 conical flask such that the volume : weight ratio was approximately 30. The contents of the flask was then refluxed for a period of one hour.

After removal of the heat source the flask was stoppered and allowed to cool in the dark for two hours.

Following this period the contents of the flask was filtered using a Whatman 542 12.5 cm diameter filter. The conical flask was washed with small aliquots of hot n-heptane until clean. The filter paper was placed in an extractor (as detailed in BS2000 Part 143) and extracted with approximately 200 cm^3 of n-heptane. The extraction was continued until the drops from the extractor exit showed no signs of containing any residue. Following this period (about $2\frac{1}{2}$ hours), the conical flask containing the n-heptane solvent was removed from the system and replaced by an identical flask containing 60 cm^3 of toluene. This was heated under reflux in order to dissolve the asphaltene component of the TJP. After

a period of $2\frac{1}{2}$ hours it was judged that all of the asphaltenes had been removed from the contents of the filter paper and the heat source was subsequently removed.

After being allowed to cool, the contents of the flask were poured into a 9 cm diameter porcelain evaporating dish. The flask was washed with small aliquots of toluene totalling 30 cm^3. The toluene was removed from the extracted asphaltenes by heating the evaporating dish and contents over a steam bath.

Following the removal of the toluene the asphaltenes were dried in an air oven at a temperature of 100°C for a period of thirty minutes.

The asphaltene content was calculated as a weight percentage based on the original sample.

2.3.3.2 <u>Extraction of porphyrin concentrate from</u>

<u>Tia Juana Pesado topped crude</u> (116)

714 cm^3 (700 g) of Tia Juana Pesado topped crude was taken and mixed with 37.5% by weight, 261 cm^3 (263 g), of synthetic heavy aromatic oil, diphenyl methane (d = 1.006).

This mixture was charged into the liquid/liquid upward displacement extractor shown in Fig. 39. The funnel, liquid delivery tube and glass sinter was placed inside the extractor and two double surface condensers were placed in series on top of the extractor.

2500 cm^3 of acetonitrile was placed in a 5 dm^3 round bottomed flask and the flask attached to the side arm of the extractor. The flask and contents were heated by means of an isomantle. Upon commencement of reflux a luminescent layer of pale yellow liquid formed at the interface

of the topped crude and the acetonitrile. As extraction proceeded the the acetonitrile turned red in colour. Following an extraction period of 15 hours, over three days, the lower layer contained in the round bottomed flask was deep red and the liquid above this was a straw colour.

After allowing the apparatus to cool, the round bottomed flask was stoppered and removed to a dark place for two days.

The acetonitrile was removed from the mixture contained in the flask by simple distillation. This was performed over a steam bath to ensure that the liquid temperature remained below 100°C at all times.

2.3.3.3   Purification of porphyrin extract using liquid/solid column chromatography (116)

2.3.3.3.1   The column

The length of the column was 150 cm while the internal diameter was 2.5 cm.

The column was fitted with stop cocks at the top and bottom. The top was fitted with a solvent delivery vessel while the bottom of the column had a solvent collection vessel.

2.3.3.3.2   Initial purification

2.3.3.3.2.1   Packing the column

The column described in Section 2.3.3.3.1 was virtually filled with 2,2,4-trimethylpentane.

Silica gel was slurried in acetonitrile and this slurry was slowly added to the column. The silica gel was allowed to settle and any excess acetonitrile was run off from the bottom of the column prior to the

addition of further slurry. Additions were made in this manner, ensuring that at all times the column packing remained wet, until the column was full.

Having packed the column, a quantity of 2,2,4-trimethylpentane was run through the column to ensure that all of the acetonitrile had been displaced.

2.3.3.3.2.2 <u>Chromatographic separation</u>

A 29 g (30.5 cm^3) aliquot of porphyrin extract was taken and diluted with 300 cm^3 of 2,2,4-trimethylpentane. No separation or precipitation occurred.This solution was charged to the top of the column and allowed to run through. The porphyrinic components, which were red in colour were retained at the top of the column in a thin band. The non-porphyrinic components, which were yellow in colour, continued to move down the column with the solvent.

Washing the column with 720 cm^3 of 2,2,4-trimethylpentane removed all of the yellow component from the column while leaving the porphyrin containing band unaffected.

The red band was subsequently eluted by passing 1050 cm^3 of aceto-nitrile through the column. Initially the porphyrin containing component moved as a thin band which slowly became more diffuse as it moved down the column.

All solvent fractions were collected and the solvents recovered by distillation.

The residue which was a dark brown viscous oil, from eight chromato-graphic runs was collected and combined in order to undertake further chromatographic separation.

2.3.3.3.3   <u>Secondary purification</u>

2.3.3.3.3.1   <u>Packing the column</u>

The column described in Section 2.3.3.3.1 was virtually filled with benzene.

Aluminium oxide 90 was slurried with benzene and this slurry was slowly added to the column. The alumina was allowed to settle and any excess benzene was run off from the bottom of the column prior to the addition of further slurry. Additions were made in this manner, ensuring that at all times the column packing remained wet, until the column was full.

2.3.3.3.3.2   <u>Chromatographic separation</u>

The combined porphyrin bearing concentrate from the chromatographic separation described in Section 2.3.3.3.2.2 was dissolved in a small quantity of benzene (1:10 v/v) and percolated onto the top of the alumina column.

A larger quantity of benzene was passed through the column in order to separate the various components of the concentrate. Three completely separate and distinct bands developed. A compact, dark brown band was retained at the top of the column. A second compact band being red in colour was observed some way down the column while a quite diffuse light yellow band developed in front of the red band.

Once the three bands had been developed such that they were completely separate, the flow of benzene was stopped and this solvent was substituted by acetonitrile. The bands were quite rapidly eluted from the bottom of the column in the order light yellow and red. The dark brown band was left

at the top of the column, retained by the alumina.

The majority of the acetonitrile was removed from the red, porphyrin bearing fraction by simple distillation. The remaining residues of solvent were removed over a steam bath.

Following this treatment a light brown/red viscous oil remained having a volume of approximately 3 cm^3.

2.3.3.4   Estimation of the total metalloporphyrin content of Tia Juana Pesado extract (63)

0.7038 g of Tia Juana Pesado concentrate was weighed out and dissolved in a small quantity of trichloromethane. This solution was then diluted to exactly 1.0 dm^3 in a graduated flask using the same solvent. A 10.0 cm^3 aliquot of this solution was taken and further diluted in a 100 cm^3 graduated flask using trichloromethane.

The UV spectrum of this solution, contained in a 1.0 cm cell, was recorded between the wavelengths of 550 and 350 nm. An estimation of the total metalloporphyrin content of the Tia Juana Pesado extract was subsequently made using the UV spectrum.

2.3.4   Preparation of supported porphyrin catalysts

2.3.4.1   Preparation of supported etioporphyrin I catalysts

0.05 g, 0.10 g, 0.25 g and 0.50 g portions (corresponding to 0.5, 1.0, 2.5 and 5.0 weight % loading) of base, nickel, vanadyl, platinum and palladium etioporphyrin I were weighed out and placed in glass jars. In each case the porphyrins were dissolved in 7.5 cm^3 of trichloromethane. To this was added 10.0 g of silica and the resulting slurry was thoroughly

mixed to ensure a homogeneous consistency. The chlorinated solvent was

subsequently allowed to evaporate, leaving the dry catalyst.

The above procedure was repeated, but alpha-alumina was substituted

for silica gel.

2.3.4.2 Preparation of supported hematoporphyrin IX catalysts

Separate portions of base, nickel and vanadyl hematoporphyrin IX

weighing 0.100 g, 0.200 g, 0.500 g and 1.000 g were each dissolved in

15 cm^3 of DMF. To each solution was added 20.00 g of 60-120 mesh silica

gel. The whole was thoroughly stirred in order to evenly distribute the

porphyrinic solution over the grains of the support material. Subsequently

the DMF was evaporated to leave the dry catalyst.

The above procedure was repeated, but alpha-alumina was substituted

for silica gel.

In this way three series of catalysts were prepared each being

founded on either base, nickel or vanadyl hematoporphyrin IX. Each series

consisted of eight discrete catalysts being either 0.5, 1.0, 2.5 or 5.0%

porphyrin (w/w) loaded on either silica or alpha-alumina.

2.3.4.3 Preparation of supported petroporphyrin catalysts

The yield of petroporphyrin concentrate, obtained from crude oil

by liquid/liquid extraction and various chromatographic procedures (see

Section 2.3.3), was 0.9092 g. Since this was a semi-solid, tar-like

substance it was considered inconvenient to accurately weigh small,

individual quantities. Thus 0.90 g of the concentrate was taken and

completely dissolved in a small quantity of tetrachloromethane. This was

then diluted to exactly 100 cm^3 using tetrachloromethane. From this

solution aliquots of 2.8, 5.5, 13.9 and 27.8 cm^3 were taken. These correspond to loadings of 0.5, 1.0, 2.5 and 5.0% by weight respectively if 5.0 g of support material is used. The larger volumes were evaporated down to approximately 3 cm^3. To each of the four solutions 5.0 g of silica was added. The whole was thoroughly stirred to form a homogeneous slurry and the remaining solvent was removed by the action of heat.

A further four aliquots were taken from the remaining 50.0 cm^3 of petroporphyrin extract in tetrachloromethane and the above procedure repeated using alpha alumina as the support material.

2.3.5   Temperature programmed decomposition

A schematic representation of the equipment used for the temperature programmed decomposition (TPD) of various materials can be seen in Fig. 40. Helium gas is passed through a number of control devices, to regulate flow, and then through the reference side of the katharometer block. The gas flows over the sample under test, which is being heated in an air oven that is controlled such that the temperature rise is linear with respect to time, through the sample side of the katharometer block and so to vent. As the temperature increases any gases formed by the thermal decomposition of the test material will be swept through the sample side of the katharometer block. The differential thermal conductivity, between the reference and sample sides of the katharometer, caused by the decomposition gases will thus be detected. The resulting signal is amplified and a hard copy given by the chart recorder.

2.3.5.1   <u>Conditions used for temperature</u>

<u>programmed decomposition tests</u>

helium flow rate	$30 \text{ cm}^3 \text{ min}^{-1}$
weight of test material	0.1 g
temperature range	ambient - 540°C
heating rate	$20^{\circ}\text{C min}^{-1}$
recorder sensitivity	20 mV

2.3.6   <u>The cracking of hydrocarbons</u>

2.3.6.1   <u>Using n-butane</u>

During the initial stages of experimentation 100% butane was used as the feed to the reactor. However, upon analysis of 0.5 cm^3 samples of the effluent gas, it was found that the chromatographic column used for product separation became overloaded. It thus proved necessary to dilute the feed gas prior to entry into the reactor. After withdrawal from their respective cylinders, both n-butane and helium were passed through various flow controllers such that upon entry to the reactor the respective flow rates were 2 and $8 \text{ cm}^3 \text{ min}^{-1}$. The gases were mixed by passing them through a 70cm length of pipe that had been packed with glass wool. The glass reaction tube used had an internal diameter of 0.45 cm and was contained in a tube furnace of length 16.5 cm and diameter 2.1 cm . Having passed through the heated zone of the furnace and been cooled to ambient temperature, the product gases were sampled by withdrawing 0.5 cm^3 portions through a septum. The remainder of the gas was then allowed to vent to the atmosphere.

2.3.6.2   Using 2,2-dimethylbutane

On using 2,2-dimethylbutane as the feed hydrocarbon, the equipment

described in Section 2.3.6.1 was modified such that after passage

through the flow controlling devices, helium gas was bubbled through

pure 2,2-dimethylbutane contained in a suitable vessel. Additionally,

a second tube furnace was incorporated in the line, before the furnace

used to heat the gas mixture to reaction temperature. This second furnace

was used as a preheater for the reaction mixture, being controlled at

about $30^{\circ}C$ lower than the onset of thermal cracking of the reactant,

in order to make the temperature gradient in the gas mixture less steep

as it passed through the cracking furnace. All other procedures were

the same as detailed in Section 2.3.6.1 (2,2-DMB TEMPERATURE
                                          = AMBIENT)

2.3.6.3   Cracking of 2,2-dimethylbutane under

                      the influence of supported phases

During the investigation of the influence of various supported

phases on the cracking of 2,2-dimethylbutane, the reactor was used as

a continuous flow, fixed bed, catalytic reactor. 0.940 g of the alumina

supported phase or 0.380 g of the silica supported phase was packed

into a reaction tube so as to form a loose plug, positioned in the

centre of the heated section of the tube furnace, supported at either

end by glass wool. These weights of material produced a bed length of

2.4 cm in the reactor. All other procedures were the same as detailed

in Section 2.3.6.2.

2.3.6.4   <u>Chromatographic separation of</u>

<u>hydrocarbon reaction products</u>

Product gases were analysed by using 0.5 cm^3 injections into a Pye

Unicam 304 series dual FID gas chromatograph linked to a Pye Unicam

DP 101 integrator and a Phillips PM 8251 chart recorder. The chromato-

graph was operated under the following conditions depending upon the

feed material used.

Column used for all separations:-

6' x 1/4" O.D. x 4 mm I.D. glass column packed with 60-120 mesh

silica gel. The silica gel was activated by heating to a temperature

of 120°C overnight prior to packing.

2.3.6.4.1   <u>Chromatograph conditions when</u>

<u>n-butane feed was used</u>

column temperature	:-	50°C for 6.5 min
		16.5°C min^{-1} for 6 min
		hold at 150°C for 3 min
detector temperature	:-	200°C
injector temperature	:-	70°C
nitrogen flow rate	:-	21 cm^3 min^{-1}
hydrogen flow rate	:-	131 cm^3 min^{-1} (19.5 psig)
air flow rate	:-	536 cm^3 min^{-1} (10.5 psig)

2.3.6.4.2   Chromatographic conditions when

2,2-dimethylbutane feed was used

column temperature	:-	50°C for 6.5 min
		10°C min^{-1} for 6 min
		Hold at 110°C for 7.5 min
detector temperature	:-	200°C
injector temperature	:-	100°C
nitrogen flow rate	:-	35 cm^3 min^{-1}
hydrogen flow rate	:-	131 cm^3 min^{-1} (19.5 psig)
air flow rate	:-	536 cm^3 min^{-1} (10.5 psig)

2.3.7   Temperature programmed reduction

The equipment used to perform the various temperature programmed reduction experiments was indentical to that used to determine the decomposition of metalloporphyrins through temperature programmed methods (Section 2.3.5).

A gaseous mixture consisting of 5% hydrogen in 95% argon was passed through a number of control devices in order to regulate flow, and then through the reference side of the katharometer block. The gas flowed over the sample under test, which was being heated in an air oven that was controlled such that the temperature rise was linear with respect to time, through the sample side of the katharometer block and so to vent.

As the temperature increases any hydrogen retained by the sample will change the composition of the gas being swept through the sample side of the katharometer block. The differential thermal conductivity, between the reference and sample sides of the katharometer, caused by the adsorption of hydrogen from the gas mixture will thus be detected.

The resulting signal was amplified and a hard copy given by the chart recorder.

2.3.7.1 **Conditions used for temperature programmed reduction tests**

5%H$_2$/95% Ar flow rate	30 cm^3 min^{-1}
weight of material under test	0.020 g
temperature range	ambient to 520°C
heating rate	20°C min^{-1}
bridge current	100 mA
recorder sensitivity	100 mV

2.3.8 **Hydrogen chemisorption**

2.3.8.1 **Hydrogen chemisorption on nickel etioporphyrin**

Two samples of nickel etioporphyrin, one the purified synthetic product and the other 5.0% (w/w) supported on silica, were submitted to Brunel University and hydrogen chemisorption experiments were performed in the Department of Chemistry.

Prior to chemisorption the samples were outgassed for 14 hours at 5 x 10^{-5} torr at room temperature and then for 20 minutes at 5 x 10^{-5} torr at 80°C. No sample decomposition was observed as a result of this pre-treatment.

2.3.8.2 **Hydrogen chemisorption on palladium etioporphyrin I**

The equipment used to perform the hydrogen chemisorption experiments was identical to that used to determine the decomposition of metalloporphyrins through temperature programmed methods (Section 2.3.5).

Gaseous hydrogen, flowing at a rate of 30 cm^3 min^{-1}, was passed through a number of flow regulation devices and then through the reference side of the katharometer block. The gas flowed over the sample, comprising 0.2g of 5.0% palladium etioporphyrin I on silica, which was heated to a temperature of $150^{\circ}C$ in an air oven, through the sample side of the katharometer block and so to vent. At $150^{\circ}C$ the gas was changed to 5% hydrogen in argon and experimental conditions allowed to stabilise prior to cooling the sample to ambient temperature.

As the temperature increases any hydrogen retained by the sample will change the composition of the gas being swept through the sample side of the katharometer block. The differential thermal conductivity, between the reference and sample sides of the katharometer, caused by the adsorption of hydrogen from the gas mixture will thus be detected. The resulting signal due to hydrogen chemisorption and subsequent desorption on cooling was amplified and a hard copy given by the chart recorder.

2.3.9   The hydrogenation of 1-hexene

Catalytic hydrogenation experiments, using 5% hydrogen/95% argon as the supply of hydrogen/diluent gas, were undertaken using the tubular reactor as described in Section 2.3.6.2. The reactor was operated in an identical manner except that 1-hexene was substituted for 2,2-dimethyl-butane as the hydrocarbon feed material and 5% hydrogen/95% argon was used instead of helium.

Gases being swept from the reactor were sampled and analysed by gas chromatography as detailed in Section 2.3.6.4.

3. <u>RESULTS</u>

3.1   <u>Product yields - etioporphyrin synthesis</u>

3.1.1   <u>Synthesis of isomeric mixture of etioporphyrin</u>

3.1.1.1   <u>Yield of methyl trans-2-pentenoate</u>

        product   -   colourless liquid

        boiling point - $142 - 143^{\circ}C$

        yield   - $82\ cm^3$

$$CH_3CH_2CH = CHCOOH + CH_3OH \longrightarrow CH_3CH_2CH = CHCOOCH_3 + H_2O$$
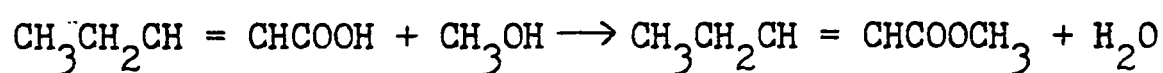
RMM	100	32	114
vol (cm^3)	92	166	82
d	0.989	0.791	0.919
wt (g)	90.988	131.306	75.358
moles	0.910	4.09	0.661

Trans-2-pentenoic acid is deficient

$$\therefore \text{yield} = \frac{0.661}{0.910} \times 100 = 72.6\%$$

3.1.1.2   <u>Yield of methyl 4-ethylpyrrole-3-carboxylate</u>

product   -   brown liquid

yield   - 32.5 cm^3

$$O=S-O-CH_2-N=C$$

$$CH_3CH_2CH=CHCOOCH_3 \xrightarrow{\quad NaH \quad}$$
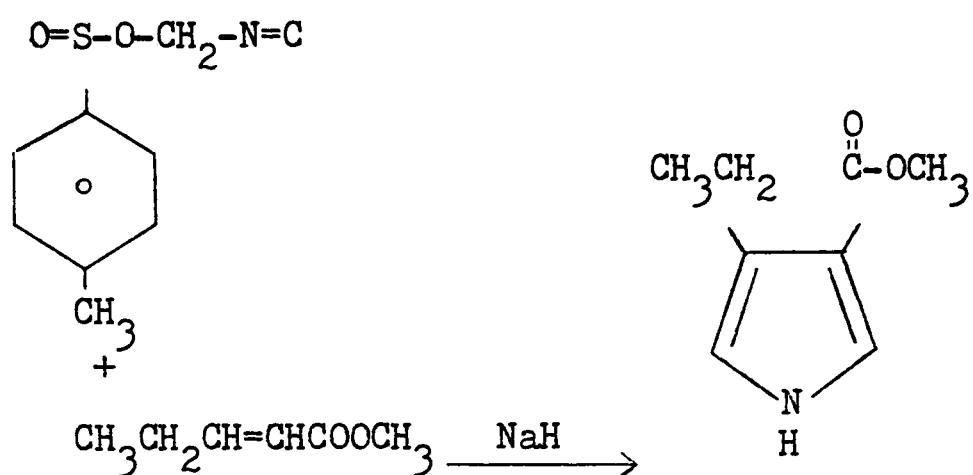
RMM	195.24	114	24	153
vol (cm^3)	-	37.2	-	32.5
d	-	0.919	-	_1.1
wt (g)	58.09	34.2	8.568	35.75
moles	0.30	0.30	0.357	0.234

Ester and tosyl methyl isocyanide are equally deficient

$$\therefore \text{ yield } = \frac{0.234}{0.30} \times 100 = 77.9\%$$

3.1.1.3   <u>Yield of 3-ethyl-4-methylpyrrole</u>

product   -   colourless oil

boiling point   -   88-89°C (under 11 mm Hg)

melting point   -   -1 to -2°C

yield   -   16.75 cm^3
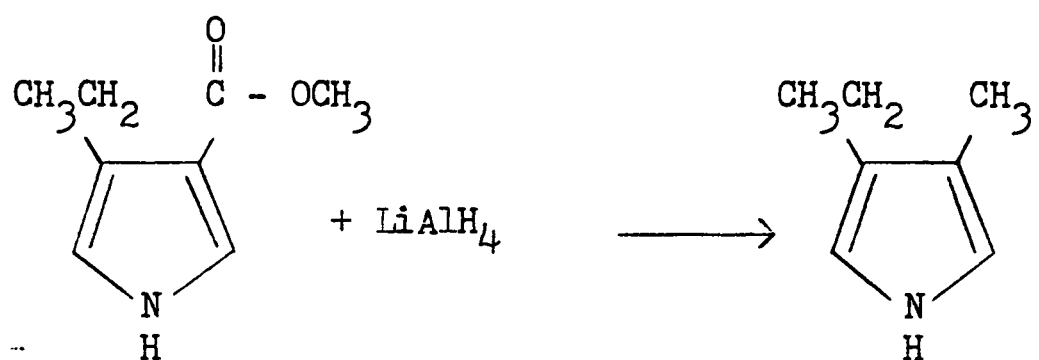
RMM	153	38	109
vol (cm^3)	49.6	-	16.75
d	1.1	-	0.9059
wt (g)	54.56	54.264	15.174
moles	0.3566	1.428	0.1392

methyl 4-ethylpyrrole-3-carboxylate is deficient

$$\therefore \text{yield} = \frac{0.1392}{0.3566} \times 100 = 39\%$$

3.1.1.4 <u>Yield of etioporphyrin</u>

product   -   purple microneedles

yield   -   3.1952 g
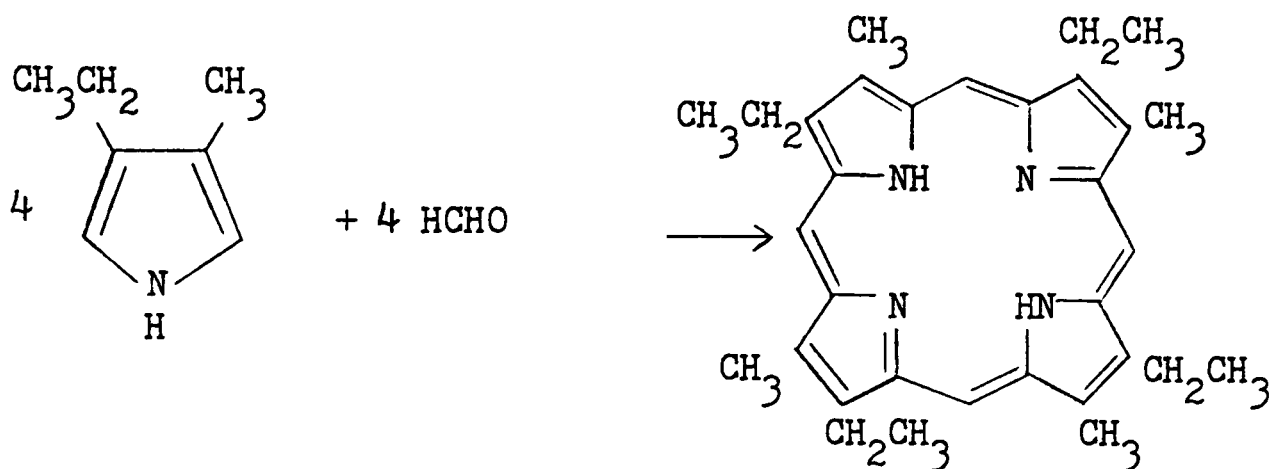
RMM	109	30	478
vol (cm^3)	13.5	122	-
d	0.9059	1.083	-
% in sol^n	-	37	-
wt (g)	12.23	132.13 at 37% =48.89 at 100%	3.1952
moles	$0.1122/4$ 2.805×10^{-2}	$1.6297/4$ 0.4074	6.6845×10^{-3}

3-ethyl-4-methylpyrrole is deficient

$$\therefore \text{ yield} = \frac{6.6845 \times 10^{-3}}{2.805 \times 10^{-2}} \times 100 = 23.8\%$$

3.1.2   Synthesis of etioporphyrin I

3.1.2.1   Yield of ethyl iodide

Product   -   homogeneous, colourless liquid

                          (turned to a light straw colour upon

                          being left to stand for 24 hours)

Boiling point   -   fraction 1 : 60-61°C

                          fraction 2 : 61-76°C

Yield   -   fraction 1 :   755 cm^3

                          fraction 2 :   1075 cm^3

Thus total yield of the combined fractions (boiling range 60-76°C)

was 1830 cm^3.

The infra red spectrum of the product collected (see Section 3.4.1.5)

indicated that it was actually a mixture of ethyl iodide and ethanol.

The suspected mixture was analysed using gas chromatography. The

conditions used for the separation are given in Section 2.3.1.2.1.3.

A calibration graph was constructed and this is shown in Fig 41.

Using this method the 60-61°C boiling fraction was shown to contain:-

. 70% ethyl iodide

30% ethanol

Assuming that no increase in volume (which would imply molecular

repulsion possibly leading to phase separation) or decrease in volume

(which would imply molecular association) takes place upon mixing ethyl

iodide and ethanol, then the algebraic manipulation of the two densities

should yield the relative amounts of each constituent in a mixture.

By using this technique the 60-61°C boiling fraction was shown to contain:-

65% ethyl iodide

35% ethanol

By use of the chromatographic technique given above, the mixture resulting from the combination of fractions 1 and 2 was shown to contain:-

63% ethyl iodide

37% ethanol

$$10C_2H_5OH + 2P + 5I_2 \longrightarrow 10C_2H_5I + 2H_3PO_4 + 2H_2O$$
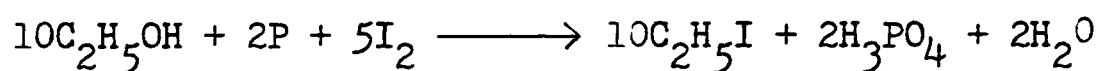
RMM	46	31	127	156
vol (cm^3)	~1800	-	-	-
d	0.789	-	-	1.936
wt (g)	1420	313	1600	1542
moles	3.09	5.05	2.52	0.988

iodine is deficient

$$\therefore \text{yield} = \frac{0.988}{2.52} \times 100 = 39.2\%$$

3.1.2.2   <u>Yield of 3-ethyl-2,4-pentandione</u>

product   -   pale yellow liquid

boiling point - $178-182^{\circ}C$

yield   - $680\ cm^3$

$$2CH_3\overset{O}{\overset{||}{C}}CH_2\overset{O}{\overset{||}{C}}CH_3 + 2CH_3CH_2I + K_2CO_3 \xrightarrow{\text{acetone solvent}} 2CH_3\overset{O}{\overset{||}{C}}\underset{\underset{CH_2CH_3}{|}}{CH}\overset{O}{\overset{||}{C}}CH_3$$

$$(+2KI + H_2CO_3)$$
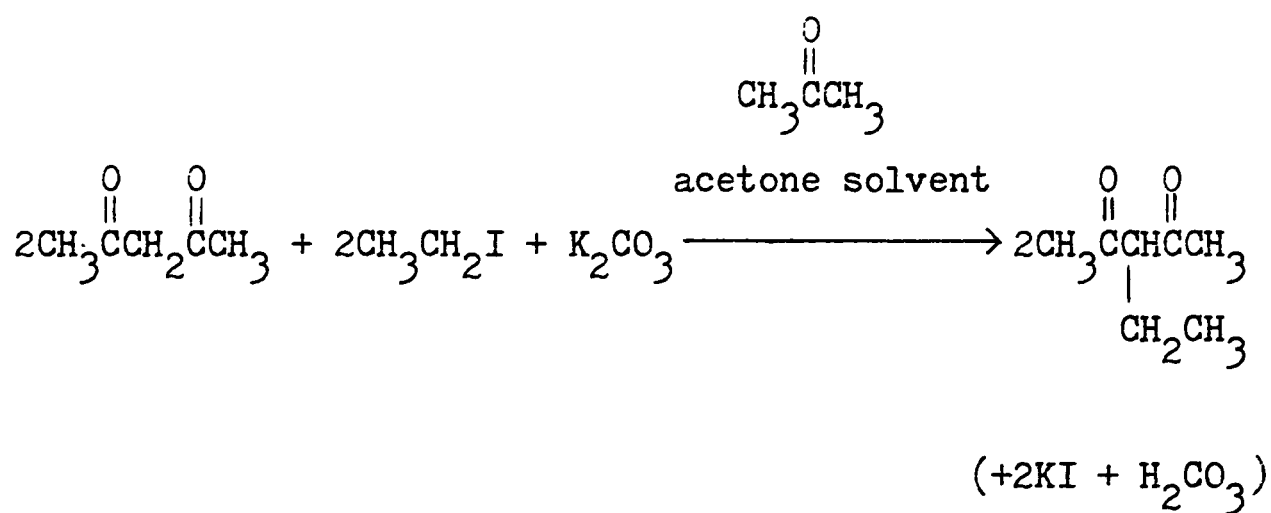
RMM	100	156	138	128
vol (cm^3)	1016	795	-	680
d	0.972	1.936	-	0.953
wt (g)	988	1539	1122	648
moles	9.88/2	9.86/2	8.13	5.06/2
=	4.94	4.93	8.13	2.53

Ethyl iodide is deficient

$$\therefore\ \text{yield} = \frac{2.53}{4.93} \times 100 = 51.3\%$$

3.1.2.3 <u>Yield of t-butyl 4-ethyl-3,5-</u>

<u>dimethylpyrrole carboxylate</u>

product   -   white needle crystals

yield   -   133 g

$$CH_3\overset{\overset{O}{\|}}{C}CH_2COOC(CH_3)_3 \; +$$

$$CH_3\overset{\overset{O}{\|}}{C}\underset{\underset{CH_2CH_3}{|}}{CH}\overset{\overset{O}{\|}}{C}CH_3 \; +$$

$$4CH_3COOH \; +$$

$$NaNO_2 \; +$$

$$2Zn \longrightarrow$$

$$(+ \; 2(CH_3COO)_2 \, Zn \; + \; CH_3COONa \; + \; 3H_2O)$$
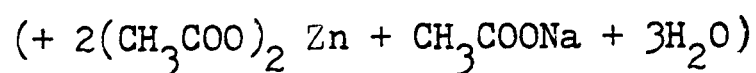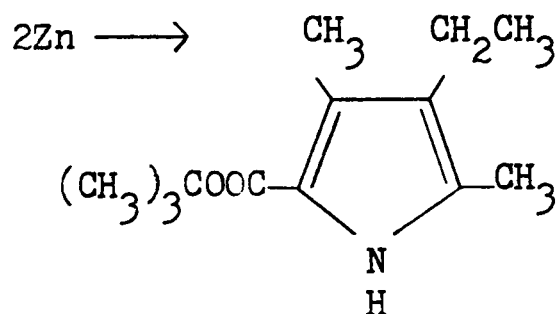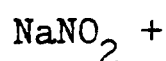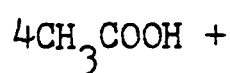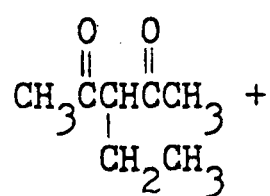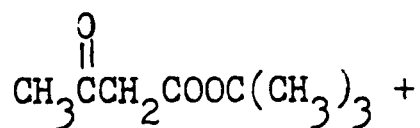
RMM	158	128	60	69	65.4	223
vol (cm³)	836	680	1128	-	-	-
d	0.9568	0.953	1.0491	-	-	-
wt (g)	800	648	1183	424	659	133
moles	5.06	5.06	$\frac{19.72}{4}$	6.14	$\frac{10.08}{2}$	0.60
=	5.06	5.06	4.93	6.14	5.04	0.60

glacial acetic acid is deficient thus yield = $\dfrac{0.60}{4.93}$ x 100 = 12.1%

3.1.2.4   <u>Yield of etioporphyrin I</u>

product   -   dark purple microneedles

yield   -   24.17 g

4

$+ 3Br_2$ $\xrightarrow[HCOOH]{CH_3COOH}$

$(+ 4HCOOC(CH_3)_3 + 6HBr)$
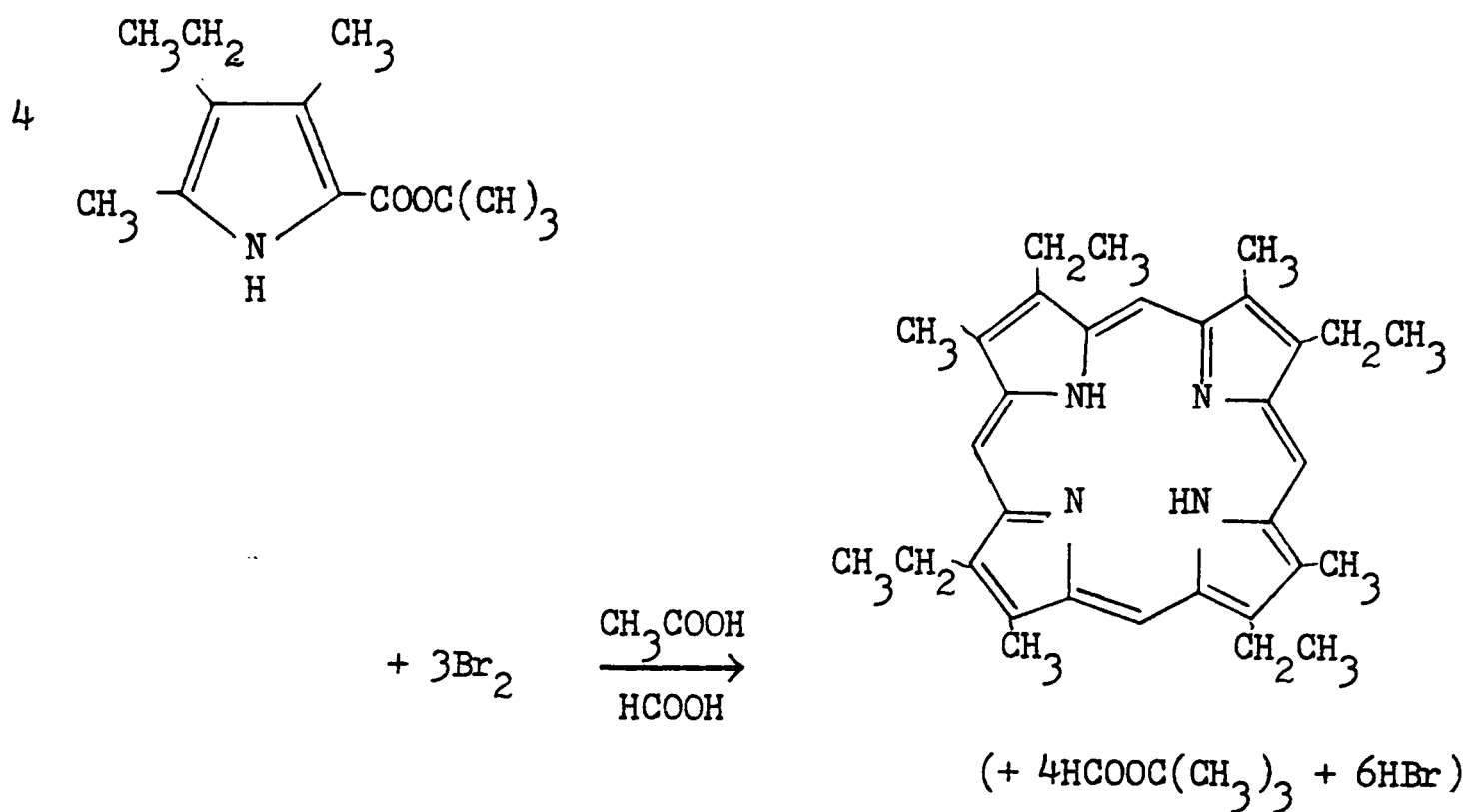
RMM	223	160	478
vol (cm^3)	-	93	-
d	-	3.12	-
wt (g)	133	290.2	24.17
moles	0.596/4	1.81/6	0.0506
=	0.15	0.30	0.0506

t-butyl 4-ethyl-3,5-dimethylpyrrole-2 carboxylate is deficient

∴ yield = 0.0506/0.15 x 100 = 33.7%

3.2   <u>Product yields - metalloporphyrin synthesis</u>

3.2.1   <u>Yield of vanadyl etioporphyrin</u>

3.2.1.1   <u>Reaction 1</u>

product   -   purple platelets

yield   -   0.5366 g

+

$$VOSO_4 5H_2O$$

+

$$CH_3COONa$$
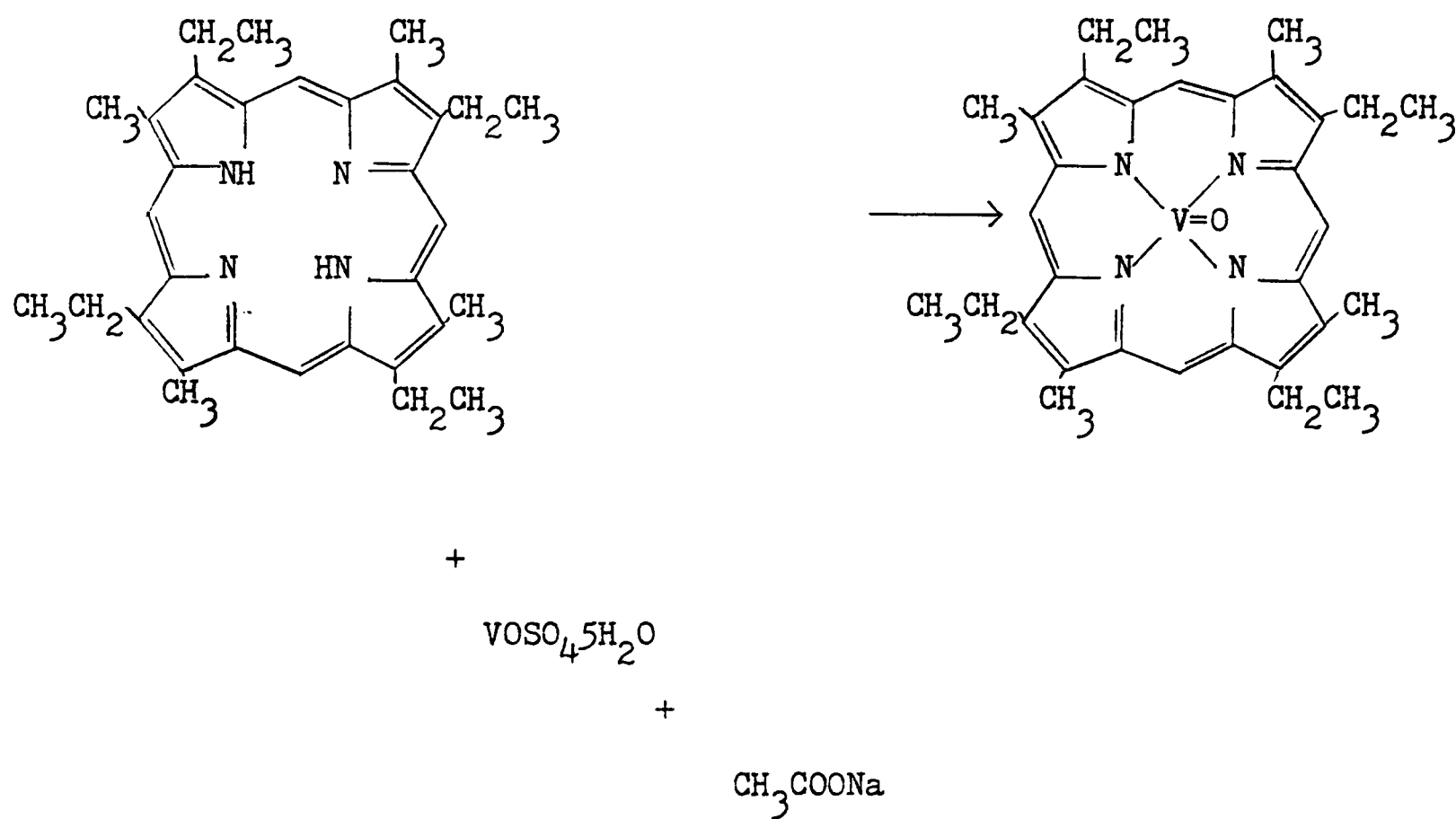
RMM	478	253	82	543
wt (g)	0.5	0.8	1.58	0.5366
moles	1.046×10^{-3}	3.162×10^{-3}	0.019	9.882×10^{-4}

etioporphyrin is deficient

$$\therefore \text{yield} = \frac{9.882 \times 10^{-4}}{1.046 \times 10^{-3}} \times 100 = 94.5\%$$

3.2.1.2   <u>Reaction 2</u>

product   -   purple platelets

yield   -   4.53 g

+

$VOSO_4 5H_2O$

+

CH_3COONa
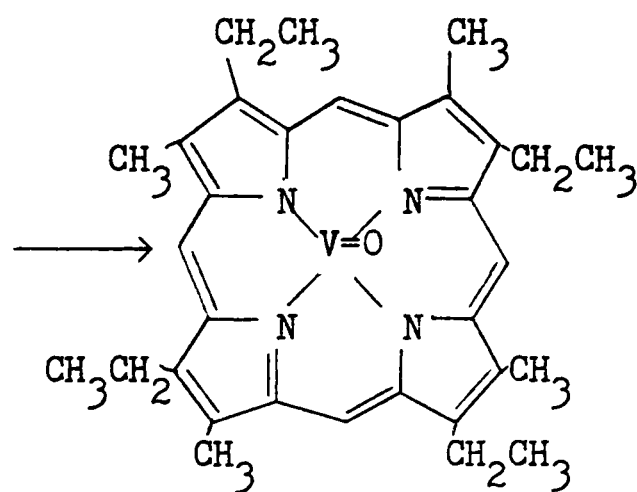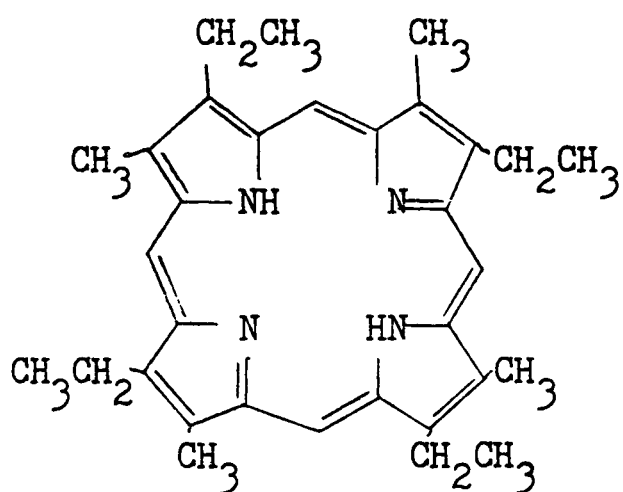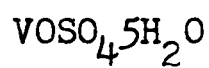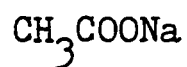
RMM	478	253	82	543
wt (g)	5.00	8.00	15.80	4.53
moles	10.460×10^{-3}	31.621×10^{-3}	0.1927	8.3425×10^{-3}

etioporphyrin is deficient

$\therefore$ yield $= \dfrac{8.3425 \times 10^{-3}}{1.046 \times 10^{-2}} \times 100 = 79.8\%$

3.2.2.   <u>Yield of nickel etioporphyrin</u>

3.2.2.1   <u>Reaction 1</u>

        product   -   purple platelets

        yield   -   0.5557 g

+

$$Ni(CH_3COO)_2 4H_2O$$
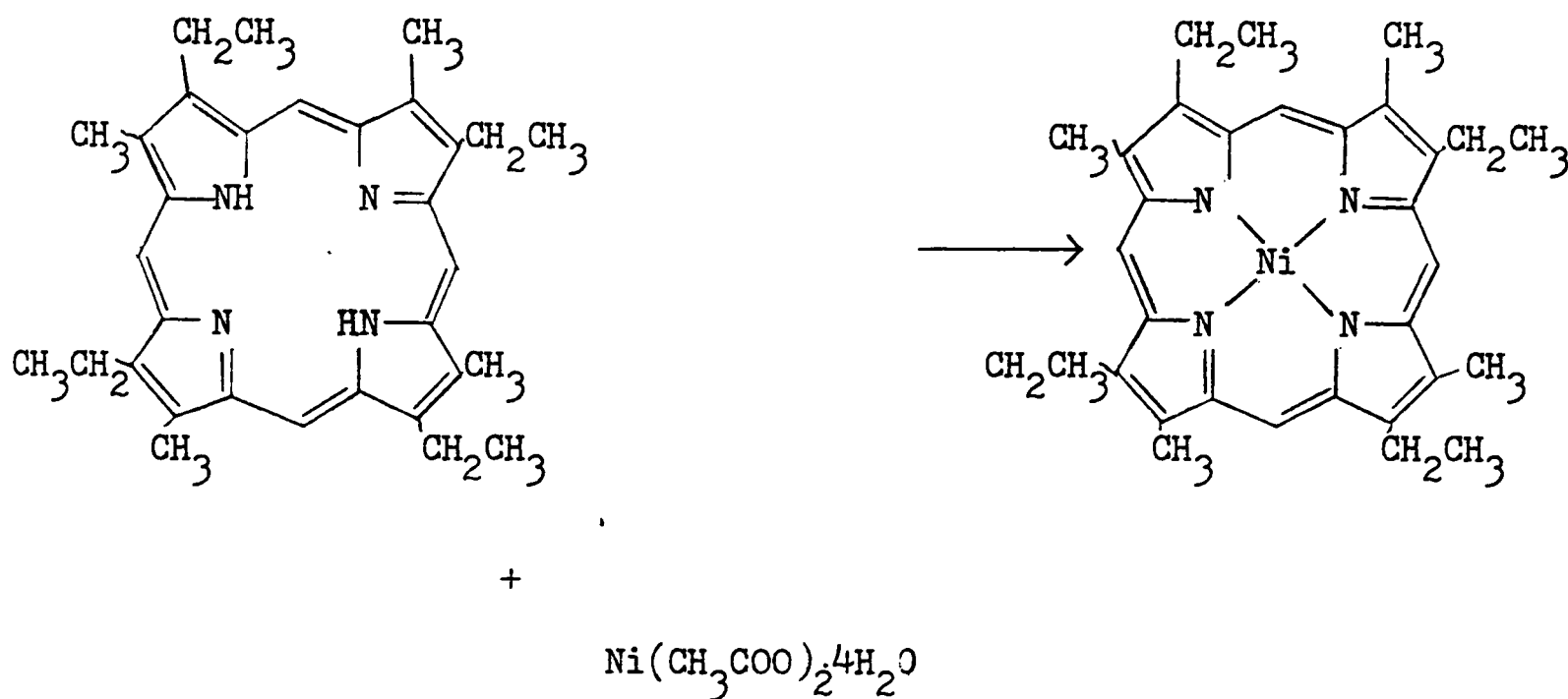
RMM	478	249	535
wt (g)	0.5015	2.6	0.5557
moles	1.049×10^{-3}	0.0104	1.0387×10^{-3}

etioporphyrin is deficient

$$\therefore \text{yield} = \frac{1.0387 \times 10^{-3}}{1.049 \times 10^{-3}} \times 100 = 99.0\%$$

3.2.2.2   <u>Reaction 2</u>

               product   -   purple platelets

               yield   -   4.36 g

$$+$$

$$Ni(CH_3COO)_2 4H_2O$$
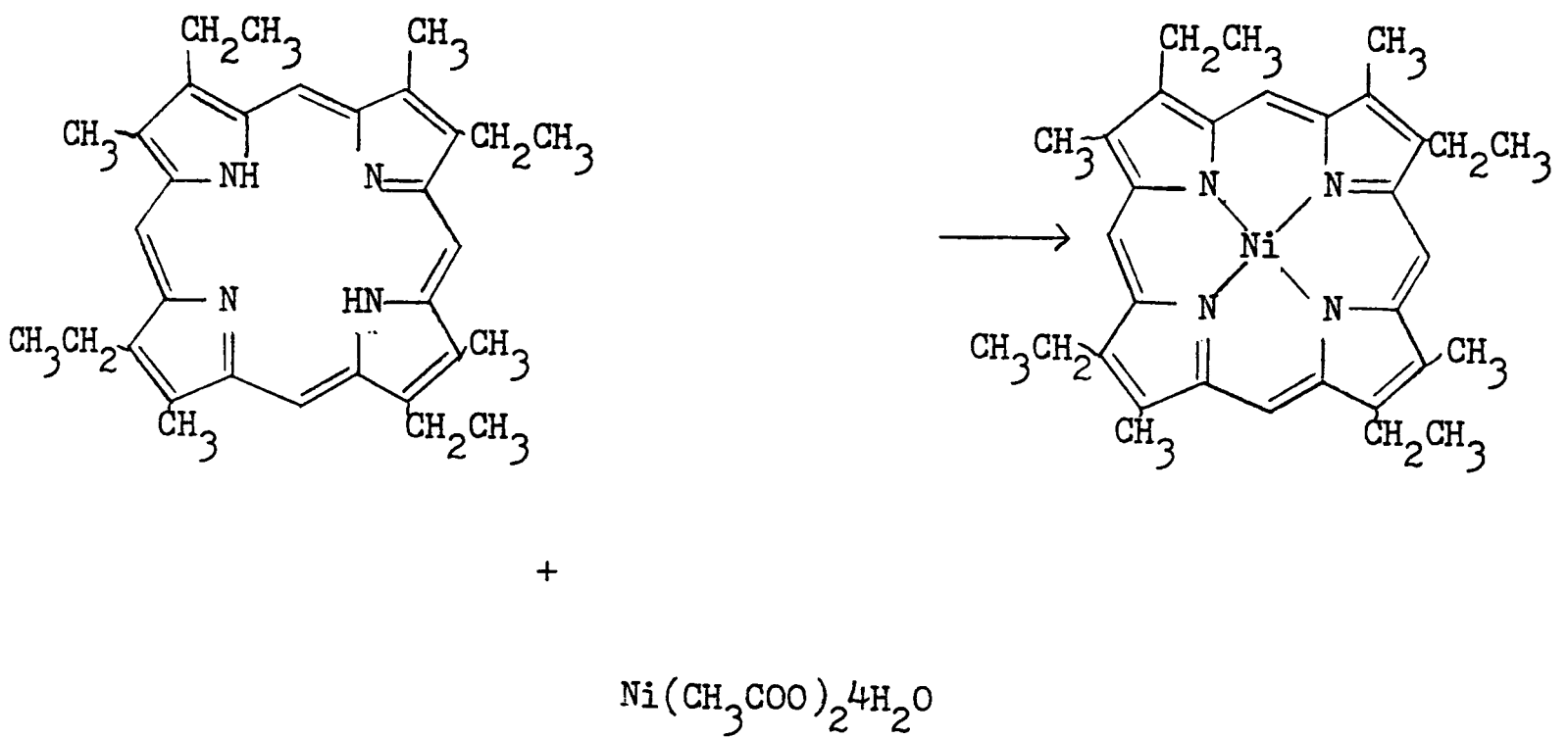
RMM	478	249	535
wt (g)	5.00	26.00	4.36
moles	1.046×10^{-2}	0.1044	8.1495×10^{-3}

etioporphyrin is deficient

$$\therefore \text{yield} = \frac{8.1495 \times 10^{-3}}{1.046 \times 10^{-2}} \times 100 = 77.9\%$$

3.2.3   <u>Yield of platinum etioporphyrin I</u>

3.2.3.1   <u>Reaction 1</u>

         product   -   small, regular purple crystals

         yield   -   1.394 g

$$+$$

$$\left[Pt(NH_3)_4\right]Cl_2$$

$$+ \ 4NH_3$$
$$+ \ 2HCl$$
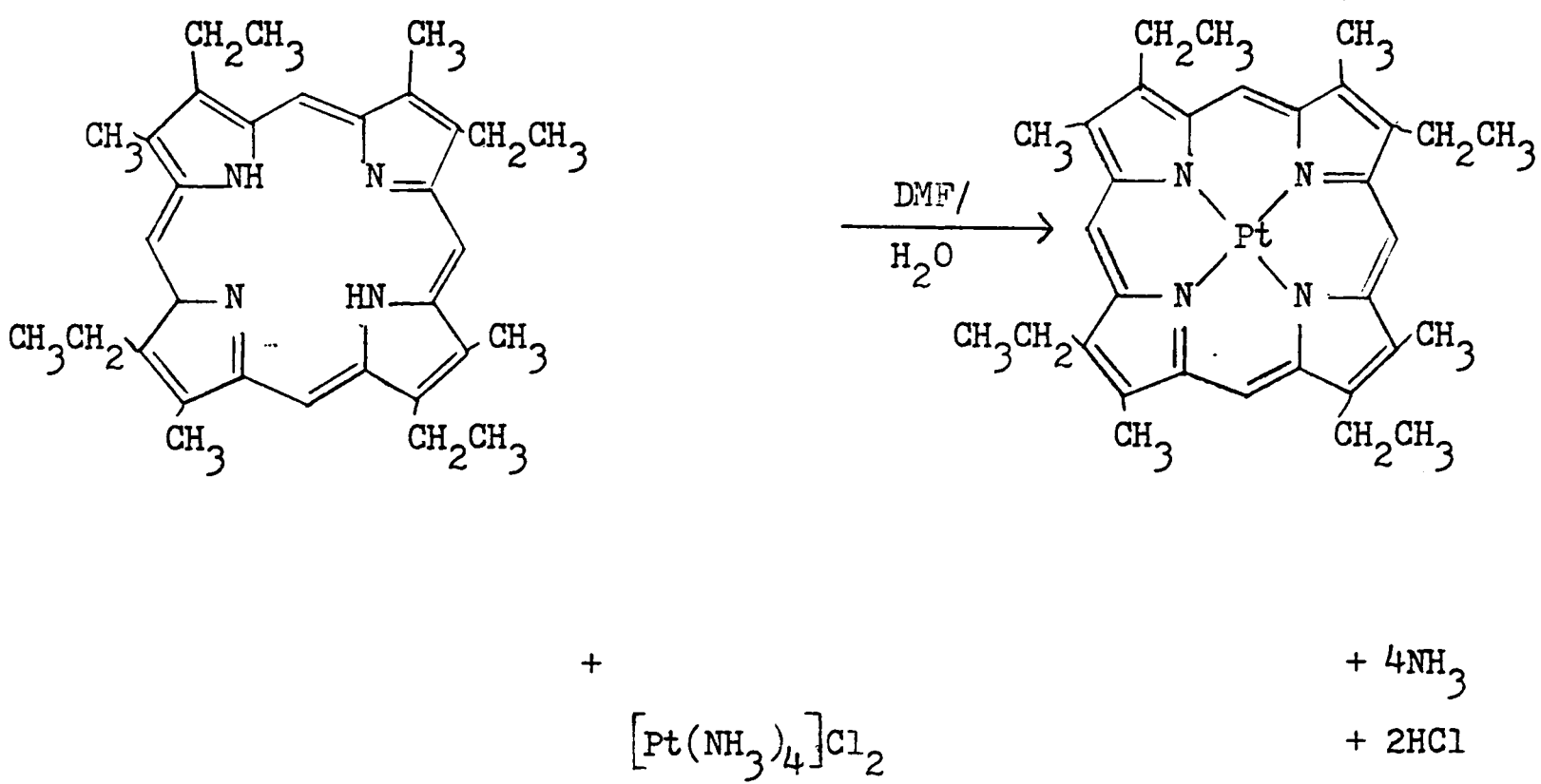
RMM	478	334	671
wt (g)	3.346	2.20	1.394
purity (%)	-	99.1	-
moles	7.00×10^{-3}	6.53×10^{-3}	2.08×10^{-3}

tetraammineplatinum (II) dichloride is deficient

$$\therefore \ \text{yield} = \frac{2.08 \times 10^{-3}}{6.53 \times 10^{-3}} \times 100 = 31.8\%$$

3.2.3.2   <u>Reaction 2</u>

product   -   small, regular purple crystals

yield   -   1.766 g

+

$$[Pt(NH_3)_4]Cl_2$$ + 4NH_3

+ 2HCl
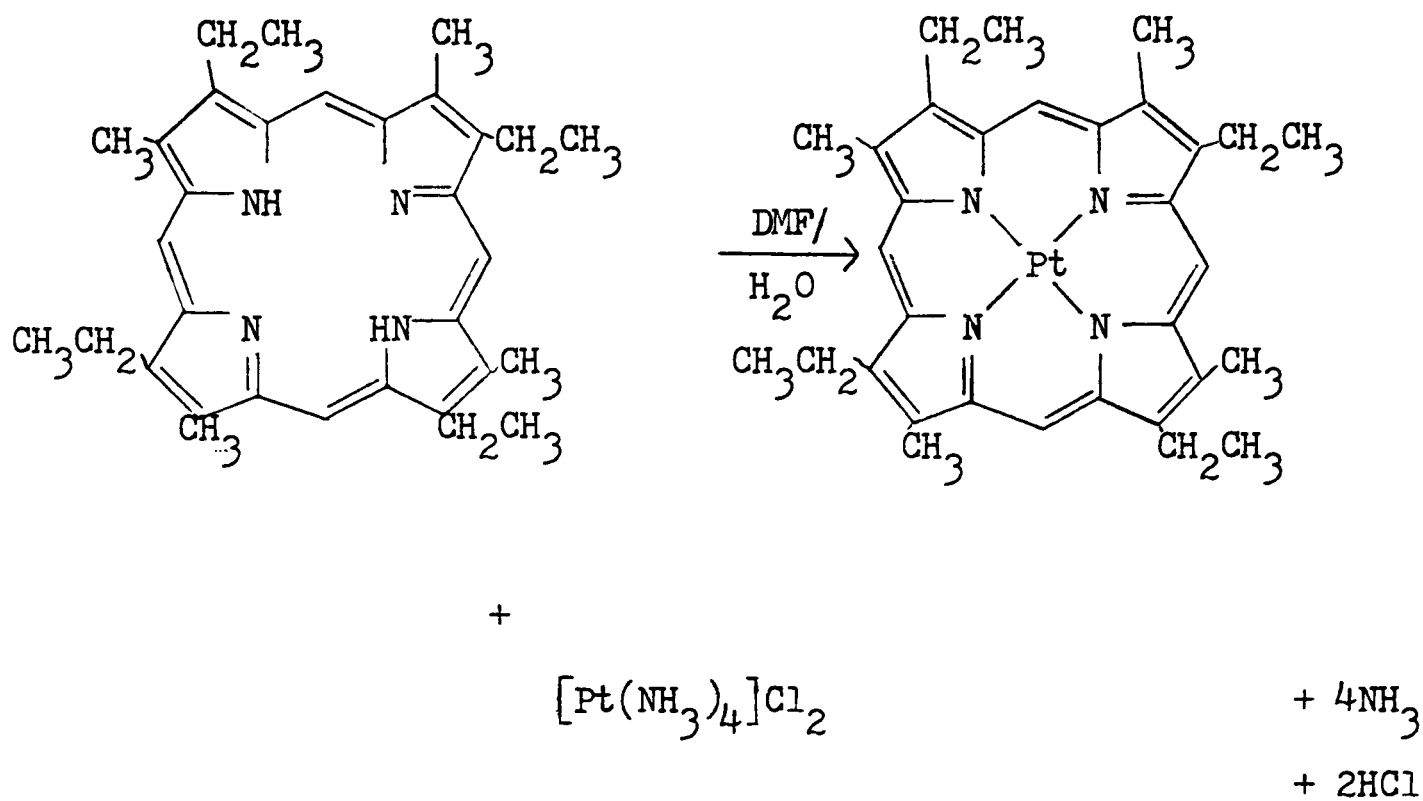
RMM	478	334	671
wt (g)	2.60	1.90	1.766
purity (%)	-	95.3	-
moles	5.44×10^{-3}	5.42×10^{-3}	2.63×10^{-3}

tetraammineplatinum (II) dichloride is deficient

$\therefore$ yield $= \dfrac{2.63 \times 10^{-3}}{5.42 \times 10^{-3}} \times 100 = 48.6\%$

3.2.4   <u>Yield of palladium etioporphyrin I</u>

product   -   small, regular purple crystals

yield   -   3.333 g

+

$[Pd(NH_3)_4]Cl_2$ + 4NH$_3$

+ 2CHl

RMM	478	245	582
wt (g)	3.346	1.81	3.333
purity (%)	-	88.40	90.63
moles	7.00×10^{-3}	6.52×10^{-3}	5.19×10^{-3}

tetraamminepalladium (II) dichloride is deficient

$$\therefore \text{yield} = \frac{5.19 \times 10^{-3}}{6.52 \times 10^{-3}} \times 100 = 79.6\%$$

3.2.4.1   Quantitative determination of palladium

1.81 g of tetraamminepalladium (II) dichloride was added to the reaction mixture. At 88.40% pure this was equivalent to 0.6938 g of palladium metal.

Quantitative gravimetric analysis was performed on the reaction filtrate according to the method given in Section 2.3.2.4.3. This determination showed that the equivalent of 0.0797 g of palladium metal remained in the reaction filtrate.

This indicated that $^{0.0797}/0.6938 \times 100 = 11.5\%$ of palladium ions remained unreacted with the etioporphyrin I.

Analysis performed by the Johnson Matthey Technology Centre indicated that the palladium etioporphyrin I prepared contained 16.54% palladium metal by weight.

By calculation, palladium etioporphyrin I theoretically contains 18.25% palladium metal by weight.

Thus the purity of the palladium etioporphyrin I prepared was $^{16.54}/18.25 \times 100 = 90.6\%$.

The two figures above correlate closely and if it is assumed that all of the porphyrin is recovered from the reaction mixture, either as unreacted base porphyrin or metalloporphyrin, then it can be seen that the purity of the palladium etioporphyrin I prepared was approximately 90%.

3.2.5 <u>Yield of vanadyl hematoporphyrin IX</u>

product   -   dark purple powder

yield   -   2.422 g

$$CH_3COOH \longrightarrow$$

+

$$VOSO_4 5H_2O$$

+

$$CH_3COONa$$
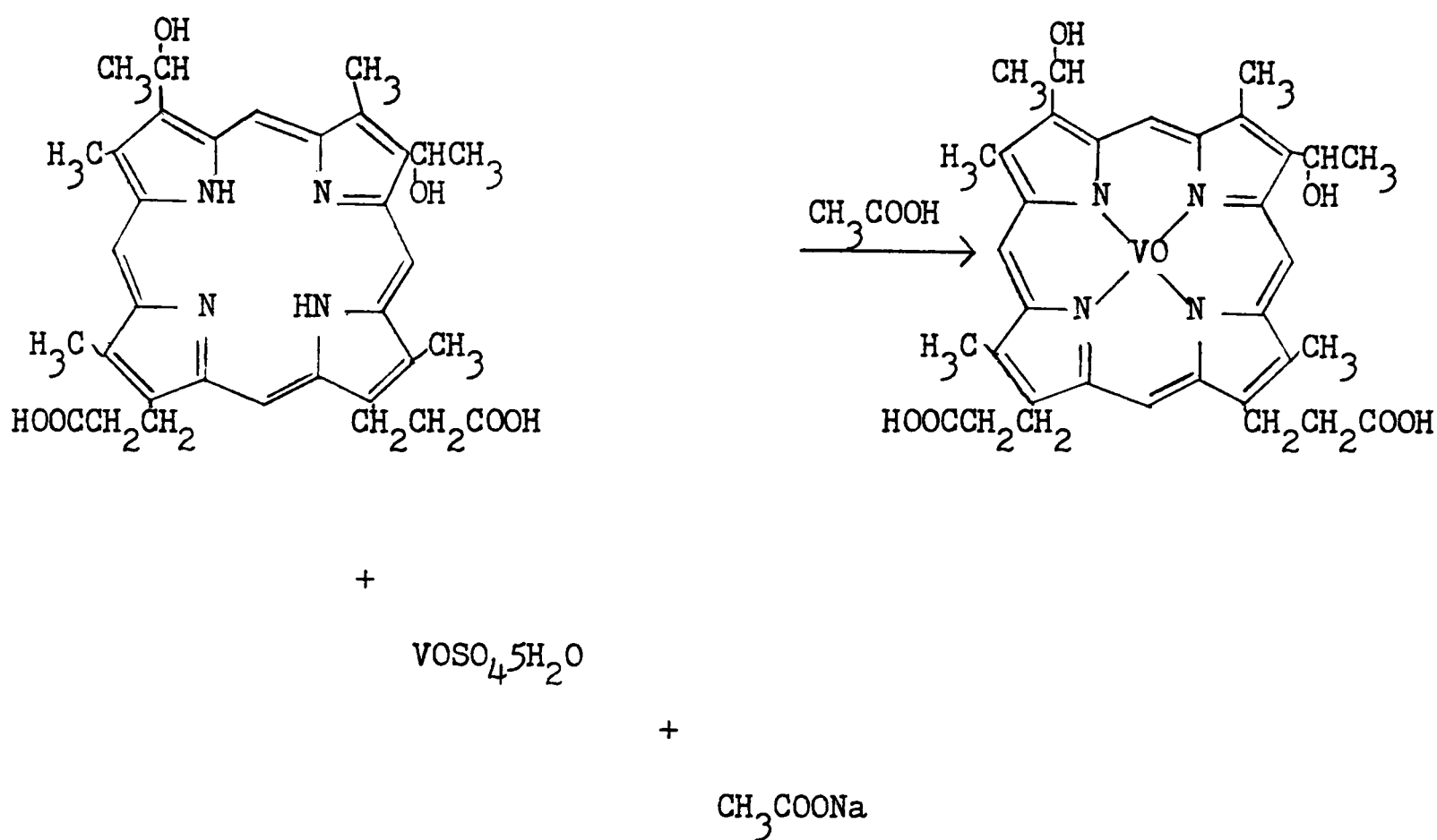
RMM	598	253	82	663
wt (ε)	3.0	3.9	7.6	2.422
moles	5.02×10^{-3}	1.5×10^{-2}	9.3×10^{-2}	3.65×10^{-3}

base hematoporphyrin IX is deficient

$$\therefore \text{yield} = \frac{3.65 \times 10^{-3}}{5.02 \times 10^{-3}} \times 100 = 72.8\%$$

3.2.6   <u>Yield of nickel hematoporphyrin IX</u>

           product   -   dark purple powder

           yield   -   2.38 g

+

$$Ni(CH_3COO)_2 4H_2O$$
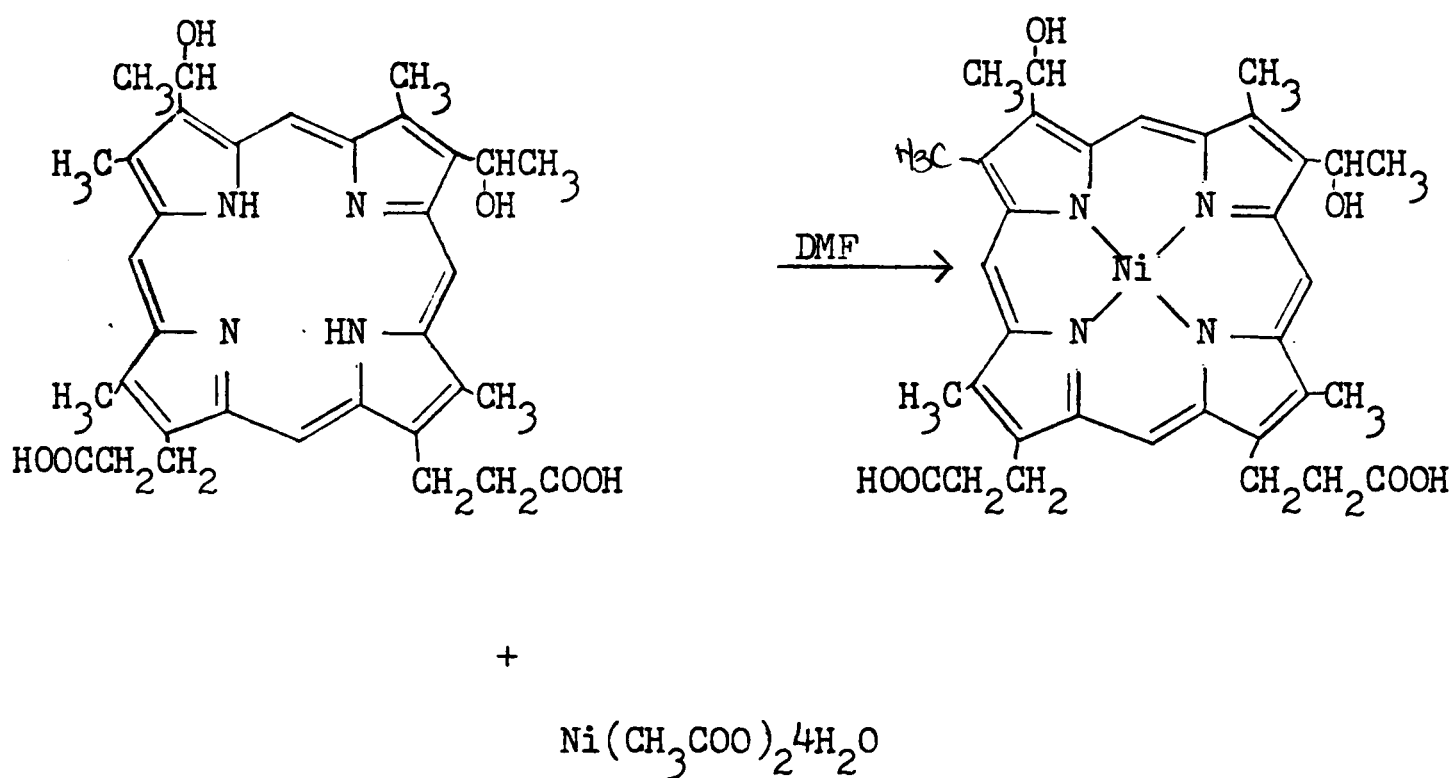
RMM	598	249	655
wt (g)	3.00	12.50	2.38
moles	5.02×10^{-3}	5.02×10^{-2}	3.63×10^{-3}

base hematoporphyrin IX is deficient

$$\therefore \text{yield} = \frac{3.63 \times 10^{-3}}{5.02 \times 10^{-3}} \times 100 = 72.3\%$$

3.3   <u>Analysis of Tia Juana Pesado topped</u>

                <u>crude and the extract from</u>

3.3.1   <u>Determination of the density of</u>

                <u>Tia Juana Pesado</u>

Using a standard volumetric technique the result shown below was obtained for the density of Tia Juana Pesado topped crude.

weight of container + TJP	(g)	86.344
weight of container	(g)	11.765
weight of TJP	(g)	74.579
container volume	(cm^3)	76.20

Thus density of TJP topped crude = 0.98

3.3.2   <u>Determination of asphaltene content</u>

                <u>of Tia Juana Pesado</u>

A duplicate determination of the asphaltene content of Tia Juana Pesado topped crude was undertaken as detailed in Section 2.3.3.1.

The results obtained are given below :-

1. weight of TJP taken   (g)   3.473

    volume of n-heptane added   (cm^3)   105

weight of asphaltenes + dish	(g)	71.4058
weight of dish only	(g)	70.8839
weight of asphaltenes	(g)	0.5219

Asphaltenes IP 143 = $\dfrac{0.5219}{3.473}$ x 100 = 15.0%

2. weight of TJP taken   (g)   3.427

    volume of n-heptane added (cm^3) 103

    weight of asphaltenes + dish   (g)   71.4024

    weight of dish only   (g)   70.8818

    weight of asphaltenes   (g)   0.5206

Asphaltenes IP 143 = $\dfrac{0.5206}{3.427}$ x 100 = 15.2%

Thus, the average result is :-

Asphaltenes IP 143 = 15.1%

3.3.3   <u>Estimation of the total metalloporphyrin</u>

<u>content of Tia Juana Pesado extract</u> (63)

The background absorbance contributing to the Soret band in the UV spectrum of the Tia Juana Pesado extract, shown in Fig. 42, was eliminated by drawing a base line tangentially through the valley on either side.

The remaining area under the Soret band was then determined as 13.03 cm^2.

Using an extinction coefficient of 4.63 x 10^6 dm^3nm $mole^{-1}cm^{-1}$ the total metalloporphyrin content of the solution of Tia Juana Pesado extract was estimated to be 2.256 x 10^{-6} moles dm^3.

Relating this back to the weight of extract sampled, the percentage metalloporphyrin in the petroporphyrin concentrate was calculated as :-

$$\frac{2.256 \times 10^{-6} \times 542.5 \times 100}{0.07038} = 1.98\%$$

3.4   <u>Analytical spectra</u>

The infrared, proton magnetic and mass spectra of the products formed during the various stages of the etioporphyrin and metalloporphyrin syntheses were resolved by consultation to correlation data in both text books (107, 117-120) and original literature (50, 121).

3.4.1   <u>Infrared spectra</u>

3.4.1.1   <u>I.R. Spectrum of methyl trans-2-pentenoate</u>

The peaks occurring in the infrared spectrum of methyl trans-2-pentenoate, shown in Fig. 43, were assigned as follows.

wavenumber (cm^{-1})	strength of absorption	arising from
990	S	C-H out of plane deformation in trans HC = CH
1190	S	C-O stretch
1300	M	C-H in plane deformation in trans HC = CH
1445	S	$-CH_3$ deformation
1465	M	$-CH_2-$ deformation
1670	S	C = C stretch
1735	S	C = O stretch
2850	W	C - H stretch
2890	W	C - H stretch in -CH=
2980	M	C - H stretch in $-CH_3$

S = strong

M = medium

W = weak

3.4.1.2   I.R. spectrum of methyl 4-ethylpyrrole-

              3-carboxylate

The peaks occurring in the infrared spectrum of methyl 4-ethyl-

pyrrole-3-carboxylate, shown in Fig 44, were assigned as follows.

wavenumber (cm^{-1})	strength of absorption	arising from
1090	M	C-O stretch
1330	S	C-N stretch
1435	S	C=C ring stretch
1560	M	overtone band of 780 cm^{-1}
1700	VS (B)	C=O stretch
2130	W	combination band of 980 cm^{-1} and 1150 cm^{-1}
2620	W	combination band of 1240 cm^{-1} and 1380 cm^{-1}
2960	VS	C-H stretch in $-CH_2-$ and $-CH_3$
3300	VS (B)	N-H stretch

VS = very strong

S = strong

M = medium

W = weak

(B)= broad

3.4.1.3   I.R. spectrum of 3-ethyl-4-methylpyrrole

The peaks occurring in the infrared spectrum of 3-ethyl-4-methyl-pyrrole, shown in Fig. 45, were assigned as follows.

wavenumber (cm^{-1})	strength of absorption	arising from
1300	M	C-N stretch
1460	S (B)	C=C ring stretch
2900	VS ⎤	C-H stretch in $-CH_2-$and$-CH_3$
2950	VS ⎬ T	C-H stretch in $-CH_2-$and$-CH_3$
2980	VS ⎦	C-H stretch in $-CH_2-$and$-CH_3$
3500	VS	N-H stretch

M = medium

S = strong

VS = very strong

(B)= broad peak

T = triplet peak

3.4.1.4   I.R. spectrum of etioporphyrin

The peaks occurring in the infrared spectrum of etioporphyrin, shown in Fig. 46, were assigned as in the table below.

Etioporphyrin is a crystalline solid and so the sample was analysed as a nujol mull. Accordingly, the infrared spectrum of nujol is given in Fig. 47 in order that the peaks arising from this substance may be readily identified and disregarded from the spectrum of etioporphyrin.

wavenumber (cm^{-1}) .	strength of absorption	arising from
740	S	N-H out of plane deformation
835	S	Cm-H out of plane deformation
900	W	$-CH_3$ rock
955	S	$-CH_3$ rock
1110	S	N-H in plane deformation
1220	M	Cm-H in plane deformation
1560	M	Cp-Cp stretch
1610	S	N-H deformation
3300	M (B)	N-H stretch

S = strong   (B) = broad

M = medium   Cm   = C methine

W = weak   Cp   = C_{1-8}

3.4.1.5   I.R. spectrum of ethyl iodide

Inspection of the spectra obtained from the 60 - 61°C (Fig 48) and

61 - 76°C (Fig 49) boiling fractions reveals that both are very similar.

Both spectra contain peaks in the same positions, the only difference being

the relative absorptions.

Comparison of the infrared spectra of the 60 - 61°C boiling fraction

with that of ethanol (Fig 50) shows that the majority of peaks are exhibited

by both spectra. However, two additional peaks (at 950 and 1200 cm^{-1}) occur

in the spectrum of the 60 - 61°C fraction. Consultation of the standard

spectrum for ethyl iodide (119) reveals that the two most intense bands

occur at 950 and 1200 cm^{-1}. All other peaks occurring in the infrared spectrum

of ethyl iodide will be masked by similar peaks due to ethanol.

Thus, in the infrared spectrum of a mixture of ethyl iodide and ethanol,

only the peaks occurring at 950 and 1200 cm^{-1} can be directly attributed to

ethyl iodide.

wavenumber cm^{-1}	arising from
1200	$-CH_2-$ wag

3.4.1.6   I.R. spectrum of 3-ethyl-2,4-pentandione

The peaks occurring in the infrared spectrum of 3-ethyl-2,4-pentandione, shown in Fig. 51, were assigned as follows.

wavenumber (cm^{-1})	strength of absorption	arising from
1170	M	$\overset{\overset{\text{O}}{\|\|}}{\text{C}}$ C-C-C stretch
1360	S	CH_3-C stretch
1420	M	CH_3-C bend
1590	M	C=O and C=C stretch of β diketone(due to enol tautomer)
1720	S (D)	C=O stretch(due to enol tautomer)
2960	M	O-H---O stretch of β diketone
3400	W	C=O stretch overtone

S = strong

M = medium

W = weak

(D) = doublet

3.4.1.7   <u>I.R. spectrum of t-butyl 4-ethyl-</u>

<u>3,5-dimethylpyrrole carboxylate</u>

The peaks occurring in the infrared spectrum of t-butyl 4-ethyl-3,5-
dimethylpyrrole carboxylate, shown in Fig. 52, were assigned as in the

table below.

t-butyl 4-ethyl-3,5-dimethylpyrrole carboxylate is a crystalline solid

and so the sample was analysed as a nujol mull. Accordingly, the infrared

spectrum of nujol is given in Fig. 47 in order that the peaks arising

from this substance may be readily identified and disregarded from the

spectrum of t-butyl 4-ethyl-3,5-dimethylpyrrole carboxylate.

wavenumber (cm^{-1})	strength of absorption	arising from
775	M	C-H bend
1160	M	C-O stretch
1250	W	$(CH_3)_3$-C stretch
1660	S (B)	C=O stretch
2900	VS	C-H stretch in $-CH_2$-and-CH_3
3300	S (B)	N-H stretch

VS = very strong   W = weak

S   = strong   (B) = broad

M   = medium

3.4.1.8   I.R. spectrum of vanadyl etioporphyrin

The peaks occurring in the infrared spectrum of vanadyl etio-

porphyrin, shown in Fig. 53 were assigned as in the table below.

Vanadyl etioporphyrin is a crystalline solid and so the sample was

analysed as a nujol mull. Accordingly, the infrared spectrum of nujol

is given in Fig. 47 in order that the peaks arising from this substance

may be readily identified and disregarded from the spectrum of vanadyl

etioporphyrin.

wavenumber (cm^{-1})	strength of absorption	arising from
840	M	Cm-H out of plane deformation
1000	S	Cp^1-Cp or Cp^1-N stretch or V-N in plane deformation
1060	M	Cp^1-N, Cp^1-Cm or Cp-Cp stretch
1150	S	Cm-H deformation
1220	W	Cm-H in plane deformation

S = strong   Cm = C methine

M = medium   Cp = C_{1-8}

W = weak Cp^1 = C linked to N, Cp and Cm

3.4.1.9   I.R. spectrum of nickel etioporphyrin

The peaks occurring in the infrared spectrum of nickel etio-

porphyrin, shown in Fig. 54, were assigned as in the table below.

Nickel etioporphyrin is a crystalline solid and so the sample was

analysed as a nujol mull. Accordingly, the infrared spectrum of nujol

is given in Fig. 47 in order that the peaks arising from this substance

may be readily identified and disregarded from the spectrum of nickel

etioporphyrin.

wavenumber (cm^{-1})	strength of absorption	arising from
705	W	C-CN or ring deformation
830	S	Cm-H out of plane deformation
1060	M	Cp^1-N, Cp^1-Cm or Cp-Cp stretch
1150	M	Cm-H deformation
1240	M	Cm-H in plane deformation

S = strong   Cm = C methine

M = medium   Cp = C_{1-8}

W = weak Cp^1 = C linked to N, Cp and Cm

3.4.1.10   I.R. spectra of base, vanadyl and

nickel hematoporphyrin IX

The three porphyrins are crystalline solids and so the samples were
analysed as nujol mulls. Accordingly, the infrared spectrum of nujol is
given in Fig. 47 in order that the peaks arising from the substance may
be readily identified and disregarded from the spectra of the above
three porphyrins.

The infrared spectra of base, vanadyl and nickel hematoporphyrin IX
are similar and poorly defined even though a small crystal size in the
nujol mull was ensured.

3.4.1.10.1   base hematoporphyrin IX

The infrared spectrum of base hematoporphyrin IX, shown in Fig.55,
exhibits a broad peak at about 1700 cm^{-1} and a small peak at 1060 cm^{-1}.

3.4.1.10.2   vanadyl hematoporphyrin IX

The infrared spectrum of vanadyl hematoporphyin IX, shown in Fig. 56,
exhibits a broad peak at about 1700 cm^{-1} and another broad band at
approximately 1600 cm^{-1}.

The small peak in the spectrum of base hematoporphyrin IX at 1060cm^{-1}
was not noted in the vanadyl hematoporphyrin IX infrared spectrum.

3.4.1.10.3   nickel hematoporphyrin IX

The infrared spectrum of nickel hematoporphyrin IX, shown in Fig.57,
exhibits a broad peak at about 1700 cm^{-1} and a small peak at 1240 cm^{-1}.

The small peak in the spectrum of base hematoporphyrin IX at 1060cm^{-1}

and the broad peak in the spectrum of vanadyl hematoporphyrin IX at about 1600 cm^{-1} were noted in the nickel hematoporphyrin IX infrared spectrum.

The broad peak occurring at 1700 cm^{-1}, which is common to all three spectra, was attributed to the -C = O stretch in the -COOH group.

No additional interpretation of the spectra was possible due to the generally poor peak definition. However, inspection of the three spectra shows that they are all different. This has allowed the conclusion that all three crystalline solids are different.

3.4.2 H^1 nuclear magnetic resonance spectra

3.4.2.1   nmr spectrum of methyl trans-2-pentenoate

The proton magnetic resonance spectrum of methyl trans-2-pentenoate in tetrachloromethane, as given in Fig. 58 was resolved as shown below.

$$
\begin{array}{ccc}
1 & a & d \\
CH_3CH_2 & & H \\
\end{array}
$$
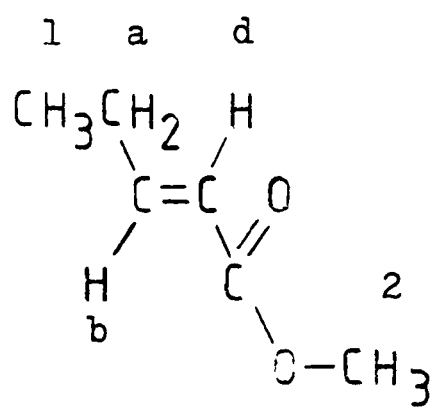
δ (ppm)	assignment	multiplicity	splitting constants, J (Hz)	relative peak areas
1.04	H1	3	7	3
2.12	Ha	10	1a=7 ab=7 ad=2	2
3.63	H2	1	-	3
5.67	Hd	2	15	1
6.86	Hb	6	bd=16 ab=6	1

3.4.2.2   nmr spectrum of methyl 4-ethyl-

pyrrole-3-carboxylate

The proton magnetic resonance spectrum of methyl 4-ethylpyrrole-

3-carboxylate in deuteriated trichloromethane, as given in Fig. 59,

was resolved as shown below.
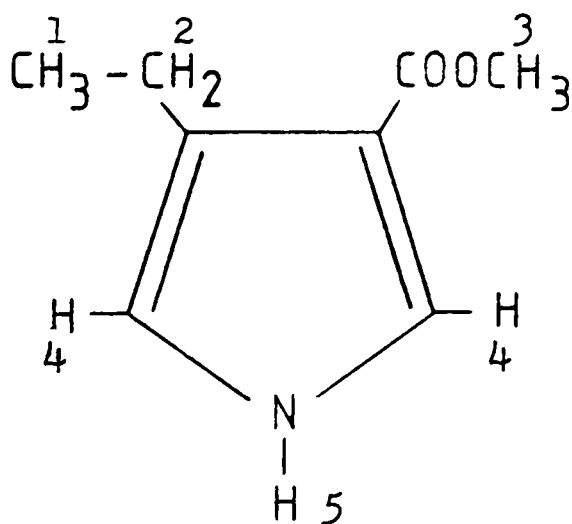
δ (ppm)	assignment	multiplicity	splitting constants, J (Hz)	relative peak areas
1.23	H1	3	8	3
2.81	H2	8	7	2
3.78	H3	1	-	3
6.54	H4	1	-	1
7.38	H5	3	2	1

The sample was apparently contaminated with a trace of diethyl ether.

Evidence for this is given by the triplet occurring at δ 0.77 ppm, which

corresponds to the $-CH_3$ group in the ether. From correlation tables the

quartet arising from the $-CH_2-$ group should be at δ 1.3 ppm. However,

this signal overlaps with the peak from the $-CH_3$ group in the pyrrolic

compound which has the effect of obscuring the former peak while slightly

increasing the integrated area of the latter.

3.4.2.3   <u>nmr spectrum of 3-ethyl-4-methylpyrrole</u>

The proton magnetic resonance spectrum of 3-ethyl-4-methylpyrrole

in deuteriated trichloromethane, as given in Fig 60, was resolved as

shown below.
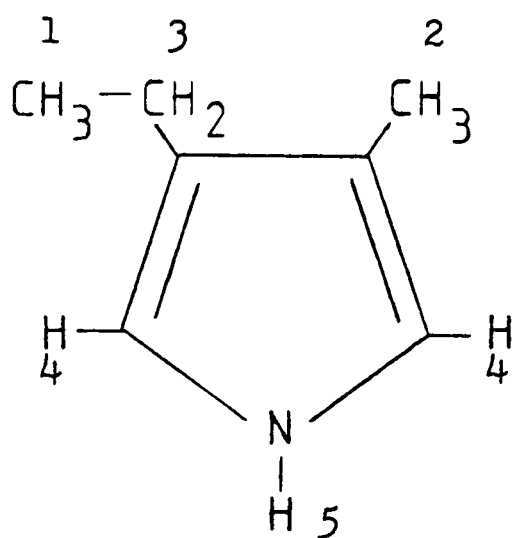
δ (ppm)	assignment	multiplicity	splitting constants, J (Hz)	relative peak areas
1.12	1	3	7	3
1.97	2	1	-	3
2.40	3	4	7	2
6.40	4	2	3	2
7.62	5	1 (VB)	-	1

VB = very broad

3.4.2.4   <u>nmr spectrum of etioporhyrin</u>

The proton magnetic resonance spectrum of etioporphyrin in

dueteriated trichloromethane, as given in Fig 61, was resolved as

shown below.

δ (ppm)	assignment	multiplicity	splitting constants, J (Hz)	relative peak areas
1.87	Hc_3	3	4	3
3.62	Hme	1	-	3
4.06	Hc_2	4	4	2
10.16	Hm	1	-	1

Hc_3 = H in $-CH_3$ of ethyl group

Hme = H in lone $-CH_3$ group

Hc_2 = H in $-CH_2-$ of ethyl group

Hm = H methine

In the case of etioporphyrin the resonance due to the hydrogen

atom in the N-H group was not seen in the nmr spectrum as, according

to correlation tables, it would occur approximately 3.75 ppm upfield

from the TMS signal.

3.4.2.5   nmr spectrum of 3-ethyl-2,4-pentandione

The proton magnetic resonance spectrum of 3-ethyl-2,4-pentandione,
as given in Fig. 62, was resolved as shown below.

$$\underset{1}{CH_3} - \underset{O}{\overset{\overset{1}{\|}}{C}} - \underset{CH}{CH} - \underset{O}{\overset{\overset{2}{\|}}{C}} - \underset{1}{CH_3}$$
$$\underset{\underset{\underset{4}{CH_3}}{|}}{\underset{3}{CH_2}}$$
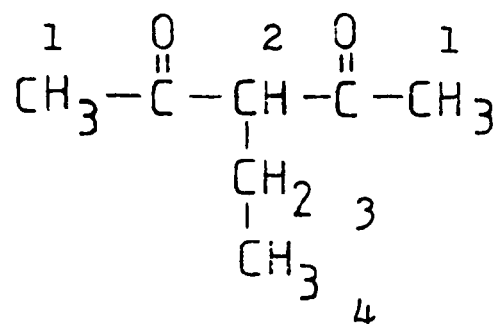
δ (ppm)	assignment	multiplicity	splitting constants, J (Hz)	relative peak areas
0.96	H3	5 (unresolved 8 due to equal J values)	$^2_3=7$ $^3_4=7$	2
1.83	H2	3	7	1
2.11	H1	1	-	6

The signals due to the H4 (methyl) group was unresolved as this
triplet was masked by the very large singlet at δ = 2.11.

3.4.2.6   <u>nmr spectrum of t-butyl 4-ethyl-</u>

<u>3,5-dimethylpyrrole carboxylate</u>

The proton magnetic resonance spectrum of t-butyl 4-ethyl-3,5-dimethylpyrrole carboxylate, as given in Fig. 63, was resolved as shown below.
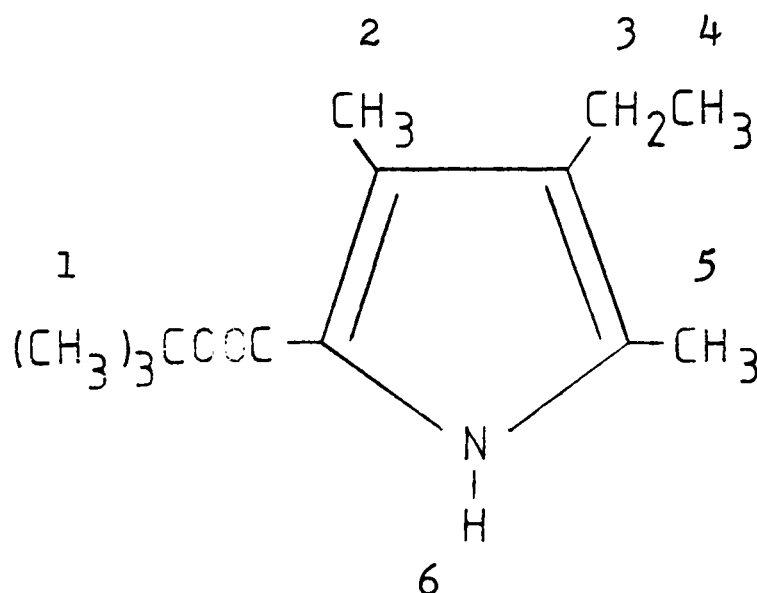
δ (ppm)	assignment	multiplicity	splitting constants, J (Hz)	relative peak areas
1.04	H4	3	7	3
1.58	H1	1	-	9
2.20	H2	1	-	3
2.26	H5	1	-	3
2.30	H3	4	7	2
8.97	H6	1	-	1

Of the four peaks in the quartet occurring at δ 2.30 the peak that is furthest upfield is masked by the singlet at δ 2.26.

3.4.2.7   nmr spectrum of vanadyl etioporphyrin

The presence of magnetic nuclei, other than hydrogen, in an organic molecule can introduce additional complications into the spectrum, since these nuclei will take up spin orientations with respect to the applied field and may cause spin-spin splitting of the proton signals (117). This effect can be seen in the proton magnetic resonance spectrum of vanadyl etioporphyrin in deuteriated trichloromethane, given in Fig. 64. The V (IV) ion has a spin quantum number of $\frac{1}{2}$ and is thus paramagnetic. This causes the spectrum to degenerate from the more usual first order appearance.

Although splitting patterns, coupling constants and peak integrations can not be obtained from this spectrum very approximate resonance positions can be determined as shown below.

Approx δ (ppm)	assignment
1.98	Hc_3
3.54	Hme
3.99	Hc_2
10.14	Hm

Hc_3 = H in $-CH_3$ of ethyl group

Hme = H in lone $-CH_3$ group

Hc_2 = H in $-CH_2-$ of ethyl group

Hm = H methine

The assignments were made by reference to other spectra and correlation tables.

3.4.2.8   <u>nmr spectrum of nickel etioporphyrin</u>

The proton magnetic resonance spectrum of nickel etioporphyrin in dueteriated trichloromethane, as given in Fig. 65, was resolved as shown below.

δ (ppm)	assignment	multiplicity	splitting constants, J (Hz)	relative peak areas
1.88	Hc_3	3	4	3
3.64	Hme	1	-	3
4.08	Hc_2	4	4	2
10.07	Hm	1	-	1

Hc_3 = H in $-CH_3$ of ethyl group

Hme = H in lone $-CH_3$ group
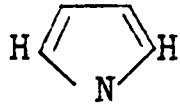
Hc_2 = H in $-CH_2-$ of ethyl group

Hm = H methine

3.4.3   <u>Mass spectra</u>

3.4.3.1   <u>Mass spectrum of methyl 4-ethyl-</u>

                                  <u>pyrrole-3-carboxylate</u>
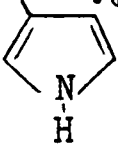
The mass spectrum of methyl 4-ethylpyrrole-3-carboxylate, shown in Fig. 66, was interpreted as shown below.

m/e	MI - m/e	groups associated with mass lost	inference
153	0	–	molecular ion
138	15	$-CH_3$	
122	31	$-OCH_3$	methyl ester
94	59	$-COOCH_3$	methyl ester
79	74	$-COOCH_3$ and $-CH_3$	methyl ester plus side chain
65	88	$-COOCH_3$ and $-C_2H_5$	pyrrolic compound as:- has a RRM = 65

3.4.3.2 <u>Mass spectrum of 3-ethyl-4-methylpyrrole</u>

The mass spectrum of 3-ethyl-4-methylpyrrole, shown in Fig. 67, was interpreted as shown below.
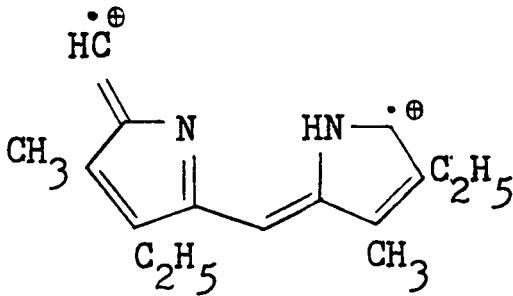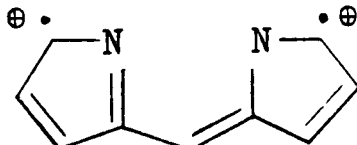
m/e	ion corresponding to m/e value
109	molecular ion
94	CH_3CH_2 ... (pyrrole ring structure)
41	$C_2H_2\overset{\cdot}{N}H^{\oplus}$
39	$C_3H_3^{\cdot\oplus}$
28	$HC \equiv \overset{\cdot}{N}H^{\oplus}$

The peak occurring at m/e 40 is due to a neutral molecule of hydrogen cyanide.

3.4.3.3   <u>Mass spectrum of etioporphyrin</u>

The mass spectrum of etioporphyrin, shown in Fig. 68, was

interpreted as shown below.

m/e	ion corresponding to m/e value
478	molecular ion
463	MI minus one $-CH_3$ group
448	ion at m/e 463 minus one $-CH_3$ group
433	ion at m/e 448 minus one $-CH_3$ group
239	half a porphyrin molecule i.e.:-
224	ion at m/e 239 minus one $-CH_3$ group
209	ion at m/e 224 minus one $-CH_3$ group
137	

The mass spectrum of etioporphyrin is typical of the type shown

by porphyrins generally. There are no prominent peaks attributable to

the fragmentation of the porphyrin ring into pyrrole subunits.

Fragmentation ions fall into two distinct groups.

1.   A high mass group of singly charged ions.

This group is separated by a relatively blank region from :-
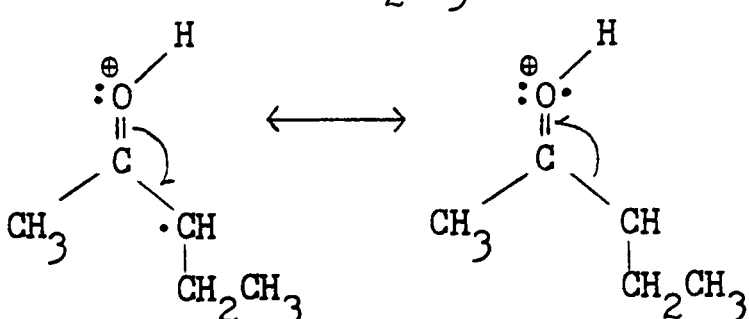
2.   A lower mass group of doubly charged ions, with the parent peak

of this group occurring at half the m/e value of the molecular ion.

The molecular ion is usually by far the most intense peak in the mass

spectrum (121).

3.4.3.4   Mass spectrum of 3-ethyl-2,4-pentandione
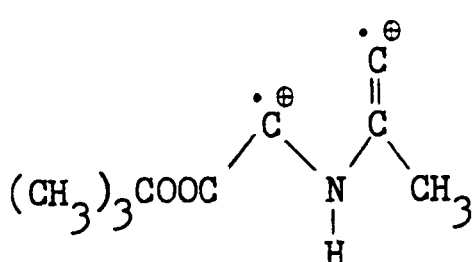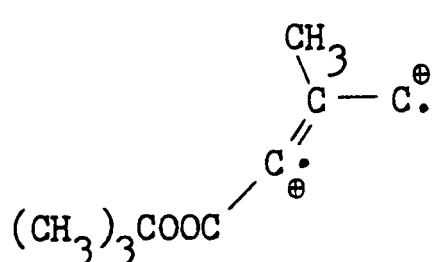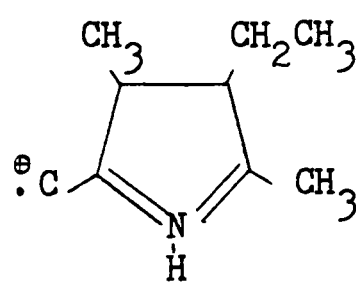
The mass spectrum of 3-ethyl-2,4-pentandione, shown in Fig.69, was interpreted as shown below.

m/e	ion corresponding to m/e value
128	molecular ion
113	MI minus one $-CH_3$ group
99	MI minus one $-CH_2CH_3$ group
86	
85	MI minus CH_3-C- $\overset{\parallel}{O}$
71	ion at m/e 86 minus one $-CH_3$ group
43	$CH_3-C = O$

3.4.3.5   <u>Mass spectrum of t-butyl 4-ethyl-</u>

<u>3,5-dimethylpyrrole carboxylate</u>

The mass spectrum of t-butyl 4-ethyl-3,5-dimethylpyrrole carboxylate, shown in Fig. 70, was interpreted as shown below.

m/e	ion corresponding to m/e value
223	molecular ion
167	$(CH_3)_3COOC$—$\overset{\bullet\oplus}{C}$—$N(H)$—$\overset{\overset{\bullet\oplus}{C}}{\underset{\parallel}{C}}$—$CH_3$
152	ion at m/e 167 minus one -CH_3 group
152	$(CH_3)_3COOC$—$\overset{\bullet}{\underset{\oplus}{C}}$=$\overset{CH_3}{\underset{}{C}}$—$\overset{\oplus}{\underset{\bullet}{C}}$
134	pyrrole ring with substituents CH_3, CH_2CH_3, $\overset{\oplus}{\underset{\bullet}{C}}$, CH_3, N–H

3.4.3.6   Mass spectrum of vanadyl etioporphyrin

The peak due to the molecular ion at m/e 543 is present in the mass
spectrum of vanadyl etioporphyrin, shown in Fig. 71. Peaks due to the
decomposition products of vanadyl etioporphyrin occurring at low m/e
values (less than 130) show a very similar distribution and intensity
to the corresponding peaks arising from etioporphyrin. Significant peaks
occurring in both spectra include those at m/e values of 55, 57, 69, 71,
81, 83, 85, 95, 97 and 123. It can be seen that the mass spectrum of
vanadyl etioporphyrin exhibits the same form as that generally shown
by porphyrins, already discussed in Section 3.4.3.3.

Due to the occurrence of isotopes a series of molecular ions of
slightly differing relative molecular masses will be obtained. By using
accepted values for the natural abundance of these isotopes it is possible
to calculate and predict, the relative intensities of the various
molecular ions in a mass spectrum. This is shown for vanadyl etio-
porphyrin in Fig. 72. Comparison of this theoretical splitting pattern
with that obtained in practice from the mass spectrum provides good
evidence for the presence of a particular compound. Such a comparison
for vanadyl etioporphyrin is shown below :-

m/e	calculated % of full scale	measured % of full scale
543	100.00	100.0
544	37.07	36.0
545	6.87	5.6
546	0.85	-

3.4.3.7   Mass spectrum of nickel etioporphyrin

The peak due to the molecular ion at m/e 534 is present in the mass

spectrum of nickel etioporphyrin, shown in Fig. 73. Although the mass

spectrum of nickel etioporphyrin shows a slightly differing distribution

of relative intensities at low m/e values (less than 130) compared to

the spectrum of etioporphyrin, both spectra have peaks in common

occurring at m/e values of 55, 57, 69, 71, 81, 83, 85, 95 and 97. In

addition, it can be seen that the mass spectrum of nickel etioporphyrin

exhibits the same form as that generally shown by porphyrins, already

discussed in Section 3.4.3.3.

Comparison of the theoretical splitting pattern, given in Fig. 74

and discussed in Section 3.4.3.6 with that measured from the spectrum

is shown below for nickel etioporphyrin.

m/e	calculated % of full scale	measured % of full scale
534	100.00	100.0
535	37.06	40.4
536	45.27	43.0
537	16.78	15.5
538	8.67	8.6
539	2.42	3.0
540	2.00	1.6
541	0.64	-

3.4.3.8   Mass spectrum of platinum etioporphyrin I

The mass spectrum of platinum etioporphyrin I is very similar in

appearance to those of nickel and vanadyl hematoporphyrin IX. The peaks

with the greatest relative abundance are due to instrumental background.

There is a group of peaks between m/e values of 28 and 100 inclusive.

Outside these m/e values there are no peaks with a relative abundance

greater than 10%. Above m/e 106 no peaks are present with a relative

abundance greater than 3%. No peak due to the molecular ion was detected.

3.4.3.9 <u>Mass spectrum of vanadyl hematoporphyrin IX</u>
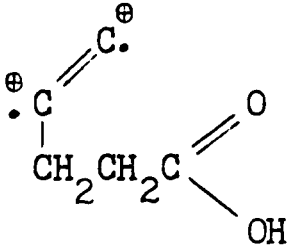
Examination of the mass spectrum of vanadyl hematoporphyrin IX, shown in Fig. 75, reveals that above an m/e value of 135 there are no peaks present with a relative abundance greater than 5%. In addition, the molecular ion was not detected.

If the mass spectrum of the instrument background, shown in Fig. 76, is compared with that of vanadyl hematoporphyrin IX it can be concluded that the peaks with m/e values of 28, 32 and 135 are due to residual elements or compounds not removed upon evacuation of the instrument.

Some of the major remaining peaks were interpreted as shown below.

m/e	groups associated with mass lost
44	
57	
83	

m/e	groups associated with mass lost
97	 $\overset{\oplus}{\underset{\bullet}{C}}$ with structure: a carbon radical cation doubly bonded to another $\overset{\oplus}{C_\bullet}$, bearing CH_2CH_2C group double bonded to O and single bonded to OH

Polar groups such as carboxyl, tend to decrease the already limited volatility of the porphyrin to such an extent that good quality mass spectra of these species are difficult to obtain (53).

3.4.3.10   <u>Mass spectrum of nickel hematoporphyrin IX</u>

Examination of the mass spectrum of nickel hematoporphyrin IX,
shown in Fig 77,reveals that above an m/e value of 60 there are no
peaks present with a relative abundance greater than 5%. In addition,
the molecular ion was not detected.

If the mass spectrum of the instrument background, shown in Fig. 76,
is compared with that of nickel hematoporphyrin IX it can be concluded
that the peaks with m/e values of 28, 32, 40 and 135 are due to residual
elements or compounds not removed upon evacuation of the instrument.

Major remaining peaks were interpreted as shown below.

m/e	groups associated with mass lost
43	$-CH_2\overset{\text{O}}{\underset{}{C}}-OH$
45	$CH_3\overset{\text{OH}}{\underset{}{CH}}$ and $C\overset{O}{\underset{OH}{}}$

3.5   Temperature programmed decomposition

               of supported metalloporphyrins

Initial temperature programmed decomposition experiments were

performed on both 1.0% (w/w) nickel and vanadyl etioporphyrin supported

on silica gel. Helium, which possesses a very high thermal conductivity,

was used as the inert carrier gas. Due to high relative differences in

thermal conductivities any gaseous decomposition products should be

easily detected. In both cases a low temperature peak, lasting from

$50^{\circ}C$ to about $210^{\circ}C$, was displayed by the traces. After this, and up

to a temperature of $540^{\circ}C$, the traces were almost horizontal, with a

very slight amount of baseline drift.

In order to identify the origins of the low temperature peak

additional thermal decomposition tests were performed on a small sample

of unsupported vanadyl etioporphyrin and a sample of silica gel. The

profile due to the unsupported porphyrin gave a straight, horizontal

line showing the absence of any low temperature peak. However, the

profile given by testing a sample of silica gel showed a peak identical

to those described above.

From these results it was concluded that the low temperature peak,

shown in the traces from the supported metalloporphyrins, was due to the

silica gel. It is probable that the low temperature peak can be attributed

to the removal of water from the support material.

In addition to the supported nickel and vanadyl etioporphyrin tested,

samples of the following porphyrins supported 1.0% w/w on silica were

examined in a similar manner.

base etioporphyrin

palladium etioporphyrin

base hematoporphyrin IX

nickel hematoporphyrin IX

vanadyl hematoporphyrin IX

In every case the above five porphyrins gave TPD traces showing
a very strong resemblance to those exhibited by supported nickel and
vanadyl etioporphyrin. In most cases the section of the trace between
$210^{\circ}C$ and $540^{\circ}C$ displayed no baseline drift at all.

From the results of these experiments it was concluded that all
of the supported metalloporphyrins tested showed no signs of decomposition
and were consequently thermally stable up to a temperature of $540^{\circ}C$

3.6.   Gas chromatographic separations

3.6.1   Calibration of the gas chromatograph

By injecting known quantities of various standard gaseous hydro-
carbon mixtures and known amounts of different liquid hydrocarbons the
FID response for the various hydrocarbons can be compared, as shown in
Fig. 78 for alkanes and Fig. 79 for n-1-alkenes, by relating the
integrator readings obtained to a reference concentration. In this way,
if the detector response for methane is assigned the arbitrary value
of 1.000, the corresponding response for other hydrocarbons can be
related to this figure. Thus the calibration factors given in Table 6
were obtained for the hydrocarbons listed.

The linearity of the FID response to increasing amounts of hydro-
carbon was checked by injecting known quantities of neat, liquid 2,2-
dimethylbutane into the gas chromatograph. From the plot of injection
size vs detector response, shown in Fig. 80, it can be seen that the FID
response is linear,and passes through the origin, as the amount of
hydrocarbon rises by an order of magnitude. From this it was assumed
that other hydrocarbons behave in a similar manner and thus quantity
vs FID response curves were deemed unnecessary.

3.6.2   Calculation of hydrocarbon concentration
                        of reactor gas effluent

Areas that are assigned to the various hydrocarbons in the reactor
gas effluent had to be converted into mole percentages. This was
achieved by dividing the area given by the integrater by the relevant
factor from Table 6, to give a corrected area. The sum of the corrected

areas may then be used to obtain mole per cent figures. i.e.:-

$$\text{corrected area} = \frac{\text{integrated area}}{\text{correction factor}}$$

$$\text{mole \%} = \frac{\text{corrected area}}{\text{sum of corrected areas}} \times 100$$

A program was written for a ZX 81 computer to perform this calculation and a listing of the program is given in Appendix 1.

3.7. Thermal cracking experiments

3.7.1 The thermal cracking of n-butane

n-butane was thermally cracked, at various temperatures ranging from $550^{\circ}C$ up to $750^{\circ}C$, according to Section 2.3.6.1.

The product gases were analysed by gas chromatography according to Section 2.3.6.4.1 and the results processed as detailed in Section 3.6.2.

The results, comprising the qualitative and quantitative product spectra arising from the thermal cracking of n-butane at various temperatures, are detailed in Table 7.

3.7.2 Mass balance

Carbon and hydrogen mass balances for the thermal decomposition of n-butane at $750^{\circ}C$ using the tubular reactor described in Section 2.3.6.1 are given in Table 8.

3.7.3   <u>Kinetic calculations for the</u>

                          <u>thermal cracking of n-butane</u>

3.7.3.1   <u>Rate constants</u>

Data obtained from the gas chromatographic analysis of the reactor gas, following the thermal cracking of n-butane at various temperatures, as given in Table 7 were used to calculate rate constants for the pyrolysis reaction.

The derivation of the rate equations used to calculate the rate constants is given in Appendix 2.

A program was written for a ZX 81 computer and used to calculate the rate constant data given in Table 9. A listing of the program is given in Appendix 3.

3.7.3.2   <u>Energy of activation</u>

The rate data in Table 9 was used to obtain the Arrhenius plot shown in Fig.81.

By graphical means the activation energy (Ea) for the first order thermal decomposition of n-butane was estimated to be 264 kJ mol^{-1}.

By calculation a corresponding value of 263 ± 17 kJ mol^{-1} was obtained.

The Arrhenius equation for the thermal decomposition of n-butane can be represented by $k_1 = (7.98 \pm 0.14) \times 10^{13} \, e^{-263 \pm 17/RT}$.

3.7.4   <u>The effect of potential catalyst supports</u>

                    <u>upon the   cracking of n-butane</u>

In order to assess their potential for use as catalyst supports, the influence on the cracking of n-butane at $653^{\circ}C$ of silica gel and two types of alumina, in various states of division, was investigated. The results, showing the influence of each material used as a reaction tube packing on the qualitative and quantitative product spectrum arising from the cracking of n-butane, are shown in Table 10.

3.7.5   <u>The thermal cracking of 2,2-dimethylbutane</u>

2,2-dimethylbutane was thermally cracked, at various temperatures ranging from $420^{\circ}C$ up to $600^{\circ}C$ and various flow rates between about 0.1 and 2.6 cm^3 min^{-1} according to Section 2.3.6.2.

The product gases were analysed by gas chromatography according to Section 2.3.6.4.2 and the results processed as detailed in Section 3.5.2.

The results, comprising the qualitative and quantitative product spectra arising from the thermal cracking of 2,2-dimethylbutane at various temperatures, are detailed in Tables 11, 12 and 13.

3.7.6   Mass balance

Carbon and hydrogen mass balances for the thermal decomposition of 2,2-dimethylbutane at $650°C$ using the tubular reactor as described in Section 2.3.6.2 are given in Table 14.

3.7.7   Kinetic calculations for the thermal
                               cracking of 2,2-dimethylbutane

3.7.7.1   Rate constants

Data obtained from the gas chromatographic analysis of the reactor gas, following the thermal cracking of 2,2-dimethylbutane at various temperatures and flow rates, as given in Tables 11, 12 and 13, was used to calculate discrete rate constants for each individual flow rate. By plotting these rate constants against the degree of cracking obtained, a series of linear plots can be obtained, one for each of the six temperature levels. The gradient of the plot is equivalent to the restraining coefficient (β) at that temperature. By plotting Log 10 β vs reciprocal absolute temperature multiplied by 1000, the temperature dependence of the restraining coefficient can be demonstrated, as shown in Fig. 82. From this graph an Arrhenius type equation can be obtained for the restraining coefficient. Thus, the equation for calculating the restraining coefficient when 2,2-dimethylbutane was cracked was derived as being :-

$$\beta = 3.555 \, (\pm 0.07) \times 10^6 e^{-108125/R.T}$$

From this equation a list of restraining coefficients at various temperatures may be obtained, as given in Table 15.

Having obtained the restraining coefficient for the cracking of 2,2-dimethylbutane, rate constants for the thermal and catalytic cracking of this particular hydrocarbon may be obtained by adopting an identical approach to that used for n-butane, as detailed in Appendix 2.

3.7.7.2 Energy of activation

The rate data in Table 16 was used to obtain the Arrhenius plot shown in Fig. 83.

By graphical means the activation energy for the first order thermal decomposition of 2,2-dimethylbutane was estimated to be 201 kJ mol^{-1}.

The Arrhenius equation for the thermal decomposition of 2,2-dimethyl-butane can be represented by $k_1 = 1.99 \, (\pm 0.93) \times 10^{12} \, e^{-201/R.T}$.

3.7.8 The effect of various supported phases on the cracking of 2,2-dimethylbutane

2,2-dimethylbutane was cracked under the influence of various phases, having a range of loadings, supported on both silica and $\propto$- alumina, at various temperatures ranging from 458°C up to 548°C, according to Section 2.3.6.3.

The product gases were analysed by gas chromatography according to Section 2.3.6.4.2 and the results processed as detailed in Section 3.5.2.

The results, comprising the qualitative and quantitative product spectra arising from the cracking of 2,2-dimethylbutane at various temperatures, can be found as detailed below.

Supported phase	Table numbers
base etioporphyrin I	17 to 20 inclusive
vanadyl etioporphyrin I	21 to 24 inclusive
nickel etioporphyrin I	25 to 28 inclusive
platinum etioporphyrin I	29 to 32 inclusive
palladium etioporphyrin I	33 to 36 inclusive
base hematoporphyrin IX	37 to 40 inclusive
vanadyl hematoporphyrin IX	41 to 44 inclusive
nickel hematoporphyrin IX	45 to 48 inclusive
petroporphyrin concentrate	49 to 52 inclusive

Typical chromatograms given by a 1.0% loading of the various phases on silica at a decomposition temperature of $497^\circ C$ are shown in Figs 84 to 92.

3.7.9   Mass balance

Carbon and hydrogen mass balances for the cracking of 2,2-dimethylbutane under the influence of vanadyl etioporphyrin and nickel etioporphyrin at $478^\circ C$ using the tubular reactor as described in Section 2.3.6.3 are given in Tables 53 and 54.

3.7.10   Kinetic calculations for the cracking of 2,2-dimethyl-
butane under the influence of various supported phases

Results obtained from the gas chromatographic analysis of the reactor gas, following the cracking of 2,2-dimethylbutane under the influence of various phases, having a range of loadings, supported on both silica and alpha-alumina, at various temperatures, as given in Tables 17 to 52 inclusive, were used to calculate kinetic data. Kinetic data similar to that obtained for the thermal decomposition of 2,2-dimethylbutane, as given in Table 16,

was derived for each loading of every phase, supported on both silica
and α-alumina. The necessary data was obtained using techniques previously
described for the thermal decomposition of both n-butane and 2,2-dimethyl-
butane. From this kinetic data Arrhenius plots were constructed which
were linear in every case. A summary of the kinetic data calculated,
including frequency factor and activation energy, can be found as
detailed below.

Supported phase	Table number
base etioporphyrin I	55
vanadyl etioporphyrin I	56
nickel etioporphyrin I	57
platinum etioporphyrin I	58
palladium etioporphyrin I	59
base hematoporphyrin IX	60
vanadyl hematoporphyrin IX	61
nickel hematoporphyrin IX	62
petroporphyrin concentrate	63

3.8. **Temperature programmed reduction**

3.8.1 **Temperature programmed reduction of
hematoporphyrins**

Temperature programmed reduction experiments were performed, as
described in Section 2.3.7, on small samples of unsupported base, vanadyl
and nickel hematoporphyrin IX.

In all cases the traces obtained from these experiments were straight

lines with virtually no baseline drift.

3.8.2   Temperature programmed reduction

                     of etioporphyrins

Temperature programmed reduction experiments were performed, as
described in Section 2.3.7, on small samples of unsupported base,
vanadyl, nickel and palladium etioporphyrin I.

In every case the traces, as given in Figs. 93, 94, 95 and 96
respectively, exhibit a high temperature adsorption peak.

3.9   Hydrogen chemisorption

3.9.1   --   Hydrogen chemisorption on synthetic

                     nickel etioporphyrin

The results of hydrogen chemisorption experiments, as detailed in
Section 2.3.8, performed on synthetic nickel etioporphyrin I are given
in Table 64 and shown graphically in Fig. 97.

At zero equilibrium pressure a monolayer is formed on the sample surface.

From the intercept of the interpolation of the linear region of the
hydrogen chemisorption graph, monolayer coverage is equivalent to
29.286 micromoles H_2 per g synthetic nickel etioporphyrin I.

MW nickel etioporphyrin I = 535.377

29.286 μmoles H_2/g porphyrin = (535.377 x 29.286) μmoles H_2/mole Ni

= 15679 μmoles H_2/mole Ni   = 0.015679 moles H_2/mole Ni

i.e. $\sim$1.57% of nickel atoms are available for hydrogen chemisorption.

3.9.2   Hydrogen chemisorption on 5.0% nickel

                         etioporphyrin on silica

The results of hydrogen chemisorption experiments, as detailed in

Section 2.3.8, performed on 5.0% nickel etioporphyrin on silica are

given in Table 65 and shown graphically in Fig. 98.

At zero equilibrium pressure a monolayer is formed on the sample

surface.

From the intercept of the interpolation of the linear region of the

hydrogen chemisorption graph, monolayer coverage is equivalent to 66.57

micromoles H_2 per g of supported nickel etioporphyrin.

66.57 µmoles H_2/g supported porphyrin =

                    1331.4 µmoles H_2/g nickel etioporphyrin

MW nickel etioporphyrin = 535.377

1331.4 µmoles H_2/g porphyrin = (535.377 x 1331.4) µmoles H_2/mole Ni

= 712801 µmoles H_2/mole Ni

= 0.712801 moles H_2/mole Ni

i.e. $\sim$ 71.3% of nickel atoms are available for hydrogen chemisorption

assuming silica support has zero adsorption and experiences no spillover.

3.9.3   <u>Hydrogen chemisorption on 5.0% palladium</u>

                            <u>etioporphyrin I on silica</u>

$1.0 cm^3$ of 5% hydrogen in argon gave a calibration peak of area 26.0 square

units. i.e. $0.05 cm^3 H_2 \equiv 26.0$ square units.

$0.2g$ of 5.0% palladium etioporphyrin I on silica gave a chemisorption peak

of 38.5 square units.

Chemisorption = $\dfrac{38.5}{26.0} \times 0.05 = 0.074 \ cm^3 H_2$

Number of atoms in $0.074 cm^3$ of hydrogen.

$\dfrac{0.074}{22413.6} \times 6.0225 \times 10^{23} \times 2 = 3.977 \times 10^{18}$ atoms.

Number of surface palladium atoms per m^2 on a polycrystalline surface

$= 1.27 \times 10^{19}$ (122).

From this value the area of one palladium atom = $\dfrac{1}{1.27 \times 10^{19}} = 7.87 \times 10^{-20} m^2$

For $0.2g$ of 5.0% palladium etioporphyrin I on silica palladium area is

$(3.977 \times 10^{18}) \times (7.87 \times 10^{-20}) = 0.313 \ m^2$

(Stoichiometry of hydrogen chemisorption on palladium = 1:1)

For 1.0g, palladium area = $\dfrac{0.313}{0.2} = 1.565 \ m^2$

Since 1.0g of catalyst $\equiv$ 0.05g of porphyrin and palladium etioporphyrin I

is 18.28% Pd and the porphyrin was 90.63% pure, 1.0g of catalyst will contain

$0.05 \times 0.1828 \times 0.9063 = 8.2836 \times 10^{-3} g$ Pd

Area of 1.0g of palladium atoms in palladium etioporphyrin I is

$\dfrac{1.565}{8.2836 \times 10^{-3}} = 189 \ m^2$

If, hypothetically, all palladium atoms were available for chemisorption then the area of 1.0g of palladium atoms is

$$\frac{6.0225 \times 10^{23}}{106.4} \times 7.87 \times 10^{-20} = 445.5 \text{ m}^2$$

Therefore, palladium atoms available for hydrogen chemisorption assuming silica support has zero adsorption and experiences no spillover

$$\frac{189}{445.5} \times 100 = 42.4\%$$

3.10   The hydrogenation of 1-hexene

Hydrogenation experiments were performed according to Section 2.3.9

using 1-hexene as the hydrocarbon feed.

The hydrocarbon feed was treated under a variety of conditions

including using helium as the carrier gas (effectively thermal cracking),

using 5% hydrogen/95% argon as the carrier gas and examining the influence

of silica as a reaction tube packing. These experiments were performed

over a range of temperatures and the results are given in Table 66.

Hydrogenation of 1-hexene over various phases supported on silica or

alpha-alumina was examined and these results can be found as detailed below.

High temperature experiments

Supported phase	Table number
base etioporphyrin I	67
vanadyl etioporphyrin I	68
nickel etioporphyrin I	69
palladium etioporphyrin I	70
base hematoporphyrin IX	71
vanadyl hematoporphyrin IX	72
nickel hematoporphyrin IX	73

Low temperature experiments

Supported phase	Table number
nickel etioporphyrin I	74
palladium etioporphyrin I	75
vanadyl hematoporphyrin IX	76

4.   DISCUSSION

4.1   Porphyrins

4.1.1   Choice of Model Compounds

The most commonly occurring and abundant trace metals in crude oils
are vanadium and nickel. Although metals other than these are sometimes
present, their concentrations will be at least an order of magnitude
lower than the total nickel and vanadium content. In addition, Barwise
and Whitehead (20) have stated that the complexes of vanadium occurring
in crude oils bond exclusively as the vanadyl ion. Thus, as the nickel
and vanadyl porphyrin complexes, which are the most thermodynamically
stable, are the two most commonly found in crude oils, it was evident
that both these metallocomplexes should be studied.

Although the group VIII transition metals are either totally absent
from crude oils or present only in very small concentrations, these
elements and their compounds are proven and well known catalysts for a
range of chemical reactions. For this reason the effect of both platinum
and palladium porphyrin complexes on the cracking of a model hydrocarbon
was studied.

The porphyrin macrocycles found in crude oil systems are usually
associated with transition metals. However, this is not exclusively the
case and the presence of free porphyrin bases in crude oils has been
reported. Since the concentration of these species is at most one percent
of the total porphyrin content of crude oil and the methods for their
detection and analysis are not well developed, very little information
is currently available (39). However, since free base porphyrins have been
positively identified in crude oil the effect of these species on the

cracking of a model hydrocarbon was studied.

Of the various porphyrins, mainly metalloporphyrins, which have been used to catalyse a whole range of reactions, including oxidation, reduction, isomerisation and decarbonylation, the vast majority of the results have been derived from work performed with the polymethine substituted porphyrin tetraphenylporphyrin (TPP) and its derivatives. Instances of the use of octaethylporphyrin and other porphyrins bearing beta substituents, are considerably less common. Thus, probably due to the relative ease of synthesis, TPP is a commonly used model compound for catalytic studies involving porphyrins. However, it has been concluded that polymethine substituted porphyrins are not present in crude oils, on the basis of the absence of certain characteristic absorption bands in electronic spectra. Thus, as these pigments do not occur in crude oils, the polymethine substituted porphyrins, as a whole group, were rejected as suitable model compounds for this study.

Of the five different homologous series of porphyrins found to be present in crude oils, namely: etio, DPEP, di-DPEP, rhodo-etio and rhodo-DPEP, the two most abundantly occurring species are etio and DPEP. Homologous series due to these porphyrins commonly span the range C_{26} to C_{40}, but of the large number of homologues and structural isomers possible within this range relatively few are found to be present in crude oil. Didyk, et al (49) have shown by oxidative degradation and mass spectrometric studies that identically beta substituted porphyrins were absent from samples of crude oil. Only unsymmetrical substitution patterns were observed and these were limited to methyl, hydrogen; ethyl, hydrogen; methyl, ethyl; methyl, propyl and ethyl, propyl. No others were experimentally determined in Lloydminster oil and the same

alkyl substitution pattern was revealed for the etio series

petroporphyrins derived from La Paz crude oil. Barwise and Whitehead (20,

31), Didyk, et al (49) and Hodgson, et al (39) have all indicated that

the most common alkyl beta substitution pattern for porphyrins of the

etio series is alternating methyl, ethyl with the series abundance

maximising at a molecular weight of 478.

Thus the choice of primary model porphyrin was narrowed to DPEP or

etio porphyrins having a methyl, ethyl beta substitution pattern. Yen

(16) has stated that the DPEP to etio ratio varies from 0.2 to 6, depending

upon the depth of the deposit. It would, therefore, seem that neither

porphyrin occurs more frequently, or at a greater concentration than the

other. Synthesis of any member of the DPEP series, with its isocyclic

ring, does present certain problems, mainly associated with the

formation of the fifth ring. These synthetic difficulties are not

insurmountable, but after consideration of the above factors it was felt

that a porphyrin from the etio series would make an ideal model compound.

Similar conclusions were reached by Bonnett, et al (48) who used vanadyl

octaethylporphyrin as a type substance for their stability studies and

Sugihara and Bean (63) who used the same porphyrin for experiments relating

to transalkylation. Although symmetrically beta substituted porphyrins

are easier to synthesise than similar compounds with an unsymmetrical

alkyl distribution, it was concluded that, since symmetrically substituted

porphyrins do not occur in crude oils, the most representative porphyrin

to take as a model would be etioporphyrin, with an alternating methyl,

ethyl substitution pattern around the ring periphery.

Hodgson, et al (27,39) have stated that the concentration of carboxy-

lated porphyrins, compared with similar species that are not carboxylated,

amounts to a maximum of 10% of the total. However, Baker, et al (57) have commented that carboxylated porphyrins are most probably too strongly held by the asphaltene fraction of the crude oil matrix to be easily recovered by methods that are currently available. Having recognised that polar porphyrins probably constitute a minor proportion of the total porphyrin content of any crude oil, this type of complex was considered worthy of investigation since their presence has been positively identified on a number of occasions. Hematoporphyrin IX was used for this aspect of the investigation.

Through the use of model complexes, information can be obtained relating to the action of porphyrins on the cracking of hydrocarbons. Although the data provided by the study of these reactions may be useful in its own right, the action that porphyrins indigenous to crude oil systems have upon the cracking of hydrocarbons can only be verified by isolation and subsequent investigation using these complexes. An attempt was thus made to obtain, in as pure a state as possible, a porphyrin rich concentrate from a sample of topped crude.

In conclusion, a total of nine different, but related, substances were defined as suitable for investigation in this study. Thus the effect that each of the following had upon the cracking of a model hydrocarbon was examined.

        Base etioporphyrin I

        Vanadyl etioporphyrin I

        Nickel etioporphyrin I

        Platinum etioporphyrin I

        Palladium etioporphyrin I

        Base hematoporphyrin IX

Vanadyl hematoporphyrin IX

Nickel hematoporphyrin IX

Petroporphyrin concentrate

4.1.2 Synthesis of etioporphyrin

Kenner and Smith (123) and Woodward (124) have stated that porphyrins bearing beta substituents, but which are unsubstituted on the methine bridges, are generally isolated from natural sources directly, or are derived from naturally occurring macrocycles by the simple transformation of one or two of the ring substituents. Porphyrins of this type may be totally synthesised but yields are generally low and the procedures tedious and time consuming. In contrast, porphyrins bearing substituents solely on the methine bridges are usually produced wholly synthetically and in quite high yields.

There are several ways of forming cyclic porphyrin systems, from monopyrroles, dipyrroles and tetrapyrrole intermediates. Evstigneeva (125) has indicated that the simplest route is a one step synthesis from mono-pyrroles. Unless the substituents around the ring are all identical, a mixture of structural isomers will be obtained by this method. This type of synthesis is very useful for the preparation of meso substituted porphyrins. Dipyrrolic species can also be used as intermediates in the synthesis of the porphyrin macrocycle, but Paine, et al (126) concluded that, in general, the yields of porphyrin obtained by using dipyrro-methenes as intermediates are usually low. Routes to porphyrins using tetrapyrroles have also been used. The linear tetrapyrroles are usually obtained by condensation of pyrrolic intermediates.

The first reaction sequence used during this study involved the formation of etioporphyrin from monopyrrole units. Having considered the above, it was felt that a reaction of this type would maximise the porphyrin yield obtained.

Initially trans-2-pentenoic acid was esterified, by reaction with methanol and concentrated sulphuric acid catalyst, to methyl trans-2-pentenoate. The general method given by Vogel (107) predicts a yield of ester in the region of 70%. A yield of 72.6% was actually obtained.

In the second step, according to van Leusen (108), tosylmethyl isocyanide, which is a stable and odourless crystalline isocyanide (127), reacted with the ester under basic conditions to give, by concomitant loss of toluene-4-sulphonic acid, methyl 4-ethylpyrrole-3-carboxylate. During the synthesis of pyrroles by this method the vinylic carbon atoms of the Michael acceptors became C_3 and C_4 of the pyrrole, and ring positions 1,2 and 5 remain free from substitution. Methyl 4-ethylpyrrole-3-carboxylate, which was prepared in a 77.9% yield, was not produced by van Leusen, et al, but the similar methyl 4-methylpyrrole-3-carboxylate was synthesised, providing a yield of 64%. Such compounds are relatively inaccessible by other methods, having previously been obtained by multi-step syntheses involving decarboxylation reactions at the nitrogen atom or C_2 position during the final stage of the reaction.

During the reduction stage, from Hinman and Theodoropulos (109), the carboxyl group attached to position three of the pyrrole ring was reduced to a hydrocarbon residue by the action of a three hundred times excess of lithium aluminium hydride. Although 3-ethyl-4-methyl pyrrole, produced in this case in a 39% yield, was not synthesised by Hinman and Theodoropulos, they did prepare 1,3,4-triscarbomethoxy pyrrole in a 50% yield, and reported that the yields of methyl pyrroles were higher from the reduction of an ester than from the corresponding acid.

Step four involved the reaction of the monopyrrole units of 3-ethyl-4-methylpyrrole with formaldehyde to form etioporphyrin in a single step

reaction. Cheng and Le Goff(110) reported that this type of acid catalysed condensation provided octasubstituted porphyrins, with no substituents on the meso positions, in high yields. They prepared octamethylporphyrin and octaethylporphyrin in 76% and 65 % yields respectively, but in this case etioporphyrin was only obtained in a 23.8% yield.

The synthetic route to etioporphyrin involving the four steps given above provided the required macrocycle in an overall yield of 5.3%.

In an effort to increase the overall yield of etioporphyrin a second synthetic route was investigated.

Although ethyl iodide is readily available and can be purchased from a number of chemical suppliers, it is a relatively expensive compound and so the synthesis of this haloalkane was undertaken according to the general method given by Vogel (107). The quantity of iodine used in the reaction was kept to a minimum while an excess of ethanol was employed. It was not foreseen that ethanol and ethyl iodide form a mixture which is inseparable by the technique of simple distillation. It was however, considered that the presence of ethanol during the subsequent step in the reaction chain would not prove detrimental, so no effort was made to separate the two components. However, it proved necessary, for the purposes of calculation of product yield, to perform an analysis of the mixture. Having done so, by both gas-liquid chromatography and liquid density measurements, the yield of ethyl iodide was calculated to be 39.2%. This figure is lower than the 90% yield predicted for this general class of reaction by Vogel (107).

Having obtained a suitable quantity of ethyl iodide, the method for the synthesis of etioporphyrin I supplied by Burr and Seddon (112) was followed.

The first step involved the reaction of ethyl iodide and 2,4-pentandione, in the presence of potassium carbonate, to give 3-ethyl-2,4-pentandione in a yield of 51.3%. This compares favourably with the 47.1% yield obtained by Burr and Seddon. Etioporphyrin I has also been prepared by Rislove, et al (111) using a very similar reaction sequence to that used in this study. Their yield of 3-ethyl-2,4-pentandione, using an identical reaction, was 79%.

The second step produced t-butyl 4-ethyl-3,5-dimethylpyrrole carboxylate via the sequence given in Fig. 34. The nitrous acid, produced by the action of acetic acid on sodium nitrite, reacts with the t-butylacetoacetate to give an oximino ester. Finely divided zinc and acetic acid together provide the nascent hydrogen required to reduce the oximino ester to an amino ester. This latter ester can then react with the 3-ethylpentan-2,4-dione to provide t-butyl 4-ethyl-3,5-dimethylpyrrole carboxylate. The pyrrolic product was obtained in a yield of 12.1%. An identical reaction performed by Barr and Seddon (112) gave a yield of 21.1%. Rislove, et al (111) synthesised the related compound ethyl 4-ethyl-3,5-dimethylpyrrole carboxylate, obtaining an overall yield of 65%.

During the third and final stage required to form etioporphyrin I, the t-butyl 4-ethyl-3,5-dimethylpyrrole carboxylate undergoes an acid catalysed condensation reaction via bromodipyrryl methene intermediates to give the desired product. Etioporphyrin I was obtained in a 33.7% yield which compares favourably with the 16.1% yield obtained by Barr and Seddon (112). From ethyl 4-ethyl-3,5-dimethylpyrrole carboxylate, Rislove, et al (111) followed a slightly differing reaction path from that described above. Their synthesis involved the isolation and subsequent purification of both a pyrrole and bromodipyrrole methene intermediate prior to the formation of the porphyrin. From the pyrrole carboxylate, Rislove, et al obtained

etioporphyrin I in a yield of 7.9%.

The second of the two synthetic routes described here gave etioporphyrin I in an overall yield of 2.1%. This compares well with the yield obtained by Barr and Seddon which totalled 1.6%. The reaction sequence followed by Rislove, et al, gave etioporphyrin I in an overall yield of 4.1%.

Etioporphyrin formed from monopyrrole units would certainly lead to an unknown mixture of structural isomers which would be inseparable and difficult to analyse. Etioporphyrin I obtained via bromodipyrrole methene intermediates would not produce such a mixture. Since there is no surety of the actual structures of petroporphyrins of a given molecular weight, the formation of an isomeric mixture of products, or otherwise, could not be viewed as being either an advantage or disadvantage.

The first route to etioporphyrin gave the desired product in an overall yield of 5.3% via four steps. The second sequence, leading to etioporphyrin I gave an overall yield of 2.1% via three steps (assuming that the formation of ethyl iodide is discounted). Although the yield of etioporphyrin obtained by the second route is only 40% of that obtained from the first method there are certain practical aspects which make the second sequence the more preferable of the two. Not only does the latter route involve one less reaction step but it also removes the necessity to handle hazardous chemicals, namely sodium hydride and lithium aluminium hydride. These are difficult compounds to manipulate and the destruction of their residues must be performed with great care.

The analytical data given by Rislove, et al (111) for 3-ethyl-2,4-pentandione, particularly boiling point and infrared spectrum and also for etioporphyrin I, specifically the ^{1}H nmr spectrum, agree particularly well with comparable data obtained during this study.

4.1.3   Synthesis of metalloporphyrins

According to Smith and Eivazi (128) metalloporphyrins have been synthesised with nearly every known metal. Complexes with the metal in a common oxidation state are usually prepared by direct reaction between the free base porphyrin and a metal compound, either simple salt, metal carbonyl, organometallic or co-ordination complex. Metalloporphyrins are virtually never synthesised by forming the porphyrin ring system around a metal ion using small molecules (metal template reactions), as is often the case with phthalocyanines, but the metal ion is inserted into the macrocycle structure following formation of the porphyrin ring. If the metal is required in an unusual oxidation state electrochemical techniques are frequently used. The ease and method of formation of metal complexes of porphyrins depends on the particular metal and its oxidation state and several general procedures have been developed. These methods have been reviewed by Ostfeld and Tsutsui (129) and include the insertion of a divalent metal ion by dissolving a suitable metal salt and the porphyrin in a refluxing solvent, either acidic or basic, such as glacial acetic acid or pyridine. However, these reaction techniques often contain some serious flaws. In an acidic medium the porphyrin exists primarily in the unreactive protonated form and these reactions typically require a large excess, usually several thousand fold and frequently higher, of the metallic species in order to force the reaction in the direction of the product. In basic media the reactivity of the metal is decreased by complexation with hydroxide ions, pyridine, etc.

It is likely that the rate of metal insertion into the porphyrin macrocycle is governed to a large degree by the dissociation of the ligands and/or solvent molecules from the first coordination sphere of

the metal. Another contributing factor to the rate, includes the proton abstraction from the base porphyrin. The higher the charge of the metal carrier, the more slowly it will react. This can be explained in terms of simple electrostatics. If a metal carries a high positive charge the anions and associated negatively polarized ligands will be strongly attracted. It therefore follows that a highly charged metal ion impedes the deconvolution of the metal carrier. For this reason it is advisable to use a metal source that contains the required metal in the lowest conveniently accessible oxidation state. Most metal insertions starting from divalent metal ions proceed quite quickly under comparatively mild reaction conditions. The incorporation of metal ions with charges between +3 and +5 usually requires prolonged heating. Preference for certain high or low coordination numbers by the metal in question also plays a role. For any given oxidation state the metal ion with the lowest coordination number will be more easily inserted. $VOSO_4 \cdot 5H_2O$ will insert vanadium smoothly, as the vanadyl ion, despite its high valancy.

The above solubility problem can sometimes be circumvented by the use of organometallic compounds for the metal source, e.g. diphenyltitanium. This requires the prior acquisition or preparation of the specific organometallic derivative, but it does allow the clean formation of a number of metalloporphyrins. Metal acetylacetonates are reasonably soluble in organic solvents, e.g. melts of phenol, quinoline and imidazole and they can be used in a ligand exchange reaction which forms a volatile product, thereby driving the reaction to completion. Instead of supplying the metal in the form of a complex, the problem of solubility can be overcome by using dimethylformamide as a solvent which, due to its high dielectric constant, is capable of dissolving both the free base porphyrin and a

metal salt. In a fairly recent development, Hermann, et al (130), inserted metal ions into porphyrins in a heterogenous reaction using solid metallic elements, or their oxides, finely divided, either in water or non-aqueous solvents. The main advantage of this method is that purification is extremely simple as any unreacted material can be filtered off as a solid. However, the metal ion in the oxide has to be in an oxidation state no higher than two and it was noted that no reaction took place with either metallic nickel or vanadium and that the insertion of nickel into octaethylporphyrin using nickel (II) oxide took in the region of two days, using a mixture of dimethylformamide and trichloromethane as solvent.

There is no direct correlation between rate of metal insertion and ionic radius. However, for an ion to be coplanar with the porphyrin the optimum ionic radius lies between 0.60 and 0.69Å.

Ions of nickel, palladium and platinum in the +2 oxidation state are all found to adopt a square planar configuration in the porphyrin system.

4.1.3.1 Vanadyl ion insertion into etioporphyrin

The classical method of vanadyl ion insertion into many porphyrins, as detailed by Erdman, et al (113), using the sulphate and glacial acetic acid, was used to prepare vanadyl etioporphyrin. Sodium acetate is added to buffer the solution and enhance deprotonation of the porphyrin. In the first of two separate reactions, which was performed on a fairly small scale, a yield of 94.5% of vanadyl etioporphyrin was obtained. The second synthesis was undertaken using a scale up factor of ten. This gave a yield of 79.8% of the single structural isomer, vanadyl etioporphyrin I.

Erdman, et al (113) produced vanadyl etioporphyrin I, using exactly

the same method, in a 95% yield.

4.1.3.2   Nickel ion insertion into etioporphyrin

In a similar method to that of Erdman, et al, the insertion of the
nickel (II) ion into etioporphyrin was attempted according to the
procedure given by McLees and Caughey (131). These authors heated a
mixture of glacial acetic acid, nickel (II) acetate and a porphyrin, to
give the nickel derivatives of mesoporphyrin IX dimethylester and deutero-
porphyrin IX dimethylester. A similar procedure was followed in an effort
to insert the nickel II ion into etioporphyrin. However, after product
work up, the supposed metalloporphyrin had exactly the same physical
appearance as the starting material. Later spectroscopic analysis confirmed
that the attempted metal ion insertion had failed and that the "product"
was unchanged etioporphyrin. As discussed previously, it was apparent that
the main problem centred around the simultaneous dissolution of both the
free base porphyrin and the metal salt under reactive conditions. Accordingly,
an alternative method was sought and that of Adler, et al (114) eventually
used. At the reflux point of dimethylformamide the solubility of both
porphyrin and metal salt is relatively high and thus both species may
readily react. Most reactions investigated by the authors gave yields in
excess of 90% with reaction times of less than five minutes. The high reflux
temperature not only facilitates rapid reaction, but readily displaces the
acidic products formed, thereby driving the reaction to completion. Although
the preparation of nickel etioporphyrin by this method was not reported,
many other metalloporphyrins were produced including seventeen derivatives
of tetraphenylporphyrin and nine other assorted metalloporphyrins. In this
case the synthesis of nickel etioporphyrin was performed twice. The first,
small scale preparation gave a yield of 99.0%. The second reaction,

undertaken using a scale up factor of ten, produced an overall yield of 77.9%.

4.1.3.3   Platinum ion insertion into etioporphyrin I

A successful attempt was made to prepare platinum etioporphyrin I using a similar technique to that employed for the formation of nickel etioporphyrin I. Refluxing DMF was used to simultaneously solvate the base etioporphyrin I and the platinum salt used, in this case tetraammine platinum (II) dichloride. Metal chlorides used by Adler, et al (114) gave high yields of the corresponding metalloporphyrin as the high reflux temperature of DMF forces the HCl evolved to escape, thus driving any reaction equilibrium to the right of the equation.

This reaction was performed on two separate occasions, providing product yields of 31.8% and 48.6% respectively. Eisner and Harding (132) prepared platinum etioporphyrin I by reacting base etioporphyrin I with bisbenzonitrile platinous chloride in refluxing benzonitrile. The required metalloporphyrin was obtained in a yield of 84% following product purification which included column chromatography and multiple recrystallisation. The above authors also attempted to prepare platinum meso-tetraphenylporphyrin by a similar method. In this case a considerably reduced yield was obtained and side reactions occurred leading to the formation of unidentified by-products.

4.1.3.4   Palladium ion insertion into etioporphyrin I

Having successfully prepared platinum etioporphyrin I, an identical approach, using refluxing DMF as solvent, was used in an effort to obtain palladium etioporphyrin I. Following reaction, the product porphyrin was filtered from the DMF solution when it was noted that the filtrate was

yellow in colour. Since the colour of the palladium/DMF solution was yellow prior to the addition of the base etioporphyrin I, the post reaction observation indicated that a residue of tetraamminepalladium II dichloride was present in the filtrate, even though a slight excess of base etioporphyrin I had been used during the synthesis. The presence of palladium in the product porphyrin was indicated by EDAX analysis, but since this instrumental technique will not detect carbon, nitrogen or hydrogen a quantitative analysis could not be undertaken. Quantitative analysis of the DMF filtrate was undertaken by employing the gravimetric method detailed in Section 2.3.2.4.3. Palladium is quantitatively precipitated by dimethyl-glyoxime from solutions of dilute mineral acids to give a yellow, water insoluble precipitate of palladium dimethylglyoxime. This compound has the same structure as the corresponding nickel complex. Since palladium is precipitated from dilute acid solutions and nickel is complexed only under very weakly acidic or ammoniacal conditions palladium may be detected by dimethylglyoxime without serious interference from other ions (115). This quantitative gravimetric analysis indicated, by difference between the quantity of palladium added to the reaction and that recovered from the filtrate, that the palladium etioporphyrin produced was 88.5% pure. Analysis performed on the solid product metalloporphyrin by the Johnson Matthey Technology Centre showed the palladium etioporphyrin to be 90.6% pure.
It can thus be concluded that palladium etioporphyrin I synthesised by the method detailed in Section 2.3.2.4.1 was obtained in a yield of 79.6% at an approximate purity of 90%.

4.1.3.5   Vanadyl ion insertion into hematoporphyrin IX

The method given by Erdman, et al (113) and detailed in Section 2.3.2.5, being generally applicable to the insertion of the vanadyl ion into porphyrins,

was used to insert this particular cation into hematoporphyrin IX. Following product purification by recrystallisation, a yield of 72.8% was obtained.

4.1.3.6   <u>Nickel ion insertion into hematoporphyrin IX</u>

Following the procedure given by Adler, et al (114) and detailed in Section 2.3.2.6 the Ni(II) ion was inserted into hematoporphyrin IX. A product yield of 72.3% was obtained after recrystallisation.

4.1.4   <u>Porphyrins from crude oil</u>

4.1.4.1   <u>Preparation of a petroporphyrin concentrate</u>
                 <u>from Tia Juana Pesado (topped crude)</u>

Since Alfred Treibs (62) positively identified the presence of metalloporphyrins in crude oil in 1934 numerous attempts have been made to isolate these tetrapyrrole pigments.

Initial attempts centred around the method given by Groennings (133). Suitable samples were treated with a mixture of hydrogen bromide and acetic acid. Porphyrins extracted by the acidic solution were transferred between ether and 20% hydrochloric acid solution before a final solvent extraction into trichloromethane. This method had a number of inherent disadvantages not least of which was due to the chemicals used during the extraction processes. These had the effect of promoting porphyrin decomposition in addition to removing the metal ions from the majority of the tetrapyrroles extracted.

Later separation techniques have employed chromatography as the almost universal tool and different methods have met with varying degrees of success.

One of the first studies employing chromatography was undertaken during 1956 by Dunning and Rabon (36). These authors deasphalted Oklahoma crude

with propane prior to chromatography using a silica gel column with hexane, cyclohexane, benzene, 10% acetone in benzene and pyridine as eluents. Three fractions were collected. The first fraction was chromatographed over alumina using hexane, cyclohexane, benzene, 10% acetone in benzene and acetone as eluents. One fraction was retained in this case and subsequently extracted with ethanol prior to further chromatography over alumina with hexane and benzene as the mobile phases. A concentrate rich in vanadium porphyrins was recovered from the extruded alumina. The second of the three fractions above was chromatographed over alumina using hexane, cyclohexane, benzene, 10% acetone in benzene and acetone to develop the column. The single fraction retained was further chromatographed over alumina with hexane and benzene developing an area rich in nickel porphyrins which was recovered from the extruded alumina. This fraction was further purified by chromatography over silica gel, the column being developed by hexane, cyclohexane, cyclohexane/benzene, benzene and benzene/acetone. The third of the three fractions obtained initially was chromatographed using an alumina column employing hexane, 70% hexane 30% trichloromethane, 40% hexane 60% trichloromethane and acetone to develop a fraction rich in vanadium porphyrins.

In 1957 Wilmington crude was chromatographically fractionated using first alumina and then magnesol-cellulose powder as adsorbents by Corwin, et al (134). Two fractions were obtained. The first contained nickel porphyrins which could not be further purified by chromatographic techniques. The second fraction contained vanadyl porphyrins which by chromatography and extraction was separated into three components. Two of these were obtained as crystalline solids.

Crystals of porphyrin exhibiting the etio type electronic spectrum were obtained by Fisher and Dunning in 1961 (38). A heavy asphaltic crude

was subjected to the removal of metals by hydrobromic acid/glacial acetic acid digestion. Extractable material was transferred to a 15% hydrochloric acid solution and then to benzene. This extract was chromatographed using an alumina column and benzene, 8% dioxane in benzene, 1% ethanol in benzene and aqueous ethanol as eluents. The first benzene fraction was further purified by passing this through a cellulose column and eluting with 2,2,4-trimethylpentane, 20% benzene in 2,2,4-trimethylpentane and benzene. The first 2,2,4-trimethylpentane cut was evaporated to dryness, dissolved in the minimum quantity of benzene and allowed to stand in order to encourage crystal formation and growth.

During 1963 Hodgson, et al (27) dissolved a sample of crude oil in the minimum quantity of benzene and exhaustively extracted this solution with methanol. The extracts were combined, evaporated to dryness, dissolved in n-hexane and chromatographed over silica gel. A fraction rich in nickel porphyrins was eluted with 50% benzene 50% hexane while vanadium porphyrins were developed with 50% trichloromethane 50% benzene.

Baker and Corwin (135) subjected a sample of Wilmington crude oil to chromatography over an alumina/magnesol-cellulose powder column. Two fractions were obtained, one containing vanadyl porphyrins, the other nickel porphyrins. The vanadyl bearing component was chromatographed over silica gel which allowed the recovery of three fractions. A solid material was not obtained in this case since additional chromatography failed to resolve the fractions further.

Nuzzi precipitated asphaltenes from the Venezuelan Bachaquero crude in 1965 by the use of pentane. 2,2,4-Trimethylpentane was employed to extract the asphaltenes and this extract was subjected to initial chromatography over silica gel. 2,2,4-Trimethylpentane, benzene, benzene/isopropyl alcohol

and ethanol provided a single fraction which was further treated using an alumina column. Benzene, benzene/isopropyl alcohol, isopropyl alcohol and ethanol eluted a vanadyl porphyrin rich fraction containing the tetrapyrrole species in a concentration of 5000 ppm (136).

During 1967 Branthaver, et al (137) obtained a concentrate very rich in vanadium petroporphyrins by using gel permeation chromatography followed by alumina and then silica gel column chromatography.

Ahwaz Iranian crude was dispersed onto silica gel and extracted with cyclohexane using a Soxhlet by Moghadam and Raisszadeh (19) during 1972. Following extraction, the silica gel was packed into the top of a chromatographic column already containing the same adsorbent and the retained material was eluted with dichloromethane. After removal of the solvent, a viscous oil was obtained which was dissolved in benzene and further chromatographed on silica gel using cyclohexane, benzene and 95% benzene/5% diethylether. The second and third cuts were shown to contain vanadyl porphyrins.

Sugihara, et al (138) took Boscan crude and deasphalted a sample using pentane precipitation during 1973. The resulting asphaltenes were dissolved in benzene and subjected to gel permeation chromatography using polystyrene cross-linked with divinylbenzene.

Filby (17) worked with two Califonian Tertiary crude oils as well as Boscan crude from Venezuela in 1973. Each of these oils was diluted with an equal quantity of benzene. After being centrifuged and filtered, asphaltenes were precipitated from the retained solid by n-pentane. The asphaltenes were fractionated by gel permeation chromatography using Sephadex LH-20 with benzene/methanol (90:10v/v). This was followed by column chromatography over silica gel with hexane/benzene (90:10v/v) being used to elute a fraction rich in nickel porphyrins. A cut containing vanadyl porphyrins was obtained by

elution with benzene. These fractions were further purified by chromatography over alumina.

Propane deasphalting of Romashkino crude with subsequent asphaltene precipitation using n-pentane was undertaken in 1975 by Sebor, et al (23). Following extraction of the asphaltenes in a Soxhlet with either acetone or acetonitrile, gel permeation chromatography over polystyrene cross-linked with divinylbenzene produced a porphyrin rich concentrate after elution with a benzene/methanol mixture.

Hungarian crude was extracted with acetonitrile by Lakatos-Szabo (26) in 1977 and deasphalted using 2,2,4-trimethylpentane to provide two fractions. The first of these cuts, which was soluble in 2,2,4-trimethylpentane, was chromatographed over silica gel. 2,2,4-trimethylpentane and acetonitrile were used to develop the column. The second of the above fractions, which was insoluble in 2,2,4-trimethylpentane, was chromatographed similarly using cyclohexane and acetonitrile as eluents. The porphyrin rich fractions from both of the above were combined and gel permeation over Sephadex LH-20 with a dimethylformamide mobile phase was used to obtain a hydrocarbon fraction that contained 2.1% porphyrins by weight.

During 1979 Sebor, et al (21) used propane to deasphalt Romashkino (USSR) crude and n-pentane to precipitate the asphaltenes present. The latter was extracted with acetone and acetonitrile prior to chromatography over silica gel using 50% n-heptane 50% benzene, 90% benzene 10% acetone and 50% benzene 50% methanol as eluents. A resulting fraction, rich in vanadyl porphyrins was further chromatographed over alumina. From this a vanadyl porphyrin concentrate was obtained of approximately 0.3% concentration with respect to the asphalt content of the crude oil.

Boscan distillate (500-650°C corrected to atmospheric pressure) was

Chromatographed over silica gel with heptane, toluene and ethyl acetate during 1980 by Barwise and Whitehead (20,31). The latter fraction, containing vanadyl porphyrins, was further chromatographed on silica gel which had previously been functionalised by an alkyl sulphonic acid (139). Elution with toluene and ethyl acetate afforded five fractions, three of which were shown to contain vanadyl porphyrins. These three cuts were further purified using silica thin layer chromatography plates. A toluene mobile phase gave both rhodo and non-rhodo porphyrins of vanadium.

Porphyrins were also separated from Boscan crude in 1980 by Martin, et al (140). A sample was dissolved in dichloromethane and chromatographed over alumina using dichloromethane, dichloromethane/methanol, and methanol. The various fractions were combined and the solvents evaporated to leave a black viscous residue. This was dissolved in toluene and run through an alumina column. Toluene/hexane, toluene, toluene/dichloromethane, dichloromethane, dichloromethane/methanol and methanol were used as eluents. One fraction was retained and the solvent was evaporated prior to dissolving the residue in dichloromethane/hexane. This solution was further purified using a silica gel column with hexane, hexane/dichloromethane and dichloromethane. Three fractions were obtained which, following work-up, provided a crystalline product.

During 1980 Chakraborty and Virendra (4) topped Darius crude from Iran at a temperature of $140^{\circ}C$, deasphalted with propane and adsorbed the resulting asphaltenes on kieselguhr prior to extraction with acetonitrile containing a small quantity of benzene. The resultant extract was chromatographed over silica gel using five different solvents to elute two fractions which were respectively nickel and vanadyl porphyrin bearing.

One of the above authors (141) extended this work on Darius crude oil

during 1981. Their separation method was initially as above. The fraction rich in vanadyl porphyrins was further chromatographed twice over silica gel, once over alumina and finally using TLC. The second fraction, of predominately nickel porphyrins, was further chromatographed three times over silica gel prior to the separation of three zones using TLC. Following extraction each of these zones was analysed and no nickel porphyrin was detected. It was assumed that any pigment that may have been present was decomposed by the action of the various chromatographic processes.

A number of salient points arise from this review of the various techniques employed to separate porphyrins from crude oils. Although many attempts have been made over a number of years to isolate solid crystalline porphyrins, very few have succeeded in this aim. Some authors provide insufficient experimental detail to reproduce exactly their findings. Barwise and Whitehead (20,31) had apparently developed a powerful separation technique using silica gel functionalised with an alkyl sulphonic acid. This aspect of their work was the subject of a British patent application (139). This application was subsequently withdrawn and as such the experimental detail has not been available. Chakraborty and Bhatia (141) demonstrated that if the separation process is protracted and convoluted there is a risk of decomposing, or otherwise losing, the porphyrins required from the method.

Having taken the above into consideration the method according to Berti, et al (116) was used to prepare a petroporphyrin concentrate from topped Tia Juana Pesado. The technique consisted of three main elements. Initial hot extraction of the topped crude using a liquid-liquid extractor with acetonitrile yielded a porphyrin enriched, substantially asphalt free extract. The second stage consisted of concentration of the extracted petroporphyrins by partition chromatography on acetonitrile inpregnated

silica gel using 2,2,4-trimethylpentane as the eluent. Final purification of the porphyrin concentrate used adsorption chromatography over alumina. It is important that the crude oil contains a considerable proportion of aromatics since these are able to peptise the asphaltenes and promote diffusion of the solvent into the latter during initial liquid-liquid extraction. The asphaltene content of Tia Juana Pesado topped crude was determined according to the method detailed in Section 2.3.3.1. The average asphaltene content was found to be 15.1%. Berti, et al added between 25% and 50% of either ditolylmethane or dixylylmethane synthetic heavy aromatic oil to the crude prior to extraction depending upon the asphaltene content. Since 15.1% asphaltenes represents a moderate amount in comparison to other crudes, diphenylmethane was added to Tia Juana Pesado crude before extraction at the level of 37.5% by weight. Quantitative extraction can be obtained by using between 5% and 15% benzene in acetonitrile. When pure acetonitrile is used extraction levels obtained range between 60% and 80% of the porphyrins present. Acetonitrile is effective and selective in the extraction of petro-porphyrins and also has a weak aptitude to extract and entrain brown asphaltous products. The use of acetonitrile/benzene mixtures ensures high yields are obtained at the expense of increased carry over of asphaltous material in to the extract such that the subsequent concentration and purification steps become considerably protracted. In consideration of the latter point pure acetonitrile was used for the extraction of petroporphyrins during this study since quantitative extraction was not vital. Following extraction, concentration and purification, this method yielded vanadium petroporphyrins in the form of a purple crystalline solid when Boscan crude was studied by Berti, et al (116). Having followed the procedure given in Fig. 99 Tia Juana Pesado topped crude provided a viscous oil that was light brown/red in colour.

4.1.4.2   Analysis of a petroporphyrin concentrate

Analysis of the petroporphyrin concentrate obtained via liquid

extraction and chromatography was performed according to Section 2.3.3.4.

From the UV spectrum, as shown in Fig. 42, it can be seen that the maximum

occurs at a wavelength of 407nm. A study of Santa Maria Valley crude by

Skinner (13) revealed a peak with a maximum in exactly the same position

as that reported above. Beach and Shewmaker (34) did not use the peak

occurring at 407nm in order to estimate the quantity of metalloporphyrins

present in Tia Juana Pesado and Bachaquero crudes because of the high

background absorption of their extracts. They concluded that the use of this

peak offered no advantage over the peaks that occurred at higher wavelengths.

A contrary deduction was reached by Costantinides, et al (51) and Sugihara

and Bean (63). Changes in groups peripheral to the porphyrin ring have much

less effect on this intense, Soret band than on the peaks in the visible

range.

Sugihara and Bean (63) adapted the method of Costantinides, et al (51)

such that metalloporphyrins in crude oil samples could be determined

directly. Accordingly, the method of the former authors was used during

this study. The direct method of determination of metalloporphyrins is

simple and quite rapid where losses of porphyrin species due to incomplete

metals removal, decomposition and incomplete extraction are eliminated. The

intensity of the Soret band is measured by integrating the area defined by

the absorption curve and a curved line which approximates as closely as

possible the background absorption. Although the Soret band is less

dependent upon structural variations, the presence of several different

molecular species in a porphyrin aggregate with absorption peaks at slightly

different wavelengths would flatten this band. Thus, when compared with

simple peak height measurement, integration of the area under the band provides more accurate quantitative analysis of porphyrin contents.

By using an appropriate extinction coefficient it is possible to calculate the concentration of metalloporphyrins present. Considerable variances in the content of polar porphyrins has only a slight effect on the magnitude of the extinction coefficient. Vanadyl and nickel porphyrins have distinctly different Soret extinction coefficients. Accordingly, a reasonable estimate of the ratio of the two types of porphyrins is necessary. Berti, et al (116) obtained a porphyrin rich extract from Tia Juana crude oil and quoted a vanadium : nickel ratio of 16:1. Sugihara and Bean (63) gave integral extinction coefficients for analytical samples of both vanadyl etioporphyrin I and nickel etioporphyrin I. If it is assumed that these two species predominate in the porphyrin concentrate obtained by extraction and chromatography, then arithmetic manipulation of the values gives an integral extinction coefficient of 4.63×10^6 $dm^3 nm$ $mole^{-1} cm^{-1}$ for Tia Juana Pesado.

4.2.   Equipment design considerations

4.2.1   Reactor

A tubular cracking furnace consists of three parts, a preheater, a cracking section and a means of quenching the reactions. The preheater raises the temperature of the feed to a value slightly lower than the required cracking temperature. In the cracking section the tube is exposed to the required temperature where the feed will have a set residue time before the effluent from the reactor is rapidly cooled in the quench section.

The cracking reactions are consecutive and usually first order, thus

crackin- should be performed as quickly as possible with the reactions being halted with similar rapidity. For this to happen a short residence time and hi-h temperatures are required. The rate of coking increases with feed pressure. This should be as low as possible with the hydrocarbon partial pressure being reduced further by dilution with an inert gas or vapour.

Wan-, et al (142) studied the thermal decomposition of n-butane in a flow reactor at a total pressure of one atmosphere, operating at low conversions and a temperature range of 460-560°C. Under these conditions, the above authors concluded that the reactor could be treated as an isothermal plug flow unit.

In order to ensure isothermal operation the pyrolysis reactor was designed such that the hydrocarbon feed could be diluted with an inert gas. By diluting the reactant gas or vapour, the volumetric changes occurring during the thermal decomposition process could also be minimised. In addition, reduction of the hydrocarbon feed partial pressure reduces the risk of coke formation.

Pacey and Purnell (143) have indicated that substantial discrepancies between rate data originating from different sources have been traced to the effects of small quantities of oxygen in the diluent gas. In order to avoid the marked influence of traces of oxygen Murata and Saito (144) used highly purified nitrogen (greater than 99.999% nitrogen) as the diluent gas for their pyrolysis studies and Sandler and Tanewala (145) reported employing helium. Accordingly it was decided that helium, having a minimum purity of 99.995%, would be a suitable diluent gas for use during this investigation.

In their study of the thermal decomposition of n-butane using an isothermal flow reactor at a total pressure of one atmosphere, Sandler and

Lanewala (145) used chromel-alumel thermocouples to measure reaction furnace temperatures. A similar device was employed by Sandler and Chung (146) in their isothermal reactor, which was also equipped with a preheating section. They measured gas stream temperatures directly and took similar readings at the reactor walls. These authors concluded that under conditions of low hydrocarbon feed conversion, any differences between the gas stream temperature and that of the reactor wall were negligible. Thus in order to simplify the construction of the reactor, temperature measurements were all taken at the wall of the reactor tube by the use of a chromel-alumel thermocouple.

4.2.2   Hydrocarbon feed

n-Butane was chosen as the hydrocarbon feed material for the initial study of thermal decomposition reactions as it is an easily handled gas, allowing simple flow control and volumetric measurement. Additionally and more importantly, as Purnell (147) commented, the pyrolysis of n-butane is almost entirely homogenous, is insensitive to the condition of reactor surfaces, is only significantly self inhibited at quite large hydrocarbon conversions, is the least affected by mechanistic complexities and is one cracking reaction where traces of oxygen have little effect. There is a large amount of kinetic data available in the literature concerned with the thermal decomposition of n-butane. This allows a comparison between experimentally obtained results and those published and accepted as correct. Additionally an assessment of the reactor construction and operating conditions, as well as the applicability of kinetic models, may be made.

Any real evidence of the thermal breakdown of n-butane did not occur until a temperature of $550^{\circ}C$ had been reached. Although temperature programmed decomposition tests indicated that both nickel and vanadyl

etioporphyrins supported on silica gel were thermally stable up to at least $540^{\circ}C$, some porphyrinic compounds start to break down at temperatures as low as $430^{\circ}C$. During this study of the effects of metalloporphyrins on the thermal decomposition of hydrocarbons it was intended to operate the reactor at a temperature corresponding to a pyrolysis level of about 10%. If n-butane was used as a reactant this would correspond to a temperature of $654^{\circ}C$, almost certainly resulting in the total thermal degradation of the metalloporphyrin over a short time scale. It was thus evident that an alternative feed material was required which would begin to decompose at a much lower temperature than n-butane. Zdonik, et al (148) have stated that the chemical reactions which occur when hydrocarbons are decomposed under the influence of heat are quite complex, the degree of complexity increasing with an increase in the molecular weight of the hydrocarbon being pyrolsed, and also with increasing conversion. Thus, it was desirable that an alternative feed material to n-butane should be a gas or liquid, for ease of handling, should start to decompose at a much lower temperature than n-butane, but that the carbon skeleton should not be too complicated or long, such that the number of products evolved on pyrolysis would be so great as to make chromatographic separation difficult.

Since carbon to carbon bonds are in the order of 67 $kJmol^{-1}$ weaker than carbon to hydrogen bonds it follows that only the homolytic cleavage of carbon to carbon bonds need be considered as being responsible for thermal decomposition reactions. According to Doue and Guiochon(149), the difference in values for the enthalpy of formation of tertiary radicals is quoted as being between 29.2 and 35.2 $kJmol^{-1}$ lower than for the formation of primary radicals. Thus as tertiary radicals are formed at a lower energy input they are more stable and hence produced more quickly,

than either secondary or primary radicals. It therefore seemed desirable that the chosen feed compound should contain a quaternary carbon atom in order to facilitate tertiary radical formation. The simplest hydrocarbon containing a quaternary carbon atom is 2,2-dimethylpropane. At the onset of pyrolysis this hydrocarbon should decompose, by the homolytic cleavage of a carbon to carbon bond, into a tertiary radical and a methyl radical. However, ethyl radicals are more stable and will therefore be formed faster than methyl radicals and the hydrocarbon 2,2-dimethylbutane should thermally decompose to give a teriary radical and an ethyl radical.

It was thus considered that 2,2-dimethylbutane would start to decompose at a suitably low temperature, without evolving an inseparable mixture of products, such that it would make a convenient feed material for a study of the effects of metalloporphyrins on the pyrolysis of hydrocarbons.

By experiment this consideration was proven. Reference to Table 11 shows that the onset of thermal decomposition of 2,2-dimethylbutane occurs at approximately $420^{\circ}C$. An extent of conversion of 10% is reached at a temperature of $478^{\circ}C$. At $550^{\circ}C$ the severity of cracking has attained a value of about 32%.

Since seven different supported porphyrins were shown to exhibit no evidence of thermal decomposition up to $540^{\circ}C$, this demonstrates that a feedstock of 2,2-dimethylbutane can be cracked in their presence, to large extents of conversion without any thermal deterioration of the supported macrocycle occurring.

4.3   Product separation by gas-liquid chromatography

Ettre (150) stated that gas-liquid chromatograph FID response for hydrocarbons is a function of the number of carbon atoms in the molecule

and that this function is linear for saturated hydrocarbons, unsaturated hydrocarbons and aromatics. However, from Figs 78 and 79 it is evident that the chromatograph used during this investigation produced some curvature of the detector response vs carbon atom number graphs. This curvature was allowed for by calculating factors from experimentally obtained chromatographic data, as shown in Table 6. These factors then allow an evaluation of product concentrations to be made from chromatograph integrator readings.

As demonstrated by Fig 80, for 2,2-dimethylbutane, detector response increases linearly as hydrocarbon concentration increases over at least an order of magnitude. It was thus considered that the above factors (single points) would be sufficient to allow the accurate estimation of the quantity of a product in the reactor effluent, rather than resorting to the construction of a calibration graph for each individual compound.

4.4   The thermal decomposition of n-butane

4.4.1   Product distributions

The pyrolysis of alkanes proceeds initially through primary reactions and then,as the temperature rises, through secondary reactions. During the first stages of cracking the primary reactions are dominant but, as conditions become increasingly severe, the products formed by the primary processes undergo thermal decomposition in secondary reactions. At incipient levels of pyrolysis the primary products of n-butane decomposition were determined, by gas-liquid chromatography, in this study to be methane, ethane, ethene and propene. Several other investigators, including Murata and Saito (144), Powers and Corcoran (151) and Purnell and Quinn (152) have also found the above four hydrocarbons to be primary products of n-butane pyrolysis.

In the temperature interval investigated, the yields of methane, ethane, ethene, propene and 1-butene all increased with increasing temperature, as shown in Table 7. This is in agreement with the findings of Zdonik, et al (148) and Sandler and Chung (146). With increased conversion the increasing yields of methane and ethane are particularly noticeable, as additional quantities of these hydrocarbons are realised due to the onset of secondary pyrolysis reactions. A similar trend was also noticed by Zdonik, et al (153).

It is generally recognised from studies such as those conducted by Sandler and Chung (146) and Zdonik, et al (148) that the yield of propene and the butenes will pass through a maximum at severity levels where the rate of disappearance just equals the formation rate. However, the pyrolysis temperatures employed in this study were too low for this effect to be noticed as it does not occur until temperatures in excess of $800^{\circ}C$ are reached.

Minor products detected include 1-butene and propane, the concentration of which remained fairly constant irrespective of temperature. Minor products noted in other investigations include propane, butenes, pentenes, hexenes, hexadienes, octadienes and depending upon the reaction conditions used, benzene and a trace of toluene. No products containing a greater number of carbon atoms than the feed material were detected during this study, but the finding that the sum total of the minor products does not exceed 2% is in agreement with previous works.

Results for the degree of conversion of n-butane at various temperatures, obtained during this study, appear to lie at the bottom end of, but within, the range of values to be found in the literature. A report by Poyhonen and Veijola (154) gave conversions ranging from 0.4 to 32.5% at temperatures of 490 and $675^{\circ}C$, compared with figures of zero and 22.3% obtained at similar

temperatures during this investigation. Powers and Corcoran (151) studied

the thermal cracking of n-butane in a gold tube reactor at temperatures of

515 and 605°C. The butane was diluted by an inert gas such that mole

fractions of between 0.01 and 0.9 were recorded for the reactor feed. Under

these conditions, conversions ranging from 0.03 to 7% were noted compared

to zero and 3.1% obtained during this study. Kitzen (155) determined the

extent of conversion to be 75.8% at a temperature of 762°C. This compares

to a value of 79.7% obtained here at the slightly lower temperature of

750°C. Kitzen (155) also reported lower yields of methane and ethene, but

higher concentrations of ethane, propane and the butenes than those quoted

in Table 7. This author also claims to have detected a trace of acetylene

and quite substantial quantities of C_{5+} compounds, none of which were

observed under the experimental conditions used here.

4.4.2   Kinetic data

The methods devised for the calculation of kinetic data relating to the

pyrolysis of alkanes and in particular n-butane, have been many and various,

being based on practical or theoretical considerations, or a mixture of both.

Voge and Good (102) derived an empirical equation for the evaluation of first

order reaction rate constants that was of general applicability to a number

of n-alkanes possessing between four and sixteen atoms in their carbon

skeletons. Purnell (147) assessed the kinetics of alkane pyrolysis by

considering the Rice free radical reaction mechanism and then taking into

account a number of secondary reactions. Kinetic calculations based on the

classical first order rate equation, but with additional terms to take into

account the energy of vibrational degrees of freedom, were used by

Partington (156). From this study it was concluded that, after propane,

the rate of thermal decomposition was almost independent of the size or

shape of the molecule. The kinetic equations formulated by Murata and Saito (144) were based upon the simulation of the experimental results which they obtained. Powers and Corcoran (151) used the kinetics devised by Pacey and Purnell (157), but adapted them by taking into account the effects of secondary reactions. Berces, et al (158) evaluated activation energies from known bond dissociation energies, assuming zero for the activation energy of the reverse reaction i.e. radical recombination. Pre-exponential factors were obtained by estimating the essential changes in the rotational, internal rotational and vibrational entropy contributions during the activation process.

Most investigators agree that there is little doubt as to the pyrolsis inhibiting nature of certain products of secondary reactions, but there is some disagreement as to the point of inhibition onset and the extent to which kinetic equations need to be modified in order to take account of this phenomenon. It has been stated that strong self inhibition appears at extents of reaction in excess of about 15% for n-butane pyrolysis. However, Purnell (147) considered that the overall reaction rate of the pyrolysis of small alkanes could be reduced by as much as an order of magnitude, with respect to the initial rate, at only a few per cent conversion. Pryor (101) attributed the mechanism of self inhibition to hydrogen atom abstraction by ethene and more importantly, propene. In order to circumvent this problem a number of workers in this area have used factors, either theoretically or empirically derived, in order to allow for this self inhibition of the pyrolysis reaction. Alternatively, according to the advice of both Sandler and Lanewala (145) and Wang, et al (142), only results obtained at low levels of conversion (typically less than 10%) should be used in the calculation of kinetic data.

Accordingly, the kinetic equations given by Illes (173), which were derived mainly through theoretical considerations, but also take into account the self inhibition discussed above through the use of an empirical restraining coefficient, were used during this study. The kinetics given by this author were considered particularly appropriate. An isothermal, isobaric continuous tubular reactor was used to pyrolyse n-butane at a total pressure of one atmosphere, over the temperature range 600 to 820°C. This equipment, and the conditions used, correspond very closely to those employed for this investigation. By the use of the kinetic equations according to Illes (173) the first order rate constants given in Table 9 were obtained. These compare favourably with thoses obtained in Zdonik, et al (148) over a wide temperature range.

Zdonik, et al (148) have stated that the rate of disappearance of a hydrocarbon feed during vapour phase pyrolysis is generally independent of both pressure and the volume to surface area ratio of the reactor. Thus, the reaction can be considered to be unimolecular and follow a first order mechanism. Sandler and Lanewala (145) have studied the effect of diluting n-butane with an inert gas, prior to pyrolysis, such that the mole fraction of n-butane varied between 0.25 and 1. The quantity of feed material cracked remained virtually constant, irrespective of initial concentration, indicating that the reaction is essentially a first order process.

From the Arrhenius plot given in Fig 81 an activation energy of 264 kJmol^{-1} was calculated for the thermal decomposition of n-butane. This result compares very favourably with activation energies obtained by other investigators. It has been reported by Sandler and Lanewala (145) and Wang, et al (142) that values appearing in the literature for the activation energy of the thermal decomposition of n-butane span the range 180 to 310 kJmol^{-1},

with figures at the lower end usually being obtained from investigations involving flow reactors. Sandler and Chung (146) state that the generally accepted value for the activation energy for the thermal cracking of n-butane is 246 kJmol^{-1}, but that in studies with flow systems results from 257 to 309 kJmol^{-1} have been obtained. Other values quoted include 213 kJmol^{-1} by Sandler and Lanewala (145) and 251 kJmol^{-1} by Sagert and Laidler (159), this figure rising to 261 kJmol^{-1} for a reaction vessel contaminated by a thin layer of coke. In addition, general figures of 247 kJmol^{-1} by Frey and Smith (160) and 272 kJmol^{-1} by Tilicheyev (161) have been quoted for the activation energies of the thermal decomposition of small alkanes.

4.4.3   Reaction mechanism

Purnell and Quinn (162) have reported that identical and reproducible reaction rates were obtained for up to a 9% conversion of n-butane using different reaction vessels that exhibited a four fold change in the surface area to volume ratio. A similar result was noted as the state of the reactor surface was varied from clean and polished, through clean and etched to potassium chloride coated pyrex. The absence of marked effects due to changes in the surface area to volume ratio and various reaction vessel surface treatments was attributed to being entirely compatible with a free radical mechanism, initiated and terminated homogeneously. Sagert and Laidler (159) also reached similar conclusions from their investigation.

If the pyrolysis of hydrocarbons is taken as being first order and homogeneous then the rate determining step, which in this case is the initiation stage, can only involve the homolytic decomposition of a single species. Since the carbon to hydrogen bond is both shorter and stronger than the carbon to carbon single bond (by 0.45 Å and 64 kJmol^{-1} respectively

(163))only the homolytic cleavage of the carbon to carbon bond need be considered during the initiation process. Therefore initiation of the thermal decomposition of n-butane may be represented by the equations given in Fig 100. The homolytic cleavage of an n-butane molecule into a methyl and a propyl radical can be regarded as the least significant of the two processes as Sagert and Laidler (159) have indicated that the dissociation energy required for this reaction is in the region of 17 kJmol^{-1} higher than for a split into two ethyl radicals.

The initial products arising from the pyrolysis of n-butane are methane, ethane, ethene and propene. Accordingly, the propagation steps of the thermal decomposition mechanism, shown in Fig 101, give these four hydrocarbons as products as well as allowing for the production of butenes. Thus, only five free radicals, hydrogen, methyl, ethyl, butyl and to a lesser extent propyl, are important in the chain propagation processes. Formation of free radicals such as $\overset{\bullet}{C}H_2$ is not likely due to energy considerations. Wang, et al (142) have indicated that free radicals larger than ethyl will decompose directly to an alkene and a smaller radical, rather than react directly with another free radical or molecule. A feature of the mechanism illustrated here is that free radicals containing more than four carbon atoms are not considered. The presence of species of this nature would lead to products such as hexane and heptane through combination and disproportionation. However, none of these higher molecular weight products were detected by experiment and these findings are in agreement with those of Blakemore and Corcoran (164).

Experimental work by Purnell and Quinn (162) points to the occurrence of heterogeneous chain termination steps at the surface of contaminated reaction vessels. Thus, pyrolysis studies should be performed using clean equipment since only then may the reaction be regarded as completely

homogeneous in character. It has been observed by Torok and Sandler (165) that the major chain termination process for the pyrolysis of n-butane is the recombination of two methyl radicals. This reaction is included in the termination scheme given in Fig 102.

The overall reaction mechanism for the thermal decomposition of n-butane proposed here is in total agreement with the scheme given by Wang, et al (142).

Several other investigators have forwarded similar pathways but some have omitted steps included here while others have added more reactions, making the mechanism unnecessarily complicated. The scheme given by Blakemore and Corcoran (164) is analagous to the one included in Figs 100 to 102, except that certain reactions attributable to secondary processes have been included. However, at low levels of conversion secondary reactions are insignificant and do not require consideration. Exactly the same mechanism was proposed by Purnell (166) and Pacey and Purnell (143), which closely resembles the scheme detailed here, except that propagation steps 4 and 5 (Fig 101) were omitted. This may be justified on the grounds that the concentration of propyl radicals,produced by initiation, will be very low and in a steady state and can therefore be neglected. This does, however, fail to provide a complete reactions scheme. Sundaram and Froment (167) not only omit propagation steps 4 and 5 but also leave out reactions 3, 6 and 9. These may be viewed as serious omissions as butenes, low as their concentration may be, are only produced by reaction 6 and hydrogen radicals, formed according to steps 3 and 4, react with a molecule of n-butane feed, as given in reaction 9, to form the butyl radical. Thus, this particular mechanism appears to be far from complete.

To summarise :

The main initiation process proceeds by reaction 1.

The major unimolecular decomposition reactions, represented by steps 7 and 8, yield propene and ethene.

The most important hydrogen abstraction reactions are numbers 10 and 11, producing methane and ethane.

Primary chain termination steps, through reactions 12 and 13, yield hydrogen and methane.

Thus, by the above seven reactions the formation of the four main hydrocarbons, which are primary reaction products from the thermal decomposition of n-butane, may be rationalised.

$$2C_4H_{10} \longrightarrow CH_4 + C_2H_4 + C_2H_6 + C_3H_6$$
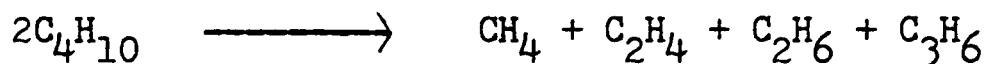
4.5   The influence of potential support materials

                     upon the   decomposition of n-butane

For the purposes of this investigation it was desirable that any material acting as a physical support for a potentially active phase should be totally inert, exerting no influence over hydrocarbon pyrolysis reactions. Silica and alumina were considered to be substances that may be used as support materials. Subsequently, a sample of gamma-alumina was obtained, in the form of 1/8 inch diameter extrudates, as used for commercial applications. Some of these small cylinders were quartered, and a further sample crushed to provide a powder. Two grades of silica gel, 6-22 mesh and 60-80 mesh, were used under test conditions and finally a small quantity of pre-powdered alpha-alumina was also assessed. Two inert materials were considered necessary as this might show the effects of any interactions between the disperse phase and support material by comparison of pyrolysis results obtained using the same compound on different supports.

Table 10 gives the product distributions obtained when n-butane was

decomposed at 653°C and the effect of potential support materials on this pyrolysis. The table shows that when coarse and fine grades of silica gel, powdered alpha-alumina and quartered gamma-alumina extrudates were used to provide a packed bed in a reaction tube, the product spectrums derived from the pyrolysis of n-butane were very similar both qualitatively and allowing for experimental error, quantitatively, to the case where no tube packing was employed. The surface area of the 6-22 mesh silica gel and the quartered extrudates of gamma-alumina was considered too low to be of practical use and therefore samples of 60-80 mesh silica gel and gamma-alumina powder were tested under identical conditions. From Table 10 it appears that surface area has very little effect on the activity of the silica gel, which remained very low, but the gamma-alumina now exhibited a strong catalytic action towards the   decomposition of n-butane. The gamma-alumina substantially reduced the quantity of n-butane in the reactor effluent and increased the concentration of every other product, as well as forming large quantities of 1,3-butadiene, a compound not detected upon pyrolysis of n-butane. Further evidence of the catalytic activity of the crushed gamma-alumina extrudates was provided by a visual examination of the reaction tube after being allowed to cool to ambient temperature. The portion of the tube which had been heated showed a heavy carbonaceous deposit on the packing material demonstrating that severe cracking had occurred in this region. Under similar experimental conditions, no other tube packing, or an empty tube, showed signs of a deposit of any kind. Slight discoloration of the grains of silica gel was noticed following the pyrolysis tests, so a similarly packed tube was heated to a temperature of 653°C with only a stream of helium gas flowing over the packing. After cooling to ambient temperature a visual examination of the packing revealed the same discoloration that was noted previously. Thus, this darkening in

colour was attributed to thermal effects, rather than a deposit accumulated as the result of hydrocarbon pyrolysis. Following decomposition tests using alpha-alumina powder as a reaction tube packing, the alumina had exactly the same physical appearance as at the beginning of the experiment.

Thus, it was concluded that as gamma-alumina greatly enhances the decomposition of n-butane it was not suitable for use as a support material during the study of the effects that various compounds have on the pyrolysis of hydrocarbons. However, as both silica gel and alpha-alumina exhibit very little or no catalytic activity towards the cracking of n-butane, both of these materials were considered to be suitable as physical supports for dispersed phases.

4.6 The thermal decomposition of 2,2-dimethylbutane

4.6.1 Product distributions

In order to acquire the data needed to calculate the restraining coefficients (Section 3.7.7.1) which were used to obtain reaction rates and the energy of activation(Section 3.7.7.2), the thermal decomposition of 2,2-dimethylbutane was investigated at five or six different residence times and six differing temperatures. From this information (Tables 11-13) a comprehensive picture concerning the cracking of 2,2-dimethylbutane can be obtained.

Illes, et al (168) have stated that the primary products arising from the thermal decomposition of 2,2-dimethylbutane include, hydrogen, methane, ethane, ethene, isobutane and isopentene. No propene was produced as a primary product and the formation of propane and butane could only be possible by chain termination reactions. Thus the concentrations of these

latter two hydrocarbons were expected to be low. From chromatographic data obtained during this study and mechanistic considerations it was considered that the primary products of 2,2-dimethylbutane pyrolysis should be ; hydrogen, methane, ethane, propane, n-butane, isobutane and the various isomers of pentene. However, no isobutane or pentene was detected at any level of hydrocarbon feed conversion and as shown in Table 13, propane and butane were only observed in small quantities under relatively severe conditions. Tables 11 to 13 show that the absolute yield of the primary products methane and ethane increases with increasing temperature and increasing residence time. It can also be seen that the rate of formation of methane and ethane increases under the above conditions. Propane was detected only at the highest temperature used during this study.

Zdonik, et al (169) stated that when hydrocarbon feedstocks containing five or more carbon atoms are pyrolysed, the reactor effluent will contain butane only in low concentrations. This observation is supported by Table 13, which shows an almost constant yield of n-butane, irrespective of temperature or hydrocarbon feed flow rate.

The decomposition of the lower molecular weight products, methane and ethane requires a high energy input. Therefore their contributions towards secondary reactions would be expected to be insignificant, even at conversions as high as 50%.

Zdonik, et al (148) stated that at high levels of conversion any pyrolysis products containing three or more carbon atoms, that were themselves formed during the early stages of decomposition, would become degraded to a signif-icant extent. In a later paper, the same authors (169) noted that butenes, and in particular 1- and 2-butenes, undergo thermal decomposition even as they are being formed and that their peak concentrations are generally lower

than for those more refractory alkenes, such as propene. This point can be demonstrated by examination of Tables 12 and 13. The yield of n-butene, while being virtually unaffected by the flow rate of the hydrocarbon feed, peaks at a temperature of 550°C. The yield of propene, formed through secondary reactions, increases linearly with temperature and remains almost static as feed flow rate changes. Propene and large quantities of ethene are formed as a result of the secondary decomposition of alkenes containing more than three carbon atoms, according to Zdonik, et al (169). Table 13 shows that the secondary product n-pentane was not detected until a temperature of 600°C was reached. n-Hexane and 2-methylbutane were not detected during the thermal decomposition of 2,2-dimethylbutane at hydrocarbon feed flow rates as low as 0.106 cm^3min^{-1} and a temperature of 600°C.

Chrysochoos and Bryce (170) quoted a figure of 23.9% for the extent of thermal decomposition of 2,2-dimethylbutane at 510°C. This compares with values varying between 16.5% and 20.2% obtained from this study at 500°C, depending on hydrocarbon feed flow rate as given in Table 12.

In addition to methane and ethene, also detected in the course of this investigation, they also found propane, isobutane and 2-methyl-2-butene to be present at 510°C. Table 12 shows that ethane, 1-butene and propene were also observed in the reactor effluent at about this temperature.

4.6.2   Reaction mechanism

Chrysochoos and Bryce (170) have reported that a ten fold change in the surface area to volume ratio of the reaction vessel used had no effect on the product distribution obtained from the thermal decomposition of 2,2-dimethylbutane. This indicates that the pyrolysis proceeds by a homogeneous free radical process. The same conclusion was reached by Doue and Guiochon (149) from their investigation.

Taking into account the same considerations as for the pyrolysis of n-butane, the initiation steps for the thermal decomposition of 2,2-dimethylbutane may be represented by the equations given in Fig 103. These vapour phase homolytic cleavages are in accord with those postulated by Purnell (147) and Chrysochoos and Bryce (171). Since tertiary radicals are more stable and therefore form more easily than either secondary or primary radicals, then by energy considerations, initiation steps 2 and 3 (fig 103) will be of greater significance than reaction 1, with regard to product formation.

From this study the primary reaction products may be listed as : hydrogen, methane, ethane, ethene, propane, n-butane, isobutene and various isomers of pentene. Thus only the formation of these compounds needs to be accounted for by the propagation and termination stages of the pyrolysis reaction. The propagation or chain carrying steps are illustrated in Fig 104. As already stated, tertiary free radicals are energetically more stable than secondary and therefore the concentration of products from reaction 4 will be very low. Wang, et al (142) have stated that free radicals larger than ethyl will decompose directly to an alkene and a smaller radical, rather than react directly with another free radical or a molecule. For this reason there will be very little, or no, 2-methylpropene (isobutene), 2-methyl-1-butene or 2-methyl-2-butene in the product stream. This observation is in agreement with the findings of this study as these hydrocarbons were not chromatographically detected upon the thermal decomposition of 2,2-dimethylbutane.

The decomposition of large free radicals to give an alkene and a smaller radical will lead to the production of significant quantities of ethene, as found here. 1-butene will also be formed by this secondary reaction process.

Thus, for reasons of stability, only hydrogen, methyl and ethyl radicals need to be considered in relation to the chain termination steps and the same set of reactions as given in Fig 102 for the pyrolysis of n-butane will serve equally well for the termination of the thermal decomposition of 2,2-dimethylbutane. It is from these six reactions that the five major reaction products of hydrogen, methane, ethane, propane and n-butane will occur.

The reaction scheme according to Purnell (147) lists the main products from the pyrolysis of 2,2-dimethylbutane as : ethene, isobutene, 2-methyl-1-butene and 2-methyl-2-butene. It would appear that the decomposition of the large radicals arising from the latter three hydrocarbons has not been taken into account. There is no suggestion that reaction products would arise from the chain termination steps, as postulated in the mechanism proposed here.

4.7   The effect of supported porphyrins on the
           decomposition of 2,2-dimethylbutane

A total of seven different porphyrins including base, nickel, vanadyl and palladium etioporphyrins and also base, nickel and vanadyl hemato-porphyrins all supported on silica gel were subjected to TPD examination. In every case the porphyrinic phase was found to be thermally stable up to a temperature of $540^{\circ}C$.

These results are in accord with those of Skinner (13), who reported that vanadyl petroporphyrins from a sample of Santa Maria Valley crude oil were stable at $400^{\circ}C$, and Barwise and Whitehead (20) who remarked that porphyrin complexes present in crude oil were sufficiently stable to appear in an unchanged state in distillate fractions that boiled in excess of $500^{\circ}C$.

Thus, having demonstrated their thermal stabilities, a range of supported porphyrins were used to investigate the influence of these macrocycles on the cracking of 2,2-dimethylbutane over a range of temperatures without thermal degradation of the disperse phase taking place. The influence of porphyrins upon the   decomposition of 2,2-dimethylbutane was investigated by using eight different porphyrins and a petroporphyrin concentrate, each supported on silica and alpha-alumina at four different loadings. These were used as packed beds in a reaction tube. A mixture of 2,2-dimethylbutane and helium gas was then passed through the tube at temperatures of 458, 478, 497, 515, 532 and 548°C, these corresponding to 2,2-dimethylbutane pyrolysis levels of about 5, 10, 15, 20, 25 and 30% respectively.

The product distributions obtained under the above conditions are given in Tables 17 to 52 inclusively and illustrated by typical chromatograms as given in Figs 84 to 92. The kinetics of these reactions are shown in Tables 55 to 63 inclusively.

4.7.1   Base etioporphyrin I

Tables 17 to 20 inclusively show the product distributions obtained when 2,2-dimethylbutane was cracked at six different temperatures over four loadings of base etioporphyrin I supported on silica and alpha-alumina.

Examination of these tables shows that for a given temperature and porphyrin loading the product distribution was very similar irrespective of the support used. From this observation it was concluded that neither silica nor alpha-alumina exerted any influence over cracking of 2,2-dimethyl-butane under these conditions.

Methane, ethane, ethene, n-pentane and n-hexane were detected at all temperatures, their level in the reactor effluent increasing with increasing temperature. Propene was also present except when 2,2-dimethylbutane was

passed over 0.5% base etioporphyrin I at a temperature of 458°C. The presence of propane was not detected until temperatures in excess of 500°C were reached.

The proportion of all reaction products, with the exception of n-hexane, increased with both temperature and porphyrin loading. The concentration of n-hexane found in the reactor effluent remained approximately constant irrespective of temperature or porphyrin loading.

Comparable results for the thermal cracking of 2,2-dimethylbutane over the same range of temperatures shows that decomposition over the porphyrin greatly increased the yield of methane, ethane, ethene, pentane and hexane.

Propane, which was not detected during the thermal cracking of 2,2-dimethylbutane, was found as a minor constituent in the reactor effluent following decomposition over base etioporphyrin.

Butane, found when 2,2-dimethylbutane was cracked at temperatures in excess of 500°C, was absent as a reaction product after catalytic decomposition.

Propene was present irrespective of decomposition conditions, the absolute quantity produced increasing only slightly with both temperature and porphyrin loading.

Although significant quantities of butene were detected after thermal cracking, this particular hydrocarbon was not evolved during decomposition over base etioporphyrin I.

2-methylbutane was not found in the reactor effluent following either thermal or catalytic cracking.

Under the influence of base etioporphyrin I the extent of decomposition of 2,2-dimethylbutane was enhanced over the thermal reaction. At 458°C this

the

increase was in order of 150%, irrespective of porphyrin loading. This figure decreased steadily with increasing temperature until the increased decomposition resulting from the influence of the porphyrin was about 10% at 548°C. The results given in Tables 17 to 20 indicate that increasing the porphyrin loading on the support had a greater effect at higher temperatures. Decomposition enhancement at 458°C increased by about 25% as the porphyrin loading increased from 0.5% to 5.0%. At a temperature of 548°C decomposition of 2,2-dimethylbutane over and above that which would be predicted for a purely thermal reaction increased from 5% to 25%, i.e. a 500% enhancement.

The above demonstrates that base etioporphyrin I exerted a positive effect on the decomposition of 2,2-dimethylbutane over the temperature range used here.

4.7.2 <u>Vanadyl etioporphyrin I</u>

Tables 21 to 24 inclusively show the product distributions obtained when 2,2-dimethylbutane was cracked at six different temperatures over four loadings of vanadyl etioporphyrin I supported on silica and alpha-alumina.

Examination of these tables shows that for a given temperature and porphyrin loading the product distribution was very similar irrespective of the support used. From this observation it was concluded that neither silica nor alpha-alumina exerted any influence over the cracking of 2,2-dimethylbutane under these conditions.

Methane, ethane, ethene, propene, n-butene and n-hexane were detected at all temperatures, their level in the reactor effluent increasing with increasing temperature. Propane was present except when 2,2-dimethylbutane was decomposed over 0.5% vanadyl etioporphyrin I at 458°C. 2-methylbutane was also detected at reaction temperatures in excess of 478°C.

The proportion of all reaction products, without exception, increased with both temperature and porphyrin loading.

Comparable results for the thermal cracking of 2,2-dimethylbutane over the same range of temperatures shows that decomposition over the porphyrin greatly increased the yield of methane, ethane, ethene, hexane and 2-methylbutane.

Propane, which was not detected during the thermal cracking of 2,2-dimethylbutane, was found as a minor constituent in the reactor effluent following decomposition over vanadyl etioporphyrin I.

Butane, found when 2,2-dimethylbutane was cracked at temperatures in excess of $500^{\circ}C$, was absent as a reaction product after catalytic decomposition.

Propene was present irrespective of decomposition conditions, the absolute quantity produced increasing with increasing porphyrin loading.

Pentane was found to be absent following both thermal and catalytic reactions.

Even at the highest loading of vanadyl etioporphyrin I the quantity of butene evolved did not reach the level obtained following thermal cracking.

Under the influence of vanadyl etioporphyrin I the extent of decomposition of 2,2-dimethylbutane was greatly enhanced over the thermal reaction. At a temperature of $458^{\circ}C$ this increase varied between 300 and 450% as porphyrin loading increased. This figure decreased steadily with increasing temperature, irrespective of porphyrin loading. At $548^{\circ}C$ the increased decomposition resulting from the influence of the porphyrin was in the range 5 to 70%. The results given in Tables 21 to 24 indicate that increasing the porphyrin

loading on the support had a greater effect at higher temperatures. Decomposition enhancement at 458°C increased by about 50% as the porphyrin loading advanced from 0.5% to 5.0%. At a temperature of 548°C decomposition of 2,2-dimethylbutane over and above that which would be expected for a purely thermal reaction increased from 5% to 70%, i.e. a 1300% increase.

These results demonstrate that vanadyl etioporphyrin I exerted a positive influence on the decomposition of 2,2-dimethylbutane over the temperature range used here.

4.7.3 Nickel etioporphyrin I

Tables 25 to 28 inclusively show the product distributions obtained when 2,2-dimethylbutane was cracked at six different temperatures over four loadings of nickel etioporphyrin I supported on silica and alpha-alumina.

Examination of these tables shows that for a given temperature and porphyrin loading the product distribution was very similar irrespective of the support used. From this observation it was concluded that neither silica nor alpha-alumina exerted any influence over the cracking of 2,2-dimethylbutane under these conditions.

Methane, ethane, ethene, propene, n-butene and n-hexane were detected at all temperatures, their level in the reactor effluent increasing with increasing temperature. Propane was detected at all temperatures when the two highest loadings of nickel etioporphyrin I were used and at temperatures in excess of 470°C when lower loadings were employed. 2-methylbutane was present except when 2,2-dimethylbutane was decomposed over 0.5% nickel etioporphyrin I at 458°C.

The proportion of both n-hexane and 2-methylbutane increased only marginally with both temperature and porphyrin loading while the

concentration of all other products increased markedly.

Comparable results for the thermal cracking of 2,2-dimethylbutane over the same range of temperatures shows that decomposition over the porphyrin greatly increased the yield of methane, ethane, ethene and propene.

Propane, which was not detected during the thermal cracking of 2,2-dimethylbutane, was found as a minor constituent in the reactor effluent following decomposition over nickel etioporphyrin I.

Butane, found when 2,2-dimethylbutane was cracked at temperatures in excess of $500^{o}C$, was absent as a reaction product after catalytic decomposition.

Pentane, was found to be absent following both thermal and catalytic reactions.

Even at the highest loading of nickel etioporphyrin I the quantity of butene evolved did not reach the level obtained following thermal cracking.

Under the influence of nickel etioporphyrin I the extent of decomposition of 2,2-dimethylbutane was greatly enhanced over the thermal reaction. At a temperature of $458^{o}C$ this increase varied between 275 and 425% as porphyrin loading increased. This figure decreased steadily with increasing temperature, irrespective of porphyrin loading. At $548^{o}C$ the increased decomposition resulting from the influence of the porphyrin was in the range 9 to 70%. The results given in Tables 25 to 28 indicate that increasing the porphyrin loading on the support had a greater effect at higher temperatures. Decomposition enhancement at $458^{o}C$ increased by about 55% as the porphyrin loading increased from 0.5 to 5.0%. At a temperature of $548^{o}C$ decomposition of 2,2-dimethylbutane over and above that which would be expected for a purely thermal reaction increased from 9 to 70%, i.e. a

675% increase.

These results demonstrate that nickel etioporphyrin I exerted a positive influence on the decomposition of 2,2-dimethylbutane over the temperature range used here.

4.7.4 Platinum etioporphyrin I

Tables 29 to 32 inclusively show the product distributions obtained when 2,2-dimethylbutane was cracked at six different temperatures over four loadings of platinum etioporphyrin I supported on silica and alpha-alumina.

Examination of these tables shows that for a given temperature and porphyrin loading the product distribution was very similar irrespective of the support used. From this observation it was concluded that neither silica nor alpha-alumina exerted any influence over the cracking of 2,2-dimethylbutane under these conditions.

Methane, ethane, ethene, propene, n-pentane and n-hexane were detected at all temperatures, their level in the reactor effluent increasing with increasing temperature. Propane was detected at temperatures in excess of 480°C.

The proportion of both propane and n-hexane increased only marginally with both temperature and porphyrin loading while the concentration of all other products increased markedly.

Comparable results for the thermal cracking of 2,2-dimethylbutane over the same range of temperatures shows that decomposition over the porphyrin greatly increased the yield of methane and ethene.

Although detected at lower temperatures, the overall yield of ethane

was not greatly enhanced by the presence of platinum etioporphyrin I.

Propane, which was not detected during the thermal cracking of 2,2-dimethylbutane, was found as a minor constituent in the reactor effluent following decomposition over platinum etioporphyrin I.

Butane, found when 2,2-dimethylbutane was cracked at temperatures in excess of $500^{\circ}C$, was absent as a reaction product after catalytic decomposition.

The yields of propene obtained were quite constant irrespective of cracking mode although porphyrin catalysed decomposition produced slightly greater quantities.

Pentane, absent following thermal cracking, was found in large amounts when 2,2-dimethylbutane was decomposed over platinum etioporphyrin I. The converse of this situation was found in the case of n-butene.

n-Hexane, detected as a minor product following the catalytic decomposition of 2,2-dimethylbutane, was absent from the reactor effluent after thermal cracking.

2-methylbutane was not found as a result of ether modes of cracking.

Under the influence of platinum etioporphyrin I the extent of decomposition of 2,2-dimethylbutane was greatly enhanced over the thermal reaction. At a temperature of $458^{\circ}C$ this increase varied between 120 and 235% as the porphyrin loading increased. This figure decreased steadily with increasing temperature, irrespective of porphyrin loading. At $548^{\circ}C$ the increased decomposition resulting from the influence of the porphyrin was in the range 9 to 30%. The results given in Tables 29 to 32 indicate that increasing porphyrin loading on the support had a greater effect at higher temperatures. Decomposition enhancement at $458^{\circ}C$ increased by about 95% as the porphyrin

loading increased from 0.5 to 5.0%. At a temperature of 548°C decomposition of 2,2-diemthylbutane over and above that which would be expected for a purely thermal reaction increased from 9 to 30%, i.e. a 230% increase.

These results demonstrate that platinum etioporphyrin I exerted a positive influence on the decomposition of 2,2-dimethylbutane over the temperature range used here.

4.7.5   Palladium etioporphyrin I

Tables 33 to 36 inclusively show the product distributions obtained when 2,2-dimethylbutane was cracked at six different temperatures over four loadings of palladium etioporphyrin I supported on silica and alpha-alumina.

Examination of these tables shows that for a given temperature and porphyrin loading the product distribution was very similar irrespective of the support used. From this observation it was concluded that neither silica nor alpha-alumina exerted any influence over the cracking of 2,2-dimethylbutane under these conditions.

Methane, ethane, ethene, propene, n-pentane and n-hexane were detected at all temperatures, their level in the reactor effluent increasing with increasing temperature. Propane was found at temperatures in excess of about 470°C for all porphyrin loadings. No hydrocarbon containing four carbon atoms was detected at any temperature or catalyst loading used during this test series. 2-Methylbutane was detected at all temperatures when the two highest loadings of palladium etioporphyrin I were used and at temperatures in excess of about 480°C when lower loadings were employed.

The proportion of both propane and 2-methylbutane increased only marginally with both temperature and porphyrin loading while the concentration of all other products increased markedly.

Comparable results for the thermal cracking of 2,2-dimethylbutane over the same range of temperatures shows that the decomposition over the porphyrin greatly increased the yield of methane, ethene, and propene.

Although the yield of ethene obtained from decomposition over palladium etioporphyrin was greater than would be expected from purely thermal cracking the increase was not as large as for methane, ethene and propene.

Propane, which was not detected during the thermal cracking of 2,2-dimethylbutane, was found as a minor constituent in the reactor effluent following decomposition over palladium etioporphyrin I.

Butane, found when 2,2-dimethylbutane was cracked at temperatures in excess of $500^{\circ}C$, was absent as a reaction product after catalytic decomposition.

Pentane was found in significant quantities following decomposition over palladium etioporphyrin although this hydrocarbon was not detected after thermal cracking. The exact opposite of this situation was found in the case of n-butene.

Both n-hexane and 2-methylbutane were both present as minor constituents of the reactor effluent following catalytic decomposition. These hydrocarbons were not detected after thermal cracking.

Under the influence of palladium etioporphyrin I the extent of decomposition of 2,2-dimethylbutane was greatly enhanced over the thermal reaction. At a temperature of $458^{\circ}C$ this increase varied between 200 and 310% as porphyrin loading increased. This figure decreased steadily with increasing temperature, irrespective of porphyrin loading. At $548^{\circ}C$ the increased decomposition resulting from the influence of the porphyrin was in the range -6 to 25%. The results given in Tables 33 to 36 indicate that increasing

the porphyrin loading on the support had a greater effect at higher temperatures. Decomposition enhancement at $458^{o}C$ increased by about 55% as the porphyin loading increased from 0.5 to 5.0%. At a temperature of $548^{o}C$ decomposition of 2,2-dimethylbutane over and above that which would be expected for a purely thermal reaction increased from -6 to 25%, i.e. a 520% increase.

These results demonstrate that palladium etioporphyrin I exerted positive influence on the decomposition of 2,2-dimethylbutane over the temperature range used here.

4.7.6   Base hematoporphyrin IX

Tables 37 to 40 inclusively show the product distributions obtained when 2,2-dimethylbutane was cracked at six different temperatures over four loadings of base hematoporphyrin IX supported on silica and alpha-alumina.

Examination of these tables shows that for a given temperature and porphyrin loading the product distribution is very similar irrespective of the support used. From this observation it was concluded that neither silica nor alpha-alumina exerted any influence over the cracking of 2,2-dimethylbutane under these conditions.

Methane, ethane, ethene, propene and n-pentane were detected at all temperatures, their level in the reactor effluent increasing with increasing temperature. n-Hexane was detected at all temperatures when the three highest loadings of base hematoporphyrin IX were used and at temperatures in excess of about $530^{o}C$ when a 0.5% loading was employed. Propane was only detected when temperatures above about $490^{o}C$ were used, irrespective of porphyrin loading.

The proportion of propane increased only marginally with both temperature and porphyrin loading while the concentration of all other products increased markedly.

Comparable results for the thermal cracking of 2,2-dimethylbutane over the same range of temperatures shows that decomposition over the porphyrin greatly increased the yield of methane, ethene, propene and n-pentane.

The increase in the quantity of ethane obtained as the porphyrin loading increased was small. Although ethane was detected at lower temperatures following decomposition over the porphyrin, overall yields at higher temperatures were comparable irrespective of cracking mode.

Propane, which was not detected during the thermal cracking of 2,2-dimethylbutane, was found as a minor constituent in the reactor effluent following decomposition over base hematoporphyrin.

Butane, found when 2,2-dimethylbutane was cracked at temperatures in excess of $500^{\circ}C$, was absent as a reaction product after catalytic decomposition.

The large quantities of butene detected following the thermal cracking of 2,2-dimethylbutane were totally absent from the reactor effluent after treatment over base hematoporphyrin.

n-Hexane was found as a minor component of the effluent stream following catalytic decomposition. This hydrocarbon was not detected as a consequence of the thermal cracking of 2,2-dimethylbutane.

2-Methylbutane was not detected after either thermal or catalytic decomposition.

Under the influence of base hematoporphyrin IX the extent of decomposition of 2,2-dimethylbutane was greatly enhanced over the thermal reaction.

At a temperature of 458°C this increase varied between 200 and 400% as porphyrin loading increased. This figure decreased steadily with increasing temperature, irrespective of porphyrin loading. At 548°C the increased decomposition resulting from the influence of the porphyrin was in the range 13 to 60%. The results given in Tables 37 to 40 indicate that increasing the porphyrin loading on the support had a greater effect at higher temperatures. Decomposition enhancement at 458°C increased by about 100% as the porphyrin loading increased from 0.5 to 5.0%. At a temperature of 548°C decomposition of 2,2-dimethylbutane over and above that which would be expected for a purely thermal reaction increased from 13 to 60%, i.e. a 360% increase.

These results demonstrate that base hematoporphyrin IX exerted a positive influence on the decomposition of 2,2-dimethylbutane over the temperature range used here.

4.7.7 <u>Vanadyl hematoporphyrin IX</u>

Tables 41 to 44 inclusively show the product distributions obtained when 2,2-dimethylbutane was cracked at six different temperatures over four loadings of vanadyl hematoporphyrin IX supported on silica and alpha-alumina.

Examination of these tables shows that for a given temperature and porphyrin loading the product distribution was very similar irrespective of the support used. From this observation it was concluded that neither silica nor alpha-alumina exerted any influence over the cracking of 2,2-dimethylbutane under these conditions.

Methane, ethane, ethene, propane and n-pentane were detected at all temperatures, their level in the reactor effluent increasing with increasing

temperature. Propane was detected at temperatures in excess of $500^{\circ}C$ except when decomposition was performed over 5.0% vanadyl hematoporphyrin IX. In this case the lower temperature limit for detection was reduced to $460^{\circ}C$. n-Hexane was found at all temperatures when the two highest loadings of vanadyl hematoporphyrin IX were used and at temperatures in excess of about $470^{\circ}C$ when lower loadings were employed.

The proportion of both propene and n-hexane increased only marginally with both temperature and porphyrin loading while the concentration of all other products increased markedly.

Comparable results for the thermal cracking of 2,2-dimethylbutane over the same range of temperatures shows that decomposition over the porphyrin greatly increased the yield of methane, ethene and propene.

The increase in the quantity of ethane obtained as the porphyrin loading increased was small. Although ethane was detected at lower temperatures following decomposition over the porphyrin, overall yields at higher temperatures were comparable irrespective of cracking mode.

Propane and n-hexane, which were not detected during the thermal cracking of 2,2-dimethylbutane, were both found as minor constituents in the reactor effluent following decomposition over vanadyl hematoprophyrin.

Butane, found when 2,2-dimethylbutane was cracked at temperatures in excess of $500^{\circ}C$, was absent as a reaction product after catalytic decomposition.

n-Pentane was evolved in large quantities during the decomposition of 2,2-dimethylbutane over vanadyl hematoporphyrin. This hydrocarbon was not detected in the reactor effluent following thermal decomposition. The exact opposite of this situation was found in the case of n-butene.

2-Methylbutane was not detected after either thermal or catalytic decomposition.

Under the influence of vanadyl hematoporphyrin IX the extent of decomposition of 2,2-dimethylbutane was greatly enhanced over the thermal reaction. At a temperature of $458^{\circ}C$ this increase varied between 205 and 425% as porphyrin loading increased. This figure decreased steadily with increasing temperature, irrespective of porphyrin loading. At $548^{\circ}C$ the increased decomposition resulting from the influence of the porphyrin was in the range 32 to 95%. The results given in Tables 41 to 44 indicate that increasing the porphyrin loading on the support had a greater effect at higher temperatures. Decomposition enhancement at $458^{\circ}C$ increased by about 105% as the porphyrin loading increased from 0.5 to 5.0%. At a temperature of $548^{\circ}C$ decomposition of 2,2-dimethylbutane over and above that which would be expected for a purely thermal reaction increased from 32 to 95%, i.e. a 195% increase.

These results demonstrate that vanadyl hematoporphyrin IX exerted a positive influence on the decomposition of 2,2-dimethylbutane over the temperature range used here.

4.7.8   Nickel hematoporphyrin IX

Tables 45 to 48 inclusively show the product distributions obtained when 2,2-dimethylbutane was cracked at six different temperatures over four loadings of nickel hematoporphyrin IX supported on silica and alpha-alumina.

Examination of these tables shows that for a given temperature and porphyrin loading the product distribution was very similar irrespective of the support used. From this observation it was concluded that neither silica nor alpha-alumina exerted any influence over the cracking of 2,2-dimethylbutane under these conditions.

Methane, ethane, ethene, propene and n-pentane were detected at all temperatures, their level in the reactor effluent increasing with increasing temperature. Propane was found at temperatures in excess of about $470^{\circ}C$. n-hexane was detected at all temperatures when the two highest loadings of nickel hematoporphyrin IX were used and at temperatures above about $500^{\circ}C$ when lower loadings were employed.

The proportion of ethane, propane and propene increased only marginally with both temperature and porphyrin loading while the concentration of all other products increased markedly.

Comparable results for the thermal cracking of 2,2-dimethylbutane over the same range of temperatures shows that decomposition over the porphyrin greatly increased the yield of methane and propene.

The quantity of both ethane and ethene obtained when 2,2-dimethylbutane was decomposed over 5% nickel hematoporphyrin IX was approximately 50% greater than that obtained for the thermal reaction. However, at the lowest porphyrin loading the yields obtained were very similar irrespective of cracking mode.

Propane and n-hexane, which were not detected during the thermal cracking of 2,2-dimethylbutane, were both found as minor constituents in the reactor effluent following decomposition over nickel hematoporphyrin IX.

Butane, found when 2,2-dimethylbutane was cracked at temperatures in excess of $500^{\circ}C$, was absent as a reaction product after catalytic decomposition.

n-Pentane was evolved in large quantities during the decomposition of 2,2-dimethylbutane over nickel hematoporphyrin IX. This hydrocarbon was not detected in the reactor effluent following thermal decomposition.

The exact opposite of this situation was found in the case of n-butene.

2-Methylbutane was not detected after either thermal or catalytic decomposition.

Under the influence of nickel hematoporphyrin IX the extent of decomposition of 2,2-dimethylbutane was greatly enhanced over the thermal reaction. At a temperature of $458^\circ C$ this increase varied between 215 and 410% as porphyrin loading increased. This figure decreased steadily with increasing temperature, irrespective of porphyrin loading. At $548^\circ C$ the increased decomposition resulting from the influence of the porphyrin was in the range 30 to 90%. The results given in Tables 45 to 48 indicate that increasing the porphyrin loading on the support had a greater effect at higher temperatures. Decomposition enhancement at $458^\circ C$ increased by about 90% as the porphyrin loading increased from 0.5 to 5.0%. At a temperature of $548^\circ C$ decomposition of 2,2-dimethylbutane over and above that which would be expected for a purely thermal reaction increased from 30 to 90%, i.e. a 200% increase.

These results demonstrate that nickel hematoporphyrin IX exerted a positive influence on the decomposition of 2,2-dimethylbutane over the temperature range used here.

4.7.9   Petroporphyrin concentrate

Tables 49 to 52 inclusively show the product distributions obtained when 2,2-dimethylbutane was cracked at six different temperatures over four loadings of petroporphyrin concentrate supported on silica and alpha-alumina.

Examination of these tables shows that for a given temperature and porphyrin loading the product distribution was very similar irrespective

of the support used. From this observation it was concluded that neither silica nor alpha-alumina exerted any influence over the cracking of 2,2-dimethylbutane under these conditions.

Methane, ethane, ethene, propene, n-pentane, n-hexane and 2-methylbutane were detected at all temperatures, their level in the reactor effluent increasing with increasing temperature. Propane was only detected when temperatures greater than about 470°C were used.

The proportion of both n-hexane and 2-methylbutane increased only marginally with both temperature and porphyrin loading while the concentration of all other products increased markedly.

Comparable results for the thermal cracking of 2,2-dimethylbutane over the same range of temperatures shows that decomposition over the petroporphyrin concentrate greatly increased the yield of methane and ethene.

The overall quantity of propene was enhanced slightly due to catalytic cracking.

The amount of ethane evolved was approximately the same irrespective of cracking mode.

Propane, n-hexane and 2-methylbutane, which were detected during the thermal cracking of 2,2-dimethylbutane, were found as minor constituents in the reactor effluent following decomposition over the petroporphyrin concentrate.

Butane, found when 2,2-dimethylbutane was cracked at temperatures in excess of 500°C, was absent as a reaction product after catalytic decomposition.

n-Pentane was evolved in large quantities during the decomposition of 2,2-dimethylbutane over the petroporphyrin concentrate. This hydrocarbon

was not detected in the reactor effluent following thermal decomposition. The exact opposite of this situation was found in the case of n-butene.

Under the influence of the petroporphyrin concentrate the extent of decomposition of 2,2-dimethylbutane was greatly enhanced over the thermal reaction. At a temperature of $458^{\circ}C$ this increase varied between 200 and 330% as petroporphyrin loading increased. This figure decreased steadily with increasing temperature, irrespective of porphyrin loading. At $548^{\circ}C$ the increased decomposition resulting from the influence of the petroporphyrin was in the range 20 to 72%. The results given in Tables 49 to 52 indicate that increasing the porphyrin loading on the support had a greater effect at higher temperatures. Decomposition enhancement at $458^{\circ}C$ increased by about 65% as the porphyrin loading increased from 0.5 to 5.0%. At a temperature of $548^{\circ}C$ decomposition of 2,2-dimethylbutane over and above that which would be expected for a purely thermal reaction increased from 20 to 72%, i.e. a 260% increase.

These results demonstrate that the petroporphyrin concentrate used during the course of these reactions exerted a positive influence on the decomposition of 2,2-dimethylbutane over the temperature range used here.

4.7.10   Comparison of the porphyrins studied

The influence that nine various porphyrins had on the decomposition of 2,2-dimethylbutane was examined using four porphyrin loadings on two different support materials at six temperature levels.

The results obtained from these experiments are exhibited in Tables 17 to 52 inclusively and illustrated by typical chromatograms as given in Figs 84 to 92. Examination of the product distributions shown in these tables highlights a number of similarities and differences with respect to the

action of these porphyrins on 2,2-dimethylbutane.

Of the five etioporphyrin derivatives studied the vanadyl and nickel homologues behaved similarly. Base, platinum and palladium etioporphyrin also gave product spectra that were similar to one another, but these three produced a slightly different range of decomposition products compared to vanadyl and nickel etioporphyrins. When 2,2-dimethylbutane was heated to temperatures in excess of 450°C in the presence of the latter two macro-cycles both n-butene and 2-methylbutane were evolved in detectable quantities. These two hydrocarbons were not found when 2,2-dimethylbutane was similarly treated in the presence of base or platinum etioporphyrins. However, when 2,2-dimethylbutane was heated over the latter two species and also palladium etioporphyrin appreciable quantities of n-pentane were detected. This compound was absent from the reactor effluent when both vanadyl and nickel etio-porphyrins were similarly tested.

The three derivatives of hematoporphyrin IX examined all behaved in an identical manner with respect to the qualitative product distributions obtained from the decomposition of 2,2-dimethylbutane. The product spectra of these three species were also very similar to those given by base and platinum etioporphyrins.

The various hydrocarbon products obtained when 2,2-dimethylbutane was decomposed over the petroporphyrin concentrate isolated from Tia Juana Pesado resembled those given by the action of palladium etioporphyrin I.

The most abundant metal found in Tia Juana Pesado is vanadium which is present in a sixteen fold excess over nickel (116). From this it might be expected that any action that the petroporphyrin concentrate, as isolated from Tia Juana Pesado, may have towards the cracking of 2,2-dimethylbutane should resemble that of vanadyl etioporphyrin. The results obtained during

this study indicate otherwise. Tia Juana Pesado topped crude has a sulphur content of 2.40%, which is relatively high when compared with other topped crudes. Since the sulphur level rises to 6.12% in the asphaltene fraction (172) it seems probable that the isolated petroporphyrin concentrate would similarly contain large quantities of sulphur. Pilcher and Winterbottom (172) have stated that the presence of sulphur exerts a moderating influence upon the extent of cracking. Thus, if it is assumed that the petroporphyrin concentrate obtained during this work from Tia Juana Pesado topped crude has high levels of decomposition retarding sulphur, then the action of this species towards the cracking of 2,2-dimethylbutane might be expected to resemble that of palladium rather than vanadyl etioporphyrin.

Upon inspection of the broadest qualitative aspects of the product distributions given in Tables 17 to 52 inclusively, it was concluded that both vanadyl and nickel etioporphyrins behaved in a similar manner to one another. The other seven porphyrins examined also provided product spectra which resembled each other but which were different from those of vanadyl and nickel etioporphyrins.

By calculating the level of decomposition, over and above that which could be attributed to thermal cracking, as obtained when 2,2-dimethylbutane was heated over the various supported porphyrins, these species could be ordered according to their effectiveness.

At a temperature of $458^{\circ}C$ the supported phase that produced the greatest decomposition enhancement was vanadyl etioporphyrin and that which gave the least was base etioporphyrin. This was found to be the case at all loadings. At a temperature of $548^{\circ}C$ the supported phase that produced the greatest decomposition enhancement was vanadyl hematoporphyrin. This was found to be the case at all loadings. At the 0.5% level palladium etioporphyrin was

found to have the least effective catalytic action at 548°C. This was the only instance where any porphyrin had a retarding effect on the decomposition of 2,2-dimethylbutane. At a temperature of 548°C and a loading of 5.0% it was found that the least effective phases with respect to enhancing the decomposition of 2,2-dimethylbutane were palladium and base etioporphyrins.

4.7.11   Kinetic data

Tables 55 to 63 inclusively give both the frequency factors and activation energies calculated for each of the eight synthetic porphyrins, togther with the petroporphyrin concentrate, for each loading and both support materials.

Generally, the activation energy for the decomposition of 2,2-dimethylbutane calculated for any one species remains fairly constant as the loading increases from 0.5 to 5.0%, while the frequency factor tends to increase. In addition, for any given porphyrin the support material appears to have little effect on either the frequency factor or activation energy.

The activation energy for the thermal reaction was calculated to be 201 kJ mol^{-1}. The porphyrin providing the lowest activation energy for the analogous reaction was vanadyl etioporphyrin which gave an average calculated value of 86 kJ mol^{-1}.

An average activation energy of 108 kJ mol^{-1} was given by platinum etioporphyrin. This was the highest value for any of the porphyrins examined. For the decomposition of 2,2-dimethylbutane four of the nine species investigated more than halved the activation energy required for the thermal cracking reaction.

The calculated frequency factor for the thermal decomposition of 2,2-dimethylbutane was 1.99×10^{12}. Of the nine porphyrins tested, vanadyl

hematoporphyrin gave the highest frequency factor which averaged 5.3 x
10^6. This compares with the lowest average value of 1.46 x 10^5 provided
by vanadyl etioporphyrin.

By using the calculated average values for both activation energy and
frequency factor the first order rate constant relating to each porphyrin
species can be estimated. The macrocycles providing the fastest reactions,
as indicated by the highest rate constants, over the temperature range
investigated (458 to 548°C) were vanadyl hematoporphyrin, nickel etio-
porphyrin and then vanadyl etioporphyrin. Base etioporphyrin gave the
slowest of any of the catalysed reactions and although the rate was
considerably higher than the corresponding thermal decomposition at 458°C,
at a temperature of 548°C the thermal reaction was the quicker of the two.
All other porphyrins provided an increased reaction rate even at the higher
temperature.

The above experimental data is consistent with the observed magnitudes
of energies of activation and frequency factors.

4.7.12 Reaction mechanism

Commercial cracking catalysts allow decomposition to proceed through
a carbonium ion mechanism. This leads to low methane and C_2 production but
maximises the yields of C_3 and C_4 compounds.

Thermal decomposition of hydrocarbons occurs via a free radical pathway
and provides a greater yield of methane, ethane and ethene than the C_3 and
C_4 analogues.

Comparison of the product distributions obtained both with (Tables 17
to 52 inclusive) and without (Tables 11 to 13 inclusive) the influence of
various porphyrin species shows product maximisation of the C_1 and C_2

hydrocarbons irrespective of experimental conditions. When 2,2-dimethyl-butane was decomposed over any of the porphyrins studied, the yield of methane and ethane was greatly enhanced over that given by the corresponding thermal reaction. The level of ethene remained constant, the yield of the C_3 hydrocarbons was slightly greater while virtually no C_4 compounds were detected as a result of catalytic decomposition. From this comparison of products given by both thermal and catalytic cracking via porphyrin species, it is evident that the reaction mechanism for hydrocarbon pyrolysis under the influence of porphyrins is quite different from that given by commercial cracking catalysts. The above comparison indicates that decomposition effected by porphyrins follows the same, or a very similar, free radical pathway as thermal degradation.

The catalytic action of the porphyrin species investigated is associated with increasing the rate of the rate determining step. In a free radical decomposition reaction this is the initiation process. Therefore, porphyrins may be responsible for an increase in the frequency of homolytic bond cleavage. It is possible that a single electron may be abstracted from the electron rich π system of the porphyrin ring and accepted by electron deficient sites present on the support materials used. This process may well be accelerated by the effect of temperature. This would lead to the formation of a porphyrin radical. This radical would be stabilised by the presence of electron donating alkyl groups around the periphery of the ring. The porphyrin radical thus formed would readily accept any electron it can capture and one readily accessible source of negative charge would be the electrons contained in the C — C σ bonds of an alkane. Electron abstraction from such bonds would lead to the formation of alkyl radicals and the initiation of free radical decomposition. Thus, in the manner described, the rate of homolytic bond cleavage may well be increased.

Significant quantities of n-pentane were detected when 2,2-dimethyl-
butane was decomposed under the influence of most porphyrinic species
whereas thermal cracking produced no identifiable C5 hydrocarbon until
temperatures between 550 and 600°C were reached. In addition to this, thermal
cracking produced small quantities of n-butane and larger amounts of n-
butene whereas C4 hydrocarbons were not detected following catalytic decomp-
osition. Examination of Table 13 shows that increasing the temperature of
the thermal reaction increased the detected levels of n-pentane while those
of n-butane decreased. This apparent difference in product spectra between
the thermal and catalytic decomposition of 2,2-dimethylbutane may be seen
as further evidence of the catalytic action of porphyrins. On a qualitative
basis, the same product mix obtained upon cracking was reached at lower
temperatures when decomposition occurred over supported porphyrins.

4.8   Hydrogenation

As indicated in Section 1.5.9.2, porphyrins are well documented
hydrogenation catalysts. Most investigations involving the use of porphyrins
have been performed in the liquid phase. As a result of their proven effects
towards the hydrogenation of various species a short study was undertaken
to examine the use of various supported porphyrins as heterogeneous catalysts
for the hydrogenation of 1-hexene vapour.

4.8.1   Temperature programmed reduction

Temperature programmed reduction tests were performed on base, vanadyl
and nickel hematoporphyrin IX and also base, vanadyl, nickel and palladium
etioporphyrin I according to Section 2.3.7.

The hematoporphyrins all behaved similarly and the absence of any peaks
in the traces obtained indicates that there had been no hydrogen uptake.

In this case the hematoporphyrins would not be expected to behave as efficient hydrogenation catalysts since there is no means whereby diatomic hydrogen can be dissociated.

The four etioporphyrins examined behaved differently from the hematoporphyrins and Figs 93 to 96 inclusive show that high temperature adsorption peaks were present in every case. The ratio of the peak areas was calculated to be as follows :-

vanadyl : base : nickel : palladium

1.0 : 1.6 : 4.0 : 11.6

From the above results alone it would be expected that the etioporphyrins examined would behave as hydrogenation catalysts. It would also be predicted that palladium etioporphyrin I would be the most effective.

4.8.2 Hydrogen chemisorption

Two samples of synthetic nickel etioporphyrin, one unsupported, the other used as a 5.0% w/w loading on silica, were subjected to hydrogen chemisorption tests at Brunel University.

The results of the hydrogen chemisorption experiments performed on the unsupported nickel etioporphyrin, given in Table 64, were manipulated as described in Section 3.9.1. It was shown that approximately 1.57% of the nickel in the sample was available for hydrogen chemisorption.

The results of the hydrogen chemisorption experiments performed on 5.0% nickel etioporphyrin supported on silica, given in Table 65, were manipulated as described in Section 3.9.2. It was shown that approximately 71.3% of the nickel in the sample was available for hydrogen chemisorption, if it is assumed that the support material has zero adsorption and that there is no spillover. The above indicates that the nickel etioporphyrin

on silica is about 45 times more active than the unsupported material.

Hydrogen chemisorption experiments were also performed on 5.0% palladium etioporphyrin I supported on silica, as outlined in Section 2.3.8.2. The results of these experiments, given in Section 3.9.3, show that 42.4% of the palladium in the sample was available for hydrogen chemisorption. This indicates that, while palladium etioporphyrin may not be as active as the nickel homologue, it should still be an effective hydrogenation catalyst.

The experimental results obtained from the hydrogen chemisorption experiments performed on supported nickel and palladium etioporphyrins were based upon different methods.While data obtained from any single method would be expected to be self consistent, it is possible that results given by differing experimental techniques may not be directly comparable. Since the same supported porphyrin was not examined by both methods of hydrogen chemisorption, it has not been possible to determine a correlation factor between the two techniques. The hydrogen chemisorption data obtained has indicated that supported nickel etioporphyrin should be approximately 1.7 times more effective as a hydrogenation catalyst than the corresponding palladium species. However, as a consequence of differing experimental methods employed for the determination of hydrogen chemisorption this may not be accurate.

On the basis of the above, the capability of seven supported porphyrins to effect the hydrogenation of 1-hexene was examined. In addition to these experiments, which were performed at temperatures of 325 and 450°C, four supported porphyrins were also examined at the lower temperature of 150°C.

4.8.3   The influence of various conditions on 1-hexene

The tubular reactor was used according to Section 2.3.9 and conditions

were varied such that their effect on 1-hexene could be assessed. The results of these experiments are given in Table 66.

Helium was bubbled through 1-hexene and the resulting gas/vapour mixture was passed through the reactor which was operated from ambient temperature up to $350^{\circ}C$. It can be seen from these results that the onset of thermal cracking occurs at about $325^{\circ}C$ and by $350^{\circ}C$ is well established.

An analogous set of experiments was performed using 5% hydrogen/95% argon as the gas used to entrain 1-hexene. The results in Table 66 illustrate that no hydrogenation has taken place under these conditions as n-hexane was not detected in the reactor effluent. It is again evident that from a temperature of $325^{\circ}C$ upwards thermal cracking was taking place.

A reaction tube was packed with silica and the reactor operated as before, using 5% hydrogen/95% argon to entrain the alkene. Comparison of the results obtained at $325^{\circ}C$ and $450^{\circ}C$, shown in Table 66, with those where there was an absence of tube packing demonstrates that the silica had no effect on the reactions occurring. No hydrogenation took place under these conditions, as illustrated by the absence of n-hexane.   Decomposition was the only reaction found, the extent of cracking with a silica tube packing being almost identical to that obtained without.

From the results given in Table 66 it can be seen that when 1-hexene in 5% hydrogen/95% argon is passed through a tubular reactor over the temperature range 325 to $450^{\circ}C$ no hydrogenation was detected and that decomposition was the major reaction, this being unaffected by the presence of silica.

4.8.4   The effect of supported porphyrins

on the hydrogenation of 1-hexene

5% hydrogen/95% argon was passed through liquid 1-hexene and the
resulting gas/vapour mixture was directed through a tubular reactor
operated at temperatures between 150 and 450°C. The alkene was passed over
a variety of supported porphyrins at different loadings. The results
obtained from these experiments are detailed in Tables 67 to 76 inclusive.

The main conclusion that can be drawn from the data contained within
Tables 67 to 73 inclusive is that since no hexane was detected in the
reactor effluent then no hydrogenation had taken place above the experi-
mental temperatures of about 320°C.

Comparison of the results contained in Table 66 with those given in
Tables 67 to 73 demonstrates that all seven of the porphyrins examined
acted as cracking catalysts. At both 325 and 450°C all seven macrocycles
gave an extent of reaction above that obtained for the purely thermal
decomposition, irrespective of loading.

At 325°C the main reaction product resulting from cracking was n-pentane.
As the temperature was increased to 450°C the product spectrum experienced
a shift towards the lighter hydrocarbon products. At the higher temperature
the total yield of C_1 to C_3 compounds was in excess of the C_4 to C_6
hydrocarbons in all but one case, the major reaction product being methane.

As was the case with the catalytic cracking of 2,2-dimethylbutane, the
higher the porphyrin loading the greater the extent of hydrocarbon decomp-
osition.

The porphyrins examined did not act as catalysts towards the hydro-
genation of 1-hexene at temperatures in excess of about 320°C but were

shown to be effective catalysts for the decomposition of this alkene.

The considerable extent of hydrogen chemisorption experienced by supported nickel and palladium etioporphyrins and the results of the TPR experiments undertaken on the four unsupported etioporphyrins provided evidence that these macrocycles should act as hydrogenation catalysts. As a consequence of this an additional set of hydrogenation experiments was conducted at the lower temperature of $150^\circ C$. The results of these experiments, using supported nickel, palladium and vanadyl porphyrins in conjunction with 1-hexene, are given in Tables 74 to 76 inclusive. Comparison of the available hydrogen chemisorption data indicates that the nickel porphyrin should have acted as a more efficient hydrogenation catalyst than the palladium species. However, the experimental results show that this was not the case, with the relative hydrogenation rates being of the same order of magnitude, but slightly higher, for the supported palladium etioporphyrin I. Inspection of the turnover numbers calculated for both supported nickel and palladium etioporphyrins, as shown in Tables 74 and 75, confirms this to be the case. The reaction rate per unit metal surface area shows that the palladium species acted in a more efficient manner towards the hydrogenation of 1-hexene than nickel etioporphyrin I.

Since two differing methods were used to obtain the given hydrogen chemisorption data for the nickel and palladium species, it is possible that the two techniques failed to yield directly comparable results as discussed in Section 4.8.2. It may also be that, although supported nickel etioporphyrin I efficiently chemisorbed hydrogen, the macrocycle : alkene interaction was not similarly effective, thus leading to a reduced rate of production of substrate-catalyst complex.

Table 76 shows that under the experimental conditions used, supported

vanadyl hematoporphyrin IX also acted as an hydrogenation catalyst. Consistent with the analysis of the TPR data, as given in Section 4.8.1, it can be seen that the vanadyl species was considerably less effective towards the hydrogenation of 1-hexene than nickel or palladium etioporphyrin I.

From the results of the hydrogenation experiments, given in Tables 67 to 76 inclusive, it can be seen that at a temperature of $150^{O}C$ supported porphyrins acted as effective hydrogenation catalysts. However, at temperatures above $320^{O}C$ no hydrogenation took place and catalytic cracking of the alkene occurred. From this it would seem possible that as the experimental temperature was increased, favourable conditions for the dehydrogenation reaction were generated, leading to the overall situation where no hydrogenation occurred. It may also be that as the reactor temperature was increased further the cracking reaction was catalysed more quickly, and to such an extent, that cracking of the alkene occurred preferentially and hydrogenation could not be detected at temperatures in excess of about $320^{O}C$.

4.9   Additional Considerations

4.9.1   Cracking Mechanism Under the Influence of Porphyrins

The reaction mechanism for the cracking of hydrocarbons under the influence of porphyrins can be regarded as a number of successive steps:-

1. Transport of the gaseous alkane, by diffusion, towards the solid-gas interface.

2. Adsorption of the gaseous alkane. This may be achieved by interaction of the electrons contained in the alkane C-C σ bonds with those in the extensive π system of the porphyrin ring.

3. Reactions at the solid-gas interface. If the decomposition of n-butane is considered, for example, then the interfacial processes may be depicted as follows:-

$$CH_3CH_2CH_2CH_3 + PM \longrightarrow \overset{\cdot}{CH_3CH_2CH_2} - PM + \overset{\cdot}{CH_3}$$

$$\overset{\cdot}{CH_3CH_2CH_2} - PM \longrightarrow CH_3CH=CH_2 + \overset{\cdot}{MPH}$$

$$\overset{\cdot}{MPH} + \overset{\cdot}{CH_3} \longrightarrow MP + CH_4$$
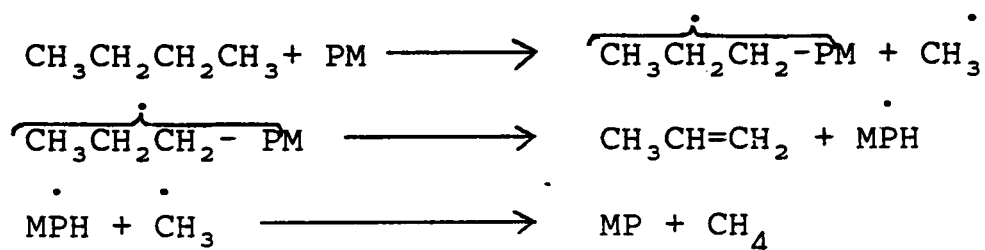
Where M = metal

P = porphyrin

4. Desorption of gaseous products.

5. Transport, by diffusion, of gaseous products away from the solid-gas interface.

It can be seen from the above that if the interfacial process is continued a high yield of methane and C2 products will be obtained. This is consistent with the reaction products, and their distribution, obtained from homogeneous thermal cracking.

The central metal atom contained in the metalloporphyrin is, on an atomic scale, a considerable distance from the porphyrin π system. For example, the average V-N bond length in vanadyl etioporphyrin is 2.102 Å.

Since the C-C σ bond is 1.54 $\overset{\circ}{A}$ it seems unlikely that the metal atom would play a major part in the catalytic decomposition of hydrocarbons. This may be particularly true since spectral evidence reveals that coupling of the metal orbitals to the π system is weak. Hence the main active centre behind the catalytic action of porphyrins towards the decomposition of hydrocarbons would be the extensive π resonance system with the central metal atom playing a secondary role.

4.9.2   Hydrogenation

4.9.2.1   Calculation of Turnover Numbers

The calculation of turnover numbers which are expressed in terms of molecules site^{-1} min^{-1} requires a reasonable estimation of the available metal surface area to be made. Hydrogen chemisorption data obtained during this study was manipulated to provide metal surface area figures on the basis that a polycrystalline metal surface exists. However, the kinetic data for the cracking of 2,2-DMB over porphyrins given in Tables 55-63 indicates that the frequency factor increases with loading for vanadyl, nickel and palladium porphyrins. This suggests that the metal porphyrin is operating as a complex and not as a set of metal crystallites. On the basis of this it may be reasonable to assume that the turnover numbers obtained during this investigation should not be used as a comparison with other values which have been published, but are self consistent for the purposes of this study. However, turnover numbers expressed as molecules site^{-1} min^{-1} calculated from available metal atoms as determined by metal surface area measurements are of the same order of magnitude as other literature values.

4.9.2.2   Reaction Mechanism

The mechanism of catalytic hydrogenation of alkenes over porphyrins may not occur via the dissociative chemisorption of hydrogen but could proceed by a pathway similar to that proposed for the cracking of alkanes. The gas-solid interfacial process may be depicted as follows:-

$$
\begin{array}{c}
R \\
\diagdown \\
C\!=\!CH_2 \;+\; MP \\
\diagup \\
R'
\end{array}
\longrightarrow
\begin{array}{c}
R \\
\diagdown \\
C\!=\!CH_2 \\
\diagup \quad | \\
R' \qquad MP
\end{array}
$$

$$
\begin{array}{c}
R \\
\diagdown \\
C\!=\!CH_2 \;+\; H_2 \\
\diagup \quad | \\
R' \qquad MP
\end{array}
\longrightarrow
\begin{array}{c}
R \\
\diagdown \\
CH\!-\!CH_3 \\
\diagup \quad | \\
R' \qquad MP
\end{array}
$$

Where R and R'
are alkyl groups

$$
\begin{array}{c}
R \\
\diagdown \\
CH\!-\!CH_3 \;+\; MP \\
\diagup \\
R'
\end{array}
$$
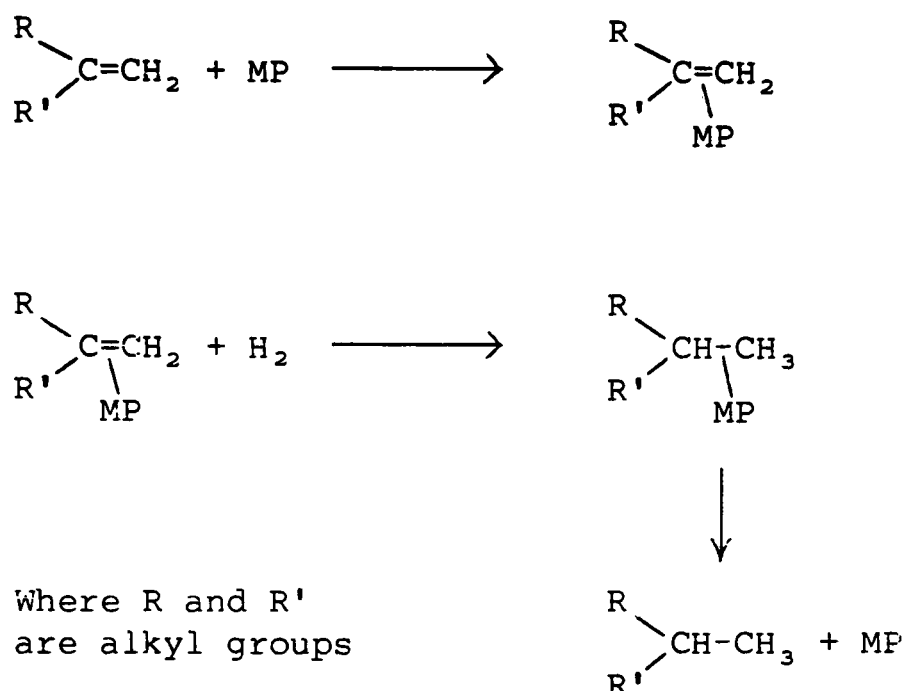
The alkene is π absorbed onto the porphyrin species and the hydrogen molecule reacts from the gas phase. The above is clearly speculative and detailed kinetic measurements and catalyst characterisation are required to elucidate this.

4.9.3   Catalyst Characterisation

If the porphyrin catalysts employed during this study were more completely characterised before, possibly during and after reaction then the mechanisms of cracking and hydrogenation postulated here may be proven. In addition to this, information may become available as to the role of the central metal ion, catalyst support, etc., during the catalytic reactions.

Some instrumental analytical methods for catalyst characterisation are suggested below.

4.9.3.1 <u>Nature of Phases</u>

X-ray diffraction (XRD) and analytical electron microscopy (AEM) can be used for the study of crystalline phases. XRD provides average information and metal particle sizes can be estimated from line broadening using the Scherrer equation. Radial electron distribution (RED) is a particular application of XRD and allows the study of the angular distribution of X-rays scattered by amorphous solids thus providing a determination of the mean distances between neighbouring atoms. AEM allows more local investigations, down to the scale of individual lattice planes when performing high-resolution electron microscopy.

4.9.3.2 <u>Size and Shape</u>

For large scale features ($\geqslant$ 100 nm) scanning electron microscopy will provide results without the need to prepare electron transparent specimens.

4.9.3.3 <u>Distribution of Composition</u>

The distribution of composition on a macroscopic scale, across a catalyst pellet can be studied using electron probe microanalysis. This analytical technique provides a lateral resolution of about 1 μm.

AEM is the major tool for the study of distribution of composition on a microscopic scale. It allows measurement of the local composition with a spatial resolution of about 10 nm.

4.9.3.4 <u>Co-ordination, Valency and Electron Energy Levels</u>

Extended X-ray absorption fine structure spectroscopy (EXAFS) provides a means of selectively probing the environment of each element by choosing the central atom and allowing the characterisation of the structure of the

outer electronic shells. In the case of amorphous solids this technique allows the determination of local structural parameters around the excited atom, such as co-ordination numbers and interatomic distances.

Infra-red spectroscopy, Fourier transform infra-red spectroscopy and Raman spectroscopy are most frequently used for the study of the nature of absorbed molecules and of their binding with the catalyst surface.

4.9.3.5   Surface Composition

X-ray photo electron spectroscopy (XPS), otherwise known as electron spectroscopy for chemical analysis (ESCA), may be used for surface analysis. This technique measures the energy distribution of electrons ejected from atoms or molecules by a source of soft X-rays. Binding energy values can identify elements present on the surface, chemical changes in the first few monolayers can be observed and shifts in binding energies are informative of atomic environments.

4.9.3.6   Dispersion

The fraction of potentially active atoms which are effectively on the surface of the solid can be determined by electron microscopy or X-ray line broadening via mean particle size when sufficiently large particles are present. Another method is to determine dispersion from surface composition, as measured by a surface sensitive technique such as XPS.

4.9.3.7   Co-ordination and Chemical State at the Surface

XPS is the only technique allowing a selective study of the valency of near-surface atoms.

CONCLUSIONS

1. The reactor and associated equipment, designed and constructed to study the thermal decomposition of hydrocarbons, gave kinetic data and product distributions for the pyrolysis of n-butane comparable to that appearing in the literature.

2. The first order rate constant for the thermal decomposition of n-butane can be represented by the equation $k_1 = 7.98(\pm 0.14) \times 10^{13} e^{-263(\pm 17)}/RT$.

3. The energy of activation for the thermal decomposition of n-butane was calculated as being 264 kJmol^{-1}.

4. Analysis of the products formed and the kinetic data given upon the pyrolysis of n-butane has allowed the proposition of a reaction mechanism. This is in accord with others in the literature.

5. 2,2-dimethylbutane was considered to be a suitable feed material for the investigation of the effects of various porphyrins upon hydrocarbon pyrolysis, since the onset of thermal decomposition occurs at a relatively low temperature.

6. The first order rate constant for the thermal decomposition of 2,2-dimethylbutane can be represented by the equation
$k_1 = 1.99 (\pm 0.93) \times 10^{12} e^{-201}/RT$.

7. The energy of activation for the thermal decomposition of 2,2-dimethyl-butane was calculated as being 201 kJ mol^{-1}.

8. Analysis of the products formed and the kinetic data given upon the pyrolysis of 2,2-dimethylbutane has allowed the proposition of a reaction mechanism differing from others found in the literature.

9. Both silica gel and alpha-alumina are suitable materials to act as

physical supports for various porphyrins to be studied under the conditions of hydrocarbon pyrolysis.

10. Base etioporphyrin was synthesised by two different routes. The first gave an overall yield of 5.3% by four steps and the second pathway gave an overall yield of 2.1% by three steps.

11. A light brown/red viscous oil was isolated from Tia Juana Pesado topped crude which contained 1.98% petroporphyrins.

12. Seven different porphyrins were shown to be thermally stable up to a temperature of 540°C.

13. The effects of nine different, but related, porphyrin species towards the decomposition of 2,2-dimethylbutane were examined. All nine were shown to act as cracking catalysts.

14. vanadyl and nickel etioporphyrins behaved similarly to each other but differently compared to the other seven porphyrin species examined.

15. The most effective cracking catalyst at a temperature of 458°C was vanadyl etioporphyrin.
   The most effective cracking catalyst at a temperature of 548°C was vanadyl hematoporphyrin IX.

16. The least effective cracking catalyst at a temperature of 458°C was base etioporphyrin.
   The least effective cracking catalysts at a temperature of 548°C were base and palladium etioporphyrins.

17. For the decomposition of 2,2-dimethylbutane the lowest activation energy was given by vanadyl etioporphyrin (86 kJ mol^{-1}).
   For the decomposition of 2,2-dimethylbutane the highest activation energy was given by platinum etioporphyrin (108 kJ mol^{-1}).

18. Four out of the nine porphyrins examined more than halved the activation energy required for the purely thermal decomposition of 2,2-dimethylbutane.

19. The highest first order rate constants (fastest reactions) for the cracking of 2,2-dimethylbutane were given by vanadyl hematoporphyrin IX, nickel etioporphyrin and vanadyl etioporphyrin.

    The lowest first order rate constant (slowest reaction) for the cracking of 2,2-dimethylbutane was given by base etioporphyrin.

20. Analysis of the products formed and the kinetic data given upon the cracking of 2,2-dimethylbutane effected by the various porphyrins has allowed the proposition of a reaction mechanism based on increasing the rate of homolytic bond cleavage.

21. Three hematoporphyrins examined gave no detectable hydrogen chemisorption. Four etioporphyrins examined all provided hydrogen chemisorption.

22. The effects that seven different porphyrins had on 1-hexene were tested over the temperature range 325 - 450°C. All species catalysed the decomposition reaction and no hydrogenation was detected.

23. At a temperature of 150°C three different porphyrins were shown to catalyse the hydrogenation of 1-hexene.

SUGGESTIONS FOR FUTURE INVESTIGATION

Temperature programmed decomposition tests have shown that porphyrins are thermally stable up to 540°C. However, visual examination of the porphyrin samples following testing revealed that a colour change from magenta to dark blue/black had occurred. No peaks were shown in the traces obtained, inferring that thermal decomposition of the porphyrin had not occurred. These two pieces of evidence would seem to be in conflict with one another. By a combination of physical and chemical methods it should be possible to determine whether any chemical change had occurred on heating.

During this investigation two different synthetic routes both yielded the crystalline solid base etioporphyrin I. In both cases the overall yield of final product was less than six per cent. As a consequence of this, large scale laboratory reactions need to be performed initially if sufficient porphyrin is to be obtained to allow detailed catalytic studies. Some of the reaction steps failed to yield the desired product in the quantities given in the literature. By critical examination of the experimental procedures and techniques used during the porphyrin synthesis it may be possible to considerably improve the final yield of base etioporphyrin.

There are a number of reported cases in the available literature where solid petroporphyrins have been isolated from a sample of crude oil. During this investigation a concentrate was obtained which contained approximately two per cent of petroporphyrins. By modifying the chromatographic procedure, or using a different approach, it may be possible to obtain a concentrate containing a higher level of petroporphyrins than above.

To assist in obtaining a concentrate containing a high level of petroporphyrins it may be advantageous to start with a material having more porphyrins than Tia Juana Pesado topped crude.

During this investigation it has been demonstrated that nine different, but related, porphyrin species acted as catalysts towards the decomposition of a single, pure hydrocarbon vapour. By dosing various porphyrins, at increasing levels, into samples of selected crude oils the action of porphyrins under these conditions may be examined. In this way design data may be obtained from the catalytic action of porphyrins towards crude oils.

It has been demonstrated during the course of this investigation that porphyrins act as hydrogenation catalysts at a temperature of $150^{\circ}C$. However, above $325^{\circ}C$ no hydrogenation of 1-hexene could be detected due to the catalytic cracking of this alkene. At a point between these two temperatures hydrogenation stops and cracking starts. Manipulation of the experimental conditions used would reveal this temperature for any given alkene.

Two etioporphyrins studied acted as efficient catalysts towards the hydrogenation of 1-hexene while one hematoporphyrin was less effective. By increasing the range of porphyrins examined at the lower temperature of $150^{\circ}C$ it would be possible to determine which species were effective hydrogenation catalysts. Examination of the product distributions and kinetic data obtained from such a study may allow elucidation of mechanistic differences.

If additional data on the effects of porphyrins towards the hydrogenation of alkenes is required it may be appropriate to use a more complex model hydrocarbon. e.g 1,3-butadiene.

Under the correct conditions it has been demonstrated that porphyrins can act as effective catalysts towards the decomposition and hydrogenation of hydrocarbons. During this study heat has been used as the driving force for these reactions. It is conceivable that porphyrins may catalyse a range of reactions where light or sound is used to replace heat as the source of

energy. If this were proven to be the case then porphyrins could be used to catalyse reactions involving temperature sensitive reactants and/or products.

There are numerous examples cited in the literature of the catalytic activities of porphyrins. During this investigation it has been demonstrated that porphyrins act as catalysts towards the decomposition and hydrogenation of hydrocarbons. Additional information on the action of porphyrins may be obtained by examination of the effects of porphyrins on other, different reaction systems. e.g. redox reactions, oxidation-reduction, etc.

16.   Rate constants at various temperatures, for the thermal cracking
        of 2,2-dimethylbutane.

17-20. Influence of base etioporphyrin I on the cracking of
        2,2-dimethylbutane.

        17.   0.5% base etioporphyrin I

        18.   1.0% base etioporphyrin I.

        19.   2.5% base etioporphyrin I.

        20.   5.0% base etioporphyrin I.

21-24. Influence of vanadyl etioporphyrin I on the cracking of
        2,2-dimethylbutane.

        21.   0.5% vanadyl etioporphyrin I.   .

        22.   1.0% vanadyl etioporphyrin I.

        23.   2.5% vanadyl etioporphyrin I.

        24.   5.0% vanadyl etioporphyrin I.

25-28. Influence of nickel etioporphyrin I on the cracking of
        2,2-dimethylbutane.

        25.   0.5% nickel etioporphyrin I.

        26.   1.0% nickel etioporphyrin I.

        27.   2.5% nickel etioporphyrin I.

        28.   5.0% nickel etioporphyrin I.

29-32. Influence of platinum etioporphyrin I on the cracking of
        2,2-dimethylbutane.

        29.   0.5% platinum etioporphyrin I.

        30.   1.0% platinum etioporphyrin I.

        31.   2.5% platinum etioporphyrin I.

        32.   5.0% platinum etioporphyrin I.

33-36.   Influence of palladium etioporphyrin I on the cracking of 2,2-dimethylbutane.

       33.   0.5% palladium etioporphyrin I.

       34.   1.0% palladium etioporphyrin I.

       35.   2.5% palladium etioporphyrin I.

       36.   5.0% palladium etioporphyrin I.

37-40.   Influence of base hematoporphyrin IX on the cracking of 2,2-dimethylbutane.

       37.   0.5% base hematoporphyrin IX.

       38.   1.0% base hematoporphyrin IX.

       39.   2.5% base hematoporphyrin IX.

       40.   5.0% base hematoporphyrin IX.

41-44.   Influence of vanadyl hematoporphyrin IX on the cracking of 2,2-dimethylbutane.

       41.   0.5% vanadyl hematoporphyrin IX.

       42.   1.0% vanadyl hematoporphyrin IX.

       43.   2.5% vanadyl hematoporphyrin IX.

       44.   5.0% vanadyl hematoporphyrin IX.

45-48.   Influence of nickel hematoporphyrin IX on the cracking of 2,2-dimethylbutane.

       45.   0.5% nickel hematoporphyrin IX.

       46.   1.0% nickel hematoporphyrin IX.

       47.   2.5% nickel hematoporphyrin IX.

       48.   5.0% nickel hematoporphyrin IX.

49-52.   Influence of petroporphyrin concentrate on the cracking of 2,2-dimethylbutane.

Table 1.   Boiling point ranges of the major fuel
            products obtained from crude oil

Product name	Boiling point range ($^{\circ}C$)
Gasoline (Petrol)	35-200
Kerosene (Paraffin)	150-260
Aviation turbine fuel (1)	60-240
(2)	160-250
Vaporising oil	140-260
Gas oil	180-350
Diesel fuel	180-350

Table 2.   Content of porphyrins and metals

in various crude oils

Oil	Ni (ppm)	V (ppm)	Total metals (ppm)	Porphyrins (ppm)
West Texas	5	23	28	12
Tia Juana, Venezuela	24	187	211	60
Coleville, Saskatchewan	32	94	126	110
Rhodes, Kansas	33	133	166	135
Tatums, Oklahoma	71	148	219	165
Lagunillas, Venezuela	41	317	358	170
Santa Maria, California	130	280	410	300
Backaquero, Venezuela	53	430	483	380

Table 3. Vanadium contents of various crude oils
and corresponding fuel oil ash

Source	V in crude oil (ppm)	V_2O_5 in resulting ash	
		ppm	%
Venezuela	250	750,000	75
Middle east	30	80,000	8
Oklahoma	50	220,000	22
Texas	2	14,000	1.4

Table 4. <u>Relative rates of formation of radicals</u>

radical formed	relative rate of formation
methyl	1
ethyl and higher primary	3
secondary	9
tertiary	27

Table 5.   Relative probabilities of bond

rupture in an alkane

compound cracked	relative probability of rupture between carbon atoms		
	1-2	2-3	3-4
n-pentane	1.0	0.78	-
n-hexane	1.0	0.50	0.25
n-heptane	1.0	0.64	0.35
n-octane	1.0	1.0	0.10

Table 6.   <u>Factors used for the calculation of the hydro-</u>

<u>carbon concentration in the product gas stream</u>

hydrocarbon	factor
methane	1.000
ethane	2.033
ethene	1.872
propane	2.596
n-butane	3.018
propene	2.966
n-pentane	2.819
1-butene	3.535
n-hexane	3.989
2-methylbutane	5.161
2,2-DMB	6.880

Table 7.　　　　　Reactor gas composition following

thermal cracking of n-butane

T (°C)	% in reactor gas effluent						
	methane	ethane	ethene	propane	n-butane	propene	1-butene
550	-	-	-	-	100.00	-	-
600	1.1	0.3	0.5	1.0	96.9	0.2	-
635	3.7	0.8	2.1	1.2	90.8	1.4	-
640	4.2	0.9	2.4	1.2	91.2	0.1	-
645	4.5	0.9	2.7	1.1	88.9	1.9	-
650	4.5	0.9	2.5	1.2	88.7	2.2	-
653	5.3	1.1	3.1	1.2	86.8	2.5	-
655	6.0	1.2	3.6	1.2	85.1	2.9	-
660	5.9	1.2	3.7	1.2	85.1	2.9	-
665	6.8	1.3	4.2	1.3	82.9	3.4	0.1
670	7.6	1.5	4.9	1.3	80.7	3.9	0.1
675	8.7	1.6	5.7	1.4	77.7	4.7	0.2
700	13.8	2.5	10.4	1.7	63.3	7.9	0.4
725	20.0	3.2	18.8	1.2	44.9	11.1	0.8
750	28.3	3.8	31.0	-	20.3	15.8	0.8

Table 8. Mass Balance for the thermal decomposition of n-butane at 750°C

Carbon Balance

Reactor			
In		Out	
Compound	Weight C	Compound	Weight C
C_4H_{10}	1.0000	CH_4	0.2565
		C_2H_6	0.0367
		C_2H_4	0.3211
		$n-C_4H_{10}$	0.2030
		C_3H_6	0.1636
		$1-C_4H_8$	0.0083
Total	1.0000	Total	0.9892

Hydrogen Balance

Reactor			
In		Out	
Compound	Weight H	Compound	Weight H
C_4H_{10}	1.0000	CH_4	0.4107
		C_2H_6	0.0441
		C_2H_4	0.2570
		$n-C_4H_{10}$	0.2030
		C_3H_6	0.1311
		$1-C_4H_8$	0.0064
Total	1.0000	Total	1.0523

Table 9.   Rate constants, at various temperatures, for the thermal cracking of n-butane

T (°C)	$\frac{1}{T}$ x10^{-3} (K)	k_1^o (sec^{-1})	Log k_1^o (sec^{-1})
600	1.1455	0.0170	-1.7675
635	1.1013	0.0687	-1.1623
640	1.0953	0.0689	-1.1613
645	1.0893	0.0897	-1.0469
650	1.0834	0.0975	-1.0107
653	1.0799	0.1202	-0.9198
655	1.0776	0.1376	-0.8612
660	1.0718	0.1482	-0.8290
665	1.0661	0.1808	-0.7426
670	1.0604	0.2177	-0.6620
675	1.0549	0.2627	-0.5805
700	1.0277	0.6314	-0.1997
725	1.0020	1.4076	0.1484
750	0.9775	3.1352	0.4958

Table 10.   Effect of various reaction tube packings upon

the _ _ cracking of n-butane at 653°C

hydrocarbon	% in product stream					
	reaction tube packing					
	1	2	3	4	5	6
methane	5.3	4.1	4.4	3.4	3.8	19.5
ethane	1.1	0.9	1.3	0.9	0.8	7.5
ethene	3.1	2.5	2.9	2.0	2.0	5.9
propane	1.2	1.2	1.4	1.3	1.1	4.2
butane	86.8	89.7	87.9	90.8	91.0	39.9
propene	2.5	1.6	2.0	1.5	1.1	6.4
1-butene	-	-	0.1	0.1	0.2	4.0
1,3-butadiene	-	-	-	-	-	12.6

Key to reaction tube packing

1   no packing

2   6-22 mesh silica gel

3   60-80 mesh silica gel

4   alpha-alumina powder

5   quartered gamma-alumina 1/8 inch extrudates

6   gamma-alumina powder

Table 11

Thermal cracking of 2,2-dimethylbutane at various flow rates

temperature (°C)	% in reactor gas effluent										
	420					440					
flow rate ($cm^3 min^{-1}$)	2.609	1.579	1.034	0.714	0.429	2.190	1.260	0.938	0.779	0.550	0.282
volume velocity ($cm^3 sec^{-1}$)	0.043	0.026	0.017	0.012	0.007	0.0365	0.021	0.016	0.013	0.009	0.005
methane	-	-	-	-	-	0.7	0.8	0.9	1.0	1.2	1.5
ethane	-	-	-	-	-	-	-	-	-	-	0.2
ethene	-	-	-	-	-	0.7	0.9	1.0	1.1	1.3	1.4
propane	-	-	-	-	-	-	-	-	-	-	-
n-butane	-	-	-	-	-	-	-	-	-	-	-
propene	-	-	-	-	-	-	-	-	-	-	-
n-pentane	-	-	-	-	-	-	-	-	-	-	-
n-butene	0.2	0.2	0.3	0.3	0.3	-	0.3	0.4	0.4	0.4	0.4
n-hexane	-	-	-	-	-	-	-	-	-	-	-
2-methylbutane	-	-	-	-	-	-	-	-	-	-	-
2,2-DMB	99.8	99.8	99.7	99.7	99.7	98.6	98.0	97.7	97.5	97.1	96.5

Table 12   Thermal cracking of 2,2-dimethylbutane at various flow rates

temperature (°C)	460						500					
flow rate (cm³min⁻¹)	1.923	1.333	1.017	0.714	0.531	0.375	1.528	1.212	0.952	0.769	0.496	0.328
volume velocity (cm³sec⁻¹)	0.032	0.022	0.017	0.012	0.009	0.006	0.026	0.020	0.016	0.012	0.008	0.006
methane	0.9	1.5	1.8	2.4	2.7	3.2	5.5	6.0	6.3	6.6	7.1	7.5
ethane	-	-	-	-	-	-	0.5	0.7	0.8	1.0	1.3	1.4
ethene	1.4	1.5	1.6	1.7	1.8	1.8	7.3	7.3	7.4	7.4	7.5	7.6
propane	-	-	-	-	-	-	-	-	-	-	-	-
n-butane	-	-	-	-	-	-	-	-	-	-	-	-
propene	-	-	-	-	-	-	0.5	0.6	0.7	0.7	0.8	0.8
n-pentane	-	-	-	-	-	-	-	-	-	-	-	-
n-butene	1.4	1.4	1.5	1.5	1.6	1.6	2.7	2.7	2.8	2.9	2.9	2.9
n-hexane	-	-	-	-	-	-	-	-	-	-	-	-
2-methylbutane	-	-	-	-	-	-	-	-	-	-	-	-
2,2-DMB	96.3	95.6	95.1	94.4	93.9	93.4	83.5	82.7	82.0	81.4	80.4	79.8

% in reactor gas effluent

Table 13   Thermal cracking of 2,2-dimethylbutane at various flow rates

temperature (°C)									
			550				600		
	% in reactor gas effluent								
flow rate (cm³min⁻¹)	1.632	1.277	1.017	0.876	0.556	0.387	2.464	1.622	1.017	0.541	0.106
volume velocity (cm³sec⁻¹)	0.027	0.021	0.017	0.015	0.009	0.007	0.041	0.027	0.017	0.009	0.002
methane	10.5	11.1	11.6	12.1	12.8	13.3	16.7	17.5	18.2	19.0	19.7
ethane	1.3	1.7	1.9	2.1	2.6	2.8	2.4	2.7	3.1	3.5	3.9
ethene	8.1	8.1	8.3	8.3	8.4	8.5	13.4	13.5	13.7	13.8	14.0
propane	-	-	-	-	-	-	0.4	0.5	0.5	0.5	0.6
n-butane	0.3	0.4	0.4	0.4	0.5	0.5	0.4	0.5	0.5	0.6	0.6
propene	1.7	1.8	1.8	1.8	1.9	1.9	2.7	2.7	2.8	2.8	2.9
n-pentane	-	-	-	-	-	-	6.9	7.1	7.2	7.4	7.5
n-butene	7.5	7.7	7.8	7.8	7.9	8.0	5.2	5.4	5.5	5.6	5.8
n-hexane	-	-	-	-	-	-	-	-	-	-	-
2-methylbutane	-	-	-	-	-	-	-	-	-	-	-
2,2-DMB	70.6	69.2	68.2	67.5	65.9	65.0	51.9	50.1	48.5	46.8	45.0

Table 14.   Mass Balance for the thermal decomposition
             of 2,2-dimethylbutane at 650°C

Carbon Balance

Reactor			
IN		OUT	
Compound	Weight C	Compound	Weight C
$CH_3C(CH_3)_2CH_2CH_3$	1.0000	CH_4	0.2087
		C_2H_6	0.0535
		C_2H_4	0.1505
		C_3H_8	0.0068
		$n-C_4H_{10}$	0.0059
		C_3H_6	0.0420
		$1-C_4H_6$	0.0727
		$n-C_5H_{12}$	0.1652
		$CH_3C(CH_3)_2CH_2CH_3$	0.2730
Total	1.0000	Total	0.9783

Hydrogen Balance

Reactor			
IN		OUT	
Compound	Weight H	Compound	Weight H
$CH_3C(CH_3)CH_2CH_3$	1.0000	CH_4	0.3578
		C_2H_6	0.0688
		C_2H_4	0.1290
		C_3H_8	0.0078
		$n-C_4H_{10}$	0.0064
		C_3H_6	0.0360
		$1-C_4H_8$	0.0623
		$n-C_5H_{12}$	0.1700
		$CH_3C(CH_3)_2CH_2CH_3$	0.2730
Total	1.0000	Total	1.1111

Table 15.   <u>The restraining coefficient for the cracking</u>

<u>of 2,2-dimethylbutane at various temperatures</u>

T($^\circ$C)	T(K)	β
458	731	0.067
478	751	0.108
497	770	0.165
515	788	0.242
532	805	0.343
548	821	0.471

Table 16.   Rate constants, at various temperatures, for

the thermal cracking of 2,2-dimethylbutane

$T(^\circ C)$	$1/T \times 10^{-3} (K)$	$k_1^\circ (sec^{-1})$	$Log\ k_1^\circ (sec^{-1})$
420	1.4430	0.0008	-3.0975
440	1.4025	0.0061	-2.2150
460	1.3643	0.0155	-1.8093
500	1.2937	0.0786	-1.1045
550	1.2151	0.2597	-0.5855
600	1.1455	0.8568	-0.0671

Table 17. Influence of 0.5% base etioporphyrin I on the cracking of 2,2-dimethylbutane

support	hydrocarbon	% in reactor gas effluent											
		silica						α -alumina					
		458°C	478°C	497°C	515°C	532°C	548°C	458°C	478°C	497°C	515°C	532°C	548°C
	methane	3.4	5.3	6.5	8.1	10.1	12.0	3.3	5.1	6.9	8.1	9.3	11.9
	ethane	0.4	0.8	1.1	1.3	1.6	1.9	0.4	0.7	0.8	1.0	1.2	1.3
	ethene	3.2	5.4	7.3	7.6	8.3	8.9	4.7	5.7	6.6	7.4	8.2	8.8
	propane	–	–	–	–	0.2	0.6	–	–	–	–	0.1	0.4
	n-butane	–	–	–	–	–	–	–	–	–	–	–	–
	propene	–	0.1	0.3	0.6	1.0	1.5	–	0.2	0.6	1.0	1.5	2.1
	n-pentane	3.1	4.4	5.4	5.7	6.0	6.4	3.7	4.3	4.7	5.4	6.0	6.5
	n-butene	–	–	–	–	–	–	–	–	–	–	–	–
	n-hexane	0.5	0.5	0.5	0.5	0.6	0.6	0.4	0.5	0.5	0.5	0.5	0.5
	2-methylbutane	–	–	–	–	–	–	–	–	–	–	–	–
	2,2-DMB	89.4	83.5	78.9	76.2	72.2	68.1	87.5	83.5	79.9	76.6	73.2	68.5

Table 18.   Influence of 1.0% base etioporphyrin I on the cracking of 2,2-dimethylbutane

support		% in reactor gas effluent											
		silica						α-alumina					
hydrocarbon		458°C	478°C	497°C	515°C	532°C	548°C	458°C	478°C	497°C	515°C	532°C	548°C
methane		3.6	5.6	7.1	8.6	10.2	11.8	3.7	5.2	6.8	8.6	10.2	11.7
ethane		0.4	0.9	1.0	1.1	1.5	1.7	0.5	0.6	0.8	1.0	1.3	1.5
ethene		3.1	4.2	5.2	6.3	7.5	8.6	3.2	4.2	5.2	6.3	7.4	8.5
propane		-	-	-	-	0.3	0.5	-	-	-	-	0.3	0.5
n-butane		-	-	-	-	-	-	-	-	-	-	-	-
propene		2.0	2.1	2.2	2.2	2.3	2.4	2.1	2.2	2.2	2.3	2.4	2.4
n-pentane		2.6	3.5	4.4	5.2	6.2	7.0	2.6	3.5	4.4	5.4	6.4	7.4
n-butene		-	-	-	-	-	-	-	-	-	-	-	-
n-hexane		0.5	0.5	0.6	0.6	0.6	0.6	0.5	0.5	0.5	0.6	0.6	0.6
2-methylbutane		-	-	-	-	-	-	-	-	-	-	-	-
2,2-DMB		87.8	83.2	79.5	76.0	71.4	67.4	87.4	83.8	80.1	75.8	71.4	67.4

Table 19. Influence of 2.5% base etioporphyrin I on the cracking of 2,2-dimethylbutane

| support | % in reactor gas effluent | | | | | | | | | | | |
| | silica | | | | | | α-alumina | | | | | |
hydrocarbon	458°C	478°C	497°C	515°C	532°C	548°C	458°C	478°C	497°C	515°C	532°C	548°C
methane	3.8	5.3	6.9	8.6	10.3	11.8	3.9	5.5	7.1	8.7	10.3	11.8
ethane	0.5	0.6	0.8	1.1	1.2	1.7	0.6	0.7	0.9	1.0	1.3	1.7
ethene	3.2	4.2	5.2	6.4	7.7	8.8	3.1	4.2	5.2	6.4	7.6	8.7
propane	-	-	-	-	-	0.4	-	-	-	-	-	0.3
n-butane	-	-	-	-	-	-	-	-	-	-	-	-
propene	2.1	2.1	2.2	2.2	2.3	2.3	2.0	2.1	2.1	2.2	2.3	2.3
n-pentane	3.1	3.7	4.6	5.5	6.5	7.2	2.9	3.6	4.6	5.6	6.4	7.3
n-butene	-	-	-	-	-	-	-	-	-	-	-	-
n-hexane	0.6	0.6	0.6	0.6	0.6	0.6	0.4	0.5	0.5	0.6	0.6	0.6
2-methylbutane	-	-	-	-	-	-	-	-	-	-	-	-
2,2-DMB	86.7	83.5	79.7	75.6	71.4	67.2	87.1	83.4	79.6	75.5	71.5	67.3

Table 20. Influence of 5.0% base etioporphyrin I on the cracking of 2,2-dimethylbutane

support	% in reactor gas effluent											
	silica						α -alumina					
hydrocarbon	458°C	478°C	497°C	515°C	532°C	548°C	458°C	478°C	497°C	515°C	532°C	548°C
methane	4.3	5.6	7.0	8.2	10.4	13.4	4.7	6.5	8.4	10.3	12.2	14.1
ethane	0.7	1.0	1.3	1.7	2.1	2.6	0.6	1.0	1.2	1.6	2.2	2.8
ethene	3.3	4.1	5.3	6.4	7.9	9.2	3.2	4.2	5.2	6.5	7.8	9.0
propane	-	-	-	0.2	0.3	0.4	-	0.3	0.3	0.4	0.5	0.6
n-butane	-	-	-	-	-	-	-	-	-	-	-	-
propene	2.9	2.9	3.0	3.0	3.0	3.0	2.7	2.7	2.7	2.8	2.8	2.8
n-pentane	3.8	4.5	5.4	6.2	7.1	7.9	3.7	4.4	5.4	6.4	7.0	7.7
n-butene	-	-	-	-	-	-	-	-	-	-	-	-
n-hexane	0.5	0.5	0.5	0.6	0.6	0.6	0.5	0.5	0.5	0.5	0.6	0.6
2-methylbutane	-	-	-	-	-	-	-	-	-	-	-	-
2,2-DMB	84.5	81.4	77.5	73.7	68.6	62.9	84.6	80.4	76.3	71.5	66.9	62.4

Table 21.   Influence of 0.5% vanadyl etioporphyrin I on the cracking of 2,2-dimethylbutane

| | % in reactor gas effluent | | | | | | | | | | | | |
| support | silica | | | | | | α -alumina | | | | | |
hydrocarbon	458°C	478°C	497°C	515°C	532°C	548°C	458°C	478°C	497°C	515°C	532°C	548°C
methane	10.4	11.2	12.2	13.4	14.6	15.6	10.0	11.0	12.1	13.1	14.2	15.4
ethane	2.9	3.1	3.3	3.6	3.8	4.1	3.0	3.1	3.3	3.5	3.6	3.8
ethene	6.0	6.3	6.7	7.2	7.6	8.0	5.7	6.1	6.4	6.9	7.4	7.9
propane	-	0.2	0.4	0.4	0.4	0.4	-	0.1	0.2	0.4	0.4	0.5
n-butane	-	-	-	-	-	-	-	-	-	-	-	-
propene	0.2	0.3	0.4	0.6	1.0	1.3	-	0.3	0.5	0.7	1.2	1.4
n-pentane	-	-	-	-	-	-	-	-	-	-	-	-
n-butene	0.9	1.0	1.2	1.4	1.7	1.8	0.8	1.0	1.2	1.5	1.7	1.9
n-hexane	0.1	0.2	0.2	0.3	0.3	0.4	0.1	0.1	0.2	0.3	0.3	0.4
2-methylbutane	-	-	0.1	0.2	0.2	0.2	-	0.1	0.1	0.2	0.2	0.3
2,2-DMB	79.5	77.7	75.5	72.9	70.4	68.2	80.4	78.2	76.0	73.4	71.0	68.4

Table 22. Influence of 1.0% vanadyl etioporphyrin I on the cracking of 2,2-dimethylbutane

support		% in reactor gas effluent											
		silica						α -alumina					
	hydrocarbon	458°C	478°C	497°C	515°C	532°C	548°C	458°C	478°C	497°C	515°C	532°C	548°C
	methane	10.9	12.5	13.9	15.4	17.0	18.6	11.1	12.5	14.1	15.8	17.6	19.1
	ethane	4.3	4.5	4.7	5.0	5.4	5.7	4.3	4.5	4.8	5.2	5.5	5.9
	ethene	6.6	6.9	7.3	7.5	7.9	8.3	6.7	6.9	7.2	7.5	7.9	8.2
	propane	0.3	0.4	0.4	0.5	0.5	0.6	0.2	0.3	0.4	0.4	0.5	0.5
	n-butane	-	-	-	-	-	-	-	-	-	-	-	-
	propene	1.0	1.3	1.5	1.9	2.3	2.6	0.9	1.1	1.3	1.8	2.2	2.5
	n-pentane	-	-	-	-	-	-	-	-	-	-	-	-
	n-butene	1.2	1.3	1.4	1.6	1.9	2.1	1.0	1.1	1.3	1.5	1.6	1.9
	n-hexane	0.3	0.4	0.4	0.5	0.6	0.6	0.2	0.3	0.3	0.5	0.6	0.6
	2-methylbutane	-	0.1	0.1	0.2	0.2	0.3	0.1	0.2	0.2	0.3	0.3	0.3
	2,2-DMB	75.4	72.6	70.3	67.4	64.2	61.2	75.5	73.1	70.4	67.0	63.8	61.0

Table 23. Influence of 2.5% vanadyl etioporphyrin I on the cracking of 2,2-dimethylbutane

% in reactor gas effluent

support hydrocarbon	silica						α-alumina					
	458°C	478°C	497°C	515°C	532°C	548°C	458°C	478°C	497°C	515°C	532°C	548°C
methane	11.0	13.0	15.2	17.9	20.2	22.6	11.4	13.6	15.9	18.3	20.7	22.9
ethane	4.5	4.7	5.0	5.4	5.8	6.2	4.4	4.7	5.0	5.4	5.9	6.4
ethene	6.9	7.2	7.4	7.8	8.3	8.7	7.1	7.4	7.7	8.1	8.5	8.9
propane	0.3	0.4	0.4	0.5	0.6	0.6	0.4	0.5	0.6	0.6	0.7	0.7
n-butane	-	-	-	-	-	-	-	-	-	-	-	-
propene	1.1	1.4	1.6	1.9	2.2	2.6	1.2	1.4	1.6	1.8	2.1	2.5
n-pentane	-	-	-	-	-	-	-	-	-	-	-	-
n-butene	1.1	1.3	1.4	1.6	1.9	2.3	1.2	1.3	1.6	1.9	2.1	2.5
n-hexane	0.4	0.5	0.7	0.7	0.9	1.0	0.3	0.4	0.4	0.6	0.7	0.9
2-methylbutane	0.3	0.3	0.4	0.6	0.7	0.7	0.2	0.3	0.3	0.6	0.6	0.7
2,2-DMB	74.4	71.2	67.9	63.6	59.4	55.3	73.8	70.4	66.9	62.7	58.7	54.5

Table 24.   Influence of 5.0% vanadyl etioporphyrin I on the cracking of 2,2-dimethylbutane

hydrocarbon	% in reactor gas effluent											
	silica						α-alumina					
	458°C	478°C	497°C	515°C	532°C	548°C	458°C	478°C	497°C	515°C	532°C	548°C
methane	12.6	15.2	18.1	21.1	24.0	26.9	13.1	15.3	18.5	21.5	24.6	27.5
ethane	4.7	5.0	5.3	5.7	6.1	6.5	4.8	5.0	5.2	5.6	6.0	6.3
ethene	7.3	7.5	7.7	8.2	8.6	9.0	7.1	7.3	7.6	8.0	8.4	8.9
propane	0.4	0.5	0.5	0.6	0.7	0.7	0.3	0.4	0.6	0.6	0.7	0.8
n-butane	-	-	-	-	-	-	-	-	-	-	-	-
propene	1.4	1.7	2.0	2.5	3.0	3.4	1.6	1.8	2.1	2.6	3.1	3.5
n-pentane	-	-	-	-	-	-	-	-	-	-	-	-
n-butene	1.2	1.4	1.6	1.9	2.1	2.4	1.3	1.4	1.6	1.8	2.1	2.4
n-hexane	0.6	0.7	0.7	0.8	0.9	1.0	0.7	0.7	0.8	1.0	1.1	1.1
2-methylbutane	0.3	0.5	0.5	0.6	0.6	0.6	0.5	0.5	0.6	0.7	0.7	0.7
2,2-DMB	71.5	67.5	63.6	58.6	54.0	49.5	70.6	67.6	63.0	58.2	53.3	48.8

Table 25. Influence of 0.5% nickel etioporphyrin I on the cracking of 2,2-dimethylbutane

% in reactor gas effluent

support	silica						α-alumina					
hydrocarbon	458°C	478°C	497°C	515°C	532°C	548°C	458°C	478°C	497°C	515°C	532°C	548°C
methane	7.7	8.6	9.6	10.7	11.8	13.0	7.5	8.6	9.7	10.8	12.0	13.1
ethane	3.6	3.7	3.8	4.0	4.2	4.4	3.5	3.7	3.9	4.0	4.2	4.3
ethene	6.6	6.8	7.0	7.4	7.8	8.1	6.2	6.5	6.9	7.4	7.8	8.1
propane	-	0.2	0.3	0.3	0.4	0.5	-	-	0.2	0.3	0.3	0.4
n-butane	-	-	-	-	-	-	-	-	-	-	-	-
propene	0.5	1.0	1.5	1.9	2.4	2.8	0.5	0.8	1.3	1.8	2.3	2.7
n-pentane	-	-	-	-	-	-	-	-	-	-	-	-
n-butene	1.1	1.5	2.1	2.8	3.3	3.8	1.2	1.6	2.0	2.6	3.2	3.7
n-hexane	0.4	0.4	0.5	0.5	0.5	0.5	0.4	0.4	0.4	0.5	0.5	0.5
2-methylbutane	-	0.1	0.1	0.2	0.2	0.2	-	0.1	0.1	0.1	0.2	0.2
2,2-DMB	80.1	77.7	75.1	72.2	69.4	66.7	80.7	78.3	75.5	72.5	69.5	67.0

Table 26. Influence of 1.0% nickel etioporphyrin I on the cracking of 2,2-dimethylbutane

support	% in reactor gas effluent											
	silica						α-alumina					
hydrocarbon	458°C	478°C	497°C	515°C	532°C	548°C	458°C	478°C	497°C	515°C	532°C	548°C
methane	9.3	10.4	11.5	12.7	14.1	15.2	9.5	10.5	11.5	12.8	13.9	15.1
ethane	4.5	4.7	4.9	5.0	5.2	5.4	4.5	4.6	4.8	5.0	5.3	5.5
ethene	7.1	7.5	7.7	8.1	8.3	8.6	7.2	7.5	7.8	8.1	8.2	8.4
propane	-	0.4	1.1	1.5	1.9	2.2	-	-	0.3	1.1	1.6	1.9
n-butane	-	-	-	-	-	-	-	-	-	-	-	-
propene	0.6	1.1	1.6	2.1	2.7	3.2	0.7	0.9	1.3	1.8	2.5	3.0
n-pentane	-	-	-	-	-	-	-	-	-	-	-	-
n-butene	1.3	1.8	2.2	2.7	3.2	3.7	1.4	1.9	2.2	2.8	3.3	3.8
n-hexane	0.4	0.5	0.6	0.6	0.6	0.6	0.3	0.3	0.4	0.5	0.6	0.6
2-methylbutane	0.1	0.1	0.2	0.3	0.3	0.3	0.2	0.2	0.2	0.3	0.3	0.3
2,2-DMB	76.7	73.5	70.2	67.0	63.7	60.8	76.2	74.1	71.5	67.6	64.3	61.4

Table 27. Influence of 2.5% nickel etioporphyrin I on the cracking of 2,2-dimethylbutane

support	silica						α-alumina					
hydrocarbon	458°C	478°C	497°C	515°C	532°C	548°C	458°C	478°C	497°C	515°C	532°C	548°C
methane	10.2	11.7	13.4	15.2	17.0	18.7	10.2	11.8	13.5	15.1	16.7	18.4
ethane	4.7	4.8	5.0	5.3	5.6	5.9	4.6	4.9	5.1	5.4	5.8	6.1
ethene	7.1	7.4	7.7	8.1	8.6	8.9	7.3	7.5	7.9	8.3	8.7	9.0
propane	0.3	0.6	1.1	1.6	2.1	2.5	0.4	0.7	1.2	1.7	2.2	2.6
n-butane	-	-	-	-	-	-	-	-	-	-	-	-
propene	0.8	1.0	1.6	2.2	2.9	3.5	0.8	1.2	1.7	2.3	2.9	3.3
n-pentane	-	-	-	-	-	-	-	-	-	-	-	-
n-butene	1.6	2.0	2.5	2.7	3.1	3.6	1.8	2.0	2.2	2.5	2.7	3.0
n-hexane	0.5	0.6	0.6	0.6	0.7	0.7	0.5	0.5	0.6	0.7	0.7	0.7
2-methylbutane	0.2	0.2	0.3	0.4	0.4	0.4	0.2	0.3	0.3	0.3	0.4	0.5
2,2-DMB	74.6	71.7	67.8	63.9	59.6	55.8	74.2	71.1	67.5	63.7	59.9	56.4

% in reactor gas effluent

Table 28. Influence of 5.0% nickel etioporphyrin I on the cracking of 2,2-dimethylbutane

| | % in reactor gas effluent | | | | | | | | | | | |
| support | silica | | | | | | α-alumina | | | | | |
hydrocarbon	458°C	478°C	497°C	515°C	532°C	548°C	458°C	478°C	497°C	515°C	532°C	548°C
methane	11.5	13.7	16.4	19.1	21.9	24.3	11.0	13.3	15.8	18.5	21.0	23.6
ethane	5.1	5.3	5.5	5.9	6.2	6.4	4.9	5.1	5.3	5.7	6.2	6.5
ethene	7.3	7.6	7.9	8.5	9.1	9.5	7.2	7.5	8.0	8.6	9.1	9.6
propane	0.4	0.8	1.3	1.7	2.3	2.7	0.4	0.7	1.2	1.7	2.2	2.6
n-butane	-	-	-	-	-	-	-	-	-	-	-	-
propene	0.6	1.1	1.9	2.7	3.4	4.2	0.8	1.4	2.1	2.7	3.5	4.1
n-pentane	-	-	-	-	-	-	-	-	-	-	-	-
n-butene	1.6	1.9	2.4	2.9	3.4	3.8	1.6	2.0	2.4	2.9	3.5	3.9
n-hexane	0.6	0.6	0.7	0.7	0.8	0.8	0.6	0.7	0.7	0.8	0.9	0.9
2-methylbutane	0.2	0.3	0.4	0.4	0.5	0.5	0.3	0.4	0.4	0.5	0.6	0.6
2,2-DMB	72.7	68.7	63.5	58.1	52.4	47.8	73.2	68.9	64.1	58.6	53.0	48.2

Table 29. Influence of 0.5% platinum etioporphyrin I on the cracking of 2,2-dimethylbutane

support		% in reactor gas effluent											
		silica						α-alumina					
	hydrocarbon	458°C	478°C	497°C	515°C	532°C	548°C	458°C	478°C	497°C	515°C	532°C	548°C
	methane	3.2	4.3	6.2	8.2	10.2	12.3	3.8	4.8	6.7	8.5	10.6	12.6
	ethane	0.4	0.6	0.9	1.3	1.5	1.8	0.3	0.6	0.8	1.2	1.6	1.9
	ethene	3.4	4.5	5.5	6.6	7.7	8.9	3.7	4.4	5.3	6.5	7.7	8.7
	propane	-	-	-	-	0.2	0.6	-	-	-	-	0.4	0.5
	n-butane	-	-	-	-	-	-	-	-	-	-	-	-
	propene	1.1	1.4	1.7	1.8	2.0	2.3	0.8	1.1	1.5	1.9	2.1	2.4
	n-pentane	3.4	3.7	4.4	5.3	6.0	6.8	2.8	3.3	4.1	5.0	5.8	6.6
	n-butene	-	-	-	-	-	-	-	-	-	-	-	-
	n-hexane	0.5	0.7	0.6	0.7	0.7	0.7	0.4	0.3	0.5	0.6	0.6	0.5
	2-methylbutane	-	-	-	-	-	-	-	-	-	-	-	-
	2,2-DMB	88.0	84.8	80.7	76.1	71.7	66.6	88.2	85.5	81.1	76.3	71.2	66.8

Table 30.   Influence of 1.0% platinum etioporphyrin I on the cracking of 2,2-dimethylbutane

% in reactor gas effluent

support	silica						α-alumina					
hydrocarbon	458°C	478°C	497°C	515°C	532°C	548°C	458°C	478°C	497°C	515°C	532°C	548°C
methane	3.4	4.7	6.6	8.6	10.5	12.6	4.1	5.4	7.3	9.2	11.1	13.2
ethane	0.5	0.6	0.9	1.2	1.5	2.0	0.7	1.0	1.0	1.2	1.4	1.9
ethene	3.5	4.4	5.4	6.5	7.6	8.7	3.7	4.3	5.4	6.6	7.6	8.9
propane	-	-	-	0.2	0.4	0.5	-	-	-	0.1	0.3	0.4
n-butane	-	-	-	-	-	-	-	-	-	-	-	-
propene	2.0	2.1	2.1	2.2	2.2	2.4	2.2	2.3	2.2	2.3	2.4	2.5
n-pentane	2.9	3.4	4.1	5.1	6.0	6.9	3.1	3.6	4.4	5.3	6.2	7.1
n-butene	-	-	-	-	-	-	-	-	-	-	-	-
n-hexane	0.5	0.6	0.8	0.9	0.8	0.9	0.4	0.6	0.7	0.8	0.9	0.8
2-methylbutane	-	-	-	-	-	-	-	-	-	-	-	-
2,2-DMB	87.2	84.2	80.1	75.3	71.0	66.0	85.8	82.8	79.0	74.5	70.1	65.2

Table 31.   Influence of 2.5% platinum etioporphyrin I on the cracking of 2,2-dimethylbutane

support	% in reactor gas effluent											
	silica						α‑alumina					
hydrocarbon	458°C	478°C	497°C	515°C	532°C	548°C	458°C	478°C	497°C	515°C	532°C	548°C
methane	4.5	5.6	7.3	9.1	11.0	12.9	4.5	5.7	7.5	9.4	11.2	13.2
ethane	0.6	0.7	0.9	2.1	2.1	2.3	0.5	0.7	0.8	2.0	2.1	2.2
ethene	4.3	5.0	5.7	6.8	7.3	8.8	4.3	4.9	5.8	6.9	7.8	8.9
propane	–	–	–	0.3	0.4	0.4	–	–	0.3	0.4	0.6	0.6
n-butane	–	–	–	–	–	–	–	–	–	–	–	–
propene	2.1	2.2	2.4	2.3	2.4	2.5	2.3	2.5	2.6	2.6	2.7	2.7
n-pentane	3.2	3.9	4.8	5.8	6.9	7.7	3.4	3.9	4.8	5.6	6.4	7.3
n-butene	–	–	–	–	–	–	–	–	–	–	–	–
n-hexane	0.7	0.6	0.7	0.7	0.7	0.8	0.5	0.7	0.6	0.7	0.6	0.7
2-methylbutane	–	–	–	–	–	–	–	–	–	–	–	–
2,2-DMB	84.6	82.0	78.2	72.9	69.2	64.6	84.5	81.6	77.6	72.4	68.6	64.4

Table 32. Influence of 5.0% platinum etioporphyrin I on the cracking of 2,2-dimethylbutane

support	silica						α -alumina					
hydrocarbon	458°C	478°C	497°C	515°C	532°C	548°C	458°C	478°C	497°C	515°C	532°C	548°C
methane	4.6	6.1	8.2	10.3	12.5	14.7	4.8	6.3	8.5	10.6	12.9	15.1
ethane	0.8	1.0	1.1	1.4	1.8	2.2	0.9	1.2	1.4	1.8	2.0	2.3
ethene	4.3	5.0	5.7	6.8	7.9	9.3	4.4	5.0	6.0	7.2	8.3	9.5
propane	-	-	0.2	0.4	0.5	0.5	-	-	0.3	0.3	0.4	0.5
n-butane	-	-	-	-	-	-	-	-	-	-	-	-
propene	3.1	3.2	3.5	3.4	3.4	3.5	2.9	2.9	3.1	3.0	3.1	3.2
n-pentane	4.3	4.6	5.4	6.4	7.3	8.2	4.6	5.0	5.5	6.4	7.4	8.1
n-butene	-	-	-	-	-	-	-	-	-	-	-	-
n-hexane	0.7	0.8	0.7	0.8	0.9	0.9	0.8	0.7	0.9	1.0	1.0	1.0
2-methylbutane	-	-	-	-	-	-	-	-	-	-	-	-
2,2-DMB	82.2	79.3	75.2	70.5	65.7	60.7	81.6	78.9	74.3	69.7	64.9	60.3

Table 33.   Influence of 0.5% palladium etioporphyrin I on the cracking of 2,2-dimethylbutane

support		silica						α-alumina					
hydrocarbon		458°C	478°C	497°C	515°C	532°C	548°C	458°C	478°C	497°C	515°C	532°C	548°C
methane		6.4	7.7	8.8	9.3	10.5	12.2	6.3	7.5	8.6	10.0	11.3	12.6
ethane		0.9	1.2	1.3	1.4	1.7	2.0	1.1	1.2	1.4	1.7	2.0	2.1
ethene		4.1	4.3	4.5	4.6	4.8	5.0	4.0	4.2	4.3	4.5	4.6	4.9
propane		-	0.3	0.2	0.2	0.3	0.4	-	0.2	0.3	0.3	0.2	0.3
n-butane		-	-	-	-	-	-	-	-	-	-	-	-
propene		0.2	0.4	0.7	1.2	1.6	2.0	0.1	0.4	0.5	0.7	1.1	1.4
n-pentane		4.0	4.3	4.7	5.3	5.7	6.2	3.7	4.1	4.5	4.9	5.4	5.9
n-butene		-	-	-	-	-	-	-	-	-	-	-	-
n-hexane		0.3	0.3	0.3	0.4	0.5	0.5	0.2	0.3	0.3	0.4	0.4	0.5
2-methylbutane		-	-	0.1	0.1	0.2	0.2	-	-	0.2	0.3	0.2	0.3
2,2-DMB		84.1	81.5	79.4	77.5	74.7	71.5	84.6	82.1	79.9	77.2	74.8	72.0

% in reactor gas effluent

Table 34. Influence of 1.0% palladium etioporphyrin I on the cracking of 2,2-dimethylbutane

% in reactor gas effluent

support	silica						α-alumina					
hydrocarbon	458°C	478°C	497°C	515°C	532°C	548°C	458°C	478°C	497°C	515°C	532°C	548°C
methane	6.9	7.9	9.2	10.6	12.0	13.4	7.0	7.8	9.1	10.3	11.6	12.9
ethane	1.2	1.3	1.5	1.8	2.1	2.5	1.3	1.5	1.7	2.0	2.3	2.7
ethene	5.3	5.8	6.4	7.2	7.9	8.6	5.1	5.6	6.3	7.1	7.9	8.7
propane	-	0.3	0.2	0.2	0.3	0.4	-	0.2	0.3	0.3	0.4	0.3
n-butane	-	-	-	-	-	-	-	-	-	-	-	-
propene	0.9	1.1	1.4	1.9	2.3	2.8	1.0	1.3	1.6	1.9	2.3	2.7
n-pentane	4.3	4.5	4.8	5.4	6.1	6.5	4.5	4.8	5.1	5.6	6.1	6.7
n-butene	-	-	-	-	-	-	-	-	-	-	-	-
n-hexane	0.3	0.3	0.4	0.4	0.6	0.6	0.2	0.2	0.3	0.4	0.5	0.5
2-methylbutane	-	0.2	0.3	0.2	0.4	0.4	-	-	0.1	0.3	0.4	0.3
2,2-DMB	81.1	78.6	75.8	72.3	68.3	64.8	80.9	78.6	75.5	72.1	68.5	65.2

Table 35. Influence of 2.5% palladium etioporphyrin I on the cracking of 2,2-dimethylbutane

% in reactor gas effluent

support	silica						α-alumina					
hydrocarbon	458°C	478°C	497°C	515°C	532°C	548°C	458°C	478°C	497°C	515°C	532°C	548°C
methane	7.4	8.5	9.7	11.1	12.6	14.0	7.2	8.4	9.7	11.2	12.7	14.1
ethane	1.3	1.5	1.7	2.0	2.3	2.7	1.4	1.6	1.8	2.1	2.4	2.8
ethene	5.9	6.4	7.0	7.8	8.5	9.4	6.0	6.4	7.0	7.8	8.5	9.2
propane	0.1	0.1	0.3	0.3	0.4	0.3	-	0.2	0.1	0.3	0.4	0.4
n-butane	-	-	-	-	-	-	-	-	-	-	-	-
propene	0.9	1.1	1.4	1.9	2.4	3.0	0.8	1.1	1.4	1.9	2.4	3.1
n-pentane	4.5	4.7	5.3	5.7	6.3	6.9	4.6	4.8	5.1	5.7	6.3	6.8
n-butene	-	-	-	-	-	-	-	-	-	-	-	-
n-hexane	0.4	0.6	0.5	0.5	0.6	0.6	0.5	0.5	0.6	0.7	0.6	0.6
2-methylbutane	0.1	0.2	0.2	0.3	0.3	0.4	0.1	0.1	0.3	0.2	0.3	0.3
2,2-DMB	79.4	76.9	73.9	70.4	66.6	62.7	79.4	76.9	74.0	70.1	66.4	62.7

Table 36. Influence of 5.0% palladium etioporphyrin I on the cracking of 2,2-dimethylbutane

support				% in reactor gas effluent									
		silica							α -alumina					
hydrocarbon	458°C	478°C	497°C	515°C	532°C	548°C	458°C	478°C	497°C	515°C	532°C	548°C	
methane	8.5	9.6	11.0	12.3	13.8	15.2	8.2	9.5	11.0	12.5	14.1	15.6	
ethane	1.3	1.6	1.9	2.2	2.6	3.1	1.4	1.7	2.0	2.4	2.8	3.3	
ethene	5.8	6.6	7.4	8.3	9.2	10.3	6.1	6.8	7.5	8.6	9.4	10.4	
propane	-	0.2	0.4	0.4	0.3	0.4	0.2	0.4	0.4	0.4	0.4	0.4	
n-butane	-	-	-	-	-	-	-	-	-	-	-	-	
propene	0.9	1.3	1.7	2.3	3.0	3.7	1.1	1.5	1.9	2.5	3.1	3.8	
n-pentane	4.8	5.2	5.7	6.3	6.9	7.4	4.8	5.1	5.5	6.1	6.8	7.6	
n-butene	-	-	-	-	-	-	-	-	-	-	-	-	
n-hexane	0.4	0.6	0.6	0.7	0.7	0.7	0.4	0.5	0.4	0.7	0.8	1.0	
2-methylbutane	0.2	0.3	0.3	0.4	0.3	0.4	0.1	0.2	0.3	0.3	0.4	0.4	
2,2-DMB	78.1	74.6	71.0	67.1	63.2	58.8	77.7	74.3	71.0	66.5	62.2	57.5	

Table 37. Influence of 0.5% base hematoporphyrin IX on the cracking of 2,2-dimethylbutane

support hydrocarbon	% in reactor gas effluent											
	silica						α-alumina					
	458°C	478°C	497°C	515°C	532°C	548°C	458°C	478°C	497°C	515°C	532°C	548°C
methane	4.9	6.1	7.5	9.0	10.4	12.0	5.0	6.3	7.5	8.9	10.4	12.1
ethane	0.4	0.5	0.7	1.0	1.4	1.9	0.6	0.7	0.7	1.0	1.3	1.8
ethene	4.5	5.3	6.0	7.0	8.3	9.0	4.6	5.5	6.4	7.2	7.9	8.8
propane	-	-	-	0.2	0.3	0.3	-	-	-	-	0.2	0.6
n-butane	-	-	-	-	-	-	-	-	-	-	-	-
propene	2.3	2.4	2.5	2.7	2.9	3.1	2.2	2.4	2.6	2.9	3.2	3.6
n-pentane	3.9	4.5	5.1	6.0	6.9	7.8	3.8	4.4	5.0	5.6	6.5	7.4
n-butene	-	-	-	-	-	-	-	-	-	-	-	-
n-hexane	-	-	-	-	0.2	0.3	-	-	-	-	-	0.2
2-methylbutane	-	-	-	-	-	-	-	-	-	-	-	-
2,2-DMB	84.0	81.2	78.2	74.1	69.6	65.6	83.8	80.7	77.8	74.4	70.5	65.5

Table 38.   Influence of 1.0% base hematoporphyrin IX on the cracking of 2,2-dimethylbutane

support	silica						α-alumina					
hydrocarbon	458°C	478°C	497°C	515°C	532°C	548°C	458°C	478°C	497°C	515°C	532°C	548°C
methane	6.2	7.4	8.8	10.2	11.7	13.3	5.9	7.2	8.5	10.0	11.6	13.1
ethane	0.5	0.7	0.9	1.2	1.5	2.2	0.6	0.8	0.9	1.3	1.6	2.2
ethene	5.0	6.0	7.0	8.1	9.2	10.4	4.8	5.8	6.8	7.9	9.0	10.2
propane	-	-	-	0.2	0.3	0.3	-	-	-	0.3	0.3	0.3
n-butane	-	-	-	-	-	-	-	-	-	-	-	-
propene	2.6	2.7	2.8	3.0	3.2	3.5	2.6	2.8	3.0	3.2	3.5	3.7
n-pentane	4.3	5.0	5.8	6.6	7.2	7.9	4.2	4.8	5.5	6.2	7.1	8.0
n-butene	-	-	-	-	-	-	-	-	-	-	-	-
n-hexane	0.1	0.2	0.4	0.4	0.6	1.0	0.2	0.1	0.3	0.5	0.6	0.7
2-methylbutane	-	-	-	-	-	-	-	-	-	-	-	-
2,2-DMB	81.3	78.0	74.3	70.3	66.3	61.4	81.7	78.5	75.0	70.6	66.3	61.8

% in reactor gas effluent

Table 39.   Influence of 2.5% base hematoporphyrin IX on the cracking of 2,2-dimethylbutane

support	silica						α-alumina					
hydrocarbon	458°C	478°C	497°C	515°C	532°C	548°C	458°C	478°C	497°C	515°C	532°C	548°C
methane	6.9	8.3	9.7	11.4	13.1	14.9	7.5	8.8	10.3	12.0	13.6	15.3
ethane	0.6	0.7	0.9	1.3	1.8	2.3	0.7	0.9	1.2	1.6	1.9	2.4
ethene	6.5	7.5	8.4	9.5	10.6	11.6	6.1	7.0	7.9	9.0	10.3	11.4
propane	-	-	0.2	0.3	0.4	0.3	-	0.1	0.2	0.2	0.4	0.4
n-butane	-	-	-	-	-	-	-	-	-	-	-	-
propene	3.2	3.2	3.4	3.5	3.7	3.9	3.0	3.1	3.2	3.4	3.6	3.8
n-pentane	5.7	6.1	6.6	7.0	7.6	8.4	5.6	6.0	6.7	7.3	7.9	8.7
n-butene	-	-	-	-	-	-	-	-	-	-	-	-
n-hexane	0.3	0.3	0.5	0.7	0.9	1.0	0.2	0.3	0.5	0.8	0.7	0.8
2-methylbutane	-	-	-	-	-	-	-	-	-	-	-	-
2,2-DMB	76.8	73.9	70.3	66.3	61.9	57.6	76.9	73.8	70.0	65.7	61.6	57.2

% in reactor gas effluent

Table 40.   Influence of 5.0% base hematoporphyrin IX on the cracking of 2,2-dimethylbutane

% in reactor gas effluent

support	silica						α -alumina					
hydrocarbon	458°C	478°C	497°C	515°C	532°C	548°C	458°C	478°C	497°C	515°C	532°C	548°C
methane	7.9	9.7	11.5	13.6	15.6	17.7	8.3	10.2	12.2	14.4	15.6	18.8
ethane	0.6	1.0	1.1	1.3	1.8	2.5	0.7	1.1	1.3	1.4	1.9	2.4
ethene	7.1	8.0	8.9	10.1	11.1	12.2	6.9	7.9	8.9	10.0	11.0	12.1
propane	-	-	-	0.2	0.3	0.4	-	-	0.1	0.2	0.3	0.5
n-butane	-	-	-	-	-	-	-	-	-	-	-	-
propene	3.7	3.8	3.9	4.1	4.3	4.5	3.9	3.9	4.0	4.2	4.3	4.4
n-pentane	5.9	6.4	7.0	7.7	8.4	9.2	6.1	6.6	7.1	7.9	8.5	9.3
n-butene	-	-	-	-	-	-	-	-	-	-	-	-
n-hexane	0.4	0.6	0.7	1.0	1.1	1.2	0.5	0.7	1.0	1.1	1.2	1.1
2-methylbutane	-	-	-	-	-	-	-	-	-	-	-	-
2,2-DMB	74.4	70.5	66.9	62.0	57.4	52.3	73.6	69.6	65.4	60.8	57.2	51.4

Table 41. Influence of 0.5% vanadyl hematoporphyrin IX on the cracking of 2,2-dimethylbutane

% in reactor gas effluent

support	silica						α-alumina					
hydrocarbon	458°C	478°C	497°C	515°C	532°C	548°C	458°C	478°C	497°C	515°C	532°C	548°C
methane	4.8	6.5	8.9	11.3	13.8	16.4	4.9	6.1	8.5	10.9	13.4	15.9
ethane	0.9	1.1	1.4	1.5	1.7	2.0	1.0	1.2	1.3	1.5	1.8	2.1
ethene	4.6	5.3	6.0	7.0	7.9	8.9	4.5	5.3	6.0	7.1	8.1	9.2
propane	-	-	-	0.3	0.4	0.3	-	-	-	0.2	0.3	0.3
n-butane	-	-	-	-	-	-	-	-	-	-	-	-
propene	2.4	2.5	2.7	2.9	3.2	3.5	2.6	2.7	2.8	3.0	3.3	3.6
n-pentane	3.2	4.1	5.0	6.1	7.2	8.4	3.6	4.4	5.2	6.1	7.2	8.3
n-butene	-	-	-	-	-	-	-	-	-	-	-	-
n-hexane	-	-	-	-	0.4	0.6	-	-	-	0.3	0.5	0.5
2-methylbutane	-	-	-	-	-	-	-	-	-	-	-	-
2,2-DMB	84.1	80.5	76.0	70.9	65.4	59.9	83.4	80.3	76.2	70.9	65.4	60.1

Table 42. Influence of 1.0% vanadyl hematoporphyrin IX on the cracking of 2,2-dimethylbutane

% in reactor gas effluent

support hydrocarbon	silica						α-alumina					
	458°C	478°C	497°C	515°C	532°C	548°C	458°C	478°C	497°C	515°C	532°C	548°C
methane	5.7	7.5	10.5	12.5	15.0	17.7	6.1	7.9	10.4	12.9	15.5	18.1
ethane	1.6	1.7	1.8	1.7	2.1	2.3	1.5	1.7	1.8	2.0	2.1	2.3
ethene	5.7	6.4	7.2	8.2	9.1	10.1	5.6	6.2	6.9	7.8	8.7	9.7
propane	-	-	-	0.2	0.3	0.5	-	-	-	0.1	0.4	0.5
n-butane	-	-	-	-	-	-	-	-	-	-	-	-
propene	2.9	3.0	3.1	3.3	3.7	4.0	3.1	3.2	3.4	3.6	3.9	4.2
n-pentane	4.6	5.5	6.4	7.5	8.6	9.7	4.4	5.2	6.1	7.2	8.3	9.5
n-butene	-	-	-	-	-	-	-	-	-	-	-	-
n-hexane	-	0.2	0.4	0.4	0.5	0.7	-	-	0.3	0.4	0.5	0.5
2-methylbutane	-	-	-	-	-	-	-	-	-	-	-	-
2,2-DMB	79.5	75.7	70.6	66.2	60.7	55.0	79.3	75.8	71.1	66.0	60.6	55.2

Table 43. Influence of 2.5% vanadyl hematoporphyrin IX on the cracking of 2,2-dimethylbutane

% in reactor gas effluent

support	silica						α-alumina					
hydrocarbon	458°C	478°C	497°C	515°C	532°C	548°C	458°C	478°C	497°C	515°C	532°C	548°C
methane	6.4	8.4	11.2	14.0	16.8	19.8	6.7	8.7	11.6	14.5	17.4	20.5
ethane	2.0	2.1	2.3	2.6	2.7	2.7	1.9	2.0	2.2	2.3	2.4	2.5
ethene	6.1	6.9	8.0	9.1	10.4	11.7	6.2	7.1	8.0	9.1	10.3	11.5
propane	-	-	-	0.3	0.4	0.6	-	-	-	0.2	0.3	0.6
n-butane	-	-	-	-	-	-	-	-	-	-	-	-
propene	2.7	2.8	3.0	3.3	3.7	4.1	3.2	3.3	3.5	3.8	3.9	4.2
n-pentane	5.0	5.8	7.0	8.2	9.6	10.9	4.8	5.8	6.8	8.1	9.4	10.7
n-butene	-	-	-	-	-	-	-	-	-	-	-	-
n-hexane	0.1	0.3	0.4	0.6	0.8	0.7	0.2	0.2	0.5	0.4	0.6	0.7
2-methylbutane	-	-	-	-	-	-	-	-	-	-	-	-
2,2-DMB	77.7	73.7	68.1	61.9	55.6	49.5	77.0	72.9	67.4	61.6	55.7	49.3

Table 44.   Influence of 5.0% vanadyl hematoporphyrin IX on the cracking of 2,2-dimethylbutane

| | % in reactor gas effluent | | | | | | | | | | | |
| | silica | | | | | | α-alumina | | | | | |
support hydrocarbon	458°C	478°C	497°C	515°C	532°C	548°C	458°C	478°C	497°C	515°C	532°C	548°C
methane	8.1	10.6	13.9	17.4	20.9	24.5	7.4	10.1	13.9	17.5	21.4	25.2
ethane	2.6	2.7	2.9	3.1	3.4	3.5	2.1	2.3	2.4	2.7	2.9	3.2
ethene	7.2	7.8	8.9	10.0	11.2	12.3	7.0	7.7	8.9	10.1	11.3	12.5
propane	–	–	0.2	0.4	0.5	0.7	–	0.1	0.3	0.4	0.6	0.7
n–butane	–	–	–	–	–	–	–	–	–	–	–	–
propene	4.0	4.2	4.2	4.4	4.6	4.9	4.3	4.6	4.7	4.7	4.9	5.1
n–pentane	6.1	7.0	8.0	9.4	10.9	12.3	5.9	6.7	8.1	9.4	10.9	12.2
n–butene	–	–	–	–	–	–	–	–	–	–	–	–
n–hexane	0.5	0.7	0.7	0.8	0.9	0.9	0.6	0.8	0.9	0.8	0.9	0.9
2–methylbutane	–	–	–	–	–	–	–	–	–	–	–	–
2,2–DMB	71.5	67.0	61.2	54.5	47.6	40.9	72.7	67.7	60.8	54.4	47.1	40.2

Table 45. Influence of 0.5% nickel hematoporphyrin IX on the cracking of 2,2-dimethylbutane

	% in reactor gas effluent											
support	silica						α-alumina					
hydrocarbon	458°C	478°C	497°C	515°C	532°C	548°C	458°C	478°C	497°C	515°C	532°C	548°C
methane	4.7	6.5	8.6	10.9	13.2	15.6	4.8	6.8	8.8	11.0	13.1	15.3
ethane	1.1	1.3	1.6	1.7	1.9	2.3	1.2	1.4	1.5	1.7	1.8	2.2
ethene	4.1	4.9	5.8	6.9	8.0	9.1	4.3	5.1	5.9	7.0	8.1	9.0
propane	-	-	-	-	0.1	0.3	-	-	-	-	0.1	0.2
n-butane	-	-	-	-	-	-	-	-	-	-	-	-
propene	2.6	2.7	2.8	3.0	3.3	3.8	2.8	2.9	3.0	3.2	3.5	3.9
n-pentane	3.9	4.6	5.4	6.3	7.4	8.3	4.1	4.8	5.5	6.5	7.4	8.4
n-butene	-	-	-	-	-	-	-	-	-	-	-	-
n-hexane	-	-	-	0.3	0.4	0.5	-	-	-	0.2	0.2	0.4
2-methylbutane	-	-	-	-	-	-	-	-	-	-	-	-
2,2-DMB	83.6	80.0.	75.8	70.9	65.7	60.1	82.8	79.0	75.3	70.4	65.8	60.6

Table 46.　Influence of 1.0% nickel hematoporphyrin IX on the cracking of 2,2-dimethylbutane

% in reactor gas effluent

support	silica						α-alumina					
hydrocarbon	458°C	478°C	497°C	515°C	532°C	548°C	458°C	478°C	497°C	515°C	532°C	548°C
methane	5.5	7.5	9.6	12.1	14.5	16.9	5.7	7.7	9.9	12.3	14.8	17.3
ethane	1.3	1.4	1.6	1.9	2.1	2.5	1.5	1.6	1.8	2.1	2.3	2.6
ethene	5.2	5.9	6.7	7.7	8.6	9.6	4.9	5.7	6.5	7.6	8.6	9.7
propane	-	-	-	-	0.2	0.5	-	-	-	-	0.2	0.4
n-butane	-	-	-	-	-	-	-	-	-	-	-	-
propene	3.1	3.2	3.4	3.5	3.7	4.0	3.0	3.1	3.3	.3.5	3.8	4.2
n-pentane	4.2	5.2	6.3	7.6	9.0	10.4	4.3	5.3	6.4	7.6	9.0	10.3
n-butene	-	-	-	-	-	-	-	-	-	-	-	-
n-hexane	-	-	-	0.2	0.4	0.5	-	-	-	0.4	0.4	0.5
2-methylbutane	-	-	-	-	-	-	-	-	-	-	-	-
2,2-DMB	80.7	76.8	72.4	67.0	61.5	55.6	80.6	76.6	72.1	66.5	60.9	55.0

Table 47.   Influence of 2.5% nickel hematoporphyrin IX on the cracking of 2,2-dimethylbutane

% in reactor gas effluent

support hydrocarbon	silica						α-alumina					
	458°C	478°C	497°C	515°C	532°C	548°C	458°C	478°C	497°C	515°C	532°C	548°C
methane	6.8	9.2	11.7	14.3	17.0	19.8	7.1	9.5	12.1	14.8	17.5	20.3
ethane	1.6	1.9	2.1	2.3	2.4	2.6	1.5	1.6	1.8	2.1	2.2	2.5
ethene	6.0	6.8	7.6	8.7	9.6	10.7	5.9	6.6	7.3	8.3	9.3	10.4
propane	-	-	-	0.2	0.5	0.4	-	-	-	0.1	0.3	0.4
n-butane	-	-	-	-	-	-	-	-	-	-	-	-
propene	3.6	3.6	3.7	3.9	4.1	4.4	3.3	3.4	3.6	3.9	4.1	4.5
n-pentane	4.6	5.9	7.3	8.6	10.2	11.8	4.7	5.8	7.1	8.5	10.0	11.5
n-butene	-	-	-	-	-	-	-	-	-	-	-	-
n-hexane	0.4	0.5	0.6	0.4	0.5	0.5	0.5	0.4	0.4	0.5	0.6	0.5
2-methylbutane	-	-	-	-	-	-	-	-	-	-	-	-
2,2-DMB	77.0	72.1	67.0	61.6	55.7	49.8	77.0	72.7	67.7	61.8	56.0	49.9

Table 48. Influence of 5.0% nickel hematoporphyrin IX on the cracking of 2,2-dimethylbutane

support	silica						α-alumina					
hydrocarbon	458°C	478°C	497°C	515°C	532°C	548°C	458°C	478°C	497°C	515°C	532°C	548°C
methane	7.4	10.0	13.7	17.2	20.9	24.7	7.6	10.3	13.9	17.6	21.3	25.2
ethane	2.0	2.3	2.4	2.6	2.9	3.2	2.1	2.2	2.4	2.7	2.9	3.1
ethene	7.3	8.1	9.0	10.1	11.1	12.2	7.1	8.0	8.9	10.0	11.1	12.4
propane	-	0.1	0.3	0.2	0.3	0.3	-	-	0.2	0.4	0.3	0.3
n-butane	-	-	-	-	-	-	-	-	-	-	-	-
propene	4.9	4.9	5.1	5.0	5.1	5.2	4.7	4.9	5.0	5.1	5.2	5.1
n-pentane	5.2	6.3	7.4	8.8	10.2	11.6	5.1	6.1	7.2	8.4	9.8	11.3
n-butene	-	-	-	-	-	-	-	-	-	-	-	-
n-hexane	0.2	0.4	0.5	0.7	0.7	0.6	0.4	0.7	0.6	0.7	0.8	0.8
2-methylbutane	-	-	-	-	-	-	-	-	-	-	-	-
2,2-DMB	73.0	67.9	61.6	55.4	48.8	42.2	73.0	67.8	61.8	55.1	48.6	41.8

% in reactor gas effluent

Table 49. Influence of 0.5% petroporphyrin concentrate on the cracking of 2,2-dimethylbutane

	% in reactor gas effluent											
support	silica						α-alumina					
hydrocarbon	458°C	478°C	497°C	515°C	532°C	548°C	458°C	478°C	497°C	515°C	532°C	548°C
methane	5.0	6.9	7.8	10.9	13.0	15.1	5.0	6.8	8.6	10.6	12.7	14.9
ethane	0.8	1.0	1.2	1.5	1.6	2.0	0.8	0.9	0.9	1.3	1.5	1.6
ethene	3.6	4.6	5.7	6.9	8.1	9.5	4.0	5.0	6.0	7.2	8.3	9.7
propane	-	-	-	0.2	0.3	0.3	-	-	-	0.1	0.2	0.2
n-butane	-	-	-	-	-	-	-	-	-	-	-	-
propene	0.2	0.4	0.6	0.9	1.3	1.7	0.4	0.6	0.8	1.1	1.4	1.6
n-pentane	5.6	5.9	6.2	6.6	7.0	7.4	5.7	6.0	6.4	6.9	7.4	8.0
n-butene	-	-	-	-	-	-	-	-	-	-	-	-
n-hexane	0.2	0.3	0.4	0.6	0.6	0.7	0.3	0.4	0.4	0.6	0.6	0.6
2-methylbutane	0.2	0.2	0.3	0.2	0.3	0.3	0.1	0.1	0.3	0.2	0.3	0.2
2,2-DMB	84.4	80.7	77.8	72.2	67.8	63.0	83.7	80.2	76.6	72.0	67.6	63.2

Table 50.   Influence of 1.0% petroporphyrin concentrate on the cracking of 2,2-dimethylbutane

% in reactor gas effluent

support	silica						α-alumina					
hydrocarbon	458°C	478°C	497°C	515°C	532°C	548°C	458°C	478°C	497°C	515°C	532°C	548°C
methane	5.6	7.6	9.6	11.8	14.0	16.3	5.8	7.9	9.8	12.2	14.5	16.9
ethane	0.9	1.1	1.3	1.4	1.7	2.0	0.9	0.9	1.0	1.2	1.5	1.9
ethene	4.9	5.9	6.9	8.1	9.3	10.5	4.8	5.8	6.8	8.0	9.3	10.6
propane	-	-	-	-	0.3	0.4	-	-	-	0.1	0.2	0.2
n-butane	-	-	-	-	-	-	-	-	-	-	-	-
propene	0.3	0.6	0.9	1.2	1.5	1.9	0.4	0.7	1.0	1.4	1.8	2.2
n-pentane	6.1	6.5	6.9	7.5	8.0	8.6	6.0	6.4	6.8	7.3	8.0	8.7
n-butene	-	-	-	-	-	-	-	-	-	-	-	-
n-hexane	0.4	0.5	0.4	0.6	0.7	0.7	0.4	0.5	0.5	0.6	0.7	0.6
2-methylbutane	0.3	0.3	0.2	0.3	0.4	0.4	0.1	0.2	0.4	0.3	0.4	0.4
2,2-DMB	81.5	77.5	73.8	69.1	64.1	59.2	81.6	77.6	73.7	68.9	63.6	58.5

Table 51.   Influence of 2.5% petroporphyrin concentrate on the cracking of 2,2-dimethylbutane

support	silica						α-alumina					
hydrocarbon	458°C	478°C	497°C	515°C	532°C	548°C	458°C	478°C	497°C	515°C	532°C	548°C
methane	6.5	8.7	10.9	13.5	16.2	18.7	6.2	8.5	11.0	13.3	15.9	18.5
ethane	1.0	1.2	1.3	1.6	1.8	2.1	1.1	1.3	1.4	1.6	1.9	2.2
ethene	4.9	6.0	7.1	8.4	9.7	11.0	5.3	6.3	7.3	8.5	9.9	11.2
propane	-	-	0.1	0.3	0.4	0.4	-	-	0.3	0.5	0.5	0.6
n-butane	-	-	-	-	-	-	-	-	-	-	-	-
propene	0.6	1.0	1.4	1.9	2.4	2.9	0.5	0.9	1.3	1.8	2.3	3.0
n-pentane	6.3	6.8	7.3	8.0	8.7	9.3	6.5	7.0	7.6	8.2	9.0	9.7
n-butene	-	-	-	-	-	-	-	-	-	-	-	-
n-hexane	0.4	0.4	0.5	0.6	0.7	0.8	0.5	0.6	0.5	0.7	0.8	0.8
2-methylbutane	0.2	0.2	0.2	0.3	0.3	0.4	0.1	0.2	0.2	0.3	0.4	0.3
2,2-DMB	80.1	75.7	71.2	65.4	59.8	54.4	79.8	75.2	70.4	65.1	59.3	53.7

% in reactor gas effluent

Table 52.   Influence of 5.0% petroporphyrin concentrate on the cracking of 2,2-dimethylbutane

% in reactor gas effluent

support	silica						α-alumina					
hydrocarbon	458°C	478°C	497°C	515°C	532°C	548°C	458°C	478°C	497°C	515°C	532°C	548°C
methane	7.9	10.1	13.0	15.9	18.9	21.8	7.2	9.9	13.0	16.1	19.3	22.6
ethane	1.0	1.2	1.4	1.7	2.0	2.4	1.1	1.4	1.4	1.6	1.9	2.3
ethene	5.8	6.9	8.0	9.5	10.8	12.2	6.1	7.1	8.2	9.5	11.0	12.3
propane	-	0.1	0.3	0.5	0.5	0.5	-	-	0.3	0.3	0.4	0.6
n-butane	-	-	-	-	-	-	-	-	-	-	-	-
propene	0.8	1.2	1.6	2.0	2.5	3.0	1.0	1.3	1.6	2.0	2.5	3.1
n-pentane	6.7	7.3	7.9	8.8	9.6	10.4	6.4	7.0	7.7	8.6	9.4	10.3
n-butene	-	-	-	-	-	-	-	-	-	-	-	-
n-hexane	0.6	0.7	0.8	0.7	0.6	0.8	0.5	0.7	0.6	0.8	0.8	0.8
2-methylbutane	0.3	0.5	0.6	0.9	0.8	0.8	0.4	0.6	0.5	0.5	0.6	0.6
2,2-DMB	76.9	72.0	66.4	60.0	54.3	48.1	77.3	72.0	66.7	60.6	54.1	47.4

Table 53.   Mass Balance for the catalytic decomposition of 2,2-dimethylbutane using vanadyl etioporphyrin at $478^{\circ}C$

Carbon Balance

Reactor			
IN		OUT	
Compound	Weight C	Compound	Weight C
$CH_3C(CH_3)_2CH_2CH_3$	1.0000	CH_4	0.1129
		C_2H_6	0.0201
		C_2H_4	0.0706
		C_3H_8	0.0489
		$n\text{-}C_4H_{10}$	0.0593
		C_3H_6	0.0123
		$1\text{-}C_4H_8$	0.0143
		$n\text{-}C_6H_{14}$	0.0040
		$CH_3CH(CH_3)CH_2CH_3$	0.0010
		$CH_3C(CH_3)_2CH_2CH_3$	0.7420
Total	1.0000	Total	1.0854

Hydrogen Balance

Reactor			
IN		OUT	
Compound	Weight H	Compound	Weight H
$CH_3C(CH_3)_2CH_2CH_3$	1.0000	CH_4	0.1935
		C_2H_6	0.0258
		C_2H_4	0.0606
		C_3H_8	0.0558
		$n\text{-}C_4H_{10}$	0.0635
		C_3H_6	0.0105
		$1\text{-}C_4H_8$	0.0123
		$n\text{-}C_6H_{14}$	0.0040
		$CH_3CH(CH_3)CH_2CH_3$	0.0010
		$CH_3C(CH_3)_2CH_2CH_3$	0.7420
Total	1.0000	Total	1.1708

Table 54. Mass Balance for the catalytic decomposition of 2,2-dimethylbutane using nickel etioporphyrin at $478^{\circ}C$

Carbon Balance

Reactor			
IN		OUT	
Compound	Weight C	Compound	Weight C
$CH_3C(CH_3)_2CH_2CH_3$	1.0000	CH_4	0.0914
		C_2H_6	0.0229
		C_2H_4	0.0809
		C_3H_8	0.0039
		$n-C_4H_{10}$	0.0040
		C_3H_6	0.0070
		$n-C_5H_{12}$	0.0169
		$1-C_4H_8$	0.0195
		$n-C_6H_{14}$	0.0060
		$CH_3CH(CH_3)CH_2CH_3$	0.0030
		$CH_3C(CH_3)_2CH_2CH_3$	0.7340
Total	1.0000	Total	0.9895

Hydrogen Balance

Reactor			
IN		OUT	
Compound	Weight H	Compound	Weight H
$CH_3C(CH_3)CH_2CH_3$	1.0000	CH_4	0.1566
		C_2H_6	0.0295
		C_2H_4	0.0693
		C_3H_8	0.0045
		$n-C_4H_{10}$	0.0042
		C_3H_6	0.0060
		$n-C_5H_{12}$	0.0174
		$1-C_4H_8$	0.0167
		$n-C_6H_{14}$	0.0060
		$CH_3CH(CH_3)CH_2CH_3$	0.0031
		$CH_3C(CH_3)_2CH_2CH_3$	0.7340
Total	1.0000	Total	1.0473

Table 55.   Summary of kinetic data for the cracking of 2,2-dimethylbutane over base etioporphyrin I

support	silica		α-alumina	
loading w/w	frequency factor	activation energy (kJ mol^{-1})	frequency factor	activation energy (kJ mol^{-1})
0.5	9.28×10^5	103	2.85×10^5	96
1.0	7.63×10^5	102	9.36×10^5	103
2.5	6.63×10^5	101	6.95×10^5	101
5.0	8.32×10^5	102	9.26×10^5	102

Table 56.   Summary of kinetic data for the cracking of 2,2-dimethylbutane over vanadyl etioporphyrin I

support	silica		α-alumina	
loading w/w	frequency factor	activation energy (kJ mol^{-1})	frequency factor	activation energy (kJ mol^{-1})
0.5	2.27×10^4	78	6.74×10^4	85
1.0	8.74×10^4	85	8.32×10^4	85
2.5	3.28×10^5	93	9.76×10^4	85
5.0	2.49×10^5	90	2.33×10^5	89

Table 57.   Summary of kinetic data for the cracking of 2,2-dimethylbutane over nickel etioporphyrin I

support	silica		α-alumina	
loading w/w	frequency factor	activation energy (kJ mol^{-1})	frequency factor	activation energy (kJ mol^{-1})
0.5	9.64×10^{4}	87	5.45×10^{4}	84
1.0	4.15×10^{4}	80	9.92×10^{4}	86
2.5	1.65×10^{5}	89	7.78×10^{4}	84
5.0	5.37×10^{5}	95	7.29×10^{5}	97

Table 58.   Summary of kinetic data for the cracking of 2,2-dimethylbutane over platinum etioporphyrin I

support	silica		α-alumina	
loading w/w	frequency factor	activation energy $(kJ\ mol^{-1})$	frequency factor	activation energy $(kJ\ mol^{-1})$
0.5	3.88×10^{6}	113	1.00×10^{7}	119
1.0	3.46×10^{6}	112	1.96×10^{6}	108
2.5	1.27×10^{6}	104	6.59×10^{5}	100
5.0	1.17×10^{6}	103	1.01×10^{6}	102

Table 59. Summary of kinetic data for the cracking of 2,2-dimethylbutane over palladium etioporphyrin I

support	silica		α-alumina	
loading w/w	frequency factor	activation energy (kJ mol^{-1})	frequency factor	activation energy (kJ mol^{-1})
0.5	1.75×10^5	92	1.47×10^5	91
1.0	5.59×10^5	98	2.60×10^5	94
2.5	4.07×10^5	96	2.54×10^5	93
5.0	3.76×10^5	95	7.60×10^5	99

Table 60.   Summary of kinetic data for the cracking of 2,2-dimethylbutane over base hematoporphyrin IX

support	silica		α-alumina	
loading w/w	frequency factor	activation energy (kJ mol^{-1})	frequency factor	activation energy (kJ mol^{-1})
0.5	6.76×10^5	100	3.88×10^5	97
1.0	3.69×10^5	95	5.05×10^5	98
2.5	1.72×10^5	89	2.03×10^5	90
5.0	2.42×10^5	91	1.80×10^5	88

Table 61. Summary of kinetic data for the cracking of 2,2-dimethylbutane over vanadyl hematoporphyrin IX

support	silica		α-alumina	
loading w/w	frequency factor	activation energy ($kJ\ mol^{-1}$)	frequency factor	activation energy ($kJ\ mol^{-1}$)
0.5	2.50×10^{7}	108	2.37×10^{6}	108
1.0	1.58×10^{6}	104	1.52×10^{6}	104
2.5	2.97×10^{6}	107	1.74×10^{6}	103
5.0	2.75×10^{6}	105	4.45×10^{6}	108

Table 62.   Summary of kinetic data for the cracking of 2,2-dimethylbutane over nickel hematoporphyrin IX

support	silica		α-alumina	
loading w/w	frequency factor	activation energy (kJ mol^{-1})	frequency factor	activation energy (kJ mol^{-1})
0.5	4.12×10^6	111	1.22×10^6	103
1.0	1.70×10^6	105	2.24×10^6	106
2.5	1.13×10^6	101	1.82×10^6	104
5.0	2.74×10^6	105	2.66×10^6	105

Table 63. Summary of kinetic data for the cracking of 2,2-dimethylbutane over petroporphyrin concentrate

support	silica		α -alumina	
loading w/w	frequency factor	activation energy (kJ mol^{-1})	frequency factor	activation energy (kJ mol^{-1})
0.5	8.85×10^5	102	8.43×10^5	101
1.0	7.99×10^5	100	8.93×10^5	101
2.5	1.60×10^6	104	1.18×10^6	103
5.0	2.18×10^6	105	2.45×10^6	105

Table 64. Hydrogen chemisorption on synthetic

nickel etioporphyrin at 292K

Equilibrium pressure (Pascals)	Hydrogen adsorption (μmoles g^{-1})
860.666	2.203
2305.324	10.226
3681.188	25.348
5469.812	29.588
7120.849	33.081
9012.663	29.945
12073.961	32.598
15204.053	34.539
19090.869	32.371
23459.239	35.561
29203.473	27.960
35876.415	26.777

Table 65.   Hydrogen chemisorption on 5.0% (w/w) nickel

etioporphyrin on silica at 292K

Equilibrium pressure (Pascals)	Hydrogen adsorption (μmoles g^{-1})
271.364	5.54
1618.33	9.72
2951.41	13.15
4025.28	27.42
6247.08	33.68
8839.17	40.84
11023.9	45.62
13579.0	53.34
17615.3	65.11
20005	67.7
22100	70.2
25000	72.7
30000	73.2
34000	73.0

Table 66.

Influence of various conditions on 1-hexene

	% in reactor gas effluent										
temperature (°C)	ambient	ambient	300	325	325	330	340	350	450	450	450
carrier gas (at a flow rate of 1 cm^3 min^{-1})	He	5% H$_2$/95% Ar	He	5% H$_2$/95% Ar	5% H$_2$/95% Ar	He	He	He	5% H$_2$/95% Ar	5% H$_2$/95% Ar	He
tube packing	-	-	-	-	silica	-	-	-	-	silica	silica
methane	-	-	-	-	-	-	-	-	-	-	-
ethane	-	-	-	-	-	-	-	-	-	-	-
ethene	-	-	-	-	0.2	0.3	0.2	0.3	0.4	0.7	0.6
propane	-	-	-	-	-	-	-	-	-	-	-
n-butane	-	-	-	-	-	-	-	-	-	-	-
propene	-	-	-	-	-	-	-	0.1	0.1	0.6	0.6
n-pentane	-	-	-	-	-	-	-	0.1	0.3	1.3	1.4
n-butene	-	-	-	-	-	-	-	-	-	-	-
n-hexane	-	-	-	-	-	-	-	-	-	-	-
1-pentene	-	-	-	-	-	0.3	0.4	0.4	0.4	1.5	1.6
1-hexene	100.0	100.0	100.0	100.0	99.8	99.7	99.5	99.2	98.8	95.9	95.8

Table 67.   Influence of base etioporphyrin I supported on silica on a hydrogen/1-hexene mixture

temperature (°C)									
		% in reactor gas effluent							
		325				450			
porphyrin loading (% w/w)		0.5	1.0	2.5	5.0	0.5	1.0	2.5	5.0
methane		0.6	0.9	1.3	1.5	1.7	2.5	3.4	4.4
ethane		-	-	-	0.3	1.4	1.6	1.7	1.9
ethene		1.4	1.7	1.9	2.3	0.8	1.8	2.9	3.9
propane		-	-	-	0.3	0.3	0.5	0.7	1.0
n-butane		-	-	-	-	-	-	-	-
propene		-	0.8	3.0	4.2	2.1	2.5	3.0	3.7
n-pentane		1.2	3.3	5.5	7.6	0.3	0.4	0.4	0.6
n-butene		-	-	-	-	-	-	-	-
n-hexane		-	-	-	-	-	-	-	-
1-pentene		0.6	0.7	0.9	1.1	1.2	1.6	1.9	2.1
1-hexene		96.2	92.6	87.4	82.7	92.2	89.1	86.0	82.4

Table 68. Influence of vanadyl etioporphyrin I supported on silica on a hydrogen/1-hexene mixture

temperature (°C)				325				450			
porphyrin loading (% w/w)				0.5	1.0	2.5	5.0	0.5	1.0	2.5	5.0
methane				-	0.8	1.0	1.0	3.6	4.0	5.4	6.9
ethane				-	-	-	-	0.7	2.0	3.0	3.9
ethene				0.3	1.3	1.8	2.3	0.7	1.3	1.7	2.0
propane				-	-	-	-	0.2	0.6	0.9	1.1
n-butane				-	-	-	-	-	0.2	0.5	0.6
propene				0.9	1.1	1.4	1.8	2.1	2.3	2.6	2.9
n-pentane				3.0	3.4	4.0	4.4	0.2	0.3	0.4	0.6
n-butene				-	-	-	-	-	-	-	-
n-hexane				-	-	-	-	-	-	-	-
1-pentene				1.4	1.6	1.6	1.7	1.1	1.3	1.5	1.6
1-hexene				94.4	91.8	90.2	88.8	91.4	88.0	84.0	80.4

% in reactor gas effluent

Table 69.   Influence of nickel etioporphyrin I supported on silica on a hydrogen/1-hexene mixture

temperature (°C)	325				450			
porphyrin loading (% w/w)	0.5	1.0	2.5	5.0	0.5	1.0	2.5	5.0
methane	-	-	-	-	0.9	1.5	2.6	3.0
ethane	-	-	-	-	0.5	0.7	1.0	1.2
ethene	-	-	1.0	1.3	1.2	1.4	1.8	2.3
propane	-	-	-	-	0.3	0.4	0.5	0.7
n-butane	-	-	-	-	-	-	0.3	0.9
propene	1.4	1.8	2.3	2.9	3.9	4.1	4.5	4.9
n-pentane	4.1	5.2	6.2	7.0	5.5	5.9	6.4	7.0
n-butene	-	-	-	-	-	-	-	-
n-hexane	-	-	-	-	-	-	-	-
1-pentene	1.4	1.5	1.6	1.6	2.0	2.2	2.8	3.1
1-hexene	93.1	91.5	88.9	87.2	85.7	83.8	80.1	76.9

% in reactor gas effluent

Table 70.   Influence of palladium etioporhyrin I supported on silica on a hydrogen/1-hexene mixture

% in reactor gas effluent

temperature (°C)	325				450			
porphyrin loading (% w/w)	0.5	1.0	2.5	5.0	0.5	1.0	2.5	5.0
methane	0.3	0.7	1.7	2.6	1.5	2.9	3.2	4.5
ethane	-	-	0.3	0.6	0.3	1.0	2.1	2.9
ethene	1.2	2.7	3.6	4.6	0.8	1.8	2.7	3.6
propane	-	-	-	0.5	0.2	0.6	1.0	1.5
n-butane	-	-	-	-	-	-	-	-
propene	1.5	2.1	2.7	3.2	2.7	3.4	4.3	5.1
n-pentane	6.1	10.4	15.7	19.4	4.3	7.0	9.5	12.3
n-butene	-	-	-	-	-	-	-	-
n-hexane	-	-	-	-	-	-	-	-
1-pentene	1.3	1.6	2.0	2.3	2.1	2.6	3.1	3.5
1-hexene	89.6	82.5	74.0	66.8	88.1	80.7	74.1	66.6

Table 71. Influence of base hematoporphyrin IX supported on silica ona hydrogen/1-hexene mixture

% in reactor gas effluent

temperature (°C)	325				450			
porphyrin loading (% w/w)	0.5	1.0	2.5	5.0	0.5	1.0	2.5	5.0
methane	-	-	-	-	1.5	2.1	2.7	3.5
ethane	-	-	-	-	0.6	0.9	1.3	1.7
ethene	-	-	0.7	1.1	0.5	1.4	2.0	2.5
propane	-	-	-	-	0.3	0.4	0.6	0.7
n-butane	-	-	-	-	-	-	-	0.2
propene	-	-	-	-	1.1	1.7	2.2	2.7
n-pentane	0.6	1.5	2.5	3.3	0.2	1.1	2.1	3.0
n-butene	-	-	-	-	-	-	-	-
n-hexane	-	-	-	-	-	-	-	-
1-pentene	0.5	0.8	1.1	1.4	0.9	1.4	2.0	2.4
1-hexene	98.9	97.7	95.7	94.2	94.9	91.0	87.1	83.3

Table 72. Influence of vanadyl hematoporphyrin IX supported on silica on a hydrogen/1-hexene mixture

| | | % in reactor gas effluent | | | | | | | |
| temperature (°C) | | 325 | | | | 450 | | | |
porphyrin loading (% w/w)		0.5	1.0	2.5	5.0	0.5	1.0	2.5	5.0
methane		-	-	-	-	0.4	0.7	1.1	1.6
ethane		-	-	-	-	0.4	0.4	0.5	0.6
ethene		-	-	-	0.3	0.6	0.7	0.8	0.8
propane		-	-	-	-	-	-	-	-
n-butane		-	-	-	-	-	-	-	-
propene		-	-	-	-	2.3	2.6	2.8	3.1
n-pentane		1.3	3.7	6.1	7.7	3.9	5.6	7.4	9.1
n-butene		-	-	-	-	-	-	-	-
n-hexane		-	-	-	-	-	-	-	-
1-pentene		0.9	0.9	1.1	1.2	1.1	1.8	2.4	3.0
1-hexene		97.8	95.4	92.8	90.8	91.3	88.2	85.0	81.8

Table 73. Influence of nickel hematoporphyrin IX supported on silica on a hydrogen/1-hexene mixture

temperature (°C)								
				% in reactor gas effluent				
porphyrin loading (% w/w)		325				450		
	0.5	1.0	2.5	5.0	0.5	1.0	2.5	5.0
methane	-	-	-	-	0.9	2.1	3.4	4.6
ethane	-	-	-	-	0.4	1.0	1.3	1.7
ethene	-	-	0.3	1.4	0.9	1.3	1.6	1.9
propane	-	-	-	-	0.3	0.5	0.6	0.6
n-butane	-	-	-	-	-	-	-	-
propene	0.6	1.6	2.7	3.6	1.1	2.1	3.3	4.5
n-pentane	1.5	1.7	2.0	2.4	1.3	2.9	4.5	6.2
n-butene	-	-	-	-	-	-	-	-
n-hexane	-	-	-	-	-	-	-	-
1-pentene	0.9	1.1	1.4	1.8	1.1	1.4	2.3	2.9
1-hexene	97.0	95.6	93.6	90.8	94.0	88.7	83.0	77.6

Table 74.   Influence of nickel etioporphyrin I supported

, on alumina on a mixture of hydrogen/1-hexene

Time on stream (min)	10	50	90	130
	% in reactor gas effluent			
1-hexene	11.8	23.4	37.4	69.4
n-hexane	88.2	76.6	62.6	30.6
Moles min^{-1} ($\times 10^{-5}$) of 1-hexene reacting	2.7	1.5	0.9	0.5
Turnover number - i) moles $min^{-1} m^{-2}$	4.6	2.6	1.5	0.9
ii) molecules $site^{-1} min^{-1}$	0.04	0.04	0.03	0.01

Inlet temperature ($^{\circ}C$)   =   22

Reaction temperature ($^{\circ}C$)   =   150

Flow rate of 1-hexene (moles min^{-1})   = 3.92×10^{-5}

Catalyst mass (g)   =   0.15

Table 75.   Influence of palladium etioporphyrin I supported
on silica on a mixture of hydrogen/1-hexene

Time on stream (min)	10	50	90	130
	% in reactor gas effluent			
1-hexene	34.7	12.5	7.2	6.3
n-hexane	65.3	87.5	92.8	93.7
Moles min^{-1} (x10^{-5}) of 1-hexene reacting	2.6	3.4	3.6	3.7
Turnover number – (i) moles min^{-1} m^{-2} s^{-1} (ii) molecules site^{-1} min^{-1}	11.1 0.08	14.5 0.10	15.3 0.11	15.7 0.11

Inlet temperature (^{o}C)   = 22

Reaction temperature (^{o}C)   = 150

Flow rate of 1-hexene (moles min^{-1})   = 3.92 x 10^{-5}

Catalyst mass (g)   = 0.15

Table 76. <u>Influence of vanadyl hematoporphyrin IX supported</u>

<u>on silica on a mixture of hydrogen/1-hexene</u>

Time on stream (min)	10	50	90
	% in reactor gas effluent		
1-hexene	98.7	97.7	98.0
n-hexane	1.3	2.3	2.0
Moles min^{-1} ($x10^{-7}$) of 1-hexene reacting	5	9	8

Inlet temperature (^{o}C) = 22

Reaction temperature (^{o}C) = 150

Flow rate of 1-hexene (moles min^{-1}) = 3.92×10^{-5}

Catalyst mass (g) = 0.15

FIGURES

Fig.1.   Structure of porphine,showing the numbering
system for the nomenclature of porphyrins.
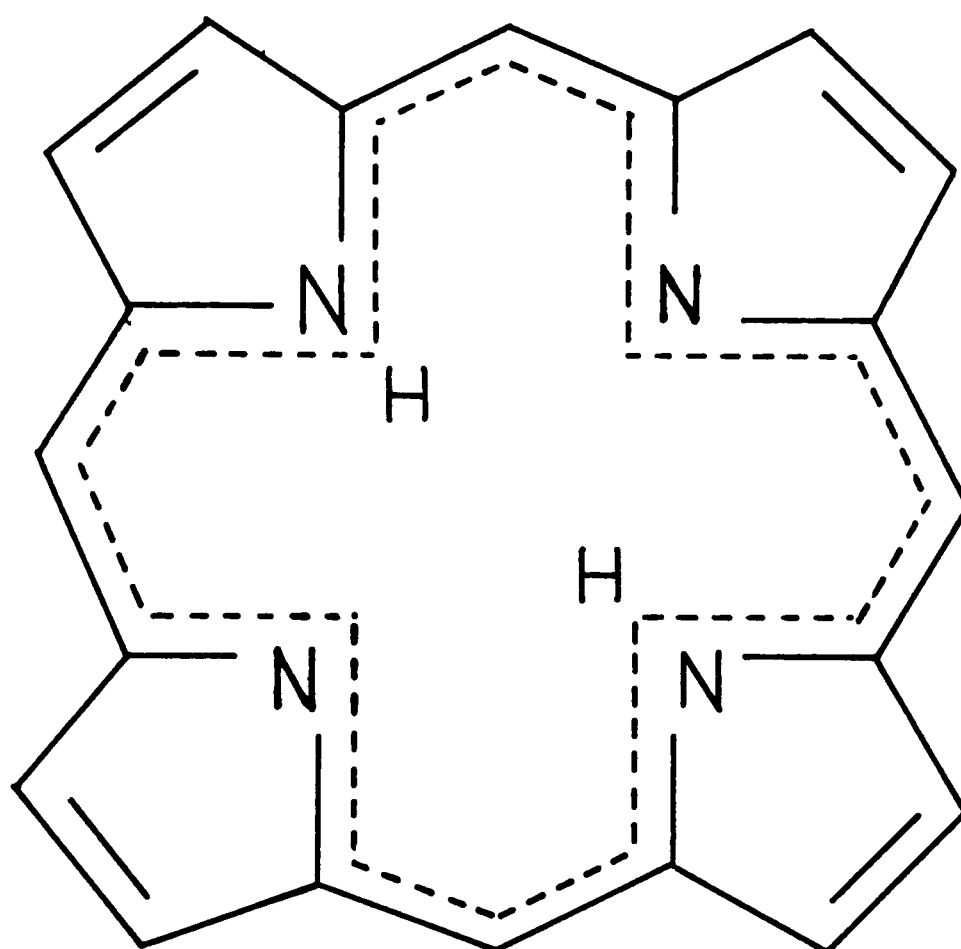
Fig.2. Structure of porphine derived from molecular orbital theory.
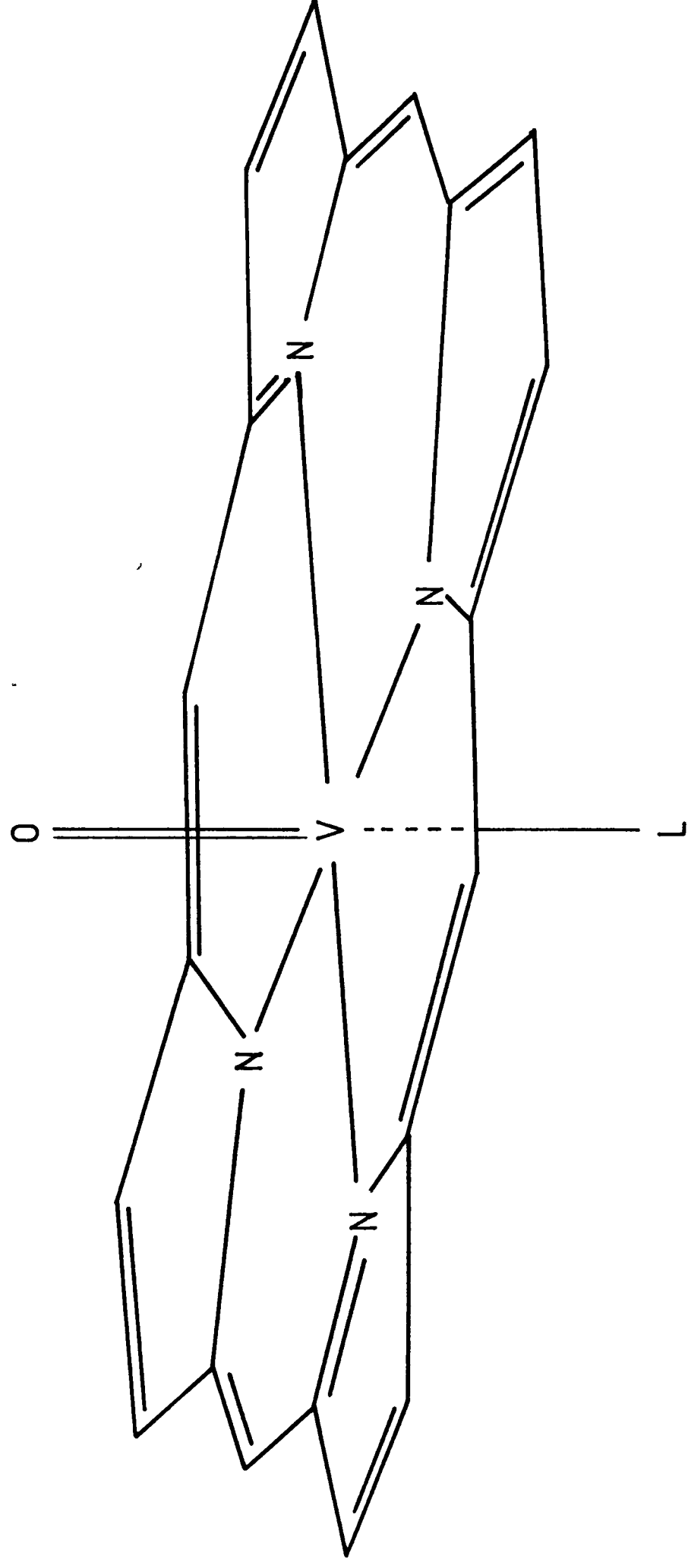
L=solvent ligand

Fig.3.   Spatial configuration of octahedral orientation.
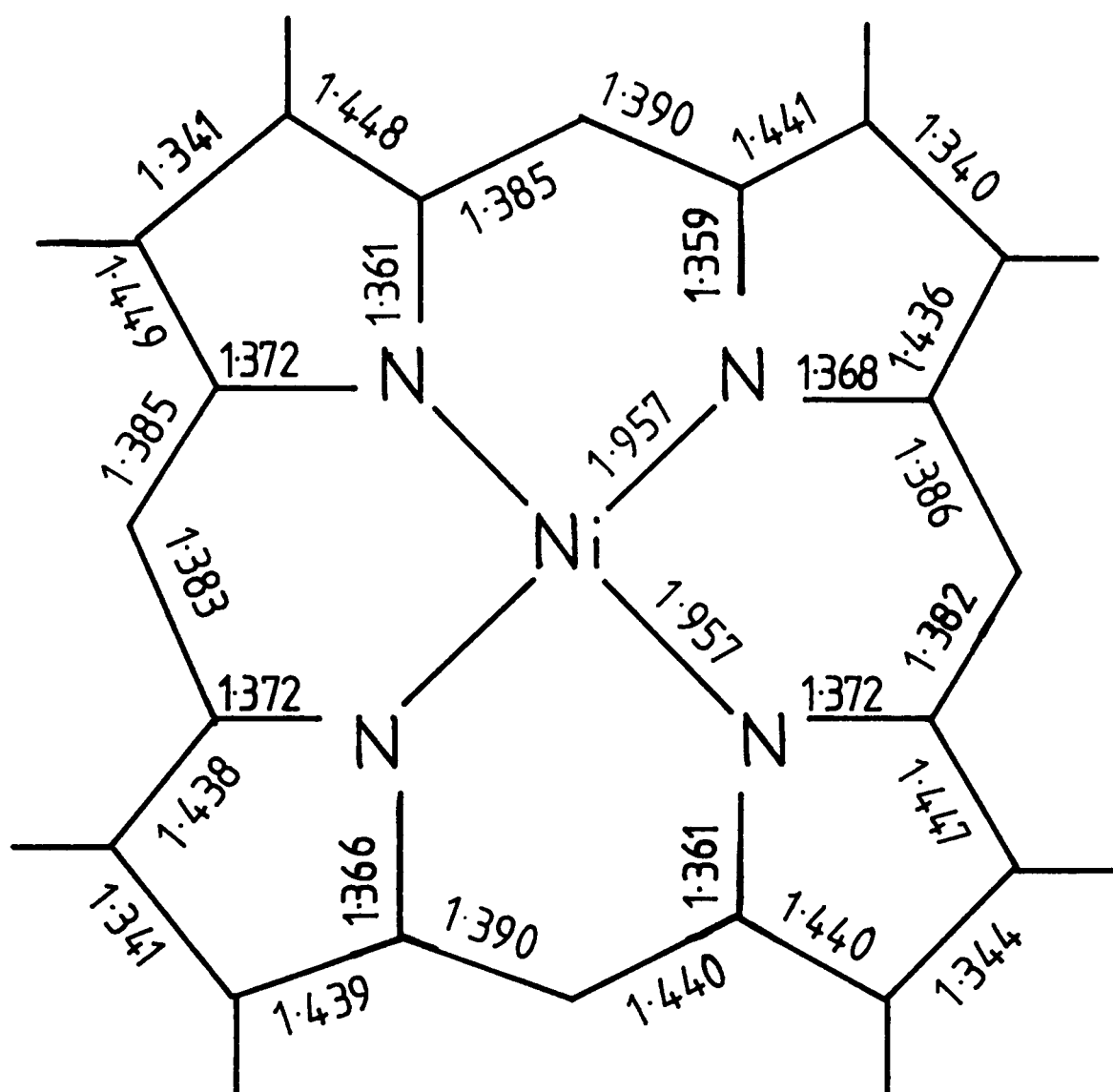
Fig.4.   Bond lengths (Å) in a nickel porphyrin
          illustrating the molecular symmetry.

Fig.5.   The thermal decomposition of a vanadyl petroporphyrin at 373°c.
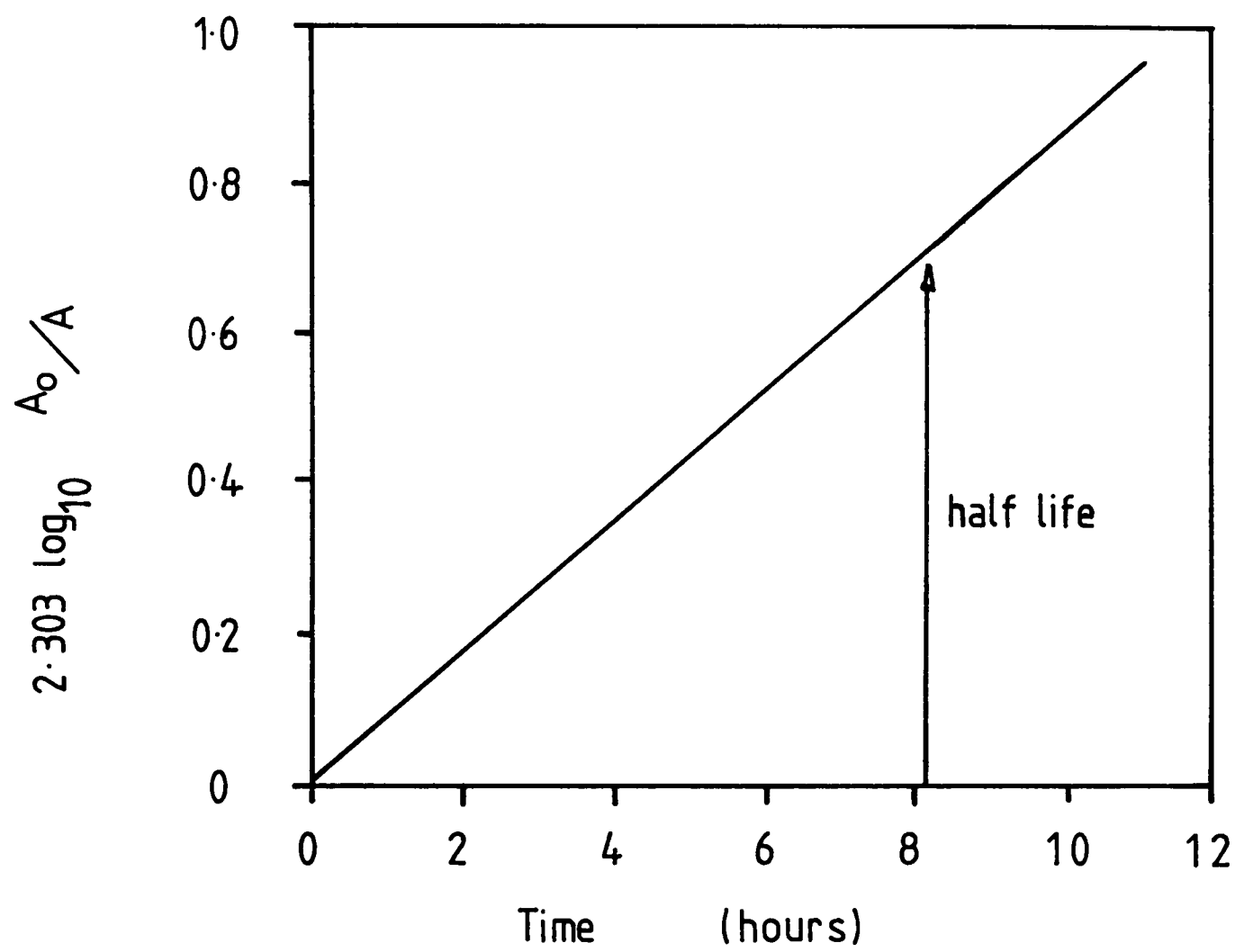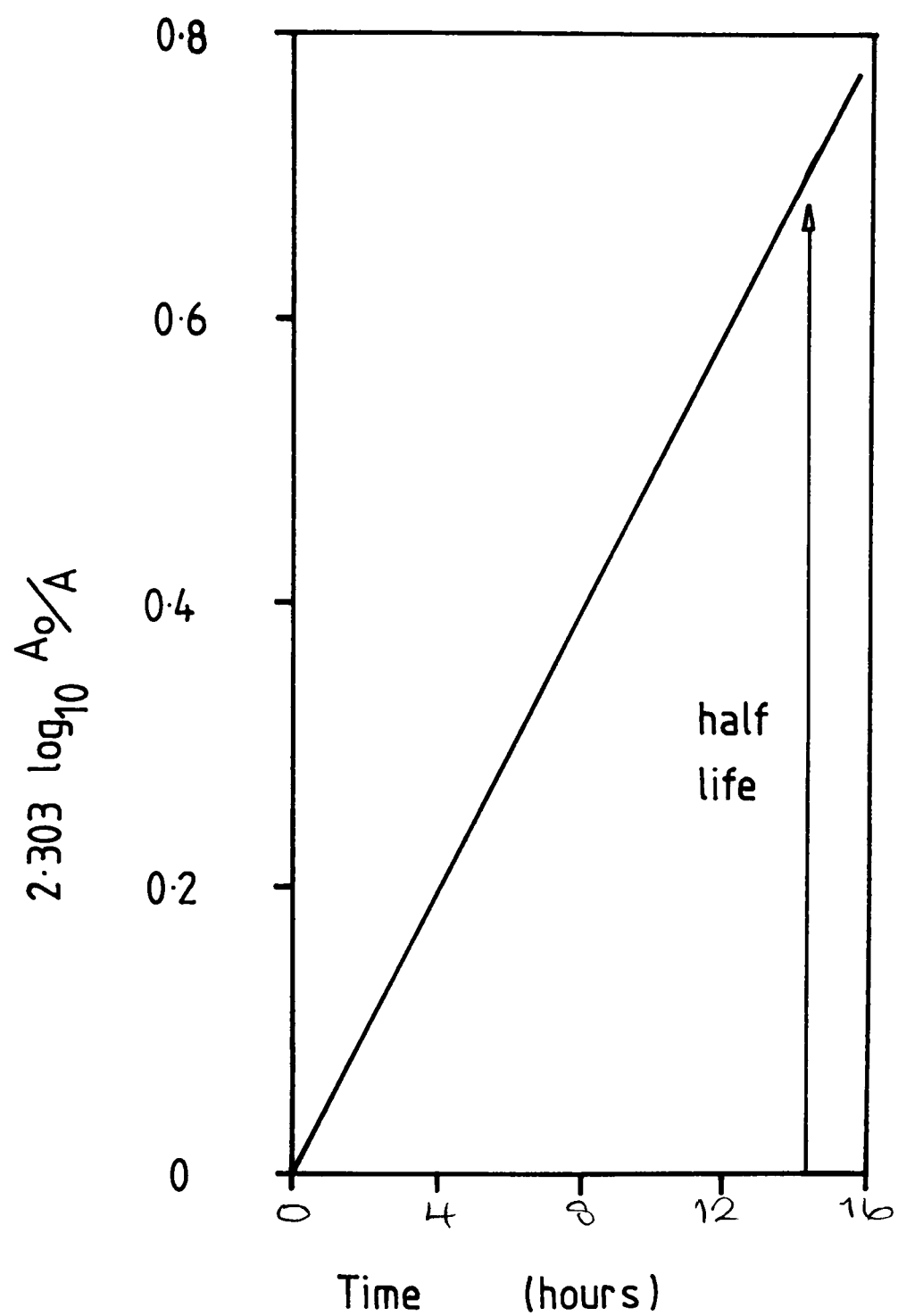
A_0 = INITIAL PORPHYRIN CONCENTRATION

A = PORPHYRIN CONCENTRATION AFTER TIME T

Fig.6. The thermal decomposition of a nickel petroporphyrin at 373°c.
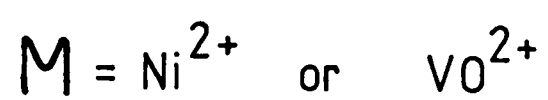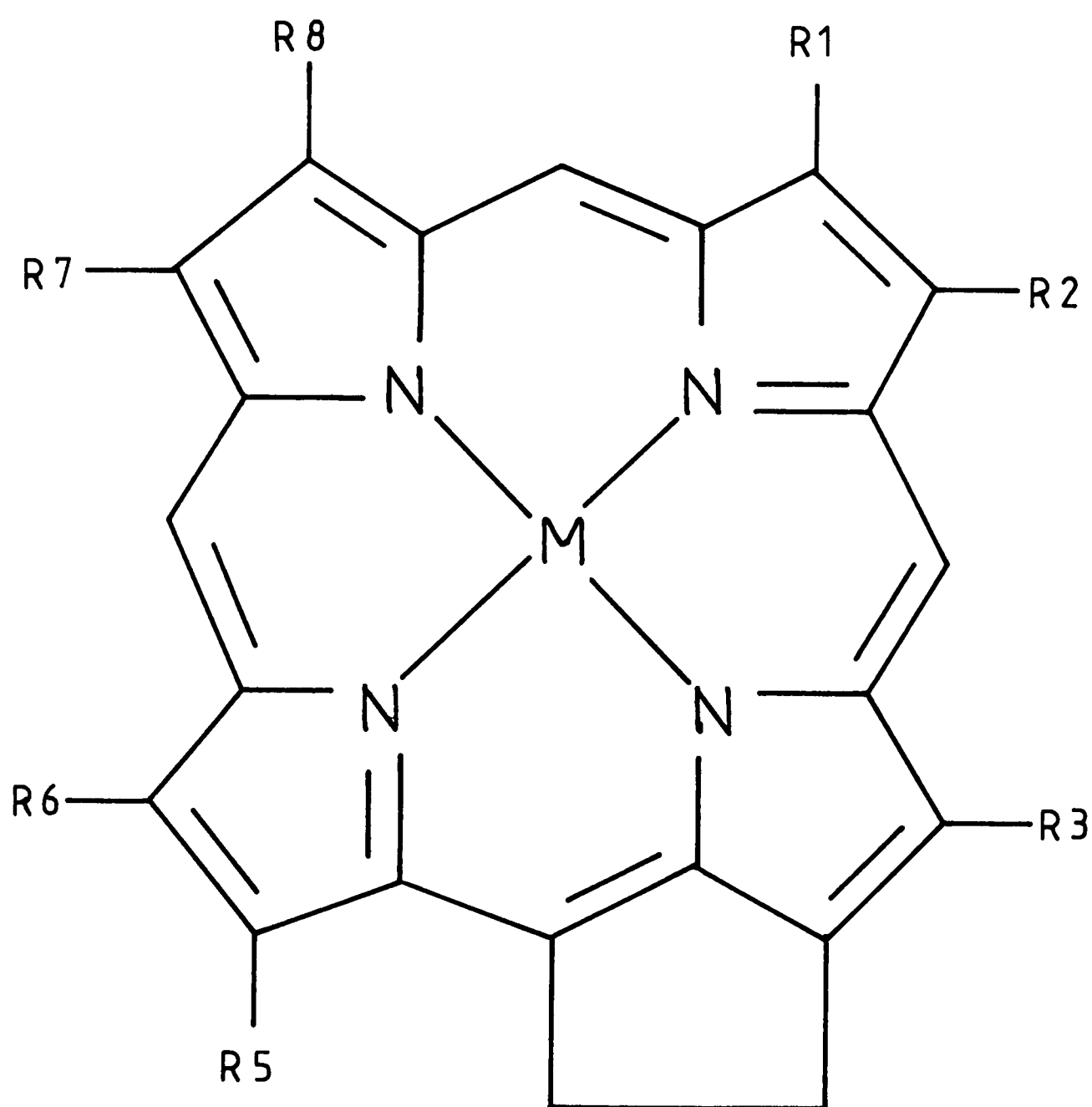
$M = Ni^{2+}$ or VO^{2+}

Fig.7. Structure of deoxophylloerythroetioporphyrin (DPEP).
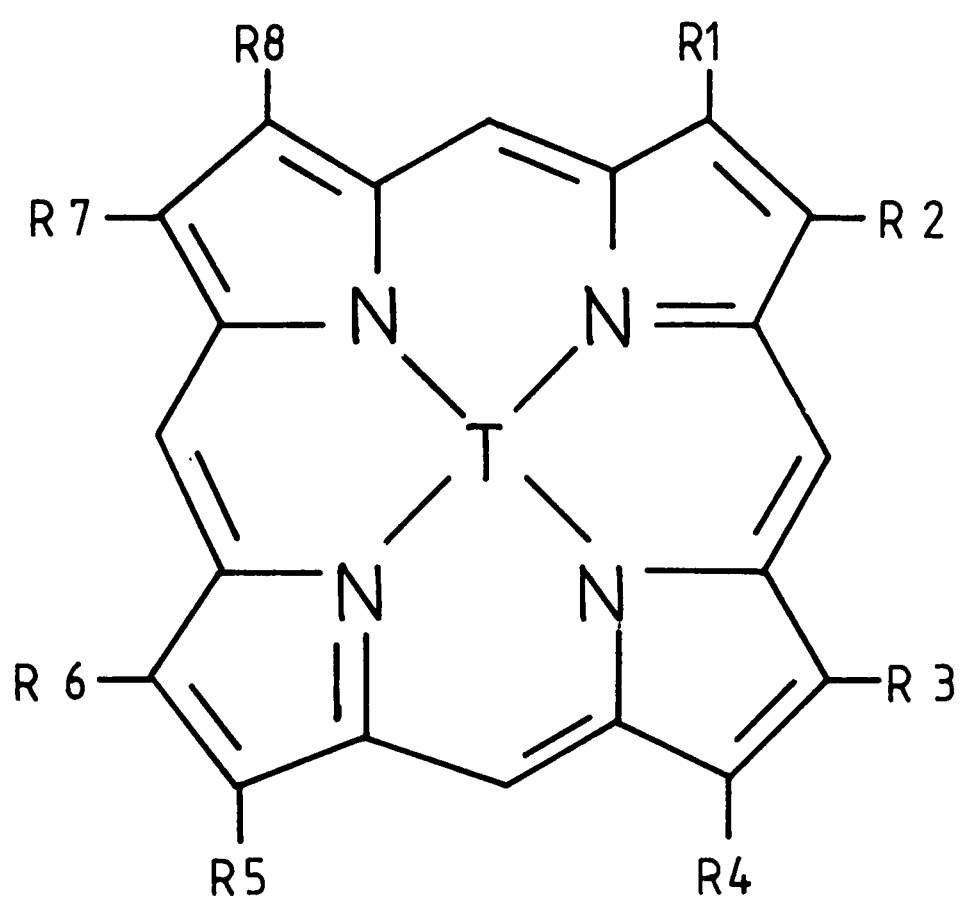
$T = Ni^{2+}$ or VO^{2+} M = methyl   E = ethyl

Porphyrin name	Peripheral substituent							
	R1	R2	R3	R4	R5	R6	R7	R8
Etioporphyrin I	M	E	M	E	M	E	M	E
Etioporphyrin II	M	E	E	M	M	E	E	M
Etioporphyrin III	M	E	M	E	M	E	E	M
Etioporphyrin IV	E	M	M	E	M	E	E	M

Fig.8. Structure and nomenclature for etioporphyrin.

$M = Ni^{2+}$ or VO^{2+}
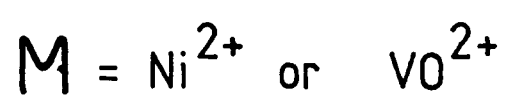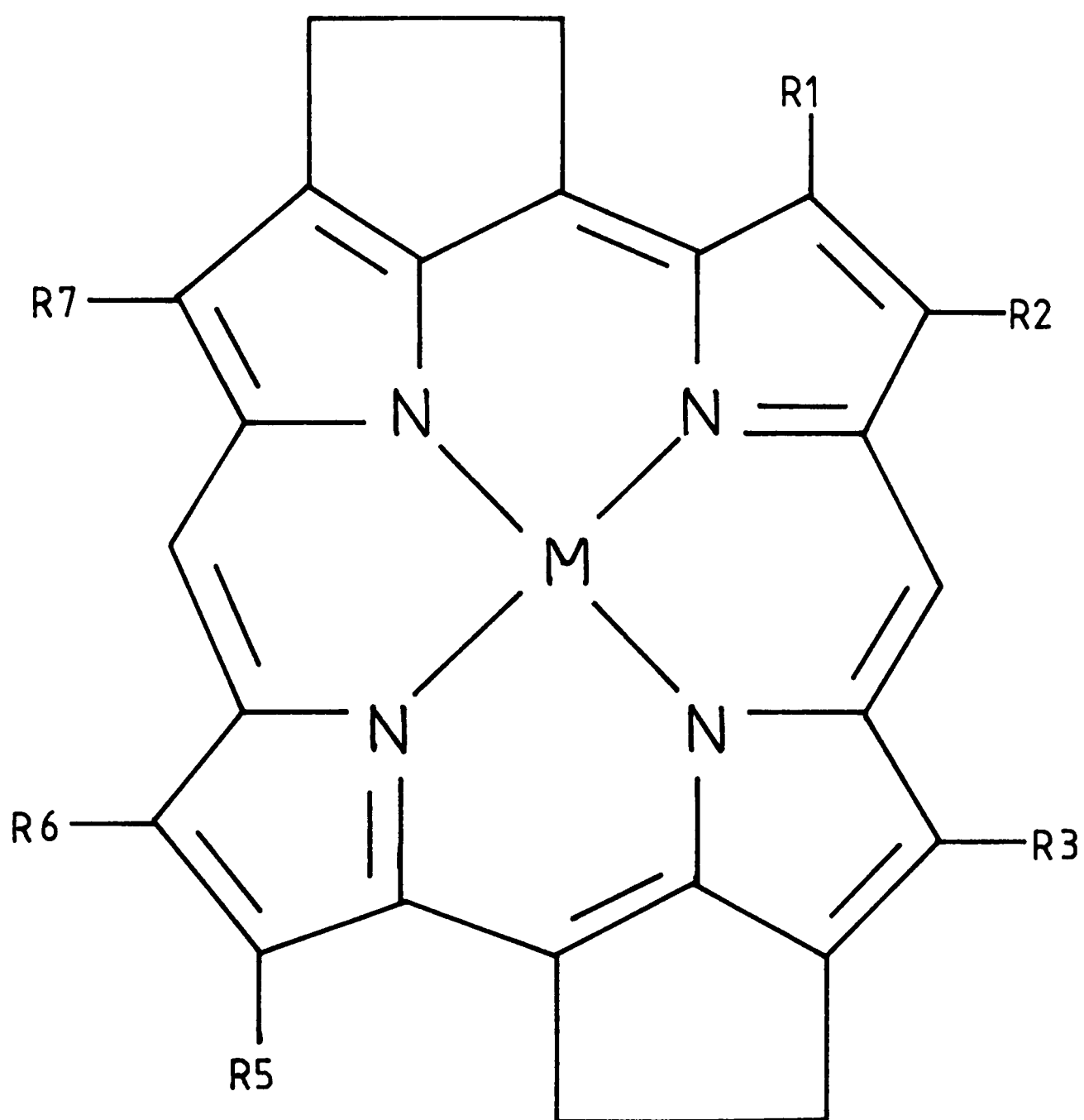
Fig.9.   Structure of di-DPEP.

$M = Ni^{2+}$ or VO^{2+}
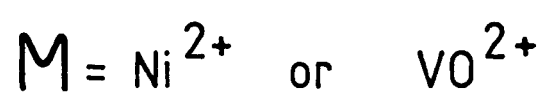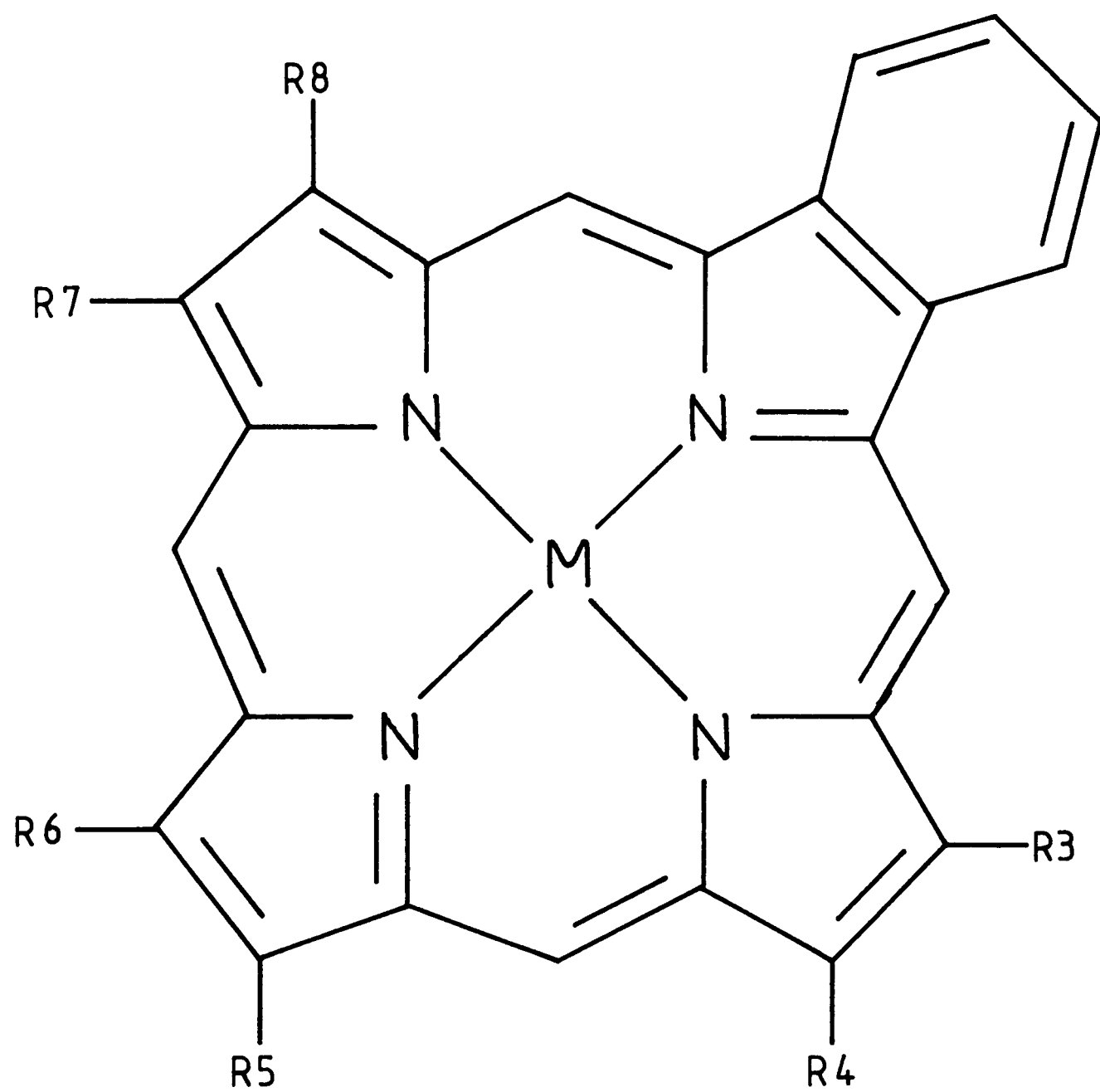
Fig.10.   Structure of rhodo-etioporphyrin.

$M = Ni^{2+}$ or VO^{2+}
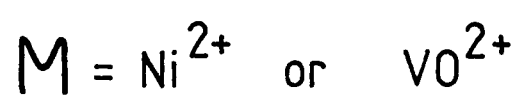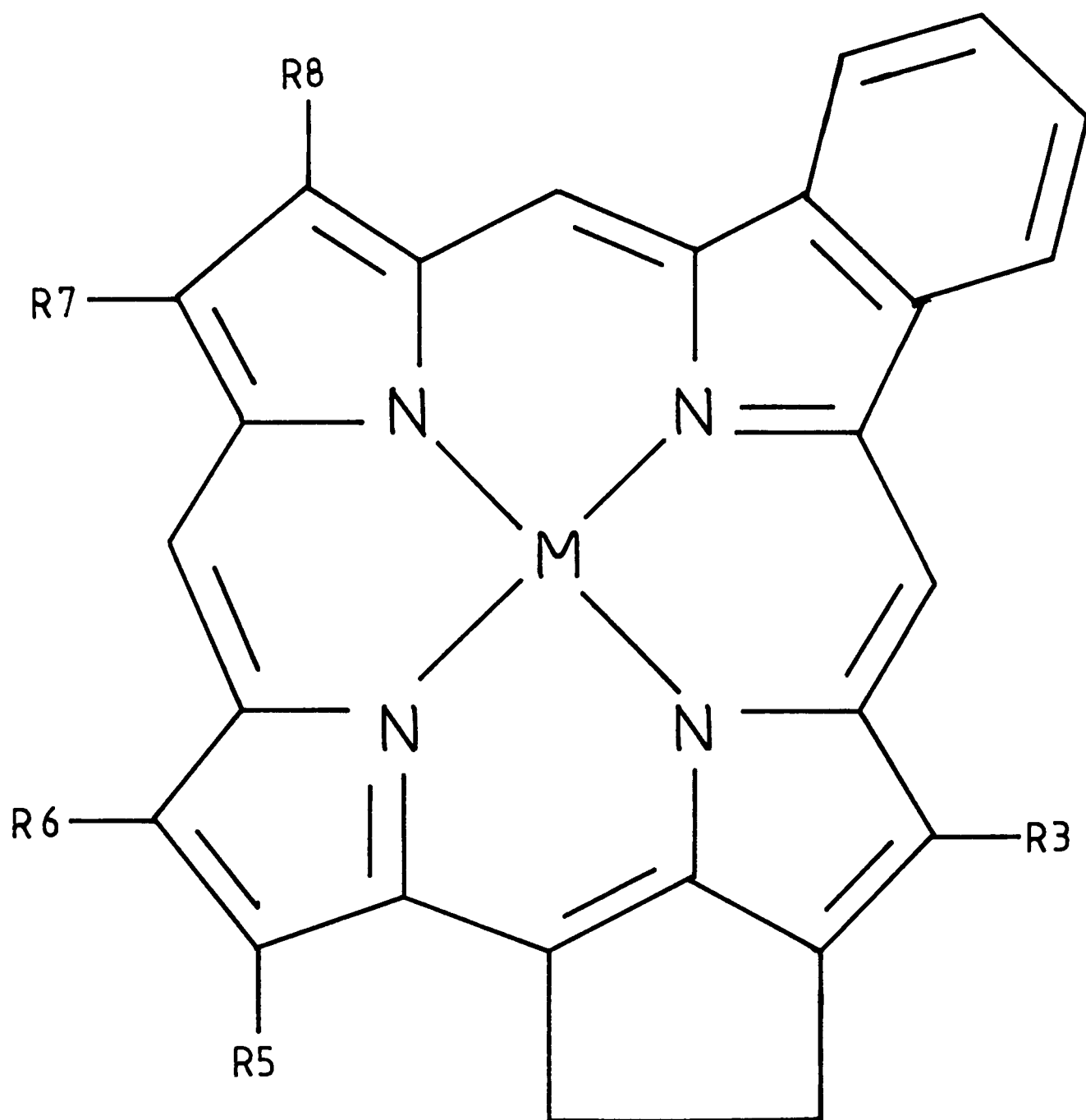
Fig.11.   Structure of rhodo-DPEP.

chlorophyll a

Demetalation

$R = 0-CH_2-CH=\underset{CH_3}{\overset{|}{C}}-C_{16}H_{33}$

pheophytin

Saponification
(and decarbomethoxylation)
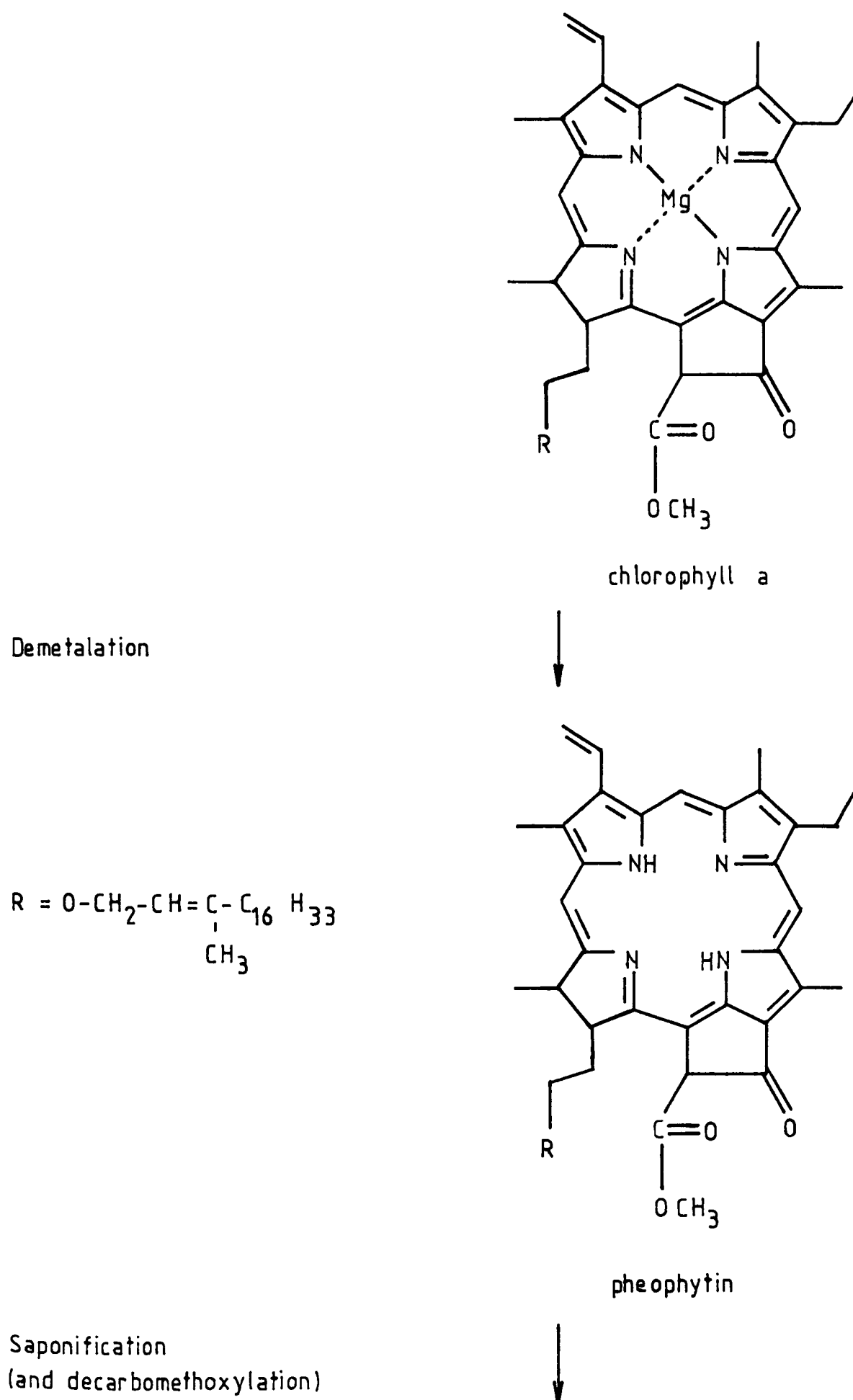
Fig.12.   The Treibs reaction scheme for the diagenic formation of deoxophylloerythroetioporphyrin from chlorophyll a.
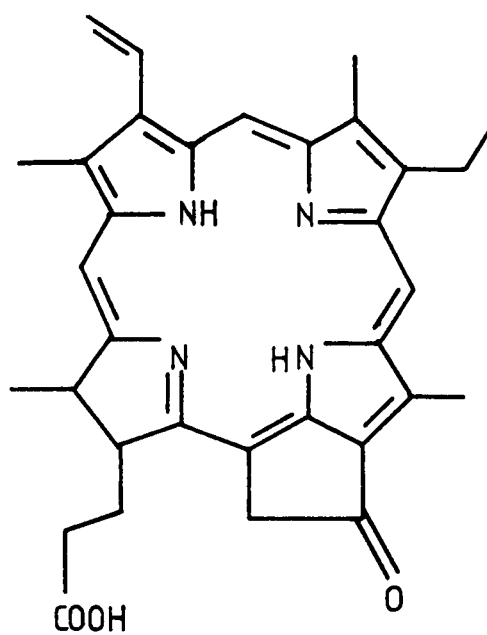
Reduction
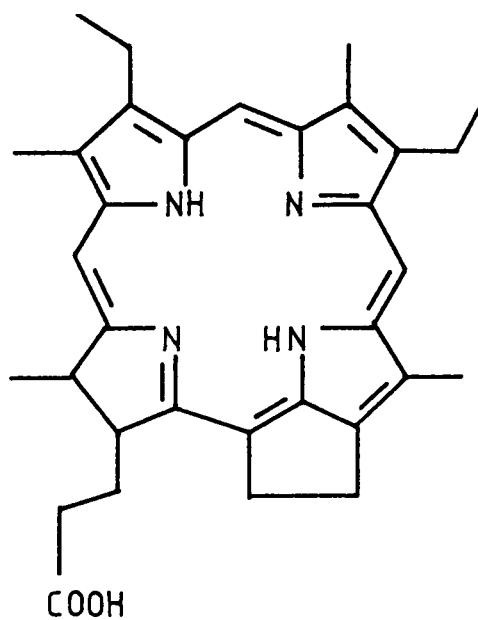
Aromatisation
(chlorin-porphyrin transition)

Fig.12.(cont.) The Treibs reaction scheme for the diagenic formation
of deoxophylloerythroetioporphyrin from chlorophyll a.
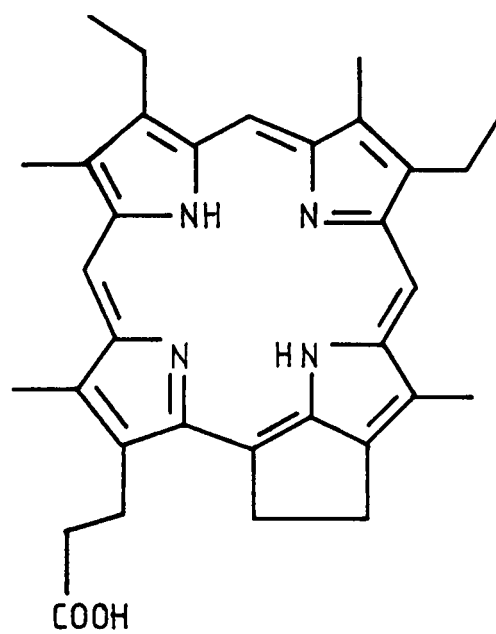
Decarboxylation
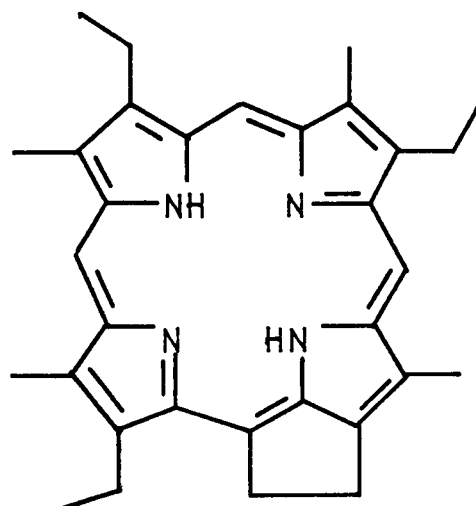
Chelation

Fig.12.(cont.)   The Treibs reaction scheme for the diagenic formation
of deoxophylloerythroetioporphyrin from chlorophyll a.
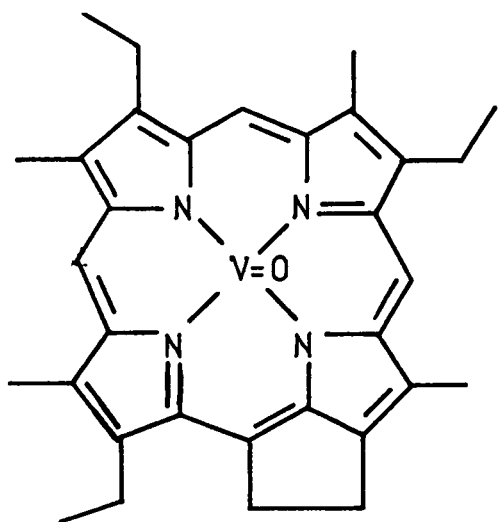
Fig.12.(cont.)   The Treibs reaction scheme for the diagenic formation
of deoxophylloerythroetioporphyrin from chlorophyll a.
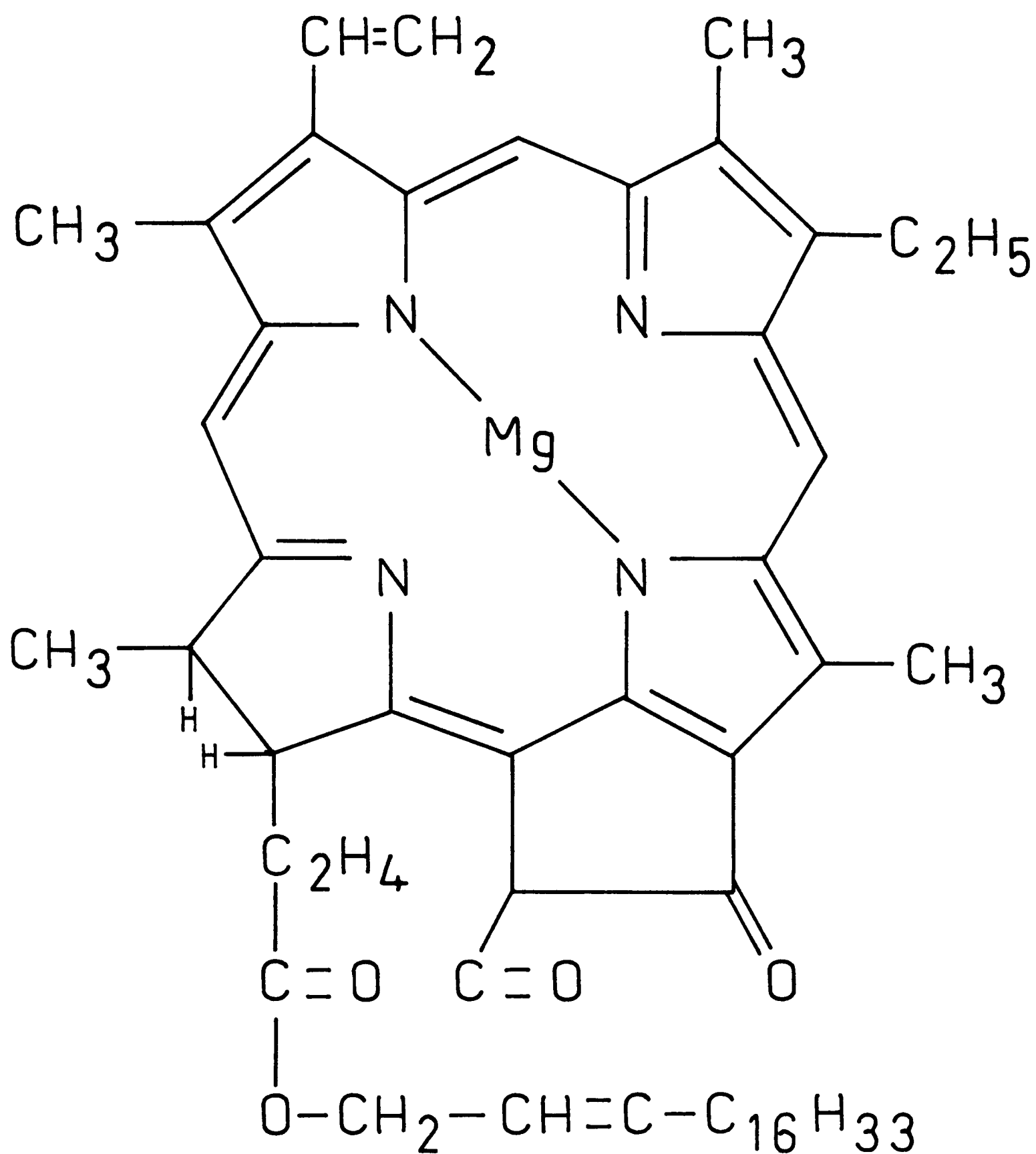
Fig.13.   The structure of chlorophyll a.

$$R-CH_2-C \underset{O-H}{\overset{O}{\lVert}} \longrightarrow R\dot{C}H_2 + CO_2 + \dot{H}$$

$$R\dot{C}H_2 \quad \begin{cases} \xrightarrow{+\dot{H}} CH_3R \\ \xrightarrow{+2[O]} RCOOH + \dot{H} \end{cases}$$
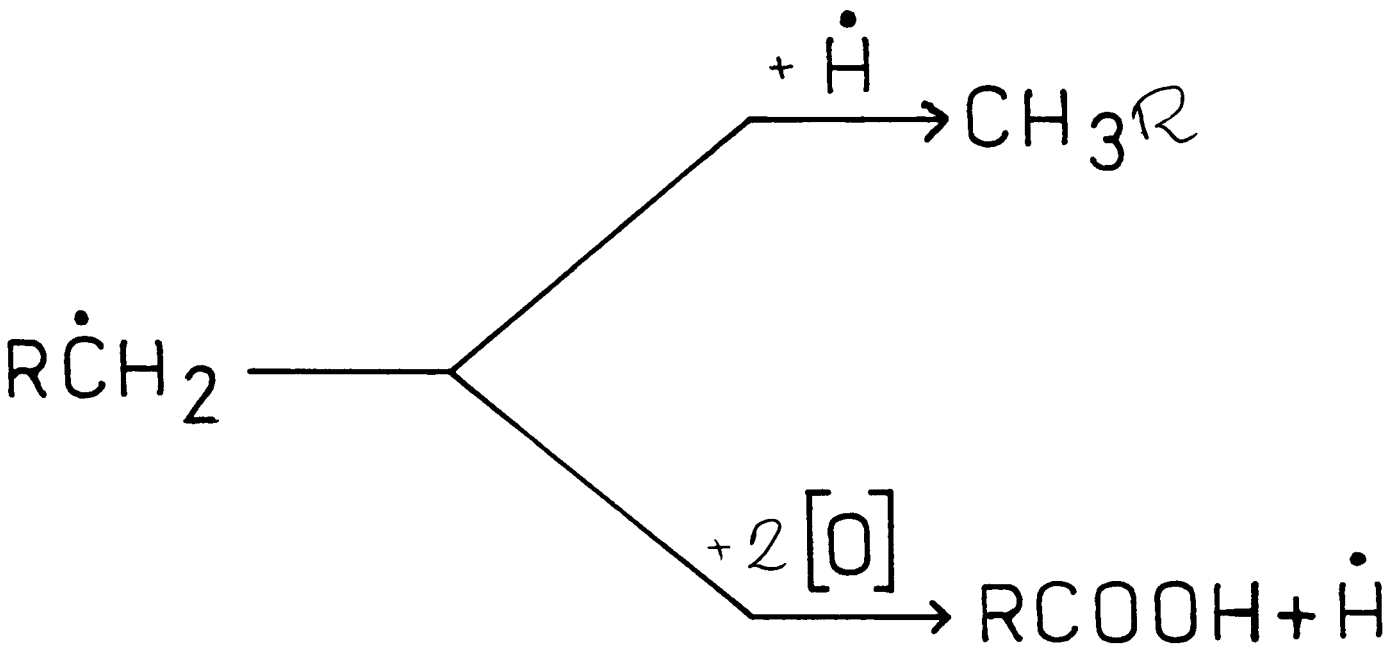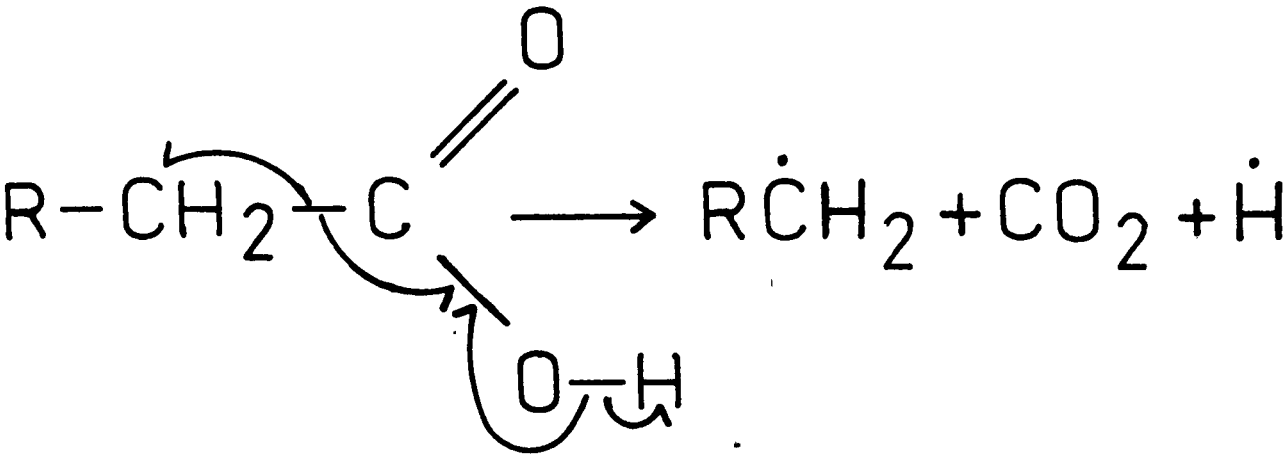
Fig.14.   Decarboxylation.
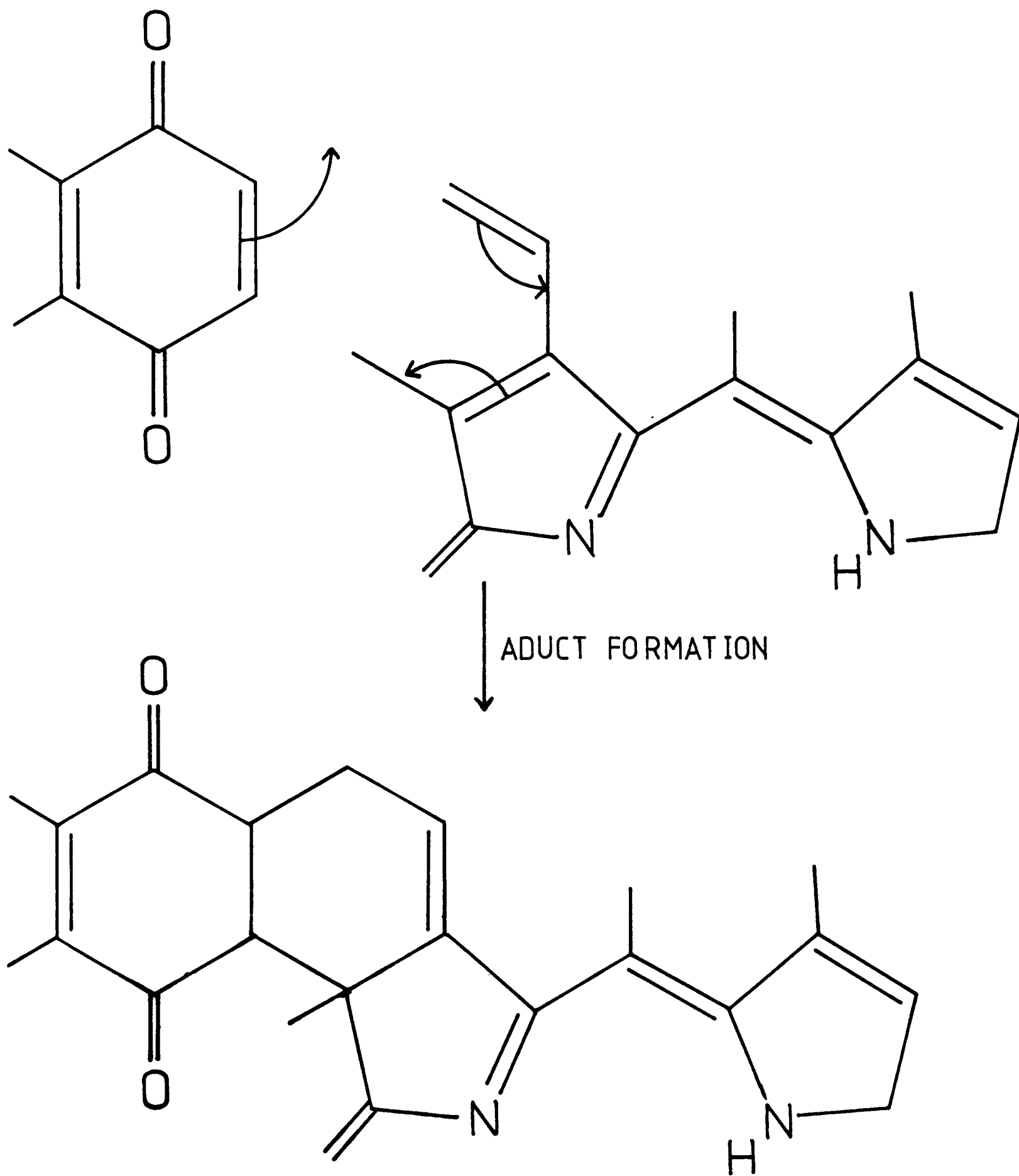
ADUCT FORMATION

Fig.15.   Benzoporphyrin formation.
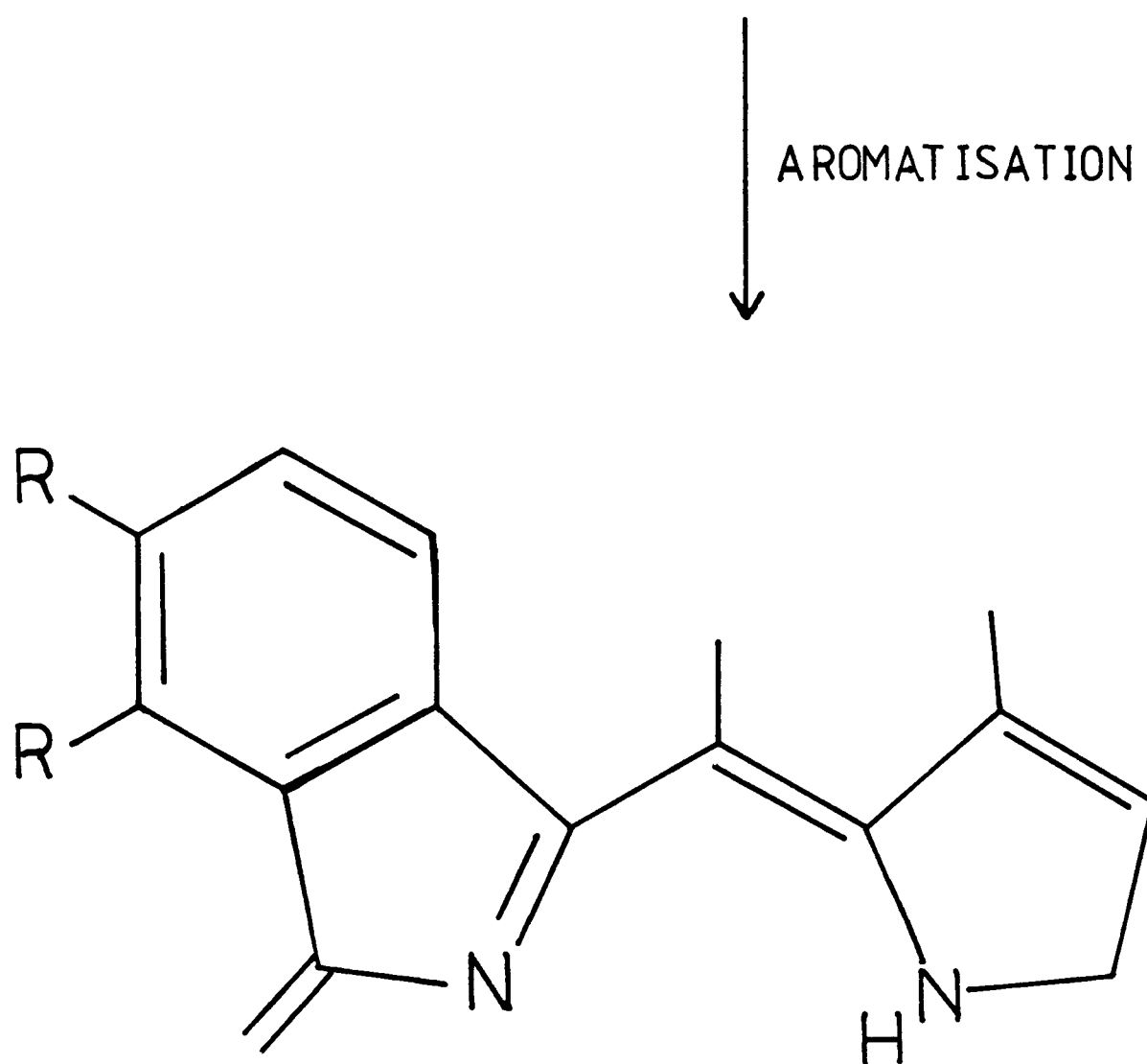
Fig.15.(cont.)   Benzoporphyrin formation.
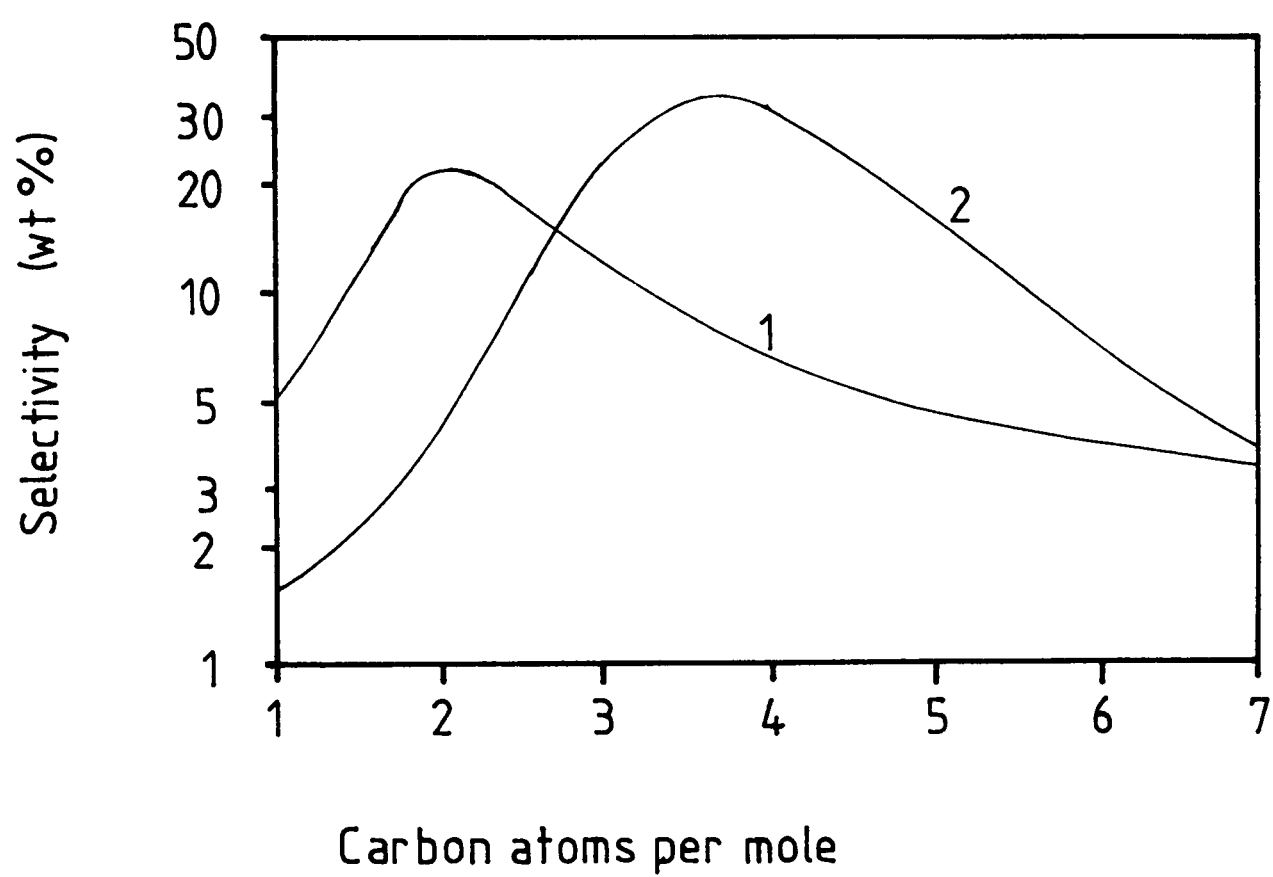
Curve 1 = Thermal cracking

Curve 2 = Cracking over silica-alumina catalyst

Fig.16.   Product spectrum for thermal and silica-alumina
          catalysed cracking reactions.

1. $$RCH_2CH=CHCH_2R + \overset{+}{H} \rightleftharpoons RCH_2\overset{+}{CH}CH_2CH_2R$$

$$RCH_2\overset{+}{CH}CH_2CH_2R \rightleftharpoons RCH=CHCH_2CH_2R + \overset{+}{H}$$

2.
$$\begin{array}{c} CH_3 \\ | \\ CH_3-CH \\ | \\ CH_3 \end{array} \underset{}{\overset{catalyst}{\rightleftharpoons}} \begin{array}{c} CH_3 \\ | \\ CH_3-\overset{+}{C} \\ | \\ CH_3 \end{array} + \ cat:\overset{-}{H}$$

3.
$$\begin{array}{cc} CH_3 & CH_3 \\ | & | \\ CH_3-CH & + \ \overset{+}{C}H \\ | & | \\ CH_3 & CH_3 \end{array} \rightleftharpoons \begin{array}{cc} CH_3 & CH_3 \\ | & | \\ CH_3-\overset{+}{C} & + \ CH_2 \\ | & | \\ CH_3 & CH_3 \end{array}$$
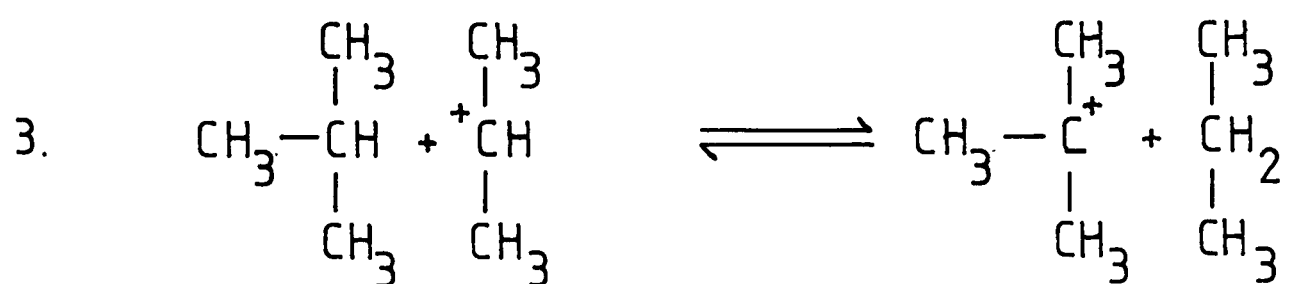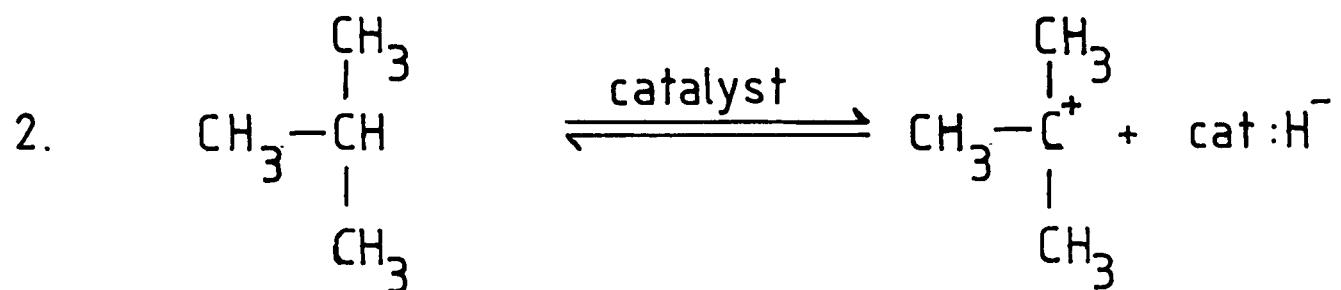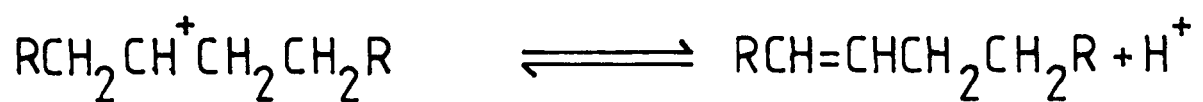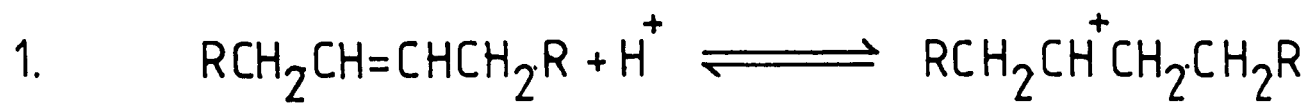
Fig.17.   Formation of carbonium ions during catalytic cracking.

$$-O-\overset{\overset{\displaystyle O}{|}}{\underset{\underset{\displaystyle O}{|}}{Si}}-O-\overset{\overset{\displaystyle O}{|}}{\underset{\underset{\displaystyle O}{|}}{Si}}-O-\overset{\overset{\displaystyle O}{|}}{\underset{\underset{\displaystyle O}{|}}{Al}}{}^{\times} \quad + \quad R{:}H \quad \longrightarrow$$

$$-O-\overset{\overset{\displaystyle O}{|}}{\underset{\underset{\displaystyle O}{|}}{Si}}-O-\overset{\overset{\displaystyle O}{|}}{\underset{\underset{\displaystyle O}{|}}{Si}}-O-\overset{\overset{\displaystyle O}{|}}{\underset{\underset{\displaystyle O}{|}}{Al}}{:}H^{-} \quad + \quad R^{+}$$
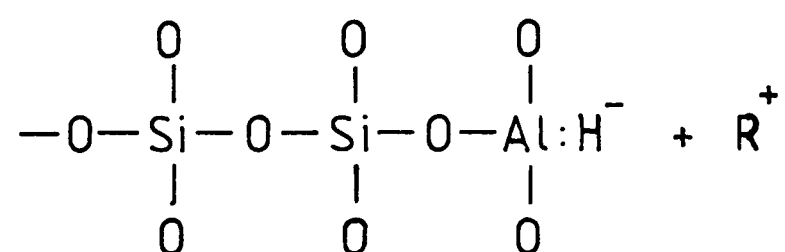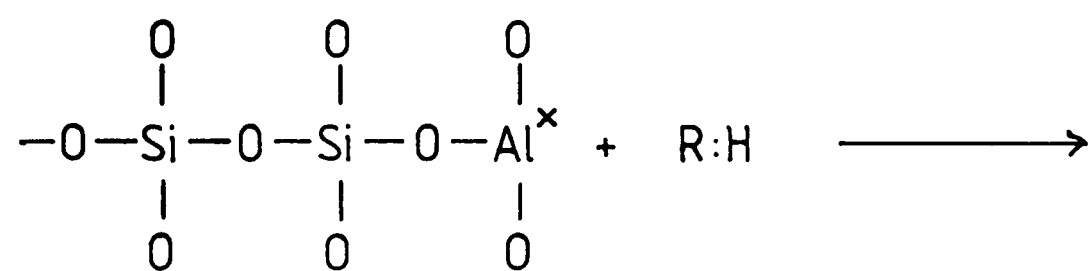
× = Lewis acid site

·Fig.18.   Hydride ion abstraction by silica-alumina catalyst.

$$-O-Si-O-Si-O-Al \ + \ :\!\overset{..}{O}-H \qquad \xrightarrow{\text{hydrated catalyst}}$$

(with O above each Si and Al, O below each Si and Al; H above the O-H)

$$-O-Si-O-Si-O-Al:\overset{..}{O}-H^{\times}$$

$$\Big\downarrow RCH{=}CHR$$

$$-O-Si-O-Si-O-Al-OH^{-}$$

+

$$RCH_2\overset{+}{C}HR$$
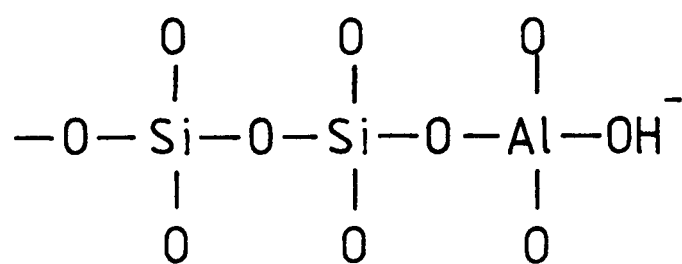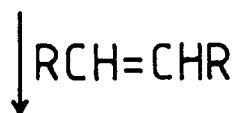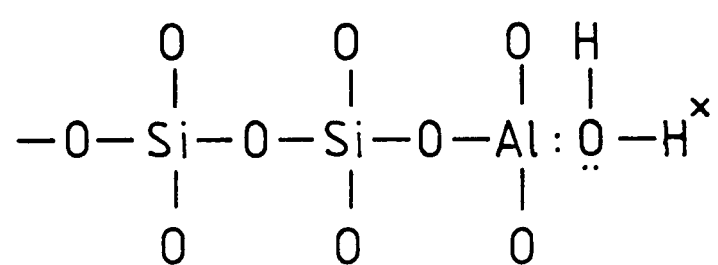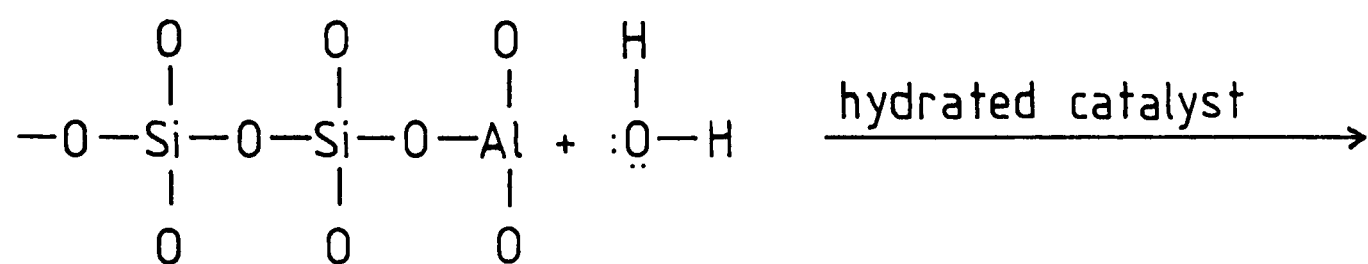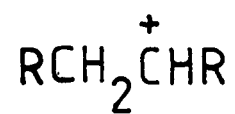
× = Bronsted acid protonic site

Fig.19.   Protonation of a carbon to carbon double
         bond by a Bronsted acid site.

Fig.20. A hydride shift.

Fig.21.   A methide shift.

$$R-CH_2-CH_2-\overset{+}{C}H-CH_2-CH_2-R'$$

$$R-\overset{+}{C}H_2 \ + \ CH_2=CH-CH_2-CH_2-R'$$

$$R-CH_2-CH_2-CH=CH_2 \ + \overset{+}{C}H_2-R'$$
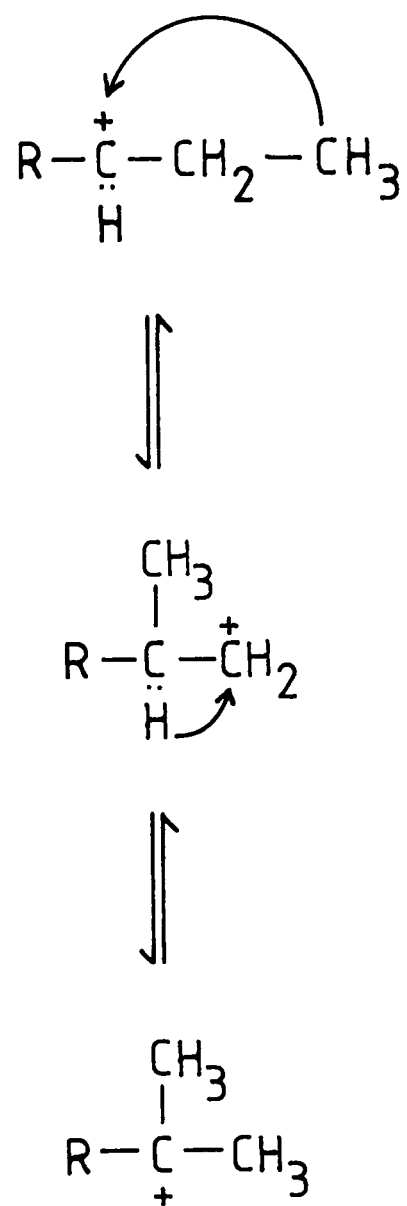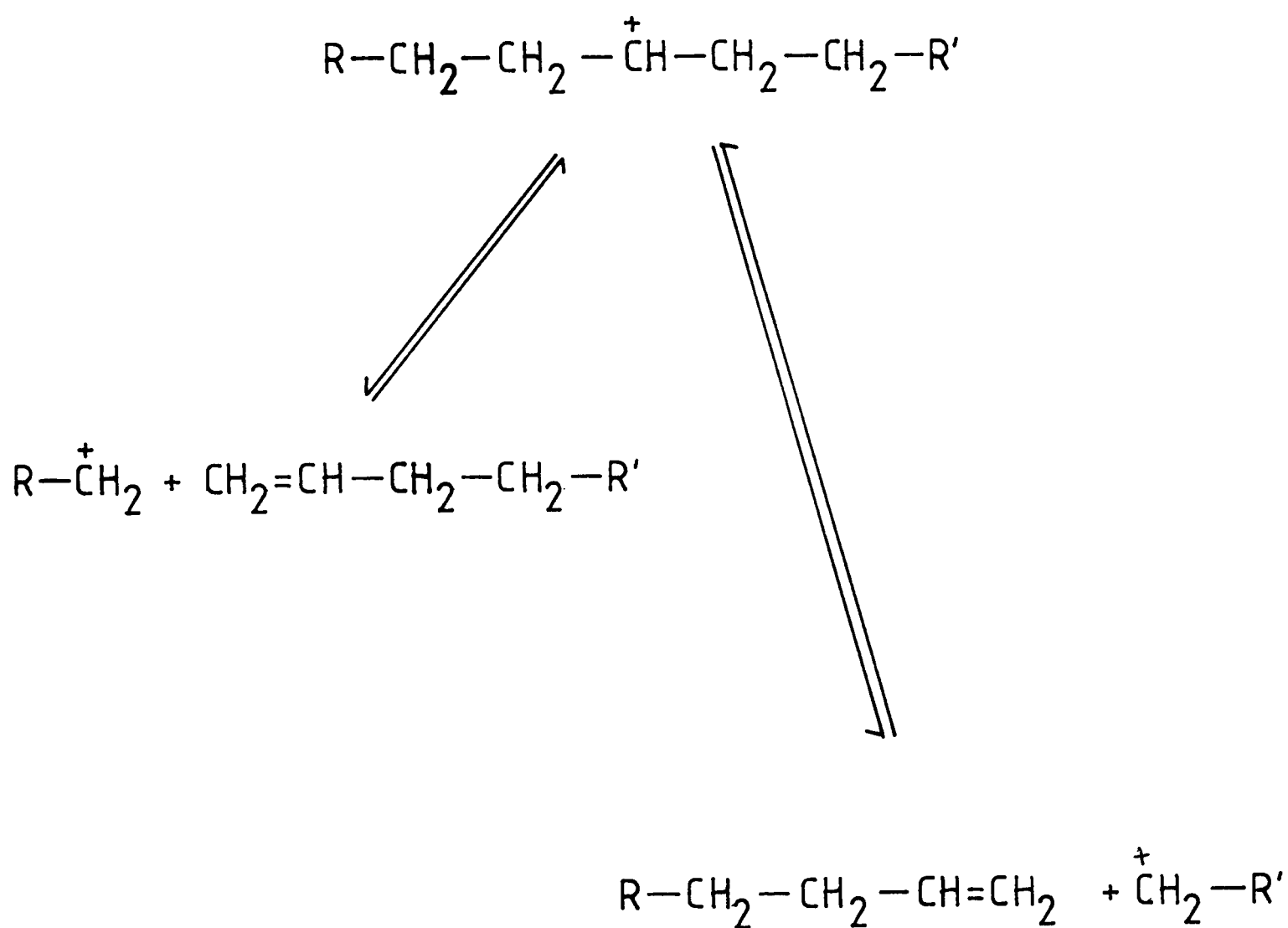
Fig.22.   Beta fission.
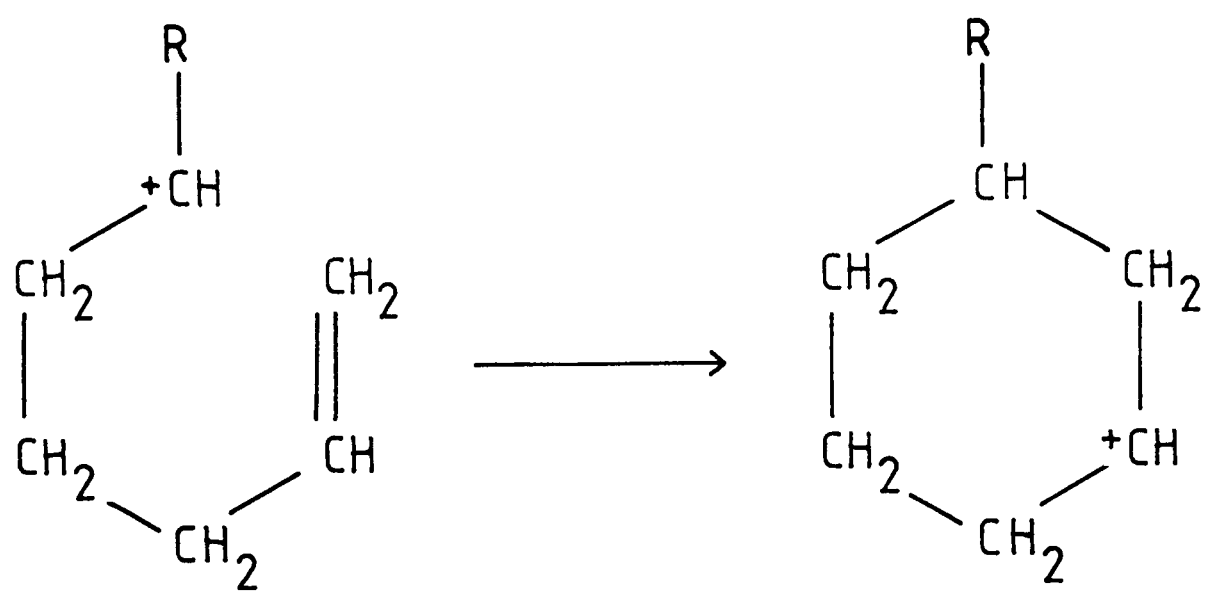
Fig.23.   Cyclisation.
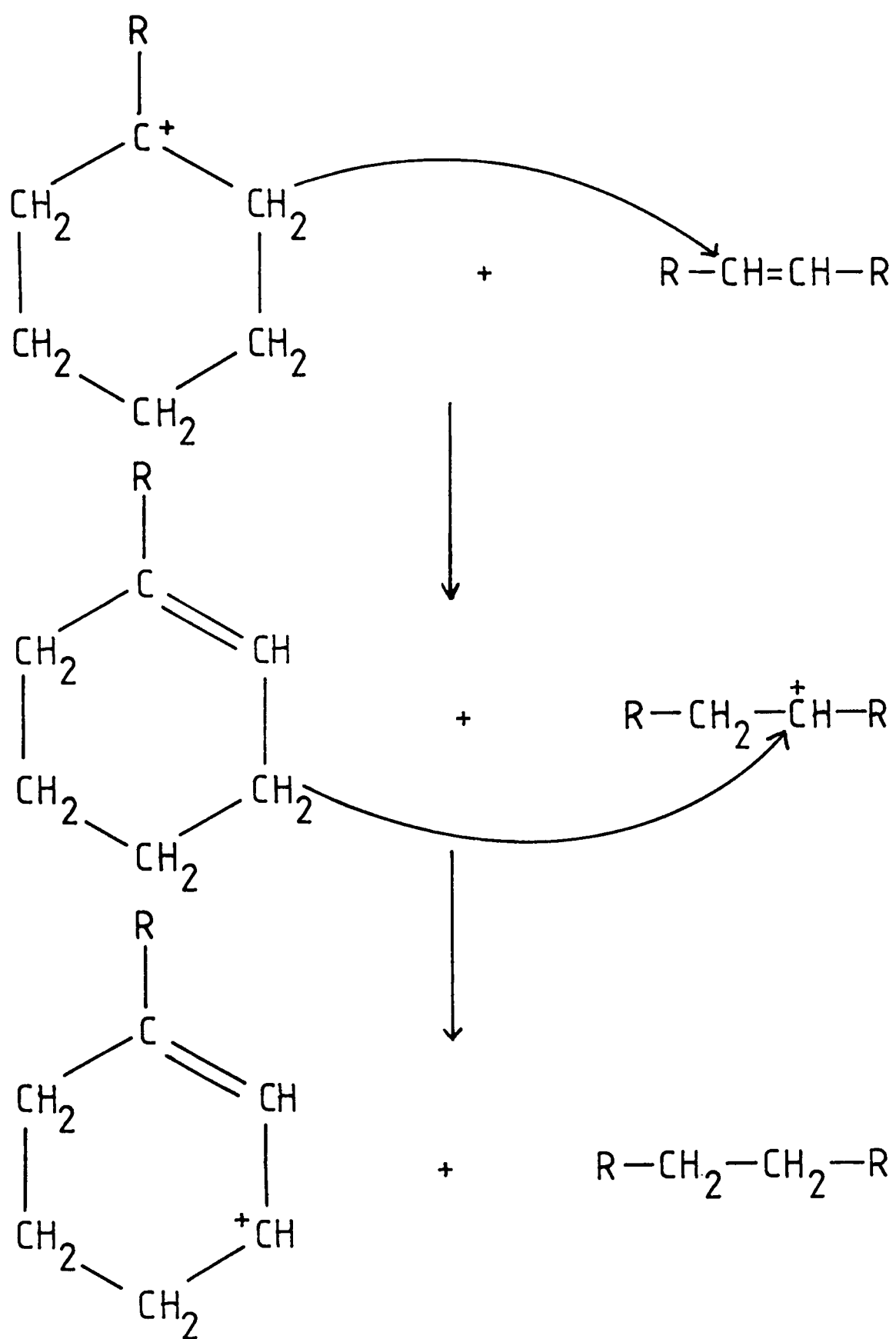
Fig.24.   Hydrogen transfer sequence.

$$CH_3CH_2CH{=}CHCOOH$$

$$+$$

$$CH_3OH$$

$$\downarrow H_2SO_4 \text{ (conc)}$$

$$CH_3CH_2CH{=}CHCOOCH_3$$

Fig.25.   Preparation of methyl trans-2-pentenoate.

$$CH_3CH_2CH=CHCOOCH_3$$

+

$$O=S-O-CH_2-N=C$$

$$CH_3$$

NaH $(Et_2O / DMSO)$

$$CH_3CH_2 \quad \overset{O}{\overset{\|}{C}}-OCH_3$$

N
H
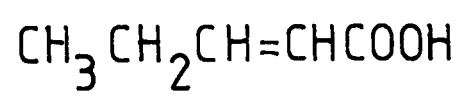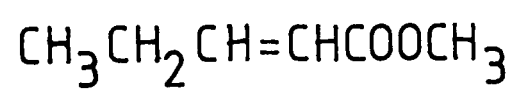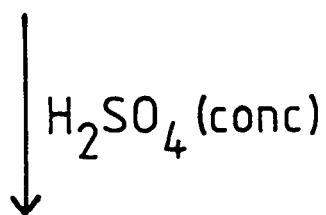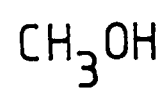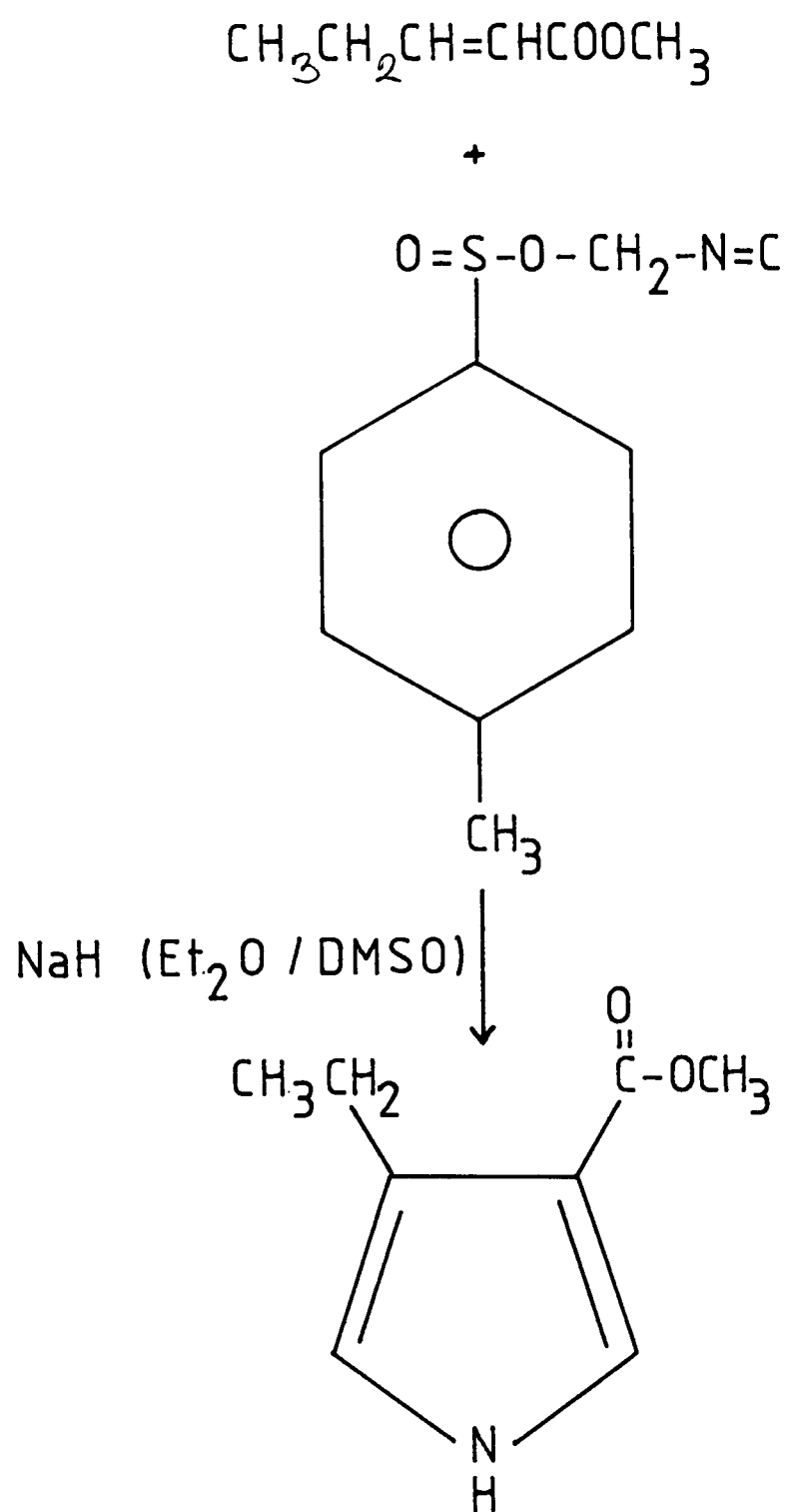
Fig.26.   Preparation of methyl 4-ethylpyrrole-3-carboxylate.
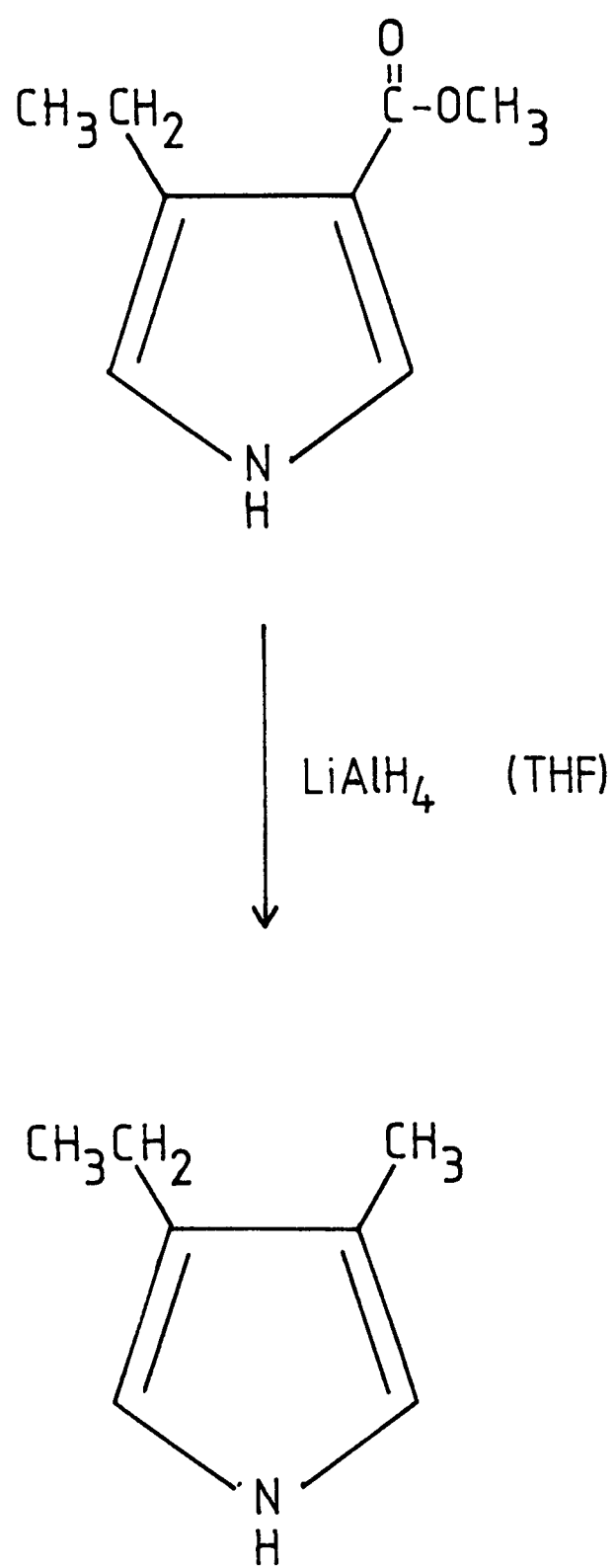
Fig.27.   Preparation of 3-ethyl-4-methyl pyrrole.

Fig.28.   Preparation of etioporphyrin.

B24

B60

5

27

97

2(O.D.)

124

20

5

82·5

B24

0·8
(O.D.)

6
(O.D.)

5 dm³
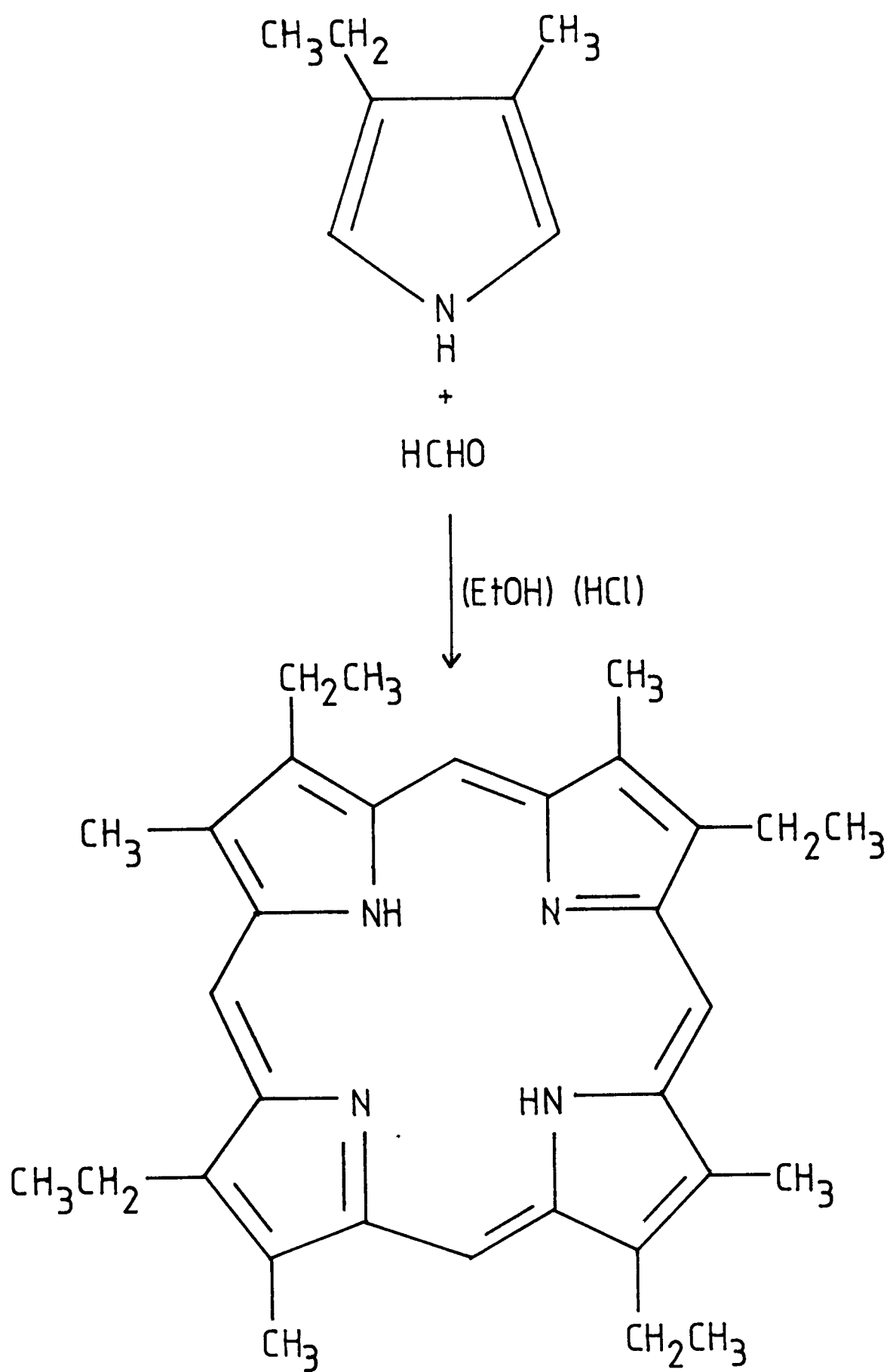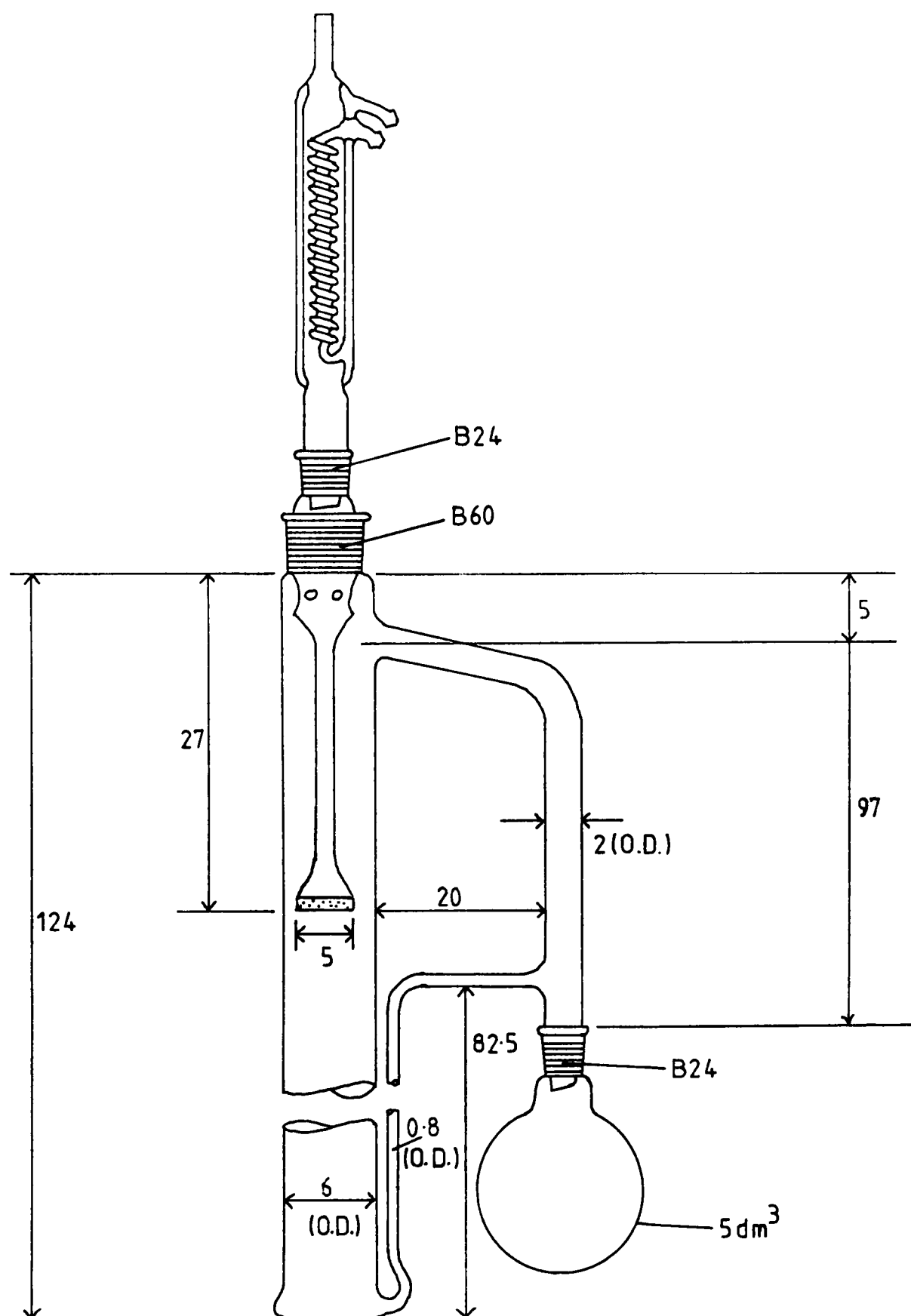
(All dimensions in cm)

Fig.29.   Downward displacement extractor used in
the preparation of etioporphyrin.

$$\underset{\text{O}}{\text{CH}_3\overset{\|}{\text{C}}\text{CH}_2\overset{\|}{\underset{\text{O}}{\text{C}}}\text{CH}_3} + \text{CH}_3\text{CH}_2\text{I} + \text{K}_2\text{CO}_3$$

acetone

$$\text{CH}_3\overset{\|}{\underset{\text{O}}{\text{C}}}\underset{\underset{\text{CH}_2\text{CH}_3}{|}}{\text{CH}}\overset{\|}{\underset{\text{O}}{\text{C}}}\text{CH}_3$$

3-ethyl-2,4 pentandione

+

$$\text{CH}_3\overset{\|}{\underset{\text{O}}{\text{C}}}\text{CH}_2\text{COOC}(\text{CH}_3)_3 + \text{CH}_3\text{COOH} + \text{NaNO}_2 + \text{Zn}$$

t-butylacetoacetate

t-butyl 4-ethyl-3,5-dimethylpyrrole carboxylate

+

Br_2

CH_3COOH | HCO OH
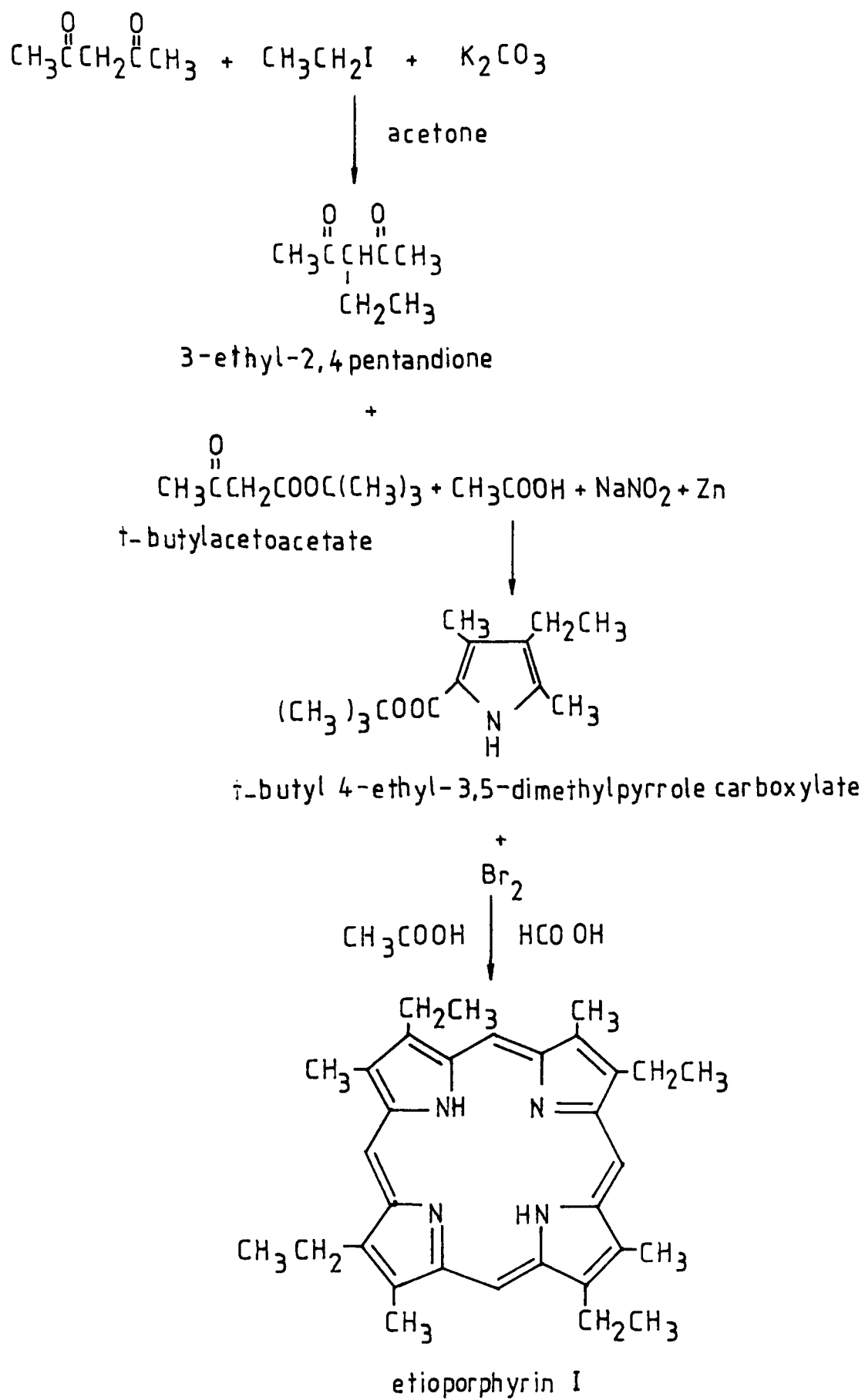
etioporphyrin I

Fig.30.   Reaction sequence for the synthesis of etioporphyrin I.

$$10C_2H_5OH + 2P + 5I_2$$

$$\downarrow$$

$$10C_2H_5I + 2H_3PO_4 + H_2O$$

Fig.31.   Preparation of ethyl iodide.

$$2CH_3\overset{\overset{\displaystyle O}{\|}}{C}CH_2\overset{\overset{\displaystyle O}{\|}}{C}CH_3 + 2CH_3CH_2I + K_2CO_3$$

2,4-pentandione

acetone | solvent

$$2CH_3\overset{\overset{\displaystyle O}{\|}}{C}\underset{\underset{\displaystyle CH_2CH_3}{|}}{C}H\overset{\overset{\displaystyle O}{\|}}{C}CH_3$$

3-ethyl-2,4-pentandione

$$(+2KI + H_2CO_3)$$

Fig.32.   Preparation of 3-ethyl-2,4-pentandione.

$$CH_3\overset{\overset{\displaystyle O}{\|}}{C}CH_2COOC(CH_3)_3 \ + \ CH_3\overset{\overset{\displaystyle O}{\|}}{C}\underset{\underset{\displaystyle CH_2CH_3}{|}}{C}H\overset{\overset{\displaystyle O}{\|}}{C}CH_3$$

t-butylacetoacetate   3-ethyl-2,4-pentandione

$$+ \ 4CH_3COOH \ + \ NaNO_2 \ + \ 2Zn$$

$$\downarrow$$

t-butyl 4-ethyl-3,5-dimethylpyrrole carboxylate

$$+ \ 2(CH_3COO)_2Zn \ + \ CH_3COONa \ + \ 3H_2O$$

Fig.33. Preparation of t-butyl 4-ethyl-3,5-dimethylpyrrole
        carboxylate.

$$CH_3COOH + NaNO_2 \xrightarrow{H_2O} HNO_2 \quad (+ CH_3COONa)$$

$$CH_3\overset{O}{\overset{\|}{C}}CH_2COOC(CH_3)_3 + HNO_2 \longrightarrow CH_3\overset{O}{\overset{\|}{C}}\underset{NOH}{\overset{\|}{C}}COOC(CH_3)_3 \quad (+ H_2O)$$

$$2Zn + 4CH_3COOH \longrightarrow 4H \quad (+ 2(CH_3COO)_2Zn)$$

$$CH_3\overset{O}{\overset{\|}{C}}\underset{NOH}{\overset{\|}{C}}COOC(CH_3)_3 + 4H \longrightarrow CH_3\overset{O}{\overset{\|}{C}}\underset{NH_2}{\overset{|}{C}}HCOOC(CH_3)_3 \quad (+ H_2O)$$

$$CH_3\overset{O}{\overset{\|}{C}}\underset{NH_2}{\overset{|}{C}}HCOOC(CH_3)_3 + CH_3\overset{O}{\overset{\|}{C}}\underset{CH_2CH_3}{\overset{|}{C}}H\overset{O}{\overset{\|}{C}}CH_3$$
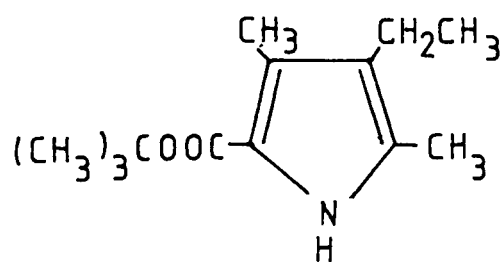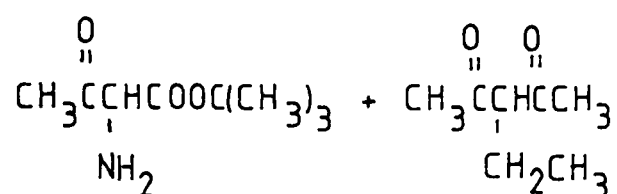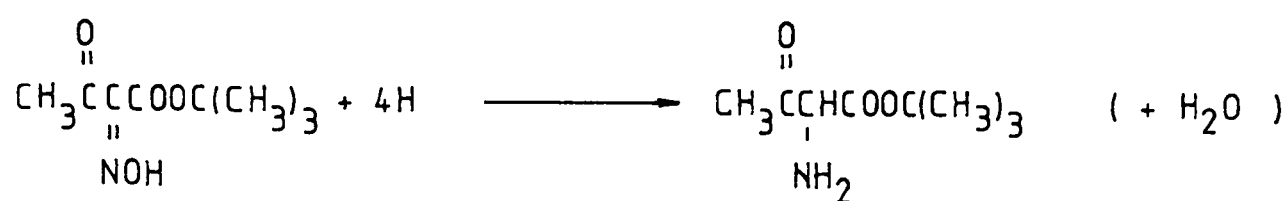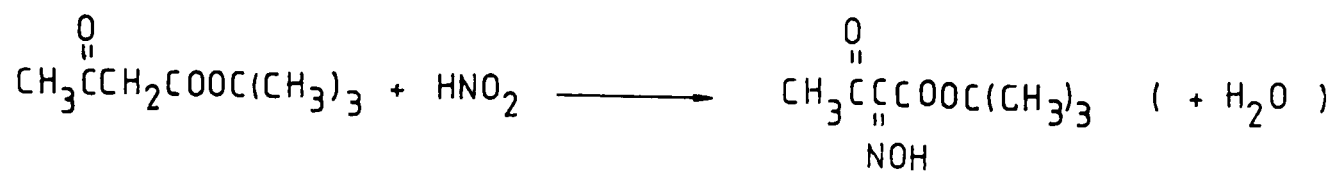
Fig.34.   Reaction sequence for the preparation of
t-butyl 4-ethyl-3,5-dimethyl pyrrole carboxylate.
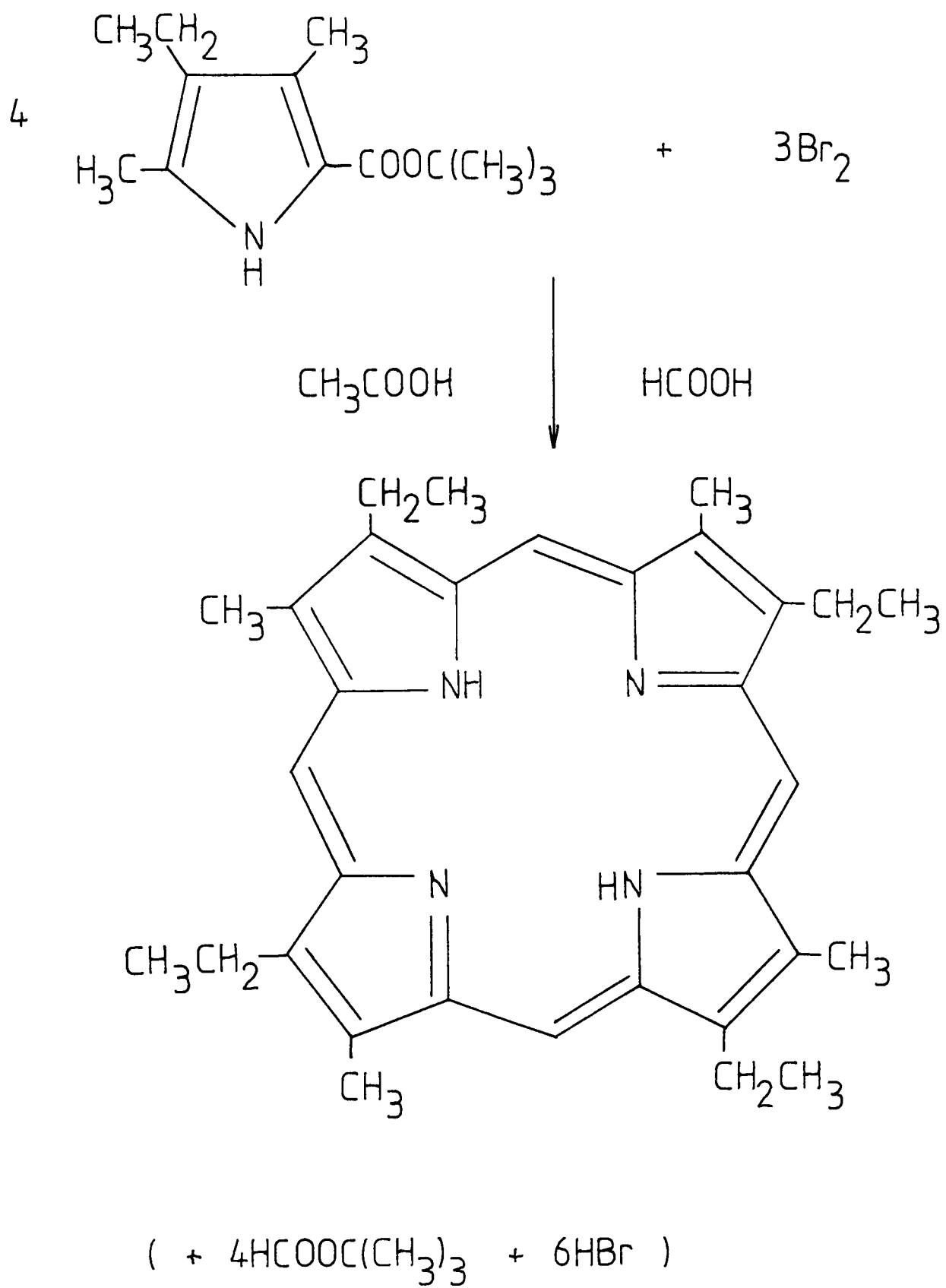
Fig.35. Preparation of etioporphyrin I.

Fig.36. Reaction sequence for the preparation of etioporphyrin I.

CH_2CH_3

CH_3

CH_3

CH_2CH_3

NH

N

N

HN

CH_3CH_2

CH_3

CH_3

CH_2CH_3

CH_3

CH_2CH_3

+

6 HBr
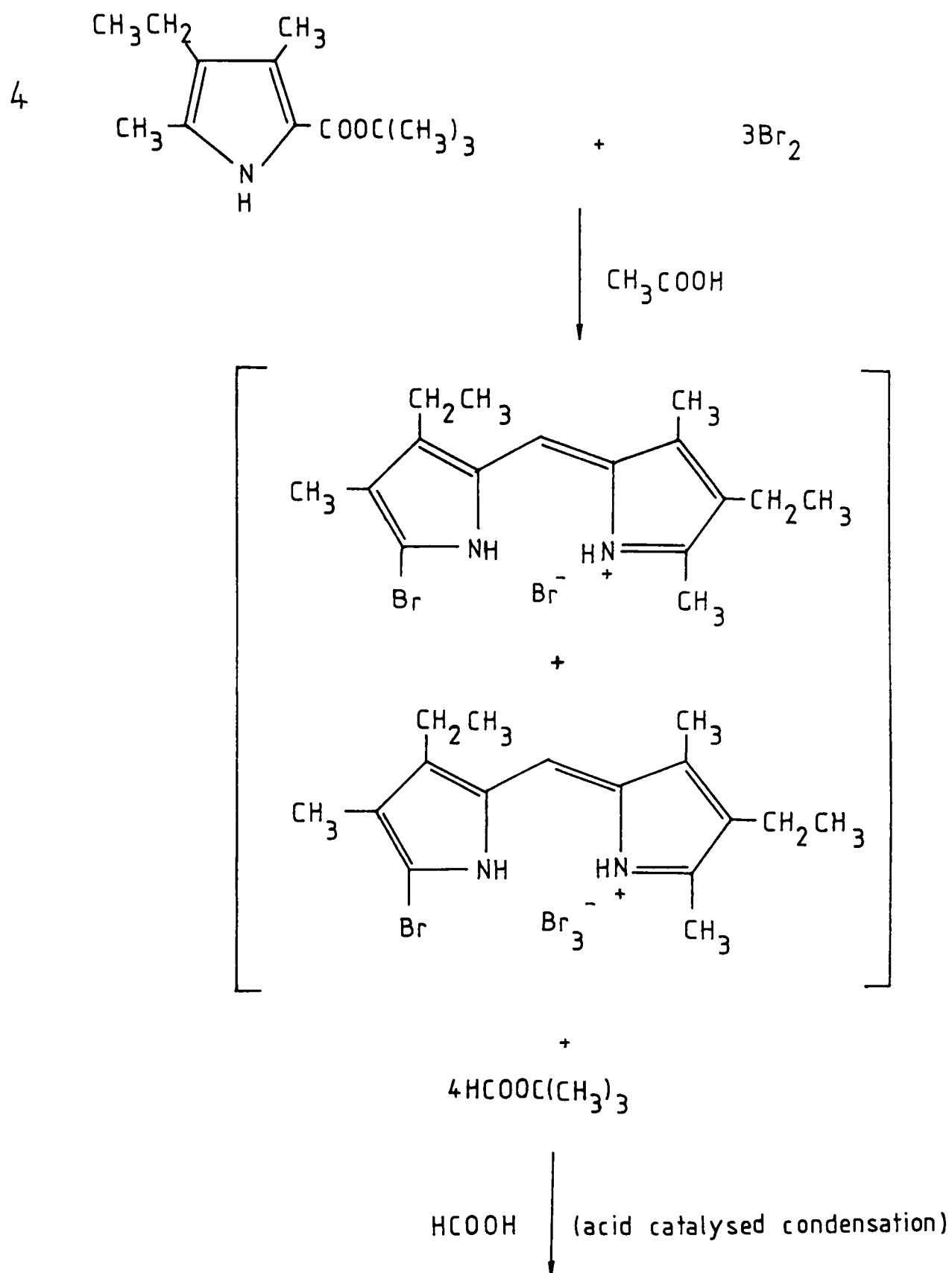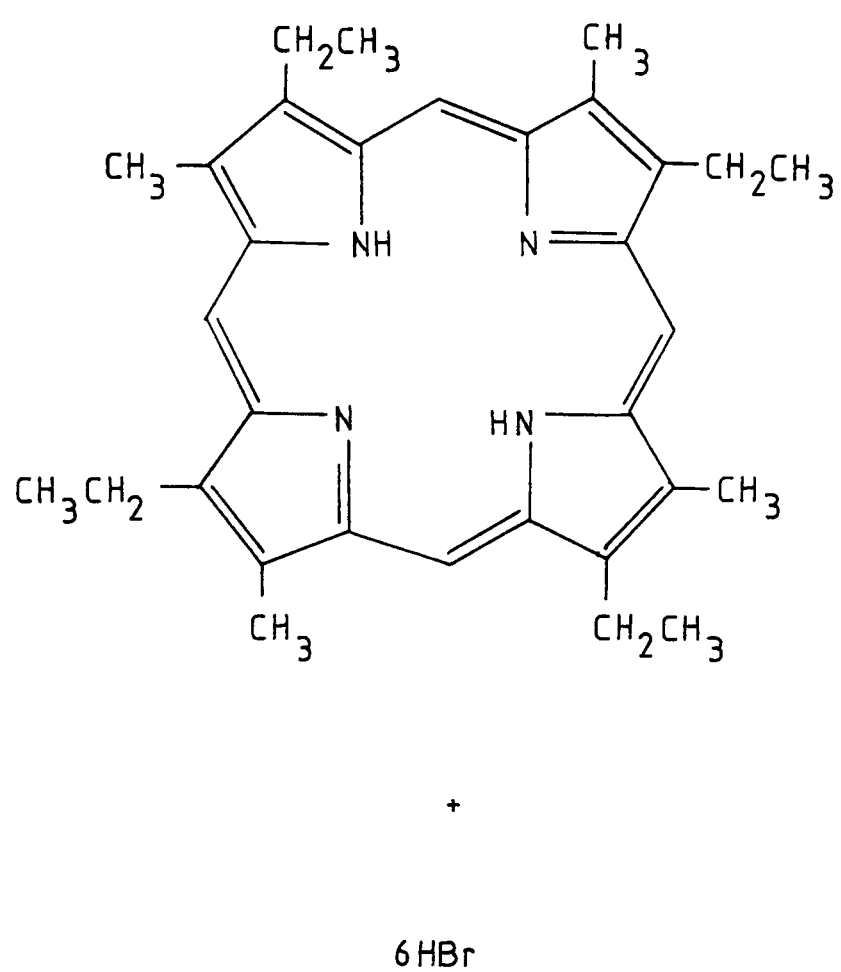
Fig.36.(cont.)   Reaction sequence for the preparation
of etioporphyrin I.
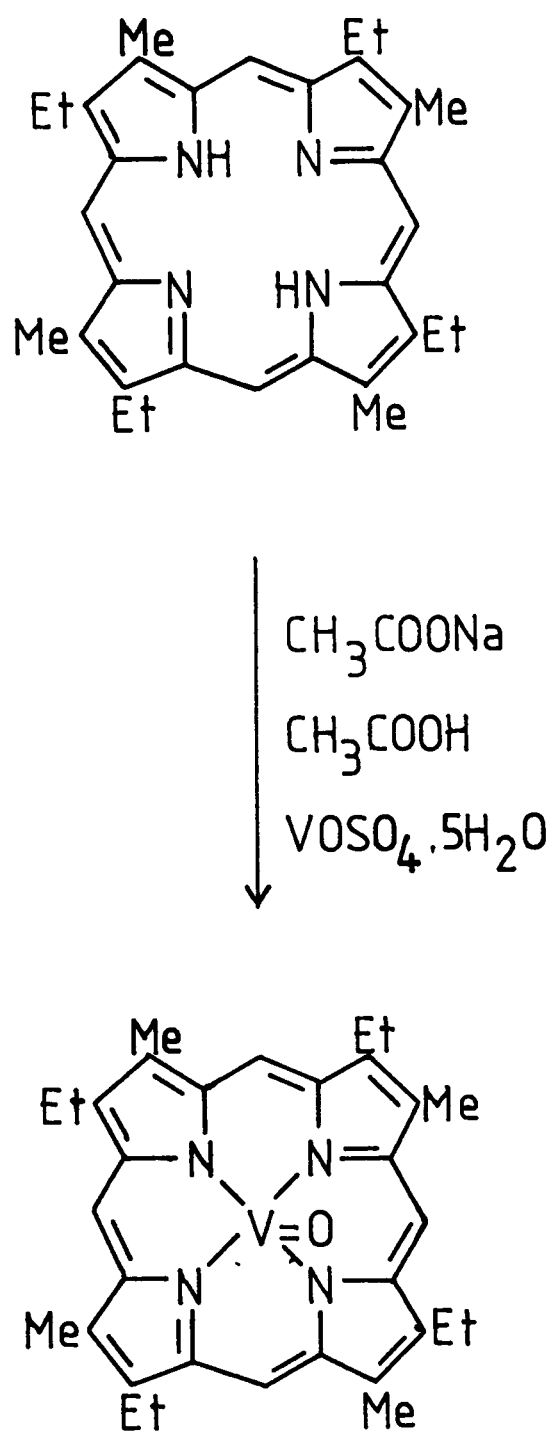
Me=methyl   Et=ethyl

Fig.37.   Vanadyl ion insertion into etioporphyrin.

$(CH_3COO)_2 Ni.4H_2O$

DMF
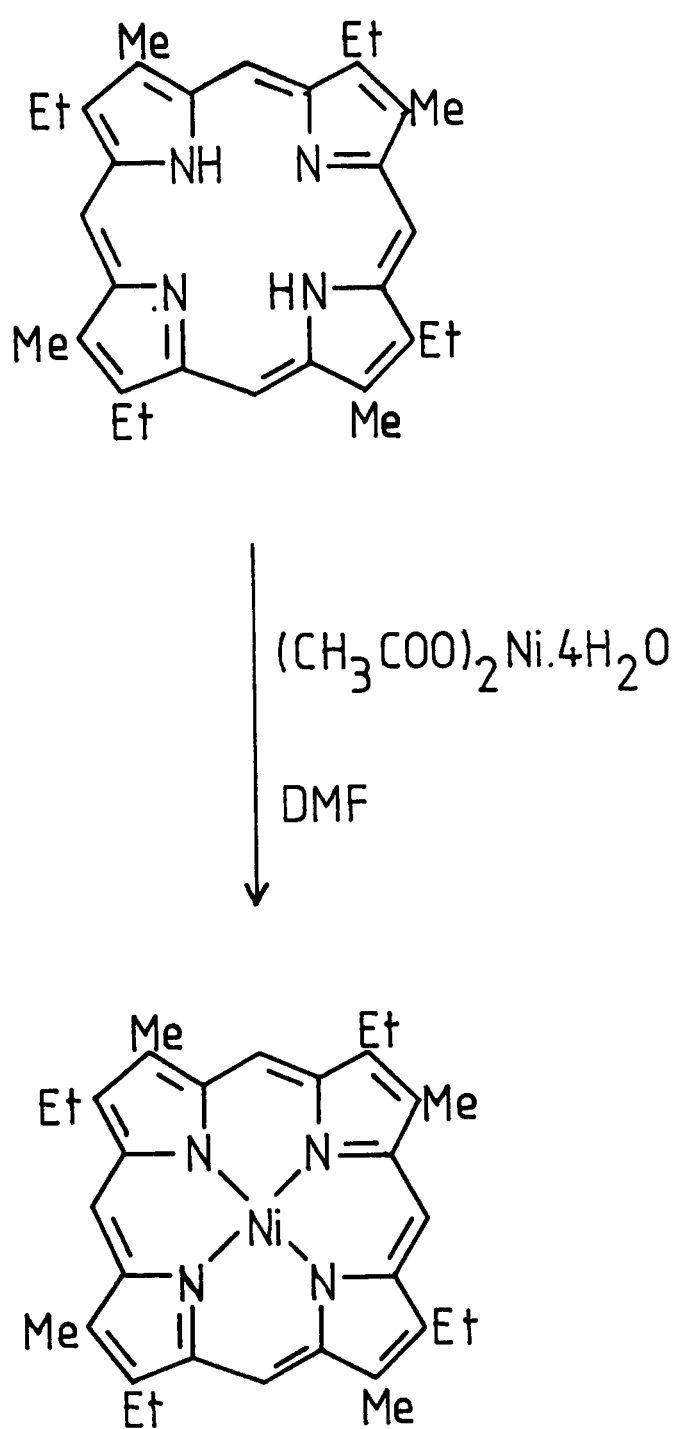
Me=methyl   Et=ethyl

Fig.38.   Nickel ion insertion into etioporphyrin.

70 cm

22 cm

5 cm

10 cm

47 cm

50mm dia
coarse glass
sinter

6cm I.D.
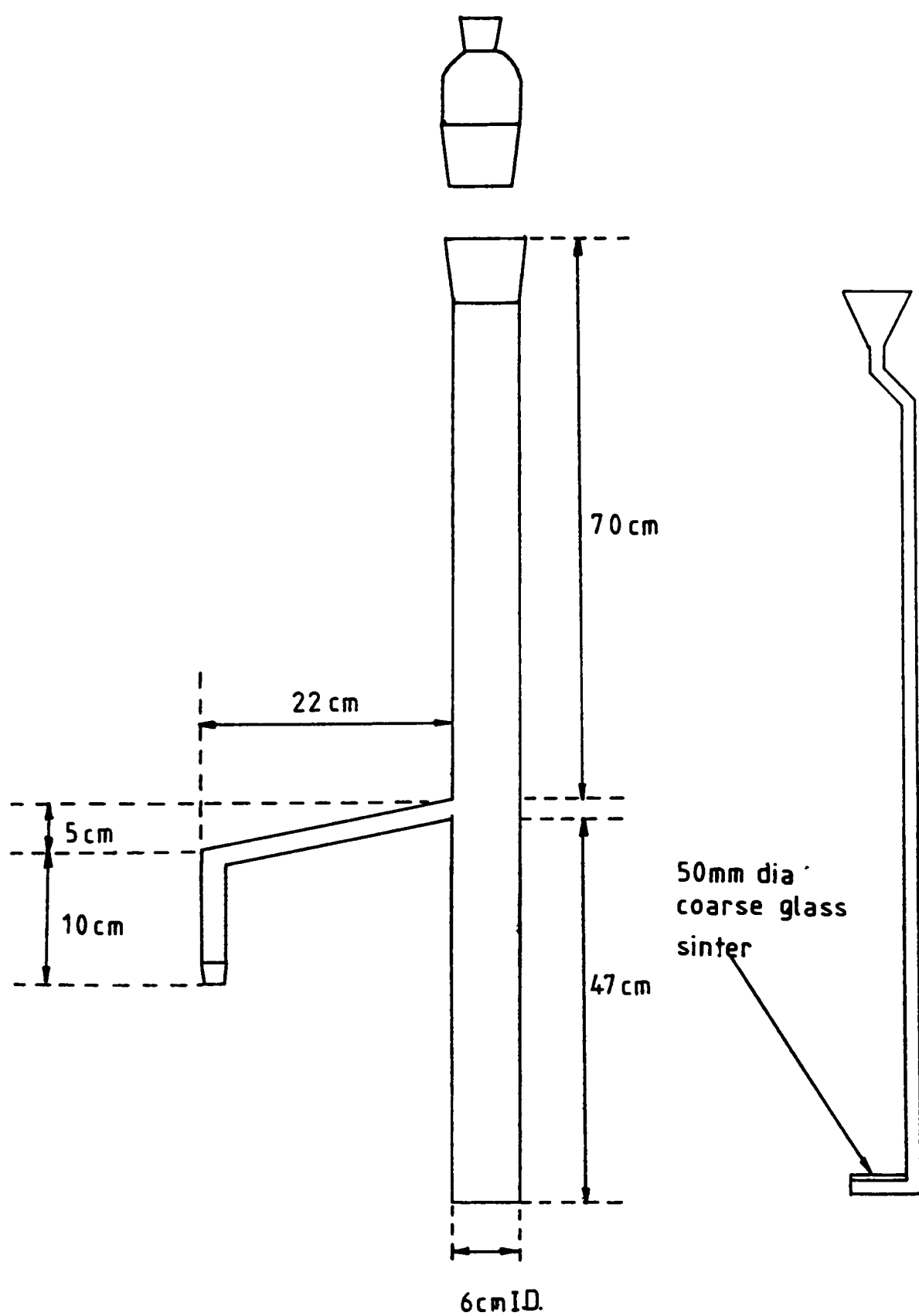
Fig.39.   Upward displacement extractor used in the preparation
of the petroporphyrin concentrate.

1. ON/OFF VALVE

2. PRESSURE REDUCTION VALVE

3. NEEDLE VALVE

4. ROTAMETER

5. MOLECULAR SIEVE (LINDE 5A)

6. KATHAROMETER BLOCK

7. AIR CIRCULATING OVEN

8. SAMPLE CELL
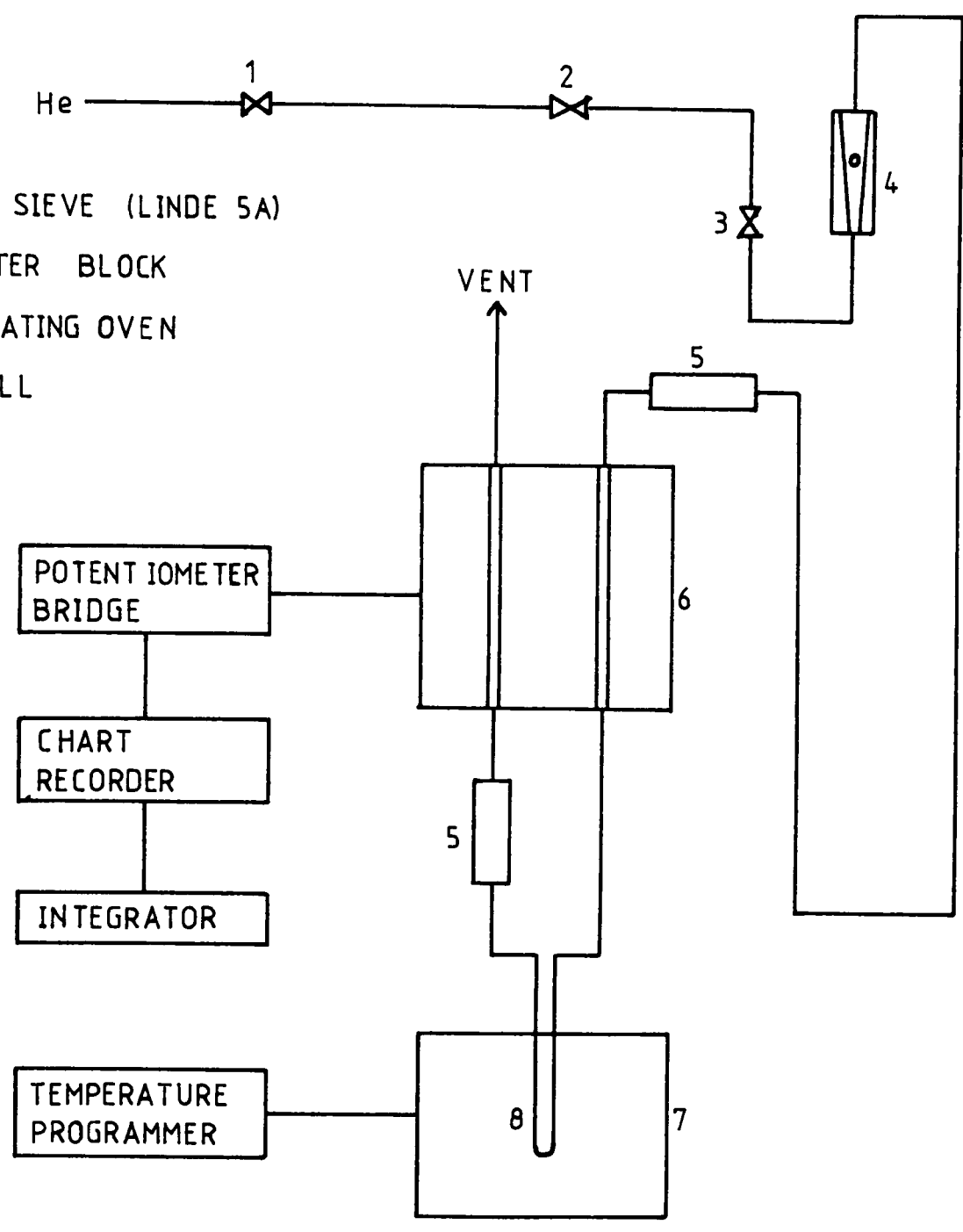
Fig.40. Schematic diagram of temperature programmed decomposition unit.
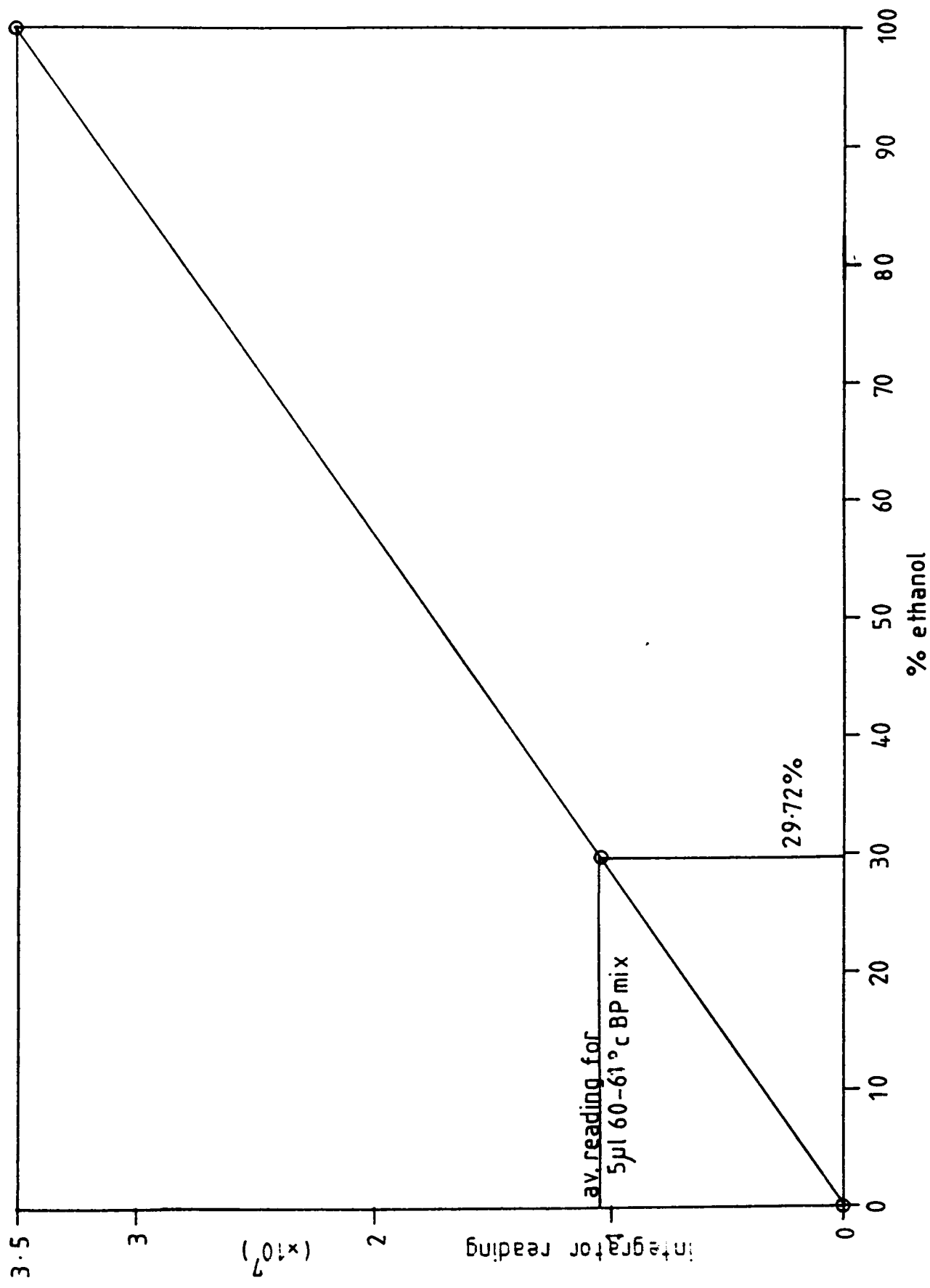
Fig. 41. Calibration graph for the chromatographic separation of ethyl iodide and ethanol.
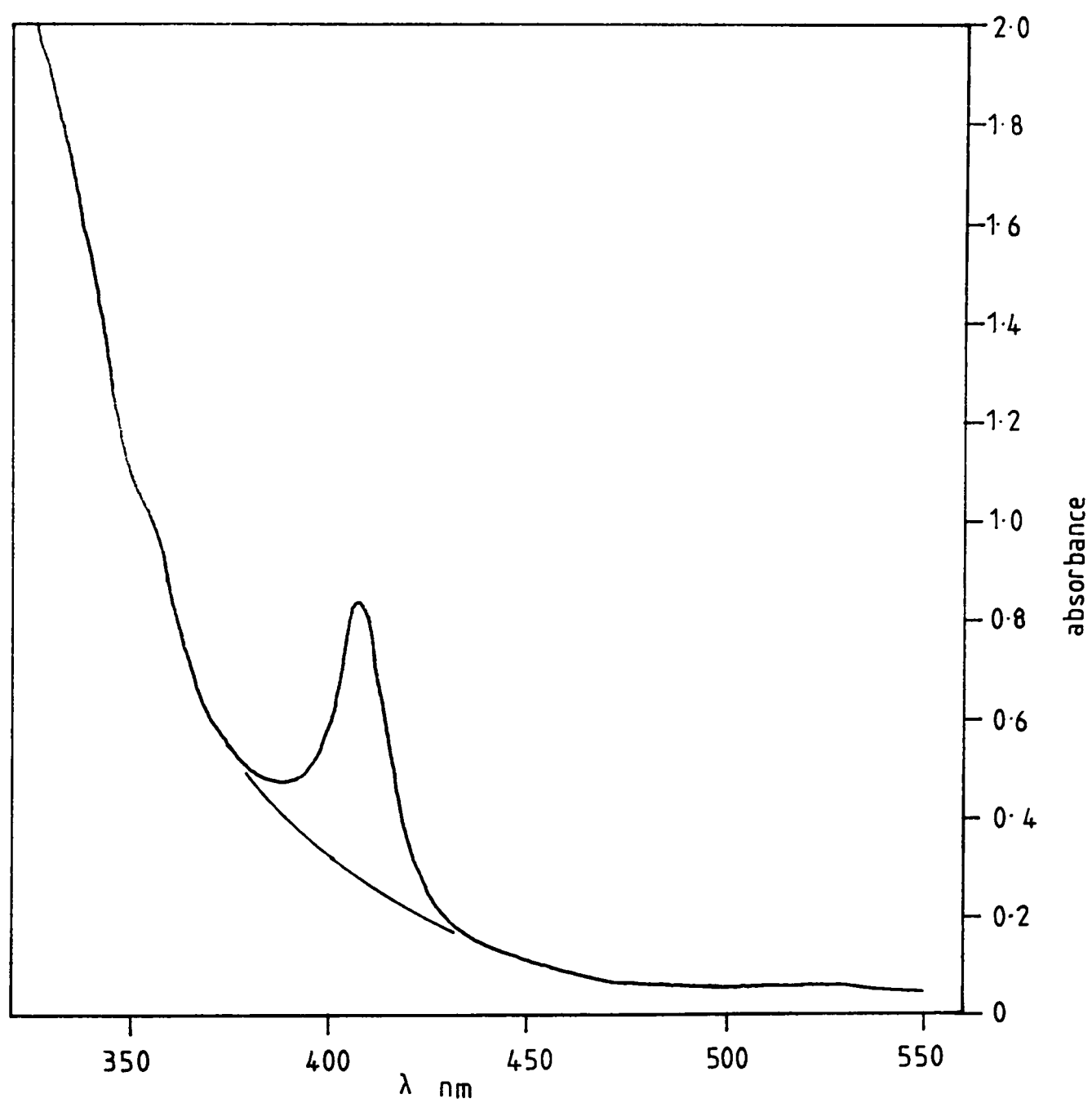
Fig.42.   UV spectrum of petroporphyrin concentrate.
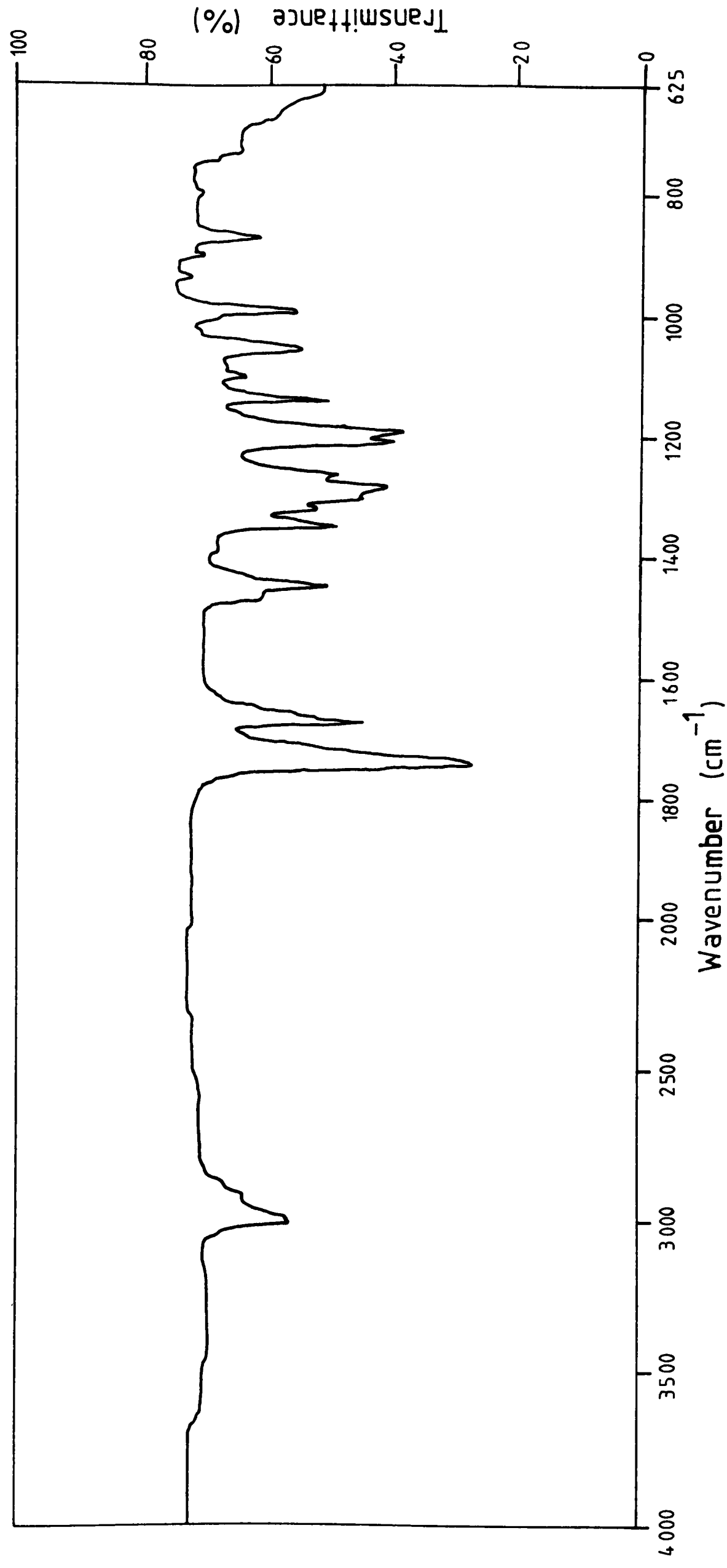
Fig. 43. Infrared spectrum of methyl trans-2-pentenoate.
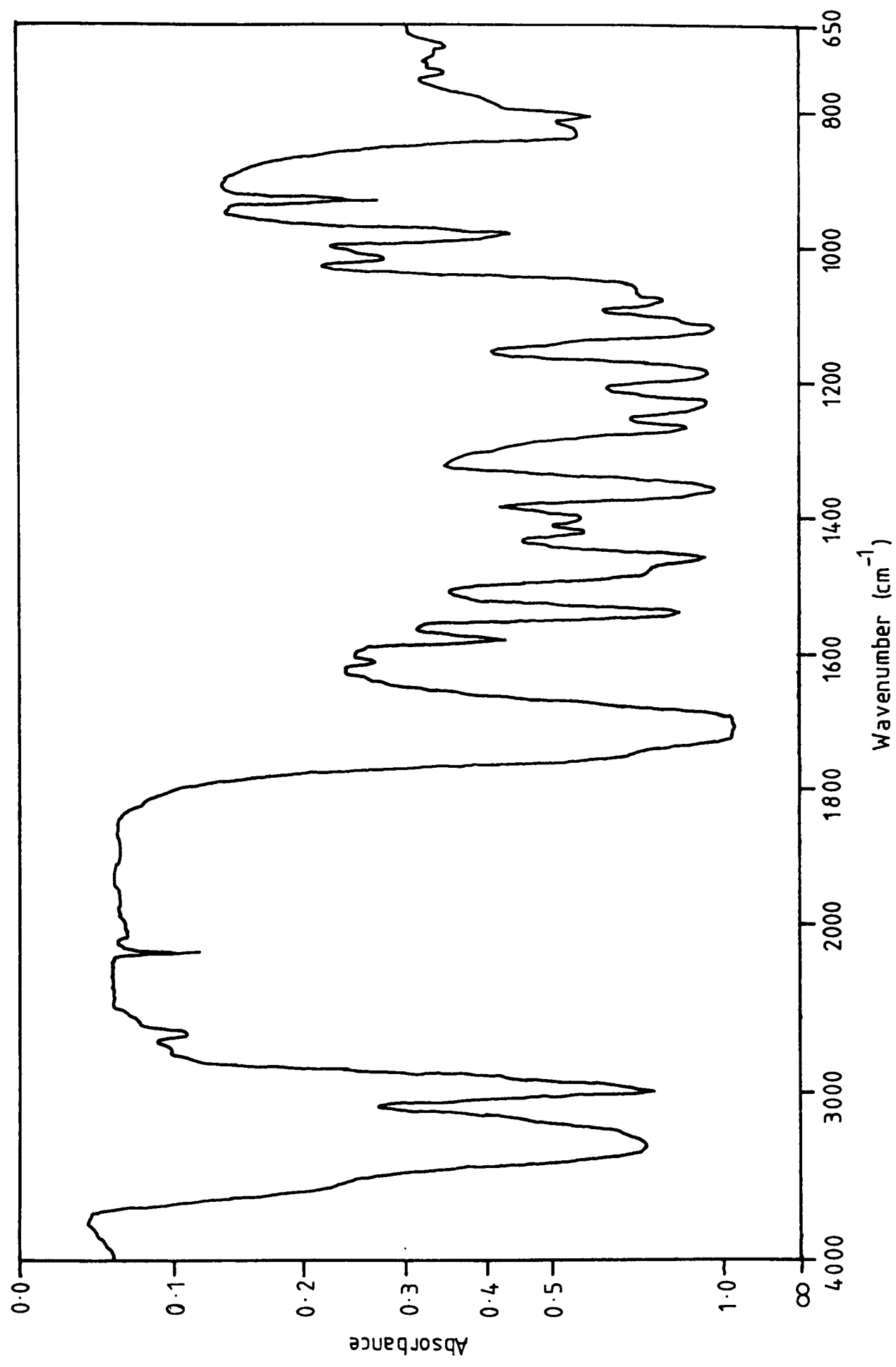
Fig. 44. Infrared spectrum of methyl 4-ethylpyrrole-3-carboxylate.
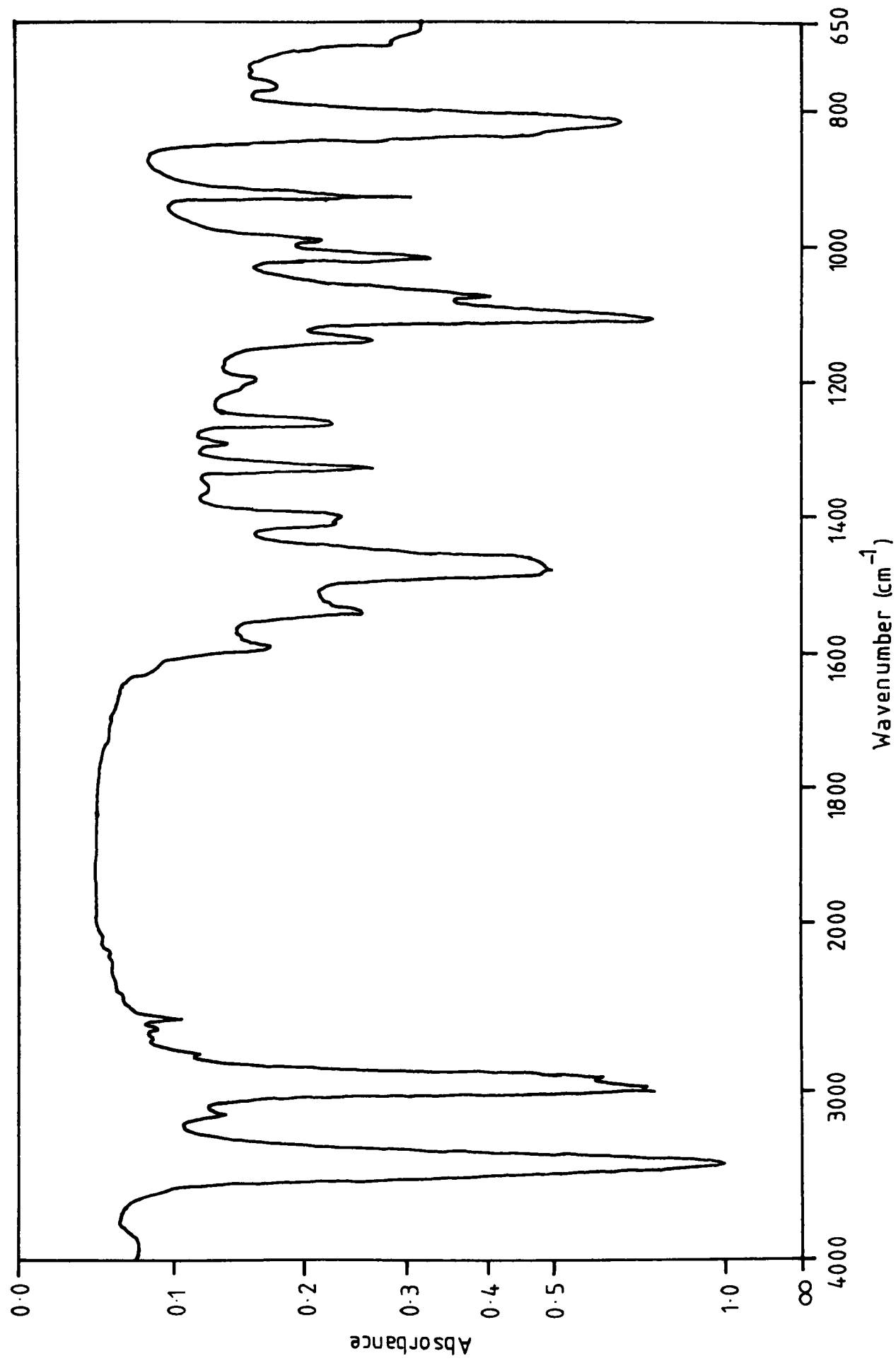
Fig. 145. Infrared spectrum of 3-ethyl-4-methylpyrrole.
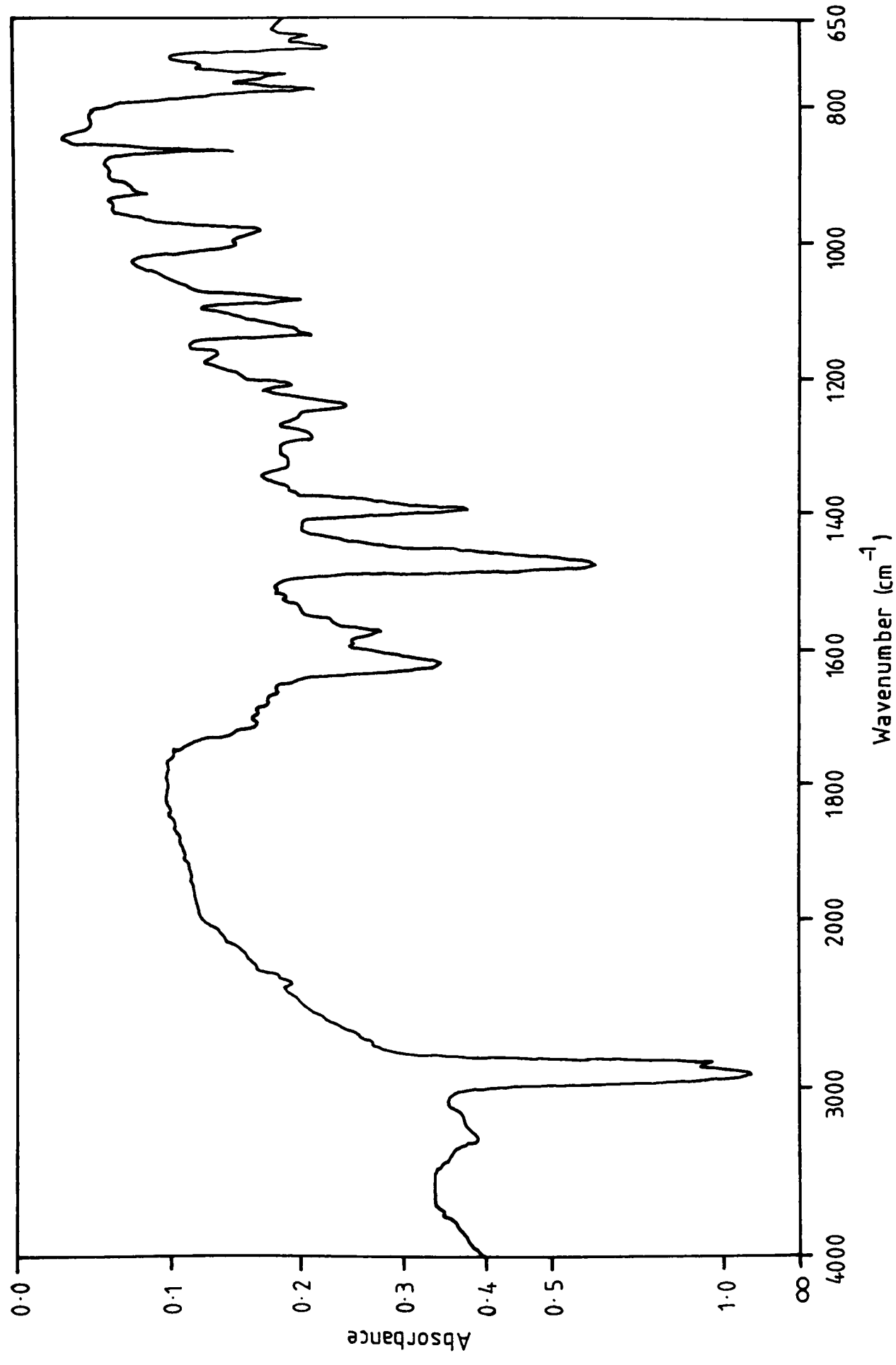
Fig. 146. Infrared spectrum of etioporphyrin.
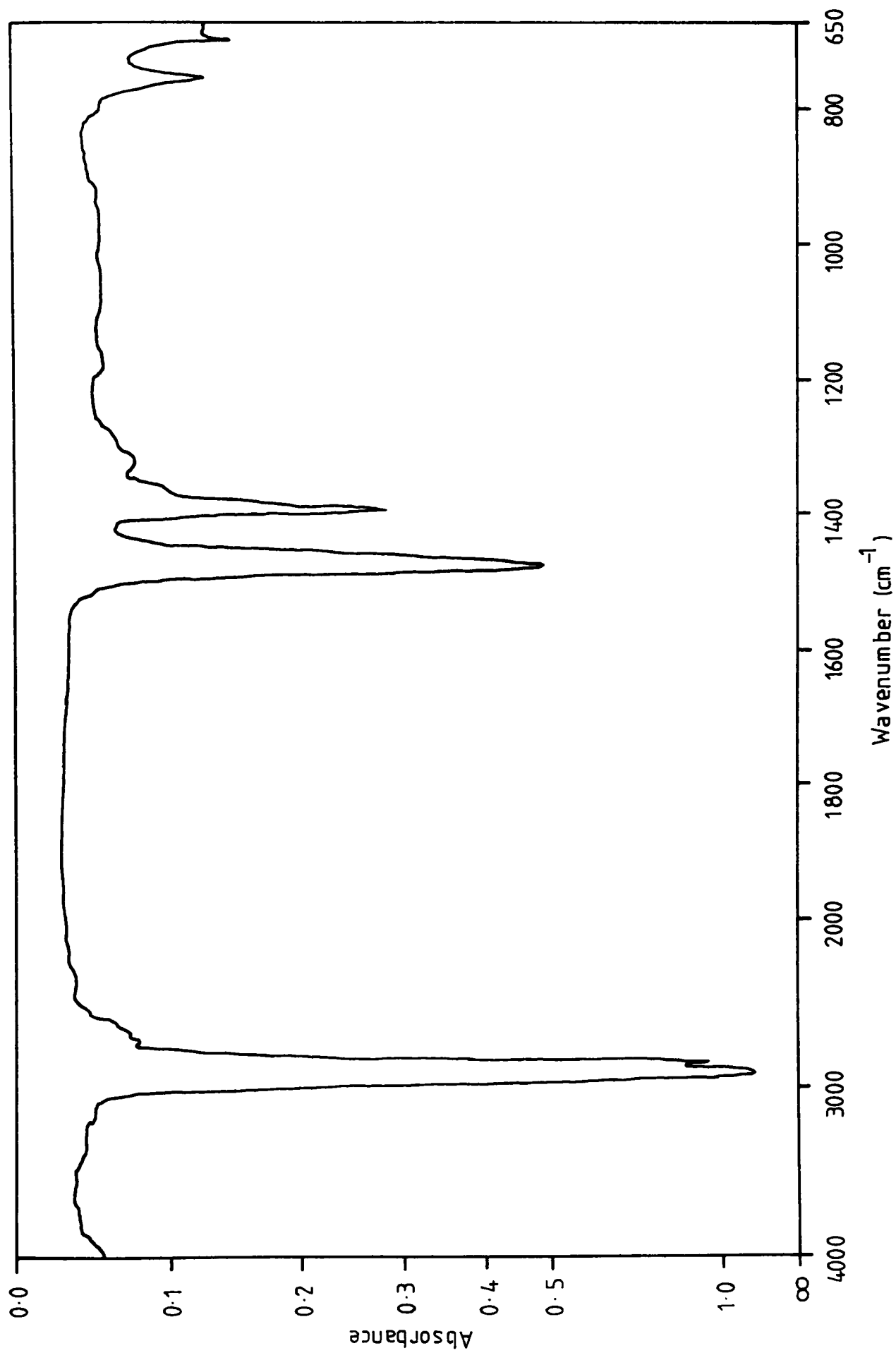
Fig. 147. Infrared spectrum of nujol.
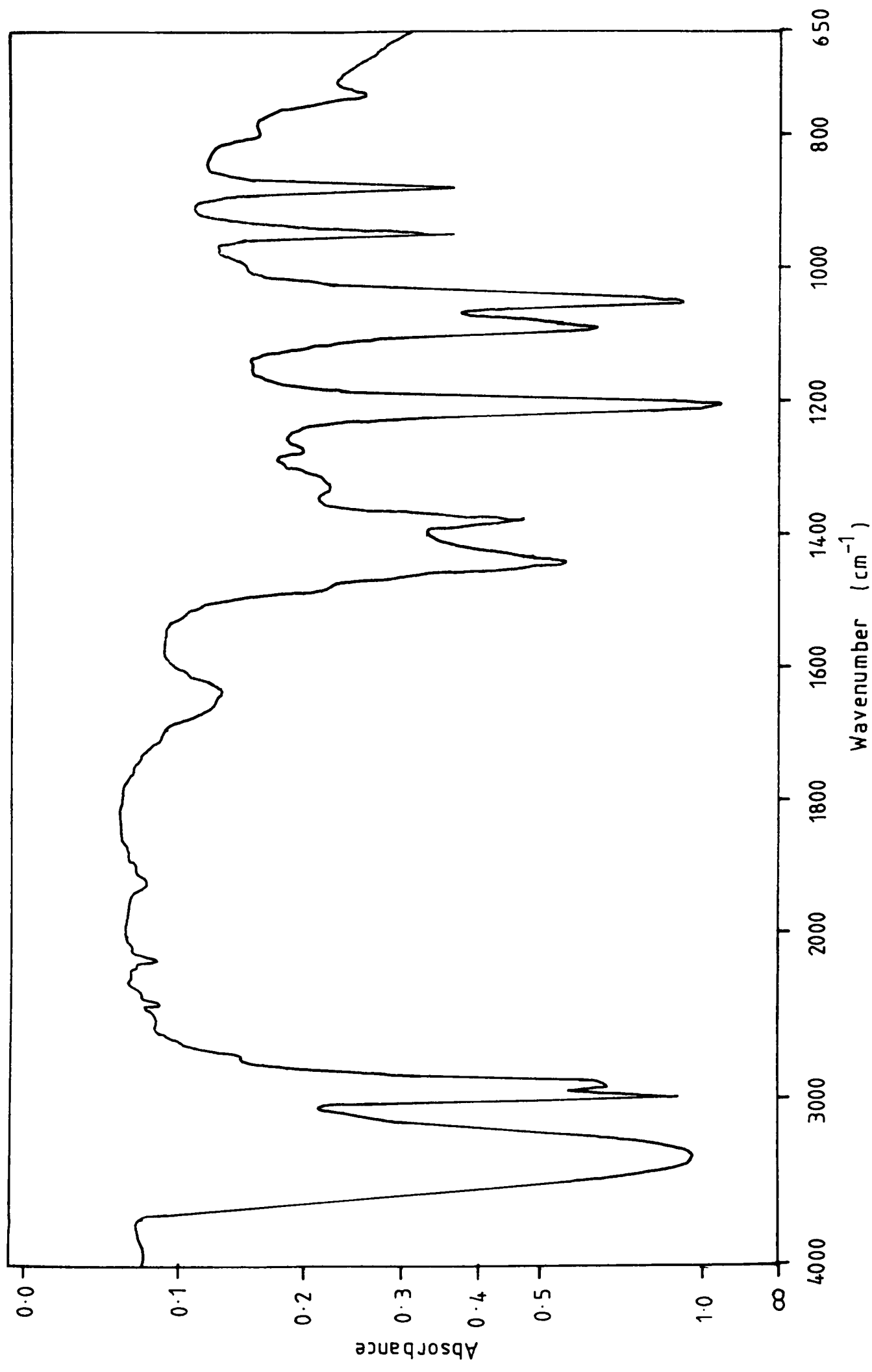
Fig. 48. Infrared spectrum of ethyl iodide/ethanol mixture (60-61°C boiling fraction).
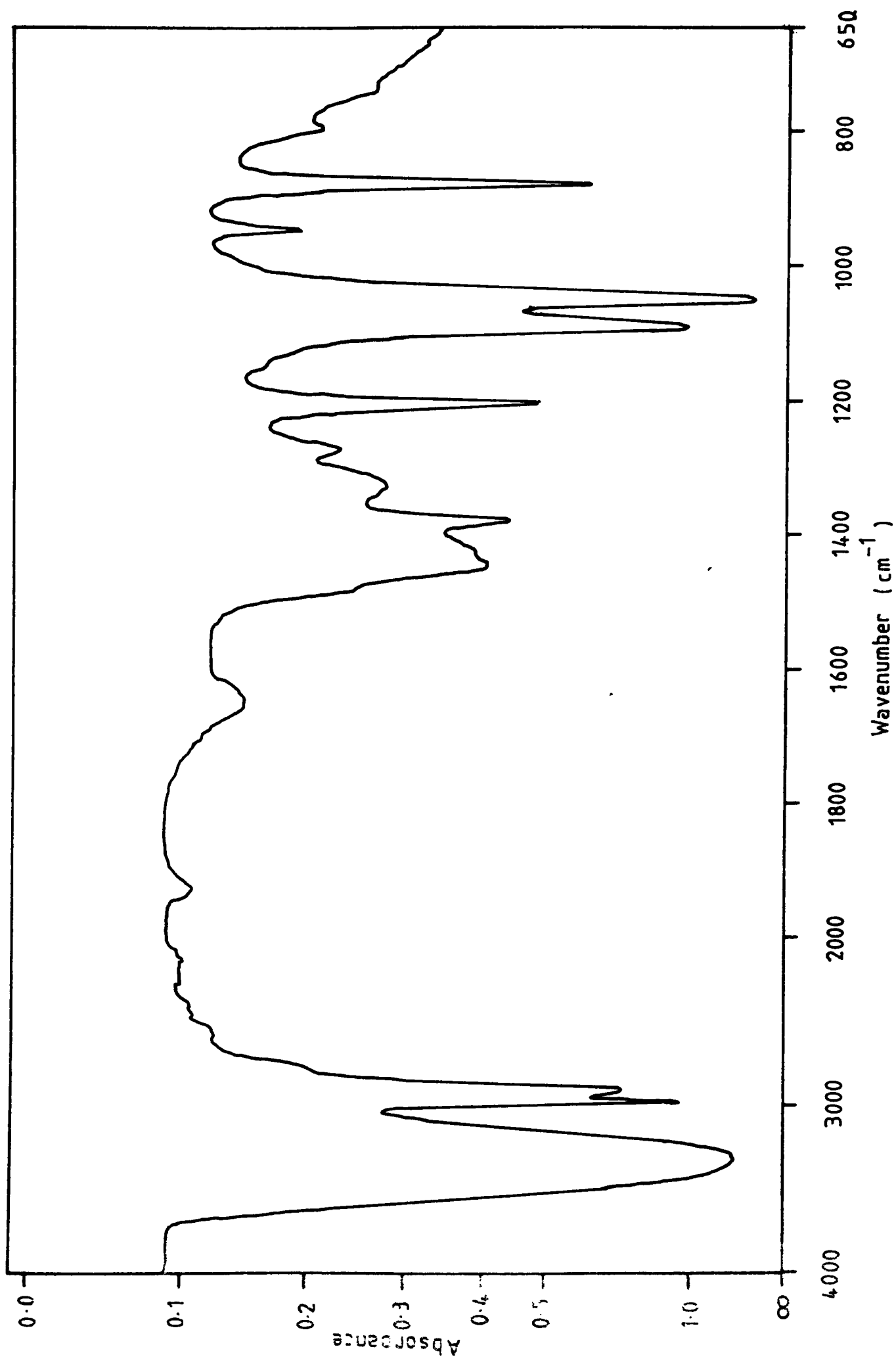
Fig. 49.   Infrared spectrum of ethyl iodide/ethanol mixture (61-67°C boiling fraction).
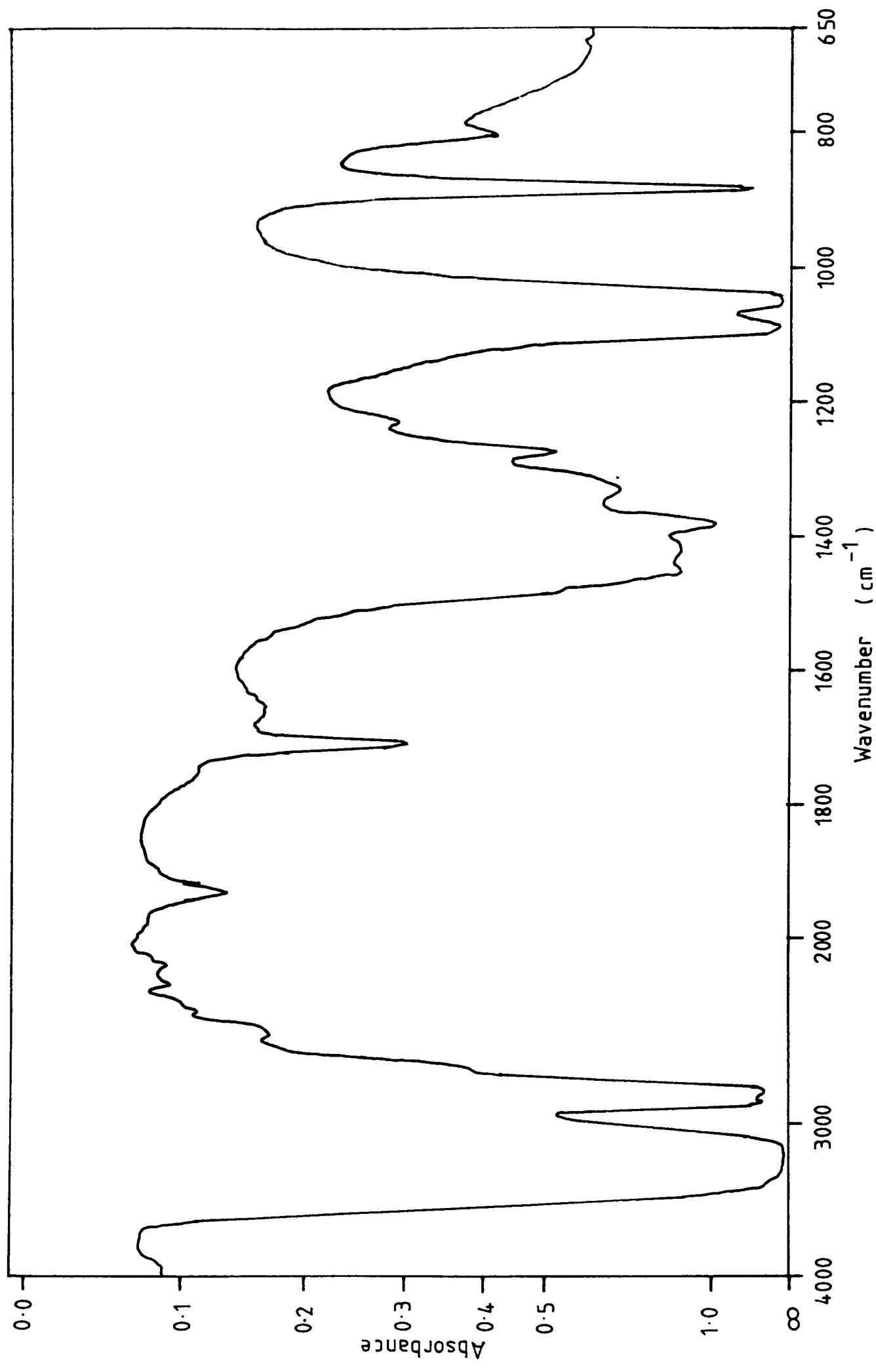
Fig. 50.   Infrared spectrum of ethanol.
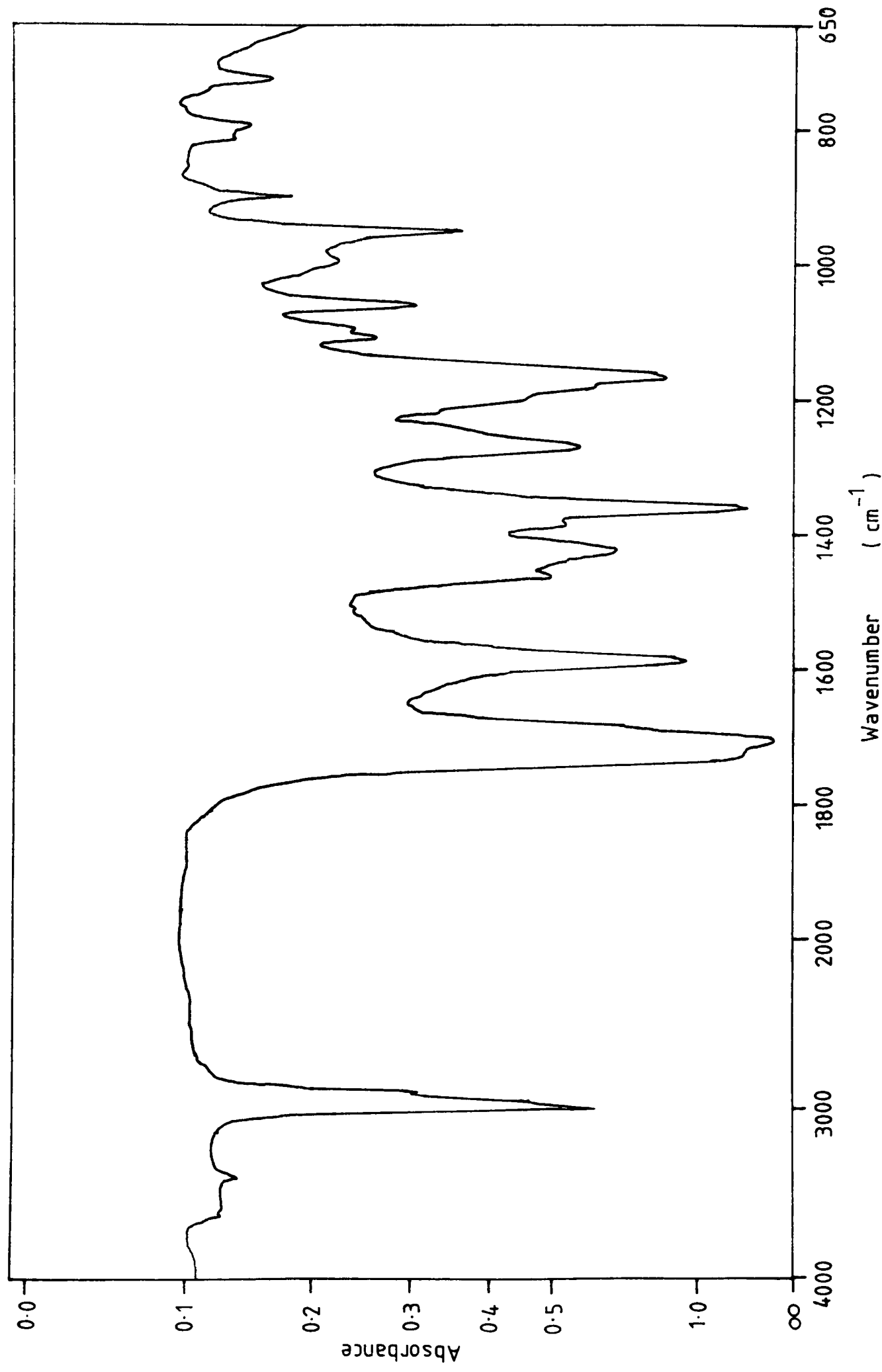
Fig. 51. Infrared spectrum of 3-ethyl-2,4-pentandione.
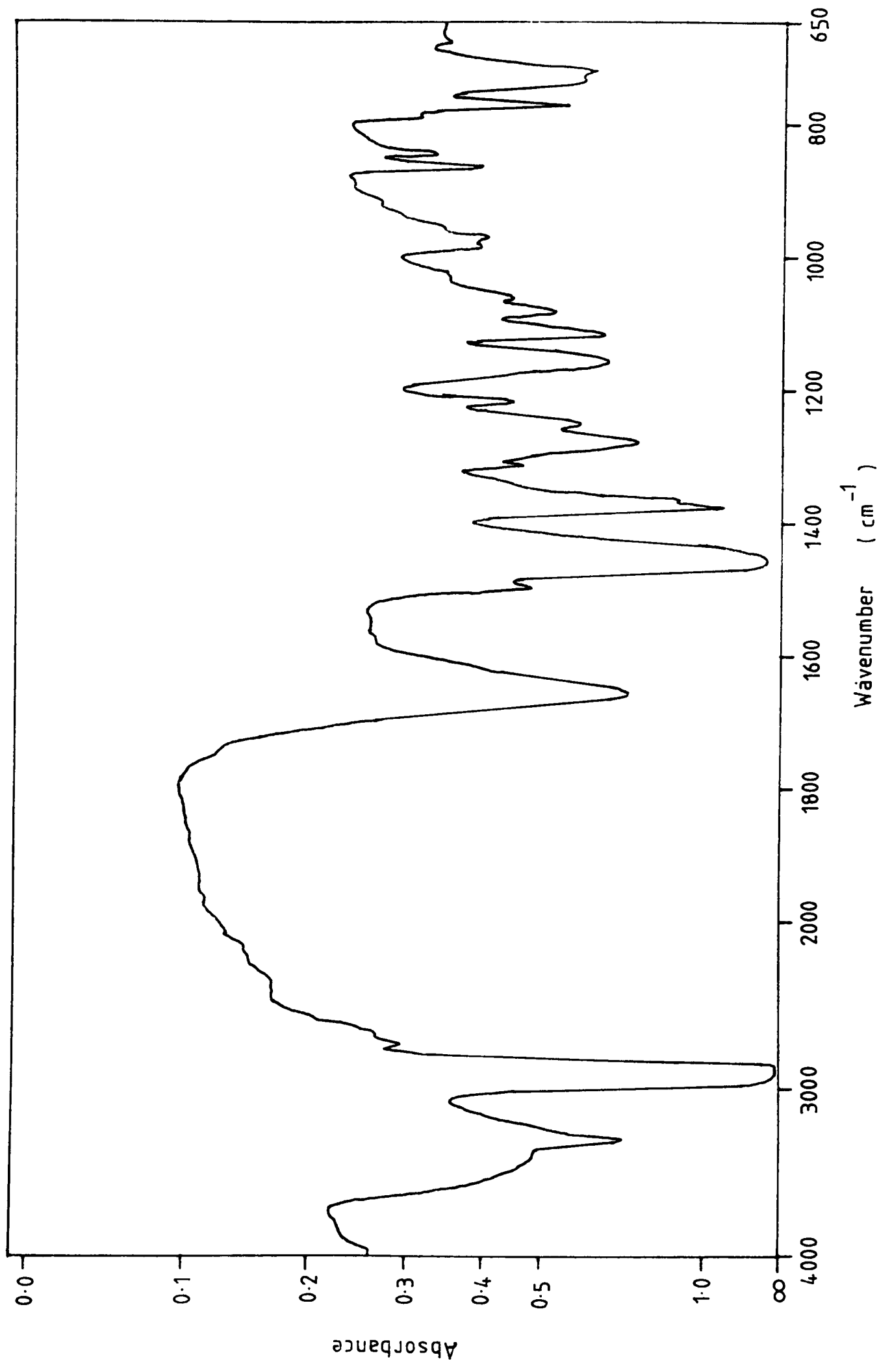
Fig. 52.   Infrared spectrum of t-butyl 4-ethyl-3,5-dimethylpyrrole carboxylate.
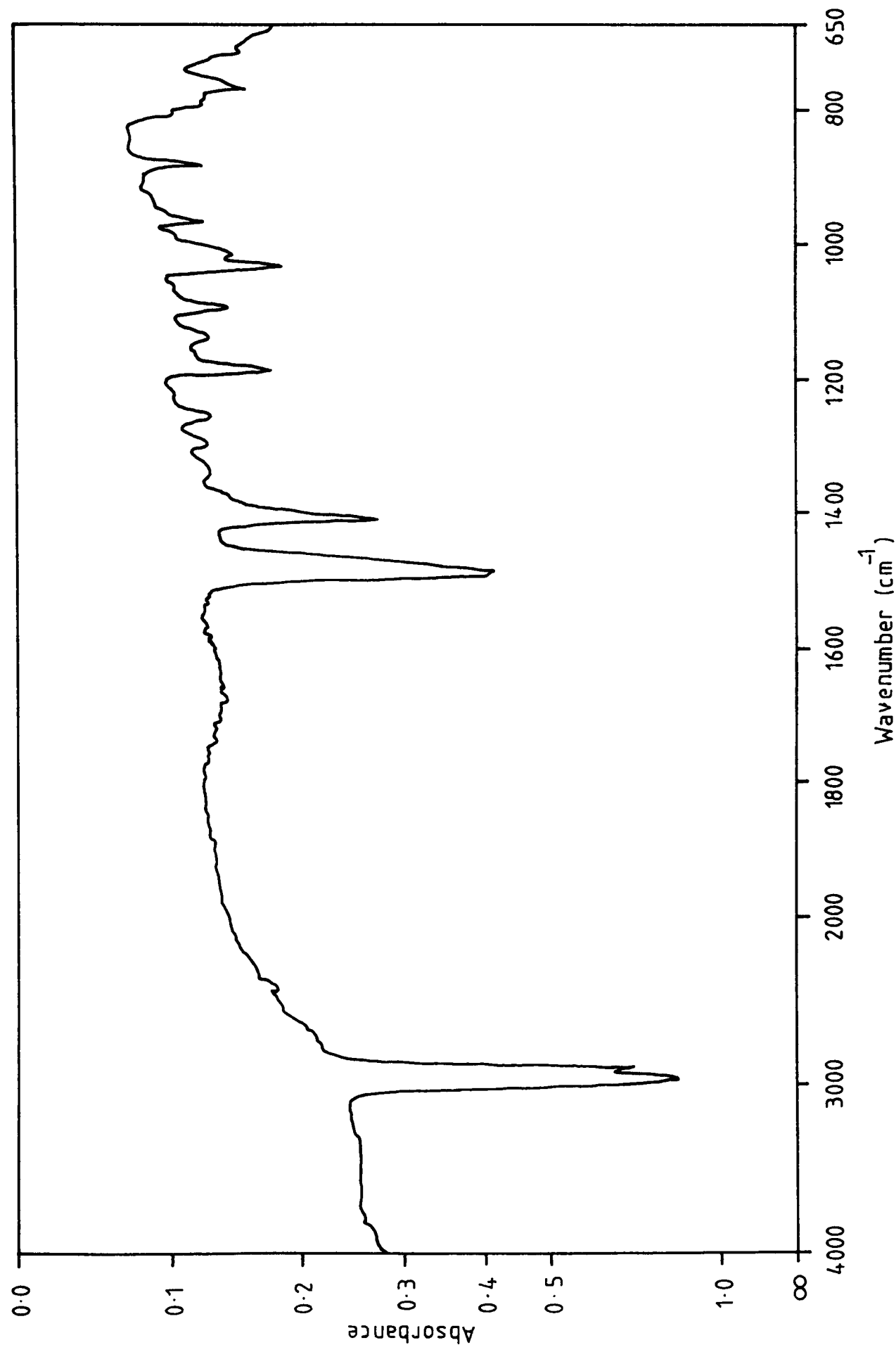
Fig.55. Infrared spectrum of vanadyl etioporphyrin.
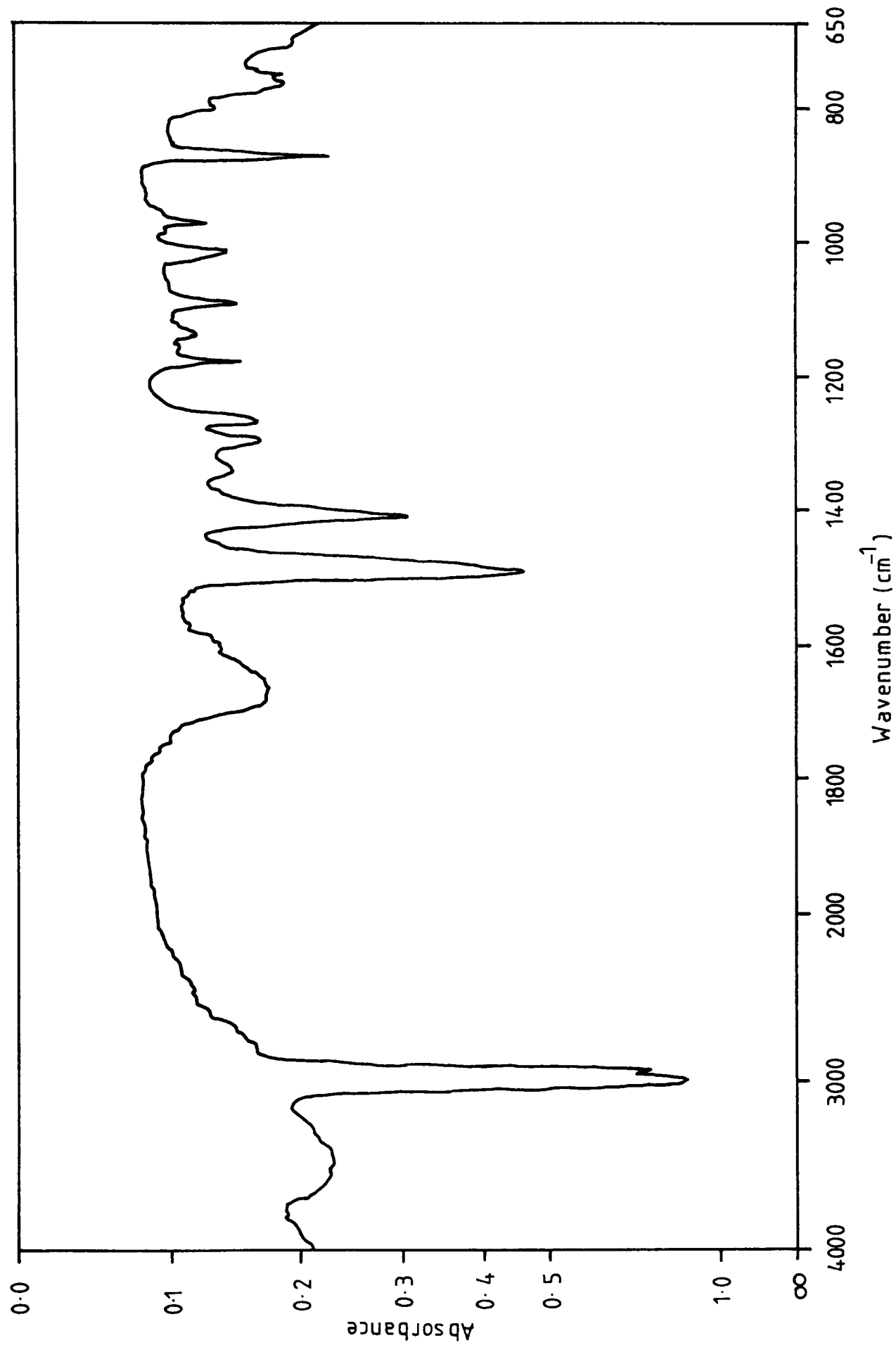
Fig. 54.   Infrared spectrum of nickel etioporphyrin.
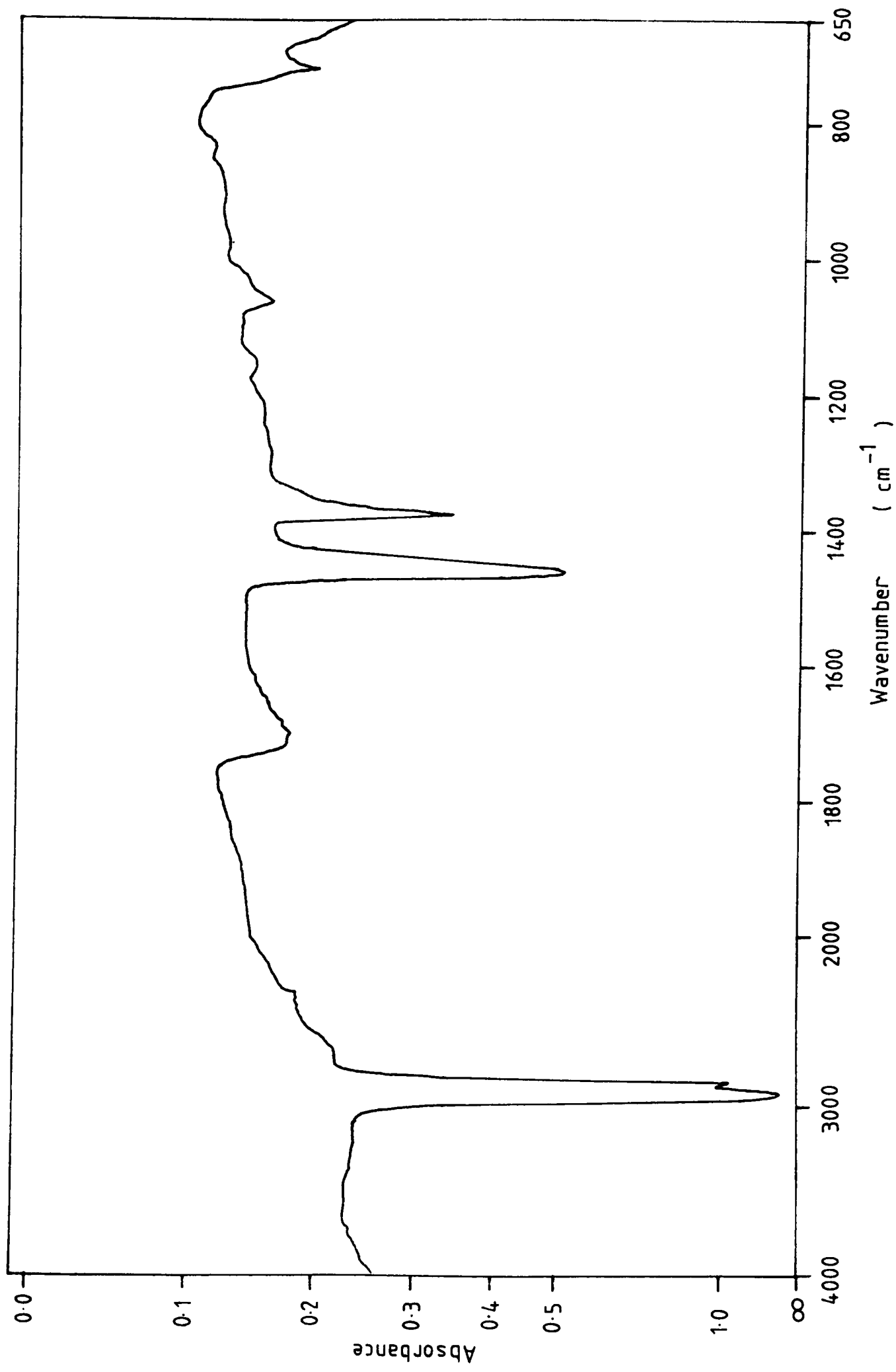
Fig. 55.   Infrared spectrum of base hematoporphyrin IX.
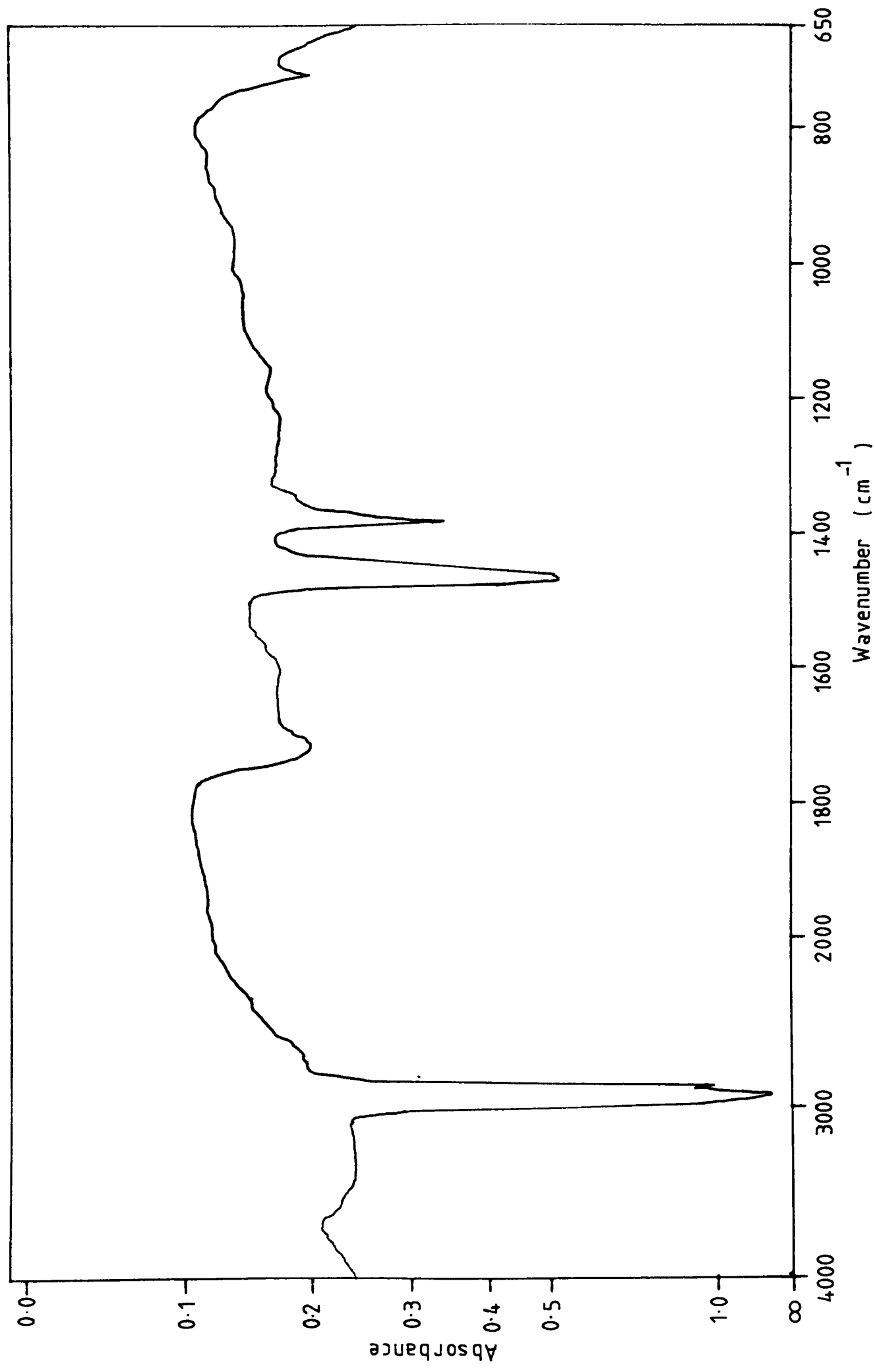
Fig. 56. Infrared spectrum of vanadyl hematoporphyrin IX.

Fig. 7/. Infrared spectrum of nickel hematoporphyrin IX.

PPM
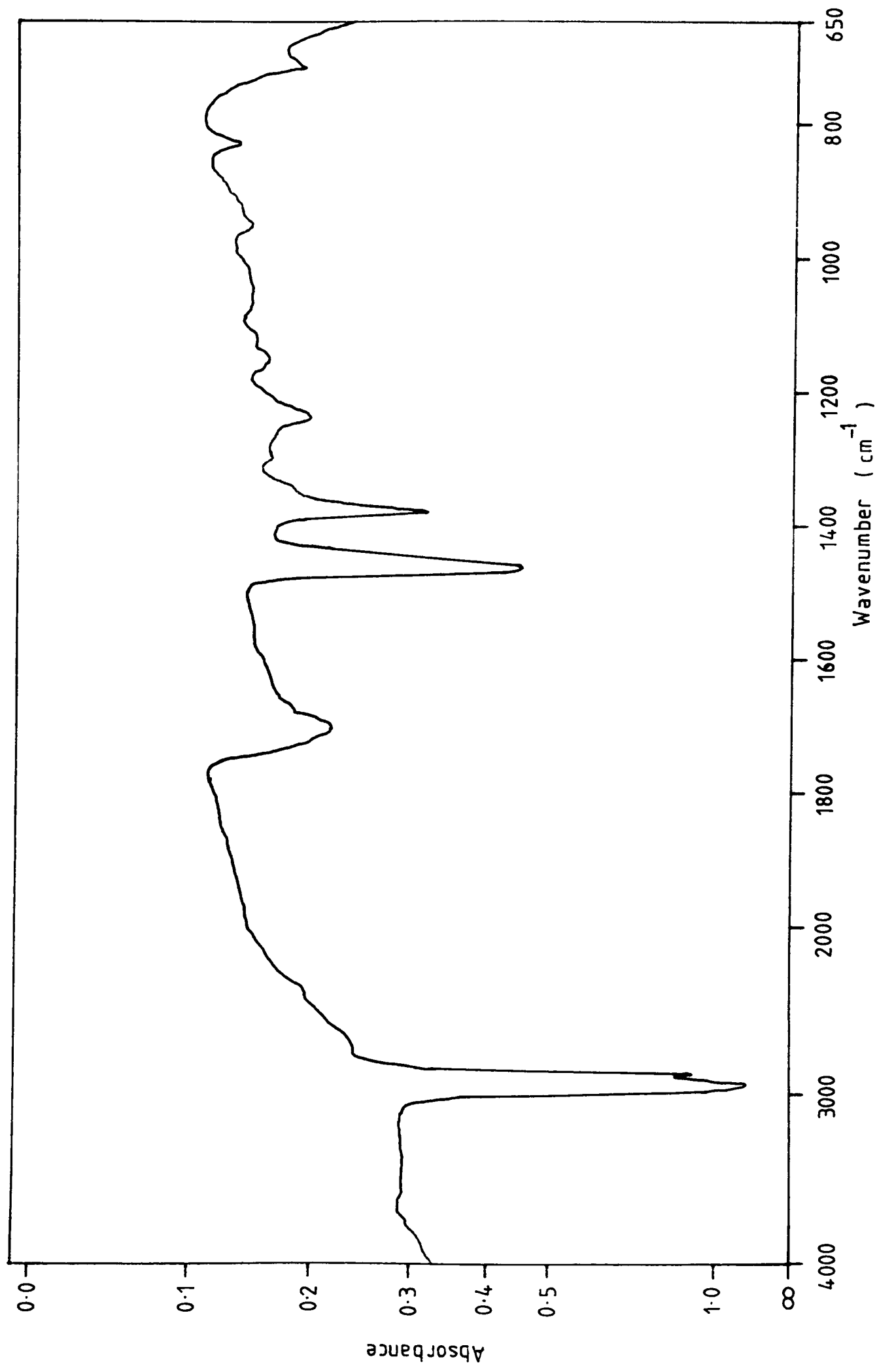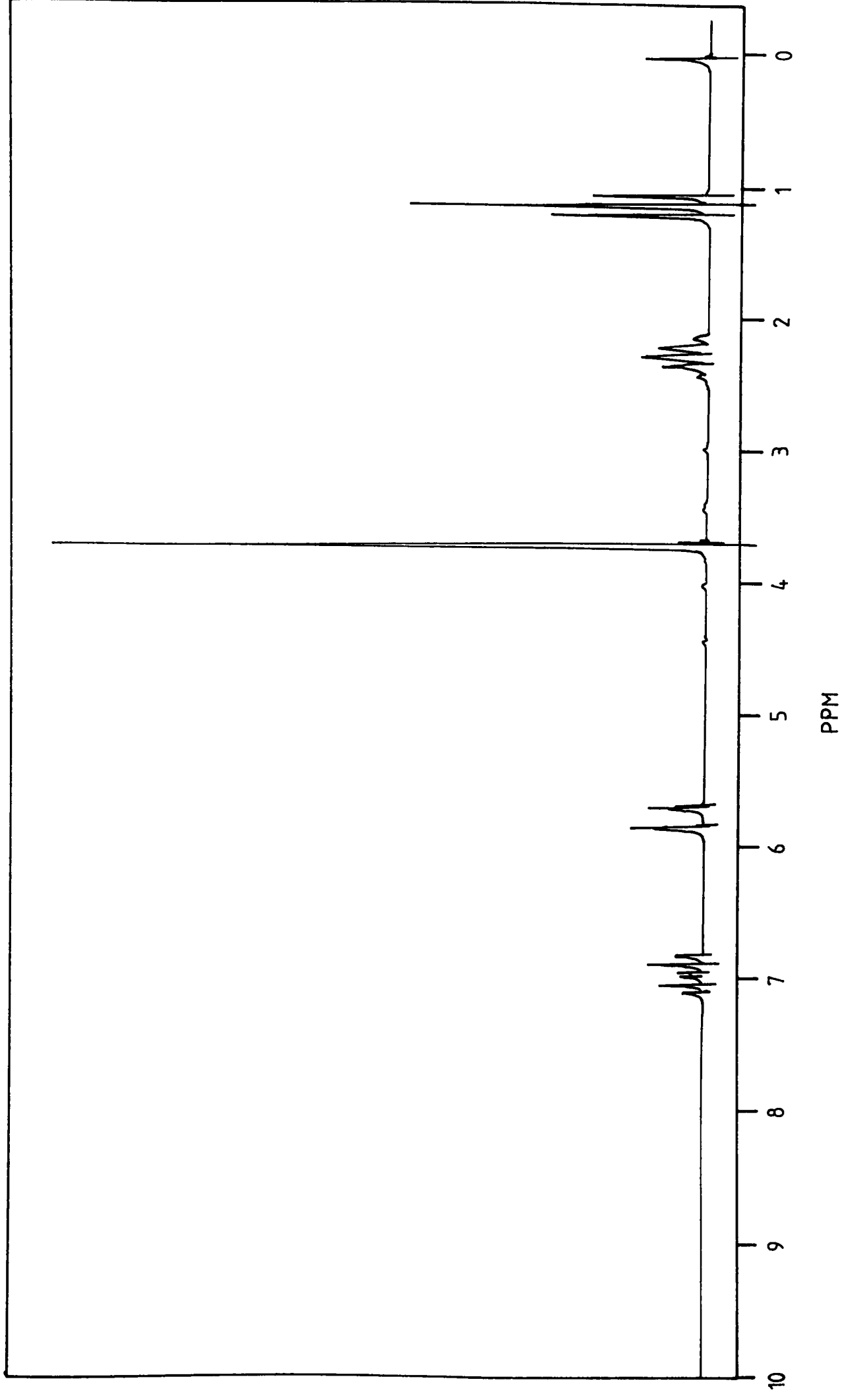
Fig. 58. ^{1}H nmr spectrum of methyl trans-2-pentenoate.
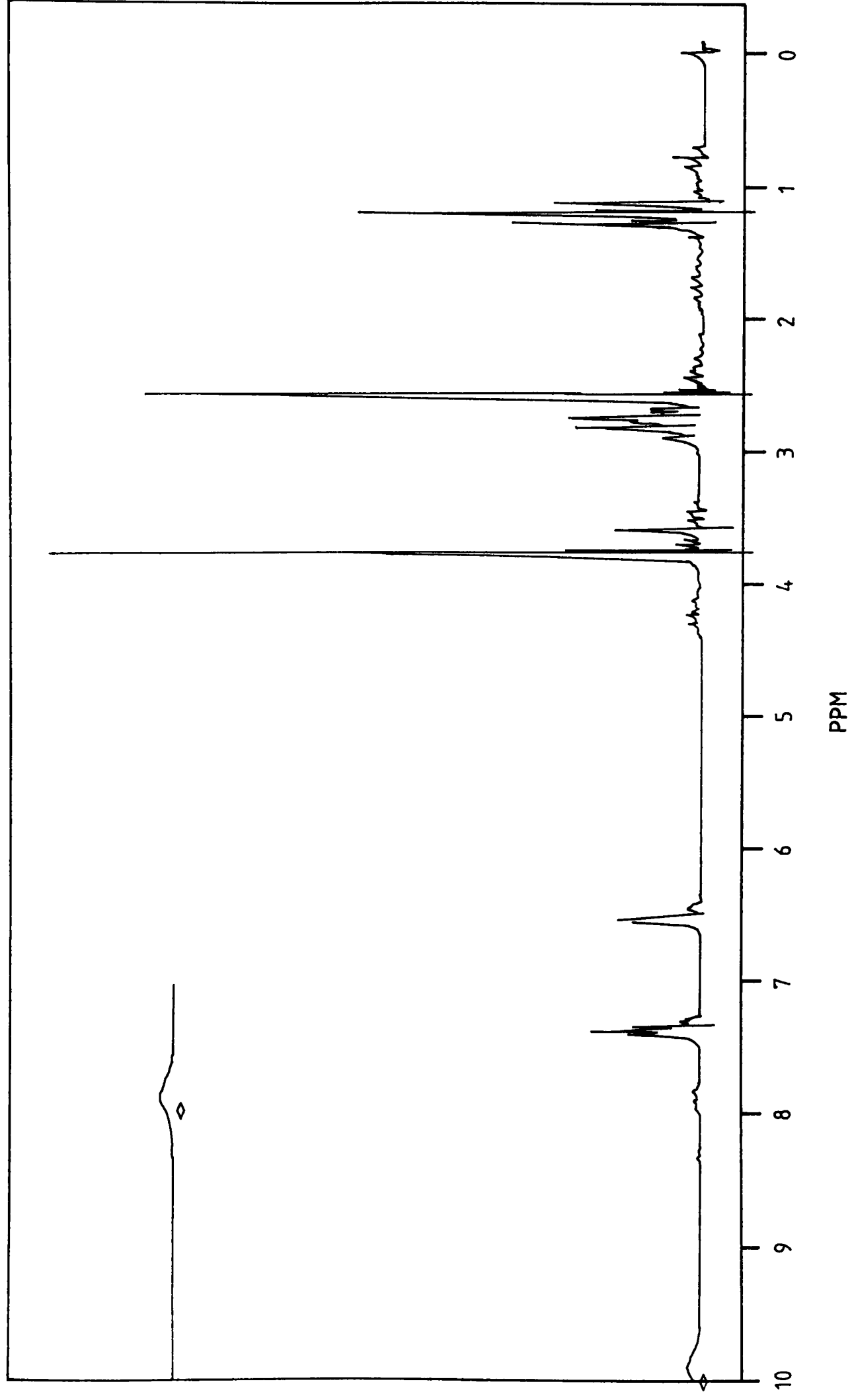
Fig.59. ^{1}H nmr spectrum of methyl 4-ethylpyrrole-3-carboxylate.

PPM
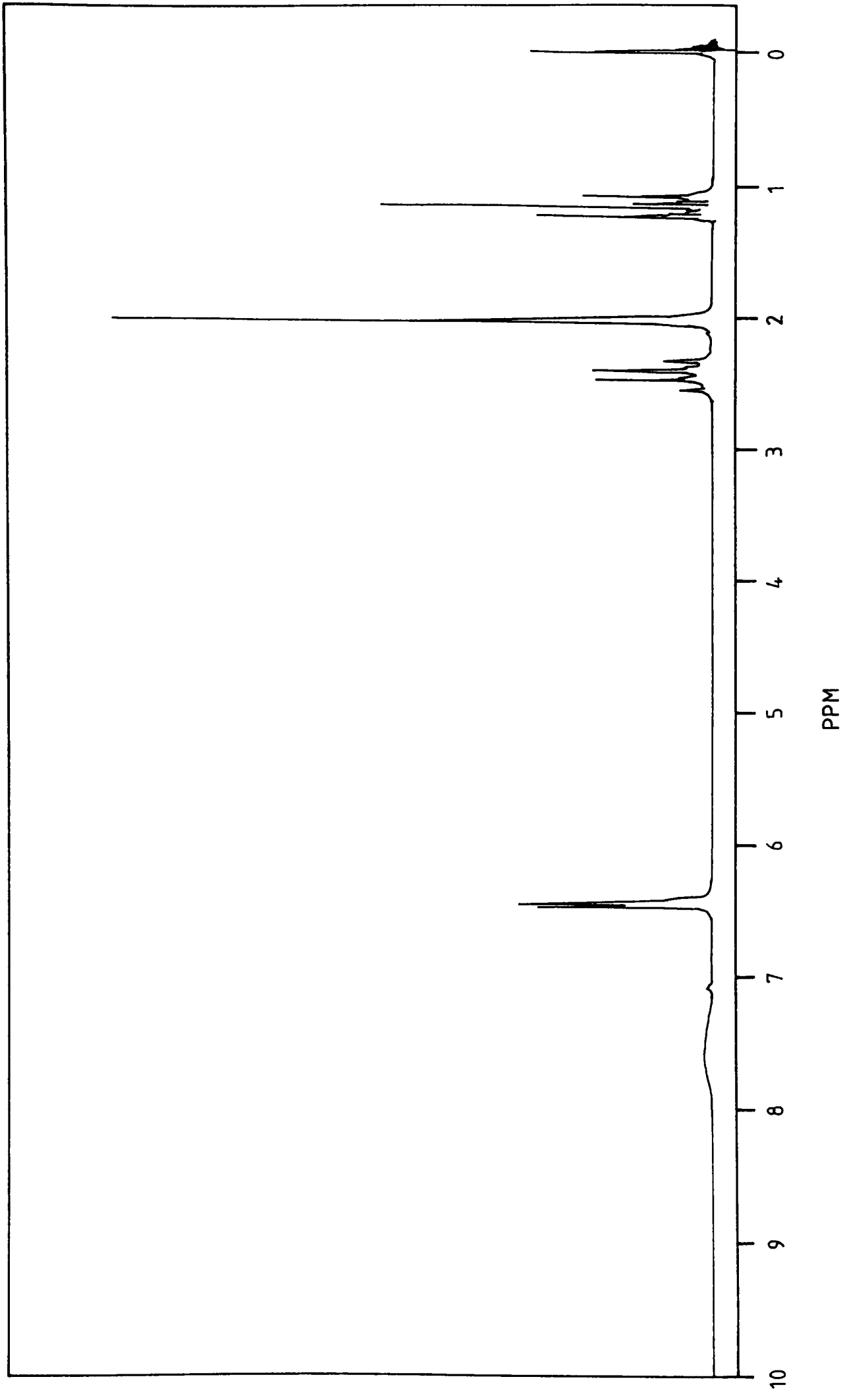
Fig. 60. ^{1}H nmr spectrum of 3-ethyl-4-methylpyrrole.
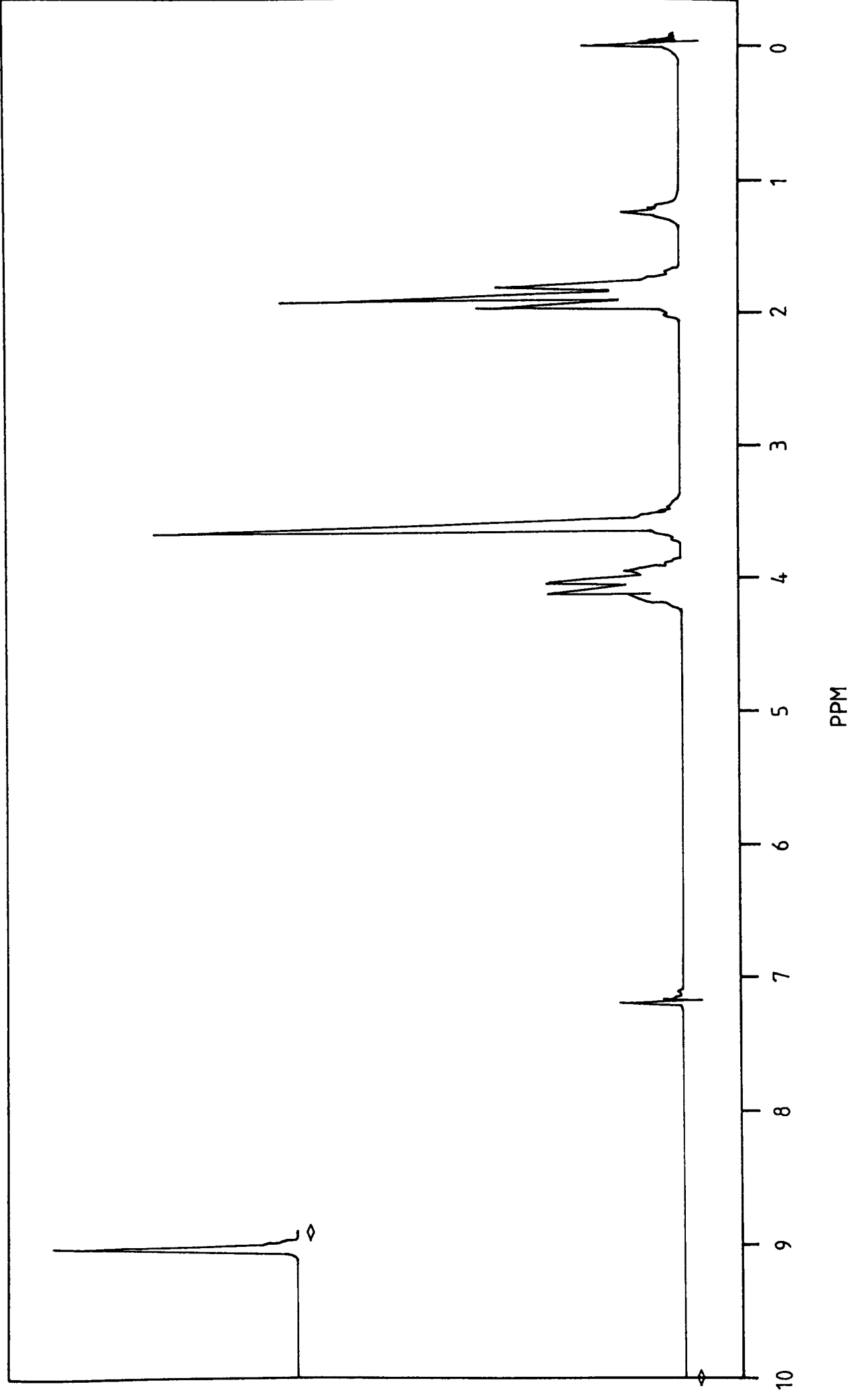
Fig.61. ^{1}H nmr spectrum of etioporphyrin.
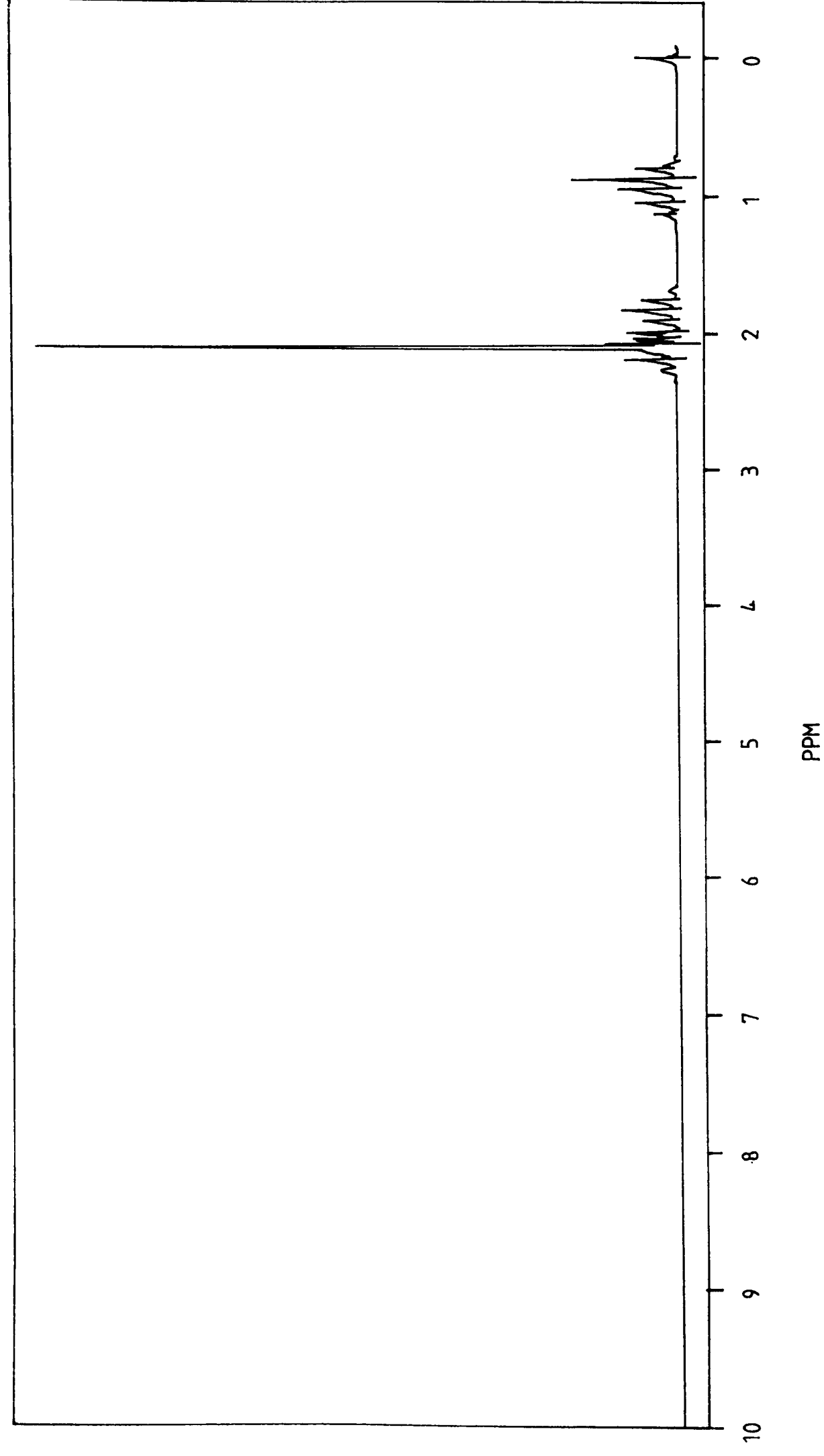
Fig. 62. ^{1}H nmr spectrum of 3-ethyl-2,4-pentandione.
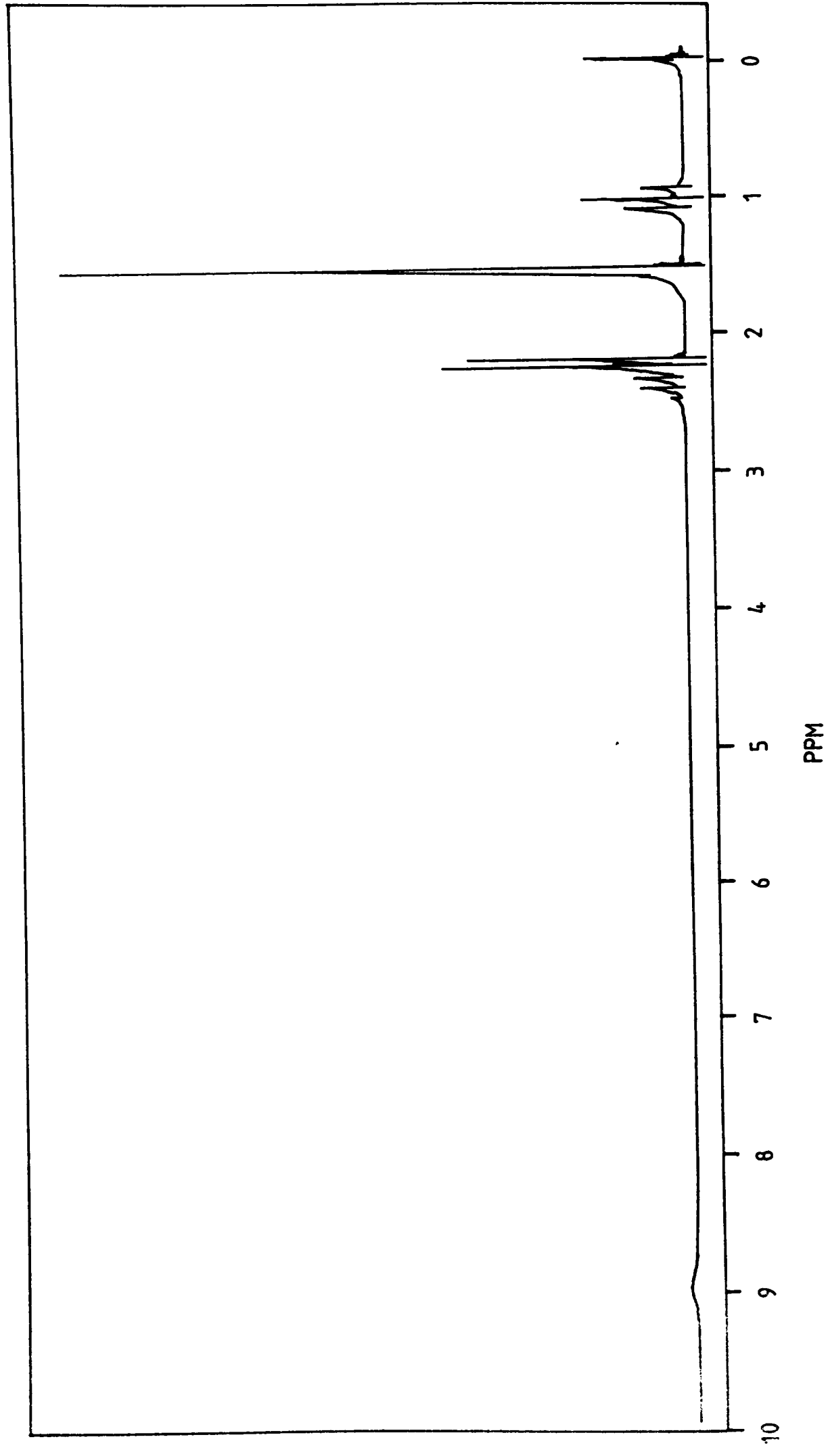
Fig. 63. ^{1}H nmr spectrum of t-butyl 4-ethyl-3,5-dimethylpyrrole carboxylate.
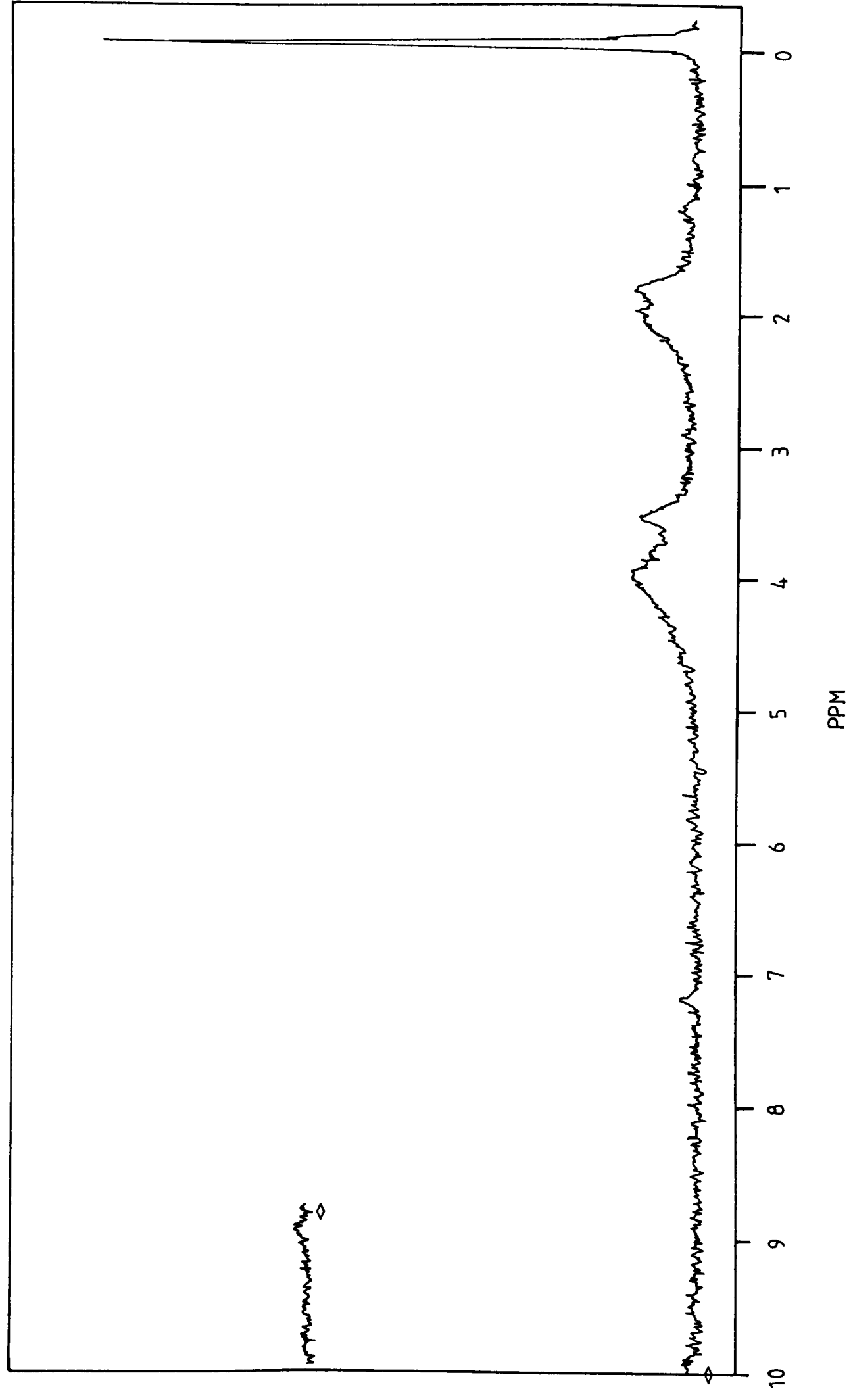
Fig. 64. ^1H nmr spectrum of vanadyl etioporphyrin.

PPM
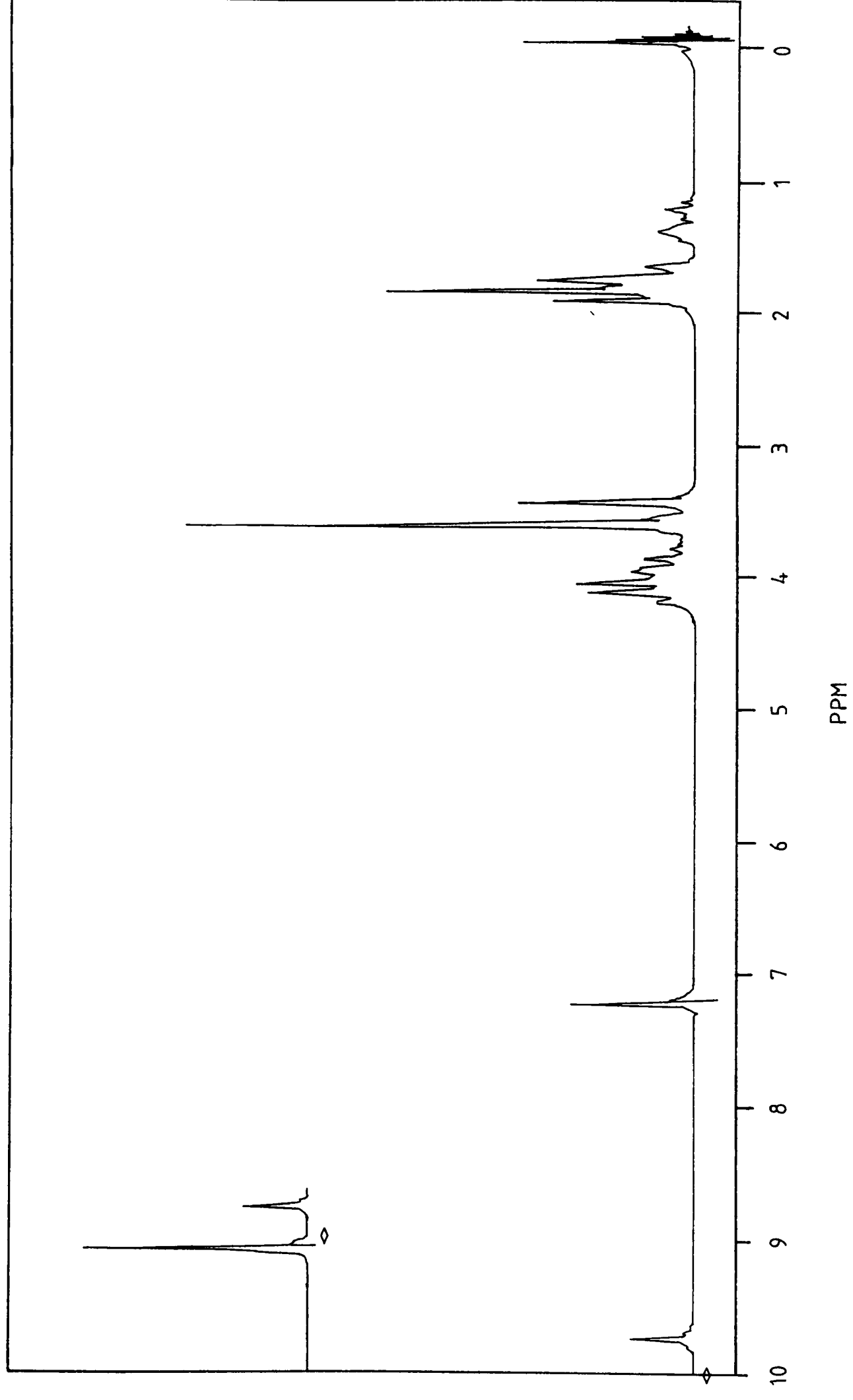
Fig. 65. ^{1}H nmr spectrum of nickel etioporphyrin.
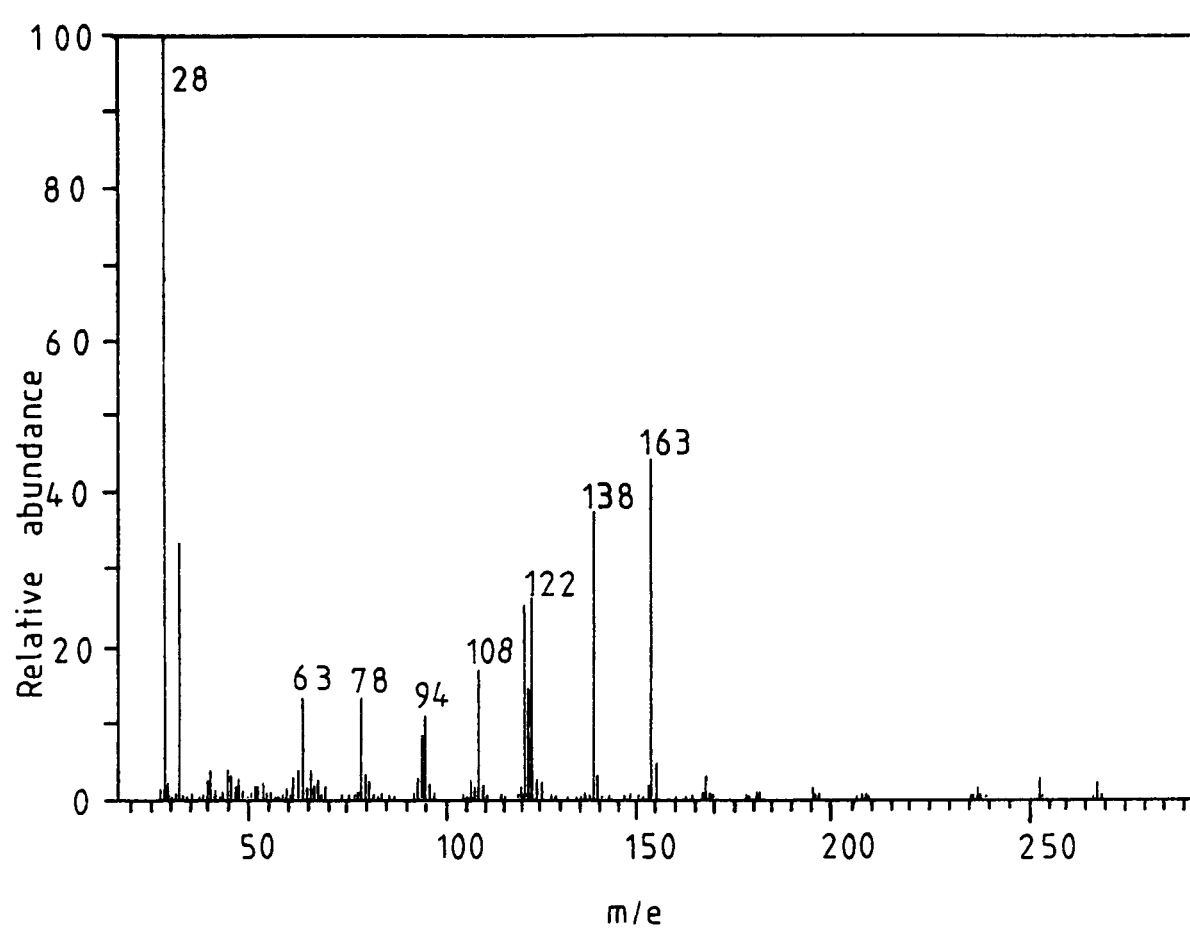
Fig.66. Mass spectrum of methyl 4-ethylpyrrole-3-carboxylate.
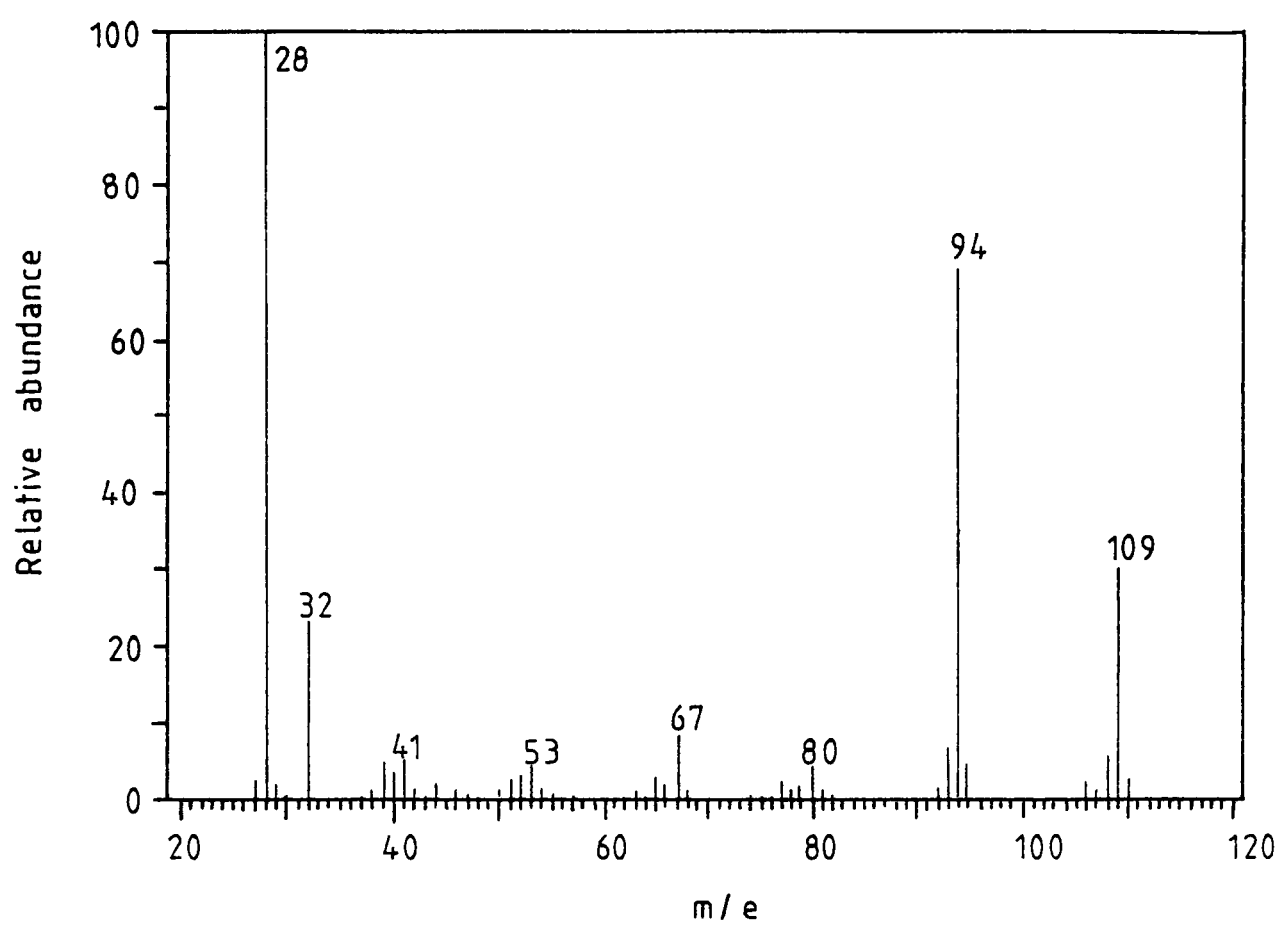
Fig.67.   Mass spectrum of 3-ethyl-4-methylpyrrole.
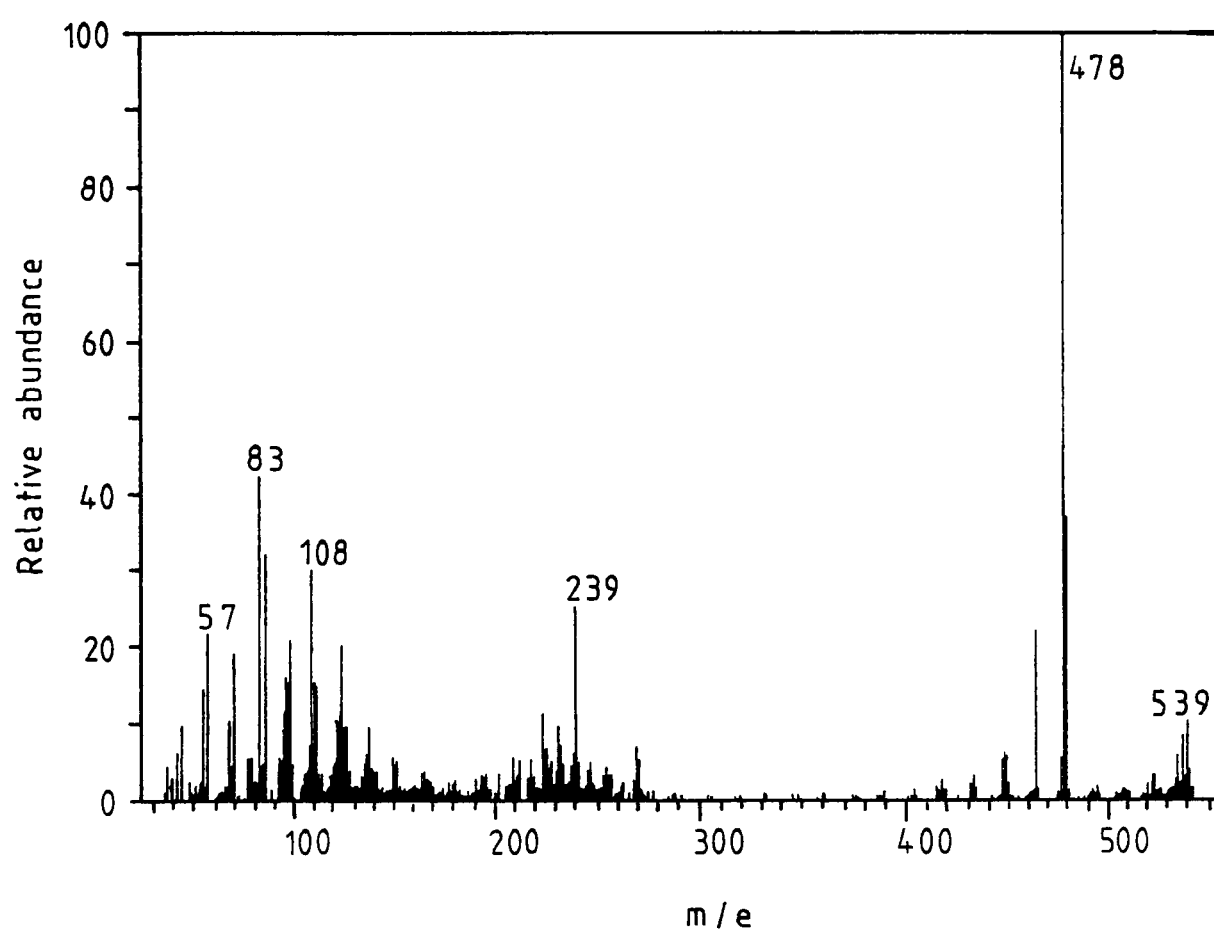
Fig.68. Mass spectrum of etioporphyrin.
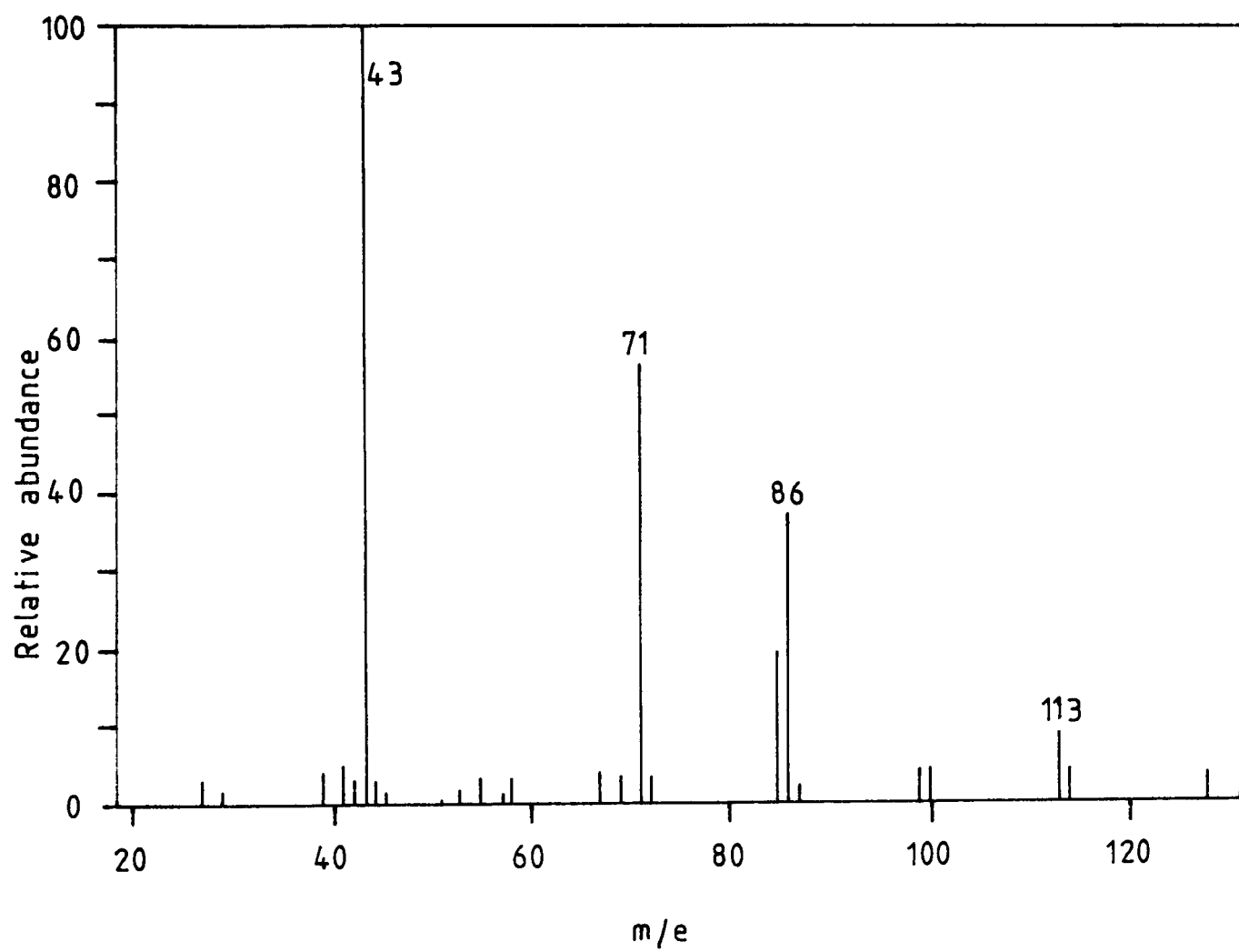
Fig.69. Mass spectrum of 3-ethyl-2,4-pentandione.
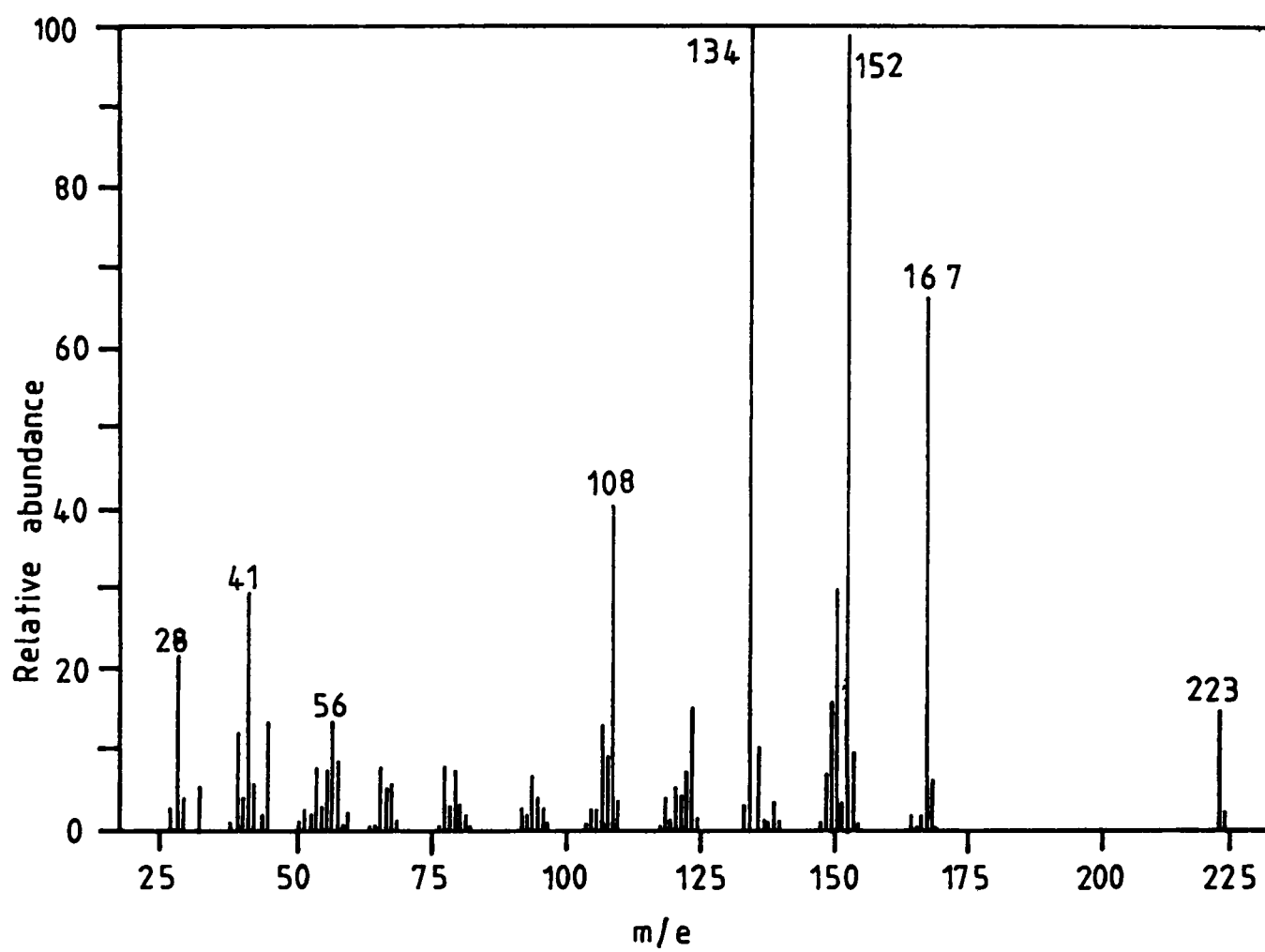
Fig.70.   Mass spectrum of t-butyl 4-ethyl-3,5-dimethylpyrrole carboxylate.
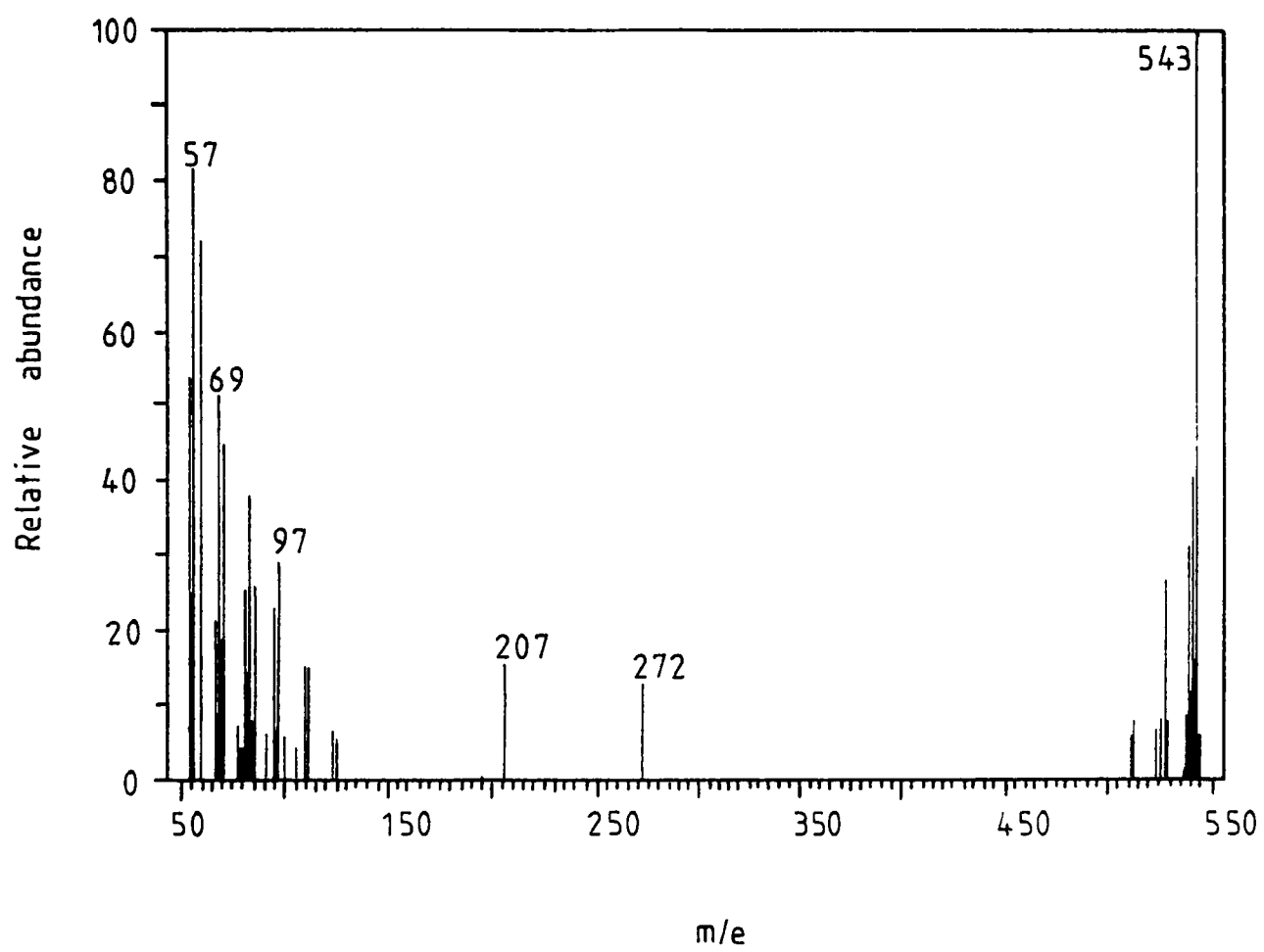
Fig.71. Mass spectrum of vanadyl etioporphyrin.

The splitting pattern of $V.C_{32}H_{36}N_4O$

is as follows :-

543	100.00
544	37.07
545	6.87
546	0.85
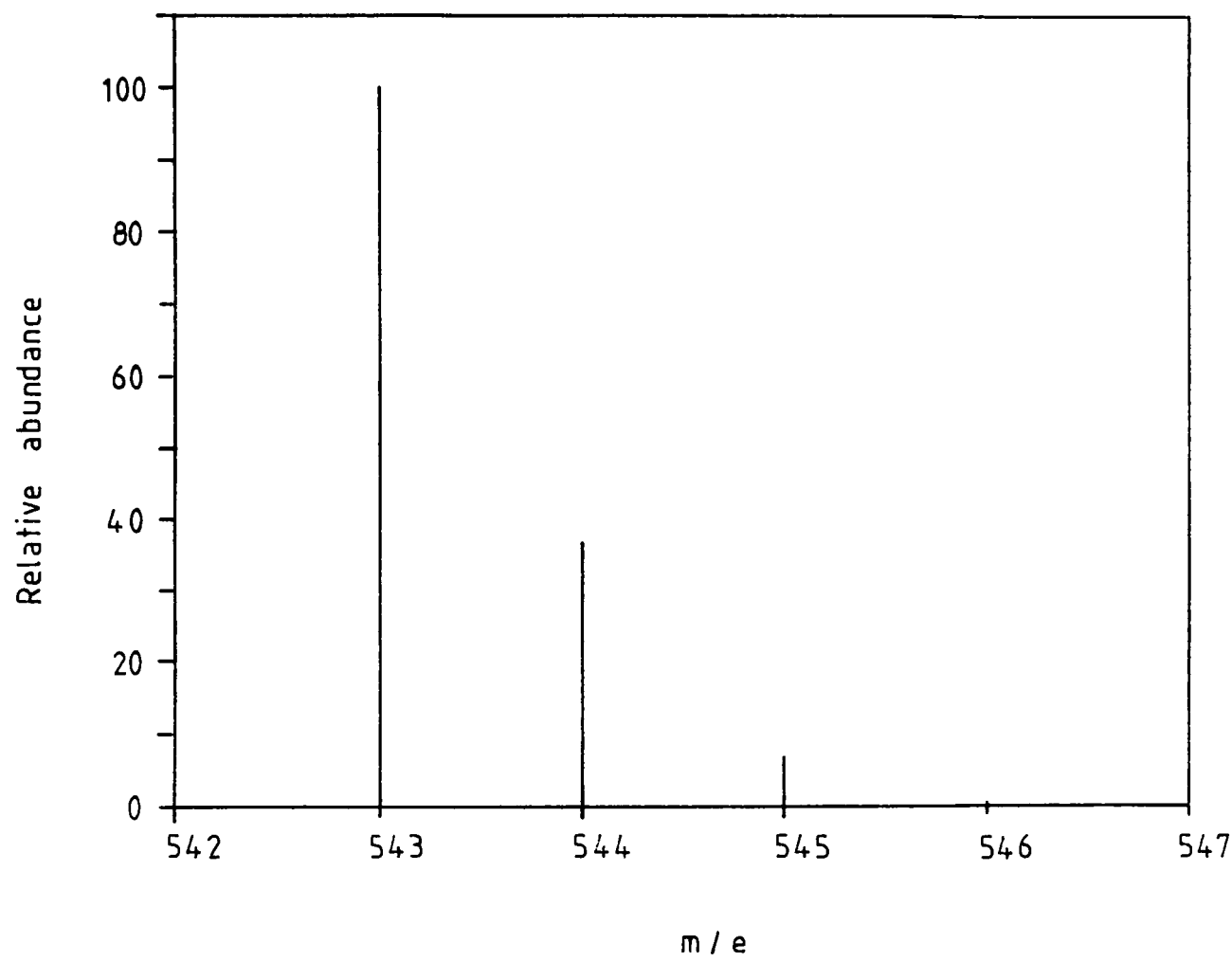
Fig.72.   Splitting pattern for the molecular ion of vanadyl etioporphyrin
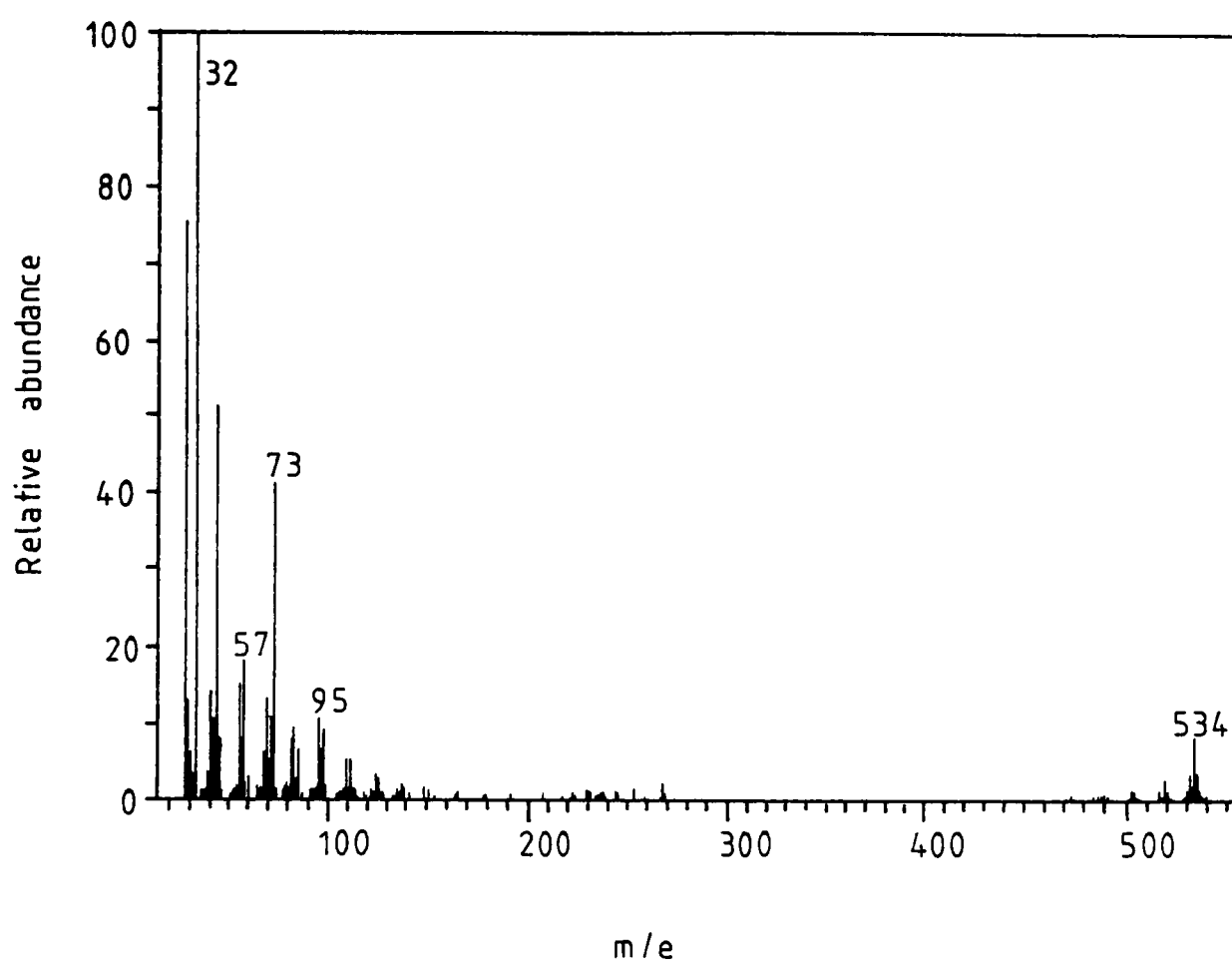
Fig.73.   Mass spectrum of nickel etioporphyrin.

The splitting pattern of $Ni.C_{32}H_{36}N_4$

is as follows :-

534	100.00
535	37.06
536	45.27
537	16.78
538	8.67
539	2.42
540	2.00
541	0.64
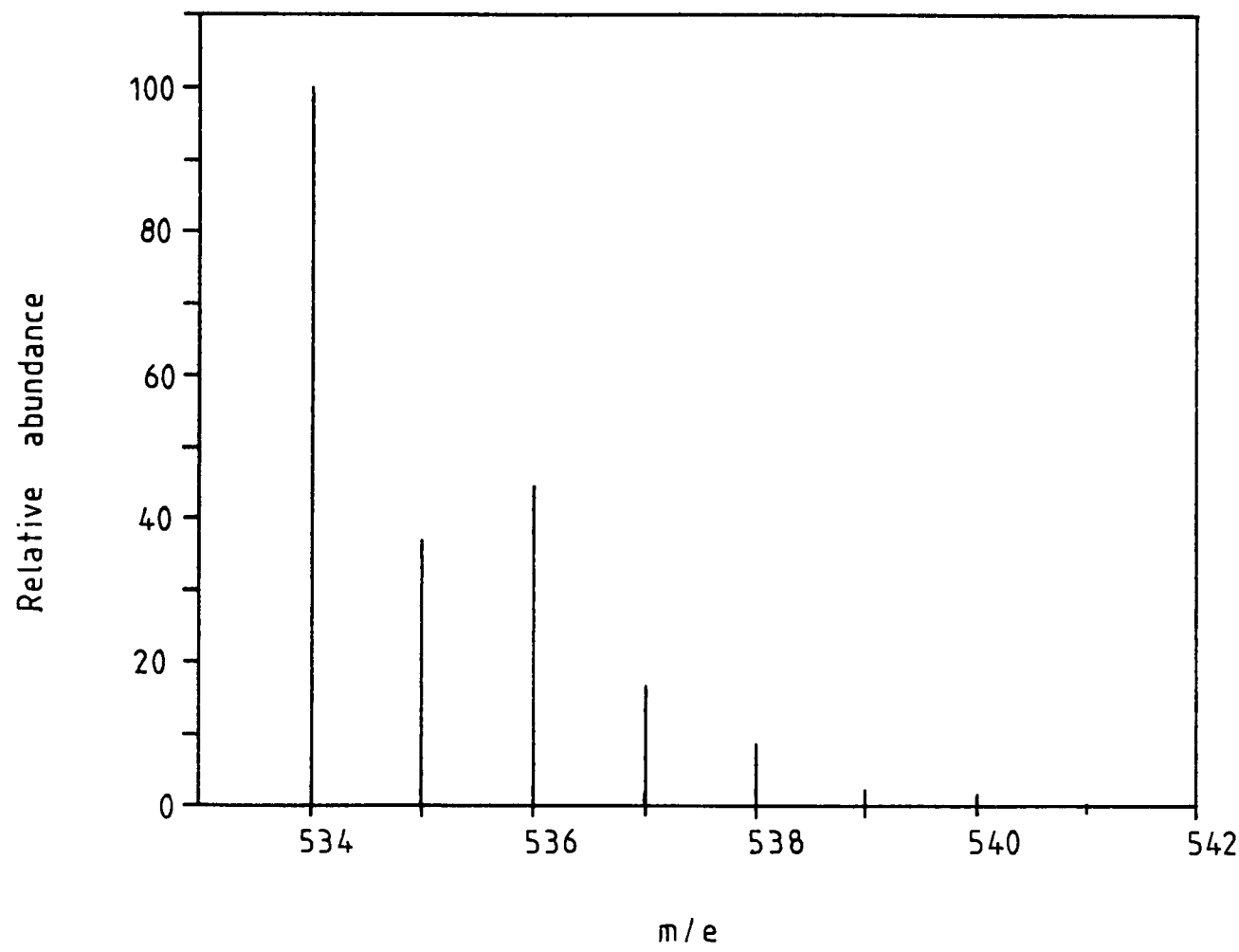
Fig.74. Splitting pattern for the molecular ion of nickel etioporphyrin.
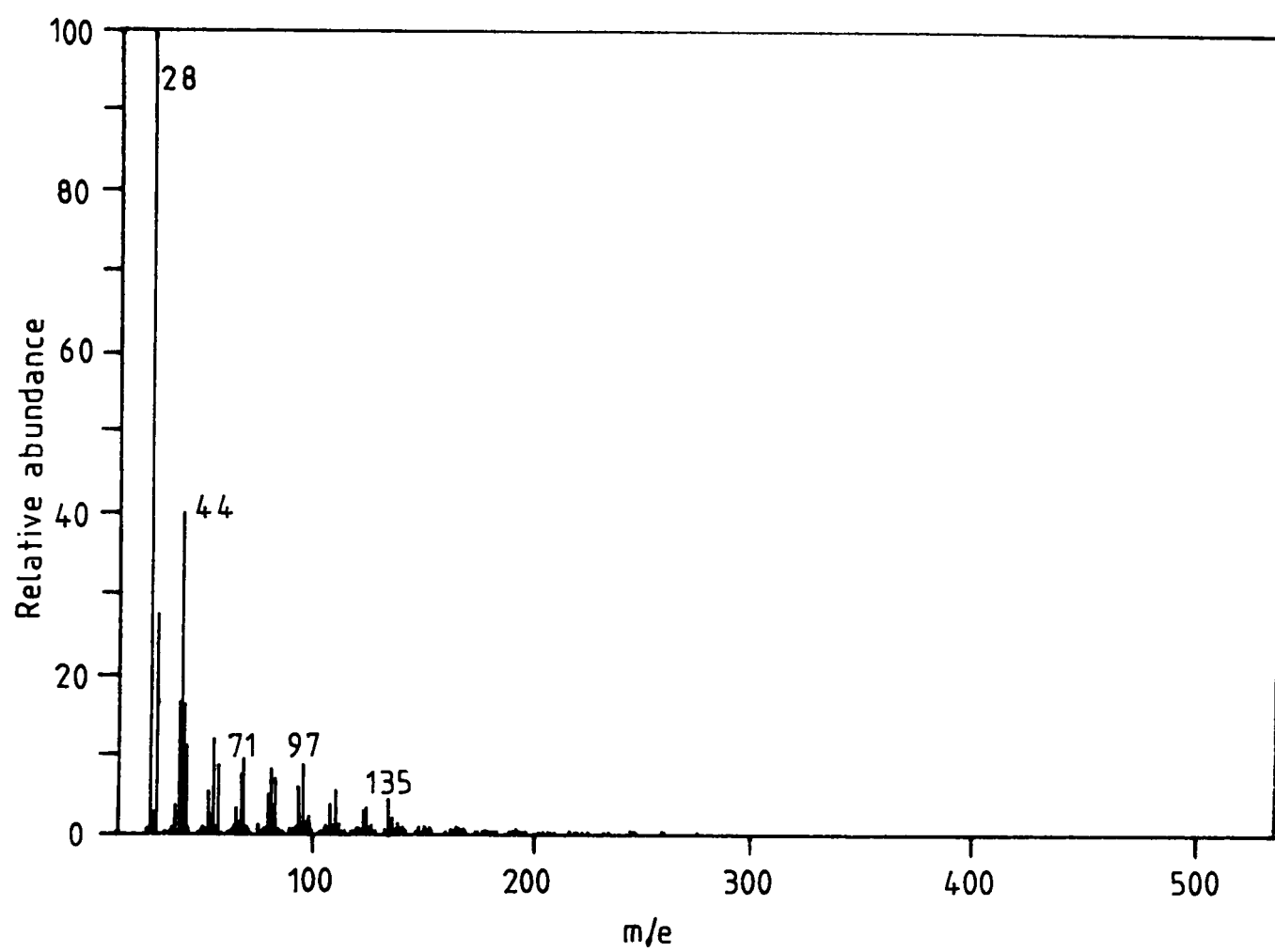
Fig.75. Mass spectrum of vanadyl hematoporphyrin IX.
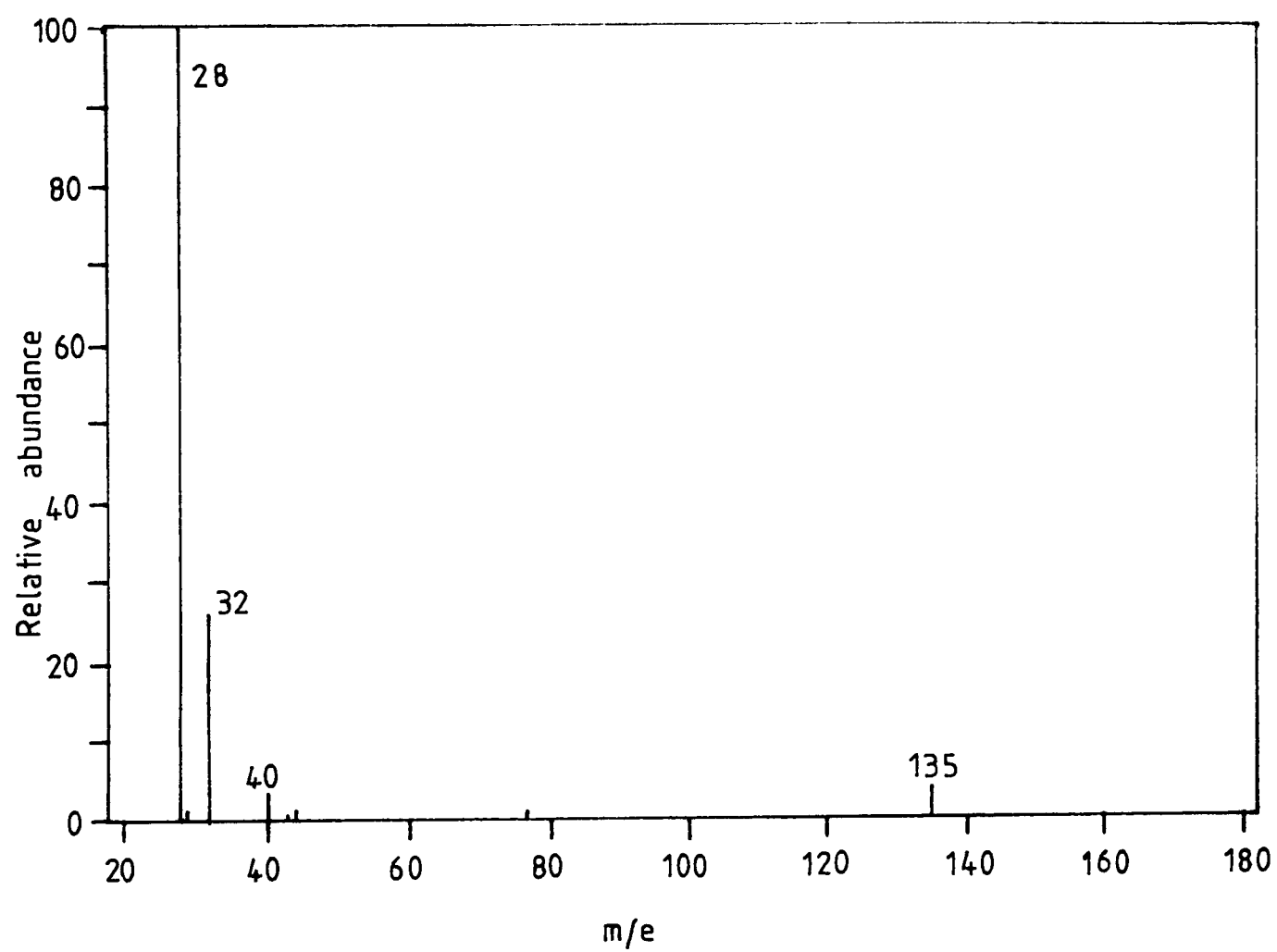
Fig.76.   Mass spectrum of instrument background.
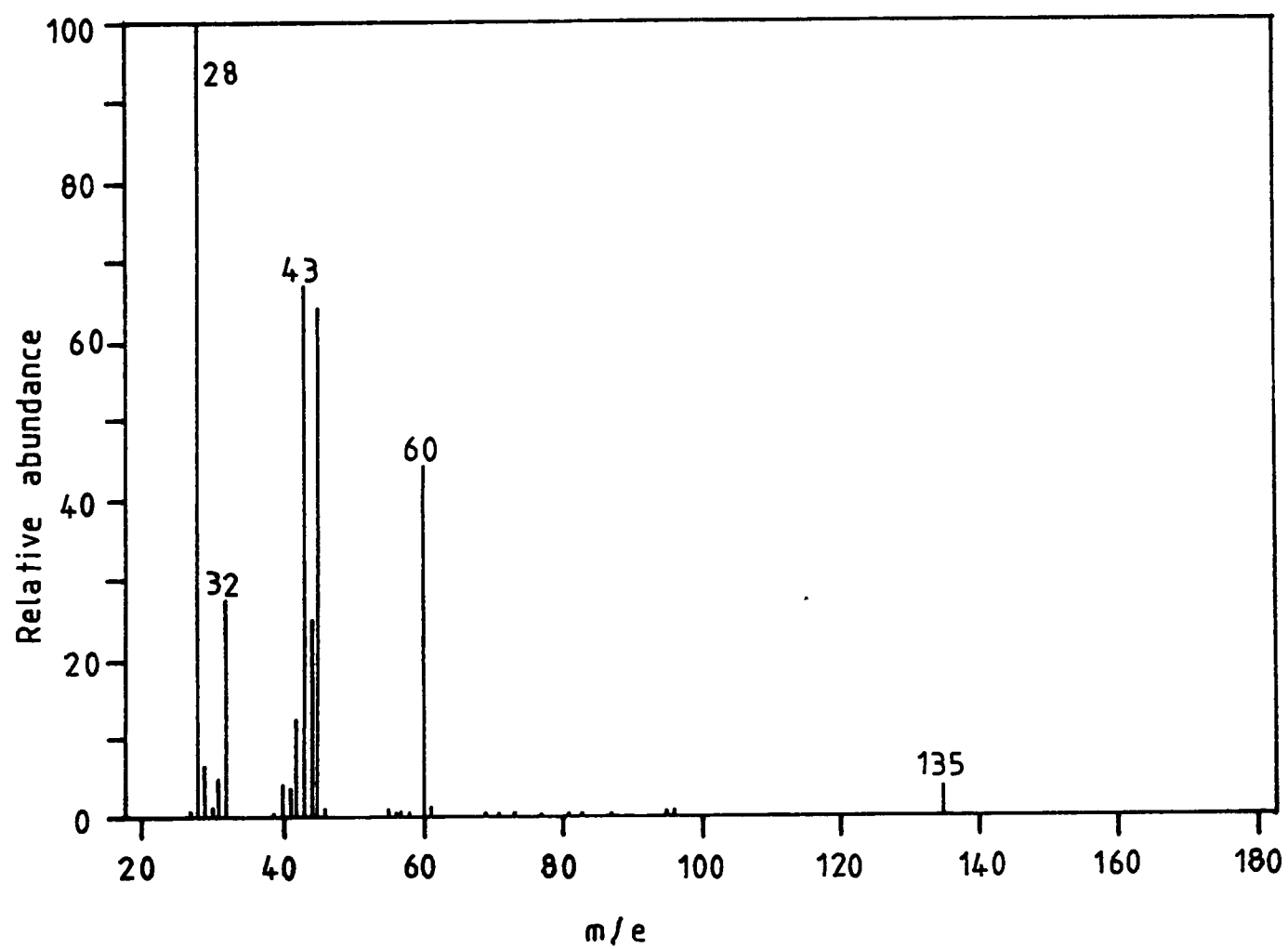
Fig.77.   Mass spectrum of nickel hematoporphyrin IX.
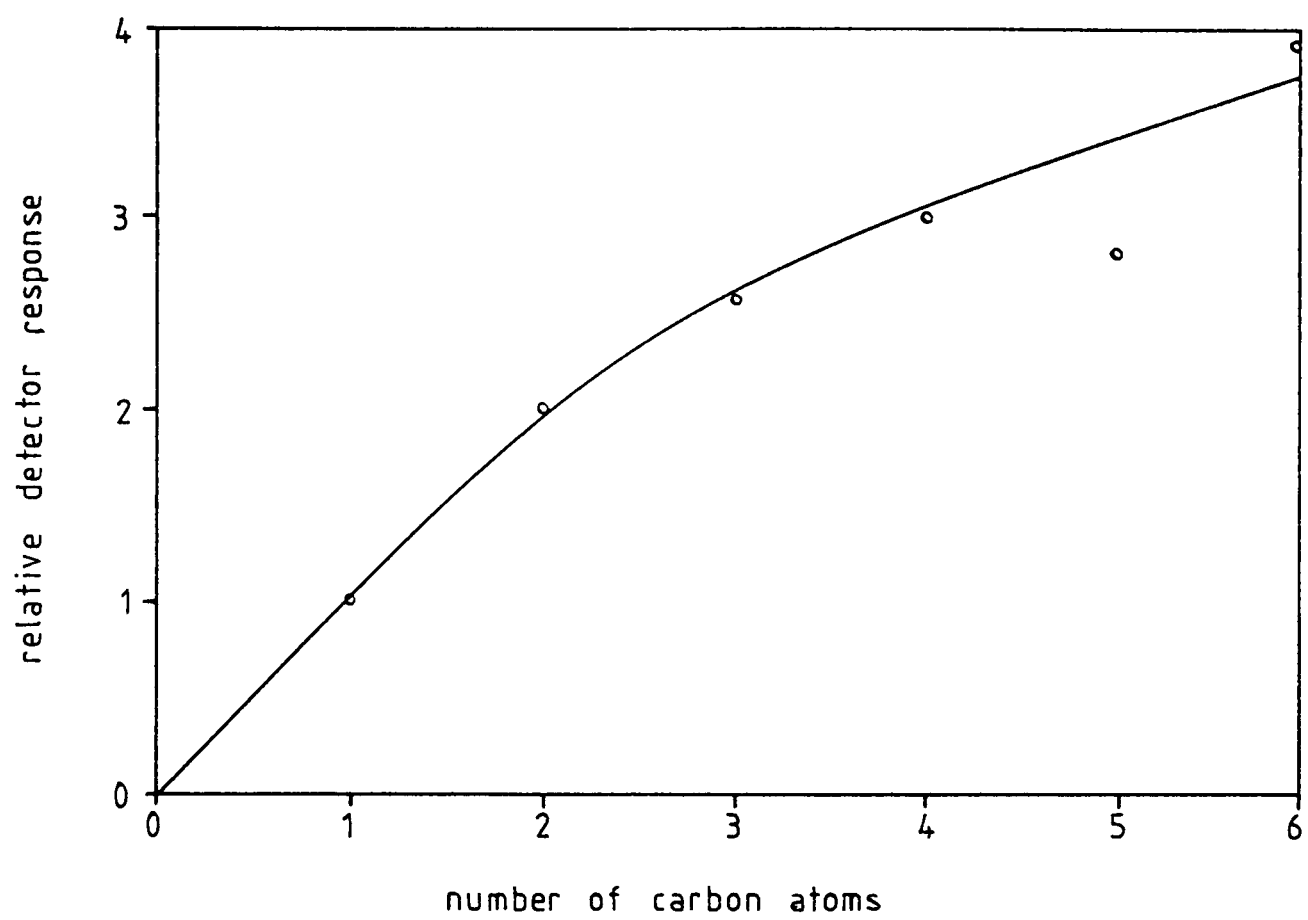
Fig.78.   Relative FID response for various n-alkanes.
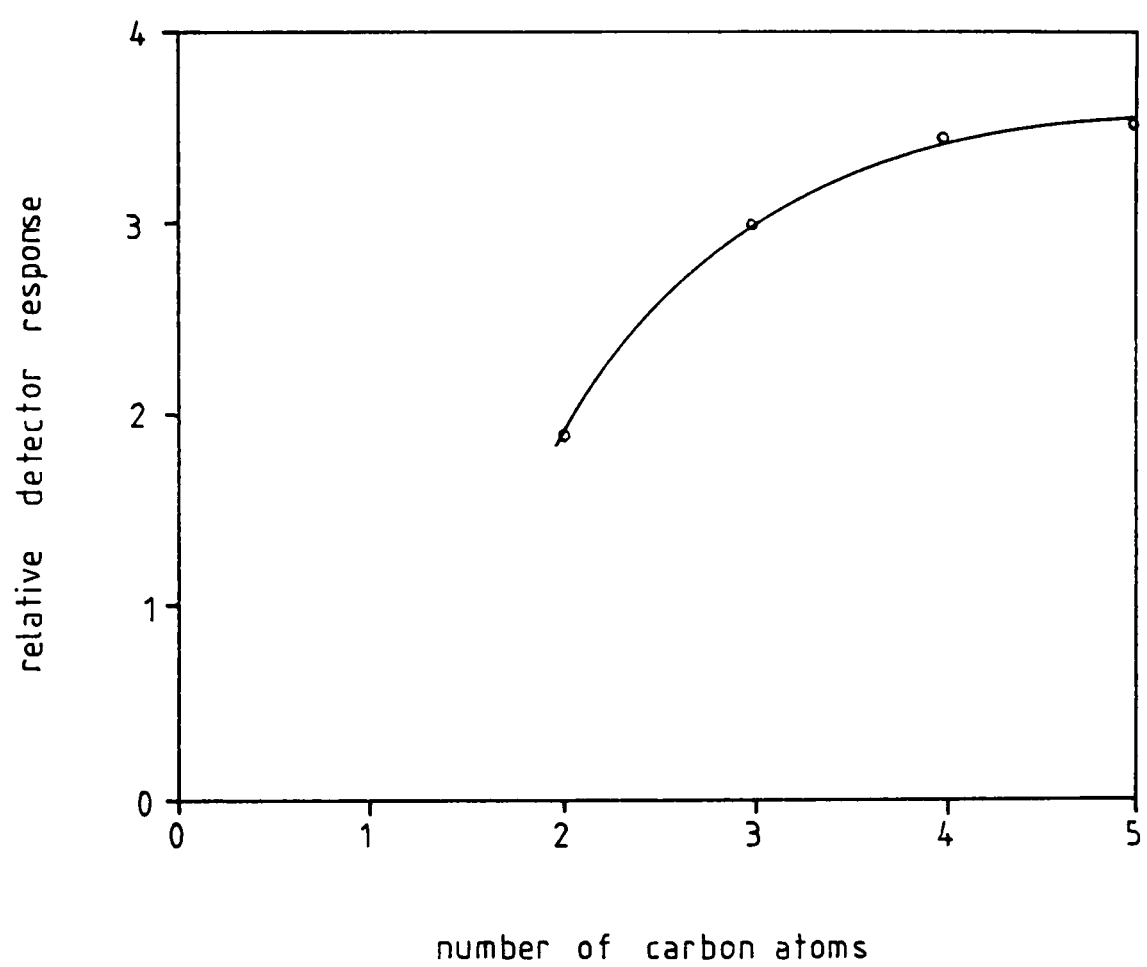
Fig.79.   Relative FID response for various n-1-alkenes.
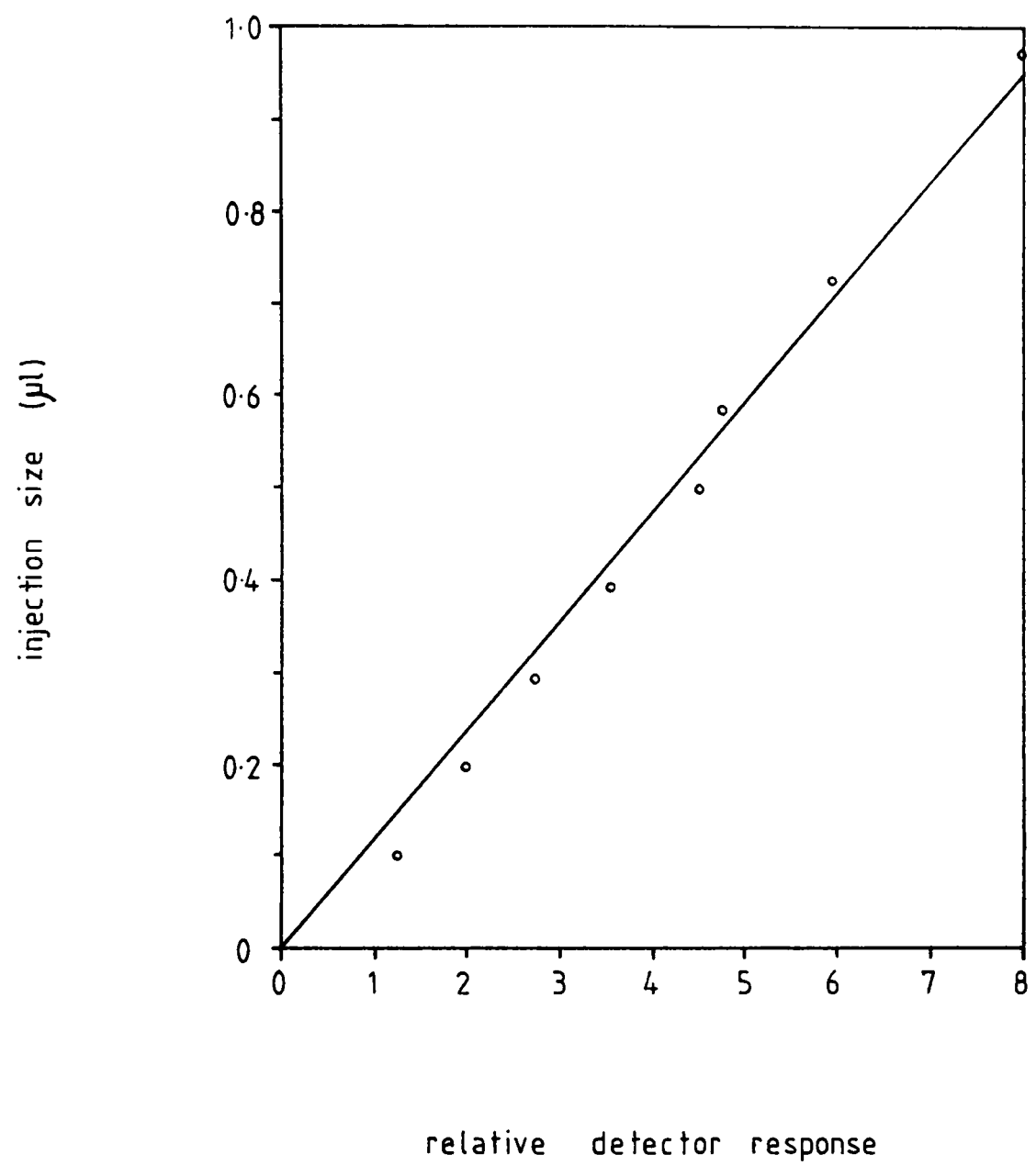
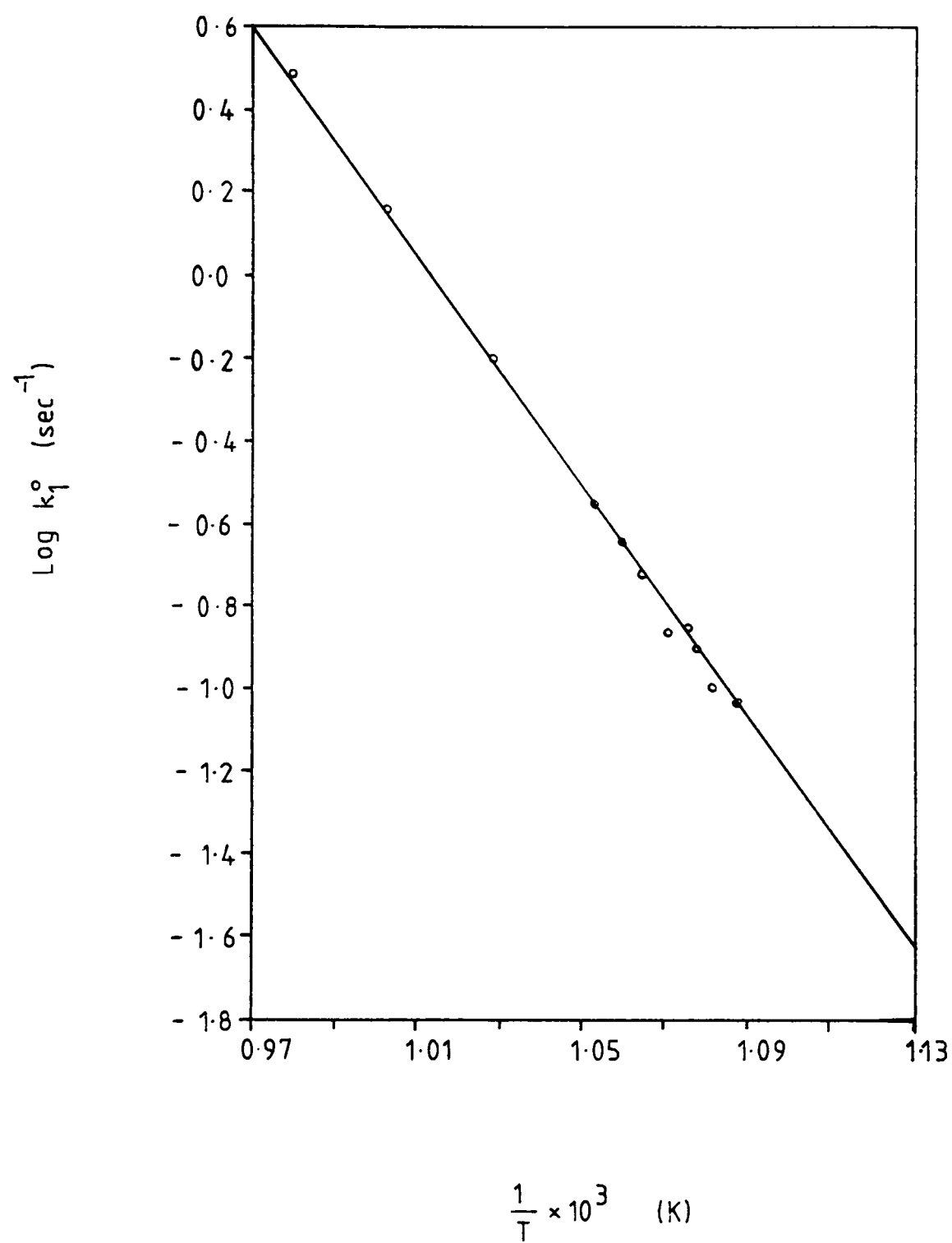Fig.80.   Chromatograph FID response to 2,2-dimethylbutane.

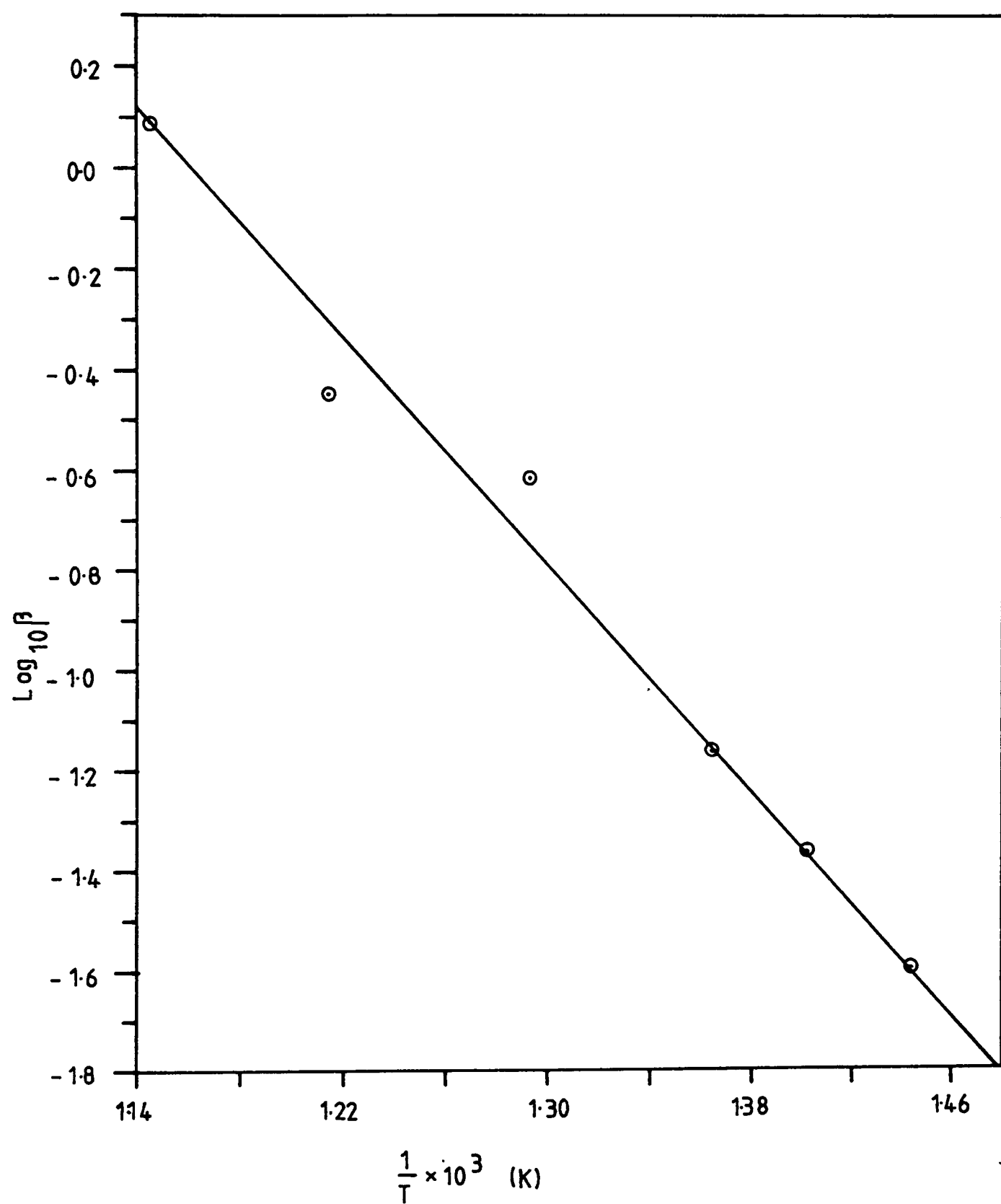Fig.81. Arrhenius plot for the thermal cracking of n-butane.

Fig.82.   The temperature dependence of the restraining coefficient
           during the thermal cracking of 2,2-dimethylbutane.
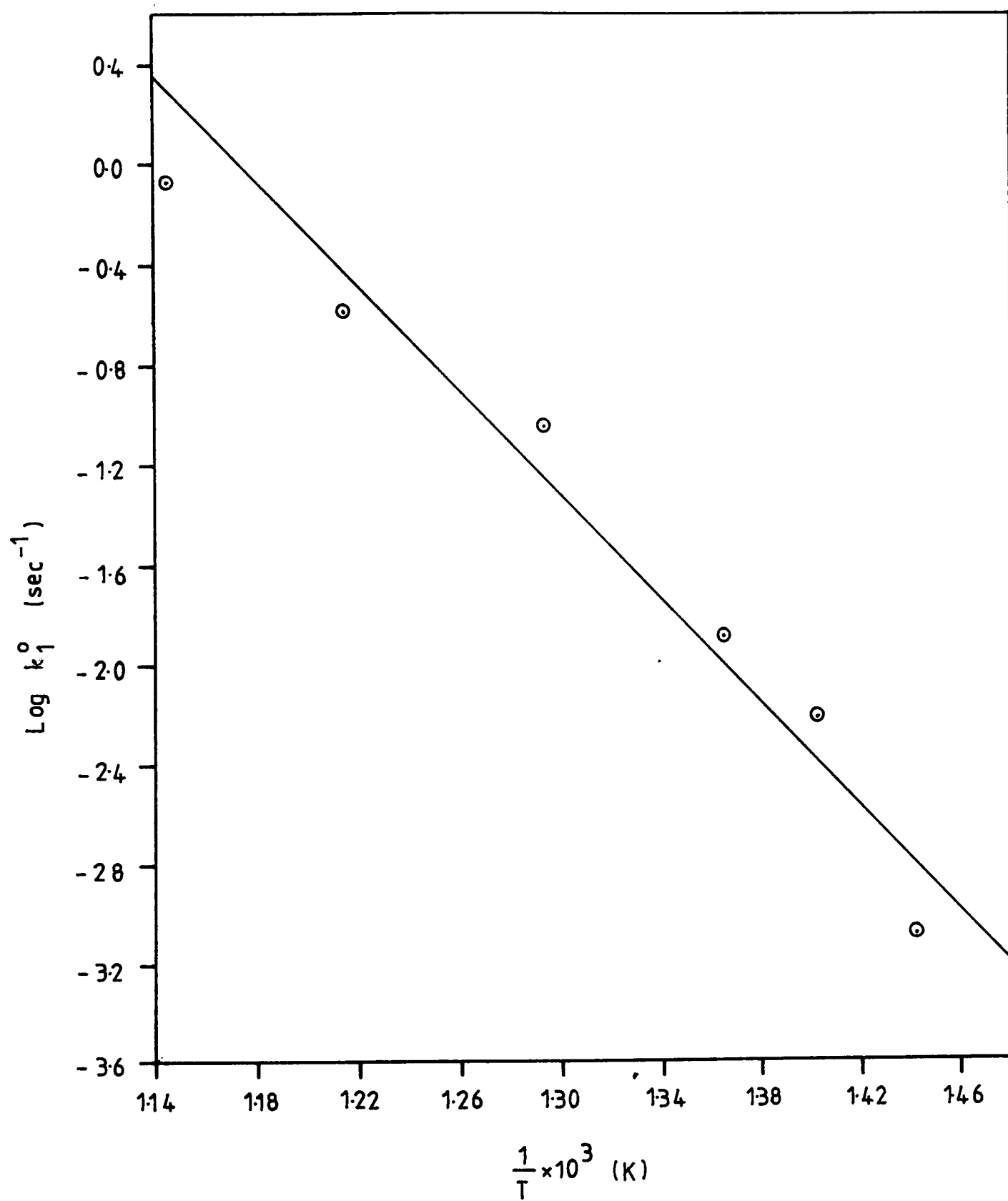
Fig.83.   Arrhenius plot for the thermal cracking
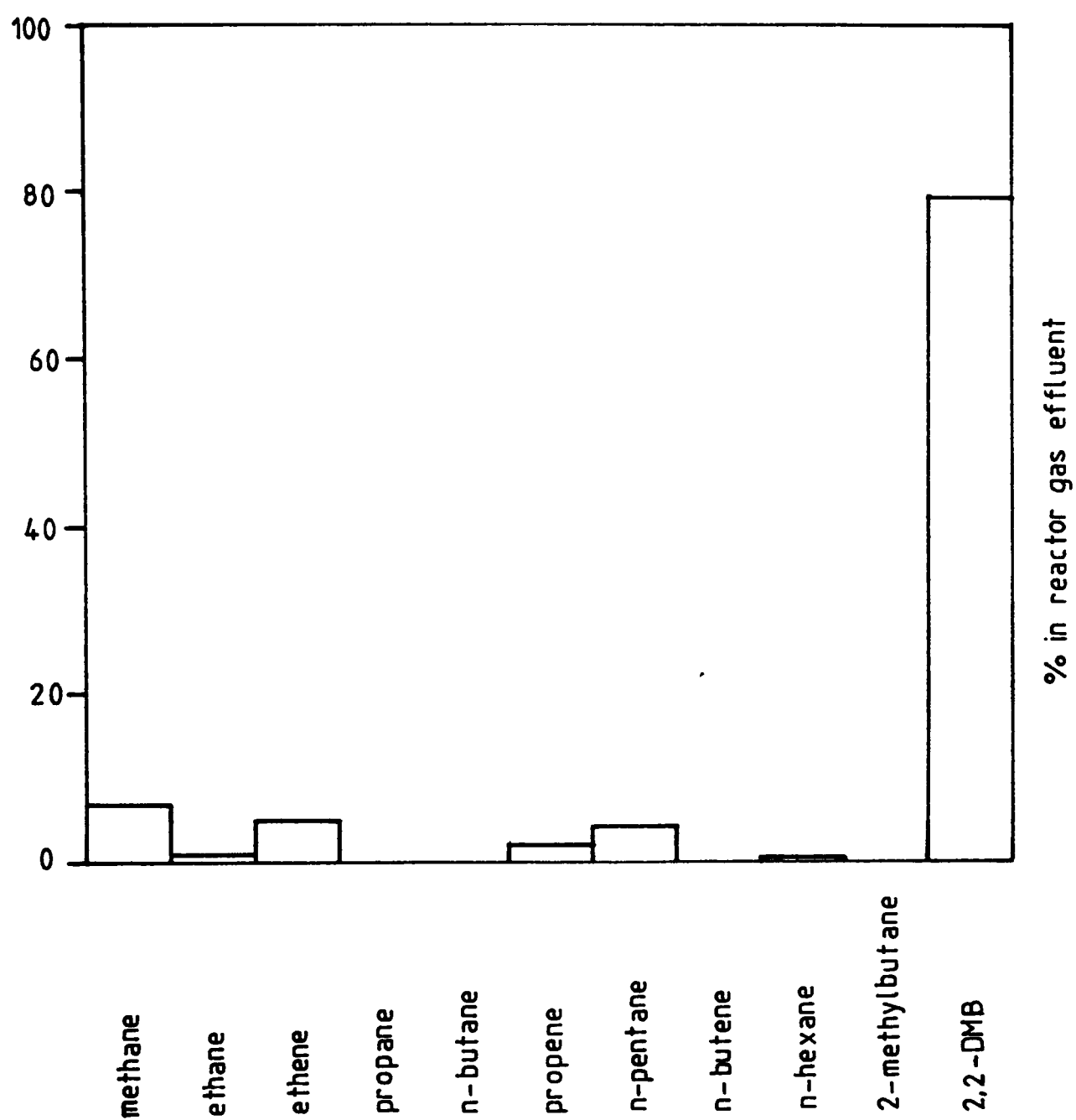   of 2,2-dimethylbutane.

Fig.84.   Chromatogram given by 2,2-dimethylbutane passed over 1.0%
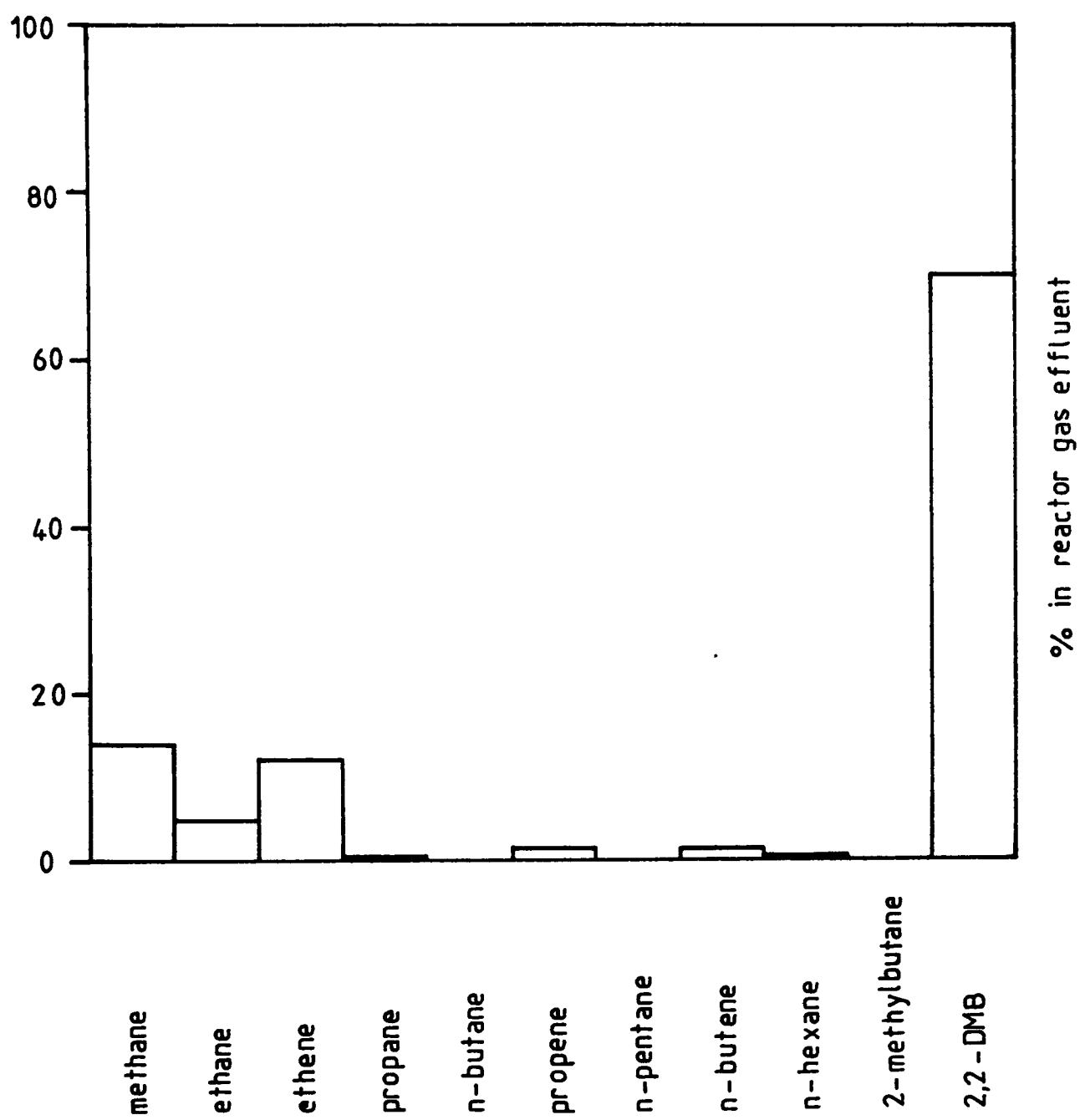base etioporphyrin I on silica at 497°C.

Fig.85. Chromatogram given by 2,2-dimethylbutane passed over 1.0% vanadyl etioporphyrin I on silica at 497°C.
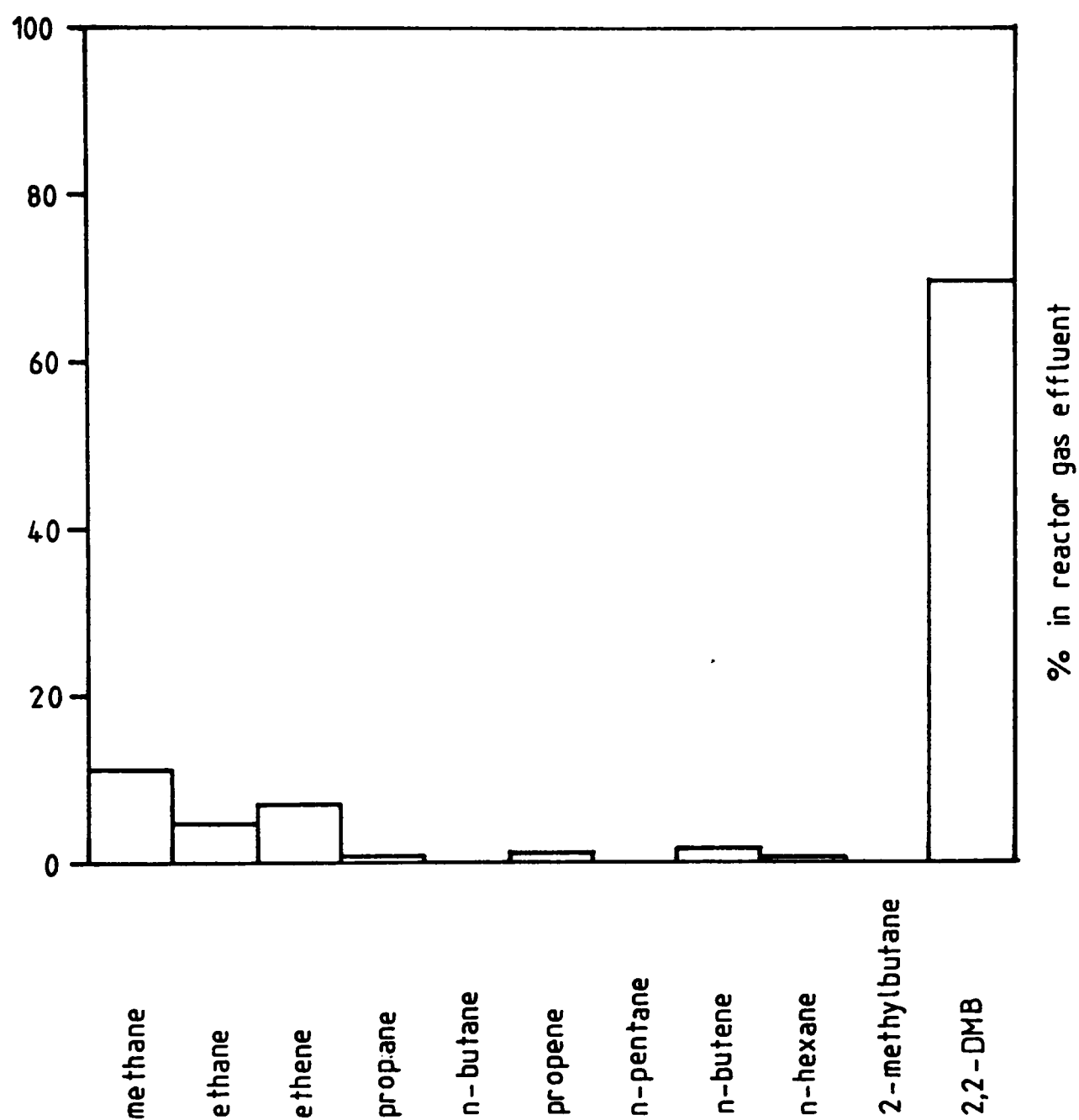
Fig.86. Chromatogram given by 2,2-dimethylbutane passed over 1.0% nickel etioporphyrin I on silica at ~97°C.
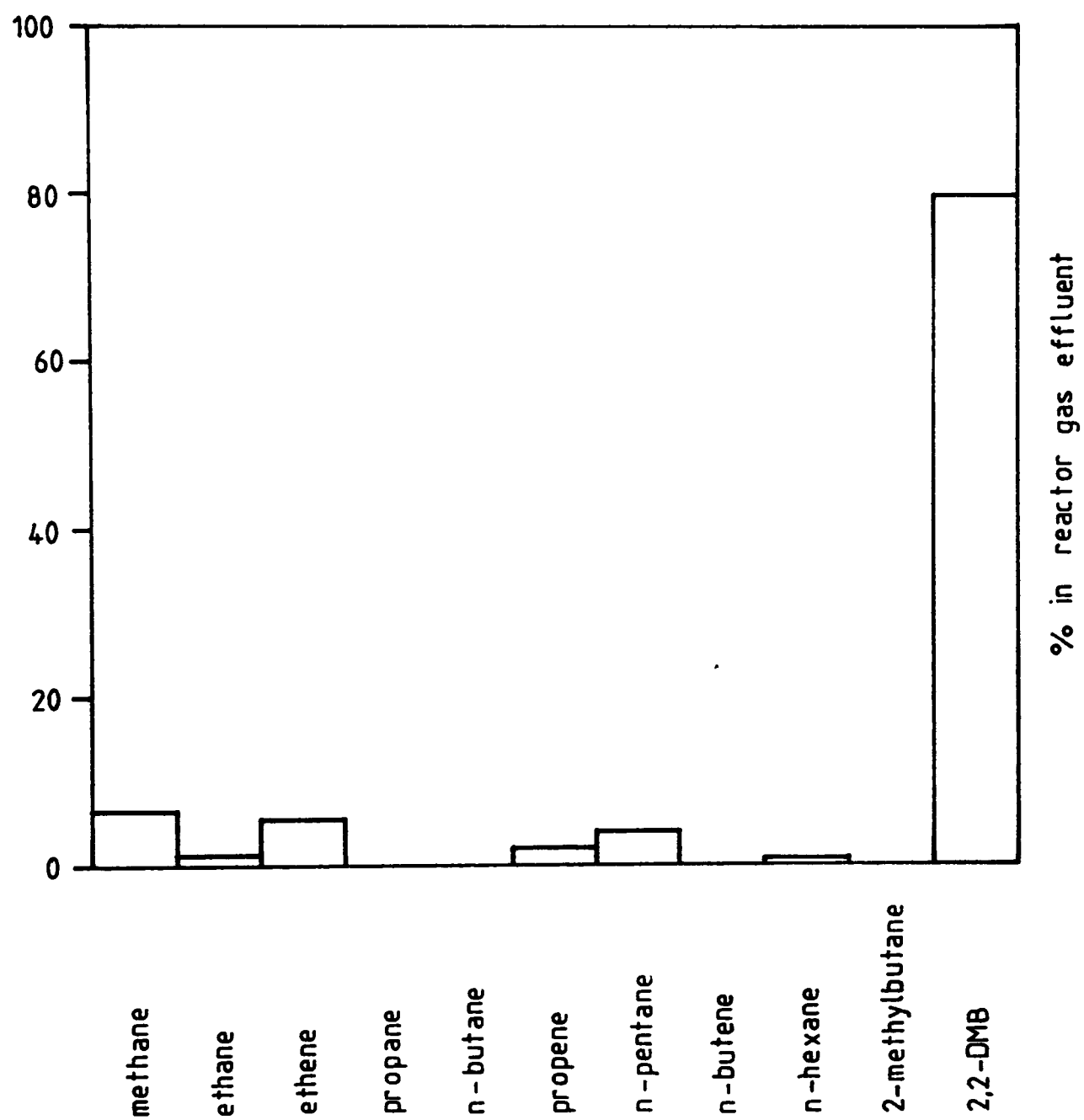
Fig.87.   Chromatogram given by 2,2-dimethylbutane passed over
1.0% platinum etioporphyrin I on silica at 497°C.

Fig.88.   Chromatogram given by 2,2-dimethylbutane passed over
          1.% palladium etioporphyrin I on silica at 497°C.

Fig.89.   Chromatogram given by 2,2-dimethylbutane passed over
1.0% base hematoporphyrin IX on silica at ~97°C.
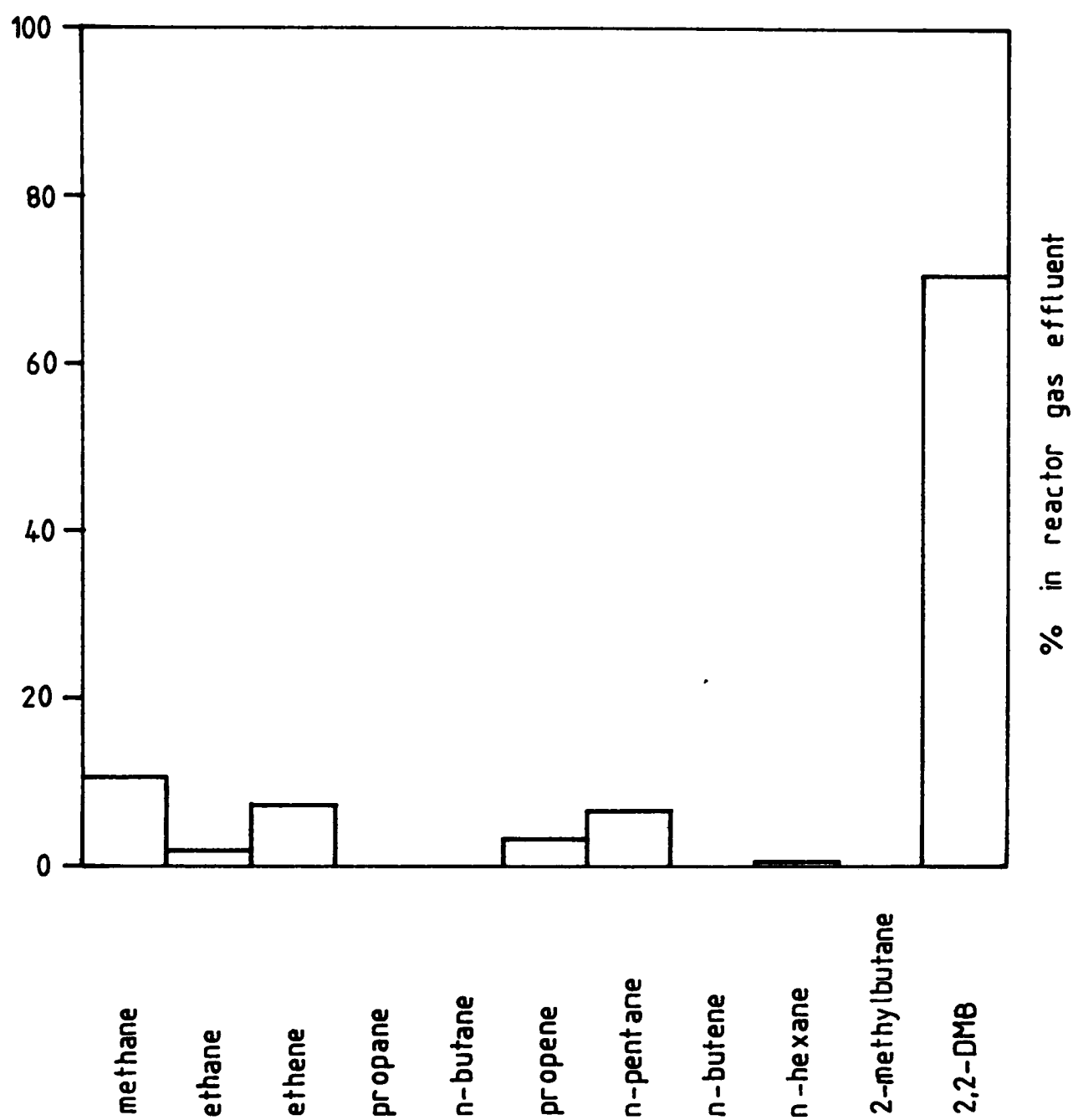
Fig. 90.   Chromatrogram given by 2,2-dimethylbutane passed over
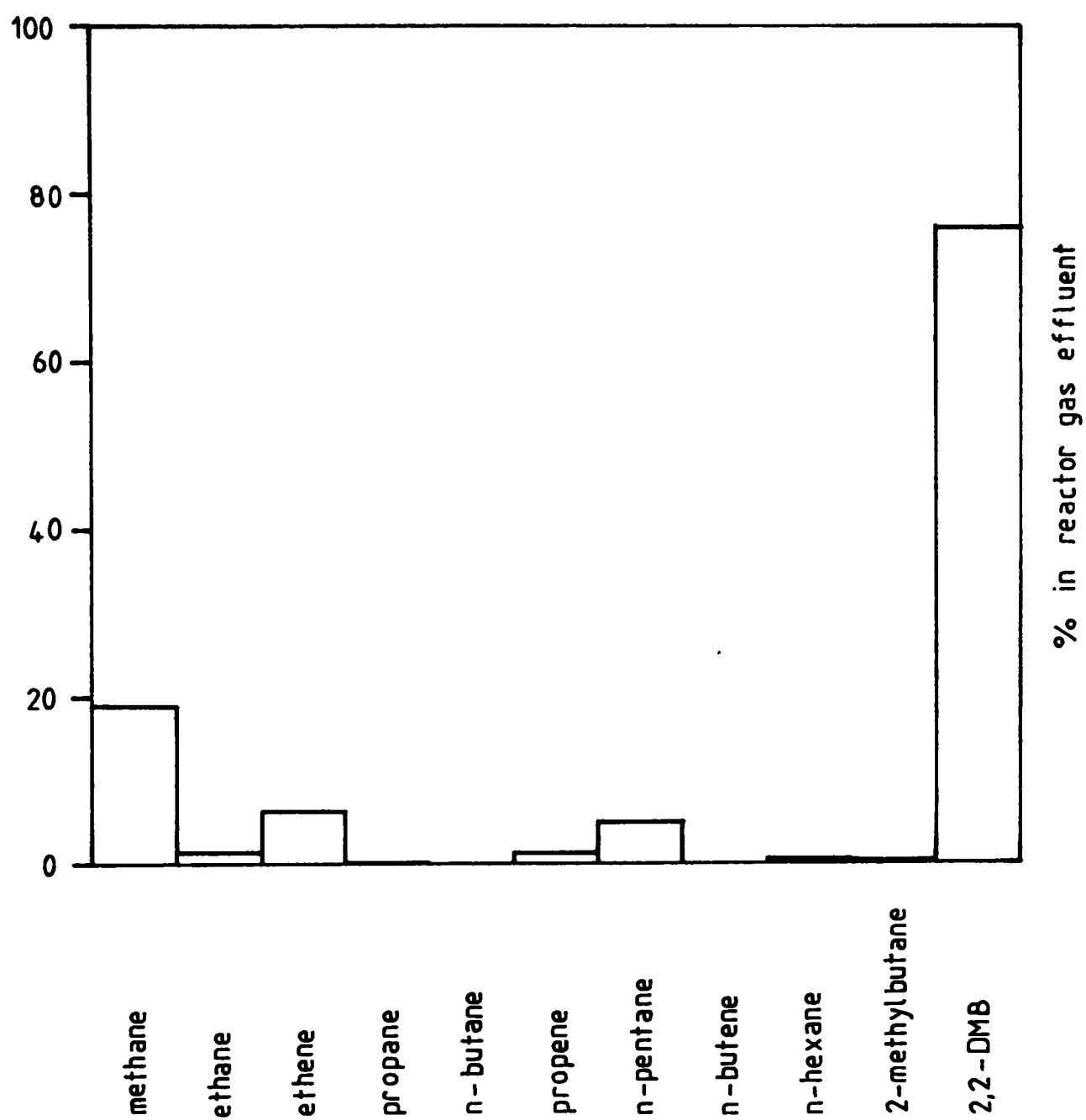1.0% vanadyl hematoporphyrin IX on silica at 497°C.
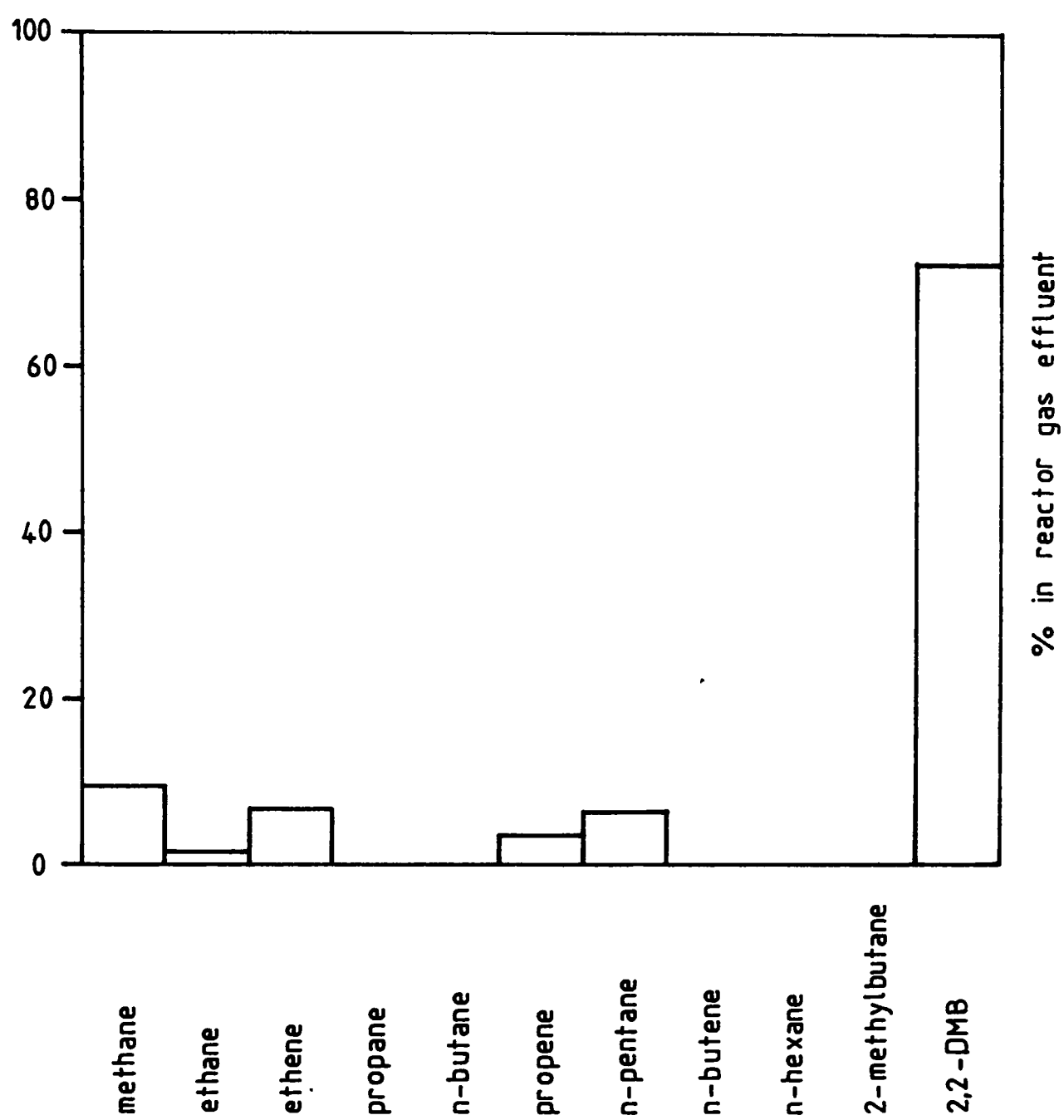
Fig.91. Chromatogram given by 2,2-dimethylbutane passed over 1.0% nickel hematoporphyrin IX on silica at 497°C.
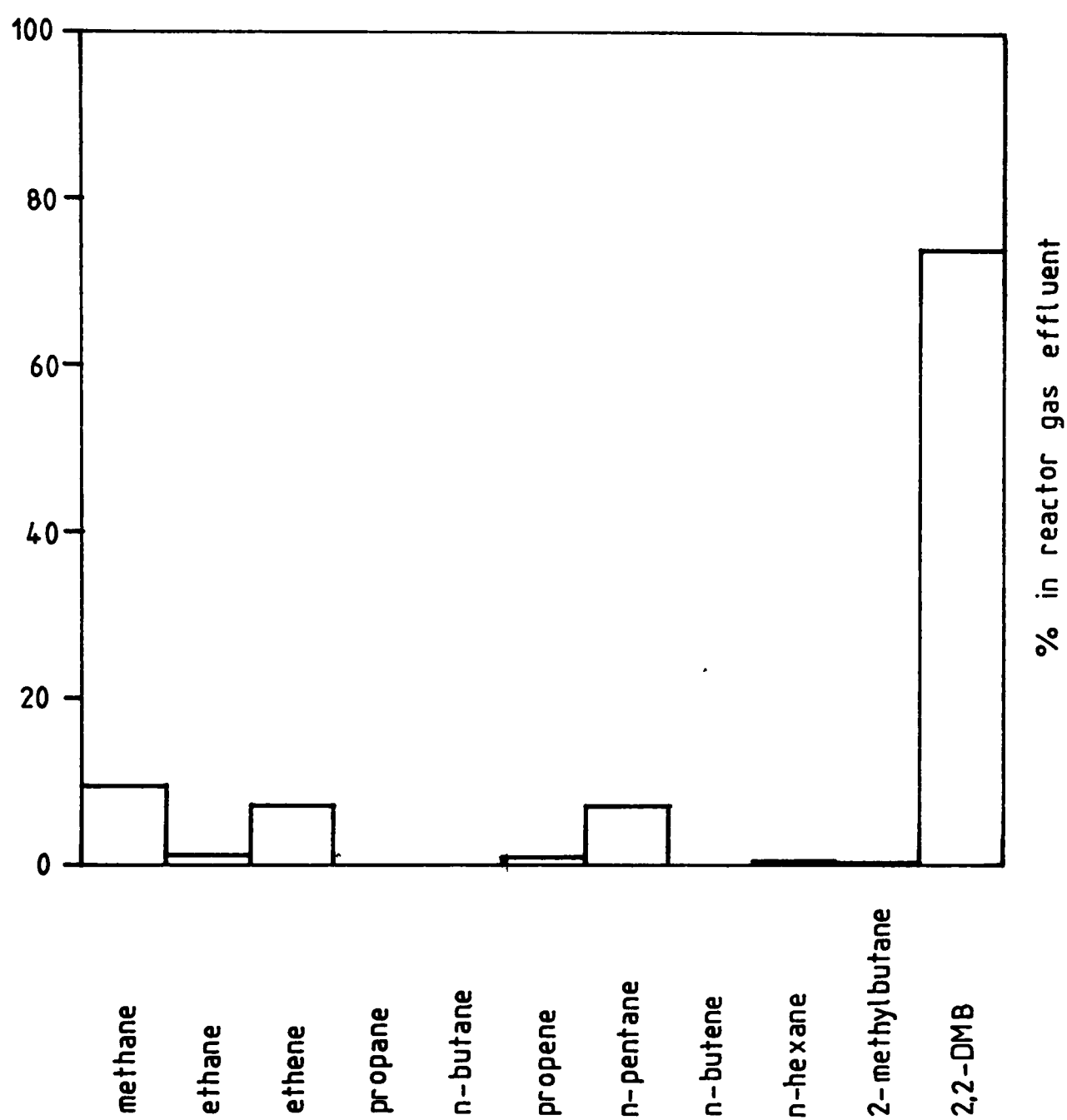
Fig.92.   Chromatogram given by 2,2-dimethylbutane passed over
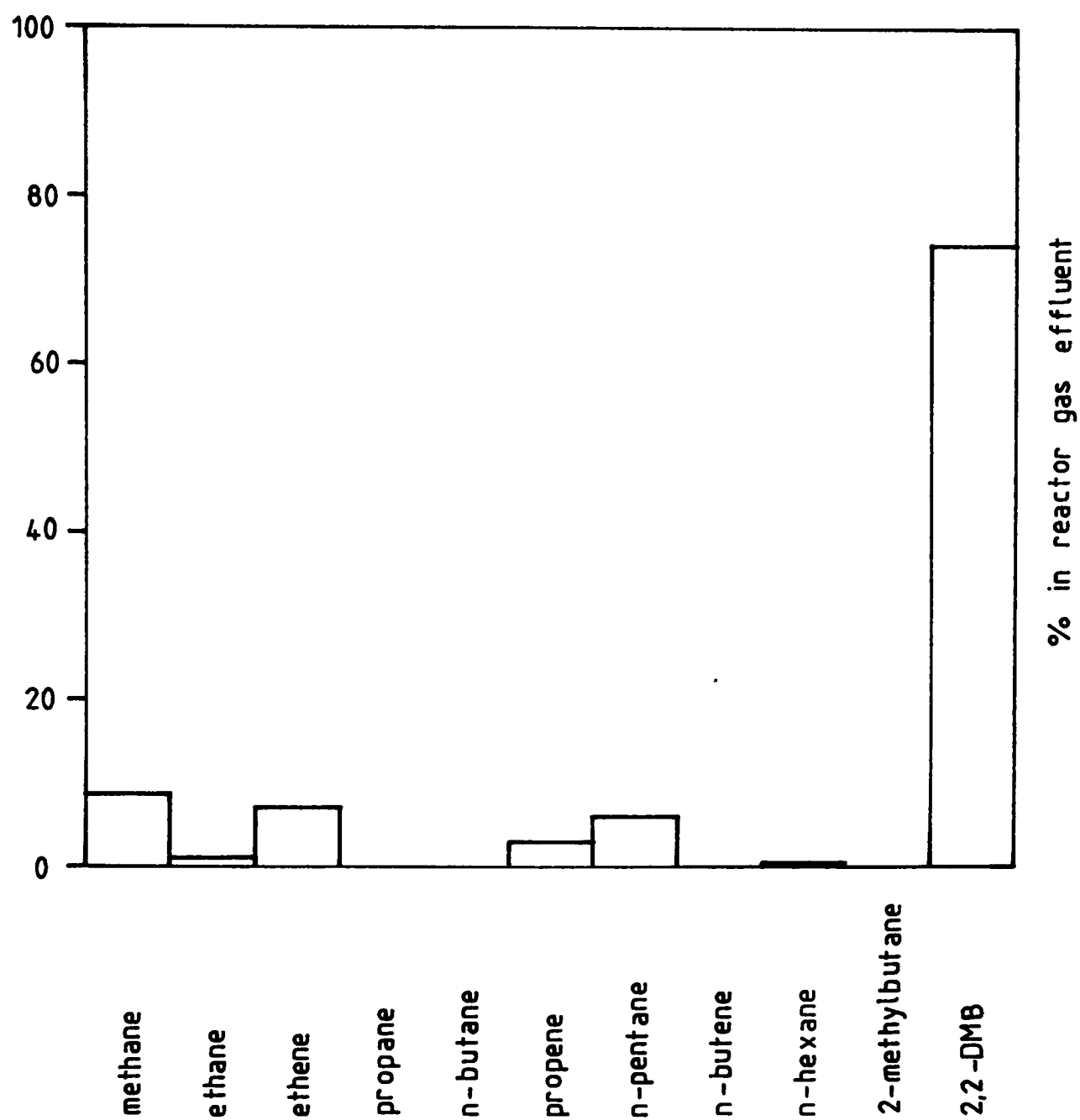   1.% petroporphyrin concentrate on silica at 497°C.
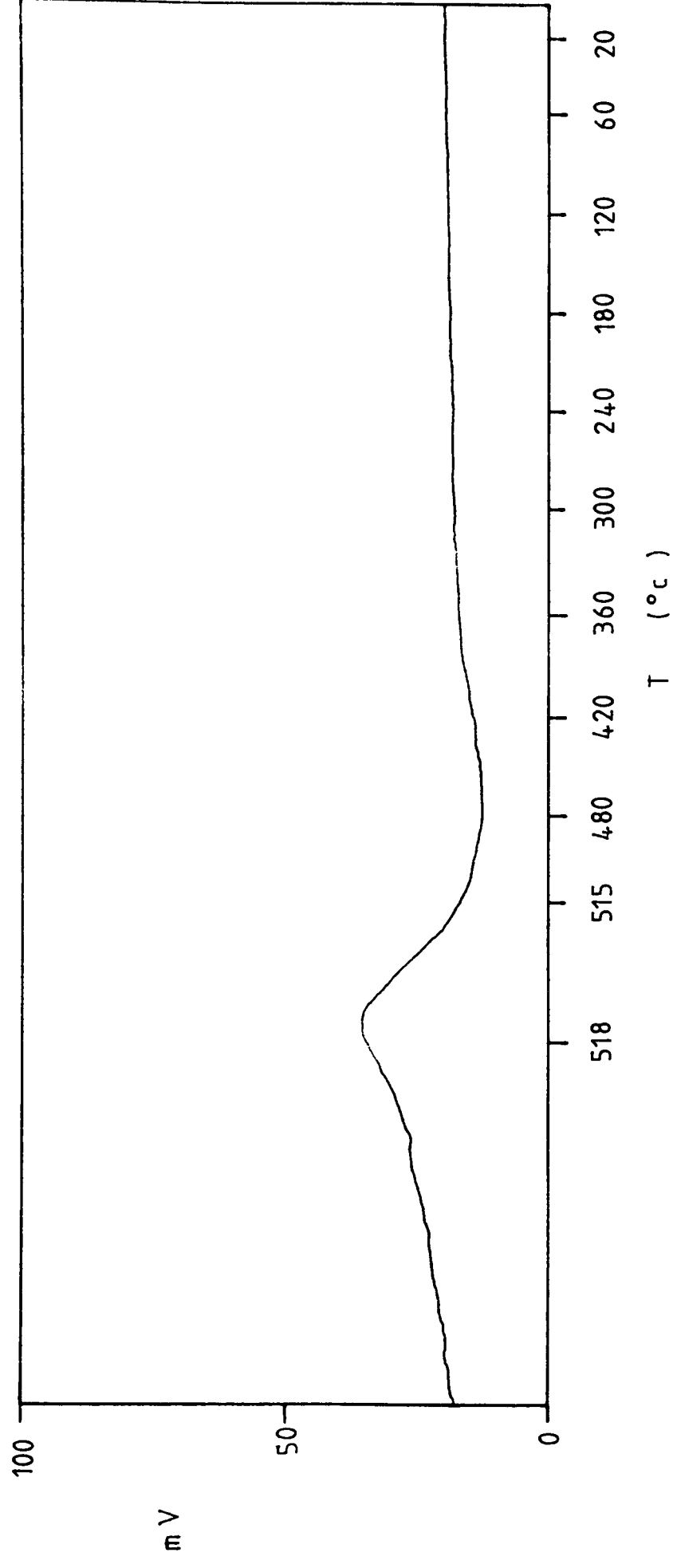
Fig. 93. TPR trace for base etioporphyrin I.
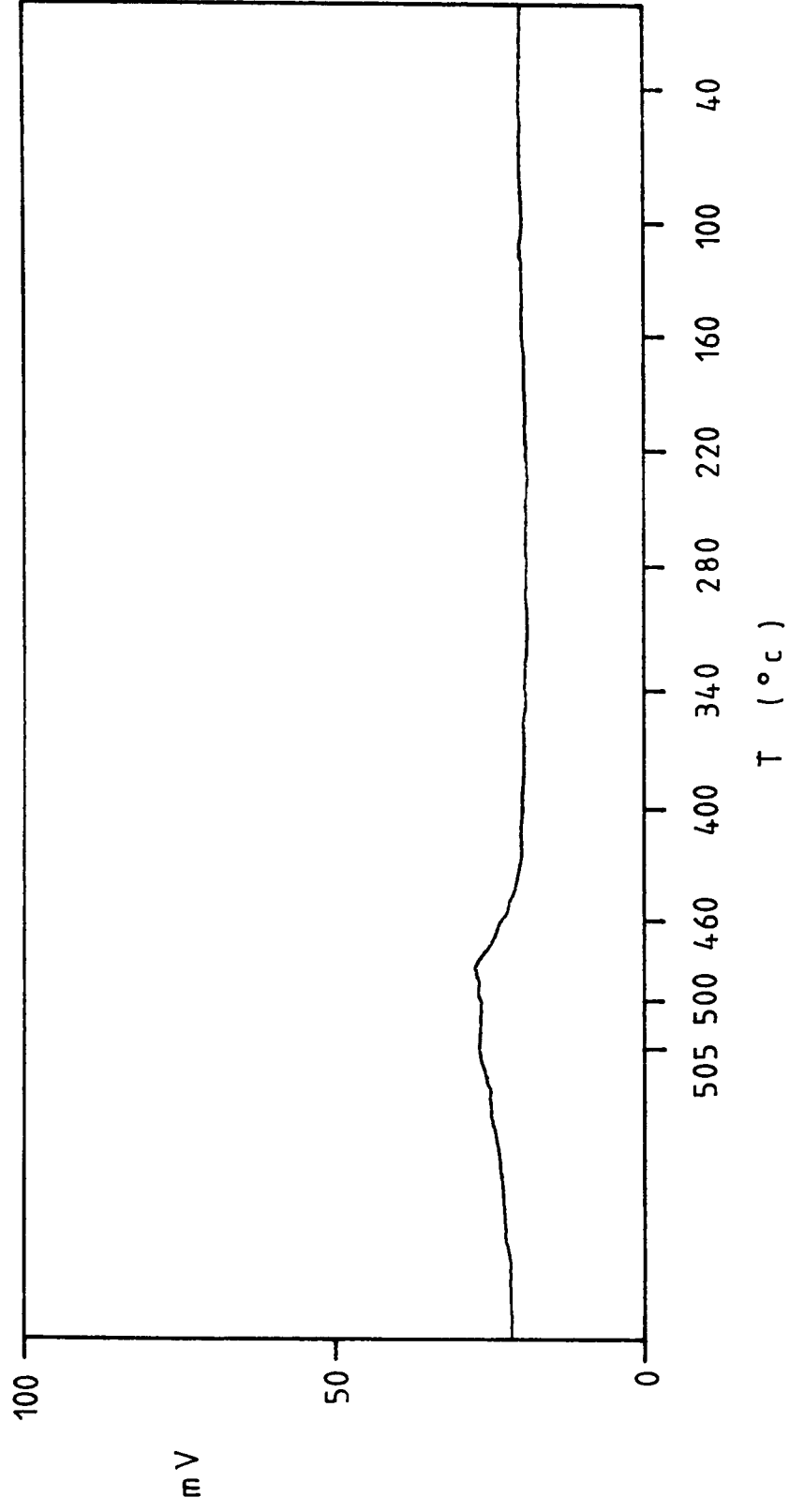
Fig.94. TPR trace for vanadyl etioporphyrin I.
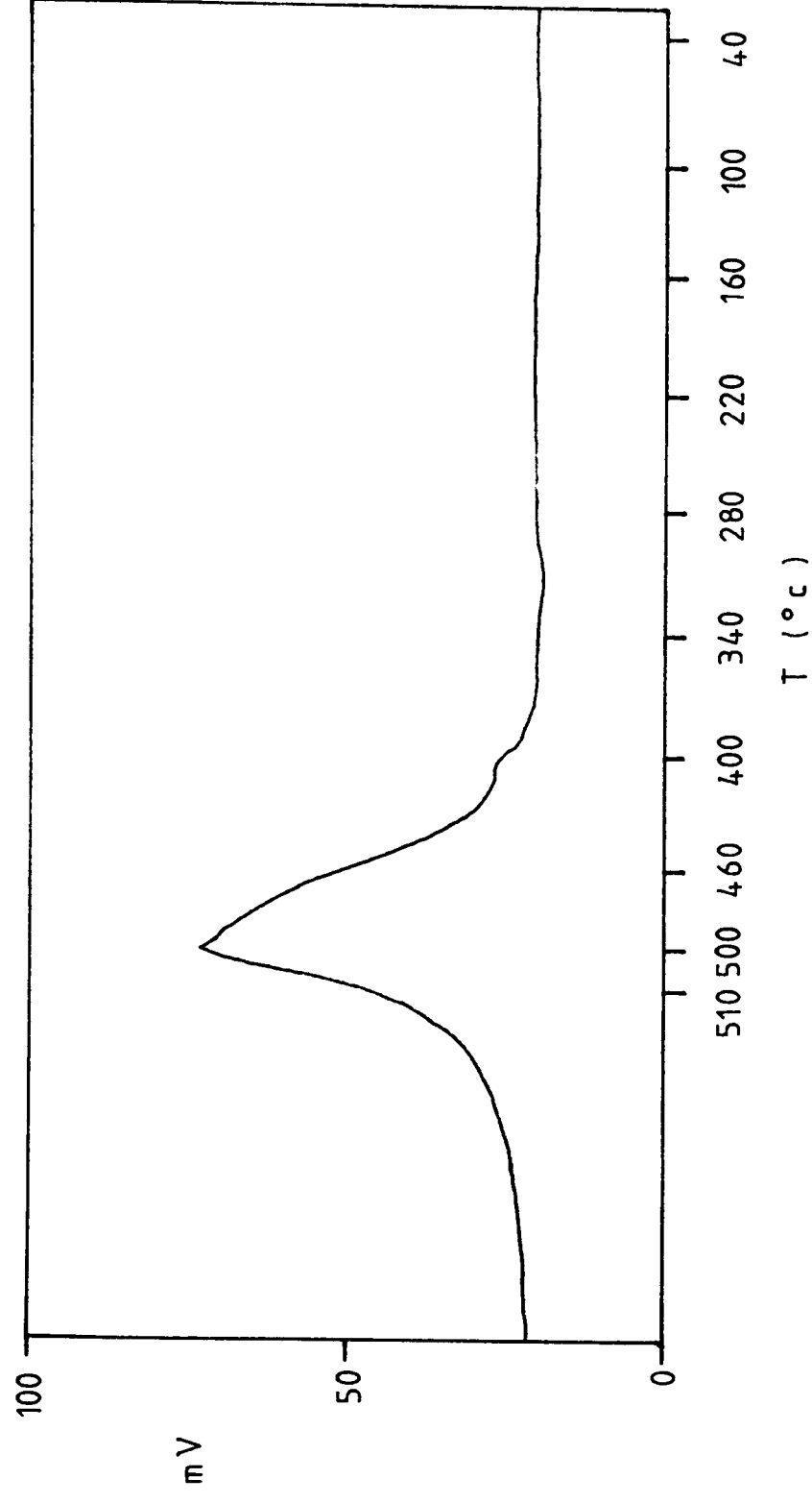
Fig.95.   TPR trace for nickel etioporphyrin I.
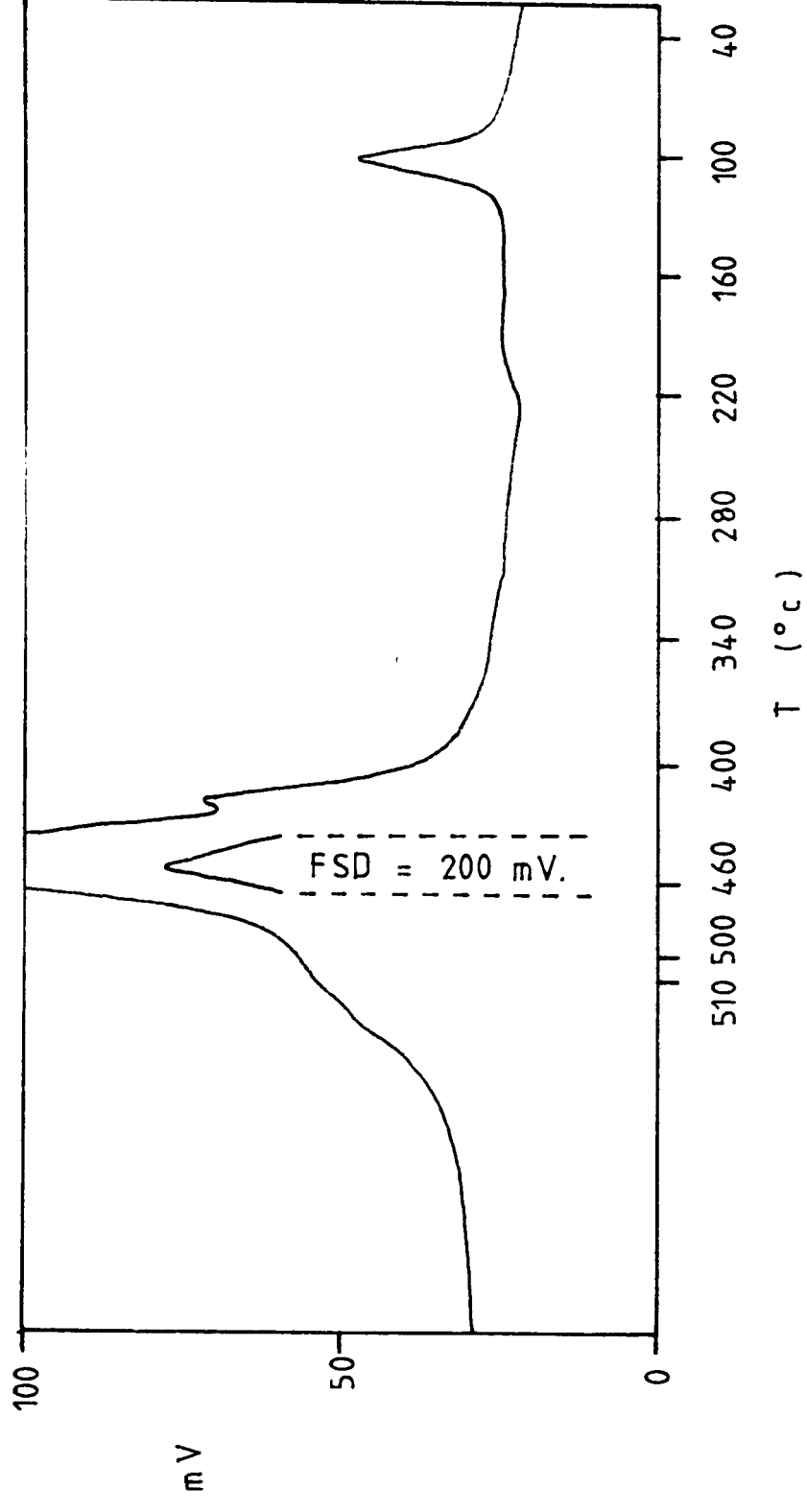
Fig. 96.   TPR trace for palladium etioporphyrin I.
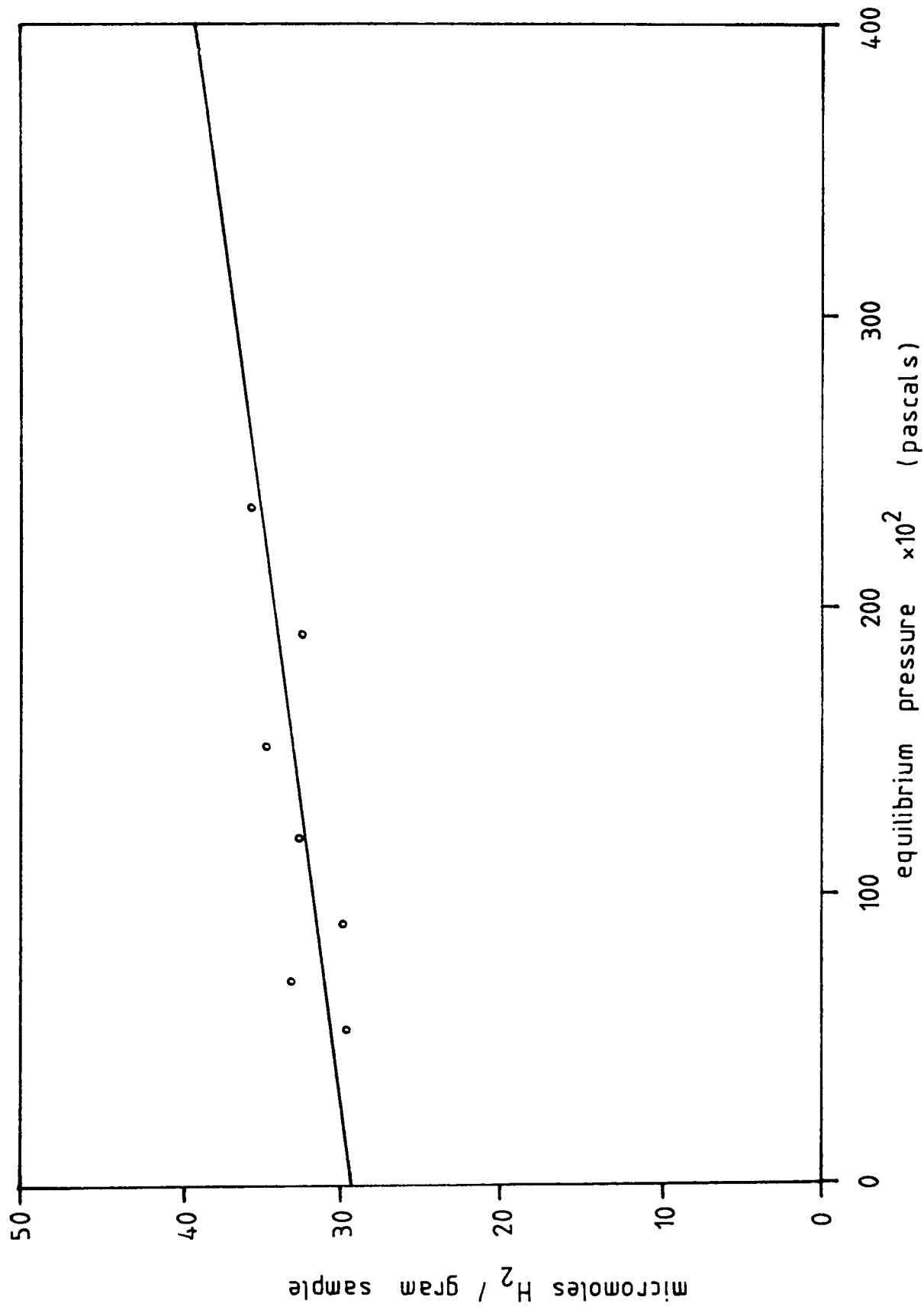
Fig. 27. Interpolation of linear region of hydrogen chemisorption graph to zero equilibrium pressure for synthetic nickel etioporphyrin.
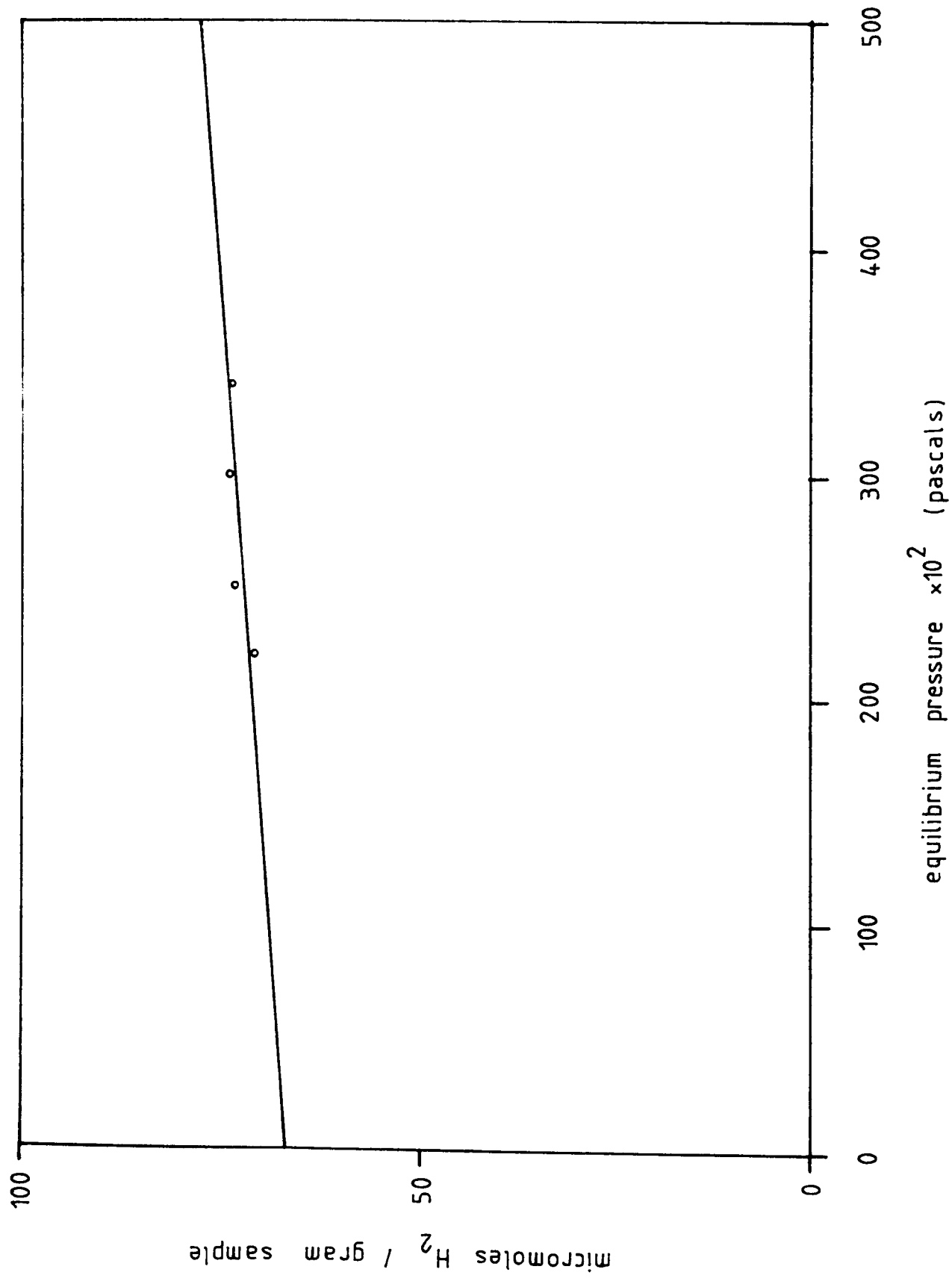
Fig. 98. Interpolation of linear region of hydrogen chemisorption graph to zero equilibrium pressure for 5.0% nickel etioporphyrin on silica.
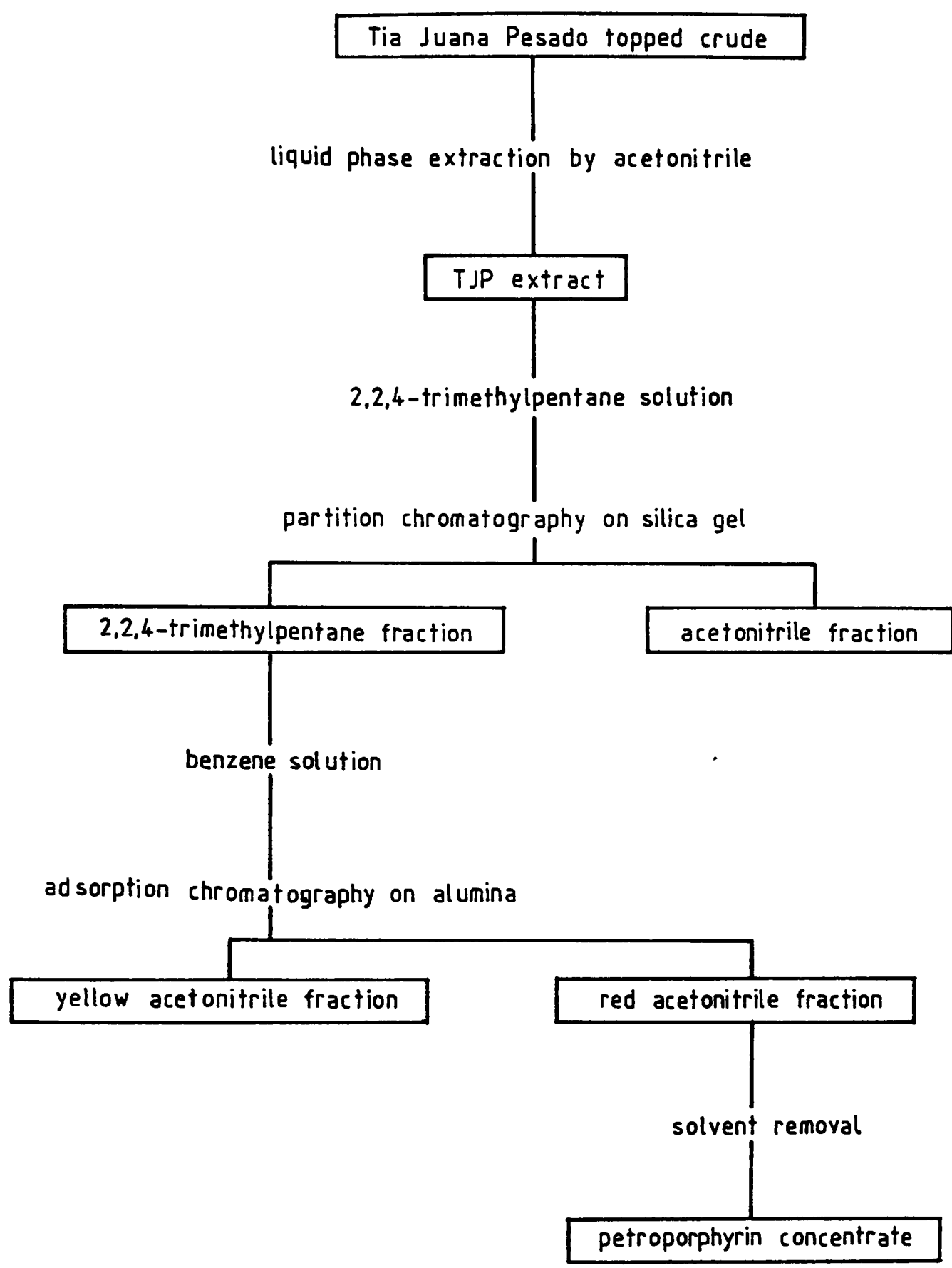
Fig. 99.   Scheme of separation and concentration of petroporphyrins
            from Tia Juana Pesado topped crude.

1. $C_4H_{10} \longrightarrow 2C_2H_5^{\bullet}$

2. $C_4H_{10} \longrightarrow CH_3^{\bullet} + C_3H_7^{\bullet}$

Fig.100. Initiation reactions for the thermal decomposition of n-butane.

3. $C_2H_5^{\bullet} \longrightarrow C_2H_4 + H^{\bullet}$

4. $C_3H_7^{\bullet} \longrightarrow C_3H_6 + H^{\bullet}$

5. $C_3H_7^{\bullet} \longrightarrow C_2H_4 + CH_3^{\bullet}$

6. $C_4H_9^{\bullet} \longrightarrow C_4H_8 + H^{\bullet}$

7. $C_4H_9^{\bullet} \longrightarrow C_3H_6 + CH_3^{\bullet}$

8. $C_4H_9^{\bullet} \longrightarrow C_2H_4 + C_2H_5^{\bullet}$

9. $C_4H_{10} + H^{\bullet} \longrightarrow C_4H_9^{\bullet} + H_2$

10. $C_4H_{10} + CH_3^{\bullet} \longrightarrow C_4H_9^{\bullet} + CH_4$

11. $C_4H_{10} + C_2H_5^{\bullet} \longrightarrow C_4H_9^{\bullet} + C_2H_6$

Fig.101.   Propagation or chain carrying reactions for
the thermal decomposition of n-butane.

12. $\overset{\bullet}{H} + \overset{\bullet}{H}$ $\longrightarrow$ H_2

13. $\overset{\bullet}{H} + \overset{\bullet}{CH_3}$ $\longrightarrow$ CH_4

14. $\overset{\bullet}{H} + \overset{\bullet}{C_2H_5}$ $\longrightarrow$ C_2H_6

15. $\overset{\bullet}{CH_3} + \overset{\bullet}{CH_3}$ $\longrightarrow$ C_2H_6

16. $\overset{\bullet}{CH_3} + \overset{\bullet}{C_2H_5}$ $\longrightarrow$ C_3H_8

17. $\overset{\bullet}{C_2H_5} \quad \overset{\bullet}{C_2H_5}$ $\longrightarrow$ C_4H_{10}
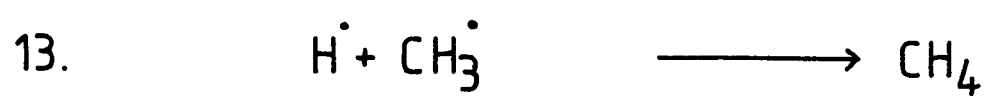
Fig.102. Chain termination reactions for the thermal decomposition of n-butane and 2,2-dimethylbutane.

1. $CH_3-\overset{\overset{\displaystyle CH_3}{|}}{\underset{\underset{\displaystyle CH_3}{|}}{C}}-CH_2CH_3 \longrightarrow CH_3-\overset{\overset{\displaystyle CH_3}{|}}{\underset{\underset{\displaystyle CH_3}{|}}{C}}-\overset{\bullet}{C}H_2 + \overset{\bullet}{C}H_3$

2. $CH_3-\overset{\overset{\displaystyle CH_3}{|}}{\underset{\underset{\displaystyle CH_3}{|}}{C}}-CH_2CH_3 \longrightarrow CH_3-\overset{\overset{\displaystyle CH_3}{|}}{\underset{\underset{\displaystyle CH_3}{|}}{\overset{\bullet}{C}}} + C_2\overset{\bullet}{H_5}$

3. $CH_3-\overset{\overset{\displaystyle CH_3}{|}}{\underset{\underset{\displaystyle CH_3}{|}}{C}}-CH_2CH_3 \longrightarrow CH_3-\overset{\overset{\displaystyle CH_3}{|}}{\underset{\underset{\displaystyle \bullet}{|}}{C}}-CH_2CH_3 + \overset{\bullet}{C}H_3$
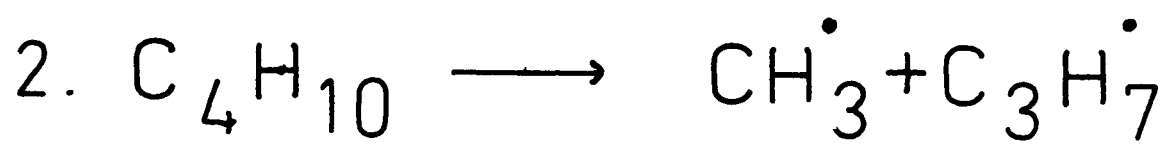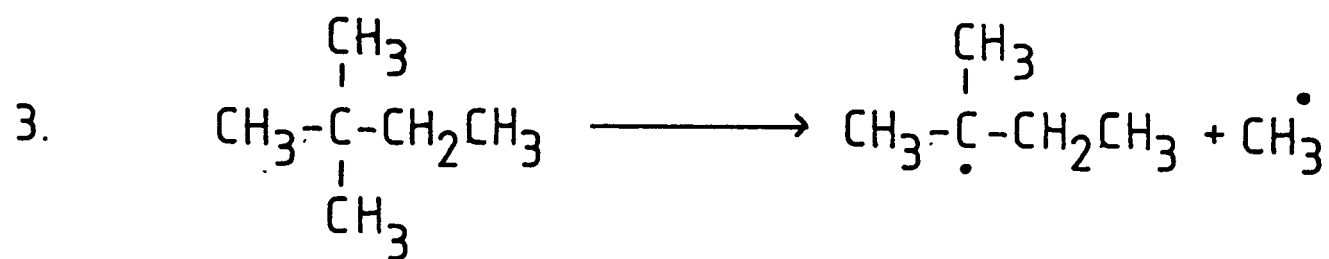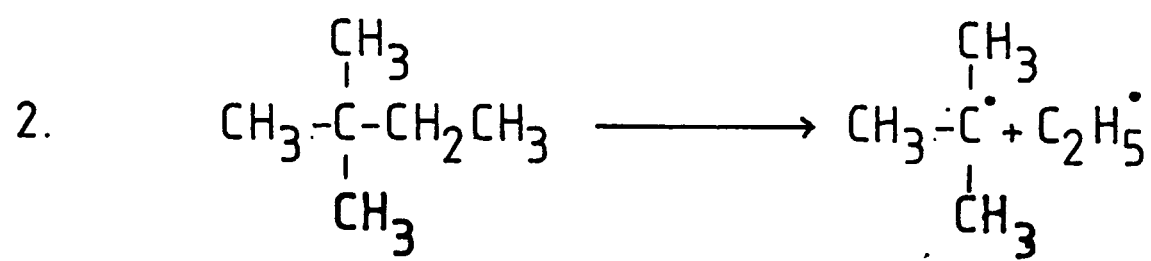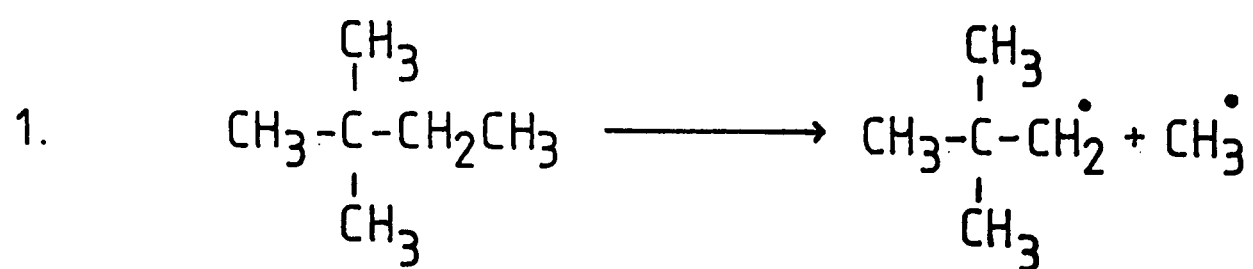
Fig.103. Initiation reactions for the thermal decomposition
of 2,2-dimethylbutane.

4. $\underset{\underset{CH_3}{|}}{\overset{\overset{CH_3}{|}}{CH_3-C-CH_2^\bullet}}$ $\longrightarrow$ $\underset{\underset{CH_3}{|}}{\overset{\overset{CH_2}{\|}}{CH_3-C}}$ $+ CH_3^\bullet$

5. $\underset{\underset{CH_3}{|}}{\overset{\overset{CH_3}{|}}{CH_3-C^\bullet}}$ $\longrightarrow$ $\underset{\underset{CH_3}{|}}{\overset{\overset{CH_2}{\|}}{CH_3-C}}$ $+ H^\bullet$

6. $\underset{\underset{\bullet}{}}{\overset{\overset{CH_3}{|}}{CH_3CH_2-C-CH_3}}$ $\longrightarrow$ $\overset{\overset{CH_3}{|}}{CH_3CH_2-C=CH_2}$ $+ H^\bullet$

7. $\underset{\underset{\bullet}{}}{\overset{\overset{CH_3}{|}}{CH_3CH_2-C-CH_3}}$ $\longrightarrow$ $\overset{\overset{CH_3}{|}}{CH_3CH=C-CH_3}$ $+ H^\bullet$

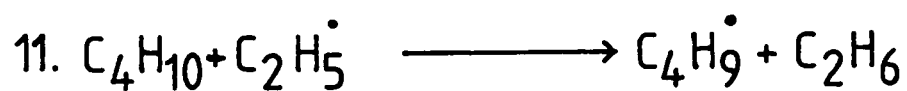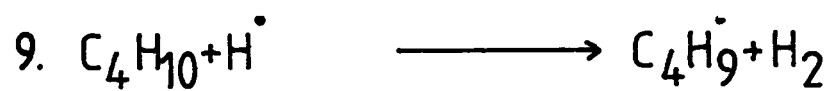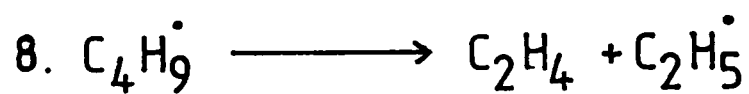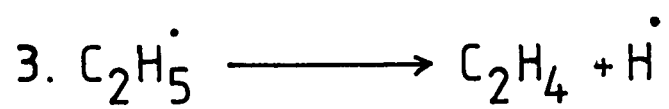8. $C_2H_5^\bullet$ $\longrightarrow$ $C_2H_4 + H^\bullet$
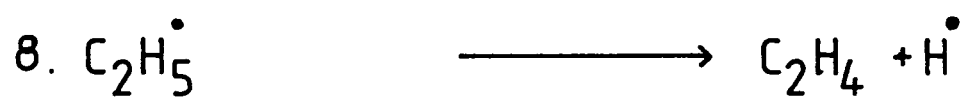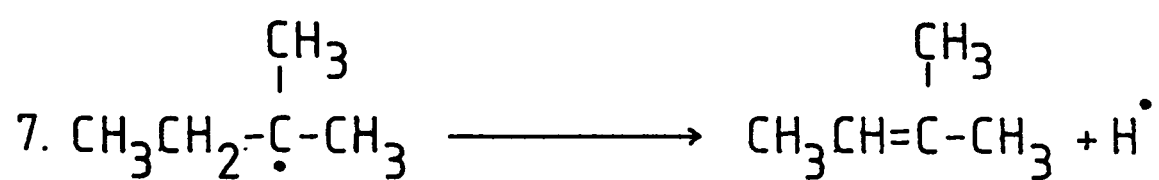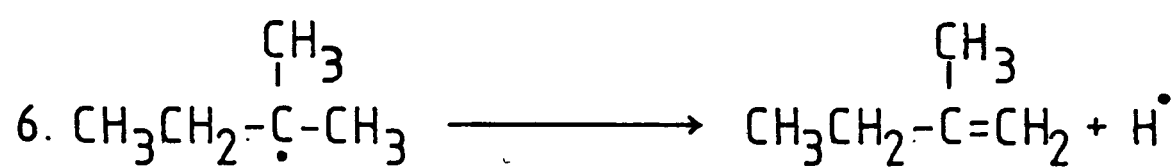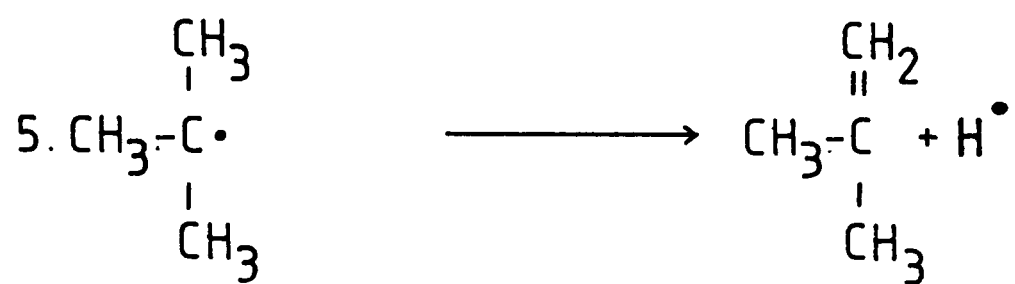
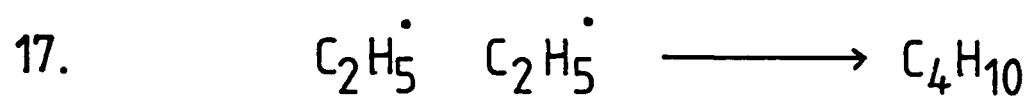Fig.104.Propagation or chain carrying reactions for the
thermal decomposition of 2,2-dimethylbutane.
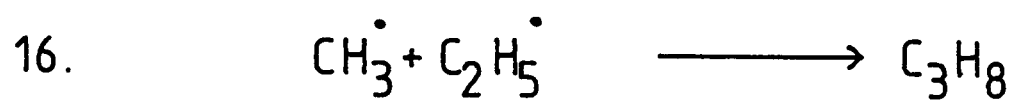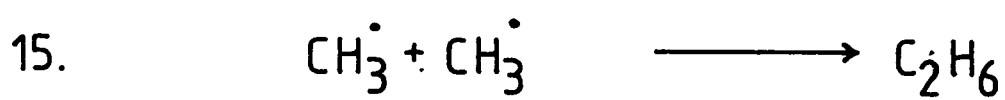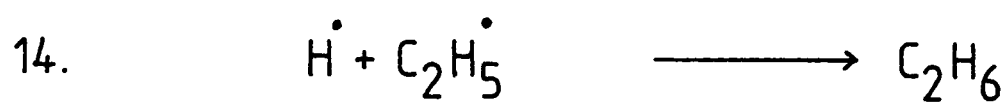
APPENDICES

Appendix No.

1.   ZX81 program for the calculation of hydrocarbon
      concentrations.

2.   Derivation of rate equation for the cracking of
      hydrocarbons.

3.   ZX81 program for the calculation of rate constant
      data for the cracking of hydrocarbons.

Appendix 1.   ZX81 program for the calculation of hydrocarbon concentrations

```
        "GC"

10      PRINT AT 5, 11; "AN IDC PROG"

20      PRINT " "

21      PRINT " "

22      PRINT " "

30      PRINT "           THIS PROG CALCULATES MOLE PERCENTAGES OF
        VARIOUS HYDROCARBONS FROM GC INTEGRATER READINGS"

31      PAUSE 200

32      CLS

40      REM F1  = METHANE FACTOR

50      REM F2  = ETHANE FACTOR

60      REM F3  = ETHENE FACTOR

70      REM F4  = PROPANE FACTOR

80      REM F5  = N-BUTANE FACTOR

90      REM F6  = PROPENE FACTOR

100     REM F7  = N-PENTANE FACTOR

110     REM F8  = N-BUTENE FACTOR

120     REM F9  = N-HEXANE FACTOR

130     REM F10 = 2-ME, BUTANE FACTOR

140     REM F11 = 2,2-DIMETHYLBUTANE FACTOR

150     LET F1  = 1.000

160     LET F2  = 2.033
```

```
17Ø        LET F3  = 1.872

18Ø        LET F4  = 2.596

19Ø        LET F5  = 3.Ø18

2ØØ        LET F6  = 2.966

21Ø        LET F7  = 2.819

22Ø        LET F8  = 3.535

23Ø        LET F9  = 3.989

24Ø        LET F1Ø = 5.161

25Ø        LET F11 = 6.88Ø

26Ø        PRINT "INPUT VALUE FOR METHANE"

27Ø        INPUT R1

271        CLS

28Ø        PRINT "INPUT VALUE FOR ETHANE"

29Ø        INPUT R2

291        CLS

3ØØ        PRINT "INPUT VALUE FOR ETHENE"

31Ø        INPUT R3

311        CLS

32Ø        PRINT "INPUT VALUE FOR PROPANE"

33Ø        INPUT R4

331.       CLS

34Ø        PRINT "INPUT VALUE FOR N-BUTANE"

35Ø        INPUT R5

36Ø        CLS

37Ø        PRINT "INPUT VALUE FOR PROPENE"

38Ø        INPUT R6

39Ø        CLS
```

```
400        PRINT "INPUT VALUE FOR N-PENTANE"

410        INPUT R7

420        CLS

430        PRINT "INPUT VALUE FOR N-BUTENE"

440        INPUT R8

450        CLS

460        PRINT "INPUT VALUE FOR N-HEXANE"

470        INPUT R9

480        CLS

490        PRINT "INPUT VALUE FOR 2-METHYLBUTANE"

500        INPUT R10

510        CLS

520        PRINT "INPUT VALUE FOR 2,2-DIME,BUTANE"

530        INPUT R11

535        PAUSE 75

536        CLS

537        LET N1  = 1

538        LET N2  = 2

539        LET N3  = 3

540        LET N4  = 4

541        LET N5  = 5

542        LET N6  = 6

543        LET N7  = 7

544        LET N8  = 8

545        LET N9  = 9

546        LET N10 = 10

547        LET N11 = 11
```

```
550     PRINT N1;   ".   METHANE          = "; R1
560     PRINT N2;   ".   ETHANE           = "; R2
570     PRINT N3;   ".   ETHENE           = "; R3
580     PRINT N4;   ".   PROPANE          = "; R4
590     PRINT N5;   ".   N-BUTANE         = "; R5
600     PRINT N6;   ".   PROPENE          = "; R6
610     PRINT N7;   ".   N-PENTANE        = "; R7
620     PRINT N8;   ".   N-BUTENE         = "; R8
630     PRINT N9;   ".   N-HEXANE         = "; R9
640     PRINT N10;  ".   2-METHYLBUTANE   = "; R10
650     PRINT N11;  ".   2,2-DIME,BUTANE  = ". R11
660     PRINT " "
670     PRINT " "
680     PRINT " "
690     PRINT "ARE THESE FIGURES CORRECT ?  Y/N"
700     INPUT B $
710     IF B $ = "N" THEN GOTO 711
711     IF B $ = "Y" THEN GOTO 891
712     PRINT " "
713     PRINT " "
720     PRINT "INPUT THE STATEMENT NUMBER THAT IS WRONG"
730     INPUT W
740     PRINT " "
750     PRINT " "
760     PRINT "INPUT THE CORRECT VALUE"
770     INPUT C
775     PAUSE 75
```

```
78Ø        CLS

79Ø        IF N1  = W THEN LET R1  = C

8ØØ        IF N2  = W THEN LET R2  = C

81Ø        IF N3  = W THEN LET R3  = C

82Ø        IF N4  = W THEN LET R4  = C

83Ø        IF N5  = W THEN LET R5  = C

84Ø        IF N6  = W THEN LET R6  = C

85Ø        IF N7  = W THEN LET R7  = C

86Ø        IF N8  = W THEN LET R8  = C

865        IF N9  = W THEN LET R9  = C

87Ø        IF N1Ø = W THEN LET R1Ø = C

88Ø        IF N11 = W THEN LET R11 = C

89Ø        GOTO 537

891        CLS

9ØØ        LET T1  = R1/F1

91Ø        LET T2  = R2/F2

92Ø        LET T3  = R3/F3

93Ø        LET T4  = R4/F4

94Ø        LET T5  = R5/F5

95Ø        LET T6  = R6/F6

96Ø        LET T7  = R7/F7

97Ø        LET T8  = R8/F8

98Ø        LET T9  = R9/F9

99Ø        LET T1Ø = R1Ø/F1Ø

1ØØØ       LET T11 = R11/F11

1Ø1Ø       LET GT = T1 + T2 + T3 + T4 + T5 + T6 + T7 + T8 + T9 + T1Ø + T11

1Ø2Ø       PRINT "TOTAL CORRECTED INTEGRATER READING = "; INT GT
```

```
1Ø3Ø      PRINT " "

1Ø4Ø      PRINT " "

1Ø5Ø      LET P1  = (T1/GT)   * 1ØØ

1Ø51      LET P2  = (T2/GT)   * 1ØØ

1Ø52      LET P3  = (T3/GT)   * 1ØØ

1Ø53      LET P4  = (T4/GT)   * 1ØØ

1Ø54      LET P5  = (T5/GT)   * 1ØØ

1Ø55      LET P6  = (T6/GT)   * 1ØØ

1Ø56      LET P7  = (T7/GT)   * 1ØØ

1Ø57      LET P8  = (T8/GT)   * 1ØØ

1Ø58      LET P9  = (T9/GT)   * 1ØØ

1Ø59      LET P1Ø = (T1Ø/GT)  * 1ØØ

1Ø6Ø      LET P11 = (T11/GT)  * 1ØØ

1Ø7Ø      LET P21 = (INT (P1  * 1ØØ)) / 1ØØ

1Ø71      LET P22 = (INT (P2  * 1ØØ)) / 1ØØ

1Ø72      LET P23 = (INT (P3  * 1ØØ)) / 1ØØ

1Ø73      LET P24 = (INT (P4  * 1ØØ)) / 1ØØ

1Ø74      LET P25 = (INT (P5  * 1ØØ)) / 1ØØ

1Ø75      LET P26 = (INT (P6  * 1ØØ)) / 1ØØ

1Ø76      LET P27 = (INT (P7  * 1ØØ)) / 1ØØ

1Ø77      LET P28 = (INT (P8  * 1ØØ)) / 1ØØ

1Ø78      LET P29 = (INT (P9  * 1ØØ)) / 1ØØ

1Ø79      LET P3Ø = (INT (P1Ø * 1ØØ)) / 1ØØ

1Ø8Ø      LET P31 = (INT (P11 * 1ØØ)) / 1ØØ

1Ø9Ø      LET TT = P21 + P22 + P23 + P24 + P25 + P26 + P27 + P28 + P29
          + P3Ø + P31
```

```
1160      PRINT "          COMPOUND          MOLE (PC)"

1170      PRINT " "

1180      PRINT "METHANE                "; P21

1190      PRINT "ETHANE                 "; P22

1200      PRINT "ETHENE                 "; P23

1210      PRINT "PROPANE                "; P24

1220      PRINT "N-BUTANE               "; P25

1230      PRINT "PROPENE                "; P26

1240      PRINT "N-PENTANE              "; P27

1250      PRINT "N-BUTENE               "; P28

1260      PRINT "N-HEXANE               "; P29

1270      PRINT "2-METHYLBUTANE         "; P30

1280      PRINT "2,2-DIME, BUTANE       "; P31

1285      PRINT AT 17, 18; " ----- "

1286      PRINT AT 18, 18; TT

1300      PRINT " "

1310      PRINT " "

1320      PRINT "PRESS ANY KEY TO CONT"

1330      INPUT C $

1340      IF C $ = " " THEN GOTO 1341

1350      CLS

9970      PRINT " "

9971      PRINT " "

9972      PRINT " "

9973      PRINT "ANY MORE DATA ?"

9974      PRINT "INPUT  Y/N"

9975      INPUT A $
```

```
9976    CLS
9977    IF A $ = "Y" THEN GOTO 40
9978    IF A $ = " " THEN GOTO 9979
9979    CLS
9980    PRINT AT 11, 11;  "ALL DONE"
9983    PRINT AT 14, 11;  "THANK YOU"
9984    STOP
```

Appendix 2.   Derivation of rate equation for the cracking

of hydrocarbons (173)

Consider the following reaction scheme :-

$$A_1 + S_1 \longrightarrow V_1 R_1 + V_2 R_2 + v_3 R_3 \ldots\ldots\ldots S_1 \qquad (1)$$
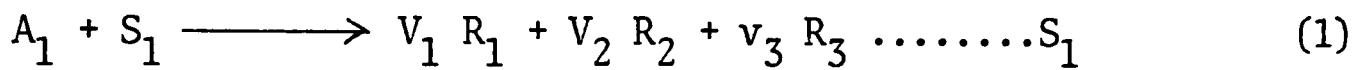
where:- A_1 =   A hydrocarbon

S_1 =   An inert substance

$R_{1,2,3}$ =   Reaction products

$v_{1,2,3}$ =   Stoichiometric coefficient of product formed

from one mole of hydrocarbon

The total number of moles and the volume of the mixture fed
into the reactor in unit time are:-

(for the total number of moles)

$$\Sigma\, n^o = n_1^o + S_1 = n_1^o\, (1 + s_1)$$

where:- n^o = total number of moles fed into the reactor.

n_1^o = quantity of hydrocarbon A_1 (mole sec^{-1}).

S_1 = quantity of inert substance S_1 (mole sec^{-1}).

s_1 = S_1/n_1^o = relative quantity of inert substance.

and :-

(for volume of mixture)

$$Bo = n_1^o \frac{RT}{P} \ (1 + s_1)$$

where:- Bo = Volume velocity of mixture fed into the reactor at

temperature = T and pressure = P

(Bo in units of $cm^3 \ sec^{-1}$)

The total number of moles and the volume of the mixture leaving the reactor in unit time at a certain conversion of the initial hydrocarbon A_1 are:-

(for the total number of moles)

$$\Sigma \ n = n_1 + \Sigma \ mi + S_1 = n_1^o \ [(1-x) + \Sigma \ vi \ x + s_1]$$

where: n = number of moles of mixture leaving the reactor in unit time.

n_1 = quantity of hydrocarbon, A_1, in the mixture leaving the reactor (mol sec^{-1})

mi = quantity of reaction product, Ri, in mixture leaving the reactor (mol sec^{-1})

x = degree of conversion

$\Sigma vi = v_1 + v_2$ .... sum of stoichiometric coefficients of the products

and :-

(for volume of mixture)

$$B = n_1^O \frac{RT}{P} \; \mathit{[}1 + s_1 + (\Sigma \; vi - 1) \; x\mathit{]} \qquad (2)$$

$$= Bo + n_1^O \frac{RT}{P} \; \mathit{[}\Sigma \; vi - 1\mathit{]} \; x$$

where:-   B = Volume velocity of mixture leaving the reactor in unit

time at temperature = T and pressure = P

(B in units of $cm^3 \; sec^{-1}$)

For gas reactions occurring with an overall change in the
mole number, the volume of the reaction mixture changes as the reaction
proceeds. This change can be expressed as the ratio of the mole number
of the mixture leaving the reactor to that fed in, or, in the case of
an isothermal, isobaric reactor, by the ratio of the volumes of this
mixture such that the ratio = expansion = E.

$$E = \Sigma n = B \qquad (3)$$

$$\Sigma n^o = Bo$$

$$= \frac{n_1^o \frac{RT}{P} (1 + s_1) + n_1^o \frac{RT}{P} [\Sigma vi - 1] x}{n_1^o \frac{RT}{P} (1 + s_1)} \qquad (4)$$

$$= 1 + (Ev - 1) x \qquad (5)$$

where:- $Ev = E$ when $x = 1$

$$Ev = 1 + \frac{\Sigma vi - 1}{1 + s_1} \qquad (6)$$

From equation (5) it can be seen that expansion changes linearly with conversion if Ev is constant. This condition holds only for simple reactions proceeding via a given stoichiometric equation, where the value of Ev can be calculated if the stoichiometric co-efficients and the quantity of inert substance are both known.

In the pyrolysis of hydrocarbons the overall stoichiometry of the reaction is dependent on the degree of conversion (due to secondary reactions). Therefore Ev is not constant and the function E(x) is not linear. However it can be experimentally shown that expansion is highly independent of temperature and that in the range $0<x<0.4$ the plot of E vs x is linear, showing that at low degrees of conversion primary decomposition reactions predominate.

Thus, from values of E, the value of Ev corresponding to a given degree of conversion can be calculated from:-

$$Ev = \frac{E - 1}{x} + 1$$

The concentrations of the single components in the reactor feed and effluent can be calculated thus:-

$$C_1^o = \frac{n_1^o}{Bo} = \frac{P}{RT\ (1-s_1)}$$

where:- C_1^o = molar concentration of hydrocarbon, A_1, in reactor feed.

$$C_1 = \frac{n_1}{B} = \frac{n_1^o\ (1-x)}{n_1^o\ \frac{RT}{P}\ [1 + s_1 + (\Sigma\ vi-1)\ x]} = \frac{C_1^o\ (1-x)}{1 + (Ev-1)\ x} \qquad (7)$$

where:- C_1 = molar concentration of hydrocarbon, A_1, in reactor effluent.

$$C_{Ri} = \frac{mi}{B} = \frac{n_1^o\ vi\ x}{n_1^o\ \frac{RT}{P}\ [1 + s_1 + (\Sigma\ vi-1)\ x]} = \frac{C_1^o\ vi\ x}{1 + (Ev-1)\ x}$$

where C_{Ri} = molar concentration of product, Ri, in reactor effluent.

If the actual concentration of the hydrocarbon, A_1, is known, the rate of conversion, (according to the reaction scheme (1)), can be written as:-

$$r = kC_1^n = k \left[\frac{C_1^0 \ (1-x)}{1 + (Ev-1)x} \right]^n \qquad (8)$$

where:- r = reaction rate, as quantity of A_1 decomposing in unit time in unit volume of the reactor.

k = temperature dependent rate constant.

n = exponent determining the overall reaction order.

However, if the stationary state hypothesis is applied to the reactor, the reaction rate is determined by the change in mole number occurring in unit time in a volume element, dV_R, of the reactor. Considering that no accumulation of substance can take place in the volume element, dV_R, the following expression applies:-

$$r dV_R = -dn_1 \qquad (9)$$

where n_1 can be defined as follows:-

From equation (5) where $E = 1 + (Ev-1)x$

and equation (7) where $C_1 = \dfrac{C_1^o (1-x)}{1 + (Ev-1)x} = \dfrac{n_1}{B}$

$$n_1 = \frac{B \; C_1^o (1-x)}{1 + (Ev-1)x}$$

$$n_1 = \frac{B}{E} \; C_1^o (1-x)$$

From equation (3) where $E = \dfrac{B}{Bo}$

$$n_1 = Bo \; C_1^o (1-x) \tag{10}$$

This represents the quantity of hydrocarbon, A_1, (in moles) entering the volume element, dV_R, in unit time.

From equation (10), by differentiation

$$dn_1 = -Bo \; C_1^o \; dx \tag{11}$$

when equation (11) is substituted into equation (9)

$$rdV_R = Bo \; C_1^o \; dx$$

therefore $\dfrac{dV_R}{Bo} = C_1^o \dfrac{dx}{r} = dw \tag{12}$

If no change in volume (and consequently mole number) occurs during the reaction, the volume flow rate is constant, and its value is the same as that of the feed rate, Bo, (in an isothermal, isobaric reactor). In this case the ratio V_R/Bo (dimension = time) gives the average time the gas takes to travel through the reactor.

If the reaction is accompanied by a mole number change, the volume of the reaction mixture and the volume flow rate will change as a function of conversion. In this case the ratio V_R/Bo will not be identical to the average time the gas takes to travel through the reactor and is thus called the fictive reaction time, denoted by w.

When the reactor volume and feed paramaters are known w can be calculated. Therefore, in chemical engineering, measured data (e.g. conversion curves) are usually plotted as a function of w or $1/w$ = the space velocity.

When the rate expression is written as a function of w, exact expressions suitable for the calculation of rate constants and conversion curves are obtained.

The actual (average) reaction time for gas reactions proceeding via a change in mole number can be expressed by the ratio of the isothermal reactor zone and the average volume velocity relating to this reaction zone such that:-

$$\tau = \frac{V_R}{\bar{B}} \qquad (13)$$

where:- τ = actual (average) reaction time (sec).

V_R = volume of isothermal reaction zone (cm^3).

$\bar{B}$ = average volume velocity of reaction mixture in reactor $(cm^3 sec^{-1})$.

$\bar{B}$ is calculated as the arithmetic mean of the volume velocities relating to the reactor inlet and outlet, thus:-

$$\bar{B} = \frac{Bo + B}{2}$$

The linear velocity of the reaction mixture at any given section of the tube reactor is:-

$$u = \frac{dl}{d\tau}$$

where:- l = the distance covered by the reaction mixture in
time = τ
(plug flow assumed)

Writing this equation in terms of volume velocity from equation (12) and introducing equation (3).

From (12) $dw = \frac{dV_R}{Bo}$ divide both sides by E

so $\frac{dw}{E} = \frac{dV_R}{BoE}$ from equation (3) - BoE = B

$\frac{dw}{E} = \frac{dV_R}{B}$

Thus from equation (13) where $\tau = \dfrac{V_R}{B}$

$$\frac{dw}{E} = d\tau \qquad (14)$$

The actual reaction time is obtained by the integration of the differential equation, (14), such that:-

$$\tau = \int_{o}^{W} \frac{dw}{E} \qquad (15)$$

The rate equation can now be written both as a function of the fictive and actual reaction time.

On substituting the reaction rate, as given by equation (8), into the fundamental equation for flow reactors, (12), the following expression for the change of conversion as a function of fictive reaction time is obtained.

From equation (12) where $C_1^o \dfrac{dx}{r} = dw$

$$\frac{dx}{dw} = \frac{r}{C_1^o}$$

From equation (8) where $r = k \left[\dfrac{C_1^o (1-x)}{1 + (Ev-1)x} \right]^n$

combining the two yields

$$\frac{dx}{dw} = \frac{k}{C_1^o} \left[\frac{C_1^o (1-x)}{1 + (Ev-1)x} \right]^n \qquad (16)$$

For actual reaction time

From equation (5) where $E = 1 + (Ev-1)x$

and equation (14) where $d\tau = \dfrac{dw}{E}$

by substituting equation (5) into equation (14)

$$d\tau = \frac{dw}{1 + (Ev-1)x}$$

Thus $dw = d\tau \; [1 + (Ev-1)x]$

substituting this equation into equation (16) gives:-

$$\frac{dx}{d\tau \; [1 + (Ev-1)x]} = \frac{k}{C_1^O} \left[\frac{C_1^O \; (1-x)}{1 + (Ev-1)x} \right]^n$$

Thus $\qquad \dfrac{dx}{d\tau} = \dfrac{k}{C_1^O} \left[\dfrac{C_1^O \; (1-x)}{1 + (Ev-1)x} \right]^n \; [1 + (Ev-1)x] \qquad\qquad$ (17)

Thus, for the determination of the overall decomposition rate it is possible to begin from either equation (16) or equation (17).

The thermal decomposition of hydrocarbons can be treated, with good approximation, as a first order reaction.

By rearrangement of equation (16) for the condition $n = 1$ the following is obtained. (For fictive time).

$$dw = \frac{1 + (Ev-1)x}{k_1 (1-x)} dx$$

where k_1 = The first order rate constant.

Integration, with Ev constant, yields:-

$$k_1 w = Ev \ln \frac{1}{1-x} - (Ev-1)x \qquad (18)$$

This equation takes into account the fact that the inert diluting substance will change the product concentration (included in the Ev value according to equation (6)).

From equation (17), when n = 1, the following differential equation is obtained. (For actual reaction time).

equation (17) is:-

$$\frac{dx}{d\tau} = \frac{k_1}{C_1^0} \cdot \frac{C_1^0 (1-x)}{1 + (Ev-1)x} \cdot [1 + (Ev-1)x] \quad \text{when } n = 1$$

Thus
$$\frac{dx}{d\tau} = k_1 (1-x)$$

and
$$d\tau = \frac{dx}{k_1 (1-x)}$$

which upon integration yields:-

$$k_1 \tau = \ln \frac{1}{1-x} \quad (19)$$

If it is assumed that overall, the decomposition reaction is first order, then the value of the rate constants can be calculated from the integrated equations (18) and (19).

Equation (18) gives exact values only if the condition Ev = constant holds true, thus equation (19) is more generally applicable.

If the values for the rate constants, calculated according to equation (19), are plotted against the degree of conversion, it can be seen that the value of k_1 (calculated on the basis of first order kinetics) decreases with increasing x. In addition, the rate of decrease was noted to be temperature dependent.

This may be explained in two ways:-

1. If n does not equal unity then the overall reaction cannot be considered to be first order.

2. Reaction products restrain the reaction.

In the pyrolysis of ethane and propane it was noticed that the value of the rate constants, calculated from a first order kinetic relationship, decreased with an increasing degree of conversion. The conclusion was drawn that the reaction products, primarily propene, inhibit the decomposition of the initial hydrocarbon.

Thus, as it stands, equation (19) is not suitable, in its present form, for the calculation of rate constants for the thermal decomposition of hydrocarbons. However, by the introduction of an empirical constant, to take into account the inhibiting effect of the reaction products, an equation suitable for the calculation of rate constants is obtained, thus:-

$$k_1^o = \frac{2.303}{\tau} \log \frac{1}{1-x} + \beta x$$

where k_1^o = first order rate constant (at a given temperature) extrapolated to zero conversion.

β = The restraining coefficient (this constant is temperature dependent).

Appendix 3.   ZX81 program for the calculation of rate constant

data for the cracking of hydrocarbons

"K"

```
10      PRINT AT 11, 9; "AN IDC PROG"

20      PRINT " "

30      PRINT " "

40      PRINT "THIS IS A KINETICS MODEL FOR THE FIRST ORDER PYROLYSIS
        OF HYDROCARBONS"

50      PAUSE 150

60      CLS

70      REM EQUATIONS FOR THE MODEL FOLLOW

71      REM

72      REM

75      REM K1 = (BØ/VR). K

80      REM K  = G.LN(1/1-X) - (G-1).X

90      REM WHERE K1 = 1ST ORDER RATE CONST (SEC-1)

100     REM        X = DEGREE OF CONVERTION (AS A FRACTION EG 0.5)

110     REM        G = (E-1/X) + 1

120     REM        E = EXPANSION

130     REM        E = N/NØ

140     REM        N = TOTAL NO MOLES HYDROCARBON LEAVING REACTOR

150     REM        NØ = TOTAL NO MOLES HYDROCARBON ENTERING REACTOR

160     REM N IS EQUIV TO ADJUSTED INTEGRATER READING AFTER CRACKING

170     REM NØ IS EQUIV TO ADJUSTED INTEGRATER READING BEFORE CRACKING

171     REM

172     REM
```

```
18Ø     REM KØ = (2.3O3/T) LOG (1/1-X) + B.X

19Ø     REM WHERE KØ = 1ST ORDER RATE CONST (AT A GIVEN TEMP) EXTRAP

        TO ZERO CONVERT (SEC-1)

2ØØ     REM        T = (1/K1) LN (1/1-X)

21Ø     REM        B = THE RESTRAINING COEFT

22Ø     REM        T = ACTUAL (AV) REACTION TIME (SEC-1)

23Ø     REM

24Ø     REM

242     PRINT "INPUT VOLUME VELOCITY OF MIXTURE FED INTO REACTOR

        (CC/SEC)"

244     INPUT BØ

245     CLS

246     LET VR = Ø.38

248     PRINT "INPUT ADJUSTED INTEGRATER READING AFTER CRACKING"

25Ø     INPUT N

251     CLS

252     PRINT "INPUT ADJUSTED INTEGRATER READING BEFORE CRACKING"

254     INPUT NØ

255     CLS

256     PRINT "INPUT EXTENT OF CONVERTION"

258     INPUT X

259     CLS

26Ø     PRINT "INPUT THE RESTRAINING COEFT"

262     INPUT B

263     PAUSE 5O

264     CLS

29Ø     LET E = N/NØ

295     LET G = ((E-1)/X) + 1
```

```
300     LET K = (G*(LN(1/(1-X)))) - ((G-1)*X)

305     LET K1 = (B0/VR)*K

310     LET T = (1/K1)*LN(1/(1-X))

315     LET K0 = ((2.303/T)*((LN(1/(1-X)))* 2.303)) + (B*X)

316     PRINT "K1 = "; K1

317     PRINT "E  = "; E

318     PRINT "T  = "; T

320     PRINT "THE FIRST ORDER RATE CONSTANT FOR THIS REACTION
        IS  ";K0;" (SEC-1)"
```

REFERENCES

1.   Eleventh World Petroleum Congress. London. 1983. Panel

      Discussion.   Paper PD 8.

2.   The Institute of Heavy Oil Processing. Heavy Oil Processing

      Handbook. Tokyo. Japan.   The Chemical Daily Co. Ltd. 1982.

3.   Aalund,   L.R.   Oil and Gas J., 1978, 76, 56.

4.   Chakraborty, S. and Virendra, K.B.   Research and Industry,

      1980, 25(2), 88-91.

      GRAY, A.M. AND LIVINGSTON, W.B.
5.   Eccles,   R.M., Oil and Gas J., 1982, 80, 121.

      STOLFA.F., HUTCHINGS,L.E., JACOBS,W.L. AND BURTON.V.P.
6.   Sikonia, J.G., Oil and Gas J., 1981, 79, 141.

      BULLINGTON.L.A., EDIT JR,C.M. AND GRGURICH.O.A.
7.   Lipuma, C.R., Selecting the right bottoms conversion

      process.   Eleventh World Petroleum Congress.   London.   1983.

8.   Tominaga, H. and Kunugi, T. Internat. Chem.Eng., 1974, 14(4),

      753.

9.   Hines, J.C. and Peniston-Bird, M.L.   Chemical Process

      Engineering, 1963, 44, 726.

10.   BS 2000 : Part 143 : 1983.

11.   Erdman, J.G. and Harju, P.H.,   J. Chem. Eng. Data, 1963, 8(2),

      252-8.

12.   Stewart, D., Ph.D. thesis, Heriot-Watt University, 1983.

13.   Skinner, D.A., Ind. Eng. Chem., 1952, 44, 1159-65.

14.   Gurwitsch, L. and Moore, H.,   The Scientific Principles of

        Petroleum Technology.   London.   Chapman and Hall.   1932.

        CO-AUTHORS NOT CITED.   July 22.

15.   Ray, B.R., ⎰   Chem. Eng. News, 1957, 35, 28.

16.   Yen, T.F., The role of Trace Metals in Petroleum.   Ann Arbor,

        Michigan.   Ann Arbor Science.   1975.

17.   Filby, R.H., Am. Chem. Soc., Div. Petrol. Chem., Preprints,

        1973, 18(4), 630-43.

18.   Rosscup, R.J. and Bowman, D.H., Symposium on Asphaltenes and

        Metals in Petroleum., Am. Chem. Soc., Div Petrol. Chem.,

        1967, A77-A81.

19.   Moghadam, P.E. and Raisszadeh, M.A.,   Proceedings of Fifth Int.

        Cong. Met. Corros. 1972, 1035-8.

20.   Barwise, A.J.G. and Whitehead, E.V., Am. Chem. Soc., Div.

        Petrol. Chem., Preprints, 1980, 25(2), 268-79.

        KUBELKA,V. AND WEISSER.O.

21.   Sebor, G., ⎰   Collect. Czech. Chem. Commun., 1979, 44(2),

        551-7.

22.   Yen, T.F.   Symposium on the Role of Trace Metals in Petroleum.,

        Am. Chem. Soc., Div. Petrol. Chem., 1973, 648-51.

        WEISSER.O. AND SESULKA.V.

23.   Sebor, G., ⎰   ' . Riv. dei Combust., 1975, 29(9), 380-6.

        BOUCHER·L.J.,DICKIE.J.P.,TYNAN.E.C. AND VAUGHAN.G.B.

24.   Yen, T.F., ⎰   - . J. Inst. Petrol., 1969, 55, 87-99.

        BRANTHAVER.J.F.,WU.G.Y. AND WEATHERBEE.C.

25.   Sugihara, J.M., ⎰⸲-   Am. Chem. Soc., Div. Petrol. Chem.,

        Preprints., 1970, 15(2), C5-C12.

26.   Lakatos-Szabo, J. Acta Chim. Acad. Sci. Hung., 1978, 98(1),

        1-11.

27. Hodgson, G.W., PEAKE.E. AND BAKER.B.L. Research Council Alberta, Canada., 1963, Information Series No. 45, 75-100.

28. Zul'fugarly, D.I., KUKLINSKII.A.Y., ORLENKO.S.F. AND PUSHKINA.R.A. Azerb. Khim. Zh., 1976, (6), 119-26.

29. Babeav, F.R. Dokl. Akad. Nauk. Az. SSR., 1980, 36(2), 60-2.

30. Babaev, F.R. Azerb. Neft. Khoz., 1975, (3), 20-2.

31. Barwise, A.J.G. and Whitehead, E.V. Phys. Chem. Earth, 1980, 12, 181-92.

32. Hodgson, G.W. Bull. Am. Assoc. Petrol. Geol., 1954, 38, 2537-54.

33. deS Brasunas, A. Corrosion, 1955, 11, 17-18.

34. Beach, L.K. and Shewmaker, J.E. Ind. Eng. Chem., 1957, 49, 1157-64.

35. Erdman, J.G., RAMSEY.V.G. AND HANSON.W.E. Science, 1956, 123, 502.

36. Dunning, H.N. and Rabon, N.A. Ind. Eng. Chem., 1956, 48, 951-5.

37. Hampel, C.A., ed. and Hawley, G.G., ed. The Encyclopeadia of Chemistry. 3rd edition. New York. Van Nostrand Reinhold. 1973.

38. Fisher, L.R. and Dunning, H.N. U.S. Bur. Mines., Report Investigation No. 5844, 1961.

39. Hodgson, G.W., BAKER.B.L. AND PEAKE.E., Fundam. Aspects. Petroleum. Geochem., 1967, 177-259.

40. Morrison, R.T. and Boyd, R.N. Organic Chemistry. Boston. Allyn and Bacon. 1976.

41. Palmer, M.H. The Structure and Reactions of Heterocyclic Compounds. London. Edward Arnold. 1967.

42.   Webb, L.E. and Fleischer, E.B.   J.Am. Chem. Soc., 1965, _87_,
        667.

43.   Fleischer, E.B.   Accounts Chem. Res., 1970, _3_, 105.

44.   Molinaro, F.S. and Ibers, J.A.   Inorg. Chem., 1976, _15_(9),
        2278-83.

45.   Fleischer, E.B.   J.Am. Chem. Soc., 1963, _85_, 146.

46.   Storm, C.B.   J. Am. Chem. Soc., 1970, _92_, 1424-5.

47.   Morandi, J.R. and Jensen, H.B.   J.Chem. Eng Data, 1966,
        _11_(1), 81-8.

48.   BRENER.P., NORO.K. AND NORO.T.
        Bonnett, R.,   Tetrahedron, 1978, _34_(3), 379-85.

49.   ALTURKI,Y.I.A., PILLINGER.C.T.AND EGLINTON.G.,
        Didyk, B.,   Chem. Geol., 1975, _15_(3), 193-208.

50.   Ueno, K. and Martell, A.E.   J. Phys. Chem., 1956, _60_, 934-8.

51.   ARICH.G. AND LOMI.C.
        Costantinides , G.,   Fifth World Petroleum Congress.
        New York. 1959. Section _V_.   Paper No. 11.

52.   Warren, H.W.   Anal. Chem., 1961, _33_, 255-60.

53.   Dolphin, D.   The Porphyrins. Vol. 1.   Part. A.   Structure and
        Synthesis.   New York.   Academic Press.   1978.

54.   Golebiowski, S.   Przegl. Geol., 1971, _19_(5), 237-42.

55.   Serbanescu, A. Petrol. Gaze., 1968, _19_(2), 116-22.

56.   Erdman, J.G. and Harju, P.H.   Am. Chem. Soc., Div. Petrol. Chem.,
        1962, Gen. Pap. 7, 43-56.

57.   YEN.T.F., DICKIE.J.P, RHODES.R.E. AND CLARK.L.F.
        Baker, E.W.,   Symposium on Asphaltenes and Metals in
        Petroleum., Am. Chem. Soc., Div. Petrol. Chem., April 9-14,

1967, A59-A71.

58.   Bonner, W.H. Jr. U.S. Pat. 2,740, 794.

59.   FLORES.J. AND BAKER.B.L.
Hodgson, G.W., . Geochim. Cosmochim. Acta, 1969, 33(4),

532-5.

60.   Corwin, A.H. Fifth World Petroleum Congress. New York. 1959.

Section V. Paper 10.

61.   ANTIPENKO.V.R., SUBOCH.V.P. AND TITOV.V.I.
Serebrennikova, O.V., . Neftekhimiya, 1975, 15(6),

909-16.

62.   Treibs, A. Annalen, 1934, 517, 103-114.

63.   Sugihara, J.M. and Bean, R.M. J. Chem. Eng. Data, 1962, 7(2),

269-71.

64.   Helberger, J.H. Naturwissenschaften, 1938, 26, 316-7.

65.   COELHO DE FIGUEIREDO.C.M. AND NOGUEIRA.L.,
Adamis, V.B. Bol. Tec., 1979, 22(3), 183-91.

66.   BACCOUCHE.M., GRABOW.H. AND ARZOUMANIAN. H.,
Fuhrhop, J.H., et al. J. Mol. Catal., 1980, 7(2), 245-56.

67.   SEKIGUCHI,O., OHKATSU.Y., AND OSA.T.,
Tezuka, M., Bull. Chem. Soc. Japan, 1976, 49(10),

2765-9.

68.   SEKIGUCHI.O. AND OSA.T.
Ohkatsu, Y. Bull. Chem. Soc. Japan, 1977, 50(3), 701-5.

69.   Akhundov, E.A. Mater. Nauchn. Konf. Aspir. Akad. Nauk. Az. SSR,

1980, 1, 246-52.

70.   Dufour-Ricroch, M.N. and Gandemer, A. Tetrahedron Lett., 1976,

(45), 4079-82.

71.   VELAPOLDI.R.A., HOFFMAN.L., SUZUKI.K. AND FERRARI.A.
Tsutsui, M., J. Am. Chem. Soc., 1969, 91(12), 3337-41.

72.   Keilin, J. Biochem. J., 1951, 49, 544-50.

73. Tabushi, I. and Koga, N. Tetrahedron Lett., 1979, (38), 3681-4.

74. U. S. Patent No. 4,202,992.

75. Fuhrhop, J. H., BACCOUCHE. M. AND PENZLIN. G. J. Mol. Catal., 1980, 7(2), 257-66.

76. Mochida, I., TAKEYOSHI. K., FUJITSU. H. AND TAKESHITA. K. Chem. Lett., 1976, (6), 589-92.

77. Tsuji, K., FUJITSU. H., TAKESHITA. K. AND MOCHIDA. I. J. Mol. Catal., 1980, 9(4), 389-98.

78. Harel, Y. and Manassen, J. J. Am. Chem. Soc., 1977, 99(17), 5817-18.

79. Domazetis, G., TARPEY. B., DOLPHIN. D. AND JAMES. B. R. J. Chem. Soc., Chem. Commun., 1980, (20), 939-40.

80. Lexa, D., SAVEANT. J. M. AND SOUFFLET. J. P. J. Electroanal. Chem. Interfacial Electrochem., 1979, 100, 159-72.

81. Eur. Pat. App. No. 19,517.

82. Eur. Pat. App. No. 4,224.

83. Wilson, H. D., HILDERBRAND. J. E. AND RINKER. R. G. J. Catal., 1978, 55(1), 116.

84. Manassen, J. J. Catal., 1970, 18(1), 38-45.

85. Vavrecka, P. and Weisser, O. Riv. dei Combust., 1978, 32(10), 331-9.

86. Ashmore, P. G. Catalysis and Inhibition of Chemical Reactions. London. Butterworths. 1963.

87. Hatch, L. F. Hydrocarbon Processing, 1969, 48(2), 77-88.

88. Rice, F. O. J. Am. Chem. Soc., 1931, 53, 1959-72.

89. Rice, F. O., JOHNSTON. W. R. AND EVERING. B. J. J. Am. Chem. Soc., 1932, 54, 3529-43.

90. Rice, F. O. J. Am. Chem. Soc., 1933, 55, 3035-40.

91.   Rice, F. O. and Dooley, M. D. J. Am. Chem. Soc., 1933, 55, 4245-7.

92.   Rice, F. O. and Johnston, W. R. J. Am. Chem. Soc., 1934, 56, 214-9.

93.   Rice, F. O. and Kerzfeld, K. F. J. Am. Chem. Soc., 1934, 56, 284-9.

94.   Rice, F. O. and Glasebrook, A. L. J. Am. Chem. Soc., 1934, 56, 741-3.

95.   Rice, F. O. and Whaley, F. R. J. Am. Chem. Soc., 1934, 56, 1311-3.

96.   Rice, F. O. and Evering, B. J. J. Am. Chem. Soc., 1934, 56, 2105-7.

97.   Rice, F. O. and Glasebrook, A. L. J. Am. Chem. Soc., 1934, 56, 2472.

98.   Rice, F. O. and Glasebrook, A. L. J. Am. Chem. Soc., 1934, 56, 2381-3.

99.   Rice, F. O. and Dooley, M. D. J. Am. Chem. Soc., 1934, 56, 2747-9.

100.   Rice, F. O. and Rodowskas, E. L. J. Am. Chem. Soc., 1935, 57, 350-2.

101.   Pryor, W. A. ed. Frontiers of Free Radical Chemistry. New York. Academic Press. 1980.

102.   Voge, H. H. and Good, G. M. J. Am. Chem. Soc., 1949, 71, 593.

103.   Kossiakoff, A. and Rice, F. O. J. Am. Chem. Soc., 1943, 65, 590.

104.   Stubbs, F. J. and Hinshelwood, C. N.   Disc. Faraday Soc.,

        1951, (10), 129.

105.   Sachanen, A. N.   Conversion of Petroleum. 2nd edition. New

        York.   Reinhold. 1948.

        DAVIS·H·G· AND EDDINGER·R·T·
106.   Oblad, A. G.   ed. Advances in Chemistry Series No. 183.

        Washington, D. C.   Am. Chem. Soc. 1979.

107.   Vogel, A. I. Textbook of Practical Organic Chemistry. London.

        Longmans.   1978.

        SIDERIUS·H·, HOOGENBOOM·B·E· AND VAN LEUSEN·O·
108.   van Leusen, A. M.,   Tetrahedron Letters, 1972, (52), 5337-40,

109.   Hinman, R. L. and Theodoropulos, S.   J. Org. Chem., 1963,

        28, 3052.

110.   Cheng, D. O. and Le Goff, E. Tetrahedron Letters, 1977, (17),

        1469.

        O'BRIEN. A.T. AND SUGIHARA·J.M
111.   Risolve, D. J.,   J. Chem. Eng. Data, 1968, 13(4), 588-90.

112.   Burr, S. H. and Seddon, K. R. Unpublished results.

        RAMSEY·V·G·, KALENDA·N·W· AND HANSON·W·E·
113.   Erdman, J. G.,   J. Am. Chem. Soc., 1956, 78, 5844-47.

        LONGO·F·R·, KAMPAS·F AND KIM·J·
114.   Adler, A. D.,   J. Inorg. Nucl. Chem., 1970, 32, 2443-45.

115.   Welcher, F. J. Organic Analytical Reagents. Vol 3. New York.

        Van Nostrand. 1947.

        LARDI·A·M·, MUZZI·M· AND MASSARA·A·
116.   Betri, V.,   Riv. Dei Combust., 1968, 22(2), 78-91.

117.   Kemp, W.   Organic Spectroscopy. London. Macmillan. 1975.

118.   Silverstein, R. M. and Bassler, G. C. Spectrometric Identification

        of Organic Compounds. 2nd edition. New York. Wiley. 1968.

119.   Pouchert, C. J. The Aldrich Library of Infrared Spectra. U.S.A.

        Aldrich Chemical Co. 1970.

120.   Fuhrhop, J. H. Smith, K. M. Laboratory Methods in Porphyrin

        and Metalloporphyrin Research. Amsterdam. Elsevier. 1975.

121.   Yen, T. F., VAUGHAN.G.B AND TYNAN.E.C. Chem. Geol., 1970, 6(5), 203-19.

122.   Anderson, J. R. Structure of Metallic Catalysts. London.

        Academic Press. 1975.

123.   Kenner, G. W. and Smith, K. M. Ann. N. Y. Acad. Sci. 1973, 206, 138.
        SEE FOOT OF THIS PAGE.

124.   Woodward, R. B. J. Am. Chem. Soc., 1960, 82, 3800-2.

125.   Evstigneeva, R. P. Pure Appl. Chem., 1981, 53(6), 1129-40.

126.   Paine, J. B., CHANG.G.W. AND DOLPHIN.D. Heterocycles, 1977, 7(2), 831-8.

127.   van Leusen, A. M., HOOGENBOOM.B.E. AND SIDERIUS.H. Tetrahedron Letters, 1972, (23), 2369-72.

128.   Smith, K. M. and Eivazi, F. J. Org. Chem., 1979, 44(14), 2591-2.

129.   Ostfeld, D. and Tsutsui, M. Acc. Chem. Res., 1974, 7(2), 52-8.

130.   Hermann, O., MEHDI.S.H. AND CORSINI.A. Can. J. Chem., 1978, 56(8), 1084-7.

131.   McLees, B. D. and Caughey, W. S. Biochem., 1968, 7(2), 642-52.

132.   Eisner, U. and Harding, M. J. C. J. Chem. Soc., 1964, 4089-4101.

133.   Groennings, S. Anal. Chem., 1953, 25, 938.

134.   Corwin, A. H., CAUGHEY,W.S., LEONE.A.M., DANIELEY.J.E. AND BAGLI.J.F. Symposium on nitrogen compounds in

        petroleum., Am. Chem. Soc., Div. Petrol. Chem., 1957, A35-A39.

135.   Baker, E. W. and Corwin, A. H., Am. Chem. Soc., Div. Petrol.

        Chem., Preprints, 1964, 9(1), 19-23.

AYER.W.A.   DUTLER.H.   LEIMGRUBER.W.
BEATON.J.M.   HANNAH.J.   LWOWSKI.W.
BICKELHAUPT.F   HAUCK.F.P.   SAUER.J.
BONNETT.R.   ITO.S.   VALENTA.Z
BUCHSCHACHER.P   LANGEMANN.A   VOLZ.H.
CLOSS.G.L.   LE GOFF.E.

136.   Nuzzi, M., Riv. dei Combust., 1965, 19(4), 171-185.

WU.G.Y. AND SUGIHARA.J.M.

137.   Branthaver, J. F., Symposium on asphaltenes and metals

in petroleum., Am. Chem. Soc., Div. Petrol. Chem., 1967,

A73-A75.

BRANTHAVER.J.F. AND WILLCOX, K.W.

138.   Sugihara, J. M., et al. Symposium on the Role of Trace Metals

in Petroleum., Am. Chem. Soc., Div. Petrol. Chem., 1973,

645-647.

139.   Brit. Pat. App. No. 35626/78, (1978).

QUIRKE.E., SHAW.G.J.,SOPER.P.D. AND MAXWELL.J.R.

140.   Martin, J., - . Tetrahedron, 1980, 36, 3261-7.

141.   Chakraborty S. and Bhatia, V. K., Indian J. Technol., 1981,

19(3), 92-99.

RINKER.R.G.AND CORCORAN.W.H.

142.   Wang, Y. L., - Ind. Eng. Chem. Fundam., 1963, 2(3), 161-8.

143.   Pacey, P. D. and Purnell, J. H. Ind. Eng. Chem. Fundam., 1972,

11(2), 233-9.

144.   Murata, M. and Saito, S.   J. Chem. Eng. Japan, 1975, 8(1), 39-45.

145.   Sandler, S. and Lanewala, M. A.   J. Chem. Eng. Data, 1963, 8,

258-60.

146.   Sandler, S. and Chung, Y. H.   Ind. Eng. Chem., 1961, 53, 391-4.

147.   Purnell, J. H.   Acta Ceint. Venez. Supl., 1973, 24(2), 40-8.

GREEN.E.J AND HALLEE.L.P.

148.   Zdonik, S. B., . Oil Gas J., 1967, 65(26), 96-101.

149.   Doue, F. and Guiochon, G.   J. Phys. Chem., 1969, 73(9), 2804-9.

150.   Ettre, L. S.   J. Chromatog., 1962, 8, 252.

151.   Powers, D. R. and Corcoran, W. H.   Ind. Eng. Chem. Fundam.,

1974, 13(4), 351-5.

152. Purnell, J. H. and Quinn, C. P. Proc. Royal Soc. (london).

Series A, 1962, <u>270</u>, 267-84.

GREEN·E·J·AND HALLEE·L·P.
153. Zdonik, S. B.,⎰⌐   Oil Gas J., 1967, <u>65</u>(30), 86-88.

154. Poyhonen, P. and Veijola, V. Kem. Teollisnus, 1970, <u>27</u>(4),

297-304.

155. Kitzen, M. R. Heat Technology, 1970, <u>1</u>(2), 8-13.

156. Partington, R. G. Disc. Faraday Soc., 1947, (2), 114-6.

157. Pacey, P. D. and Purnell, J. H. Int. J. Chem. Kinet., 1972, <u>4</u>, 657.

SERES·L· AND MARTA·F.
158. Berces, T.,⎰   . Acta Chim. (Budapest), 1972, <u>71</u>(1), 31-45.

159. Sagert, N. H. and Laidler, K. J. Can. J. Chem., 1963, <u>41</u>, 838-47.

160. Frey, F. E. and Smith, D. F. Ind. Eng. Chem., 1928, <u>20</u>, 948.

161. Tilicheyev, M. D. Foreign Petrol. Tech., 1939, <u>7</u>(5/6), 209-24.

162. Purnell, J. H. and Quinn, C. P. J. Chem. Soc., 1961, 4128-32.

163. Stark, J. G. and Wallace, H. G. Chemistry Data Book. London.

John Murray. 1978.

164. Blakemore, J. E. and Corcoran, W. H. Ind. Eng. Chem., Process

Des. Devel., 1969, <u>8</u>(2), 206-9.

165. Torok, J. and Sandler, S. Can. J. Chem., 1969, <u>47</u>(14), 2707-12.

166. Purnell, J. H. J. Chem. Soc., Faraday Trans. I. 1974, <u>70</u>(3), 594-9.

167. Sundaram, K. M. and Froment, G. F. Chem. Eng. Sci., 1977,

<u>32</u>(6), 609-17.

WELTHER·K· AND SZEPESY·L.
168. Illes, V.,⎰et al. Acta Chim. (Budapest), 1974, <u>80</u>(1), 1-17.

GREEN·E·J·AND HALLEE·L·P.
169. Zdonik, S. B.,⎰   Oil Gas J., 1967, <u>65</u>(32), 133-8.

170. Chrysochoos, J. and Bryce, W. A. Can. J. Chem., 1965, 43(9), 2457-64.

171. Chrysochoos, J. and Bryce, W. A. Trans. Faraday Soc., 1965, 61(515), 2447-55.

172. Pilcher, K. A. and Winterbottom, J. M., Chem. Eng. Technol., 1988, 11(2), 89-94.

173. Illes, V. Acta Chim. Acad. Sci. Hung., 1969, 59(1), 35-55.